

IRIDIUM CATALYZED C–H 1,2-DIBORYLATION AND 1,2,3-TRIBORYLATION OF ARENES THROUGH THE USE  
OF ANTI-AROMATIC PYRAZINE BASED LIGANDS AND OTHER BORON RELATED STUDIES

By

Thomas Jonathan Oleskey

A DISSERTATION

Submitted to  
Michigan State University  
in partial fulfillment of the requirements  
for the degree of

Chemistry – Doctor of Philosophy

2025

## ABSTRACT

During the last few decades iridium catalyzed C–H borylations have become an important method to access aryl boronic esters. As aryl C–H borylations are governed predominately by sterics, this reaction offers a complementary regiochemical approach to traditional synthetic routes accessing aromatic boronic esters such as metal halogen exchange and Miyaura borylation.

As these reactions can be reliably directed away from positions ortho to any functionality other than hydrogen, fluorine, and nitriles, iridium catalyzed borylations find ample use in industry and total synthesis.

Since this reaction is directed sterically and not electronically, regiochemical selectivity can become challenging in cases where multiple activation sites are available, especially in the case of 1,2-disubstituted arenes. To overcome this challenge, we developed a method for para selective borylation of phenols and anilines utilizing alkyl ammonium cations as steric shields to direct borylation. We further show how this methodology can be expanded to utilize in situ heteroatom borylation in place of the alkyl ammonium cations to access the same para selectivity.

We further utilized existing 4,4,5,5-tetramethyl-1,3,2-dioxaborolane (Bpin) functionalities to guide the regiochemistry of iridium catalyzed C–H borylation ortho to itself to access 1,2-diborylated arenes as well as new 1,2,3-triborylated arenes.

As borylated compounds are important synthetic intermediates, being able to study C–H borylations mechanistically offers important insights into reactions utilizing these compounds. We therefore investigated developing a method to measure boron heavy atom isotope effects using fluorine reporters and NMR to observe boron isotopic distributions.

## TABLE OF CONTENTS

<b>Chapter 1: Introduction to Iridium Catalyzed C–H Borylations.....</b>	<b>1</b>
REFERENCES .....	10
<b>Chapter 2: 1,2 and 1,2,3 Di and TriBorylation Through the Use of Novel Antiaromatic Pyrazine Based Ligands .....</b>	<b>12</b>
Experimental Procedures .....	23
REFERENCES .....	43
<b>Chapter 3: <i>Para</i> Selective C–H Borylation of Sulfonated Phenols, Anilines, and Benzyl Alcohols Equipped with a Tetraalkylammonium Steric Shield .....</b>	<b>45</b>
Experimental Procedures .....	54
REFERENCES .....	73
<b>Chapter 4: Steric Shielding Effects induced by Intramolecular C–H•••O Hydrogen Bonding: Remote Borylation Directed by Bpin Groups.....</b>	<b>76</b>
Experimental Procedures .....	92
REFERENCES .....	98
<b>Chapter 5: Measurement of Isotopic Distribution of Boron.....</b>	<b>102</b>
Experimental Procedures .....	110
REFERENCES .....	114
<b>APPENDIX A: NMR SPECTRA .....</b>	<b>115</b>
<b>APPENDIX B: CRYSTALLOGRAPHIC DATA.....</b>	<b>355</b>

## Chapter 1: Introduction to Iridium Catalyzed C–H Borylations

It is hard to find a type of substrate as useful as an aryl boronic acid or ester. When it comes to aryl couplings there is hardly a reaction as ubiquitous as the Suzuki coupling.<sup>1</sup> In 2011 a review was published characterizing all the palladium catalyzed C–C coupling reactions wherein it was found by no small margin, the Suzuki coupling was the most used reaction reported.<sup>2</sup> This speaks volumes to the importance of aryl boronic acids and esters as starting materials. Additionally, these functionalities can undergo a multitude of reactions to generate a myriad of functionalities as shown in Figure 1-1.<sup>1,3-11</sup> Because of this utility, I like to affectionately refer to boronic esters as the stem cells of chemistry.

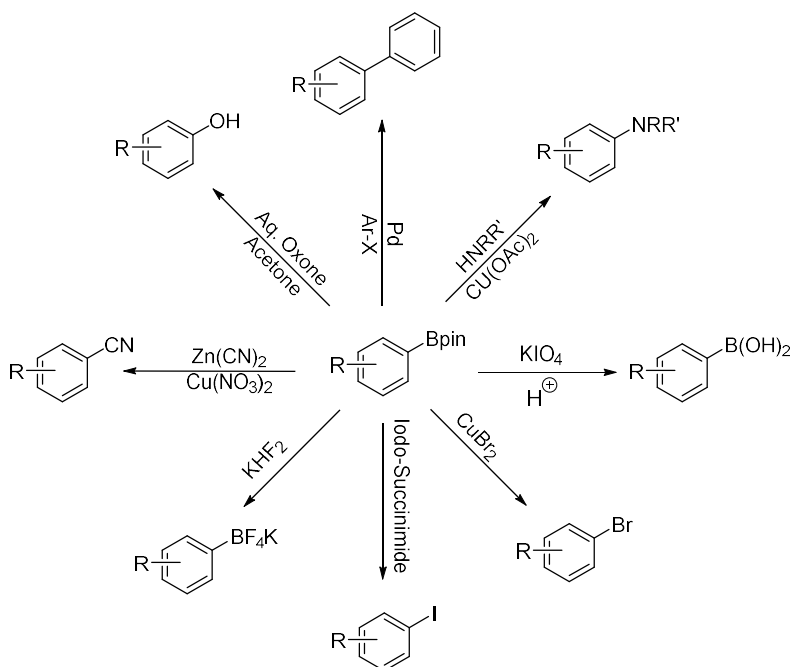


Figure 1-1 Derivatization Paths for Aryl Boronic Pinacolate Esters

Between boronic acids and esters, both exhibit extraordinarily similar reactivities, to the point that they are often used interchangeably throughout the literature. The more useful of these is generally regarded to be boronic esters, notably as the pinacolate ester, as they tend to be more stable than their corresponding boronic acid counterparts while also often exhibiting superior solubility in organic solvents.

Traditionally, aryl boronic esters have been synthesized directly from aryl halides via metal halogen exchange followed by quenching with an isopropyl borate.<sup>12</sup> This, however, is a non-ideal way to synthesize these reagents as the metalated intermediate is a highly reactive species that is not tolerant of many functional groups. Therefore, this approach is greatly limited in the products that it can access.



Additionally metal halogen exchange is dependent on the availability of halogenated starting materials, further limiting the compounds that can be practically synthesized. Because of this, many alternative routes to aryl boronic esters have been developed. The most notable of these is the Miyaura borylation (Figure 1-2), which can safely be said to be the predominant route to these materials in synthetic literature.

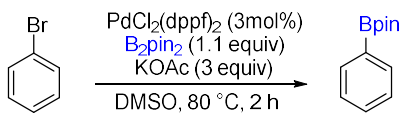


Figure 1-2 A Representative Example of a Typical Miyaura Borylation

In the Miyaura borylation, an aryl halide is coupled with a borane or diboron reagent most often 4,4,4',4',5,5,5',5'-octamethyl-2,2'-bi(1,3,2-dioxaborolane) ( $\text{B}_2\text{pin}_2$ ) to generate a boronic ester via palladium catalyzed cross coupling.<sup>13</sup> Like metal halogen exchange, Miyaura borylations also suffer from the same problem in the fact that they are reliant on access to an initial halogenated starting material. This often limits the accessible boronic esters to positions that are accessible to electrophilic aromatic substitution type halogenation reactions. While extraordinarily useful, it is inherently limited. Ideally aryl boronic esters would be able to be installed directly from C–H bonds, avoiding reliance on halogenated starting materials, and allowing access to positions not accessible by electrophilic aromatic substitution regioselectivity. This brings us to the rise of Iridium catalyzed borylations.

While iridium catalyzed C–H borylations were predated by photochemical tungsten C–H borylations,<sup>14</sup> the birth of a thermal catalytic method for C–H borylation allowed for the proliferation of C–H borylations in synthesis. The first thermal catalytic C–H borylation was discovered by the Smith group in 1999 of which Smith affectionately referred to it as “*The worst catalyst ever published in JACS*” (Figure 1-3).<sup>15</sup> Despite having a turnover of approximately 3, this reaction was a landmark in boron chemistry.

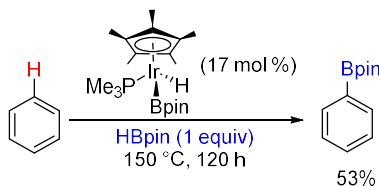
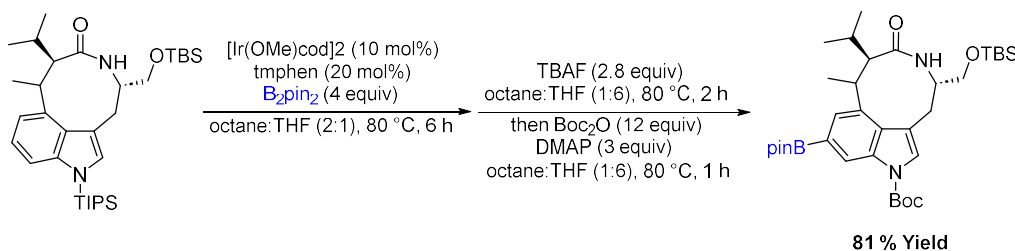


Figure 1-3 First Published Thermal Catalytic C–H Borylation

This iridium catalyst was quickly improved first by the institution of phosphine ligands followed by transition to dipyrindine ligands instituted by Hartwig, which brought the catalytic turnover from 3 all the way to 14000.<sup>16,17</sup> This reactivity makes this catalyst industrially relevant. This coupled with how tolerant

iridium catalyzed borylations are of functional groups, makes this reaction particularly useful for late-stage functionalization. This was demonstrated by the Baran research group who used this chemistry to install a boronic ester on an indole scaffold late in the synthesis of teleocidins and even on a gram scale.<sup>18</sup> This systems robust utility is further demonstrated by Merck which utilized an iridium catalyzed borylation on a 85 Kg scale to in the presence of chlorine and iodine functionalities who are typically activated in most metal catalysis (Figure1-4).<sup>19</sup>

### C–H Borylation Utilized by Baran in the Synthesis of Teleocidins



### C–H Borylation Utilized by Merck in the Synthesis of c-Met/ALK Inhibitor HS-10168

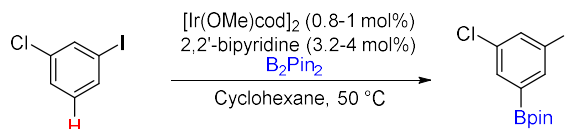


*Figure 1-4 Synthesis towards Teleocidins using Iridium Catalyzed Borylations by Phil Baran and the Kg Scale C–H Borylation of 1-Chloro-3-Iodobenzene by Merck*

Having developed the current method for iridium catalyzed CH borylation, studies were undertaken by Hartwig to understand the general mechanism of the catalytic cycle. It was debated whether the catalytic cycle was III–V or I–III before it was definitively shown to be III–V by Hartwig in 2009 as shown in Figure 1-5.<sup>17</sup> Even more is that the Hartwig group was able to isolate and characterize the resting catalyst which provided an unusual insight into this methodology.

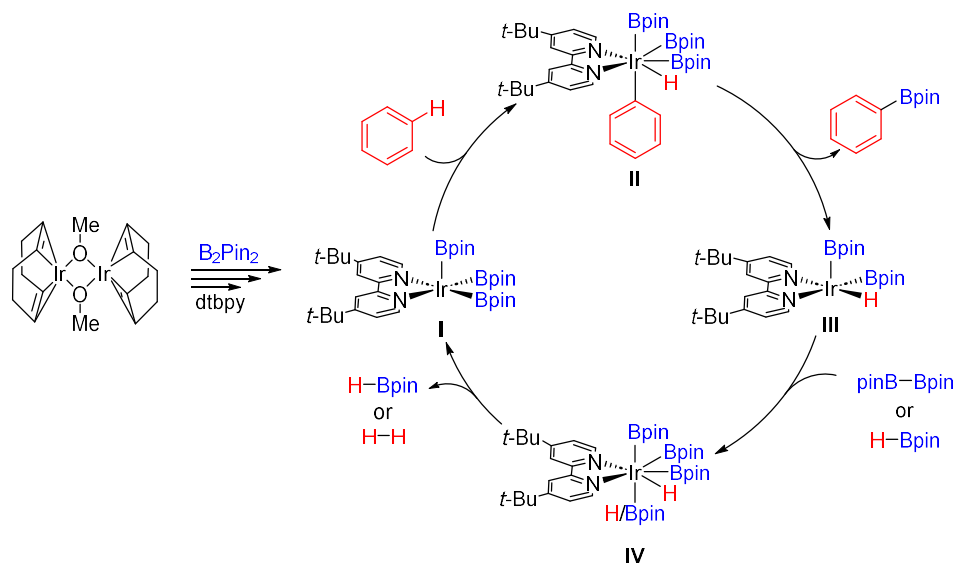


*Figure 1-5 C–H Borylation Catalytic Cycle as Established by Hartwig*

In the catalytic cycle, an iridium(I) catalyst is used which when treated with boron source (either HBpin or the preferred  $B_2pin_2$ ) and a ligand, undergoes oxidative addition with the boron source and assembles into the active resting catalyst (structure I in Figure 1-5). This active resting catalyst, often referred to as the tris-boryl, is then able to undergo oxidative addition with an aryl C–H bond (Structure II in Figure 1-5), which subsequently undergoes reductive elimination to generate a borylated arene. The resulting iridium(III) catalyst (Structure III Figure 1-5) once again can undergo oxidative addition with a boron source to generate the iridium(V) intermediate (Structure IV Figure 1-5), which can undergo reductive elimination to release either HBpin or  $H_2$  gas thus completing the catalytic cycle. It is important to note that the side product of this catalytic cycle when using  $B_2pin_2$  is HBpin, which can itself act as a boron source for this reaction. Because of this it is possible to run these reactions at half stoichiometric loadings of  $B_2pin_2$  or stoichiometric loadings of HBpin.

Ligands were also investigated for activity in this system wherein it became evident that iridium metal centers ligated with bipyridine ligands containing electron withdrawing groups were less active than those with donating groups. It is important to note that the pyridine rings of ligands can be borylated. As boronic esters are electron withdrawing this can also lead to lower activity of the catalyst over the course of a reaction.<sup>20</sup> Because of this, most ligands have a substituent in the 4 and 4' position of the pyridine rings such as in 4,4'-di-tert-butyl-2,2'-dipyridine (dtbpy) which has become one of the most commonly used ligands for iridium catalyzed CH borylations along with 3,4,7,8-tetramethyl-1,10-phenanthroline (tmphen).

With an active catalyst able to initiate C–H activation followed by borylation, the question becomes which C–H position will be activated? For example, observe anisole shown in Figure 1-6, which hydrogen will be activated? The answer is surprisingly simple. As a rule, unless directed iridium catalyzed C–H borylations are sterically guided. They can only borylate sterically accessible positions or positions that have no groups other than hydrogen, fluorine, or nitriles adjacent to them. In the case of anisole, the hydrogens denoted in red in Figure 1-6 are not active to iridium catalyzed borylations as they are adjacent to the methoxy group.

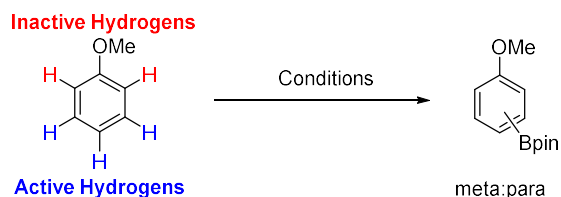


Figure 1-6 Borylation of Anisole

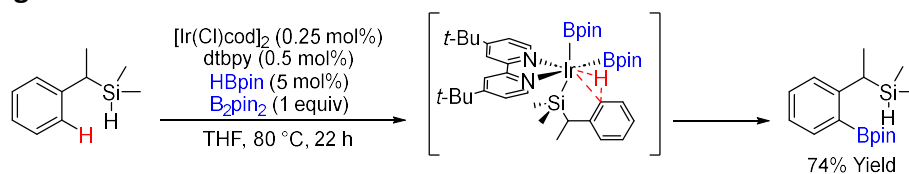
Fluorine and nitriles due to their small steric presence, and in the case of nitriles, linear shape can undergo C–H borylation adjacent to themselves, therefore, it is possible and sometimes favorable to borylate positions next to these groups. Two groups worth mentioning as well are chlorine and methoxy. While it is “possible” to borylate adjacent to these groups as well, it is rather unfavorable and rarely observed. This regioselectivity does however have a severe shortcoming, and that is in the case of substrates with more than one sterically accessible hydrogen present. In these cases, both positions will be borylated equally leading to a statistical distribution of regioisomers as also illustrated in Figure 1-6. While steric environment is typically the determining factor in iridium catalyzed borylations, many groups have devoted research to further improving regioselectivity, especially in systems where multiple accessible borylation positions are available. These guided borylations are typically placed into three categories: ortho borylation, *meta* borylation, and para borylation.

Ortho borylation typically refers to borylation ortho to a directing group. These directing groups may be inherent to the target of interest or installed prior to borylation. The first published example of ortho borylation was by the Hartwig group who utilized silyl groups to direct borylation ortho to themselves.<sup>21</sup> Hartwig was able to utilize a silane iridium binding interaction to direct borylations. This strategy was then mirrored by Ishiyama who developed a monodentate phosphine ligand that was able to easily dissociate providing a spot for imines to coordinate to direct borylations ortho to themselves. This approach has since been applied to other groups such as esters and phosphates.

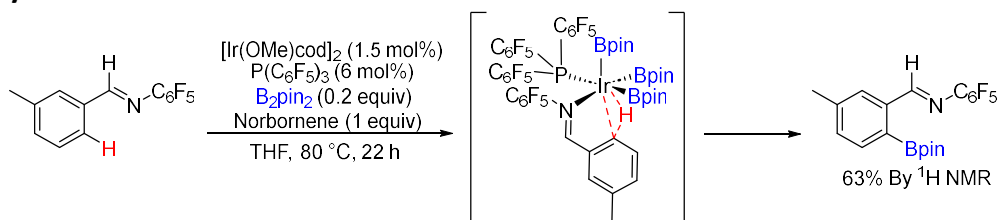
For a substrate to coordinate to a metal center, the catalyst first must have an open coordination position available. Common bipyridine borylation ligands do not allow for this as they are very rigid and strongly donating and therefore do not allow for two open coordination positions. Unfortunately, the iridium catalyst cannot be easily stabilized with monodentate ligands.

This led to the idea of utilizing hemilabile ligands or bidentate ligands with a labile half.<sup>30</sup> These hemilabile ligands can dissociate part of themselves from the metal center in solution thus freeing a second coordination spot on the iridium metal center. This allows for chelation to the iridium thus directing borylation ortho to the chelating group. This strategy has since been applied to substrates containing many other functional groups such as thioethers, hydrazones, aldehydes, and benzylamines. If borylations can be directed by attaching a substrate to the metal center, it should be possible to direct borylations by attaching starting materials to the ligand of the active catalyst. This was the approach that a few groups also took to achieve ortho borylations. By utilizing interactions such as electrostatics, Lewis's acid-base interactions, and hydrogen bonding, borylations were able to be directed ortho to.

**[A] Hartwig 2008<sup>21</sup>**



**[B] Ishiyama 2014<sup>16</sup>**



**[C] Lassaletta 2011<sup>30</sup>**

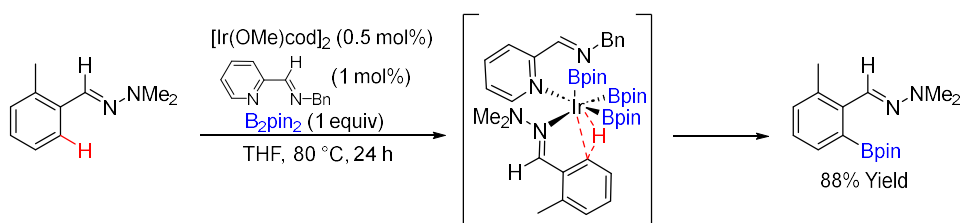
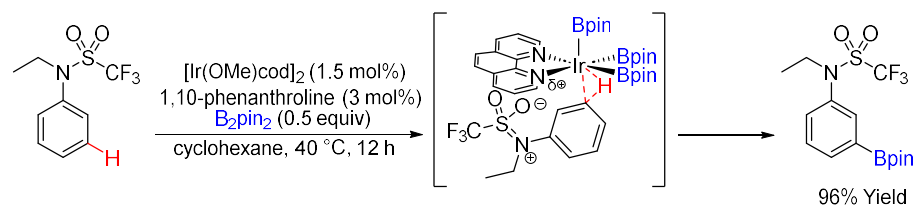


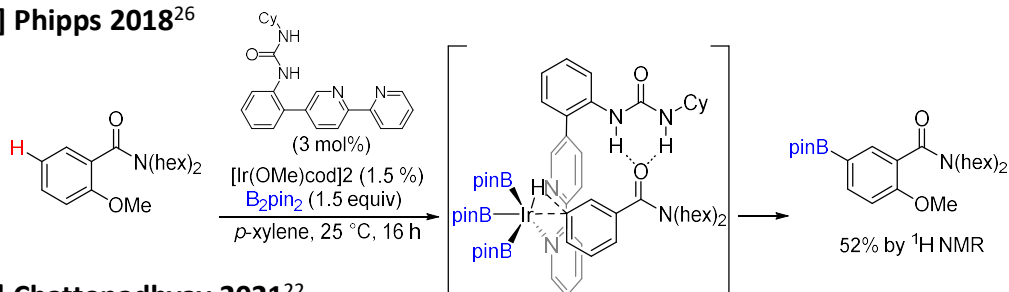
Figure 1-7 Select Examples of ortho-Borylations

*Meta* directed borylations are the easiest position to borylate in the case of 1,3- disubstituted arenes, however, when there is no 3 substituent, to achieve selectively is a bit trickier. In these systems para borylation is possible as well. The trick is differentiating between the *meta* and *para* positions. Many of the *meta* direction strategies mimic that of ortho borylation strategies such as using ligand substrate interactions to guide reactivity. In the *meta* directed substrates, the same strategies are used albeit with longer tethering groups to push borylation to the *meta* position as opposed to *ortho*.<sup>22,23</sup> In addition to what was used in ortho borylations a new strategy appeared here; wherein ionic attraction was utilized by the Phipps group to be used to attract quaternary ammonium salts to a sulfate ligand guiding *meta* selectivity.<sup>24-26</sup>

**[A] Kuninobu and Kanai 2015<sup>29</sup>**



**[B] Phipps 2018<sup>26</sup>**



**[C] Chattopadhyay 2021<sup>22</sup>**

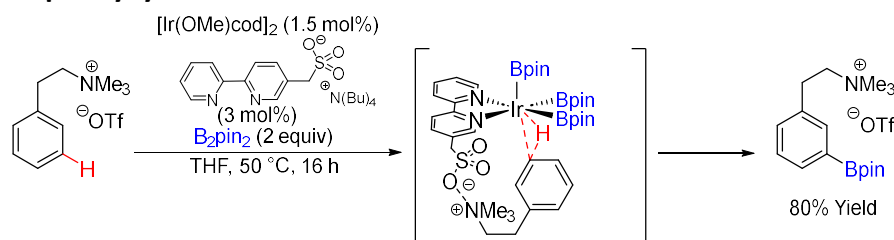
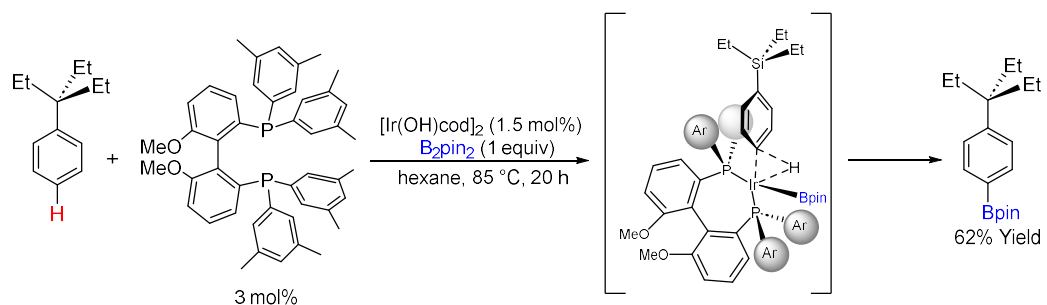


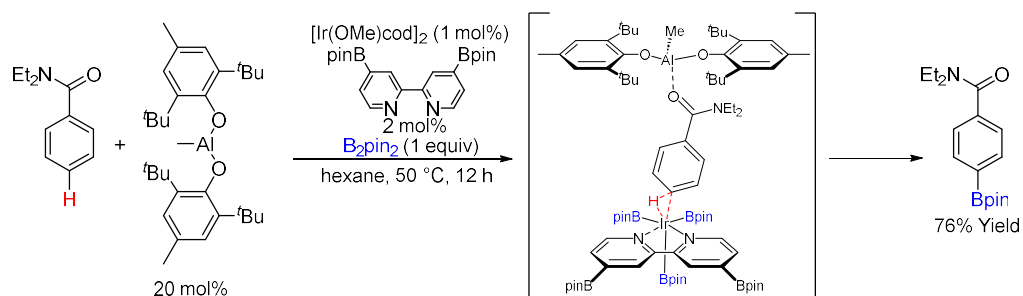
*Figure 1-8 Select Examples of meta-Borylations*

Para borylation is easily the hardest to target selectively. This is because it falls squarely in the domain of remote functionalization, meaning there is no directing group close to the position of interest. That coupled by the competition with the *meta* position mentioned above makes these positions difficult to target selectively. So far only a handful of strategies have been developed to target these positions. One method is a strategy by Chattopadhyay, where he implemented an unusually long ligand with a potassium alkoxide group to guide borylation para to aryl esters.<sup>23</sup> Other methods targeting para borylation take advantage of the high steric selectivity seen in iridium catalyzed borylations. In 2017, two methods were published utilizing modified steric environments to guide selectivity. Nakao utilized bulky aluminum Lewis acids to coordinate to amides to greatly exaggerate their steric presence pushing borylation to the para position.<sup>27</sup> This was further expanded to pyridines. The other method of doing this was demonstrated by Itami who developed a particularly bulky diphosphine ligand that when coordinated with an iridium metal center formed a pseudo active pocket only allowing unencumbered arenes access to the metal center and therefore borylate at the para position.<sup>28</sup>

**[A] Segawa and Itami 2015<sup>28</sup>**



**[B] Nakao 2017<sup>27</sup>**



**[C] Chattopadhyay 2017<sup>23</sup>**

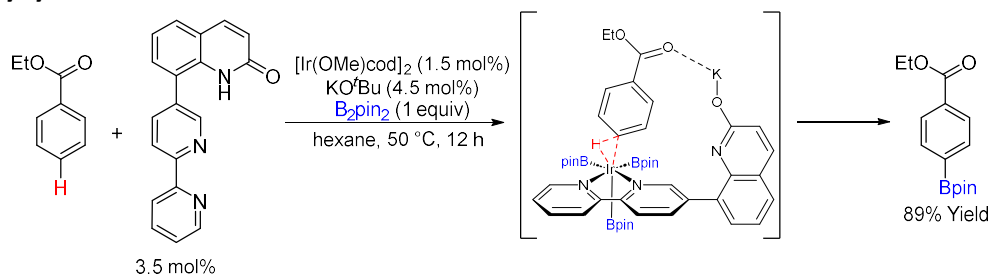


*Figure 1-9 Select Examples of para-Borylations*

Iridium catalyzed borylations are one of the most important catalytic reactions developed in the twenty first century. It gives predictable selectivity while being a robust reaction capable of tolerating many functional groups even at low catalytic loadings. This is exemplified by its use in industry and total synthesis by groups other than its developers. As it is one of the most well understood catalytic cycles, much work has been done to push the capabilities of this reaction to their highest potential through guidance of selectivity as well as optimization of catalytic conditions. Despite the work that has already been done, there are ample opportunities to further expand this field of chemistry as well as the selectivity possible with this reaction.



## REFERENCES

- (1) Miyaoura, N.; Yamada, K.; Suzuki, A. A New Stereospecific Cross-Coupling by the Palladium-Catalyzed Reaction of 1-Alkenylboranes with 1-Alkenyl or 1-Alkynyl Halides. *Tetrahedron Lett.* **1979**, *20*, 3437–3440.
- (2) Colacot, T. J. The 2010 Nobel Prize in Chemistry: Palladium-Catalysed Cross-Coupling. *Platin. Met. Rev.* **2011**, *55*, 84–90.
- (3) Thiebes, C.; Petasis, N. A.; Olah, G. A. Mild Preparation of Haloarenes by Ipso-Substitution of Arylboronic Acids with N-Halosuccinimides *Synlett* **1998**, *2*, 141-142.
- (4) Chan, D. M. T.; Monaco, K. L. Wang, R. P.; Winters, M. P. New N- and O-arylations with Phenylboronic Acids and Cupric Acetate *Tetrahedron Letters*, **1998**, *39*, 2933-2936.
- (5) Evans, D. A.; Katz, J. L.; West, T. R. Synthesis of diaryl ethers through the copper-promoted arylation of phenols with arylboronic acids. An expedient synthesis of thyroxine *Tetrahedron Letters*, **1998**, *39*, 2937-2940.
- (6) Lam, P. Y. S.; Clark, C. G.; Saubern, S.; Adams, J.; Winters, M. P.; Chan, D. M. T.; Combs, A. New Aryl/Heteroaryl C-N Bond Cross-coupling Reactions via Arylboronic Acid/Cupric Acetate Arylation *Tetrahedron Letters*, **1998**, *39*, 2941-2944.
- (7) Yuen, A. K. L.; Hutton, C. A. Deprotection of Pinacolyl Boronate Esters via Hydrolysis of Intermediate Potassium Trifluoroborates *Tetrahedron Letters*, **2005**, *49*, 7899-7903.
- (8) Tang, Y. L.; Xia, X. S.; Gao, J. C.; Li, M. X.; Mao, Z. W. Direct bromodeboronation of arylboronic acids with CuBr<sub>2</sub> in water *Tetrahedron Letters*, **2021**, *64*, 152738.
- (9) Molander, G. A.; Fumagalli, T. Palladium(0)-catalyzed Suzuki-Miyaura cross-coupling reactions of potassium aryl- and heteroaryltrifluoroborates with alkenyl bromides *J. Org. Chem.* **2006**, *71*, 5743-5747.
- (10) Liskey, C. W.; Liao, X.; Hartwig, J. F. Cyanation of Arenes via Iridium-Catalyzed Borylation. *J. Am. Chem. Soc.* **2010**, *132*, 11389–11391.
- (11) Molloy, J. J.; Thomas, A.; Irving, C. Anderson, N. A.; Lloyd-Jones, G. C. Chemoselective Oxidation of Aryl Organoboron Systems Enabled by Boronic Acid-Selective Phase Transfer *Chemical Science*, **2017**, *8*, 1551-1559.
- (12) Brown, H.; Cole, T. E. Organoboranes. 31. A Simple Preparation of Boronic Esters From Organolithium Reagents and Selected Trialkoxyboranes *Organometallics*, **1983**, *2*, 1316-1319.
- (13) Ishiyama, T.; Murata, M.; Miyaoura, N. Palladium(0)-Catalyzed Cross-Coupling Reaction of Alkoxydiboron with Haloarenes: A Direct Procedure for Arylboronic Esters *J. Org. Chem.* **1995**, *60*, 7508-7510.
- (14) Chen, H.; Hartwig, J. F. Catalytic, Regiospecific End-Functionalization of Alkanes : Rhenium-Catalyzed Borylation under Photochemical Conditions *Angew. Chem. Int. Ed.* **1999**, *38*, 3391-3393.
- (15) Iverson, C. N.; Smith III, M. R. Stoichiometric and Catalytic B–C Bond Formation from Unactivated Hydrocarbons and Boranes *J. Am. Chem. Soc.* **1999**, *121*, 7696-7697
- (16) A.) Ishiyama, T.; Isou, H.; Kikuchi, T.; Miyaoura, N. Ortho-C–H Borylation of Benzoate Esters with Bis(Pinacolato)Diboron Catalyzed by Iridium–Phosphine Complexes. *Chem. Commun.* **2010**, *46*, 159–161. B.) Sasaki, I.; Amou, T.; Ito, H.; Ishiyama, T. Iridium-catalyzed ortho-C–H

Borylation of Aromatic Aldimines Derived from Pentafluoroaniline with bis(pinacolate)diboron *org. Biomol. Chem.* **2014**, *12*, 2041-2044.

- (17) Boller, T. M.; Murphy, J. M.; Hapke, M.; Ishiyama, T.; Miyaura, N.; Hartwig, J. F. Mechanism of the Mild Functionalization of Arenes by Diboron Reagents Catalyzed by Iridium Complexes. Intermediacy and Chemistry of Bipyridine-Ligated Iridium Trisboryl Complexes *J. Am. Chem. Soc.* **2005**, *127*, 14263 – 14278
- (18) Nakamura, H.; Yasui, K.; Kanda, Y.; Baran, P. S. 11-Step Total Synthesis of Teleocidins B1-B-4. *J. Am. Chem. Soc.* **2019**, *141*, 1494–1497.
- (19) Campeau, L. C.; Chen, Q.; Gauvreau, D.; Girardin, M.; Belyk, K.; Maligres, P.; Zhou, G.; Gu, C.; Zhang, W. Tan, L.; O'Shea, P. D. A Robust Kilo-Scale Synthesis of Doravirine *Org. Process Res. Dev.* **2016**, *20*, 1476–1481.
- (20) Larsen, M. A.; Oeschger, R. J.; Hartwig, J. F. Effect of Ligand Structure on the Electron Density and Activity of Iridium Catalysts for the Borylation of Alkanes *ACS Catal.* **2020**, *10*, 3415-3424.
- (21) Boebel, T. A.; Hartwig, J. F. Silyl-Directed, Iridium-Catalyzed Ortho-Borylation of Arenes. A One-Pot Ortho-Borylation of Phenols, Arylamines, and Alkylarenes *J. Am. Chem. Soc.* **2008**, *130*, 7534–7535
- (22) Chaturvedi, J.; Haldar, C.; Bisht, R.; Pandey, G. Chattopadhyay, B. *Meta* Selective C–H Borylation of Sterically Biased and Unbiased Substrates Directed by Electrostatic Interaction *J. Am. Chem. Soc.* **2021**, *143*, 7604–7611.
- (23) Hoque, D.; Bisht, R.; Haldar, C.; Chattopadhyay, B. Noncovalent Interactions in Ir-Catalyzed C–H Activation: L-Shaped Ligand for Para-Selective Borylation of Aromatic Esters *J. Am. Chem. Soc.* **2017**, *139*, 7745–7748.
- (24) Davis, H. J.; Genov, G. R.; Phipps, R. *meta*-Selective C–H Borylation of Benzylamine-, Phenethylamine-, and Phenylpropylamine-Derived Amides Enabled by a Single Anionic Ligand *J. Angew. Chem. Int. Ed.* **2017**, *56*, 13351–13355.
- (25) Davis, H. J.; Mihai, M. T.; Phipps, R. J. Ion Pair-Directed Regiocontrol in Transition-Metal Catalysis: A *Meta*-Selective C–H Borylation of Aromatic Quaternary Ammonium Salts *J. Am. Chem. Soc.* **2016**, *138*, 12759–12762.
- (26) Mihai, M. T.; Davis, H. J.; Genov, G. R.; Phipps, R. Ion Pair-Directed C–H Activation on Flexible Ammonium Salts: *meta*-Selective Borylation of Quaternized Phenethylamines and Phenylpropylamines *J. ACS Catalysis.* **2018**, *8*, 3764–3769.
- (27) Yang, L.; Semba, K.; Nakao, Y. para-Selective C–H Borylation of (Hetero)Arenes by Cooperative Iridium/Aluminum Catalysis *Angew. Chem.* **2017**, *129*, 4931 –4935.
- (28) Saito, Y.; Segawa, Y.; Itami, K. para-C–H Borylation of Benzene Derivatives by a Bulky Iridium Catalyst *J. Am. Chem. Soc.* **2015**, *137*, 5193–5198.
- (29) Kuninobu, Y.; Ida, H.; Nishi, M.; Kanai, M. A *meta*-Selective C–H borylation Directed by a Secondary Interaction Between Ligand and Substrate *Nature Chemistry* **2015**, *7*, 712-717.
- (30) Ros, A.; Estepa, B.; Lopez-Rodriguez, R.; Alvarez, E.; Fernandez, R.; Lassaletta, J. M. Use of Hemilabile N,N Ligands in Nitrogen-Directed Iridium- Catalyzed Borylations of Arenes *Angew. Chem. Int. Ed.* **2011**, *50*, 11724-11728.

## Chapter 2: 1,2 and 1,2,3 Di and TriBorylation Through the Use of Novel Antiaromatic Pyrazine Based Ligands

1,2-Diborylated arenes are interesting starting materials. They can be derivatized like traditional aryl borates and they are amenable for the rapid assembly of polycyclic aromatics through Suzuki couplings.<sup>1</sup> With polycyclic aromatics being used in the synthesis of organic semiconductors and ligands such as those shown in Figure 2-1, access to a variety of 1,2 borylated arenes would be useful for the assembly of polycyclic aromatics containing a variety of functional groups.<sup>2-4</sup>

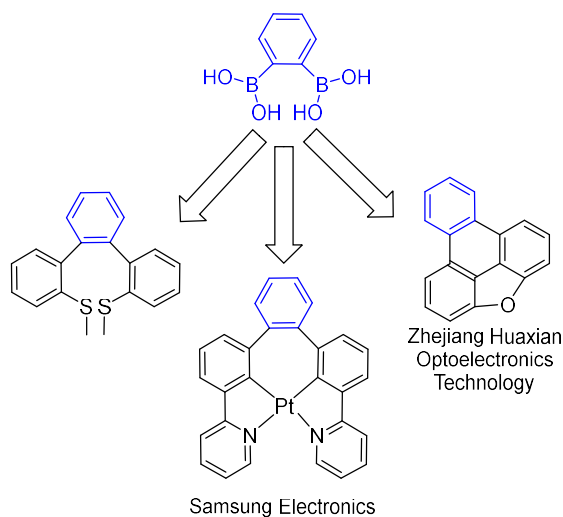


*Figure 2-1 Organic Semiconductors and Ligands Derived from 1,2-Benzenediboronic Acid bis(Pinacol)  
Ester*

Traditionally, formation of 1,2-Diborylated arenes were synthesized via halogen metal exchange of 1,2-dihalogenated arenes with magnesium or lithium followed by addition of an isopropyl borate to form the 1,2-diborylated species.<sup>5</sup> As this method relies on the presence of preexisting halogens it can be limited by the availability of starting materials halogenated in the correct positions. Additionally metal halogen exchange is a non-ideal route to 1,2-diborylated aryl structures as the reactive intermediates are highly reactive functionalities and do not tolerate a wide variety of functional groups and risk initiating side reactions such as the halogen dance reaction. This greatly limits the practical utility of these methodologies, especially for late-stage functionalization. Because of this, other routes to 1,2-diborylated arenes have since been developed including benzyne chemistry<sup>6,7</sup>, earth abundant metal catalysis<sup>7,8</sup>, electrochemistry<sup>10</sup>, and photochemistry<sup>11</sup>. The most notable route to these compounds by far however is Miyaura borylation<sup>12</sup>. Akin to metal halogen exchange, Miyaura borylation also relies on halogenated

starting materials which often means that one is limited to electrophilic aromatic substitution (EAS) halogenation patterns due to availability of halogenated starting materials. Additionally with these methods synthesis of some compounds such as 1,2-diborylated arenes containing iodine functionalities is impossible. Ideally, 1,2-diborylated arenes could be directly synthesized utilizing iridium catalyzed C–H borylation.

As previously established in Chapter 1, general selectivity of iridium aryl C–H borylations is well understood. Therefore, it is no surprise that aryl borylation *ortho* to existing boronic pinacol esters do not happen, due to the steric presence of the existing Bpin. Because of this, synthesis of 1,2 di-borylated arenes are almost impossible to synthesize via C–H borylation.

To date, iridium catalyzed C–H aryl borylations *ortho* to existing boronic pinacolate esters are practically unheard of, with no methods of undirected 1,2 diborylations having been developed. Only one method of accessing this selectivity with iridium C–H borylation has been developed in which the Suginome group mirrored the approach for silylation *ortho* to aryl boronic acids.<sup>13,14</sup> In both cases the starting boronic acids were converted into azaborolidines with pyrazol-5-ylaniline to form the Bpza group that acts as a directing group (Figure 2-2). It is theorized that the Bpza binds to the catalyst metal center to guide C–H activation *ortho* to itself. While this is impressive, it adds an additional 2 steps to the borylation process: adding and removing the Bpza directing / protecting group. This methodology is limited to accessing 1,2-diborylated compounds and no 1,2,3-triborylation was observed.

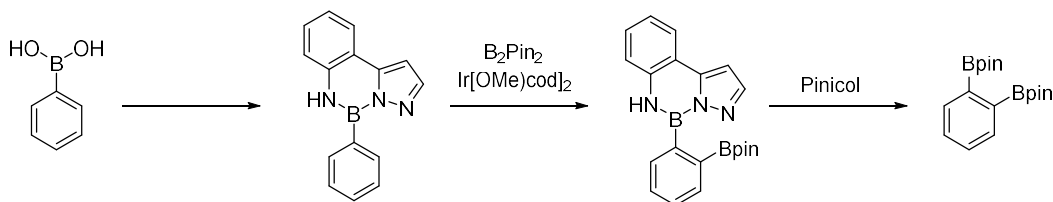
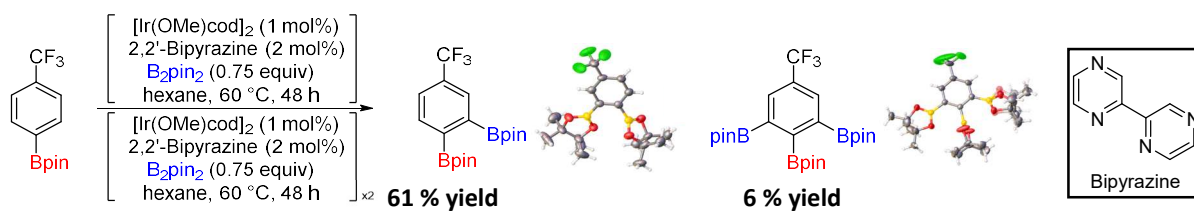


Figure 2-2 C–H Borylation *Ortho* to a Boronic Pinacolate Ester as Reported by Suginome

Previously, while screening ligands for ones that favors electronically activated positions, my prior group member Jayasundara found that iridium C–H borylations using 2,2'-bipyrazine as a ligand generated 1,2 diborylation and 1,2,3-triborylated products (Figure 2-3).<sup>15</sup>



*Figure 2-3 1,2-Diborylated and 1,2,3-Triborylated Product Observed by Jayasundara*

As this selectivity was exceedingly unusual, we elected to further investigate this reaction. We did this by utilizing the bipyrazine ligand to borylate a variety of substrates as shown in Figure 2-4.

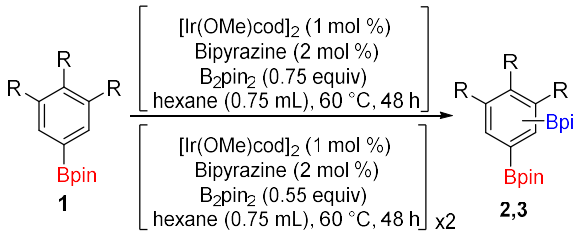
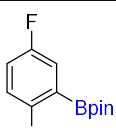
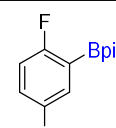
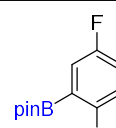
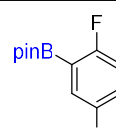
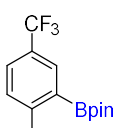
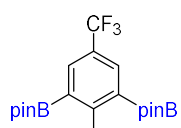
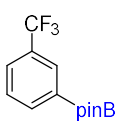
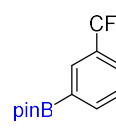
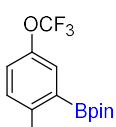
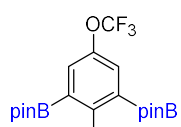
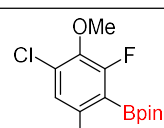
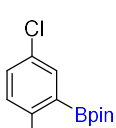
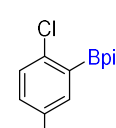
	
Entry	Products
1.	<div>  <b>2a</b>  <b>53 %</b>            (37 %)         </div> <div>  <b>2a'</b>  <b>16 %</b>            (12 %)         </div> <div>  <b>3a</b>  <b>6 %</b>            (4 %)         </div> <div>  <b>3a'</b>  <b>16 %</b>            (3 %)         </div>
2.	<div>  <b>2b</b>  <b>73 %</b>            (56 %)         </div> <div>  <b>3b</b>  <b>9 %</b>            (8 %)         </div> <div>  <b>1b'</b>  <b>2 %</b>            (1 %)         </div> <div>  <b>2b'</b>  <b>1 %</b>            (1 %)         </div>
3.	<div>  <b>2c</b>  <b>57 %</b>            (47 %)         </div> <div>  <b>3c</b>  <b>4 %</b>            (3 %)         </div>
4.	<div>  <b>2d</b>  <b>100 %</b>            (84 %)         </div>
5.	<div>  <b>2e</b>  <b>20 %</b>            (1 %)         </div> <div>  <b>2e'</b>  <b>2 %</b>            (1 %)         </div>

Figure 2-4 C–H Borylation of Arenes Using 2,2'-Bipyrazine as a Ligand

(Bolded Percentiles Represent Yields by <sup>1</sup>H NMR and Percentiles in Parentheses Represent Isolated Yields.)

A few interesting notes emerged from examining this substrate scope. First and most interesting is the regioselectivity seen. While this methodology is notable for being able to borylate ortho to existing boronic pinacolate ester it was not expected to see a preference for borylation ortho to these groups even in cases where traditionally accessible borylation positions are available such as in entries 1 and 5 in Figure 2-4. More notable though, was the difficulty in achieving high conversion of starting material to product.

In previous studies it was found that achieving high conversion of starting material to product was not as simple as just raising the catalyst loadings. Even running a reaction with 15 mol%  $[\text{Ir}(\text{OMe})\text{cod}]_2$  did not give complete conversion. This initially led us to believe the catalyst was poisoning itself and that multiple catalyst loadings were needed to achieve high conversion. This theory, however, was not pursued as the 2,2'-bipyrazine system ultimately proved to be too irreproducible. Although the 2,2'-bipyrazine ligand was consistently able to produce the same products, it often gave low conversion or no conversion at all. A few hypotheses were formed to explain the observed inconsistencies seen in this reaction: Impurities in the starting material mainly looking at palladium, poor glove box atmosphere, and polymerization of the ligand.

Reagent purity was looked at as the original 2,2'-bipyrazine used had a tan color despite being reported to have been originally observed to be neon yellow. As 2,2'-bipyrazine is white solid, this was immediately seen to be a potential issue for the reproducibility of this system. After rigorously purifying the 2,2'-bipyrazine and all other starting materials, the following three test reactions shown in Figure 2-5 were completed.

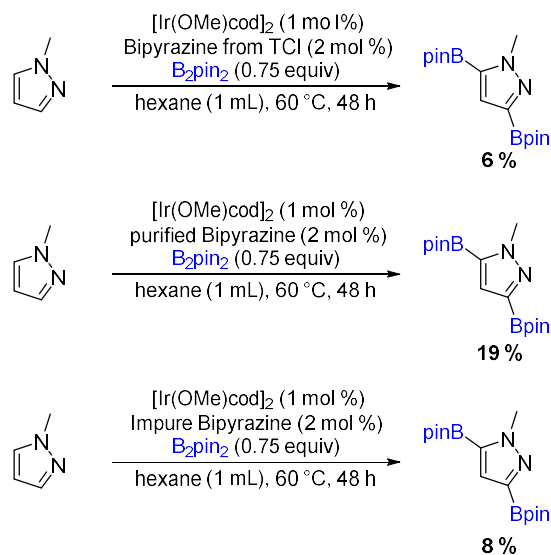


*Figure 2-5 Test Reactions and Measured Conversions, Run to Evaluate the Role of 2,2'-Bipyrazine Impurities for C–H Borylations*

As a control the first reaction was run with the original 2,2'-bipyrazine obtained through TCI. A second reaction was run with 2,2'-bipyrazine that had been purified by sublimation to remove any palladium impurities followed by multiple recrystallizations resulting in a spectroscopically pure white flake like crystalline powder. The third and final reaction was run with 2,2'-bipyrazine synthesized via palladium homo-coupling, which after initial work up was yellow in color (thought to be due to palladium impurities from the coupling conditions) and reminiscent of the reported color of the TCI bipyrazine. Unsurprisingly, the rigorously purified starting materials performed the best in this set of test reactions. Unfortunately, despite showing a higher reactivity than the initial 2,2'-bipyrazine provided by TCI, rigorous purification of the starting reagents did not alleviate the reproducibility problem. Inspired by work done by Suginome, we elected to look at the pyrazine substructure as Suginome showed that pyrazines dearomatize in the presence of  $\text{B}_2\text{pin}_2$  while in solution.<sup>16,17</sup> Looking at the 2,2'-bipyrazine scaffold by NMR (shown in Figure 2-6), we found that treating 2,2'-bipyrazine with  $\text{B}_2\text{pin}_2$ , resulted in the de-aromatization of the pyrazine substructure.



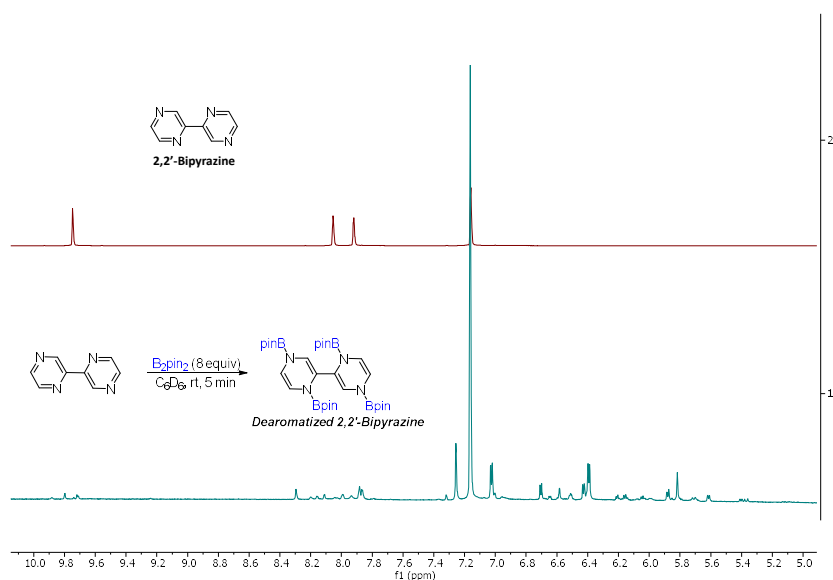


Figure 2-6 The Result of De-Aromatization of 2,2'-Bipyrazine with  $B_2pin_2$  (NMR 1) and the NMR of Pure 2,2'-Bipyrazine (NMR 2)

The bipyrazine took on a deep green color when it was converted to the 1,1',4,4'-tetrahydro-2,2'-bipyrazine that quickly turned red in the presence of air indicating auto air oxidation. Noticeably in the case of bipyrazine, the dearomatization failed to give a clean spectrum. It was postulated that this was due to polymerization induced by trace oxygen. When opened to air the solution formed a red precipitate that was unable to be characterized, and all peaks save for bipyrazine disappeared. From this we concluded that bipyrazine is merely a pre-ligand to the active catalytic ligand responsible for the selectivity seen in this system. Since the theorized active dearomatized ligand is formally anti-aromatic we postulated that the inconsistency in the reactions could be due to trace oxygen in the reaction atmosphere poisoning the active catalyst through oxidation and polymerization. We attempted to remedy these problems by designing our own pyrazine-based ligand which we designated as Ligand-213.

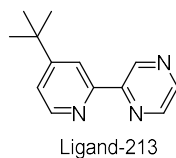
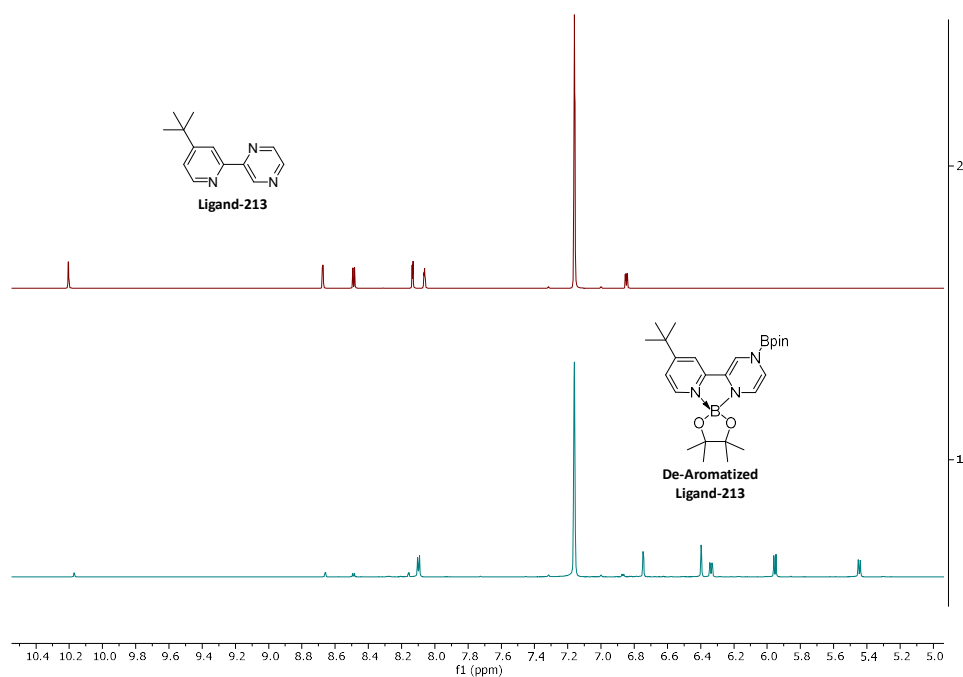


Figure 2-7 Our Designed Ligand (Ligand-213)

We based our ligand around the pyrazine scaffold as it was obvious to us that this substructure is clearly responsible for the unusual regioselectivity seen. We desymmetrized the ligand by replacing one of the pyrazines handles with that of a pyridine. This was done for two reasons. By adding a pyridine half, we in

turn stabilize the dearomatized pyrazine. This is accompanied by dative bonding to the N-borylated dihydro pyrazine through the pyridine lone pair. Additionally, it aids in discouraging metal ligand oligomerization by eliminating one of the nitrogens capable of binding to a second metal center.<sup>18</sup> Furthermore, by introducing a *t*-butyl group in the 4 position of the pyridine we can further discourage coordination of the active iridium catalyst with a second metal center. Incidentally, by including a *t*-butyl group in the 4 position of the pyridine we additionally prevent borylation of the pyridine half of the ligand which has been known to deactivate other common bipyridine ligands.<sup>19</sup> With ligand-213 (Figure 2-7) in hand we initially tested its ability to dearomatize. We found that ligand-213 dearomatizes far slower than 2,2'-bipyrazine (Figure 2-8). Once dearomatized however, it is stable for extended periods of time when kept under nitrogen. 2,2'-Bipyrazine, once dearomatized, quickly degrades into unidentifiable products over the course of a few days, even when stored under nitrogen, as opposed to ligand-213 which once dearomatized is stable in solution for weeks under nitrogen.



*Figure 2-8 The Result of De-Aromatization of Ligand-213 with B<sub>2</sub>pin<sub>2</sub> (NMR 1) and the NMR of pure Ligand-213 (NMR 2)*

Having established that Ligand-213 can undergo dearomatization like bipyrazine, we started investigating its reactivity (Figure 2-9). Utilizing this ligand, we found that it was active and gave moderate to good reactivity and yield in a single catalyst loading achieving 1,2-diborylation and 1,2,3-triborylation.

Entry	Products
1.	<div> </div>
2.	<div> </div>
3.	<div> </div>
4.	<div> </div>

Figure 2-9 C–H Borylation of Arenes Using Ligand-213 as a Ligand

(Bolded Percentiles Represent Yields by <sup>1</sup>H NMR and Percentiles in Parentheses Represent Isolated Yields.)

Even though ligand-213 was able to generate the same regiochemical products as bipyrazine, the selectivity seen differed significantly in entry 1. Ligand-213 did not favor 1,2-diborylation as heavily as bipyrazine. The reason for the difference in selectivity may be explained by the higher activity of the ligand. The more reactive a borylation system is the higher the likelihood that kinetics can override direction. This observation could provide helpful insight into the mechanism responsible for the regiochemical outcome pyrazine-based ligands. The improved reactivity of ligand-213 over bipyrazine may possibly be due to increased resistance to oxidation. However, the reproducibility problem that has

become characteristic for antiaromatic pyrazine-based ligands remained. Despite the increased stability, we once again propose that trace oxygen in the reaction conditions is responsible for the variance in reactivity, especially due to the anti-aromatic nature of the active ligand. This was evidenced by the qualitative observation that when the glovebox used for these reactions saw low usage, reactions using 2,2'-bipyrazine and Ligand-213 tended to give noticeably more favorable results.

With the unusual products that this system is able to produce, it became of great interest to investigate the chemical mechanism behind this selectivity. Initially the mechanism was proposed to be a hemilabile ligand<sup>15</sup>, however with the insights gained through the two substrate scopes studies we now propose that this system utilizes a Lewis acid-base interaction to guide regioselectivity as shown in Figure 2-10.

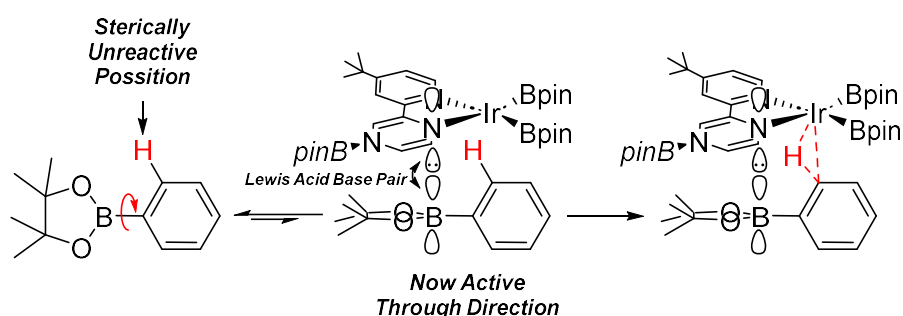


*Figure 2-10 The Proposed Lewis Acid - Base Interaction Thought to be Responsible for Guiding Regioselectivity*

As the active ligand (the dearomatized pyrazine scaffold) contains an enamine functionality in the form of the 1,4-dihydropyrazine, it can be viewed rather as an amine where in it is possible for it to form a Lewis adduct with a boronic pinacolate ester. The resultant geometry of the adduct allows the arene to adopt the proper orientation to undergo C–H activation ortho to an existing boronic pinacolate ester. The ability of the arene to adopt this geometry, however, will be heavily dependent on the rotational barrier of the preexisting boronic pinacolate ester, which in turn will be dependent on the aryl C–B bond order. Therefore, we would expect to see an increase in selectivity and reactivity as the C–B bond weakens. This should be heavily dependent on the electron density of the arene due to resonance donation into the boronic ester. More electron donation into the boronic pinacolate ester would rigidify the bond as the C–B bond takes on more and more bonding character. This results in higher reactivity in electron deficient substrates and a decrease in reactivity of electron rich substrates which is exactly what we observe. Substrates containing electron donating substituents lack reactivity such as with 4-isopropylphenylboronic acid pinacol ester and 4-methoxyphenylboronic acid pinacol ester showing no reactivity.

The only exception to this observation is substrate **1d** shown in entry 4 of Figure 2-4 and Figure 2-9. This substrate shows an unusually high reactivity despite containing an electron donating methoxy functionality. It is important to note however, that in this case the boronic pinacolate ester is ortho to a fluorine functionality. This is expected to cause an electronic repulsion between the boronic pinacolate's oxygen lone pairs and that of fluorine which should largely decrease the boronic pinacolate's rotational barrier as illustrated in Figure 2-11.

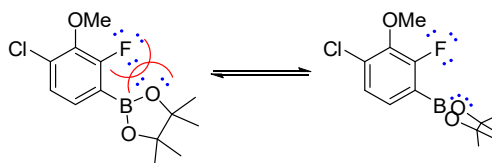


*Figure 2-11 Electronic Repulsion Between the Fluorine and Boronic Pinacolate of Substrate 1d*

Because of this, it is important to note that electronics of the arene is not the only factor governing this reaction and that any interaction influencing the C–B rotational barrier will play an important role in the reactivity of this methodology.

While characterizing some of the new compounds made, we made a second interesting discovery. In isolating a triborylated species we noticed we had inadvertently crystalized an orange/red compound. Intrigued by these crystals, we found that they corresponded to a boryl iridium trimer with a molecular formula of  $[\text{Ir}(\text{Bpin})_3]_3$  (Figure 2-12). While we do not know how this this compound formed, it may be interesting to the community at large. This compound may show activity as a C–H borylation catalyst or may be the product of the death of the active iridium borylation catalysts. Future work will further explore the formation of  $[\text{Ir}(\text{Bpin})_3]_3$  and its role in iridium catalyzed C–H borylations.

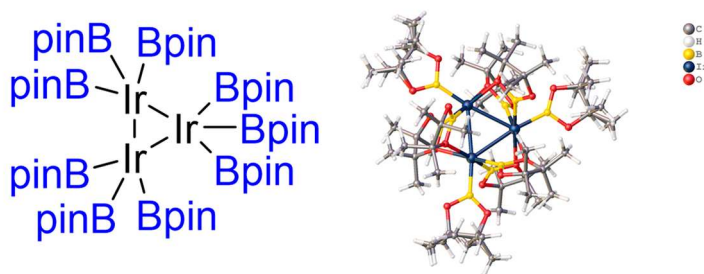


*Figure 2-12  $[\text{Ir}(\text{Bpin})_3]_3$  Crystalized from a Reaction Mixture*

In conclusion it is herein reported the ability of pyrazine containing ligands to influence borylation ortho to existing aryl pinacol boronic esters to synthesize 1,2-di and 1,2,3-tri borylated compounds directly through iridium catalyzed C–H activation. This methodology is the first ligand guided C–H borylation *ortho*

to aryl boronic pinacolate esters through iridium catalysis. By taking advantage of what we believe is a Lewis acid base interaction between the substrate and active dearomatized pyrazine ligand, we are able to direct borylation to traditionally unavailable positions. Utilizing this approach 1,2-di and 1,2,3-triborylation can be achieved to synthesize compounds that are impossible to directly synthesize efficiently through known methods.

## Experimental Procedures

### General Information

All available reagents were purchased through Combi-blocks and used as received unless otherwise indicated. Bis(pinacolato)diborn ( $B_2pin_2$ ) was generously supplied by BoroPharm. Hexane was refluxed over  $CaH_2$  and distilled. Column chromatography was done using 240-400 mesh silica P-Flash silica gel. TLC was done on 0.25 mm thick aluminum backed silica gel plates and visualized with UV light ( $\lambda = 254$  nm) with alizarin stain.<sup>58</sup>

$^1H$ ,  $^{13}C$ ,  $^{11}B$  and  $^{19}F$  NMR spectra were recorded on a Varian 500 MHz DD2 Spectrometer equipped with a  $^1H$ - $^{19}F$ / $^{15}N$ - $^{31}P$  5 mm Pulsed Field Gradient (PFG) Probe. Spectra taken in  $CDCl_3$  were referenced to 7.26 ppm in  $^1H$  NMR and 77.2 ppm in  $^{13}C$  NMR. Spectra taken in  $C_6D_6$  were referenced to 7.16 ppm in  $^1H$  NMR and 128.1 ppm in  $^{13}C$ .  $^{11}B$  NMR spectra were referenced to neat  $BF_3 \cdot Et_2O$  as the external standard. NMR spectra were processed for display using the MNova software program with only phasing and baseline corrections applied. High-resolution mass spectra (HRMS) were obtained at the Molecular Metabolism and Disease Mass Spectrometry Core facility and at the Mass Spectrometry Service Center at Michigan State University using electrospray ionization (ESI+ or ESI-) on quadrupole time-of-flight (Q-TOF) instruments.

### Synthesis of $[Ir(OMe)cod]_2$

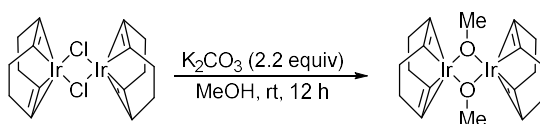


Figure 2-13 Synthesis of  $[Ir(OMe)cod]_2$

A 100 mL Schlenk flask was charged with a stir bar and  $[Ir(OMe)cod]_2$  (0.8418 g, 1.25 mmol) then sealed with a ribbed rubber septa. The flask was then purged with nitrogen. A second 100 mL round bottom flask was charged with methanol (80 mL, 63.3600 g, 1.98 mol) and  $K_2CO_3$  (0.3810 g, 2.76 mmol) then sealed with a rubber septum. The methanol solution was stirred for 12 hours over which the  $K_2CO_3$  dissolved. The  $K_2CO_3$  solution was sparged with nitrogen for 3 hours before being canula transferred into the Schlenk flask containing the  $[Ir(cod)Cl]_2$  with the strongest magnetic stirring possible. The Schlenk

flask was covered with aluminum foil and stirred for 12 hours under a positive pressure of nitrogen. Over the 12 hours the reaction turned from an orange suspension to a yellow suspension. The Schlenk flask was then opened, and the contained suspension was filtered using a water aspirator. The resulting yellow solid was then washed with ice cold methanol (3x, 3 mL). The solid was then dried under vacuum to yield  $[\text{Ir}(\text{OMe})\text{cod}]_2$  (0.6713 g, 1.01 mmol) as a fine yellow solid resulting in a yield of 81% yield.

#### Data for $[\text{Ir}(\text{OMe})\text{cod}]_2$

$^1\text{H}$  NMR (500 MHz,  $\text{C}_6\text{D}_6$ )  $\delta$  3.56 (d,  $J$  = 2.7 Hz, 4H), 3.17 (s, 3H), 2.15 (m, 4H), 1.31 (q,  $J$  = 7.7 Hz, 4H).

$^{13}\text{C}$  NMR (126 MHz,  $\text{C}_6\text{D}_6$ )  $\delta$  56.0, 54.1, 31.8.

#### Synthesis of Bipyrazine

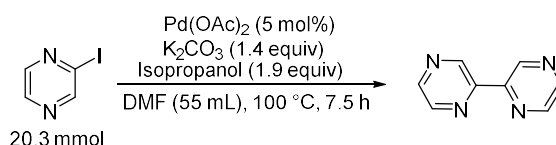


Figure 2-14 Synthesis of Bipyrazine

A 100 mL round bottom flask was charged with  $\text{K}_2\text{CO}_3$  (4.0200 g, 29.09 mmol),  $\text{Pd}(\text{OAc})_2$  (221.1 mg, 0.99 mmol), and a stir bar. The flask was sealed with a rubber septum and purged with nitrogen. DMF (55 mL) was added along with isopropanol (3 mL, 39.20 mmol) and 2-iodopyrazine (2 mL, 4.1720 g, 20.30 mmol). The reaction was stirred at  $100^\circ\text{C}$  in an oil bath for 7.5 h. The reaction was then allowed to cool to room temperature, and 40 mL of brine was added. The reaction was extracted with EtOAc (3x, 75 mL). The EtOAc layer was washed 3x with aqueous sodium thiosulfate (50 g in 100 mL of  $\text{H}_2\text{O}$ ). The EtOAc layer was then dried over  $\text{Na}_2\text{SO}_4$ , filtered, and dried to yield a brown solid. The solid was then sublimated under vacuum at  $78^\circ\text{C}$  to yield 0.7059 g of a yellow solid consisting of bipyrazine giving a yield of 44%. The product was further purified before use by recrystallization by dissolution of the yellow solid in 50 mL of boiling hexane on an oil bath. EtOAc was then slowly added until all the solid had dissolved. Stirring was stopped and the oil bath was turned off allowing the solution in the oil bath to come to room temperature together over 3 hours allowing crystals to form. The crystals were collected by filtration and washed with 10 mL of cold hexane. Bipyrazine (249.3 mg, 1.60 mmol) was collected as perfectly white flake like crystals giving a yield of 19%. The bipyrazine was dried under Dean-Stark conditions prior to use.

#### Data for Bipyrazine

$^1\text{H}$  NMR (500 MHz,  $\text{CDCl}_3$ )  $\delta$  9.59 (d,  $J$  = 1.1 Hz, 1H), 8.66 (m, 2H).

$^1\text{H}$  NMR (500 MHz,  $\text{C}_6\text{D}_6$ )  $\delta$  9.75 (s, 1H), 8.05 (s, 1H), 7.92 (s, 1H).

$^{13}\text{C}$  NMR (126 MHz,  $\text{CDCl}_3$ )  $\delta$  149.4, 145.4, 143.9, 143.6.

Melting Point: 187.3-187.9  $^\circ\text{C}$ .

### Synthesis of 4-(tert-butyl)-2-(tributylstannyl)pyridine (**S1**)

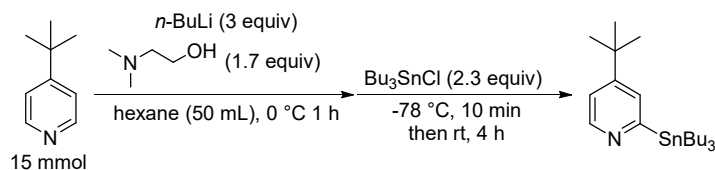


Figure 2-15 Synthesis of 4-(tert-butyl)-2-(tributylstannyl)pyridine (**S1**)

A stir bar was added to a 100 mL three neck round bottom flask which was then sealed with a septa. The flask was purged with nitrogen then charged with 50 mL of hexane and dimethylethanolamine (2.25 mL, 2.2150 g, 24.80 mmol) via a syringe and needle. The solution was cooled with stirring to  $0\text{ }^\circ\text{C}$  in an ice water bath.  $n\text{-BuLi}$  (2.5M in hexane, 19 mL, 2.2150 g, 47.50 mmol) was then added causing the solution to take on a yellow color. The reaction was allowed to stir at  $0\text{ }^\circ\text{C}$  for 15 minutes. 4- $t$ Butylpyridine (2.2 mL, 2.0306 g, 15.00 mmol) was then added via syringe dropwise over the course of 5 minutes causing the reaction to turn orange after which it eventually took on a red / orange hue. The reaction was stirred at  $0\text{ }^\circ\text{C}$  for 1 hour. The reaction was then cooled to  $-78\text{ }^\circ\text{C}$  with a dry ice acetone bath.  $\text{Bu}_3\text{SnCl}$  (9.25 mL, 11.1000 g, 34.00 mmol) was then added dropwise with a syringe over 5 minutes with strong stirring, causing a white precipitate to form. The reaction was stirred for an additional 30 minutes at  $-78\text{ }^\circ\text{C}$  before being allowed to warm to room temperature and stirred for an additional 7 hours. The reaction was then filtered, and the precipitate washed with 20 mL of diethyl ether. The filtrate was concentrated under vacuum to yield **S1** as a yellow oil. The product was used without further purification.



### Synthesis of Ligand-213 (2-(4-(tert-butyl)pyridin-2-yl)pyrazine)

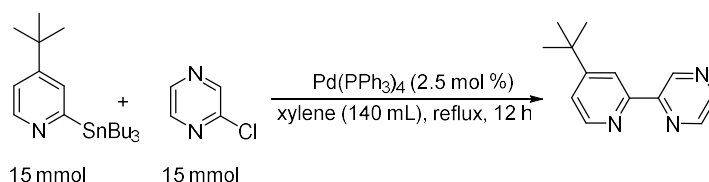


Figure 2-16 Synthesis of Ligand-213 (2-(4-(tert-butyl)pyridine-2-yl)pyrazine)

A 500 mL Schlenk flask was charged with  $\text{Pd(PPh}_3)_4$  (0.4330 g, 0.38 mmol, 2.5 mol %) and a stir bar. It is worth noting that the  $\text{Pd(PPh}_3)_4$  was in poor condition and had a black appearance. An Alan reflux condenser was fitted to the flask and the apparatus sealed with a septum. The flask was purged with nitrogen through the sidearm and out through a needle in the septum. Xylene (120 mL) was then added via a syringe to the flask along with 2-chloropyrazine (1.34 mL, 1.7200 g, 15.00 mmol). The reaction was then stirred for 12 hours at reflux. After refluxing the reaction was allowed to cool and gravity filtered. The filtrate was then concentrated under vacuum to yield an oil. The oil was then dissolved in 250 mL of hexane during which bipyrazine precipitated out. This was collected and purified as described in the synthesis of bipyrazine. The hexane layer was then washed with 200 mL of water with 5 g of NaF dissolved in it to remove any residual tin. After being allowed to sit a fine precipitate settled and the reaction was filtered, and the solvent evaporated. The remaining oil was redissolved in 75 mL of hexane. The hexane solution was then extracted with acetonitrile (3x, 75 mL). The acetonitrile was evaporated to give an oil. 2/3 of the oil by weight was purified via silica column chromatography (31cm x 2 cm) using 8:2 hexane:EtOAc as the eluent to yield Ligand-213 as a brown oil (fractions were chosen by GCMS). The brown oil was dissolved in 20 mL of hexane and placed in the freezer overnight over which Ligand-213 crystallized out. This was recrystallized by dissolving in hexane and placing in the freezer to crystallize. Ligand-213 (291.2 mg, 1.40 mmol) was collected as the product giving a yield of 9%. The adjusted yield for the product collected after chromatography was 14%.

### Data for Ligand-213 (2-(4-(tert-butyl)pyridine-2-yl)pyrazine)

$^1\text{H}$  NMR (500 MHz,  $\text{CDCl}_3$ )  $\delta$  9.63 (d,  $J$  = 1.3 Hz, 1H), 8.65-8.61 (m, 2H), 8.59 (d,  $J$  = 2.5 Hz, 1H), 8.38 (d,  $J$  = 1.9 Hz, 1H), 7.37 (dd,  $J$  = 5.2, 1.9 Hz, 1H), 1.40 (s, 9H).

$^{13}\text{C}$  NMR (126 MHz,  $\text{CDCl}_3$ )  $\delta$  161.5, 154.2, 151.7, 149.6, 144.4, 143.7, 143.6, 121.8, 118.6, 35.2, 30.7.

Melting Point: 74.6-75.4 °C.

### Synthesis of 4,4,5,5-tetramethyl-2-(4-(trifluoromethyl)phenyl)-1,3,2-dioxaborolane (**1b**)

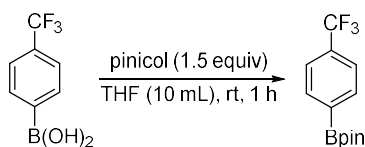


Figure 2-17 Synthesis of 4,4,5,5-tetramethyl-2-(4-(trifluoromethyl)phenyl)-1,3,2-dioxaborolane (**1b**)

A 20 mL scintillation vial was charged with (4-(trifluoromethyl)phenyl)boronic acid (3.0009 g, 15.80 mmol) and pinacol (2.8007 g, 23.70 mmol). 10 mL of THF was then added, and the vial closed. The vial was stirred at room temperature for 1 hour. The vial was then opened and the THF evaporated. The remaining oil was redissolved in 10 mL of DCM and the solution washed with water (7x, 10 mL). The organic layer was then dried over  $\text{MgSO}_4$  before being evaporated. **1b** (3.7286 g, 13.70 mmol) was collected as a white waxy solid giving a yield of 86.7%.

### Data for 4,4,5,5-tetramethyl-2-(4-(trifluoromethyl)phenyl)-1,3,2-dioxaborolane (**1b**)

$^1\text{H}$  NMR (500 MHz,  $\text{CDCl}_3$ )  $\delta$  7.91 (d,  $J$  = 7.7 Hz, 2H), 7.61 (d,  $J$  = 7.7 Hz, 2H), 1.36 (s, 12H).

$^{13}\text{C}$  NMR (126 MHz,  $\text{CDCl}_3$ )  $\delta$  135.1, 133.0 (q,  $J$  = 32.1 Hz), 124.5 (q,  $J$  = 3.8 Hz), 124.3 (q,  $J$  = 272.4 Hz), 84.4, 25.0.

$^{11}\text{B}$  NMR (160 MHz,  $\text{CDCl}_3$ )  $\delta$  30.5.

$^{19}\text{F}$  NMR (470 MHz,  $\text{CDCl}_3$ )  $\delta$  -64.97 (s).

Melting Point: 72.1 – 73.3 °C.

### Synthesis of 4,4,5,5-tetramethyl-2-(4-(trifluoromethoxy)phenyl)-1,3,2-dioxaborolane (**1c**)

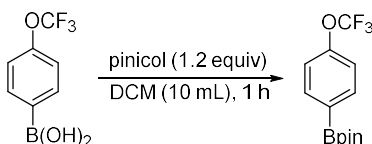


Figure 2-18 Synthesis of 4,4,5,5-tetramethyl-2-(4-(trifluoromethoxy)phenyl)-1,3,2-dioxaborolane (**1c**)

A 20 mL scintillation vial was charged with (4-(trifluoromethoxy)phenyl)boronic acid (1.9996 g, 9.71 mmol) and pinacol (1.3770 g, 11.65 mmol). 10 mL of dichloromethane was then added, and the vial closed. The vial was placed in a pocket and carried for 1 hour of general laboratory work. The vial was then opened, and the solution washed with water (5x, 10 mL). The organic layer was then dried over  $\text{MgSO}_4$  before being evaporated. **1c** (2.5028 g, 8.69 mmol) was collected as a white waxy solid giving a yield of 89%.

**Data for 4,4,5,5-tetramethyl-2-(4-(trifluoromethoxy)phenyl)-1,3,2-dioxaborolane (1c)**

$^1\text{H}$  NMR (500 MHz,  $\text{CDCl}_3$ )  $\delta$  7.84 (d,  $J$  = 8.1 Hz, 2H), 7.20 (d,  $J$  = 8.3 Hz, 2H), 1.35 (s, 12H).

$^{13}\text{C}$  NMR (126 MHz,  $\text{CDCl}_3$ )  $\delta$  151.8 (q,  $J$  = 1.7 Hz), 136.7, 120.4 (q,  $J$  = 257.6 Hz), 84.2, 25.0.

$^{19}\text{F}$  NMR (470 MHz,  $\text{CDCl}_3$ )  $\delta$  -57.50 (s).

$^{11}\text{B}$  NMR (160 MHz,  $\text{CDCl}_3$ )  $\delta$  30.4.

Melting Point: 61.5 – 62.3 °C.

**Synthesis of 2-(4-chloro-2-fluoro-3-methoxyphenyl)-4,4,5,5-tetramethyl-1,3,2-dioxaborolane (1d)**

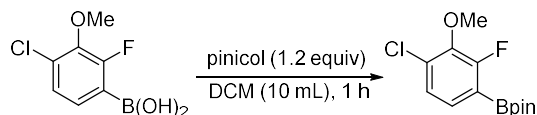


*Figure 2-19 Synthesis of 2-(4-chloro-2-fluoro-3-methoxyphenyl)-4,4,5,5-tetramethyl-1,3,2-dioxaborolane (1d)*

A 20 mL scintillation vial was charged with (4-(trifluoromethoxy)phenyl)boronic acid (3.0045 g, 14.70 mmol) and pinacol (2.0814 g, 17.61 mmol). 10 mL of dichloromethane was then added, and the vial closed. The vial was placed in a pocket and carried for 1 hour of general laboratory work. The vial was then opened, and the solution washed with water (5x, 10 mL). The organic layer was then dried over  $\text{Na}_2\text{SO}_4$  before being evaporated. 1d (3.6270 g, 12.66 mmol) was collected as a white waxy solid giving a yield of 86.11%.

**Data for 2-(4-chloro-2-fluoro-3-methoxyphenyl)-4,4,5,5-tetramethyl-1,3,2-dioxaborolane (1d)**

$^1\text{H}$  NMR (500 MHz,  $\text{CDCl}_3$ )  $\delta$  7.35 (dd,  $J$  = 8.1, 5.7 Hz, 1H), 7.14 (dd,  $J$  = 8.1, 1.3 Hz, 1H), 3.96 (d,  $J$  = 1.4 Hz, 3H), 1.36 (s, 12H).

$^{13}\text{C}$  NMR (126 MHz,  $\text{CDCl}_3$ )  $\delta$  160.5 (d,  $J$  = 254.3 Hz), 144.3 (d,  $J$  = 15.3 Hz), 131.9 (d,  $J$  = 4.2), 130.6 (d,  $J$  = 9.1 Hz), 125.3 (d,  $J$  = 3.5 Hz), 84.3, 61.6 (d,  $J$  = 4.9 Hz), 25.0.

$^{19}\text{F}$  NMR (470 MHz,  $\text{CDCl}_3$ )  $\delta$  -118.07 (m, 1F).

$^{11}\text{B}$  NMR (160 MHz,  $\text{CDCl}_3$ )  $\delta$  29.7.

Melting Point: 63.1-63.8°C

**Independent Synthesis of 2,2',2''-(2-fluorobenzene-1,3,5-triyl)tris(4,4,5,5-tetramethyl-1,3,2-dioxaborolane) (3a'')**

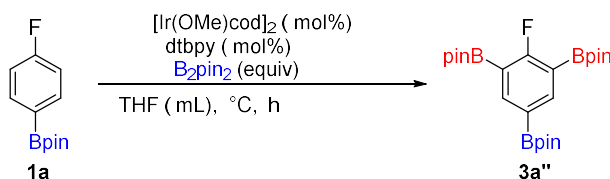


*Figure 2-20 Synthesis of 2,2',2''-(2-fluorobenzene-1,3,5-triyl)tris(4,4,5,5-tetramethyl-1,3,2-dioxaborolane) (3a'')*

In a glove box under nitrogen a 5 mL Wheaton conical vial with a triangular stir bar was charged with  $[\text{Ir}(\text{OMe})\text{cod}]_2$  (33.0 mg, 0.05 mmol) and  $\text{B}_2\text{pin}_2$  (0.5590 g, 2.20 mmol). THF (1 mL, 0.8890 g, 12.33 mmol) was added and the reaction was stirred at room temperature for 5 minutes over which the solution turned a golden-brown color. Then  $\text{dtbpy}$  (27.0 mg, 0.10 mmol) was then added along with THF (1 mL, 0.8890 g, 12.33 mmol) causing the reaction to a dark color. The reaction was stirred for an additional 5 minutes at room temperature. 2-(4-fluorophenyl)-4,4,5,5-tetramethyl-1,3,2-dioxaborolane (0.2220 g, 1.00 mmol) was added and the reaction vial capped and removed from the glove box. The reaction was heated in an aluminum heating block at  $80^\circ\text{C}$  with stirring for 48 hours. After heating the vial was allowed to cool. The solvent was then removed under a vacuum to yield a reddish black oil. The oil was then purified via flash column chromatography (2 cm x 18 cm) using hexane : ethyl acetate (8:2) as an eluent. A significant amount of solid, however, did remain on the sand on top of the column. A brown oil was then collected as the product. The oil was dissolved in 10 mL of DCM and washed with 10 mL of  $\text{H}_2\text{O}$ . The oil was then subjected to column chromatography a second time (2 cm x 25 cm) using hexane : ethyl acetate (8:2) as an eluent. After evaporation, **3a''** (0.1183 g, 0.25 mmol) was collected as a white solid resulting in a yield of 25%.

**Data for 2,2',2''-(2-fluorobenzene-1,3,5-triyl)tris(4,4,5,5-tetramethyl-1,3,2-dioxaborolane) (3a'')**

$^1\text{H}$  NMR (500 MHz,  $\text{CDCl}_3$ )  $\delta$  8.28 (d,  $J$  = 6.4 Hz, 2H), 1.33 (s, 24H), 1.33 (s, 12H). Referenced with  $\text{CDCl}_3$  = 7.26 ppm.

$^{13}\text{C}$  NMR (126 MHz,  $\text{CDCl}_3$ )  $\delta$  173.9 (d,  $J$  = 260.0 Hz), 147.3 (d,  $J$  = 9.2 Hz), 84.0, 83.9, 25.0, 25.0.

$^{19}\text{F}$  NMR (470 MHz,  $\text{CDCl}_3$ )  $\delta$  -87.27(t,  $J$  = 6.2 Hz, 1F), -87.28 (t,  $J$  = 6.4 Hz, 1F). Two overlapping triplets were seen. This was believed to be an isotopic effect between  $^{10}\text{B}$  and  $^{11}\text{B}$ .

$^{11}\text{B}$  NMR (160 MHz,  $\text{CDCl}_3$ )  $\delta$  30.2.

Melting Point:  $282.9 - 286.6^\circ\text{C}$

### Experimental for Figure 2-4 Entry 1

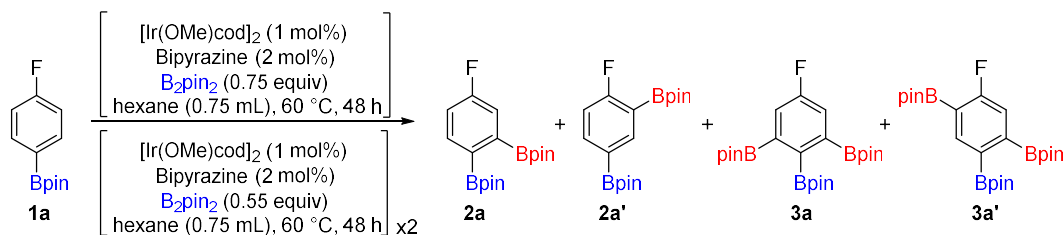


Figure 2-21 Experimental for Figure 2-4 Entry 1

In a glove box under nitrogen a 5 mL Wheaton conical vial with a triangular stir bar was charged with  $[\text{Ir}(\text{OMe})\text{cod}]_2$  (3.0 mg, 0.05 mmol) and  $\text{B}_2\text{pin}_2$  (0.0950 g, 0.37 mmol). Hexane (0.5 mL, 0.3325 g, 3.86 mmol) was added and the reaction was stirred at room temperature for 5 minutes over which the solution turned a golden-brown color. Bipyrazine (1.5 mg, 0.01 mmol) was then added along with hexane (0.25 mL, 0.1663 g, 1.93 mmol) causing the reaction to turn green. The reaction was stirred for an additional 5 minutes at room temperature. 2-(4-fluorophenyl)-4,4,5,5-tetramethyl-1,3,2-dioxaborolane (0.1110 g, 0.50 mmol) was added and the reaction vial capped and removed from the glove box. The reaction was heated in an aluminum heating block at 60 °C with stirring for 48 hours. The vial was then returned to the glove box and opened.  $[\text{Ir}(\text{OMe})\text{cod}]_2$  (3.0 mg, 0.05 mmol) and  $\text{B}_2\text{pin}_2$  (0.0711 g, 0.28 mmol) was then added with hexane (0.5 mL, 0.3325 g, 3.86 mmol). The reaction was stirred at room temperature for 5 minutes. Bipyrazine (1.5 mg, 0.01 mmol) was then added along with hexane (0.25 mL, 0.1663 g, 1.93 mmol). The reaction was capped and stirred for an additional 5 minutes at room temperature before being removed from the glove box and stirred at 60 °C in an aluminum heating block for an additional 48 hours. The vial was then returned to the glove box and opened.  $[\text{Ir}(\text{OMe})\text{cod}]_2$  (3.0 mg, 0.05 mmol) and  $\text{B}_2\text{pin}_2$  (0.0711 g, 0.28 mmol) was then added with hexane (0.5 mL, 0.3325 g, 3.86 mmol). The reaction was stirred at room temperature for 5 minutes. Bipyrazine (1.5 mg, 0.01 mmol) was then added along with hexane (0.25 mL, 0.1663 g, 1.93 mmol). The reaction was capped and stirred for an additional 5 minutes at room temperature before being removed from the glove box and stirred at 60 °C in an aluminum heating block for an additional 48 hours. After heating for the third time, the vial was allowed to cool. The solvent was then removed under a vacuum to yield a reddish black oil. The oil was then purified via flash column chromatography (2 cm x 18 cm) using hexane : ethyl acetate (8:2) as an eluent to yield **2a**, **2a'**, **3a**, **3a'** as a mixture of regio-isomers (116.5mg). This results in a yield of **2a** (64.4 mg, 0.19 mmol, ), **2a'** (21.7 mg, 0.06 mmol), **3a** (9.9 mg, 0.03 mmol), **3a'** (7.3 mg, 0.15 mmol). In a subsequent reaction run the same as described above a small amount of brown precipitate formed. This

was found to be compound **3a**. This was further purified by flash column chromatography (2 cm x 18 cm) using hexane : ethyl acetate (8:2) as an eluent to yield pure **3a** as a white solid (3.6 mg, 0.01 mmol).

**Data for Figure 2-4 Entry 1 Compound 2a**

$^1\text{H}$  NMR (500 MHz,  $\text{CDCl}_3$ )  $\delta$  7.67 (dd,  $J$  = 8.3, 6.0 Hz, 1H), 7.29 (dd,  $J$  = 9.5, 2.6 Hz, 1H), 7.04 (m, 1H), 1.370 (s, 12H), 1.351 (s, 12H).

$^{13}\text{C}$  NMR (126 MHz,  $\text{CDCl}_3$ )  $\delta$  163.9 (d,  $J$  = 250.3 Hz), 136.4 (d,  $J$  = 7.4 Hz), 120.1 (d,  $J$  = 18.8 Hz), 116.1 (d,  $J$  = 19.9 Hz), 84.1, 84.0, 25.0, 25.0.

$^{19}\text{F}$  NMR (470 MHz,  $\text{CDCl}_3$ )  $\delta$  -111.35 (dt,  $J$  = 9.3, 6.1).

$^{11}\text{B}$  NMR (160 MHz,  $\text{CDCl}_3$ )  $\delta$  30.9.

**Data for Figure 2-4 Entry 1 Compound 2a'**

$^1\text{H}$  NMR (500 MHz,  $\text{CDCl}_3$ )  $\delta$  8.20 (dd,  $J$  = 6.5, 1.7 Hz, 1H), 7.88 (ddd,  $J$  = 8.1, 6.0, 1.8 Hz, 1H), 7.02 (dd,  $J$  = 9.5, 8.4 Hz, 1H), 1.35 (s, 12H), 1.33 (s, 12H).

$^{13}\text{C}$  NMR (126 MHz,  $\text{CDCl}_3$ )  $\delta$  169.6 (d,  $J$  = 255.3 Hz), 144.1 (d,  $J$  = 8.4 Hz), 140.3 (d,  $J$  = 9.2 Hz), 115.0 (d,  $J$  = 23.5 Hz), 84.0, 25.0, 25.0.

$^{19}\text{F}$  NMR (470 MHz,  $\text{CDCl}_3$ )  $\delta$  -98.10 (m).

$^{11}\text{B}$  NMR (160 MHz,  $\text{CDCl}_3$ )  $\delta$  30.9.

**Data for Figure 2-4 Entry 1 Compound 3a**

$^1\text{H}$  NMR (500 MHz,  $\text{CDCl}_3$ )  $\delta$  7.60 (d,  $J$  = 9.5 Hz, 2H), 1.47 (s, 12H), 1.33 (s, 24H).

$^{13}\text{C}$  NMR (126 MHz,  $\text{CDCl}_3$ )  $\delta$  162.5 (d,  $J$  = 248.5 Hz), 124.2 (d,  $J$  = 18.1 Hz), 84.3, 25.939, 24.9.

$^{19}\text{F}$  NMR (470 MHz,  $\text{CDCl}_3$ )  $\delta$  -115.39 (t,  $J$  = 9.5 Hz, 1F). Referenced with  $\text{C}_6\text{F}_6$  = -161.64 ppm.

$^{11}\text{B}$  NMR (160 MHz,  $\text{CDCl}_3$ )  $\delta$  30.8.

**Data for Figure 2-4 Entry 1 Compound 3a'**

$^1\text{H}$  NMR (500 MHz,  $\text{CDCl}_3$ )  $\delta$  8.02 (d,  $J$  = 6.3 Hz, 1H), 7.25 (d,  $J$  = 10.3 Hz, 1H),

$^{19}\text{F}$  NMR (470 MHz,  $\text{CDCl}_3$ )  $\delta$  101.29 (dd,  $J$  = 9.9, 6.4 Hz, 1F).

$^{11}\text{B}$  NMR (160 MHz,  $\text{CDCl}_3$ )  $\delta$  30.9

### Experimental for Figure 2-4 Entry 2

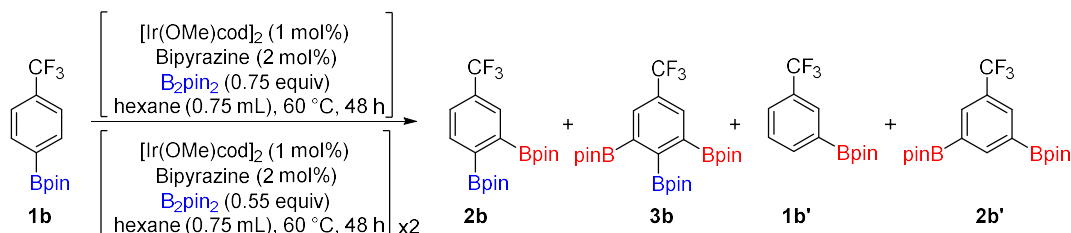


Figure 2-22 Experimental for Figure 2-4 Entry 2

In a glove box under nitrogen a 5 mL Wheaton conical vial with a triangular stir bar was charged with  $[\text{Ir}(\text{OMe})\text{cod}]_2$  (3 mg, 0.05 mmol) and  $\text{B}_2\text{pin}_2$  (0.0950 g, 0.37 mmol). Hexane (0.5 mL, 0.3325 g, 3.86 mmol) was added and the reaction was stirred at room temperature for 5 minutes over which the solution turned a golden-brown color. Bipyrazine (1.5 mg, 0.01 mmol) was then added along with hexane (0.25 mL, 0.1663 g, 1.93 mmol) causing the reaction to turn green. The reaction was stirred for an additional 5 minutes at room temperature. 4,4,5,5-tetramethyl-2-(4-(trifluoromethyl)phenyl)-1,3,2-dioxaborolane (0.1366 g, 0.50 mmol) was added and the reaction vial capped and removed from the glove box. The reaction was heated in an aluminum heating block at 60 °C with stirring for 48 hours. The vial was then returned to the glove box and opened.  $[\text{Ir}(\text{OMe})\text{cod}]_2$  (3.0 mg, 0.05 mmol) and  $\text{B}_2\text{pin}_2$  (0.0711 g, 0.28 mmol) was then added with hexane (0.5 mL, 0.3325 g, 3.86 mmol). The reaction was stirred at room temperature for 5 minutes. Bipyrazine (1.5 mg, 0.01 mmol) was then added along with hexane (0.25 mL, 0.1663 g, 1.93 mmol). The reaction was capped and stirred for an additional 5 minutes at room temperature before being removed from the glove box and stirred at 60 °C in an aluminum heating block for an additional 48 hours. The vial was then returned to the glove box and opened.  $[\text{Ir}(\text{OMe})\text{cod}]_2$  (3.0 mg, 0.05 mmol) and  $\text{B}_2\text{pin}_2$  (0.0711 g, 0.28 mmol) was then added with hexane (0.5 mL, 0.3325 g, 3.86 mmol). The reaction was stirred at room temperature for 5 minutes. Bipyrazine (1.5 mg, 0.01 mmol) was then added along with hexane (0.25 mL, 0.1663 g, 1.93 mmol). The reaction was capped and stirred for an additional 5 minutes at room temperature before being removed from the glove box and stirred at 60 °C in an aluminum heating block for an additional 48 hours. After heating for the third time, the vial was allowed to cool. The solvent was then removed under a vacuum to yield a reddish black oil. The oil was then purified via flash column chromatography (2 cm x 18 cm) using hexane : ethyl acetate (8:2) as an eluent. The products were collected in 3 fractions as clear oil and consisted of a mixture of regio-isomers. This results in a yield of **1b'** (1.4 mg, 0.01 mmol), **2b** (111.9 mg, 0.28 mmol), **2b'** (2.7 mg, 0.01 mmol), and **3b** (22.2 mg, 0.04 mmol).

**Data for Figure 2-4 Entry 2 Compound 1b'**

$^1\text{H}$  NMR (500 MHz,  $\text{CDCl}_3$ )  $\delta$  8.06 (s, 1H), 7.97 (d,  $J$  = 7.3 Hz, 1H), 7.48 (t,  $J$  = 7.6 Hz, 1H), 1.35 (s, 12H).

$^{13}\text{C}$  NMR (126 MHz,  $\text{CDCl}_3$ )  $\delta$  138.1, 131.5 (q,  $J$  = 3.8 Hz), 130.1 (q,  $J$  = 3.6 Hz), 128.2, 127.9 (q,  $J$  = 3.8 Hz), 84.4, 25.0.

$^{19}\text{F}$  NMR (470 MHz,  $\text{CDCl}_3$ )  $\delta$  -62.61 (s)

$^{11}\text{B}$  NMR (160 MHz,  $\text{CDCl}_3$ )  $\delta$  31.1.

**Data for Figure 2-4 Entry 2 Compound 2b**

$^1\text{H}$  NMR (500 MHz,  $\text{CDCl}_3$ )  $\delta$  7.90 (s, 1H), 7.73 (d,  $J$  = 7.8 Hz, 1H), 7.61 (d,  $J$  = 7.8 Hz, 1H), 1.37 (s, 12H), 1.37 (s, 12H).

$^{13}\text{C}$  NMR (126 MHz,  $\text{CDCl}_3$ )  $\delta$  133.6, 130.9, 130.1 (q,  $J$  = 3.8 Hz), 125.8 (q,  $J$  = 3.7 Hz), 124.4 (q,  $J$  = 3.8 Hz), 124.4 (d,  $J$  = 272.4 Hz), 84.4, 25.0.

$^{19}\text{F}$  NMR (470 MHz,  $\text{CDCl}_3$ )  $\delta$  -62.93 (s, 3F).

$^{11}\text{B}$  NMR (160 MHz,  $\text{CDCl}_3$ )  $\delta$  31.1.

**Data for Figure 2-4 Entry 2 Compound 2b'**

$^1\text{H}$  NMR (500 MHz,  $\text{CDCl}_3$ )  $\delta$  8.42 (s, 1H), 8.13 (s, 2H), 1.35 (s, 24H).

$^{19}\text{F}$  NMR (470 MHz,  $\text{CDCl}_3$ )  $\delta$  -62.51.

$^{11}\text{B}$  NMR (160 MHz,  $\text{CDCl}_3$ )  $\delta$  31.1.

**Data for Figure 2-4 Entry 2 Compound 3b**

$^1\text{H}$  NMR (500 MHz,  $\text{CDCl}_3$ )  $\delta$  134.02 (q,  $J$  = 3.62 Hz), 84.59, 84.46, 25.97, 25.91.

$^{13}\text{C}$  NMR (126 MHz,  $\text{CDCl}_3$ )  $\delta$  134.0 (q,  $J$  = 3.62 Hz), 84.6, 84.5, 26.0, 25.9.

$^{19}\text{F}$  NMR (470 MHz,  $\text{CDCl}_3$ )  $\delta$  -62.79 (s, 1F).

$^{11}\text{B}$  NMR (160 MHz,  $\text{CDCl}_3$ )  $\delta$  31.0.

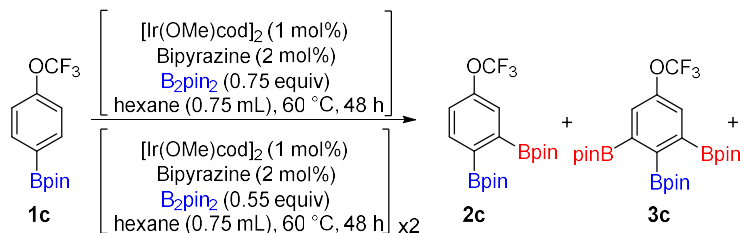
**Experimental for Figure 2-4 Entry 3**

Figure 2-23 Experimental for Figure 2-4 Entry 3

In a glove box under nitrogen a 5 mL Wheaton conical vial with a triangular stir bar was charged with  $[\text{Ir}(\text{OMe})\text{cod}]_2$  (3.0 mg, 0.05 mmol) and  $\text{B}_2\text{pin}_2$  (0.0950 g, 0.37 mmol). Hexane (0.5 mL, 0.3325 g, 3.86



mmol) was added and the reaction was stirred at room temperature for 5 minutes over which the solution turned a golden-brown color. Bipyrazine (1.5 mg, 0.01 mmol) was then added along with hexane (0.25 mL, 0.1663 g, 1.93 mmol) causing the reaction to turn green. The reaction was stirred for an additional 5 minutes at room temperature. 4,4,5,5-tetramethyl-2-(4-(trifluoromethoxy)phenyl)-1,3,2-dioxaborolane (0.1440 g, 0.50 mmol) was added and the reaction vial capped and removed from the glove box. The reaction was heated in an aluminum heating block at 60 °C with stirring for 48 hours. The vial was then returned to the glove box and opened.  $[\text{Ir}(\text{OMe})\text{cod}]_2$  (3.0 mg, 0.05 mmol) and  $\text{B}_2\text{pin}_2$  (0.0711 g, 0.28 mmol) was then added with hexane (0.5 mL, 0.3325 g, 3.86 mmol). The reaction was stirred at room temperature for 5 minutes. Bipyrazine (1.5 mg, 0.01 mmol) was then added along with hexane (0.25 mL, 0.1663 g, 1.93 mmol). The reaction was capped and stirred for an additional 5 minutes at room temperature before being removed from the glove box and stirred at 60 °C in an aluminum heating block for an additional 48 hours. The vial was then returned to the glove box and opened.  $[\text{Ir}(\text{OMe})\text{cod}]_2$  (3.0 mg, 0.05 mmol) and  $\text{B}_2\text{pin}_2$  (0.0711 g, 0.28 mmol) was then added with hexane (0.5 mL, 0.3325 g, 3.86 mmol). The reaction was stirred at room temperature for 5 minutes. Bipyrazine (1.5 mg, 0.01 mmol) was then added along with hexane (0.25 mL, 0.1663 g, 1.93 mmol). The reaction was capped and stirred for an additional 5 minutes at room temperature before being removed from the glove box and stirred at 60 °C in an aluminum heating block for an additional 48 hours. After heating for the third time, the vial was allowed to cool. The solvent was then removed under a vacuum to yield a reddish black oil. The oil was then purified via flash column chromatography (2 cm x 18 cm) using hexane : ethyl acetate (8:2) as an eluent.

**Data for Figure 2-4 Entry 3 Compound 2c**

$^1\text{H}$  NMR (500 MHz,  $\text{CDCl}_3$ )  $\delta$  7.70 (d,  $J$  = 8.2 Hz, 1H), 7.461 (s, 1H), 7.21 (m, 1H), 1.37 (s, 1H), 1.36 (s, 12H).

$^{13}\text{C}$  NMR (126 MHz,  $\text{CDCl}_3$ )  $\delta$  150.4, 135.6, 125.6, 121.4, 120.0, 84.3, 84.2, 25.0.

$^{19}\text{F}$  NMR (470 MHz,  $\text{CDCl}_3$ )  $\delta$  -57.48 (s, 3F).

$^{11}\text{B}$  NMR (160 MHz,  $\text{CDCl}_3$ )  $\delta$  31.0.

**Data for Figure 2-4 Entry 3 Compound 3c**

$^1\text{H}$  NMR (500 MHz,  $\text{CDCl}_3$ )  $\delta$  7.75 (s, 2H), 1.48 (s, 12H), 1.33 (s, 12H).

$^{19}\text{F}$  NMR (470 MHz,  $\text{CDCl}_3$ )  $\delta$  -57.36.

$^{11}\text{B}$  NMR (160 MHz,  $\text{CDCl}_3$ )  $\delta$  31.0.

## Experimental for Figure 2-4 Entry 4

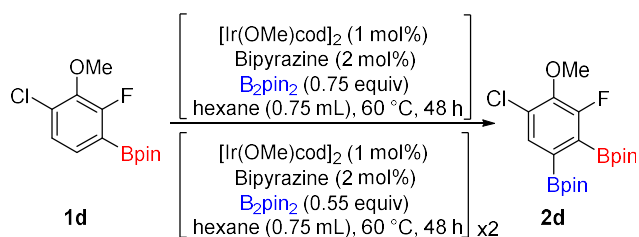


Figure 2-24 Experimental for Figure 2-4 Entry 4

In a glove box under nitrogen a 5 mL Wheaton conical vial with a triangular stir bar was charged with  $[\text{Ir}(\text{OMe})\text{cod}]_2$  (3 mg, 0.0045 mmol) and  $\text{B}_2\text{pin}_2$  (0.0950 g, 0.37 mmol). Hexane (0.5 mL, 0.3325 g, 3.86 mmol) was added and the reaction was stirred at room temperature for 5 minutes over which the solution turned a golden-brown color. Bipyrazine (1.5 mg, 0.01 mmol) was then added along with hexane (0.25 mL, 0.1663 g, 1.93 mmol) causing the reaction to turn green. The reaction was stirred for an additional 5 minutes at room temperature. 2-(4-chloro-2-fluoro-3-methoxyphenyl)-4,4,5,5-tetramethyl-1,3,2-dioxaborolane (0.1430 g, 0.50 mmol) was added and the reaction vial capped and removed from the glove box. The reaction was heated in an aluminum heating block at 60 °C with stirring for 48 hours. The vial was then returned to the glove box and opened.  $[\text{Ir}(\text{OMe})\text{cod}]_2$  (3.0 mg, 0.05 mmol) and  $\text{B}_2\text{pin}_2$  (0.0711 g, 0.28 mmol) was then added with hexane (0.5 mL, 0.3325 g, 3.86 mmol). The reaction was stirred at room temperature for 5 minutes. Bipyrazine (1.5 mg, 0.01 mmol) was then added along with hexane (0.25 mL, 0.1663 g, 1.93 mmol). The reaction was capped and stirred for an additional 5 minutes at room temperature before being removed from the glove box and stirred at 60 °C in an aluminum heating block for an additional 48 hours. The vial was then returned to the glove box and opened.  $[\text{Ir}(\text{OMe})\text{cod}]_2$  (3.0 mg, 0.05 mmol) and  $\text{B}_2\text{pin}_2$  (0.0711 g, 0.28 mmol) was then added with hexane (0.5 mL, 0.3325 g, 3.86 mmol). The reaction was stirred at room temperature for 5 minutes. Bipyrazine (1.5 mg, 0.01 mmol) was then added along with hexane (0.25 mL, 0.1663 g, 1.93 mmol). The reaction was capped and stirred for an additional 5 minutes at room temperature before being removed from the glove box and stirred at 60 °C in an aluminum heating block for an additional 48 hours. After heating for the third time, the vial was allowed to cool. The solvent was then removed under a vacuum to yield a reddish black oil. The oil was then purified via flash column chromatography (2 cm x 18 cm) using hexane : ethyl acetate (8:2) as an eluent. 2,2'-(5-chloro-3-fluoro-4-methoxy-1,2-phenylene)bis(4,4,5,5-tetramethyl-1,3,2-dioxaborolane) was collected as a white waxy solid (0.1732g, 0.42 mmol) resulting in a yield of 84%.

#### Data for Figure 2-4 Entry 4 Compound 2d

$^1\text{H}$  NMR (500 MHz,  $\text{CDCl}_3$ )  $\delta$  7.59 (d,  $J$  = 0.9 Hz, 1H), 3.96 (d,  $J$  = 1.8 Hz, 3H), 1.41 (s, 12H), 1.31 (s, 12H).

$^{13}\text{C}$  NMR (126 MHz,  $\text{CDCl}_3$ )  $\delta$  158.2 (d,  $J$  = 244.8 Hz), 145.8 (d,  $J$  = 15.4 Hz), 132.6 (d,  $J$  = 2.8 Hz), 128.6 (d,  $J$  = 3.9 Hz), 84.7, 84.600, 61.5 (d,  $J$  = 5.4 Hz), 25.1, 25.9.

$^{19}\text{F}$  NMR (470 MHz,  $\text{CDCl}_3$ )  $\delta$  -121.69 (s, 1F).

$^{11}\text{B}$  NMR (160 MHz,  $\text{CDCl}_3$ )  $\delta$  30.4.

#### Experimental for Figure 2-4 Entry 5

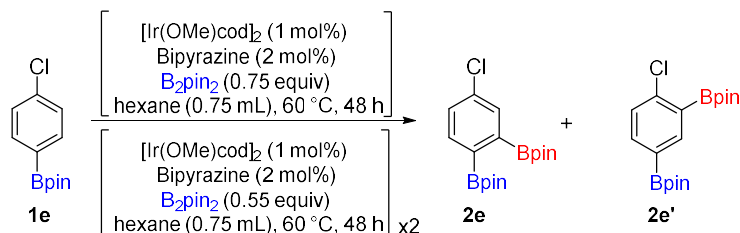


Figure 2-25 Experimental for Figure 2-4 Entry 5

In a glove box under nitrogen a 5 mL Wheaton conical vial with a triangular stir bar was charged with  $[\text{Ir}(\text{OMe})\text{cod}]_2$  (3.0 mg, 0.05 mmol) and  $\text{B}_2\text{pin}_2$  (0.0950 g, 0.37 mmol). Hexane (0.5 mL, 0.3325 g, 3.86 mmol) was added and the reaction was stirred at room temperature for 5 minutes over which the solution turned a golden-brown color. Bipyrazine (1.5 mg, 0.01 mmol) was then added along with hexane (0.25 mL, 0.1663 g, 1.93 mmol) causing the reaction to turn green. The reaction was stirred for an additional 5 minutes at room temperature. 2-(4-chlorophenyl)-4,4,5,5-tetramethyl-1,3,2-dioxaborolane (0.1190 g, 0.50 mmol) was added and the reaction vial capped and removed from the glove box. The reaction was heated in an aluminum heating block at 60 °C with stirring for 48 hours. The vial was then returned to the glove box and opened.  $[\text{Ir}(\text{OMe})\text{cod}]_2$  (3.0 mg, 0.05 mmol) and  $\text{B}_2\text{pin}_2$  (0.0711 g, 0.28 mmol) was then added with hexane (0.5 mL, 0.3325 g, 3.86 mmol). The reaction was stirred at room temperature for 5 minutes. Bipyrazine (1.5 mg, 0.01 mmol) was then added along with hexane (0.25 mL, 0.1663 g, 1.93 mmol). The reaction was capped and stirred for an additional 5 minutes at room temperature before being removed from the glove box and stirred at 60 °C in an aluminum heating block for an additional 48 hours. The vial was then returned to the glove box and opened.  $[\text{Ir}(\text{OMe})\text{cod}]_2$  (3.0 mg, 0.05 mmol) and  $\text{B}_2\text{pin}_2$  (0.0711 g, 0.28 mmol) was then added with hexane (0.5 mL, 0.3325 g, 3.86 mmol). The reaction was stirred at room temperature for 5 minutes. Bipyrazine (1.5 mg, 0.01 mmol) was then added along with hexane (0.25 mL, 0.1663 g, 1.93 mmol). The reaction was capped and stirred for an additional 5 minutes at room temperature before being removed from the glove box and stirred at 60

°C in an aluminum heating block for an additional 48 hours. After heating for the third time, the vial was allowed to cool. The solvent was then removed under a vacuum to yield a reddish black oil. The oil was then purified via flash column chromatography (2 cm x 18 cm) using hexane : ethyl acetate (8:2) as an eluent to give 61.1 mg of a clear oil consisting of a mixture of mixture of isomers.

**Data for Figure 2-4 Entry 4 Compound 2e**

$^1\text{H}$  NMR (500 MHz,  $\text{CDCl}_3$ )  $\delta$  7.59 (s, 1H), 7.58 (d,  $J$  = 5.0 Hz, 1H), 7.33 (d,  $J$  = 8.2 Hz, 1H), 1.36 (s, 12H), 1.35 (s, 12H).

$^{13}\text{C}$  NMR (126 MHz,  $\text{CDCl}_3$ ) 136.1, 135.3, 133.3, 129.3, 84.3, 84.2, 25.0.

$^{11}\text{B}$  NMR (160 MHz,  $\text{CDCl}_3$ )  $\delta$  30.1.

**Data for Figure 2-4 Entry 4 Compound 2e'**

$^1\text{H}$  NMR (500 MHz,  $\text{CDCl}_3$ )  $\delta$  8.10 (d,  $J$  = 1.6 Hz, 1H), 7.73 (1H), 7.34 (1H), 1.37 (s, 12H), 1.33 (s, 12H).

$^{13}\text{C}$  NMR (126 MHz,  $\text{CDCl}_3$ )  $\delta$  142.9, 142.8, 138.3, 128.9, 84.2, 84.1, 24.7.

$^{11}\text{B}$  NMR (160 MHz,  $\text{CDCl}_3$ )  $\delta$  30.1.

**Experimental for Figure 2-9 Entry 1**

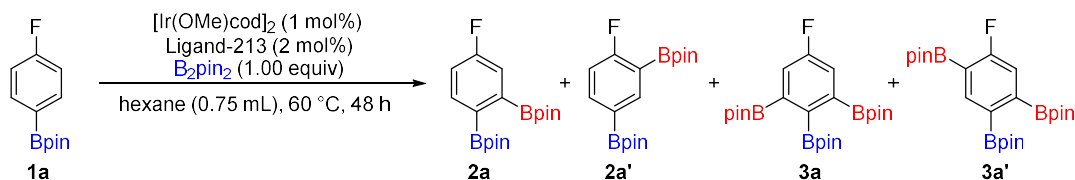


Figure 2-26 Experimental for Figure 2-9 Entry 1

In a glove box under nitrogen a 5 mL Wheaton conical vial with a triangular stir bar was charged with  $[\text{Ir}(\text{OMe})\text{cod}]_2$  (3.0 mg, 0.05 mmol) and  $\text{B}_2\text{pin}_2$  (0.1270 g, 0.50 mmol). Hexane (0.5 mL, 0.3325 g, 3.86 mmol) was added and the reaction was stirred at room temperature for 5 minutes over which the solution turned a golden-brown color. Ligand-213 (1.5 mg, 0.01 mmol) was then added along with hexane (0.25 mL, 0.1663 g, 1.93 mmol) causing the reaction to turn green. The reaction was stirred for an additional 5 minutes at room temperature. 4,4,5,5-tetramethyl-2-(4-(trifluoromethyl)phenyl)-1,3,2-dioxaborolane (0.1366 g, 0.50 mmol) was added and the reaction vial capped and removed from the glove box. The reaction was heated in an aluminum heating block at 60 °C with stirring for 48 hours after which the reaction vial was cooled to room temperature and opened. The solvent was removed under vacuum to yield a red, black oil. The oil was purified via flash column chromatography (2 cm x 18) using hexane : ethyl acetate (8:2) as the eluent.

**Data for Figure 2-9 Entry 1 Compound 2a**

$^1\text{H}$  NMR (500 MHz,  $\text{CDCl}_3$ )  $\delta$  7.67 (dd,  $J$  = 8.2, 6.0 Hz, 1H), 7.29 (dd,  $J$  = 9.6, 2.6 Hz, 1H), 7.05 (dt,  $J$  = 8.7, 2.6 Hz, 1H), 1.37 (s, 12H), 1.35 (s, 12H).

$^{13}\text{C}$  NMR (126 MHz,  $\text{CDCl}_3$ )  $\delta$  136.4 (d,  $J$  = 7.3 Hz), 120.1 (d,  $J$  = 18.7 Hz), 116.2 (d,  $J$  = 19.9 Hz), 84.3, 84.2, 24.9, 24.8.

$^{19}\text{F}$  NMR (470 MHz,  $\text{CDCl}_3$ )  $\delta$  -111.35 (dt,  $J$  = 9.3, 6.1, 1F).

$^{11}\text{B}$  NMR (160 MHz,  $\text{CDCl}_3$ )  $\delta$  30.6.

**Data for Figure 2-9 Entry 1 Compound 2a'**

$^1\text{H}$  NMR (500 MHz,  $\text{CDCl}_3$ )  $\delta$  8.20 (dd,  $J$  = 6.5, 1.7 Hz, 1H), 7.88 (ddd,  $J$  = 8.1, 6.0, 1.8 Hz, 1H), 7.02 (dd,  $J$  = 9.5, 8.4 Hz, 1H), 1.37 (s, 12H), 1.35 (s, 12H).

$^{13}\text{C}$  NMR (126 MHz,  $\text{CDCl}_3$ )  $\delta$  169.6 (d,  $J$  = 255.3 Hz), 144.1 (d,  $J$  = 8.4 Hz), 140.4 (d,  $J$  = 9.2 Hz), 114.9 (d,  $J$  = 23.2 Hz), 84.0, 25.0, 25.0.

$^{19}\text{F}$  NMR (470 MHz,  $\text{CDCl}_3$ )  $\delta$  -98.11 (m). This peak was characterized as a multiplet although it seemed to be two peaks overlapped with one peak representing compound **2a'** with  $^{10}\text{B}$  and the other representing compound **2a'** with  $^{11}\text{B}$ .

$^{11}\text{B}$  NMR (160 MHz,  $\text{CDCl}_3$ )  $\delta$  30.6.

**Data for Figure 2-9 Entry 1 Compound 3a**

$^1\text{H}$  NMR (500 MHz,  $\text{CDCl}_3$ )  $\delta$  7.60 (d,  $J$  = 9.5 Hz, 2H), 1.47 (s, 12H), 1.33 (s, 24H).

$^{13}\text{C}$  NMR (126 MHz,  $\text{CDCl}_3$ )  $\delta$  162.5 (d,  $J$  = 248.5 Hz), 124.2 (d,  $J$  = 18.1 Hz), 84.3, 25.9, 24.9.

$^{19}\text{F}$  NMR (470 MHz,  $\text{CDCl}_3$ )  $\delta$  -115.39 (t,  $J$  = 9.5 Hz, 1F). Referenced with  $\text{C}_6\text{F}_6$  = -161.64 ppm.

$^{11}\text{B}$  NMR (160 MHz,  $\text{CDCl}_3$ )  $\delta$  30.8.

**Data for Figure 2-9 Entry 1 Compound 3a'**

$^1\text{H}$  NMR (500 MHz,  $\text{CDCl}_3$ )  $\delta$  8.02 (d,  $J$  = 6.3 Hz, 1H), 7.25 (d,  $J$  = 10.3 Hz, 1H),

$^{19}\text{F}$  NMR (470 MHz,  $\text{CDCl}_3$ )  $\delta$  101.29 (dd,  $J$  = 9.9, 6.4 Hz, 1F).

$^{11}\text{B}$  NMR (160 MHz,  $\text{CDCl}_3$ )  $\delta$  30.6

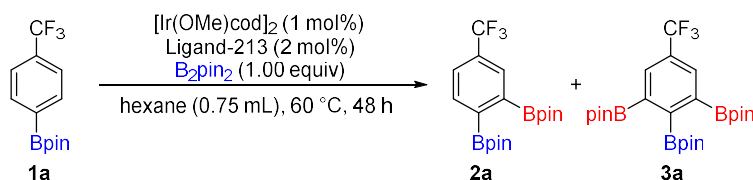
**Experimental for Figure 2-9 Entry 2**

Figure 2-27 Experimental for Figure 2-9 Entry 2

In a glove box under nitrogen a 5 mL Wheaton conical vial with a triangular stir bar was charged with  $[\text{Ir}(\text{OMe})\text{cod}]_2$  (3.0 mg, 0.05 mmol) and  $\text{B}_2\text{pin}_2$  (0.1270 g, 0.50 mmol). Hexane (0.5 mL, 0.3325 g, 3.8595 mmol) was added and the reaction was stirred at room temperature for 5 minutes over which the solution turned a golden-brown color. Ligand-213 (1.5 mg, 0.01 mmol) was then added along with hexane (0.25 mL, 0.1663 g, 1.93 mmol) causing the reaction to turn green. The reaction was stirred for an additional 5 minutes at room temperature. 4,4,5,5-tetramethyl-2-(4-(trifluoromethyl)phenyl)-1,3,2-dioxaborolane (0.1366 g, 0.50 mmol)

was added and the reaction vial capped and removed from the glove box. The reaction was heated in an aluminum heating block at 60 °C with stirring for 48 hours after which the reaction vial was cooled to room temperature and opened. The solvent was removed under vacuum to yield a red, black oil. The oil was purified via flash column chromatography (2 cm x 18) using hexane : ethyl acetate (8:2) as the eluent.

**Data for Figure 2-9 Entry 2 Compound 1b'**

$^1\text{H}$  NMR (500 MHz,  $\text{CDCl}_3$ )  $\delta$  8.06 (s, 1H), 7.97 (d,  $J$  = 7.3 Hz, 1H), 7.48 (t,  $J$  = 7.6 Hz, 1H), 1.35 (s, 12H).

$^{13}\text{C}$  NMR (126 MHz,  $\text{CDCl}_3$ )  $\delta$  138.1, 131.5 (q,  $J$  = 3.8 Hz), 130.1 (q,  $J$  = 3.6 Hz), 128.2, 127.9 (q,  $J$  = 3.8 Hz), 84.4, 25.0.

$^{19}\text{F}$  NMR (470 MHz,  $\text{CDCl}_3$ )  $\delta$  -62.61 (s, 13F)

$^{11}\text{B}$  NMR (160 MHz,  $\text{CDCl}_3$ )  $\delta$  31.1.

**Data for Figure 2-9 Entry 2 Compound 2b**

$^1\text{H}$  NMR (500 MHz,  $\text{CDCl}_3$ )  $\delta$  7.90 (s, 1H), 7.73 (d,  $J$  = 7.8 Hz, 1H), 7.61 (d,  $J$  = 7.8 Hz, 1H), 1.374 (s, 12H), 1.37 (s, 12H).

$^{13}\text{C}$  NMR (126 MHz,  $\text{CDCl}_3$ )  $\delta$  133.6, 130.9, 130.1 (q,  $J$  = 3.8 Hz), 125.8 (q,  $J$  = 3.7 Hz), 124.4 (q,  $J$  = 3.8 Hz), 124.4 (d,  $J$  = 272.4 Hz), 84.4, 25.0.

$^{19}\text{F}$  NMR (470 MHz,  $\text{CDCl}_3$ )  $\delta$  -62.93 (s, 3F).

$^{11}\text{B}$  NMR (160 MHz,  $\text{CDCl}_3$ )  $\delta$  31.1.

**Data for Figure 2-9 Entry 2 Compound 2b'**

$^1\text{H}$  NMR (500 MHz,  $\text{CDCl}_3$ )  $\delta$  8.42 (s, 1H), 8.13 (s, 2H), 1.35 (s, 24H).

$^{19}\text{F}$  NMR (470 MHz,  $\text{CDCl}_3$ )  $\delta$  -62.51.

$^{11}\text{B}$  NMR (160 MHz,  $\text{CDCl}_3$ )  $\delta$  31.1.

**Data for Figure 2-9 Entry 2 Compound 3b**

$^1\text{H}$  NMR (500 MHz,  $\text{CDCl}_3$ )  $\delta$  134.02 (q,  $J$  = 3.62 Hz), 84.59, 84.46, 25.97, 25.91.

$^{13}\text{C}$  NMR (126 MHz,  $\text{CDCl}_3$ )  $\delta$  134.0 (q,  $J$  = 3.62 Hz), 84.6, 84.5, 25.0, 25.9.

$^{19}\text{F}$  NMR (470 MHz,  $\text{CDCl}_3$ )  $\delta$  -62.79 (s, 1F).

$^{11}\text{B}$  NMR (160 MHz,  $\text{CDCl}_3$ )  $\delta$  31.0.

### Experimental for Figure 2-9 Entry 3

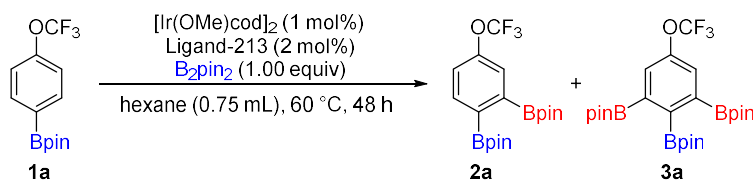


Figure 2-28 Experimental for Figure 2-9 Entry 3

In a glove box under nitrogen a 5 mL Wheaton conical vial with a triangular stir bar was charged with  $[\text{Ir}(\text{OMe})\text{cod}]_2$  (3.0 mg, 0.05 mmol) and  $\text{B}_2\text{pin}_2$  (0.1270 g, 0.50 mmol). Hexane (0.5 mL, 0.3325 g, 3.86 mmol) was added and the reaction was stirred at room temperature for 5 minutes over which the solution turned a golden-brown color. Ligand-213 (1.5 mg, 0.01 mmol) was then added along with hexane (0.25 mL, 0.1663 g, 1.93 mmol) causing the reaction to turn green. The reaction was stirred for an additional 5 minutes at room temperature. 4,4,5,5-tetramethyl-2-(4-(trifluoromethoxy)phenyl)-1,3,2-dioxaborolane (0.1440 g, 0.50 mmol) was added and the reaction vial capped and removed from the glove box. The reaction was heated in an aluminum heating block at 60 °C with stirring for 48 hours after which the reaction vial was cooled to room temperature and opened. The solvent was removed under vacuum to yield a red, black oil. The oil was purified via flash column chromatography (2 cm x 18) using hexane : ethyl acetate (8:2) as the eluent.

### Data for Figure 2-9 Entry 3 Compound 2c

$^1\text{H}$  NMR (500 MHz,  $\text{CDCl}_3$ )  $\delta$  7.70 (d,  $J$  = 8.2 Hz, 1H), 7.46 (s, 1H), 7.21 (m, 1H), 1.37 (s, 1H), 1.36 (s, 12H).

$^{13}\text{C}$  NMR (126 MHz,  $\text{CDCl}_3$ )  $\delta$  150.4, 135.6, 125.6, 121.4, 120.0, 84.3, 84.2, 25.0.

$^{19}\text{F}$  NMR (470 MHz,  $\text{CDCl}_3$ )  $\delta$  -57.45 (s, 3F).

$^{11}\text{B}$  NMR (160 MHz,  $\text{CDCl}_3$ )  $\delta$  31.0.

### Data for Figure 2-9 Entry 3 Compound 3c

$^1\text{H}$  NMR (500 MHz,  $\text{CDCl}_3$ )  $\delta$  7.75 (s, 2H), 1.48 (s, 12H), 1.33 (s, 12H).

$^{19}\text{F}$  NMR (470 MHz,  $\text{CDCl}_3$ )  $\delta$  -57.36.

$^{11}\text{B}$  NMR (160 MHz,  $\text{CDCl}_3$ )  $\delta$  31.0.

#### Experimental for Figure 2-9 Entry 4

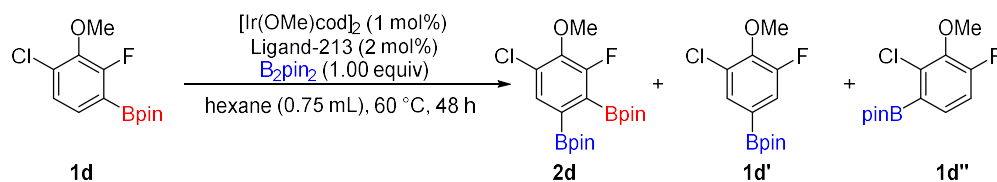


Figure 2-29 Experimental for Figure 2-9 Entry 4

In a glove box under nitrogen a 5 mL Wheaton conical vial with a triangular stir bar was charged with  $[\text{Ir}(\text{OMe})\text{cod}]_2$  (3.0 mg, 0.05 mmol) and  $\text{B}_2\text{pin}_2$  (0.1270 g, 0.50 mmol). Hexane (0.5 mL, 0.3325 g, 3.86 mmol) was added and the reaction was stirred at room temperature for 5 minutes over which the solution turned a golden-brown color. Ligand-213 (1.5 mg, 0.01 mmol) was then added along with hexane (0.25 mL, 0.1663 g, 1.93 mmol) causing the reaction to turn green. The reaction was stirred for an additional 5 minutes at room temperature. 2-(4-chloro-2-fluoro-3-methoxyphenyl)-4,4,5,5-tetramethyl-1,3,2-dioxaborolane (0.1430 g, 0.50 mmol) was added and the reaction vial capped and removed from the glove box. The reaction was heated in an aluminum heating block at 60 °C with stirring for 48 hours after which the reaction vial was cooled to room temperature and opened. The solvent was removed under vacuum to yield a red, black oil. The oil was purified via flash column chromatography (2 cm x 18) using hexane : ethyl acetate (8:2) as the eluent.

#### Data for Figure 2-9 Entry 4 Compound **2d**

$^1\text{H}$  NMR (500 MHz,  $\text{CDCl}_3$ )  $\delta$  7.59 (d,  $J$  = 0.9 Hz, 1H), 3.96 (d,  $J$  = 1.8 Hz, 3H), 1.41 (s, 12H), 1.31 (s, 12H).

$^{13}\text{C}$  NMR (126 MHz,  $\text{CDCl}_3$ )  $\delta$  158.2 (d,  $J$  = 244.8 Hz), 145.8 (d,  $J$  = 15.4 Hz), 132.6 (d,  $J$  = 2.8 Hz), 128.6 (d,  $J$  = 3.9 Hz), 84.7, 84.6, 61.5 (d,  $J$  = 5.4 Hz), 25.1, 25.9.

$^{19}\text{F}$  NMR (470 MHz,  $\text{CDCl}_3$ )  $\delta$  -121.69 (s, 1F).

$^{11}\text{B}$  NMR (160 MHz,  $\text{CDCl}_3$ )  $\delta$  30.4.

#### Data for Figure 2-9 Entry 4 Compound **1d'**

$^1\text{H}$  NMR (500 MHz,  $\text{CDCl}_3$ )  $\delta$  7.58 (s, 1H), 7.41 (d,  $J$  = 11.1 Hz, 1H), 1.32 (s, 12H).

$^{19}\text{F}$  NMR (470 MHz,  $\text{CDCl}_3$ )  $\delta$  -129.13 (dt,  $J$  = 11.0, 1.5 Hz, 1F).

$^{11}\text{B}$  NMR (160 MHz,  $\text{CDCl}_3$ )  $\delta$  30.0.

#### Data for Figure 2-9 Entry 4 Compound **1d''**

$^{19}\text{F}$  NMR (470 MHz,  $\text{CDCl}_3$ )  $\delta$  -114.53 (d,  $J$  = 6.1 Hz, 1F).



### Synthesis and Isolation of 3a and [IrBpin<sub>3</sub>]<sub>3</sub>

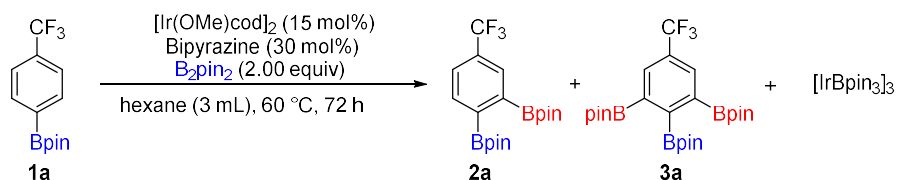


Figure 2-30 Synthesis and Isolation of 3a and [IrBpin<sub>3</sub>]<sub>3</sub>

In a glove box under nitrogen a 5 mL Wheaton conical vial with a triangular stir bar was charged with [Ir(OMe)cod]<sub>2</sub> (233.0 mg, 0.35 mmol) and B<sub>2</sub>pin<sub>2</sub> (1.0158 g, 4.00 mmol). Hexane (2 mL, 1.3300 g, 15.44 mmol) was added and the reaction was stirred at room temperature for 5 minutes over which the solution turned black. Bipyrazine (90 mg, 0.57 mmol) was then added along with hexane (1 mL, 0.6650 g, 7.72 mmol). The reaction was stirred for an additional 5 minutes at room temperature. 4,4,5,5-tetramethyl-2-(4-(trifluoromethyl)phenyl)-1,3,2-dioxaborolane (0.5440 g, 2.00 mmol) was added and the reaction vial capped and removed from the glove box. The reaction was heated in an aluminum heating block at 60 °C with stirring for 72 hours after which the reaction vial was cooled to room temperature and opened. The solvent was removed under vacuum to yield a red, black oil. The oil was purified via flash column chromatography (2 cm x 12 cm) using hexane : ethyl acetate (8:2) as the eluent yielding a tan oil. The oil was further purified by passing through a silica plug (2 cm x 3 cm) using hexane : ethyl acetate (8:2) which yielded a less tan oil. The oil was re-dissolved in hexane and placed in a freezer at -30 °C for 1 week over which red / orange crystals formed. The crystals were filtered out and washed with hexane to yield [IrBpin<sub>3</sub>]<sub>3</sub> (0.8 mg).

## REFERENCES

- (1) Teo, W. J.; Ge, S. Cobalt-Catalyzed Diborylation of 1,1-disubstituted Vinylarenes: A Practical Route to Branched *gem*-Bis(boryl)alkanes *Angew. Chem. Int. Ed.* **2018**, *57*, 1654-1658.
- (2) Choi, J.; Kwak, S.; Kwak Y.; Kwon, O.; Kim, J.; Lee, K.; Lee, S. Organic Light-Emitting Device Including The Same U.S. Patent 2018/0097189 A1, April 5, 2018.
- (3) CN 111978355A, June 6, 2015
- (4) Liao, G.; Zhang, T.; Jin, L.; Wang, B. J.; X., C. K.; Lan, Y.; Zhao, Y.; Shi, B. F. Experimental and Computational Studies on the Directing Ability of Chalcogenoethers in Palladium-Catalyzed Atroposelective C-H Olefination and Allylation *Angew. Chem.* **2022**, *134*, e2021152.
- (5) Seven, O.; Bolte, M.; Lerner, H. W.; Wagner, M. High-Yield Syntheses and Reactivity Studies of 1,2-Diborylated and 1,2,4,5-Tetraborylated Benzenes *Organometallics*, **2014**, *33*, 1291-1299.
- (6) Yoshida, H.; Okada, K.; Kawashima, S.; Tanino, K.; Oshita, J. Platinum-Catalysed Diborylation of Arynes: Synthesis and Reaction of 1,2-Diborylarenes *Chem. Commun.* **2010**, *46*, 1763-1765.
- (7) Yoshida, H.; Kawahima, S.; Takemoto, Y.; Okada, K.; Ohshita, J.; Takaki, K. Copper-Catalyzed Borylation Reactions of Alkynes and Arynes *Angew. Chem.* **2012**, *124*, 239-242.
- (8) Moldoveanu, C.; Wilson, D. A.; Wilson C. J.; Leowanawat, P.; Resmerita, A. M.; Liu, C.; Rosen, B. M.; Percec, V. Neopentylglycolborylation of ortho-Substituted Aryl Halides Catalyzed by NiCl<sub>2</sub>-Based Mixed-Ligand Systems *J.Org.Chem.* **2010**, *75*, 5438–5452.
- (9) Niwa, T; Ochiai, H.; Hosoya, T. Copper-Catalyzed ipso-Borylation of Fluoroarenes *ACS Catal.* **2017**, *7*, 4535-4541.
- (10) Laza, C.; Pintaric, C.; Dunach, E. Electrochemical Reduction of Polyhalogenated Aryl Derivatives in the Presence of Pinacolborane: Electrosynthesis of Functionalised Arylboronic Esters *Electrochimica Acta.* **2005**, *50*, 4897–4901.
- (11) Mfuh, A. M.; Nguyen V. T.; Chhetri, B.; Burch, J. E. Doyle, J. D.; Nesterov, V. N.; Arman, H. D.; Larionov, O. V. Additive- and Metal-Free, Predictably 1,2- and 1,3-Regioselective, Photoinduced Dual C–H/C–X Borylation of Haloarenes *J. Am. Chem. Soc.* **2016**, *138*, 8408–8411.
- (12) Shimizu, M.; Tomioka, Y.; Nagao, I.; Hiyama, T. Palladium-Catalyzed Double Cross-Coupling Reaction of vic-Diborylalkenes and -arenes with vic-Bromo(bromomethyl)arenes *Synlett.* **2009**, *19*, 3147-3150.
- (13) Yamamoto, T.; Suginome, M.; Regioselective Synthesis of o-Benzenediboronic Acids via Ir-Catalyzed o-C–H Borylation Directed by a Pyrazolylaniline Modified Boronyl Group *Org. Lett.* **2017**, *19*, 886-889.
- (14) Ihara, H.; Suginome, M.; Easily Attachable and Detachable ortho-Directing Agent for Arylboronic Acids in Ruthenium-Catalyzed Aromatic C- H Silylation *J. Am. Chem. Soc.* **2009**, *131*, 7502-7503.
- (15) Jayasundara, C. R. K. Iridium Catalyzed C-H Activation Borylations of Fluorine Bearing Arenes and Related Studies Ph.D. Dissertation, Michigan State University, East Lansing, MI, **2018**.

- (16) Oshima, K.; Ohmura, T.; Suginome, M. Dearomatizing Conversion of Pyrazines to 1,4-Dihydropyrazine Derivatives via Transition-Metal-Free Diboration, Silaboration, and Hydroboration. *Chem. Commun.* **2012**, 48 (68), 8571–8573.
- (17) Ohmura, T.; Morimasa, Y.; Suginome, M. Organocatalytic Diboration Involving “Reductive Addition” of a Boron–Boron  $\sigma$ -Bond to 4,4'-Bipyridine. *J. Am. Chem. Soc.* **2015**, 137 (8), 2852–2855.
- (18) Galstyan, A.; Shen, W.; Freisinger, E.; Alkam, H.; Hiller, W.; Sanz Miguel, P. J.; Schürmann, M.; Lippert, B. Supramolecular Isomerism of 2,2'-Bipyrazine Complexes with  $\text{Cis}-(\text{NH}_3)_2 \text{Pt II}$ : Ligand Rotational State and Sequential Orientation Determine the 3D Shape of Metallacycles. *Chem. Eur. J.* **2011**, 17 (38), 10771–10780.
- (19) Larsen, M. A.; Oeschger, R. J.; Hartwig, J. F. Effect of Ligand Structure on the Electron Density and Activity of Iridium Catalysts for the Borylation of Alkanes *ACS Catal.* **2020**, 10, 3415–3424.

## Chapter 3: *Para* Selective C–H Borylation of Sulfonated Phenols, Anilines, and Benzyl Alcohols Equipped with a Tetraalkylammonium Steric Shield

Parts of this chapter were taken from “*Para-Selective, Iridium-Catalyzed C–H Borylations of Sulfated Phenols, Benzyl Alcohols, and Anilines Directed by Ion-Pair Electrostatic Interactions*”

J. Am. Chem. Soc. **2019**, *141*, 15483-15487.

For two competing pathways, a difference in barrier heights of 2.5 kcal·mol<sup>-1</sup> is sufficient for 99% of the reactants to follow the favored pathway in a chemical reaction. This is lower than the barrier for converting the anti-conformer of butane to the gauche form.<sup>1</sup> In transition-metal mediated reactions, a classic mode for selectively functionalizing bonds in a substrate relies on the coordination of an atom in a reactant functional group to the metal center of a compound or catalytic intermediate. The magnitudes of the ligand–metal interactions are at least an order of magnitude greater than the difference in barrier heights necessary for 99:1 selectivity. Consequently, design of catalysts where selectivity is conferred by weakly coordinating groups,<sup>2</sup> as well as catalysts that leverage even weaker interactions (e.g., hydrogen-bonding, ion-pairing, dipole–dipole, etc.) for selective transformations,<sup>3,4</sup> is attracting significant attention.

C–H functionalization offer both atom and step economical means of converting ubiquitous C–H bonds to a range of functional groups.<sup>5,6</sup> C–H borylations (CHB) convert C–H bonds to C–B bonds and are mediated by both metal and metal-free catalysts.<sup>7-9</sup> CHB reactions are valuable due to (i) facile substitution of the boron moiety by numerous functional groups and (ii) functional group tolerance of C–H borylation catalysts, particularly those containing iridium.

The first iridium C–H borylation catalysts enabled C(sp<sup>2</sup>)–H functionalization with high selectivity for the most sterically accessible C–H bonds.<sup>10-12</sup> In substrates where multiple C–H bonds are sterically accessible, early generation catalysts often give isomer mixtures, as well as multiple borylated products. To overcome these limitations, more selective iridium catalysts have been designed. The first examples were ortho-selective,<sup>13</sup> relying on strongly coordinating functional groups in the substrate,<sup>14,15</sup> while later reports exploited weaker interactions for ortho selectivity.<sup>16-17</sup>

By comparison, *meta* and *para* C–H borylations pose different challenges because their C–H bonds are farther from the functional group. One *meta*-selective C–H borylation has been ascribed to a classical chelate-directed mechanism,<sup>18</sup> while others rely on iridium ligands bearing groups that engage in noncovalent interactions with substrate functional groups to effect *meta* C–H borylations.<sup>19-24</sup>

Figure 3-1 depicts approaches for *para* selective C–H borylations. The first C–H borylation with high *para* selectivity involved electrophilic additions of borenium cations to arenes bearing ortho, *para*-directors.<sup>25</sup>

Sterically directed C–H borylations rely on hindered phosphine ligands and substrates with large substituents.<sup>26,27</sup> More recently, para borylations of esters and amides have been achieved through noncovalent interactions with potassium ions or coordination of the amide oxygen to hindered Lewis acids.<sup>28,29</sup>

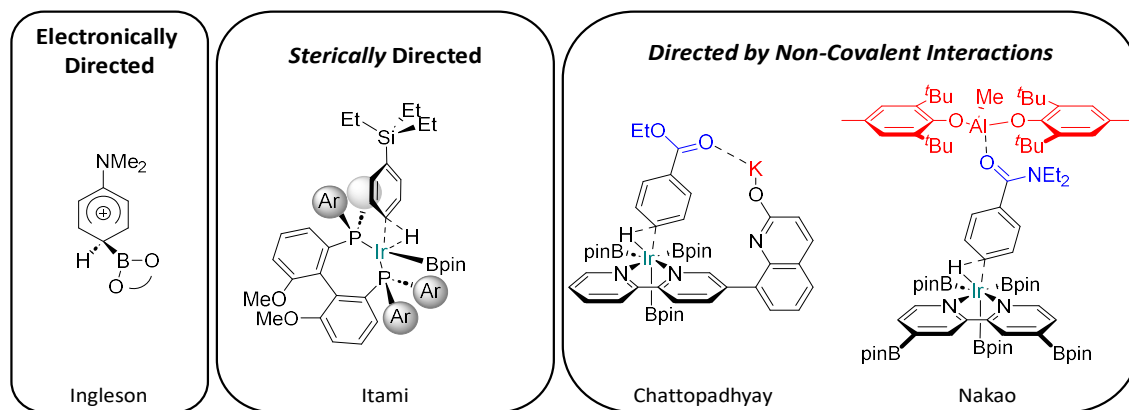


Figure 3-1 Examples of para Selective C–H Borylations

Our inspiration was based on the Phipps' group ion-pair directed C–H borylations with one key difference.<sup>20,22</sup> Instead of using oppositely charged groups on the ligand and substrate, combinations where groups on the ligand and substrate had the same charge were surveyed with the expectation that para borylation would be favored because electrostatic repulsions between the ligand and substrate would be minimized. However, a control experiment where tetrabutylammonium 2-chlorophenyl sulfate (4a) was subjected to standard borylation conditions with a neutral 4,4'-di-tert-butyl-2,2'-bipyridine (dtbpy) (3 mol%) with B<sub>2</sub>pin<sub>2</sub>, and [Ir(cod)OMe]<sub>2</sub> (1.5 mol%), in THF at 80 °C showed promising results with 6:1 para to meta regioselectivity (Figure 3-2).

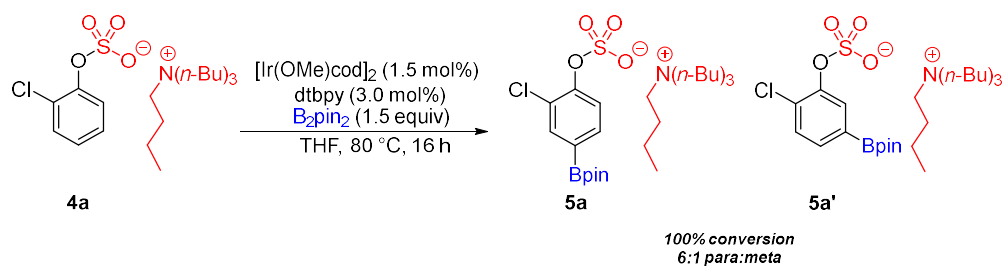
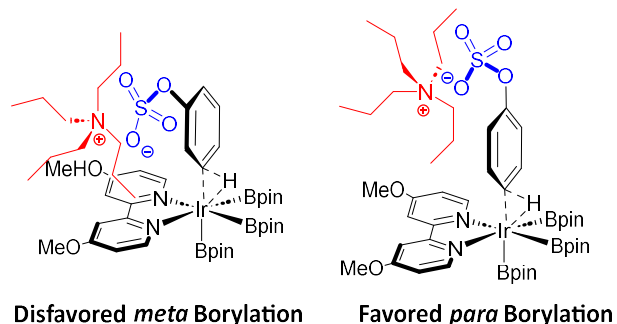


Figure 3-2 Initial para Selectivity Observed in Substrates Containing Tetraalkylammonium Cations

We hypothesized that substrate ion-pairing interactions, where the *n*-butyl groups of the cation shield the meta C–H bonds of the counter-anions, accounted for the para selectivity (Figure 3-3).

*Sterically Directed by Ion-Pair Electrostatic Interactions*



*Figure 3-3 Hypothesized Ion-Pairing Interaction Shielding meta Borylation Thus Promoting para Borylation*

In Nakao's study, ligand geometry played a key role in enhancement of the para selectivity.<sup>29</sup> Similarly, we have observed that ligand choice can impact CHB regiochemistry where there is little steric differentiation between different arene C–H bonds.<sup>30</sup>

Therefore, we tested commercially available substituted bipyridine and phenanthroline ligands (Figure 3-4) in C–H borylation reactions run at 80 °C. The reactivity of the ligands is in accordance with previously noted electronic effects,<sup>31</sup> with electron-rich ligands affording a more active system relative to electron poor ligands. The borylation in THF with 4,4'-dimethoxy-2,2'-bipyridine (**L3**) as the ligand went to >95% conversion and afforded the best para selectivity (13:1). This observation is notable in that 4,4'-dimethoxy-2,2'-bipyridine (**L3**) is a nontraditional C–H borylation ligand. Switching the solvent to 1,4-dioxane slightly increased the para selectivity (14:1), whereas other apolar solvents worsened regioselectivity.

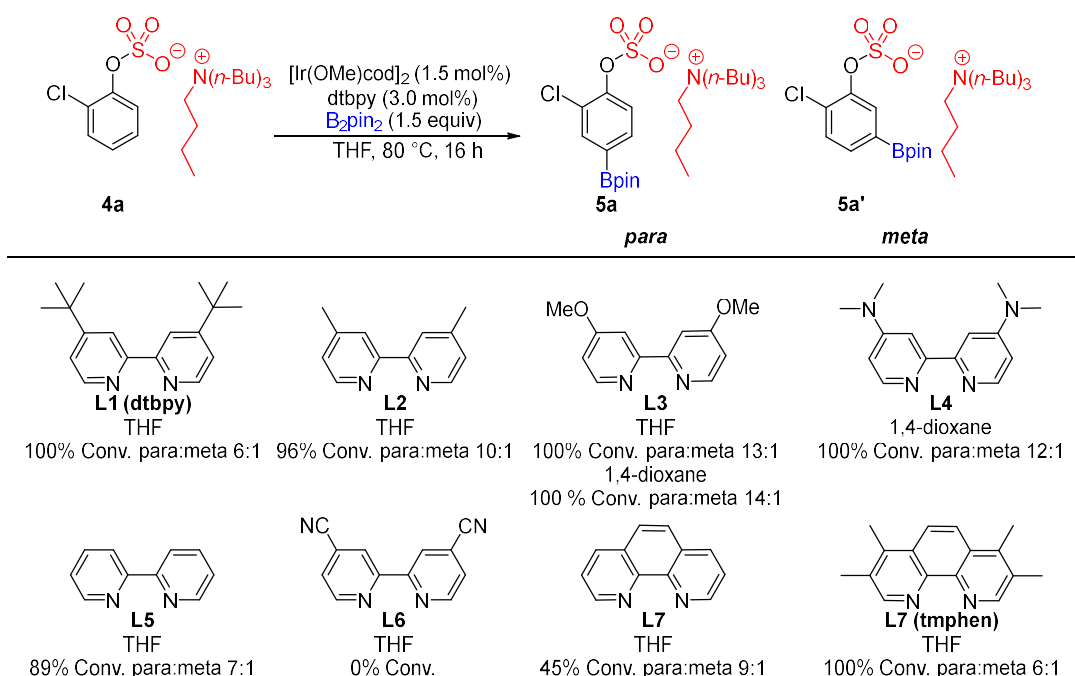


Figure 3-4 para meta Ratio of C–H Borylations of **4a** Utilizing Different Ligands

Running the reactions at lower temperature (60 °C and 40 °C) further improved the para selectivity while still allowing for full conversion (Figure 3-5). The reaction at room temperature afforded 21:1 para selectivity, but starting material remained even after 50 h.

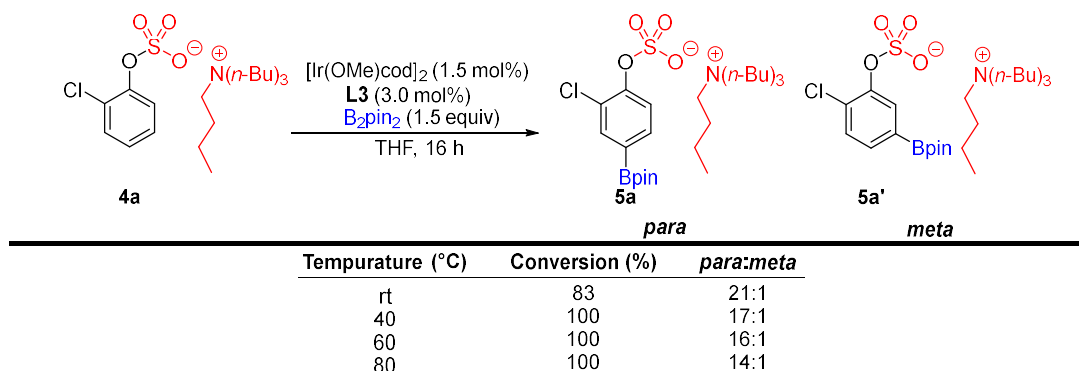


Figure 3-5 C–H Borylation of **4a** at Different Temperatures Using **L3**

With the experiments in Figure 3-4 and Figure 3-5 establishing 4,4'-dimethoxy-2,2'-bipyridine (**L3**) and 1,4-dioxane as our ligand and solvent of choice, we next investigated the effect of the tetraalkylammonium salt on para selectivity. DFT geometry optimization of **4a**, using the B3LYP functional and 6-31G\* basis set for all the atoms suggested to us that a slightly shorter alkyl chain would still block the *meta* position but leave the para position more exposed leading to improved para selectivity. Because of this we decided to

try shorter chained alkyl ammonium cations in an attempt to obtain better para selectivity. Additionally, it was noticed that there was a particularly short distance between the alpha hydrogens of the alkyl ammonium counterion with the oxygens of the sulfate suggesting the presence of hydrogen bonding. This is a known phenomenon with tetraalkylammonium cations as they are known hydrogen bond donors.<sup>32</sup> This potential hydrogen bonding may help maintain the optimal conformation needed for the steric shielding effect seen in borylation.

As shown in Figure 3-6, the C–H borylation of tetra propylammonium 2-chlorophenyl sulfate validated this hypothesis, as running the reaction with ligand 4,4'-dimethoxy-2,2'-bipyridine (**L3**) in 1,4-dioxane at 40 °C pushed the para selectivity to 22:1. We also examined tetraethylammonium 2-chlorophenyl sulfate as a substrate. In terms of chain shortening, clearly diminishing returns had set in as the para selectivity decreased to 17:1.

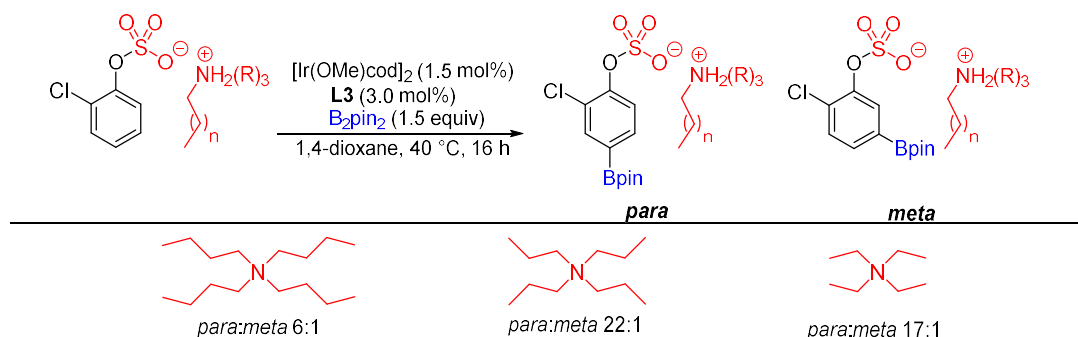


Figure 3-6 Effect of the Tetraalkylammonium Chain Length of para Selectivity in the Borylation of **4a**

Based on our results, we chose to test a series of phenol derived sulfates with  $n\text{-Pr}_4\text{N}$  as the counterion to determine substrate scope (Figure 3-7).

As illustrated in Figure 3-7, borylations of a series of 2-substituted phenol derived sulfates produced the para regioisomer as the major isomer, often with >20:1 selectivity. Most isolated yields were in the 70–80% range. Notably upon isolation the para to *meta* isomer was enhanced, in some cases to >50:1.



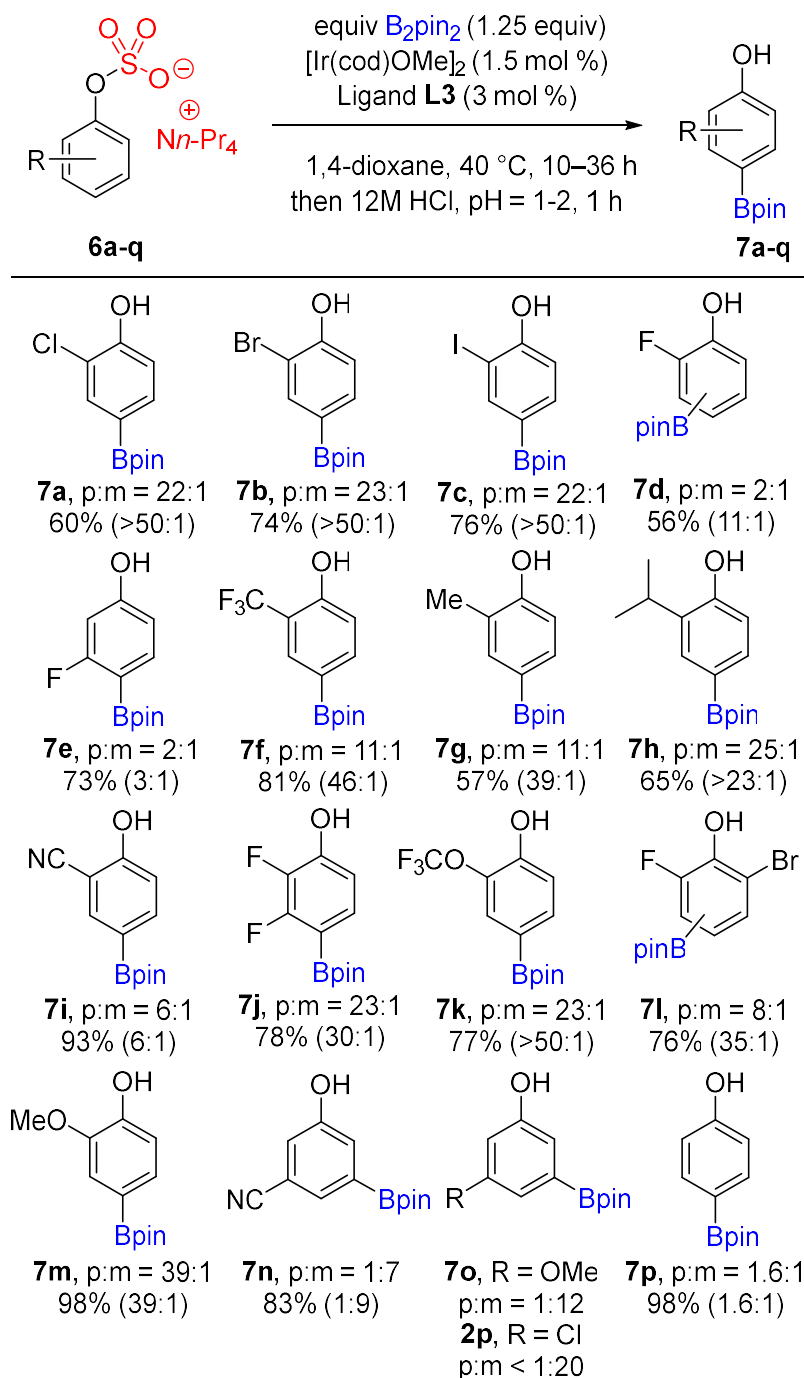


Figure 3-7 C–H Borylation Substrate Scope of  $n\text{-Pr}_4\text{N}^+$  Aryl Sulfates

It is clear that the ortho substituents of the phenolic arenes play a role in the selectivity. Those with lone pairs favor the para selectivity (substrates **7a–c**) resembling prior work showing that these groups favoring *meta* C–H borylations<sup>33</sup> which in our case is para with respect to the sulfated group. This selectivity decreases significantly without lone pairs in the ortho substituent as seen in **7f** and **7g**. Additionally, larger

ortho substituents improve selectivity irrespective of their electronic withdrawing character. This is illustrated in Figure 3-8 with **7f**, **7g**, **7h** where in **7f** and **7g** are approximately the same size show the same selectivity while being drastically different electronically. This indicates that the ortho substituent impacts the selectivity by helping to lock the arene sulfate conformation so as it is pointed away from the ortho substituent and towards the *meta* position to be shielded by the ammonium ion.

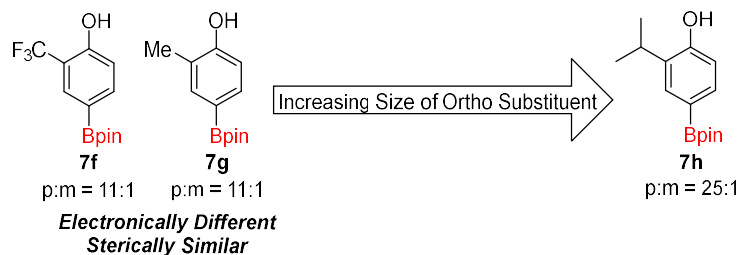


Figure 3-8 Steric Effects of the ortho Substituent on Regioselectivity

Indeed, analysis of the crude reaction mixture indicated that **6i** gave a mixture of the para to 5-Bpin to 3,5-diBpin products in a ratio of approximately 7.5:1:0.4. For substrates **6d** and **6l**, the observed minor isomer was that with the Bpin ortho to the fluoro group and no diborylation was observed. Given this preference, it was perhaps somewhat surprising that 3-fluorophenol sulfate (**6e**) produced a relatively large amount of the *meta* regioisomer.

Not surprising was that the C–H borylation of 3-substituted phenol sulfates (**6n–p**) gave the *meta* isomer as the major product, showing that such ion-pair interactions are limited in their ability to overcome steric crowding of the *para* C–H position. Last, we borylated the sulfate of phenol (**6p**) and observed the para, *meta*, and 3,5-*dimeta* Borylated products in a ratio of 4.4:1:1.8, or a *para:meta* ratio of 1.6:1. This result is consistent with the assumption that the ion pairing can only block one *meta* site and thus the reactions need a 2-substituent to sterically block the second *meta* C–H bond.

Looking at anilines (Figure 3-9), we subjected tetrapropylammonium 2-chlorophenylsulfamate (**8a'**) to our standard conditions. The para selectivity (40:1) was even better than that observed for **6a**. Questioning if the chain length of the tetraalkylammonium salt would also impact the para selectivity for aniline derivatives, we prepared and reacted the tetrabutylammonium salt (**8a**). In contrast to the phenol sulfates, employing this counterion met with 43:1 para selectivity and a higher isolated yield. Owing to this result and that the tetrabutylammonium salts are somewhat easier to prepare and isolate, we chose *n*-Bu<sub>4</sub>N<sup>+</sup> as the counterion for C–H borylations of a series of aniline sulfamates. The para selectivities for **8b** and **8d** were excellent, while again selectivity for a 3-fluoro substrate (**38c**) suffered, giving only a 2.4:1 94 *para:meta* ratio.

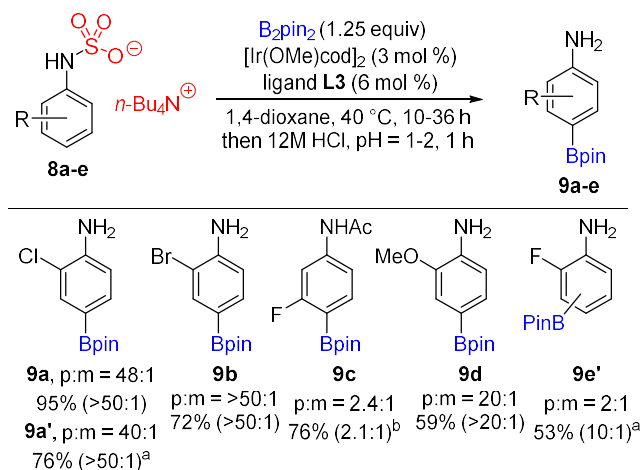


Figure 3-9 C–H Borylation Substrate Scope of  $n-Bu_4N^+$  Aryl Sulfamates <sup>a</sup> Substrate was Run as the  $n-Pr_4N^+$  Salt <sup>b</sup> The Product was Isolated as the Acetamide

Finally, we surveyed benzyl alcohol derived sulfates and found selectivity for the para position. Surprisingly we found that despite the increased distance from the additional methylene,  $n-Pr_4N^+$  was still the optimal shielding group as opposed to  $n-Bu_4N^+$ .

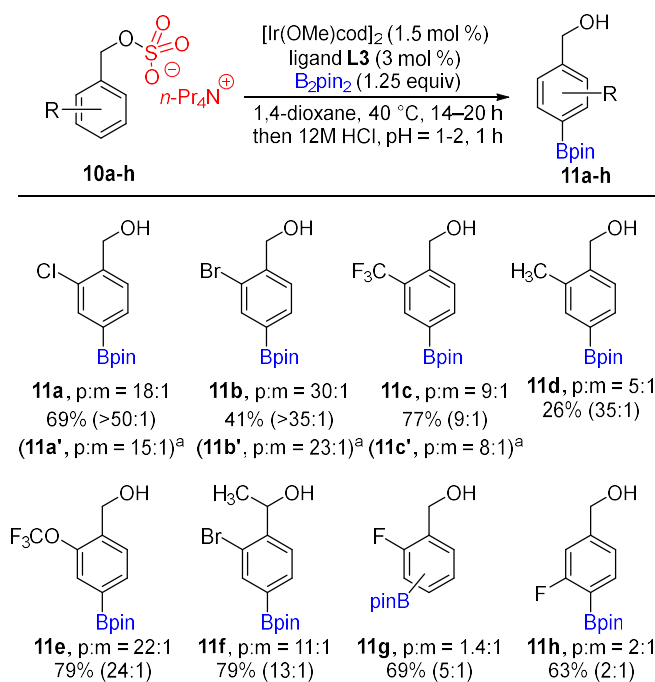


Figure 3-10 C–H Borylation Substrate Scope of  $n-Pr_4N^+$  Benzyl Sulfates <sup>a</sup> Substrate was Run as the  $n-Bu_4N^+$  Salt

Generally, benzyl sulfates reacted with somewhat diminished para selectivity relative to their phenol and aniline counterparts (Figure 3-10). Products **11b** and **11d** were generated in lower yields owing in part to lower conversions and, for **11d**, loss of the *meta* isomer upon isolation. Again, borylation of a substrate with fluorine in the 2-position (**10g**) afforded a significant amount of product with the Bpin ortho to the fluorine. By applying the C–H borylation conditions to the *n*-Bu<sub>4</sub>N<sup>+</sup> counterion, **10a–10c** revealed that the counterion has a similar influence on the regioselectivity as observed for the phenols.

During the course of our work we became aware that the Phipps group had developed the same strategy, using tetraalkylammonium cations as steric shields to direct borylations para to phenols, anilines, benzyl alcohols, benzyl amines, and benzyl sulfones.<sup>34</sup> Despite using the same method, the Phipps group focused on substrate exploration whereas we delved deeper into reaction optimization with regards to ligand, solvent, temperature and most importantly ammonium alkyl chain length. Because of this optimization we were able to achieve far more impressive selectivity. As the Phipps group expanded the methodology to additional substrate scaffolds, our work and the work done by Phipps provides a complimentary report and together a better understanding of the method. We are thankful to Phipps for allowing us to publish in a back-to-back manner and for that we are eternally grateful.<sup>35</sup> Since the conclusion of our work on this project, Phipps has since expanded use of ionic interactions to direct borylations to the use of chiral cationic shielding groups to de-symmetrize symmetric di-aryl systems by selective borylation of aryl rings based on chirality.<sup>36</sup>

In summary, ion-pair electrostatic interactions can be used to direct iridium catalyzed borylation to the para position of sulfates and sulfamates derived from phenols, anilines, and benzyl alcohols. We show that the source of the para selectivity is through the steric presence created by the carbon chain of the tetraalkylammonium counterion and is augmented by the ortho substituent. We found that *n*-Pr<sub>4</sub>N<sup>+</sup> salts gave better selectivity than their *n*-Bu<sub>4</sub>N<sup>+</sup> counterparts. The chain length of tetraalkylammonium salt however was not as influential on the borylation of the sulfamates derived from anilines. Notably, optimal results were observed with the nontraditional C–H borylation ligand 4,4'-dimethoxy-2,2'-bipyridine (**L3**) serving to remind the community to look beyond 4,4'-di-*tert*-butyl-2,2'-bipyridine (dtbpy) (**L1**) or 3,4,7,8-tetramethyl-1,10-phenanthroline (tmphen) (**L7**) when optimizing C–H borylation reactions.

## Experimental Procedures

### General Information

All available reagents were used as received unless otherwise indicated. Bis(pinacolato)diboron ( $B_2pin_2$ ) was generously supplied by BoroPharm. THF was refluxed over Na/benzophenone ketyl and distilled. Anhydrous 1,4-dioxane was obtained through Sigma-Aldrich and used as received. 3,4,7,8-tetramethyl-1,10-phenanthroline (tmphen) and neocuproine were purchased from Combi-blocks and recrystallized from ethanol. 2-chloroaniline, 2-methoxyaniline, 2-methylaniline, 2-ethylaniline, 2-tertbutylaniline and tetrahydroquinoline were distilled over molecular sieves prior to use. Column chromatography was done using 240-400 mesh silica P-Flash silica gel. TLC was done on 0.25 mm thick aluminum backed silica gel plates and visualized with UV light ( $\lambda = 254$  nm) with alizarin stain.<sup>58</sup>

$^1H$ ,  $^{13}C$ ,  $^{11}B$  and  $^{19}F$  NMR spectra were recorded on a Varian 500 MHz DD2 Spectrometer equipped with a  $^1H$ - $^{19}F$ / $^{15}N$ - $^{31}P$  5 mm Pulsed Field Gradient (PFG) Probe. Spectra taken in  $CDCl_3$  were referenced to 7.26 ppm in  $^1H$  NMR and 77.2 ppm in  $^{13}C$  NMR. Spectra taken in  $C_6D_6$  were referenced to 7.16 ppm in  $^1H$  NMR and 128.1 ppm in  $^{13}C$ .  $^{11}B$  NMR spectra were referenced to neat  $BF_3 \cdot Et_2O$  as the external standard. NMR spectra were processed for display using the MNova software program with only phasing and baseline corrections applied. High-resolution mass spectra (HRMS) were obtained at the Molecular Metabolism and Disease Mass Spectrometry Core facility and at the Mass Spectrometry Service Center at Michigan State University using electrospray ionization (ESI+ or ESI-) on quadrupole time-of-flight (Q-TOF) instruments.

Parts of this chapter were reprinted with permission from Montero Bastidas, J. R.; Oleskey, T. J.; Miller, S. L.; Smith, M. R., III; Maleczka, R. E., Jr. Para-Selective, Iridium-Catalyzed C–H Borylations of Sulfated Phenols, Benzyl Alcohols, and Anilines Directed by Ion-Pair Electrostatic Interactions. *J. Am. Chem. Soc.* **2019**, *141*, 15483-15487. Copyright 2021 American Chemical Society

The work presented in this chapter was not all conducted by Thomas Oleskey. Substrate exploration was a team effort with Montero Bastidas, J. R. and Miller, S. L.

### Synthesis of tetrapropylammonium 2-iodophenylsulfate (6c)

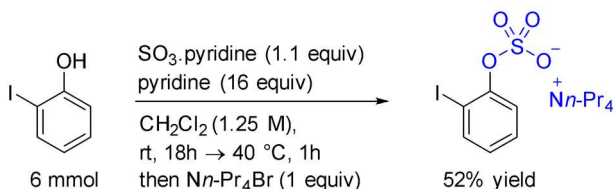


Figure 3-11 Synthesis of tetrapropylammonium 2-iodophenylsulfate (6c)

2-Iodophenol (1.3200 g, 6.00 mmol) and  $\text{SO}_3 \cdot \text{pyridine}$  complex (1.0500 g, 6.60 mmol) were placed in a 100 mL round bottom flask. Pyridine (8 mL) and dry dichloromethane (5 mL) were added and the mixture was stirred at rt for 18 h. After this time, the reaction was heated to 40 °C for 1 h. Water (70 mL) was added and the mixture was washed once with dichloromethane (1 x 70 mL). The aqueous phase was treated with tetrapropyl ammonium bromide (1.6000 g, 6.00 mmol) and stirred for 1 h. The solution was extracted with dichloromethane (3 x 70 mL). The organic layer was dried over  $\text{MgSO}_4$ , filtered, and concentrated. Diethyl ether and hexanes were added to evaporate the solvent to dryness and the product was obtained as a white solid (1.5100 g, 52% yield).

**Data for tetrapropylammonium 2-iodophenylsulfate (6c)**

$^1\text{H}$  NMR (500 MHz,  $\text{CDCl}_3$ ) 7.65 (m, 2H), 7.17 (ddd,  $J = 8.6, 7.3, 1.6$  Hz, 1H), 6.70 (td,  $J = 7.6, 1.5$  Hz, 1H), 3.15–2.81 (m, 8H), 1.68–1.22 (m, 8H), 0.84 (t,  $J = 7.3$  Hz, 12H).

$^{13}\text{C}$  NMR (126 MHz,  $\text{CDCl}_3$ )  $\delta$  153.4, 138.9, 129.05, 124.8, 120.7, 89.5, 60.2, 15.5, 10.8.

HRMS (ESI)  $m/z$  calcd. for  $\text{C}_6\text{H}_4\text{IO}_4\text{S} [\text{M}-n\text{-Pr}_4]^+$  298.8875, found 298.8890.

**Synthesis of tetrapropylammonium 3-fluorophenyl sulfate (6e)**

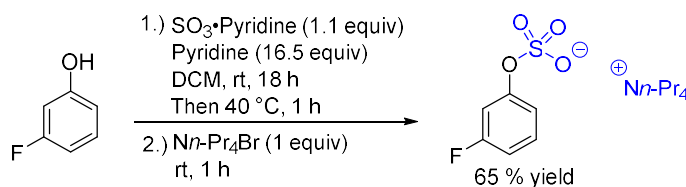


*Figure 3-12 Synthesis of tetrapropylammonium 3-fluorophenyl sulfate (6e)*

3-Fluorophenol (0.6730 g, 6.00 mmol) and  $\text{SO}_3 \cdot \text{pyridine}$  complex (1.0500 g, 6.60 mmol) was placed in a 100 mL round bottom flask. Pyridine (8 mL) and dry dichloromethane (5 mL) were added, and the mixture was stirred at rt for 18 h. After this time, the reaction was heated to 40 °C for 1 h. Water (70 mL) was added, and the mixture was washed once with dichloromethane (1 x 70 mL). The aqueous phase was treated with tetrapropyl ammonium bromide (1.6000 g, 6.00 mmol) and stirred for 1 h. The solution was extracted with dichloromethane (3 x 70 mL). The organic layer was dried over  $\text{MgSO}_4$ , filtered, and concentrated, resulting in a clear oil. To the concentrated oil, hexanes were added, and the suspension was concentrated by rotary evaporation. This process was repeated until the product was obtained as a white solid. After overnight drying under high vacuum (**6e**) was obtained as a white solid (1.4600 g, 64% yield).

#### Data for tetrapropylammonium 3-fluorophenyl sulfate (6e)

$^1\text{H}$  NMR (500 MHz,  $\text{CDCl}_3$ )  $\delta$  7.19 (td,  $J = 8.2, 6.8$  Hz, 1H), 7.14 (dt,  $J = 10.6, 2.4$  Hz, 1H), 7.07 (ddd,  $J = 8.2, 2.4, 0.9$  Hz, 1H), 6.74 (tdd,  $J = 8.2, 2.4, 0.9$  Hz, 1H), 3.15–2.90 (m, 8H), 1.68–1.51 (m, 8H), 0.94 (t,  $J = 7.3$  Hz, 12H).

$^{13}\text{C}$  NMR (126 MHz,  $\text{CDCl}_3$ )  $\delta$  162.8 (d,  $J = 244.6$  Hz), 154.8 (d,  $J = 11.2$  Hz), 129.6 (d,  $J = 9.6$  Hz), 116.5 (d,  $J = 2.9$  Hz), 110.1 (d,  $J = 21.1$  Hz), 108.3 (d,  $J = 24.3$  Hz), 60.3, 15.5, 10.7.

$^{19}\text{F}$  NMR (470 MHz,  $\text{CDCl}_3$ )  $\delta$  -115.73 (m).

HRMS (ESI)  $m/z$  calcd. for  $\text{C}_6\text{H}_4\text{FO}_4\text{S} [\text{M}-\text{Nn-Pr}_4]^+$  190.9814, found 190.9821

#### Synthesis of tetrapropylammonium 2-cyanophenyl sulfate (6i)

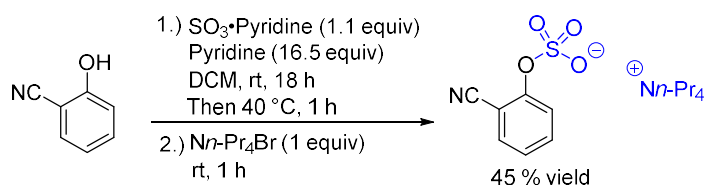


Figure 3-13 Synthesis of tetrapropylammonium 2-cyanophenyl sulfate (6i)

2-Cyanophenol (0.7140 g, 6.00 mmol) and  $\text{SO}_3 \cdot \text{pyridine}$  complex (1.0500 g, 6.60 mmol) were placed in a 100 mL round bottom flask. Pyridine (8 mL) and dry dichloromethane (5 mL) were added and the mixture was stirred at rt for 18 h. After this time, the reaction was heated to 40 °C for 1 h. Water (70 mL) was added and the mixture was washed once with dichloromethane (1 x 70 mL). The aqueous phase was treated with tetrapropyl ammonium bromide (1.6000 g, 6.00 mmol) and stirred for 1 h. The solution was extracted with dichloromethane (3 x 70 mL). The organic layer was dried over  $\text{MgSO}_4$ , filtered, and concentrated, resulting in a clear oil. To the concentrated oil, hexanes and ether were added and the suspension was again concentrated by rotary evaporation. This process was repeated until the product was obtained as a white solid. After overnight drying under high vacuum (6i) was obtained as a white solid (1.0300 g, 45% yield).

#### Data for tetrapropylammonium 2-cyanophenyl sulfate (6i)

$^1\text{H}$  NMR (500 MHz,  $\text{CDCl}_3$ )  $\delta$  7.79 (dd,  $J = 7.6, 1.1$  Hz, 1H), 7.46 (dd,  $J = 7.6, 1.8$  Hz, 1H), 7.45 (td,  $J = 7.6, 1.8$  Hz, 1H), 7.05 (td,  $J = 7.6, 1.1$  Hz, 1H), 3.26 – 2.73 (m, 8H), 1.61 (m, 8H), 0.90 (t,  $J = 7.3$  Hz, 12H).

$^{13}\text{C}$  NMR (126 MHz,  $\text{CDCl}_3$ )  $\delta$  155.7, 133.9, 132.9, 123.2, 121.0, 116.9, 104.6, 60.2, 15.5, 10.7.

HRMS (ESI)  $m/z$  calcd. for  $\text{C}_7\text{H}_4\text{NO}_4\text{S} [\text{M}-\text{Nn-Pr}_4]^+$  197.9861, found 197.8931.

### Synthesis of tetrapropylammonium 2-(trifluoromethoxy)phenyl sulfate (6k)

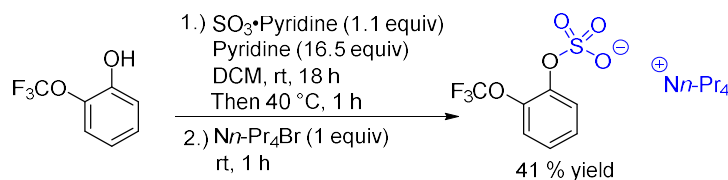


Figure 3-14 Synthesis of tetrapropylammonium 2-(trifluoromethoxy)phenyl sulfate (6k)

2-(trifluoromethoxy)phenol (1.0700 g, 6 mmol) and  $\text{SO}_3 \cdot \text{pyridine}$  complex (1.0500 g, 6.6 mmol) were placed in a 100 mL round bottom flask. Pyridine (8 mL) and dry dichloromethane (5 mL) were added, and the flask sealed with a glass stopper. The mixture was stirred at rt for 18 h. After this time, the reaction was heated to 40 °C for 1 h. Water (70 mL) was added, and the mixture was washed once with dichloromethane (70 mL) and the aqueous phase transferred to a 250 mL round bottom flask.  $\text{Nn-Pr}_4\text{Br}$  (1.6000 g, 6 mmol) was added to the aqueous phase and the flask sealed with a glass stopper. The mixture was stirred for 1 h. The solution was extracted with dichloromethane (3x, 70 mL). The organic layer was dried over  $\text{MgSO}_4$ , filtered, and concentrated. Hexanes (7 mL) were added to the product and the suspension evaporated. This was repeated until no pyridine was seen via NMR. Diethyl ether (7 mL) was added to the product, and the suspension evaporated until no dichloromethane was seen via NMR. After the pyridine and dichloromethane were removed a white solid was collected, which was crushed then dried overnight under high vacuum. **6k** was obtained as a white solid (1.0900 g, 41% yield). The NMR values were consistent with previously reported values.<sup>6</sup>

### Data for tetrapropylammonium 2-(trifluoromethoxy)phenyl sulfate (6k)

$^1\text{H}$  NMR (500 MHz,  $\text{CDCl}_3$ )  $\delta$  7.80 (dd,  $J=8.7, 1.4$  Hz, 1H), 7.20-7.12 (m, 2H), 6.99 (td,  $J=7.9, 1.7$  Hz, 1H), 3.11 (p,  $J=4.2$  Hz, 8H), 1.59 (hept,  $J=7.6$  Hz, 8H), 0.89 (t,  $J=7.3$  Hz, 12H).

$^{13}\text{C}$  NMR (126 MHz,  $\text{CDCl}_3$ )  $\delta$  151.9 (q,  $J=1.8$  Hz), 132.8 (s), 126.2 (q,  $J=5.0$  Hz), 123.5 (q,  $J=272.4$  Hz), 122.2 (s), 120.7 (s), 120.4 (q,  $J=30.6$  Hz), 60.1, 15.4, 10.5.

$^{19}\text{F}$  NMR (470 MHz,  $\text{CDCl}_3$ )  $\delta$  -57.4 (s, 3F).

HRMS (ESI)  $m/z$  calcd. For  $\text{C}_7\text{H}_4\text{F}_3\text{O}_4\text{S} [\text{M}-\text{Nn-Pr}_4]$  -240.9782, found 240.9784.



### Synthesis of tetrapropylammonium 2-bromo-6-fluorophenyl sulfate (6I)

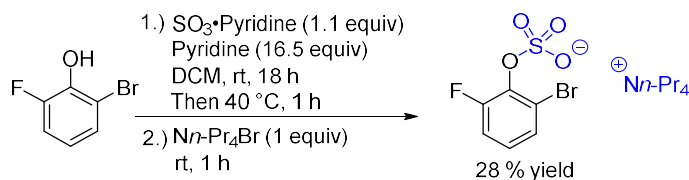


Figure 3-15 Synthesis of tetrapropylammonium 2-bromo-6-fluorophenyl sulfate (6I)

2-bromo-6-fluorophenol (1.1500 g, 6.00 mmol) and  $\text{SO}_3 \cdot \text{pyridine}$  complex (1.0500 g, 6.60 mmol) were placed in a 100 mL round bottom flask. Pyridine (8 mL) and dry dichloromethane (5 mL) were added, and the flask sealed with a glass stopper. The mixture was stirred at rt for 18 h. After this time, the reaction was heated to 40°C for 1h. Water (70 mL) was added, and the mixture was washed once with dichloromethane (70 mL) and the aqueous phase transferred to a 250 mL round bottom flask.  $\text{Nn-Pr}_4\text{Br}$  (1.6000 g, 6.00 mmol) was added to the aqueous phase and the flask sealed with a glass stopper. The mixture was stirred for 1h. The solution was extracted with dichloromethane (3x, 70 mL). The organic layer was dried over  $\text{MgSO}_4$ , filtered, and concentrated. Hexanes (7 mL) were added to the product and the suspension evaporated. This was repeated until no pyridine was seen via NMR. Diethyl ether (7 mL) was added to the product, and the suspension evaporated until no dichloromethane was seen via NMR. After the pyridine and dichloromethane were removed a white solid was collected, which was crushed then dried overnight under high vacuum. **6I** was obtained as a white solid (0.7800 g, 28% yield). The NMR values were consistent with previously reported values.

#### Data for tetrapropylammonium 2-bromo-6-fluorophenyl sulfate (6I)

$^1\text{H}$  NMR (500 MHz,  $\text{CDCl}_3$ )  $\delta$  7.24 (d,  $J=8.0$  Hz, 1H), 6.97 (t,  $J=8.7$  Hz, 1H), 6.89 (td,  $J=8.1, 5.3$  Hz, 1H), 3.10 (p,  $J=4.31$  Hz, 8H), 1.58 (hept,  $J=8.12$  Hz, 8H), 0.89 (t,  $J=7.3$  Hz, 12H).

$^{13}\text{C}$  NMR (126 MHz,  $\text{CDCl}_3$ )  $\delta$  156.8 (d,  $J=253.8$  Hz), 139.7 (d,  $J=14.4$  Hz), 128.3 (d,  $J=3.5$  Hz), 125.5 (d,  $J=8.1$  Hz), 119.8 (d,  $J=1.9$  Hz), 115.7 (d,  $J=19.9$  Hz), 60.2, 15.5, 10.7.

$^{19}\text{F}$  NMR (470 MHz,  $\text{CDCl}_3$ )  $\delta$  -124.4 (dd,  $J=9.5, 5.1$  Hz).

HRMS (ESI)  $m/z$  calcd. For  $\text{C}_6\text{H}_3\text{BrFO}_4\text{S}$  [ $\text{M}-\text{Nn-Pr}_4$ ]- 268.8919, found 268.8919.

### Synthesis of tetrapropylammonium phenyl sulfate (6p)

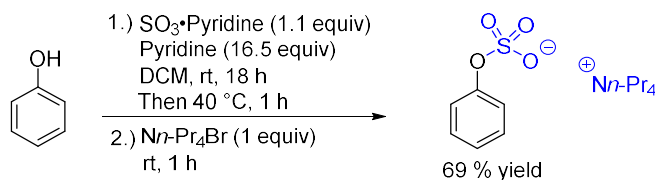


Figure 3-16 Synthesis of tetrapropylammonium phenyl sulfate (6p)

Phenol (1.0700 g, 6.00 mmol) and  $\text{SO}_3 \cdot \text{pyridine}$  complex (1.0500 g, 6.60 mmol) were placed in a 100 mL round bottom flask. Pyridine (8 mL) and dry dichloromethane (5 mL) were added, and the flask sealed with a glass stopper. The mixture was stirred at 40 °C for 8 h. Water (70 mL) was added, and the mixture was washed once with dichloromethane (70 mL) and the aqueous phase transferred to a 250 mL round bottom flask.  $\text{Nn-Pr}_4\text{Br}$  (1.6000 g, 6.00 mmol) was added to the aqueous phase and the flask sealed with a glass stopper. The mixture was stirred for 1 h. The solution was extracted with dichloromethane (3x, 70 mL). The organic layer was dried over  $\text{MgSO}_4$ , filtered, and concentrated. Hexanes (7 mL) were added to the product and the suspension evaporated. This was repeated until no pyridine was seen via NMR. Diethyl ether (7 mL) was added to the product, and the suspension evaporated until no dichloromethane was seen via NMR. After the pyridine and dichloromethane were removed a white solid was collected, which was crushed then dried overnight under high vacuum. **6p** was obtained as a white solid (1.5000 g, 69% yield). The NMR values were consistent with previously reported values.<sup>6</sup>

### Data for tetrapropylammonium phenyl sulfate (6p)

$^1\text{H}$  NMR (500 MHz,  $\text{CDCl}_3$ )  $\delta$  7.32 (d,  $J=8.1$  Hz, 2H), 7.23 (t,  $J=8.1$  Hz, 2H), 7.02 (t,  $J=7.3$  Hz, 1H), 3.08 (p,  $J=3.8$  Hz, 8H), 1.57 (hept, 7.8 Hz, 8H), 0.92 (t,  $J=7.3$  Hz, 12H).

$^{13}\text{C}$  NMR (126 MHz,  $\text{CDCl}_3$ )  $\delta$  153.6, 128.8, 123.4, 121.0, 60.1, 15.4, 10.7.

HRMS (ESI)  $m/z$  calcd. For  $\text{C}_6\text{H}_5\text{O}_4\text{S} [\text{M}-\text{Nn-Pr}_4]^+$ – 172.9909, found 173.0117.

### Synthesis of tetrabutylammonium 2-chlorophenyl sulfamate (9a)

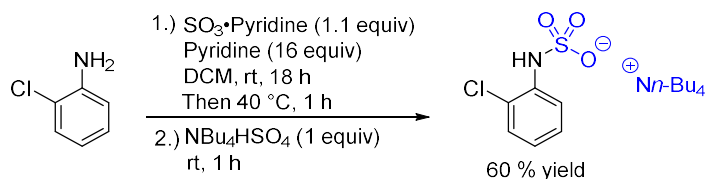


Figure 3-17 Synthesis of tetrabutylammonium 2-chlorophenyl sulfamate (9a)

In an open 100 mL round bottom flask in air, 2-chloroaniline (1.6300 g, 12.74 mmol) was added along with 17 mL pyridine, 10 mL dichloromethane, and  $\text{SO}_3 \cdot \text{Pyridine}$  (2.1900 g, 13.75 mmol). A stir bar was

added, and the flask capped with a rubber septum. The solution was stirred at room temperature for 18 hours. The temperature was then raised to 40 °C in an oil bath and the reaction stirred for an additional hour. 150 mL of water was then added. The resulting solution was washed with 150 mL of DCM. The aqueous phase was transferred to a 250 mL round bottom flask and  $\text{NBu}_4\text{HSO}_4$  (4.2400 g, 12.50 mmol) added. The flask was capped with a glass stopper. This solution was stirred for 1 hour over which the solution cleared, and a brown oil formed. The aqueous layer was extracted 3x with 150 mL dichloromethane. The organic phase was dried over anhydrous  $\text{MgSO}_4$ . The organic phase was evaporated forming a tan oil. To the oil, approximately 7 mL of hexanes were added, and the oil suspension evaporated. This was repeated until no pyridine was seen via NMR. Diethyl ether was also added, and the oil and the suspension evaporated until no dichloromethane was seen via NMR. After the pyridine and dichloromethane were removed the oil solidified into a light tan solid that was then dried overnight under high vacuum. **9a** was collected as a tan solid (3.8200 g, 60 % yield). The NMR values were consistent with previously reported values.<sup>6</sup>

#### Data for tetrabutylammonium 2-chlorophenyl sulfamate (**9a**)

$^1\text{H}$  NMR (500M Hz,  $\text{CDCl}_3$ )  $\delta$  7.80 (d,  $J=8.3$  Hz, 1H), 7.19 (d,  $J=7.9$  Hz, 1H), 7.11 (t,  $J=7.8$  Hz, 1H), 6.71 (t,  $J=7.6$  Hz, 1H), 6.65 (bs, 1H), 3.16 (t,  $J=8.3$  Hz, 8H), 1.54 (p,  $J=7.2$  Hz, 8H), 1.35 (h,  $J=7.0$  Hz, 8H), 0.94 (t,  $J=7.4$  Hz, 12H).

$^{13}\text{C}$  NMR (126 MHz,  $\text{CDCl}_3$ )  $\delta$  139.2, 128.7, 127.6, 120.0, 120.0, 117.7, 58.7, 24.0, 19.8, 13.8.

HRMS (ESI)  $m/z$  calcd. for  $\text{C}_6\text{H}_5\text{ClNO}_3\text{S}$  [ $\text{M}-\text{Nn}-\text{Bu}_4$ ] $^-$  205.9679, found 205.9897.

#### Synthesis of tetrabutylammonium 2-bromophenyl sulfamate (**9b**)

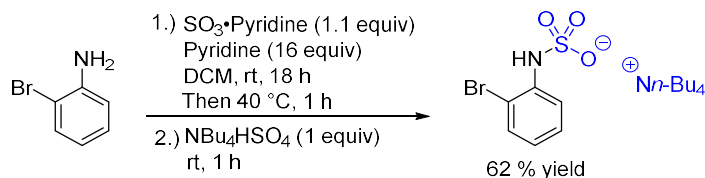


Figure 3-18 Synthesis of tetrabutylammonium 2-bromophenyl sulfamate (**9b**)

In a 100 mL round bottom flask in air, 2-bromoaniline (2.1400 g, 12.50 mmol) was added along with pyridine (17 mL), dichloromethane (10 mL), and  $\text{SO}_3 \cdot \text{Pyridine}$  (2.1900 g, 13.75 mmol). A stir bar was added, and the flask sealed with a glass stopper. The solution was stirred at room temperature for 18 hours. The temperature was then raised to 40 °C in an oil bath and the reaction stirred for an additional hour. Water (150 mL) was then added. The resulting solution was washed with dichloromethane (150 mL). The aqueous phase was transferred to a 250 mL round bottom flask and  $\text{NBu}_4\text{HSO}_4$  (4.2400 g, 12.50

mmol) added turning the solution an opaque white. The flask was sealed with a glass stopper. This solution was stirred for an hour over which the solution cleared, and a brown oil formed. The reaction was extracted with dichloromethane (3x, 150 mL). The organic phase was dried over anhydrous  $\text{MgSO}_4$ . The organic phase was evaporated forming a tan oil. To the oil, hexanes (7 mL) were added, and the oil suspension evaporated. This was repeated until no pyridine was seen via NMR. Diethyl ether (7 mL) was added to the oil, and the oil suspension evaporated until no dichloromethane was seen via NMR. After the pyridine and dichloromethane were removed the oil solidified into a white solid that was crushed then dried overnight under high vacuum. **9b** was collected as an off-white solid (3.8400 g, 62 % yield). The NMR values were consistent with previously reported values.

#### Data for tetrabutylammonium 2-bromophenyl sulfamate (**9b**)

$^1\text{H}$  NMR (500 MHz,  $\text{CDCl}_3$ )  $\delta$  7.81 (dd,  $J=8.5, 1.4$  Hz, 1H), 7.37 (dd,  $J=8.0, 1.3$  Hz, 1H), 7.16 (td,  $J=7.3, 1.2$  Hz, 1H), 6.66 (m, 2H), 3.18 (t,  $J=8.2$  Hz, 8H), 1.57 (p,  $J=7.8$  Hz, 8H), 1.37 (h,  $J=7.3$ , 8H), 0.96 (t,  $J=7.3$  Hz, 12H).

$^{13}\text{C}$  NMR (126 MHz,  $\text{CDCl}_3$ )  $\delta$  140.3, 131.9, 128.3, 120.5, 117.7, 110.5, 58.6, 24.0, 19.8, 13.8.

HRMS (ESI)  $m/z$  calcd for  $\text{C}_6\text{H}_5\text{BrNO}_3\text{S}$  [ $\text{M}-\text{Nn}-\text{Bu}_4$ ] $^-$  249.9173, found 249.8044.

#### Synthesis of tetrabutylammonium 3-fluorophenyl sulfamate (**9c**)

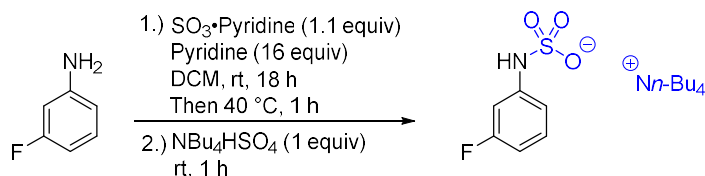


Figure 3-19 Synthesis of tetrabutylammonium 3-fluorophenyl sulfamate (**9c**)

In an open 100 mL round bottom flask in air, 2-bromoaniline (1.3900 g, 12.50 mmol) was added along with 17 mL pyridine, 10 mL dichloromethane, and  $\text{SO}_3\cdot\text{Pyridine}$  (2.1900 g, 13.75 mmol). A stir bar was added, and the flask capped with a rubber septum. The solution was stirred at room temperature for 18 hours. The temperature was then raised to 40 °C in an oil bath and the reaction stirred for an additional hour. 150 mL of water was then added. The resulting solution was washed with 150 mL of DCM. The aqueous phase was transferred to a 250 mL round bottom flask and  $\text{NBu}_4\text{HSO}_4$  (4.2400 g, 12.50 mmol) added turning the solution an opaque white. The flask was capped with a glass stopper. This solution was stirred for 1 hour over which the solution cleared, and a brown oil formed. The aqueous layer was extracted 3x with 150 mL dichloromethane. The organic phase was dried over anhydrous  $\text{MgSO}_4$ . The organic phase was evaporated forming a tan oil. To the oil, approximately 7 mL of hexanes were added, and the oil suspension evaporated. This was repeated until no pyridine was seen via NMR. Diethyl ether

was also added, and the oil and the suspension evaporated until no dichloromethane was seen via NMR. After the pyridine and dichloromethane were removed the oil solidified into a pink solid that was then dried overnight under high vacuum. **9c** was collected as a pink solid (4.1200 g, 71 % yield). The NMR values were consistent with previously reported values.

#### Data for 3-fluorophenyl sulfamate (9c)

$^1\text{H}$  NMR (500MHz,  $\text{CDCl}_3$ )  $\delta$  7.07 (bs, 1H), 7.12–6.96 (m, 2H), 6.78 (dt,  $J=8.2$ , 0.83 Hz, 1H), 6.44 (td,  $J=8.5, 2.2$  Hz, 1H), 3.16 (t,  $J=8.4$  Hz, 8H), 1.51 (p,  $J=7.9$  Hz, 8H), 1.33 (h,  $J=7.3$ , 8H), 0.91 (t,  $J=7.3$  Hz, 12H).

$^{13}\text{C}$  NMR (126 MHz,  $\text{CDCl}_3$ )  $\delta$  163.2 (d,  $J=241.6$  Hz), 144.5 (d,  $J=11.1$  Hz), 129.3 (d,  $J=9.8$  Hz), 112.1 (d,  $J=1.7$  Hz), 105.5 (dd,  $J=21.4$ , 1.7 Hz), 103.4 (d,  $J=25.4$  Hz), 58.0, 23.5, 19.3, 13.4.

$^{19}\text{F}$  NMR (470 MHz,  $\text{CDCl}_3$ )  $\delta$  -113.56 (dt,  $J=11.8$ , 8.3 Hz).

HRMS (ESI)  $m/z$  calcd. for  $\text{C}_6\text{H}_5\text{FNO}_3\text{S}$  [ $\text{M}-\text{Nn}-\text{Bu}_4$ ]- 189.9974, found 189.9108.

#### Synthesis of tetrabutylammonium (2-chlorophenyl)methane sulfamate (10a')

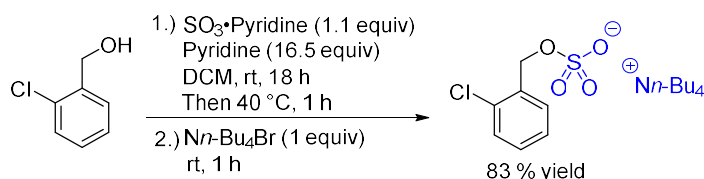


Figure 3-20 Synthesis of tetrabutylammonium (2-chlorophenyl)methane sulfamate (10a')

2-Chlorobenzyl alcohol (0.8600 g, 6.00 mmol) and  $\text{SO}_3 \cdot \text{pyridine}$  complex (1.0500 g, 6.60 mmol) were placed in a 100 mL round bottom flask. Pyridine (8 mL) and dry dichloromethane (5 mL) were added, and the flask sealed with a glass stopper. The mixture was stirred at rt for 18 h. After this time, the reaction was heated to 40°C for 1h. Water (70 mL) was added, and the mixture was washed once with dichloromethane (70 mL) and the aqueous phase transferred to a 250 mL round bottom flask. Tetrabutylammonium hydrogen sulfate (2.1300 g, 6.00 mmol) was added to the aqueous phase and the flask sealed with a glass stopper. The mixture was stirred for 1 hour. The solution was extracted with dichloromethane (3x, 70 mL). The organic layer was dried over  $\text{MgSO}_4$ , filtered, and concentrated. Hexanes (7 mL) were added to the product and the suspension evaporated. This was repeated until no pyridine was seen via NMR. Diethyl ether (7 mL) was added to the product, and the suspension evaporated until no dichloromethane was seen via NMR. After the pyridine and dichloromethane were removed a white solid was collected, which was crushed then dried overnight under high vacuum. **10a'** was obtained as a white solid (2.2800 g, 83% yield). The NMR values were consistent with previously reported values.

**Data for tetrabutylammonium (2-chlorophenyl)methane sulfamate (11a')**

$^1\text{H}$  NMR (500 MHz,  $\text{CDCl}_3$ )  $\delta$  7.63 (d,  $J=7.4$  Hz, 1H), 7.18 (d,  $J=7.5$  Hz, 1H), 7.10 (m, 2H), 5.02 (s, 2H), 3.10 (t,  $J=7.1$  Hz, 8H), 1.46 (p,  $J=7.3$  Hz, 8H), 1.25 (h,  $J=6.5$  Hz, 8H), 0.82 (t,  $J=6.7$  Hz, 12H).

$^{13}\text{C}$  NMR (126 MHz,  $\text{CDCl}_3$ )  $\delta$  135.5, 132.0, 129.1, 128.8, 128.6, 128.2, 126.4, 65.4, 58.1, 23.6, 19.4, 13.4.

HRMS (ESI)  $m/z$  calcd for  $\text{C}_7\text{H}_6\text{ClO}_4\text{S}$  [ $\text{M}-\text{Nn}-\text{Bu}_4$ ] $^-$  220.9675, found 220.9689.

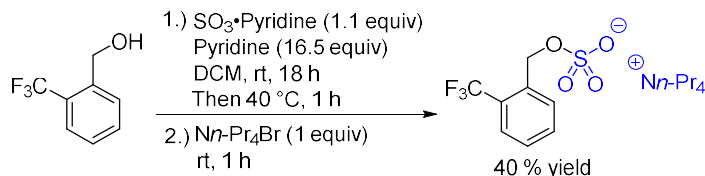
**Synthesis of tetrapropylammonium 2-(trifluoromethyl)benzyl sulfate (11c)**

Figure 3-21 Synthesis of tetrapropylammonium 2-(trichloromethyl)benzyl sulfate (11c)

(2-(trifluoromethyl)phenyl)methanol (0.8600 g, 6.00 mmol) and  $\text{SO}_3 \cdot \text{pyridine}$  complex (1.0500 g, 6.60 mmol) were placed in a 100 mL round bottom flask. Pyridine (8 mL) and dry dichloromethane (5 mL) were added, and the flask sealed with a glass stopper. The mixture was stirred at rt for 18 h. After this time, the reaction was heated to 40°C for 1h. Water (70 mL) was added, and the mixture was washed once with dichloromethane (70 mL) and the aqueous phase transferred to a 250 mL round bottom flask.  $\text{Nn-Pr}_4\text{Br}$  (1.6000 g, 6.00 mmol) was added to the aqueous phase and the flask sealed with a glass stopper. The mixture was stirred for 1h. The solution was extracted with dichloromethane (3x, 70 mL). The organic layer was dried over  $\text{MgSO}_4$ , filtered, and concentrated. Hexanes (7 mL) were added to the product and the suspension evaporated. This was repeated until no pyridine was seen via NMR. Diethyl ether (7 mL) was added to the product, and the suspension evaporated until no dichloromethane was seen via NMR. After the pyridine and dichloromethane were removed a white solid was collected, which was crushed then dried overnight under high vacuum. **11c** was obtained as a white solid (1.2000 g, 40% yield). The NMR values were consistent with previously reported values.

**Data for tetrapropylammonium 2-(trifluoromethyl)benzyl sulfate (11c)**

$^1\text{H}$  NMR (500 MHz,  $\text{CDCl}_3$ )  $\delta$  7.86 (d,  $J=7.7$ Hz, 1H), 7.55 (dd,  $J=7.7$ , 1.2 Hz, 1H), 7.47 (td,  $J=7.7$ , 1.2 Hz, 1H), 7.30 (t,  $J=7.7$  Hz, 1H), 5.22 (s, 2H), 3.36–3.09 (m, 8H), 1.61–1.50 (m, 8H), 1.39–1.29 (m, 8H), 0.91 (t,  $J=7.4$  Hz, 12H).

$^{13}\text{C}$  NMR (126 MHz,  $\text{CDCl}_3$ )  $\delta$  136.7 (q,  $J=1.9$ Hz), 131.7, 129.1, 126.9, 126.7 (q,  $J=30.6$ Hz), 125.1(q,  $J=5.8$  Hz), 124.3 (q,  $J=273.7$  Hz), 64.5 (q,  $J=3.1$  Hz), 58.5, 23.8, 19.6, 13.6.

$^{19}\text{F}$  NMR (470 MHz,  $\text{CDCl}_3$ )  $\delta$ -63.3.

HRMS (ESI)  $m/z$  calcd. for  $C_8H_6F_3O_4S$  [M– $Nn$ -Bu $_4$ ]– 254.9939, found 255.0028.

#### Synthesis of tetrapropylammonium *o*-tolymethane sulfonate (**11d**)

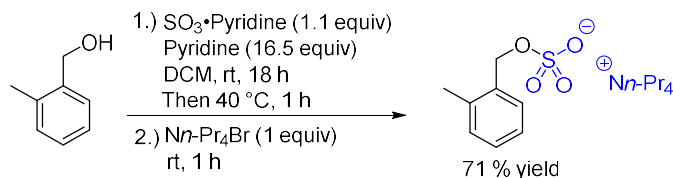


Figure 3-22 Synthesis of tetrabutylammonium *o*-tolymethane sulfonate (**11d**)

*o*-tolymethanol (0.7300 g, 6.00 mmol) and  $SO_3 \cdot \text{pyridine}$  complex (1.0500 g, 6.60 mmol) were placed in a 100 mL round bottom flask. Pyridine (8 mL) and dry dichloromethane (5 mL) were added, and the flask sealed with a glass stopper. The mixture was stirred at rt for 18 h. After this time, the reaction was heated to 40°C for 1h. Water (70 mL) was added, and the mixture was washed once with dichloromethane (70 mL) and the aqueous phase transferred to a 250 mL round bottom flask.  $Nn\text{-}Pr_4Br$  (1.6000 g, 6.00 mmol) was added to the aqueous phase and the flask sealed with a glass stopper. The mixture was stirred for 1h. The solution was extracted with dichloromethane (3x, 70 mL). The organic layer was dried over  $MgSO_4$ , filtered, and concentrated. Hexanes (7 mL) were added to the product and the suspension evaporated. This was repeated until no pyridine was seen via NMR. Diethyl ether (7 mL) was added to the product, and the suspension evaporated until no dichloromethane was seen via NMR. After the pyridine and dichloromethane were removed a white solid was collected, which was crushed then dried overnight under high vacuum. **11d** was obtained as a white solid (1.4100 g, 71% yield). The NMR values were consistent with previously reported values.

#### Data for tetrapropylammonium *o*-tolymethane sulfonate (**11d**)

$^1H$  NMR (500 MHz,  $CDCl_3$ )  $\delta$  7.33–7.28 (m, 1H), 7.13–7.01 (m, 3H), 4.96 (s, 2H), 3.06 (p,  $J=3.6$  Hz, 8H), 2.29 (s, 3H), 1.53 (hept,  $J=7.3$  Hz, 8H), 0.88 (t,  $J=7.3$  Hz, 12H).

$^{13}C$  NMR (126 MHz,  $CDCl_3$ )  $\delta$  136.9, 135.5, 129.9, 128.8, 127.7, 125.5, 67.0, 60.1, 18.8, 15.4, 10.7.

HRMS (ESI)  $m/z$  calcd for  $C_8H_9O_4S$  [M– $Nn$ -Pr $_4$ ]– 201.0222, found 201.0271.

#### Synthesis of tetrapropylammonium (2-fluorophenyl)methane sulfonate (**11g**)

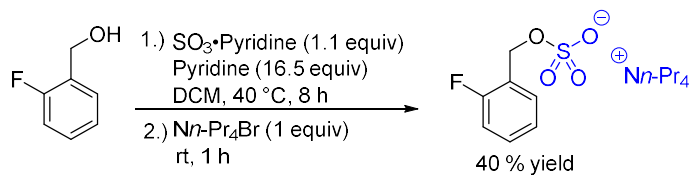


Figure 3-23 Synthesis of tetrabutylammonium (2-fluorophenyl)methane sulfonate (**11g**)

(2-fluorophenyl)methanol (0.7600 g, 6.00 mmol) and  $\text{SO}_3 \cdot \text{pyridine}$  complex (1.0500 g, 6.60 mmol) were placed in a 100 mL round bottom flask. Pyridine (8 mL) and dry dichloromethane (5 mL) were added, and the flask sealed with a glass stopper. The mixture was stirred at 40 °C for 8 h. After this time, the reaction was heated to 40°C for 1 hour. Water (70 mL) was added, and the mixture was washed once with dichloromethane (70 mL) and the aqueous phase transferred to a 250 mL round bottom flask.  $\text{Nn-Pr}_4\text{Br}$  (1.6000 g, 6.00 mmol) was added to the aqueous phase and the flask sealed with a glass stopper. The mixture was stirred for 1 hour. The solution was extracted with dichloromethane (3 x 70 mL). The organic layer was dried over  $\text{MgSO}_4$ , filtered, and concentrated. Hexanes (7 mL) were added to the product and the suspension evaporated. This was repeated until no pyridine was seen via NMR. Diethyl ether (7 mL) was added to the product, and the suspension evaporated until no dichloromethane was seen via NMR. After the pyridine and dichloromethane were removed a white solid was collected, which was crushed then dried overnight under high vacuum. **11g** was obtained as a white solid (0.9400 g, 40% yield). The NMR values were consistent with previously reported values.

#### Data for tetrapropylammonium (2-fluorophenyl)methane sulfonate (**11g**)

$^1\text{H}$  NMR (500 MHz,  $\text{CDCl}_3$ )  $\delta$  7.48 (td,  $J=7.5, 1.7$  Hz, 1H), 7.18 (dtd,  $J=7.6, 5.2, 1.8$  Hz, 1H), 7.03 (td,  $J=7.5, 1.1$  Hz, 1H), 6.92 (ddd,  $J=9.5, 8.3, 1.0$  Hz, 1H), 5.03 (s, 1H), 3.11 (p,  $J=4.82$  Hz, 8H), 1.58 (hept,  $J=7.36$  Hz, 8H), 0.89 (t,  $J=7.3$  Hz, 8H).

$^{13}\text{C}$  NMR (126 MHz,  $\text{CDCl}_3$ )  $\delta$  160.4 (d,  $J=246.9$  Hz), 130.5 (d,  $J=4.1$  Hz), 129.2 (d,  $J=8.0$  Hz), 124.8 (d,  $J=14.4$  Hz), 123.9 (d,  $J=3.6$  Hz), 114.8 (d,  $J=21.3$  Hz), 62.3 (d,  $J=4.5$  Hz), 60.2, 15.4, 10.7.

$^{19}\text{F}$  NMR (470 MHz,  $\text{CDCl}_3$ )  $\delta$  -118.9-12.96 (m).

HRMS (ESI)  $m/z$  calcd for  $\text{C}_7\text{H}_6\text{FO}_4\text{S} [\text{M}-\text{Nn-Pr}_4]^+$  204.9971, found 205.0033.

#### Synthesis of tetrapropylammonium (3-fluorophenyl)methane sulfonate (**11h**)

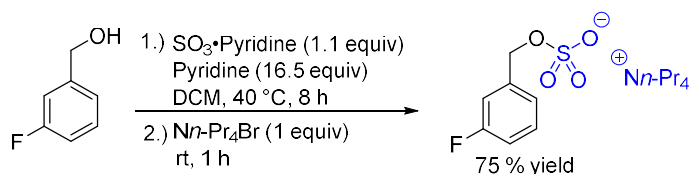


Figure 3-24 Synthesis of tetrapropylammonium (3-fluorophenyl)methane sulfonate (**11h**)

(2-fluorophenyl)methanol (0.7600 g, 6.00 mmol) and  $\text{SO}_3 \cdot \text{pyridine}$  complex (1.0500 g, 6.60 mmol) were placed in a 100 mL round bottom flask. Pyridine (8 mL) and dry dichloromethane (5 mL) were added, and the flask sealed with a glass stopper. The mixture was stirred at 40 °C for 8 h. After this time, the reaction was heated to 40°C for 1h. Water (70 mL) was added, and the mixture was washed once with



dichloromethane (70 mL) and the aqueous phase transferred to a 250 mL round bottom flask. *Nn*-Pr<sub>4</sub>Br (1.6000 g, 6.00 mmol) was added to the aqueous phase and the flask sealed with a glass stopper. The mixture was stirred for 1 hour. The solution was extracted with dichloromethane (3 x 70 mL). The organic layer was dried over MgSO<sub>4</sub>, filtered, and concentrated. Hexanes (7 mL) were added to the product and the suspension evaporated. This was repeated until no pyridine was seen via NMR. Diethyl ether (7 mL) was added to the product, and the suspension evaporated until no dichloromethane was seen via NMR. After the pyridine and dichloromethane were removed a white solid was collected, which was crushed then dried overnight under high vacuum. **11h** was obtained as a white solid (1.7500 g, 75% yield). The NMR values were consistent with previously reported values.

#### Data for tetrapropylammonium (3-fluorophenyl)methane sulfonate (**11h**)

<sup>1</sup>H NMR (500 MHz, CDCl<sub>3</sub>) δ 7.2–7.13 (m, 1H), 7.09–7.00 (m, 2H), 6.83 (td, J=8.4, 1.9 Hz, 1H), 4.92 (s, 2H), 3.08 (p, J=4.3 Hz, 8H), 1.56 (hept, J=4.6 Hz, 8H), 0.87 (t, J=7.3 Hz, 12H).

<sup>13</sup>C NMR (126 MHz, CDCl<sub>3</sub>) δ 162.6 (d, J=245.0 Hz), 140.4 (d, J=7.5 Hz), 129.6 (d, J=8.2 Hz), 123.1 (d, J=2.8 Hz), 114.4 (d, J=19.5 Hz), 114.1 (d, J=21.1 Hz), 67.8, 60.1, 15.4, 10.6.

<sup>19</sup>F NMR (470 MHz, CDCl<sub>3</sub>) δ –117.07 (dt, J=9.16, 6.4 Hz).

HRMS (ESI) m/z calcd for C<sub>7</sub>H<sub>6</sub>FO<sub>4</sub>S [M–*Nn*-Pr<sub>4</sub>]<sup>–</sup> 204.9971, found 205.0026.

#### Para borylation of tetrapropyl ammonium 2-fluorophenyl sulfate (**6e**)

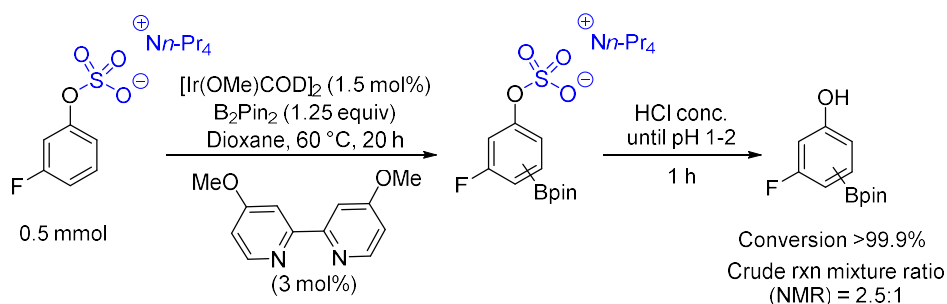


Figure 3-25 Para borylation of tetrapropyl ammonium 2-fluorophenyl sulfate (**6e**)

In a glovebox, a 5.0 mL Wheaton micro reactor was charged with tetrapropylammonium 3-fluorophenyl sulfate (189.0 mg, 0.50 mmol), [Ir(OMe)COD]<sub>2</sub> (5.0 mg, 1.5 mol%), B<sub>2</sub>pin<sub>2</sub> (159.0 mg, 0.63 mmol), and dioxane (1 mL) and stirred at rt. for 5 minutes. Then 4,4'-dimethoxy-2,2'-bipyridine (3.3 mg, 3.0 mol%) and dioxane (0.5 mL) were added. The micro reactor was capped with a Teflon pressure cap and placed into an aluminum block pre-heated to 40 °C. After 20 h, an aliquot of the reaction mixture was taken and analyzed directly by <sup>1</sup>H NMR to find the conversion and *para:meta* ratio which was determined to be 2.45:1 *para:meta*. HCl (12M) was added drop wise until pH=1–2 and the resultant mixture was stirred for

1 h. Copious bubbling was observed with the addition of HCl. The solution was concentrated and washed with hexanes (0.5 mL). The remaining solution subjected to chromatographic separation with silica gel (12% EtOAc in CHCl<sub>3</sub> as eluent) to give 87.0 mg of a mixture para borylated 3-fluorophenol (**7e**) with the *meta* isomer (**7e'**) (para:*meta*=3:1) as a white solid (73% yield, mp 89.4-91.2 °C). The NMR values were consistent with previously reported values.

**Data for 3-fluoro-4-(4,4,5,5-tetramethyl-1,3,2-dioxaborolan-2-yl)phenol (**7e**)**

**Para:**

<sup>1</sup>H NMR (500 MHz, CDCl<sub>3</sub>) δ 7.58 (t, J=7.7 Hz, 1H), 6.76 (bs, 1H), 6.61 (dd, J=8.2, 2.2 Hz, 1H), 6.50 (dd, J=10.9, 2.1Hz, 1H), 1.34 (s, 12H).

<sup>13</sup>C NMR (126 MHz, CDCl<sub>3</sub>) δ 168.6 (d, J=250.4 Hz), 160.8 (d, J=12.4 Hz), 138.0 (d, J=10.3 Hz), 111.6 (d, J=2.6 Hz), 103.1 (d, J=27.2 Hz), 84.2, 24.8.

<sup>11</sup>B NMR (160 MHz, CDCl<sub>3</sub>) δ 31.4.

<sup>19</sup>F NMR (470 MHz, CDCl<sub>3</sub>) δ -104.14 – -104.26 (m).

HRMS (ESI) m/z calcd. for C<sub>12</sub>H<sub>15</sub>BFO<sub>3</sub> [M-H]–237.1098, found 237.1320.

**Data for 3-fluoro-5-(4,4,5,5-tetramethyl-1,3,2-dioxaborolan-2-yl)phenol (**7e'**)**

**Meta:**

<sup>1</sup>H NMR (500 MHz, CDCl<sub>3</sub>) δ 7.04 (s, 1H), 7.03 (d, J=2.0 Hz, 1H), 6.67 (dt, J=10.2, 2.3 Hz, 1H), 1.33 (s, 12H).

<sup>13</sup>C NMR (126 MHz, CDCl<sub>3</sub>) δ 163.4 (d, J=246.6Hz), 156.8 (d, J=10.6 Hz), 117.2 (d, J=2.5 Hz), 113.1 (d, J=19.8 Hz), 106.3 (d, J=24.4 Hz), 84.5, 24.9.

<sup>11</sup>B NMR (160 MHz, CDCl<sub>3</sub>) δ 31.4.

<sup>19</sup>F NMR (470MHz, CDCl<sub>3</sub>) δ -116.3 – -116.4 (m).

HRMS (ESI) m/z calcd. for C<sub>12</sub>H<sub>15</sub>BFO<sub>3</sub> [M-H]– 237.1098, found 237.1320.

**Para borylation of tetrapropyl ammonium 2-methylphenyl sulfate (**6g**)**

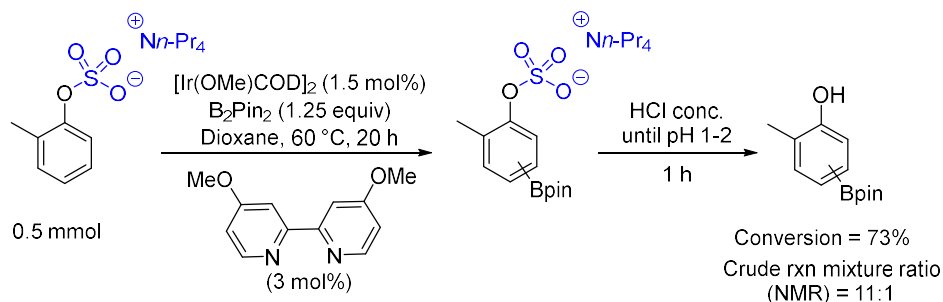


Figure 3-26 Para borylation of tetrapropyl ammonium 2-methylphenyl sulfate (**6g**)

In a glovebox, a 5.0 mL Wheaton micro reactor was charged with 2-Methylphenylsulfate (187.0 mg, 0.50 mmol),  $[\text{Ir}(\text{OMe})\text{COD}]_2$  (5.0 mg, 1.5 mol%),  $\text{B}_2\text{pin}_2$  (159.0 mg, 0.63 mmol), and dioxane (1 mL) and stirred at rt. for 5 minutes. Then 4,4'-dimethoxy-2,2'-bipyridine (3.3 mg, 3.0 mol%) and dioxane (0.5 mL) were added. The micro reactor was capped with a Teflon pressure cap and placed into an aluminum block pre-heated to 40°C. After 20 h, an aliquot of the reaction mixture was taken and analyzed directly by  $^1\text{H}$  NMR to find the conversion and *para:meta* ratio which was determined to be 10:1 *para:meta*. HCl (12M) was added drop wise until pH=1–2 and the resultant mixture was stirred for 1 h. Copious bubbling was observed with the addition of HCl. The solution was concentrated and washed with hexanes (0.5 mL). The remaining solution subjected to chromatographic separation with silica gel ( $\text{CHCl}_3$  as eluent) to give 67.0 mg of a mixture *para* borylated 2-methylphenol (**7g**) with the *meta* isomer (**7g'**) (*para:meta*=39:1) as a white solid (57% yield, mp 100.0–102.4 °C). NMR values were consistent with previously reported NMR values.

**Data for 2-methyl-4-(4,4,5,5-tetramethyl-1,3,2-dioxaborolan-2-yl)phenol (**7g**)**

**Para:**

$^1\text{H}$  NMR (500 MHz,  $\text{CDCl}_3$ )  $\delta$  7.61 (s, 1H), 7.54 (dd,  $J=8.0, 1.2$  Hz, 1H), 6.76 (d,  $J=8.0$  Hz, 1H), 5.81 (bs, 1H), 2.24 (s, 3H), 1.35 (s, 12H).

$^{13}\text{C}$  NMR (126 MHz,  $\text{CDCl}_3$ )  $\delta$  157.0, 138.0, 134.4, 123.5, 114.6, 83.8, 24.9, 15.6.

$^{11}\text{B}$  NMR (160 MHz,  $\text{CDCl}_3$ )  $\delta$  31.4.

HRMS(ESI)  $m/z$  calcd. for  $\text{C}_{13}\text{H}_{18}\text{BO}_3$   $[\text{M}-\text{H}]^-$  233.1349, found 233.1367.

**Data for 2-methyl-5-(4,4,5,5-tetramethyl-1,3,2-dioxaborolan-2-yl)phenol (**7g'**)**

**Meta:**

$^1\text{H}$  NMR (500 MHz,  $\text{CDCl}_3$ )  $\delta$  7.30 (d,  $J=7.3$  Hz, 1H), 7.20 (s, 1H), 7.14 (d,  $J=7.3$  Hz, 1H), 5.31 (bs, 1H), 2.08 (s, 3H), 1.34 (s, 12H).

**Para borylation of tetrapropyl ammonium 2-isopropylphenyl sulfate (**6h**)**

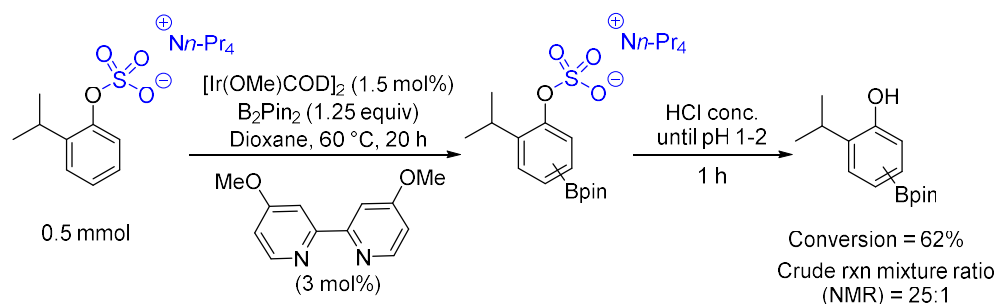


Figure 3-27 Para borylation of tetrapropyl ammonium 2-isopropylphenyl sulfate (**6h**)

In a glovebox, a 5.0 mL Wheaton micro reactor was charged with 2-isopropylphenylsulfate (201.0 mg, 0.50 mmol),  $[\text{Ir}(\text{OMe})\text{COD}]_2$  (5.0 mg, 1.5 mol%),  $\text{B}_2\text{pin}_2$  (159.0 mg, 0.63 mmol), and dioxane (1 mL) and stirred at rt. for 5 minutes. Then 4,4'-dimethoxy-2,2'-bipyridine (3.3 mg, 3.0 mol%) and dioxane (0.5 mL) were added. The micro reactor was capped with a teflon pressure cap and placed into an aluminum block pre-heated to 40°C. After 20h, an aliquot of the reaction mixture was taken and analyzed directly by  $^1\text{H}$  NMR to find the conversion and *para:meta* ratio which was determined to be 25:1 *para:meta*. HCl (12M) was added drop wise until pH=1–2 and the resultant mixture was stirred for 1 h. Copious bubbling was observed with the addition of HCl. The solution was concentrated and washed with hexanes (0.5 mL). The remaining solution subjected to chromatographic separation with silica gel (2 % EtOAc in  $\text{CHCl}_3$  as eluent) to give 81.0 mg of a mixture *para* borylated 2-methylphenol (**7h**) with the meta isomer (**7h'**) (*para:meta*=23:1) as a white solid (62 % yield, mp 138.3–145.9 °C). NMR values were consistent with previously reported NMR values.

#### Data for 2-isopropyl-4-(4,4,5,5-tetramethyl-1,3,2-dioxaborolan-2-yl)phenol (**7h**)

##### Para:

$^1\text{H}$  NMR (500 MHz,  $\text{CDCl}_3$ )  $\delta$  7.68 (s, 1H), 7.54 (d,  $J=7.9$  Hz, 1H), 6.74 (d,  $J=7.9$  Hz, 1H), 5.82 (s, 1H), 3.23 (hept,  $J=6.8$  Hz, 1H), 1.36 (s, 12H), 1.26 (d,  $J=6.9$  Hz, 6H).

$^{13}\text{C}$  NMR (126 MHz,  $\text{CDCl}_3$ )  $\delta$  156.2, 134.1, 134.1, 133.5, 115.0, 83.8, 27.2, 24.9, 22.6.

$^{11}\text{B}$  NMR (160 MHz,  $\text{CDCl}_3$ )  $\delta$  31.48.

HRMS (ESI)  $m/z$  calcd. for  $\text{C}_{15}\text{H}_{22}\text{BO}_3$   $[\text{M}-\text{H}]^-$  261.1662, found 261.1696.

#### Para borylation of tetrapropyl ammonium 2-trifluoromethylphenyl sulfate (**6k**)

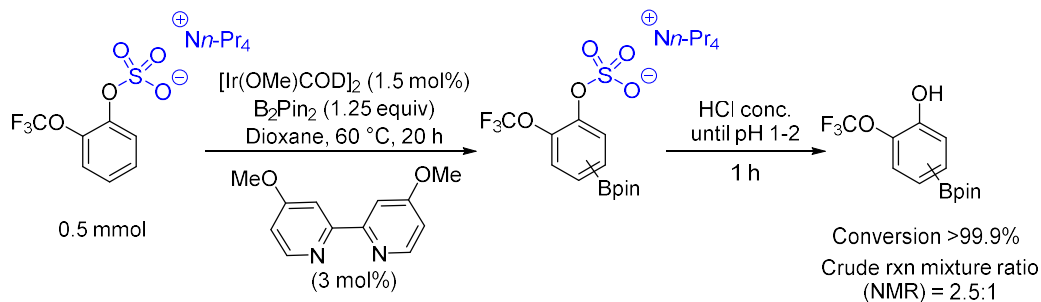


Figure 3-28 Para borylation of tetrapropyl ammonium 2-trifluoromethylphenyl sulfate (**6k**)

In a glovebox, a 5.0 mL Wheaton micro reactor was charged with tetrapropylammonium 2-trifluoromethylsulfate (189mg, 0.50 mmol),  $[\text{Ir}(\text{OMe})\text{COD}]_2$  (5.0 mg, 1.5 mol%),  $\text{B}_2\text{pin}_2$  (159.0 mg, 0.63 mmol), and dioxane (1 mL) and stirred at rt. for 5 minutes. Then 4,4'-dimethoxy-2,2'-bipyridine (3.3 mg, 3.0 mol%) and dioxane (0.5 mL) were added. The micro reactor was capped with a Teflon pressure cap

and placed into an aluminum block pre-heated to 40°C. After 20 h, an aliquot of the reaction mixture was taken and analyzed directly by  $^1\text{H}$  NMR to find the conversion and *para:meta* ratio which was determined to be 2.45:1 *para:meta*. HCl (12M) was added drop wise until pH=1–2 and the resultant mixture was stirred for 1 h. Copious bubbling was observed with the addition of HCl. The solution was concentrated and washed with hexanes (0.5 mL). The remaining solution subjected to chromatographic separation with silica gel (4% EtOAc in  $\text{CHCl}_3$  as eluent) to give 117.0 mg of a mixture *para* borylated 3-fluorophenol (**7k**) with the *meta* isomer (**7k'**) (>2%) as a white solid (77% yield, mp 129.6–131.9 °C). The NMR values were consistent with previously reported values.

**Data for 4-(4,4,5,5-tetramethyl-1,3,2-dioxaborolan-2-yl)-2-(trifluoromethoxy)phenol (**7k**)**

$^1\text{H}$  NMR (500 MHz,  $\text{CDCl}_3$ )  $\delta$  7.65 (s, 1H), 7.63 (d,  $J=8.2$  Hz, 1H), 7.01 (d,  $J=8.1$  Hz, 1H), 5.97 (bs, 1H), 1.33 (s, 12H).

$^{13}\text{C}$  NMR (126 MHz,  $\text{CDCl}_3$ )  $\delta$  150.6, 136.4, 135.1, 127.8, 120.9 (q,  $J=259.0$  Hz), 117., 84.2, 24.9.

$^{19}\text{F}$  NMR (470 MHz,  $\text{CDCl}_3$ )  $\delta$  -60.98 (s, 3F).

$^{11}\text{B}$  NMR (160 MHz,  $\text{CDCl}_3$ )  $\delta$  30.5.

HRMS (ESI)  $m/z$  calcd. for  $\text{C}_{13}\text{H}_{15}\text{BF}_3\text{O}_4$  [ $\text{M}-\text{H}$ ]-303.1015, found 303.1244.

**Para borylation of tetrapropyl ammonium 2-bromobenzyl sulfate (**10b**)**

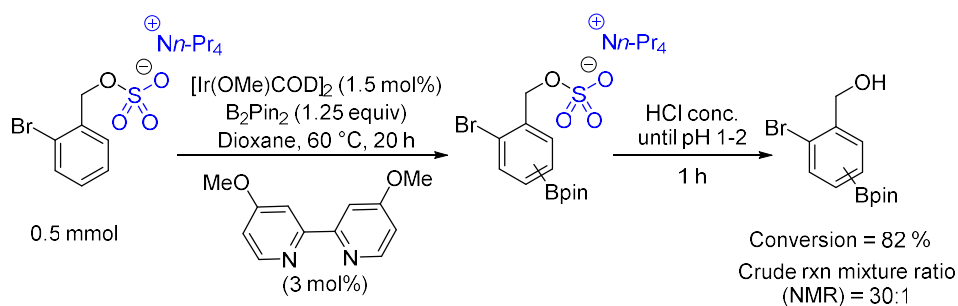


*Figure 3-29 Para borylation of tetrapropyl ammonium 2-bromobenzyl sulfate (**10b**)*

In a glovebox, a 5.0 mL Wheaton micro reactor was charged with tetrapropylammonium 2-bromobenzyl sulfate (226.0 mg, 0.50 mmol),  $[\text{Ir}(\text{OMe})\text{COD}]_2$  (5.0 mg, 1.5 mol %),  $\text{B}_2\text{pin}_2$  (159.0 mg, 0.63 mmol), and dioxane (1 mL) and stirred at rt. for 5 minutes. Then 4,4'-dimethoxy-2,2'-bipyridine (3.3 mg, 3.0 mol%) and dioxane (0.5 mL) were added. The micro reactor was capped with a Teflon pressure cap and placed into an aluminum block pre-heated to 40°C. After 20 h, an aliquot of the reaction mixture was taken and analyzed directly by  $^1\text{H}$  NMR to find the conversion and *para:meta* ratio which was determined to be 30:1 *para:meta*. HCl (12M) was added drop wise until pH=1–2 and the resultant mixture was stirred for 1 h. Copious bubbling was observed with the addition of HCl. The solution was concentrated and washed

with hexanes (0.5 mL). The remaining solution subjected to chromatographic separation with silica gel (10 % EtOAc in CHCl<sub>3</sub> as eluent) to give 64.0 mg of a mixture *para* borylated 3-fluorophenol (**10b**) with the *meta* isomer (**10b**) (*para:meta*=35:1) as a white solid (82 % yield, mp 89.4-91.2 °C). The NMR values were consistent with previously reported values.

**Data for (2-bromo-4-(4,4,5,5-tetramethyl-1,3,2-dioxaborolan-2-yl)phenyl)methanol (**11b**)**

***Para*:**

<sup>1</sup>H NMR (500 MHz, CDCl<sub>3</sub>) δ 7.95 (s, 1H), 7.73 (d, J=7.5 Hz, 1H), 7.48 (s, 1H), 4.74 (s, 2H), 2.31 (bs, 1H) 1.34 (s, 12H).

<sup>13</sup>C NMR (126 MHz, CDCl<sub>3</sub>) δ 142.8, 138.7, 134.0, 128.1, 122.3, 84.3, 65.1, 25.0.

<sup>11</sup>B NMR (160 MHz, CDCl<sub>3</sub>) 30.6.

HRMS (APCI+) m/z calcd. for C<sub>13</sub>H<sub>17</sub>BBro<sub>2</sub> [M–OH–] 295.0505, found 295.0595.

**Para borylation of tetrapropyl ammonium 2-fluorobenzyl sulfate (**10g**)**

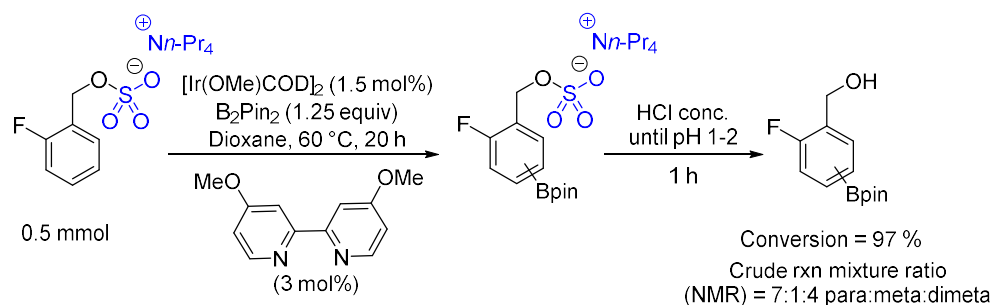


*Figure 3-30 Para borylation of tetrapropyl ammonium 2-fluorobenzyl sulfate (**10g**)*

In a glovebox, a 5.0 mL Wheaton micro reactor was charged with tetrapropylammonium 2-fluorobenzyl sulfate (196.0 mg, 0.50 mmol), [Ir(OMe)COD]<sub>2</sub> (5.0 mg, 1.5 mol %), B<sub>2</sub>pin<sub>2</sub> (159.0 mg, 0.63 mmol), and dioxane (1 mL) and stirred at rt. for 5 minutes. Then 4,4'-dimethoxy-2,2'-bipyridine (3.3 mg, 3.0 mol%) and dioxane (0.5 mL) were added. The micro reactor was capped with a teflon pressure cap and placed into an aluminum block pre-heated to 40°C. After 36 h, an aliquot of the reaction mixture was taken and analyzed directly by <sup>1</sup>H NMR to find the conversion and *para:meta* ratio which was determined to be 7:1:4 *para:meta:dimeta*. HCl (12M) was added drop wise until pH=1–2 and the resultant mixture was stirred for 1 h. Copious bubbling was observed with the addition of HCl. The solution was concentrated and washed with hexanes (0.5 mL). The remaining solution subjected to chromatographic separation with silica gel (5 % EtOAc in CHCl<sub>3</sub> as eluent) to give 91.0 mg of a mixture *para* borylated (2-fluorophenyl)methanol (**11g**) with the *meta* isomer (**11g**) and *dimeta* isomer (**11g**)

(*para:meta:dimeta*=10.6:1:1.2) as an oil (69 % yield). NMR values were consistent with previously reported values.

**Data for (2-fluoro-4-(4,4,5,5-tetramethyl-1,3,2-dioxaborolan-2-yl)phenyl)methanol (11g)**

<sup>1</sup>H NMR (500 MHz, CDCl<sub>3</sub>) δ 7.61–7.52 (m, 1H), 7.48–7.37 (m, 2H), 4.75 (d, J=12.7 Hz, 3H), 2.17 (bs, 1H), 1.34 (s, 12H).

<sup>13</sup>C NMR (126 MHz, CDCl<sub>3</sub>) δ 160.1 (d, J=246.6 Hz), 130.9 (d, J=14.7 Hz), 130.6 (d, J=3.4 Hz), 128.5 (d, J=3.9 Hz), 120.8 (d, J=19.5 Hz), 84.1, 59.2 (d, J=4.6 Hz), 24.8.

<sup>11</sup>B NMR (160 MHz, CDCl<sub>3</sub>) δ 30.47.

<sup>19</sup>F NMR (470 MHz, CDCl<sub>3</sub>) δ –108.48, –112.94 (d, J=6.6 Hz), –124.36, –164.90 (t, J=0.9 Hz).

HRMS (APCI+) m/z calcd. for C<sub>13</sub>H<sub>17</sub>BFO<sub>2</sub> [M–OH–] 235.1306, found 235.1337.

## REFERENCES

- (1) Anslyn, E. V.; Dougherty, D. A. *Modern Physical Organic Chemistry*; University Science Books: Sausalito, CA, 2005.
- (2) Engle, K. M.; Mei, T.-S.; Wasa, M.; Yu, J.-Q. Weak Coordination as a Powerful Means for Developing Broadly Useful C-H Functionalization Reactions. *Acc. Chem. Res.* **2012**, *45*, 788–802
- (3) Raynal, M.; Ballester, P.; Ferran, A. V.; van Leeuwen, P. W. N. M. Supramolecular catalysis. Part 1: non-covalent interactions as a tool for building and modifying homogeneous catalysts *Chem. Soc. Rev.* **2014**, *43*, 1660–1733
- (4) Davis, H. J.; Phipps, R. J. Harnessing non-covalent interactions to exert control over regioselectivity and site-selectivity in catalytic reactions *Chem. Sci.* **2017**, *8*, 864–877.
- (5) C-H Bond Activation and Catalytic Functionalization I; Dixneuf, P. H., Doucet, H., Eds.; Topics in Organometallic Chemistry; Springer International Publishing: Cham, Switzerland, 2018
- (6) C-H Bond Activation and Catalytic Functionalization II; Dixneuf, P. H., Doucet, H., Eds.; Topics in Organometallic Chemistry; Springer Nature: Cham, Switzerland, 2018
- (7) Mkhalid, I. A.; Barnard, J. H.; Marder, T. B.; Murphys, J. M.; Hartwig, J. F. C–H Activation for the Construction of C–B Bonds *Chem. Rev.* **2010**, *110*, 890–931
- (8) Xu, L.; Wang, G.; Zhang, S.; Wang, H.; Wang, L.; Lu, L.; Jiao, J.; Li, P. Recent advances in catalytic C–H borylation reactions *Tetrahedron* **2017**, *73*, 7123–7157.
- (9) Fontaine, F. G.; Rochette, E. Ambiphilic Molecules: From Organometallic Curiosity to Metal-Free Catalysts *Acc. Chem. Res.* **2018**, *51*, 454–464.
- (10) Cho, J. Y.; Iverson, C. N.; Smith, M. R. Steric and Chelate Directing Effects in Aromatic Borylation *J. Am. Chem. Soc.* **2000**, *122*, 12868–12869.
- (11) Cho, J. Y.; Tse, M. K.; Holmes, D.; Maleczka, R. E.; Smith, M. R. Remarkably selective iridium catalysts for the elaboration of aromatic C–H bonds *Science* **2002**, *295*, 305–308.
- (12) Ishiyama, T.; Takagi, J.; Ishida, K.; Miyaura, N.; Anastasi, N. R.; Hartwig, J. F. Mild Iridium-Catalyzed Borylation of Arenes. High Turnover Numbers, Room Temperature Reactions, and Isolation of a Potential Intermediate *J. Am. Chem. Soc.* **2002**, *124*, 390–391.
- (13) Ros, A.; Fernandes, R.; Lassaletta, J. M. Functional group directed C–H borylation *Chem. Soc. Rev.* **2014**, *43*, 3229–3243.
- (14) Kawamori, S.; Ohmiya, H.; Hara, K.; Fukuoka, A.; Sawamura, M. Directed Ortho Borylation of Functionalized Arenes Catalyzed by a Silica-Supported Compact Phosphine–Iridium System *J. Am. Chem. Soc.* **2009**, *131*, 5058–5059.
- (15) Ishiyama, T.; Isou, H.; Kikuchi, T.; Miyaura, N. Ortho-C–H Borylation of Benzoate Esters with Bis(Pinacolato)Diboron Catalyzed by Iridium–Phosphine Complexes. *Chem. Commun.* **2010**, *46*, 159–161.
- (16) Roosen, P. C.; Kallepalli, V. A.; Chattopadhyay, B.; Singleton, D. A.; Maleczka, R. E.; Smith, M. R. Outer-Sphere Direction in Iridium C–H Borylation *J. Am. Chem. Soc.* **2012**, *134*, 11350–11353.
- (17) Chattopadhyay, B.; Dannatt, J. E.; Sanctis, I. L. A.; Gore, K. A.; Maleczka, R. E.; Singleton, D. A.; Smith, M. R. Ir-Catalyzed ortho-Borylation of Phenols Directed by Substrate–Ligand



Electrostatic Interactions: A Combined Experimental/in Silico Strategy for Optimizing Weak Interactions *J. Am. Chem. Soc.* **2017**, *139*, 7864–7871.

- (18) Bisht, R.; Chattopadhyay, B. Formal Ir-Catalyzed Ligand-Enabled Ortho and *Meta* Borylation of Aromatic Aldehydes via in Situ-Generated Imines *J. Am. Chem. Soc.* **2016**, *138*, 84–87.
- (19) Kuninobu, Y.; Ida, H.; Mishi, M.; Kanai, M. A *meta*-selective C–H borylation directed by a secondary interaction between ligand and substrate *Nat. Chem.* **2015**, *7*, 712–717.
- (20) Davis, H. J.; Mihai, M. T.; Phipps, R. J. Ion Pair-Directed Regiocontrol in Transition-Metal Catalysis: A *Meta*-Selective C–H Borylation of Aromatic Quaternary Ammonium Salts *J. Am. Chem. Soc.* **2016**, *138*, 12759–12762.
- (21) Yang, L.; Uemura, N.; Nakao, Y. *meta*-Selective C–H Borylation of Benzamides and Pyridines by an Iridium–Lewis Acid Bifunctional Catalyst *J. Am. Chem. Soc.* **2019**, *141*, 7972–7979.
- (22) Mihai, M. T.; Davis, H. J.; Genov, G. R.; Phipps, R. Ion Pair-Directed C–H Activation on Flexible Ammonium Salts: *meta*-Selective Borylation of Quaternized Phenethylamines and Phenylpropylamines *J. ACS Catalysis*. **2018**, *8*, 3764–3769.
- (23) Davis, H. J.; Genov, G. R.; Phipps, R. *meta*-Selective C–H Borylation of Benzylamine-, Phenethylamine-, and Phenylpropylamine-Derived Amides Enabled by a Single Anionic Ligand *J. Angew. Chem. Int. Ed.* **2017**, *56*, 13351–13355.
- (24) Lee, B.; Mihai, T. M.; Stojalnikova, V.; Phipps, R. J. Ion-Pair-Directed Borylation of Aromatic Phosphonium Salts *J. Org. Chem.* **2019**, *84*, 13124–13134.
- (25) Grosso, R. D.; Singleton, P. J.; Muryn, C. A.; Ingleson, M. J. Pinacol Boronates by Direct Arene Borylation with Borenium Cations *Angew. Chem. Int. Ed.* **2011**, *50*, 2102–2106.
- (26) Saito, Y.; Segawa, Y.; Itami, K. *para*-C–H Borylation of Benzene Derivatives by a Bulky Iridium Catalyst *J. Am. Chem. Soc.* **2015**, *137*, 5193–5198.
- (27) Saito, Y.; Yamanoue, K.; Segawa, Y.; Itami, K. Selective Transformation of Strychnine and 1,2-Disubstituted Benzenes by C–H Borylation *Chem* **2020**, *6*, 985–993.
- (28) Hoque, D.; Bisht, R.; Haldar, C.; Chattopadhyay, B. Noncovalent Interactions in Ir-Catalyzed C–H Activation: L-Shaped Ligand for *Para*-Selective Borylation of Aromatic Esters *J. Am. Chem. Soc.* **2017**, *139*, 7745–7748.
- (29) Yang, L.; Semba, K.; Nakao, Y. *para*-Selective C–H Borylation of (Hetero)Arenes by Cooperative Iridium/Aluminum Catalysis *Angew. Chem. Int. Ed.* **2017**, *56*, 4853–4857.
- (30) Miller, S. L.; Chotana, G. A.; Ritz, J. A.; Chattopadhyay, B.; Maleczka, R. E.; Smith, M. R. C–H Borylation Catalysts that Distinguish Between Similarly Sized Substituents Like Fluorine and Hydrogen *Org. Lett.* **2019**, *21*, 6388–6392.
- (31) Ishiyama, T.; Takagi, J.; Hartwig, J. F.; Miyaura, N. A Stoichiometric Aromatic C–H Borylation Catalyzed by Iridium(I)/2,2'-Bipyridine Complexes at Room Temperature *Angew. Chem. Int. Ed.* **2002**, *41*, 3056–3058.
- (32) Shirakawa, S.; Liu, S.; Kaneko, S.; Kumatabara, Y.; Fukuda, A.; Omagari, R.; Maruoka, K. Tetraalkylammonium Salts as Hydrogen-Bonding Catalysts *Angew. Chem. Int. Ed.* **2015**, *54*, 15767–15770.
- (33) Tajuddin, H.; Harrisson, P.; Bitterlich, B.; Collings, J. C.; Sim, N.; Batsanov, A. S.; Cheung M. S.; Kawamorita, A.; Maxwell, A. C.; Shukla, L.; Morris, J.; Lin, Z.; Marder, T. B.; Steel, P. G. Iridium-

catalyzed C–H borylation of quinolines and unsymmetrical 1,2-disubstituted benzenes: insights into steric and electronic effects on selectivity *Chem. Sci.* **2012**, 3, 3505–3515.

- (34) Mihai, M. T.; Williams, b. D.; Phipps, R. J. Para-Selective C–H Borylation of Common Arene Building Blocks Enabled by Ion-Pairing with a Bulky Counteranion *J. Am. Chem. Soc.* **2019**, 141, 15477–15482.
- (35) <https://www.chemistryworld.com/news/steric-shield-leads-boron-to-aromatic-rings-most-remote-region/4010603.article> Accessed 12-5-2023.
- (36) Genov, G. R.; Douthwaite, J. L.; Lahdenpera, A. S. K.; Gibson, D. C.; Phipps, R. J. Enantioselective remote C–H activation directed by a chiral cation *Science*, **2020**, 367, 1246–1251.

## Chapter 4: Steric Shielding Effects induced by Intramolecular C–H...O Hydrogen Bonding: Remote Borylation Directed by Bpin Groups

Parts of this chapter were taken from “Steric Shielding Effects Induced by Intramolecular C–H...O Hydrogen Bonding: Remote Borylation Directed by Bpin Groups”

*ACS Catalysis*. **2022**, *12*, 2694–2705.

C–H bonds can be diversified via different C–H functionalization methods. Yet, targeting one C–H reactive site in the presence of similar C–H bonds remains challenging.<sup>1,2</sup> Although considered weak, noncovalent interactions can differentiate the energetics and therefore relative reactivity of otherwise similar reactive sites. For example, an interaction where  $\Delta G^0 \leq -3.5$  kcal/mol will be in force for  $\geq 99\%$  of the molecules at 100 °C. In the area of  $sp_2$  C–H activation, preinstalled directing groups can interact with the catalyst via hydrogen bonding, Lewis acid–base, or electrostatic interactions to selectively functionalize *ortho*, *meta*, or *para* positions of arenes.<sup>3–9</sup> However, selective reactions at distal C–H sites often require the construction of complex directing groups/ligands.<sup>7–11</sup> A different strategy uses steric shields to block nearby C–H bonds, thus leaving the distal position as the only accessible reactive site. For example, Nakao’s group used Lewis acidic additives that interact with aryl amides and shield the *meta* positions, enabling selective *para* functionalizations.<sup>12–15</sup> In contrast, a complementary approach where intramolecular noncovalent interactions create steric shields leading to remote functionalization is far less common.

Iridium catalyzed C–H borylation is currently a standard protocol to make aryl boronic esters.<sup>16–18</sup> In the last decade, *ortho* regioselective  $sp_2$  C–H borylation has been achieved by means of chelating and relay directing groups as well as outer-sphere interactions.<sup>4,7,19</sup> In 2013, our group reported that *meta* and *para*-substituted anilines yield the corresponding *ortho* borylated product courtesy of a N–H hydrogen bonding with the catalyst.<sup>20</sup> Unexpectedly, 2-methoxyaniline was selectively borylated *para* to nitrogen. A similar result was reported by the Phipps group during their C–H borylation of 2-chloroaniline (Figure 4-1).<sup>21</sup> It was proposed that electronic effects might play a role in the change of selectivity for 2-chloro and 2-methoxyaniline, but there was no experimental corroboration of this hypothesis. Based on some of our prior work, it seems likely that this could be due to a steric shielding effect of the N borylated aniline pushing borylation *para* to itself by blocking the *meta* position.

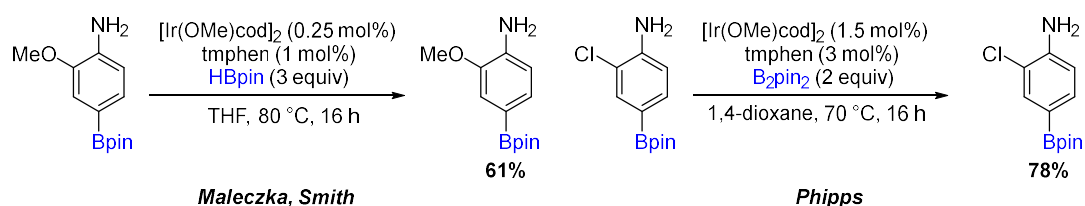


**Figure 4-1 Unexpected para Selectivity Seen in the C–H Borylation of 2-Methoxyaniline and 2-Chloroaniline**

Previously in conjunction with the Phipps group, we independently discovered a method for achieving para C–H borylation of phenols, anilines, and benzylic alcohols utilizing ion-pairing interactions of sulfates and sulfamates with alkylammonium cations. (Figure 4-2)<sup>21,22</sup>

By sterically shielding the C–H bonds *ortho* and *meta* to the sulfonated alcohol or aniline, we were able to use the alkyl chains of the tetraalkylammonium cation as a shield. Coupled with our previous reported borylations of anilines and amino pyridines<sup>20</sup>, we envisioned using in situ borylation of hetero atoms to act as a steric shield and thus allow us to access para selectivity.

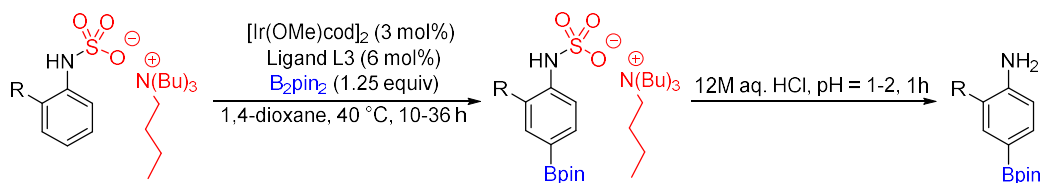


**Figure 4-2 Previous Ion-Pair Directed para Borylation of Tetrabutylammonium Sulfamates**

It is well documented that N–borylation of N–unsubstituted anilines occurs rapidly under C–H borylation conditions.<sup>20</sup> We expected that in the presence of an electron rich or bulky *ortho* substituent such as methoxy, chloro, or *tert*-butyl, the N–Bpin group could be forced in a conformation in which the Bpin is oriented toward the *meta* C–H where it would act as a steric shield, leading to para selective C–H borylation (Figure 4-2). Bpin would be an attractive steric shield for primary or secondary anilines since in situ N–borylation with B<sub>2</sub>pin<sub>2</sub> or HBpin is rapid, and the aniline N–H is easily restored during workup by exposing the reaction to water or adding methanol, which rapidly breaks the B–N bond. This contrasts with our previous approach to accessing para-borylated anilines, which required a step to install the sulfamate group and a step where highly acidic conditions were required to remove it from the product.

**Para C–H Borylation of Anilines, N-Alkylated Anilines, and Indoles.** We set out to examine whether para selectivity after N-borylation of anilines and allied substrates was a general phenomenon. To do so, we first looked to optimize the reaction on 2-chloroaniline. Starting with our previously reported conditions,

we compared the regioselectivity when B<sub>2</sub>pin<sub>2</sub> was used in place of HBpin and found that the former yielded an improved *para* to *meta* ratio: 5.6 to 1 vs 4.5 to 1. With B<sub>2</sub>pin<sub>2</sub> as the new boron partner, we then explored temperature and solvent effects on selectivity (Figure 4-3). Cyclohexane and THF gave higher *para* selectivity at lower temperatures, but conversion dropped especially with cyclohexane. The best balance between reactivity and selectivity was found with THF at 40 °C. After 4 h, the conversion was 61 and >90% after 24 h.

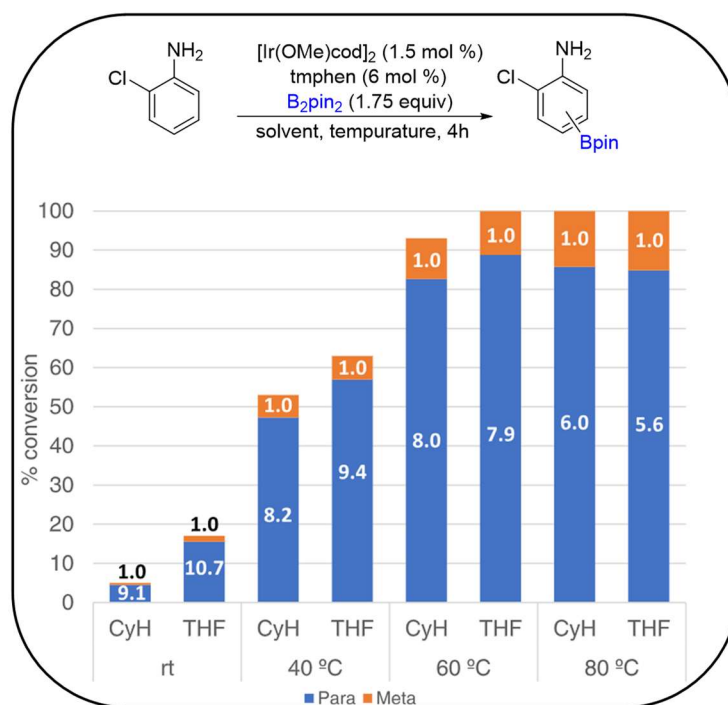


Figure 4-3 Solvent and Temperature Effects on *para* Selectivity of C–H Borylation of 2-Chloroaniline

With these conditions in hand, we evaluated the effect of the ligand (Figure 4-4). Bipyridine ligands (**L1–L3**) gave modest *para:meta* ratios (~5:1). Notably, 4,4'-dimethoxy-2,2'-bipyridine (**L3**), which was optimal in our previous *para*-directed C–H borylation of sulfamate salts,<sup>22</sup> did not prove superior in this scenario. Selectivity with ligand **L9** was similar but yield suffered. In contrast, the *para:meta* ratio doubled with phenanthrolines **L8** and **L7**, while yields remained high. We chose 3,4,7,8-tetramethyl-1,10-phenanthroline (tmphen) (**L7**) to continue our studies due to it being slightly better than **L8** in terms of regioselectivity and yield.

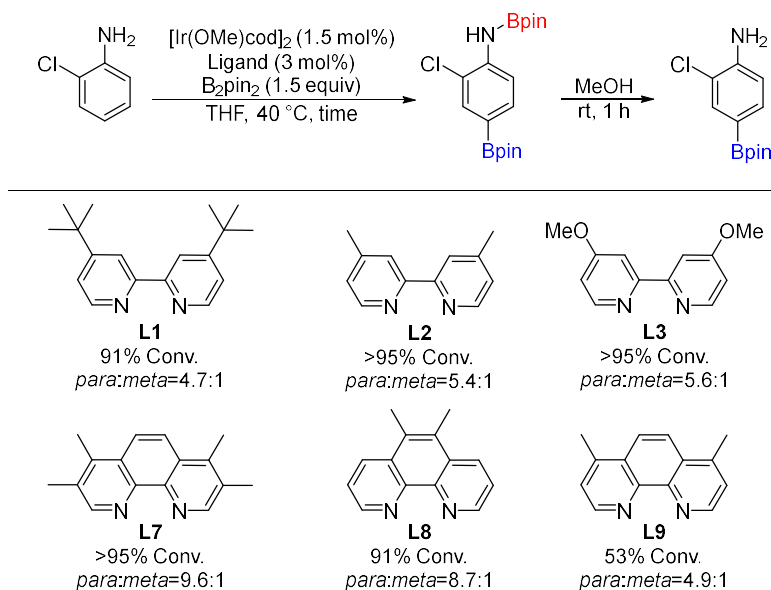
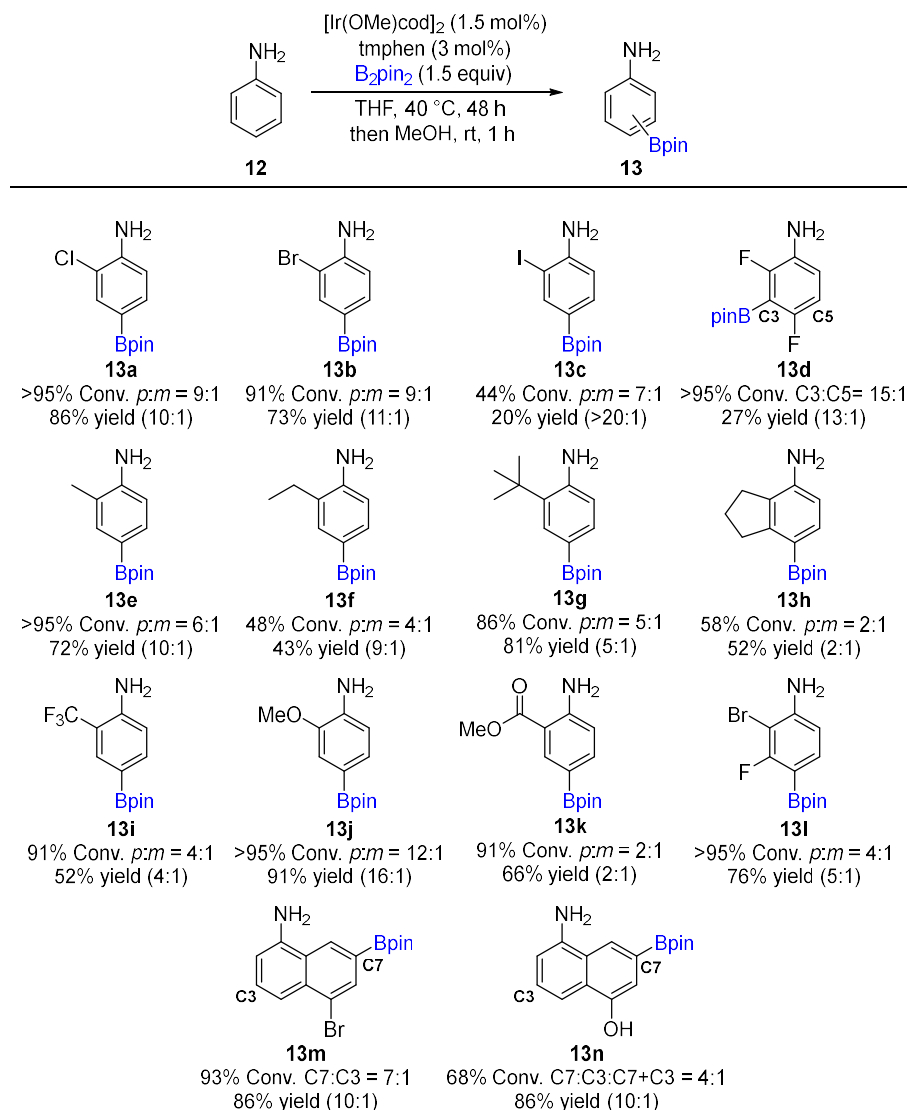


Figure 4-4 Ligand Effects on *para* Selectivity of C–H Borylation of 2-Chloroaniline

Next, we evaluated the *para* borylation of different anilines, all of which are substituted at the 2-position (Figure 4-5). The highest *para* selectivity ( $\text{C}_4:\text{C}_5 > 7:1$ ) was observed in C–H borylations for substrates, where *ortho* substituents have electron lone pairs (**13a**, **13b**, **13c**, **13j**). Given that C–H borylations are enhanced at the *meta* positions in monosubstituted benzenes  $\text{C}_6\text{H}_5\text{X}$  when  $\text{X} = \text{Br}$ ,<sup>23</sup>  $\text{I}$ ,<sup>17</sup> or  $\text{OMe}$ ,<sup>24</sup> the 2-substituents are enhancing selectivity *para* to N. In contrast, **13i** with a trifluoromethyl *ortho* substituent saw selectivity drop to 4:1. Benzoate **13k** with an electron- withdrawing group by resonance gave an even lower ratio of 2 to 1 *para* to *meta*. This result bears some relationship to previous reports of ester groups favoring *para* C–H borylation. In our case, that position is *meta* with respect to aniline nitrogen.<sup>25,26</sup>



*Figure 4-5 C–H Borylation Substrate Scope of Anilines*

The size of alkyl *ortho* substituents (**13e–13h**) showed little effect, as *para* to *meta* ratios only ranged from 4:1 to 6:1. It should be noted that the 6:1 observed for 2-methylaniline (**13e**) was achieved by forming the N–Bpin bond prior to the C–H borylation. In contrast, a selectivity of 4:1 is achieved with in situ N–Bpin bond formation of **13e**, which suggests a slow formation of the N-borylated intermediate in this case. C–H borylation at C4 was preferred for anilines when C3 was fluorine-substituted (substrate **13l**). This is consistent with an electronic preference for C–H borylation *ortho* to F and attenuated steric interference from F since H, and its isotopes are the only substituents that are less sterically demanding.<sup>27,28</sup> Para selectivity for substrate **13h**, albeit modest, is more significant since the only literature report where C–H

borylation at C4/C7 of an indane structure is preferred has a tert-butyl group at C5, obstructing C4/C6 positions.<sup>29</sup>

Our hypothesis implies that the Bpin steric shield can only block one *meta* position of arene. This can explain the necessity of an *ortho* substituent to block the other *meta* position. C–H borylation of unsubstituted aniline supports this statement as no para to *meta* selectivity was observed.<sup>30</sup>

This feature can allow a *meta* selective C–H borylation if the para position bears a small substituent. As stated above, fluorine atoms are relatively small and C–H borylation next to them is observed. C–H borylation of 2,4-difluoroaniline (**13d**) presented a more interesting scenario. In this case, where the N–Bpin orientated away from the *ortho* fluorine, the resultant steric shield would block C5 leaving 3-borylation as the only option. This was the result as C3 borylation occurred with a 15:1 preference over C5 borylation. It can be argued that **13d**'s is electronically biased to favor 3-selective C–H borylation. C–H borylation of 2,4-difluorotoluene shows a modest 3 to 1 preference for the 3-borylated product. The C3-selectivity of **13d**' is 5 times more than that of 2,4-difluorotoluene, which shows that both electronics and the Bpin steric shield play a role in the C3-selectivity of **13d**'. To probe other substrates with substituents at the *ortho* and *meta* C–H positions, we examined the C–H borylation of N-borylated 5- substituted 1-naphthylamines **13m** and **13n**. In these substrates, C2, C4, C6, and C8 would be blocked from C–H borylation by substituents, leaving only C3 and C7 sterically unencumbered. However, were our hypothesis correct, the N–Bpin would sterically shield C3, thus favoring C7 in a CHB. Indeed, borylation of **13m** and **13n** yield their 7-borylated product selectively (C7/C3 7:1 and 24:1, respectively). In the case of **13n**, a small amount of diborylation was observed.

We next turned our attention to other in situ borylated scaffolds, namely, N-alkylated anilines (Figure 4-6). Unfortunately, C–H borylation of 2-chloro-N-methylaniline **14a** was not para selective under the optimized conditions. A slow rate of N–Bpin formation could explain the lack of selectivity. However, even after formation of the N–Bpin bond, no selectivity was observed. Thus, we considered other explanations. This led us to propose that a reluctance of N-borylated **14a** to orientate in the same plane as the aromatic ring, which per our hypothesis creates the N–Bpin steric shield, is responsible for the observed regiochemical result. Such a hypothesized planar conformation is supported by modeling the lowest energy conformation of N-borylated intermediates of N-unsubstituted anilines. In contrast, N-borylated 2-chloro-N-methylaniline does not adopt a planar conformation owing to an A (1,3) interaction between the N-methyl with the *ortho* chlorine. As N-borylated N-alkyl-2-amino- pyridines should lack this steric clash, **14b** and **14c** should be para selective. This proved to be the case with **15b** and **15c** both being the major (4:1) C–H borylation products.



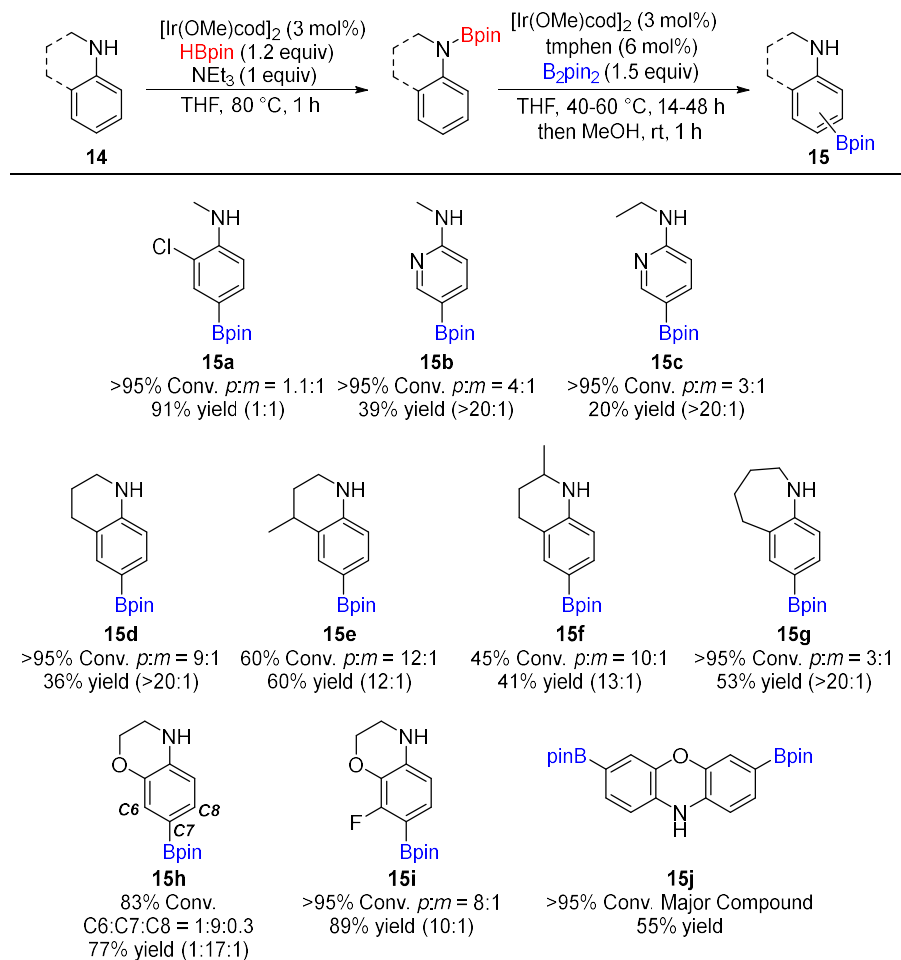


Figure 4-6 C–H Borylation Substrate Scope of N-Alkylated Anilines

1,2,3,4-Tetrahydroquinolines also drew our attention as in these N-alkylated anilines, the covalent chain that links the aromatic ring with nitrogen should allow the N-borylated intermediate to achieve a pseudo planar conformation. Para products **15d–15j** were obtained as the major regioisomer from their corresponding 1,2,3,4-tetrahydroquinolines. The size of the saturated ring does influence the level of selectivity, as illustrated in **15g** where the selectivity was only 3:1. Adding a methyl group about the saturated ring did not significantly change the selectivity, as shown by products **15d–15f**. With 3h, borylation next to oxygen was also observed, but the para product still predominated (para:others = 7:1). The fluorinated version of **14h**, namely, **14i**, was equally selective. Diborylation of phenoxazine **14j** mainly yielded the bis para compound along with multiple minor products.

N-Borylation of indoles is known to block C2 C–H borylation normally seen in the parent compounds, instead yielding the corresponding 3-borylated product.<sup>20</sup> We asked if in a N-borylated 3-substituted indole, the N–Bpin would shield the closer C6-position, leading to the corresponding 5-borylated indoles. C5 and

C6 indole functionalization remains rare. Baran's group reported that C–H borylation of 3-substituted N-TIPS-indoles yield the 6-borylated product using phenanthroline as ligand.<sup>31</sup> C5 borylation of indoles has been elusive besides some specific examples employing electrophilic borylation with borenium cations. The examples are limited to N-methyl carbazole or are triggered by the use of an amine pivaloate directing group at the 4 position.<sup>32,33</sup> A protocol to access 3,5-diborylated indoles has been reported, but suffers from low conversions (<30%).<sup>34</sup> Under our optimized conditions (Figure 4-7) and after the formation of the N–Bpin intermediate, 3-methyl-indole **16a** yielded the 5-borylated product with a modest 3:1 selectivity over the minor 6-borylated isomer. Replacement of the methyl group by a methyl ester as in **16c** resulted in the loss of selectivity. However, the presence of substituents at both C2 and C3 impacted selectivity little, as shown in **17b** and **17d**. It should be stated that for **16b** and **16d**, formation of the N–Bpin intermediate was slow and additional HBpin and triethylamine as well as a 3 h reaction time was needed to afford full N-borylation.

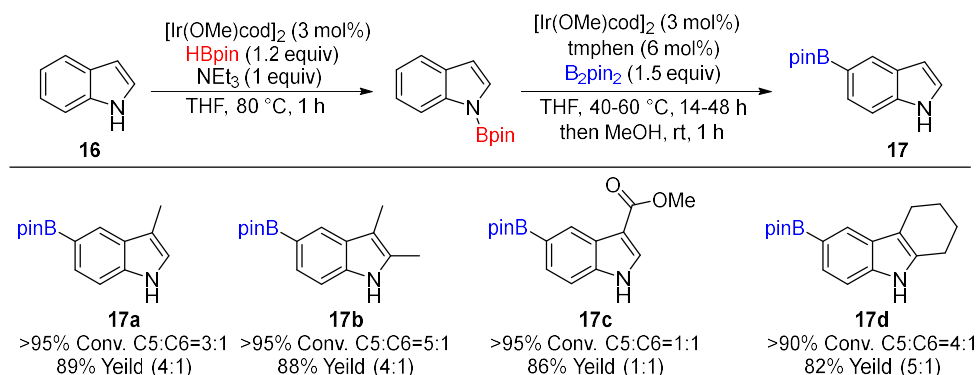


Figure 4-7 C–H Borylation Substrate Scope of Indoles

In our efforts to expand the Bpin steric effect to phenols, we found that the C–H borylation of 2-chlorophenol did not show selectivity. Neither QTAIM nor  $\Delta\delta$  data (vide infra) show any evidence of intra molecular hydrogen bonding, which explains this experimental result.

We speculated that Bpin groups could create a steric shield even when not part of a N–Bpin moiety. We thus focused on 1-borylated naphthalenes, which could bear geometries similar to those of N-borylated 2-substituted anilines and N-borylated tetrahydroquinolines (Figure 4-8). If so, the Bpin derived steric shield would block the C7-position leaving the C6-position available for C–H borylation. The borylation of 1-borylated naphthalene **7a** supported our proposition and yielded the 1,6-diborylated product selectively. A ligand screening showed that 4,4'-dimethoxy-2,2'-bipyridine (**L3**) was the best choice for the C6 borylation of 1-borylated naphthalenes. This result is potentially valuable as C6 functionalization

of naphthalenes remains rare.<sup>35</sup> A notable exception comes from Nakao's group where a 1-naphthyl amide was made to undergo C6-alkylation using an aluminum Lewis acid as a steric shield.<sup>13,14</sup>

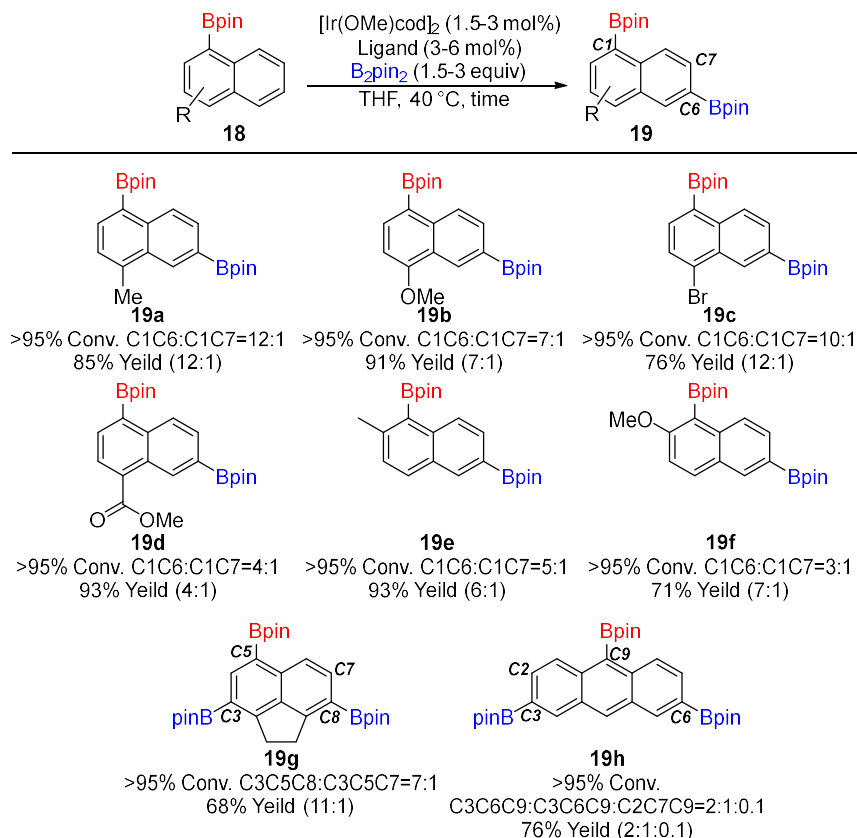


Figure 4-8 C–H Borylation Substrate Scope of Naphthalenes

As shown in Scheme 3, a substituent on the C2- or C4- position is needed to avoid borylation at C3 (**18a–18f**). 5-Bpin dihydroacenaphthene **18g** was borylated at both the expected C8 position and at C3. Under conditions that promote diborylation, 3,5,8-triborylated product **18g** was obtained as the major product along with the 3,5,7-triborylated product as a minor isomer. The Bpin shield in 9-borylated anthracene **18h** enabled remote borylation of both sides of the molecule leading to a 2:1 mixture of 3,6,9-triborylated and 2,6,9-triborylated products (**19h**).

We began this study by suggesting that the unusual para selective C–H borylation of 2-methoxy and 2-chloroaniline came about by virtue of a N–Bpin steric shielding in contrast to the previously evoked electronic drivers. This steric shielding hypothesis could be understandably challenged as free rotation around the C–N and N–B bonds can avoid any steric perturbation caused by the N–Bpin group. Moreover, even in the orientation that maximizes the putative steric shield, one could question if the N–Bpin group

is close enough to the *meta* C–H so as to block its borylation. To address these questions and better understand the observed selectivities, we performed the experiments described below.

Steel and Marder have shown that  $^1\text{H}$  NMR chemical shifts can be qualitative predictors of C–H borylation selectivity when there is not a steric difference between two reactive sites.<sup>25</sup> More de-shielded hydrogens are expected to be more acidic and more reactive toward C–H borylation. Based on 1D-NOE and 2D NMR experiments, we assigned the  $^1\text{H}$  NMR chemical shifts of N-borylated 2-chloro (**12a\***) and 2-tertbutylaniline (**12g\***)(Figure 4-9). We acquired the spectra in THF- $d_8$  so as to best simulate solution structures present during the C–H borylation. Spectra for both compounds had the *meta* proton appearing more downfield than the *para* proton. Per Steel and Marder, this would suggest the *meta* position should be electronically favored in a C–H borylation. However, a preference for *para* borylation is the experimentally observed result. This points to factors besides electronic effects being responsible for the *para* preference.

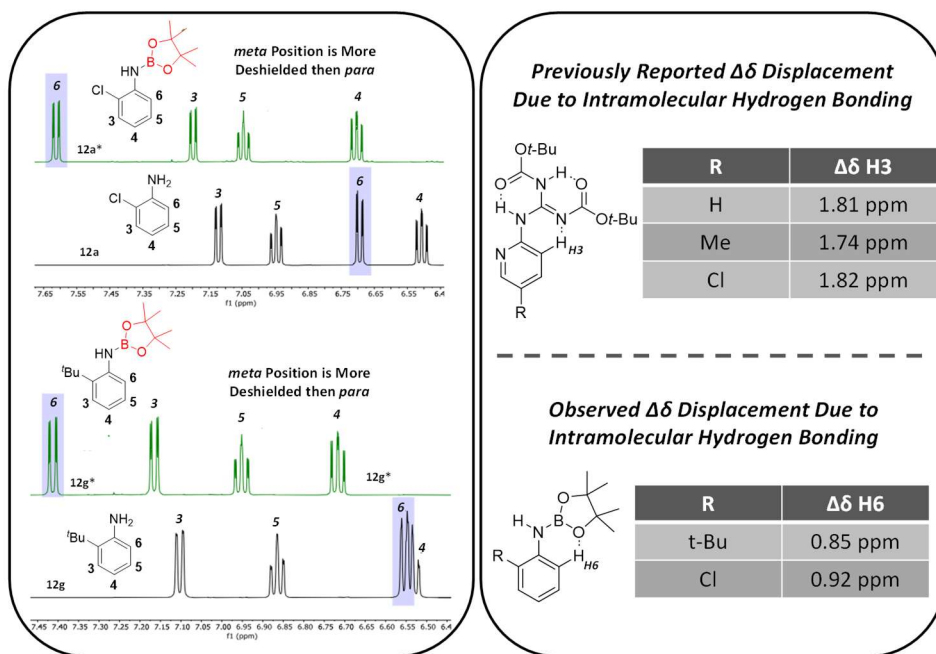


Figure 4-9 Intramolecular Hydrogen Bonding as Seen by  $^1\text{H}$  NMR

A closer comparison of the  $^1\text{H}$  NMR of the N-borylated intermediate vs the nonborylated version of 2-chloro and 2-tertbutylaniline revealed a surprising de-shielding effect on the chemical shift of the *ortho* proton after N-borylation (Figure 4-9). This displacement was also observed in other NMR solvents ( $\text{C}_6\text{D}_6$ , acetone- $d_6$ ,  $\text{CDCl}_3$ , pyridine- $d_5$ ). We attribute the downfield chemical shift movement to an intramolecular C–H $\cdots$ O hydrogen bond (IMHB) between the oxygen of the N–Bpin group and the *ortho* hydrogen in the

aniline. De-shielding effects on chemical shifts caused by hydrogen bonds are well documented,<sup>36-38</sup> and one of the closest examples to our system is the intramolecular hydrogen bond present in N1,N'-diBoc-protected pyridine-2-yl guanidine (Figure 4-9).<sup>39</sup> In this scenario, a C-H...N IMHB is said to change the conformation, vs analogous compound lacking a Boc group, to one where the pertinent protons are de-shielded.

While NMR studies argued against electronic effects being responsible for the para borylation of anilines, those studies did not shed light on the question of whether the N-Bpin group is actually close enough to the *meta* position to act as a steric shield. To begin addressing this question, we ran C-H borylation reactions with larger diboron partners such as B<sub>2</sub>hg<sub>2</sub> and B<sub>2</sub>pp<sub>2</sub> (Figure 4-9 entry [A]). B<sub>2</sub>hg<sub>2</sub> proved less reactive than B<sub>2</sub>pin<sub>2</sub> in accordance with a previous report;<sup>40</sup> however, the selectivity for the para position improved. We tested a novel diboron partner for C-H borylation, B<sub>2</sub>pp<sub>2</sub>, and interestingly the conversion to the borylated product was greater than with B<sub>2</sub>hg<sub>2</sub>. The largest *para* to *meta* ratio was also found with B<sub>2</sub>pp<sub>2</sub>, which is consistent with our steric shield hypothesis. While this improved selectivity could be due to the size of the installed N-Bpp group, a B<sub>2</sub>pp<sub>2</sub>-derived trisboryl active catalyst could also influence regiochemistry. Thus, we generated N-Bpin and N-Bpp compounds from 2-chloro and 2-methylaniline. These intermediates were then independently reacted under the same C-H borylation conditions with B<sub>2</sub>pin<sub>2</sub> as the diboron partner (Figure 4-9 Entry [B] and [C]). For 2-chloroaniline, the N-Bpp borylated derivative yielded a higher *para:meta* ratio as compared to the N-Bpin substrate. For 2-methylaniline, there was no observable change in selectivity; this may be a reflection of 2-methylaniline being inherently less para selective than 2-chloroaniline. We wondered if a smaller steric shield would reduce para selectivity. However, C-H borylation of N-Beg borylated 2-chloroaniline with B<sub>2</sub>pin<sub>2</sub> as the diboron partner yielded mainly the *ortho* product in accordance with the previously reported *ortho* C-H borylation of anilines along with only trace amounts of the *para* and *meta* isomers.<sup>30</sup> Switching the steric shield and diboron partner, i.e., C-H borylation of N-Bpin borylated 2-chloroaniline with B<sub>2</sub>eg<sub>2</sub> lead to similar results.

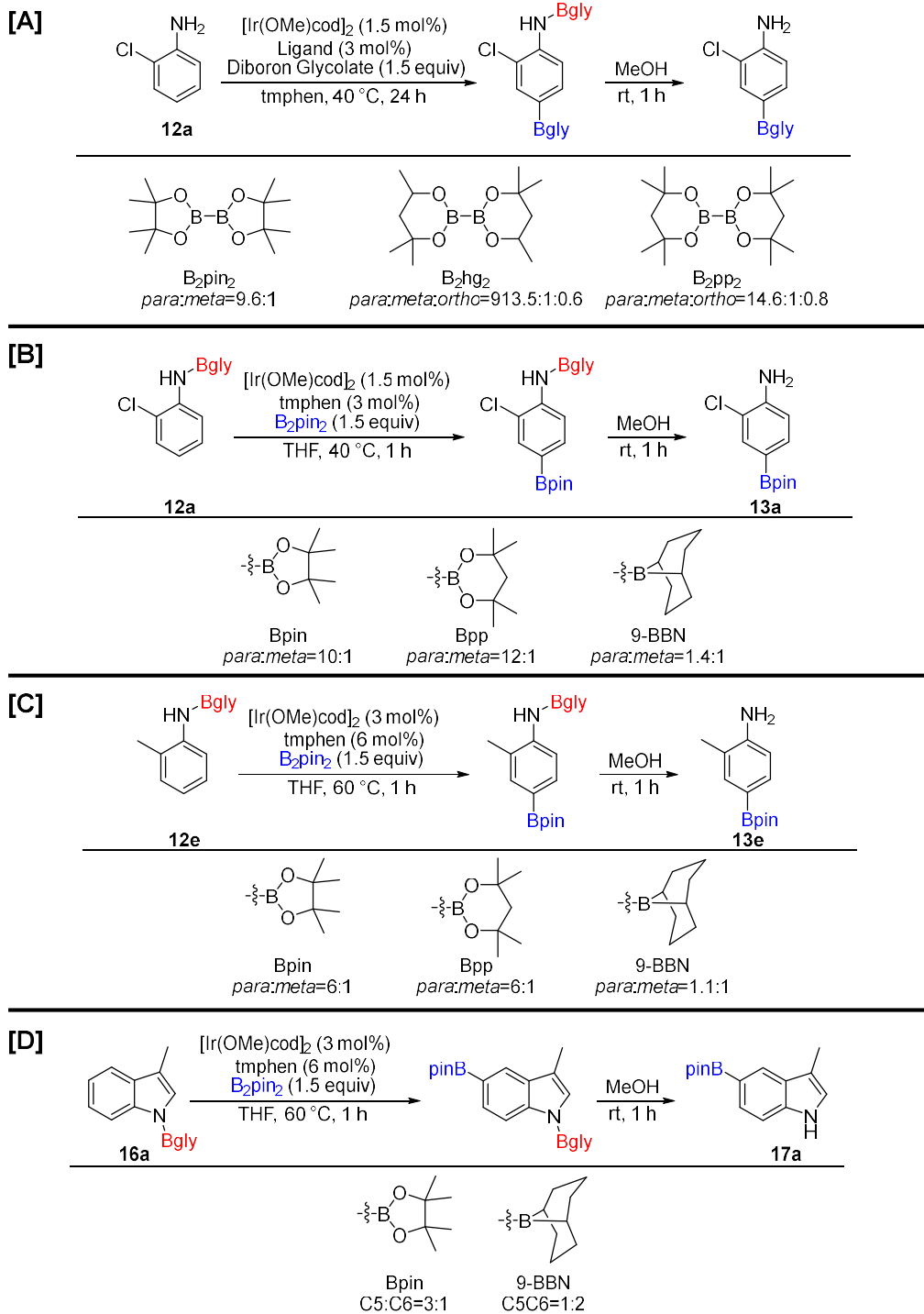


Figure 4-10 Effect of Diboron Partners on Regioselectivity

To probe the significance of the intramolecular hydrogen bond acceptor ability of N-Bpin toward selectivity, we decided to generate N-BBN, a boron group without oxygen, on aniline. With a N-BBN in place, the *para* selectivity dramatically drops for both 2-chloro and 2-methylaniline. This further supports

intramolecular hydrogen bonds playing a direct role in selectivity. With N-BBN generated from 3-methylindole, the C–H borylation regiochemical preference flips and the C6-borylated isomer is major (2:1) as opposed to the C5 selectivity (3:1) seen with N-Bpin.

We further evaluated computationally the proximity of the Bpin steric shield to the *meta* position. We used a B3LYP functional and 6-311++G(d,p) basis set to optimize the geometry of N-borylated 2-chloro (**12a\***) and 2-methylaniline (**12e\***) (Figure 4-11 Entry [A]). This basis set has been previously reported to work well when intramolecular hydrogen bonding is present.<sup>41</sup> Solid angles around the *meta* and *para* positions of **12a\*** and **12e\*** show that the *meta* position is more shielded than the *para* position supporting our hypothesis.<sup>42</sup>

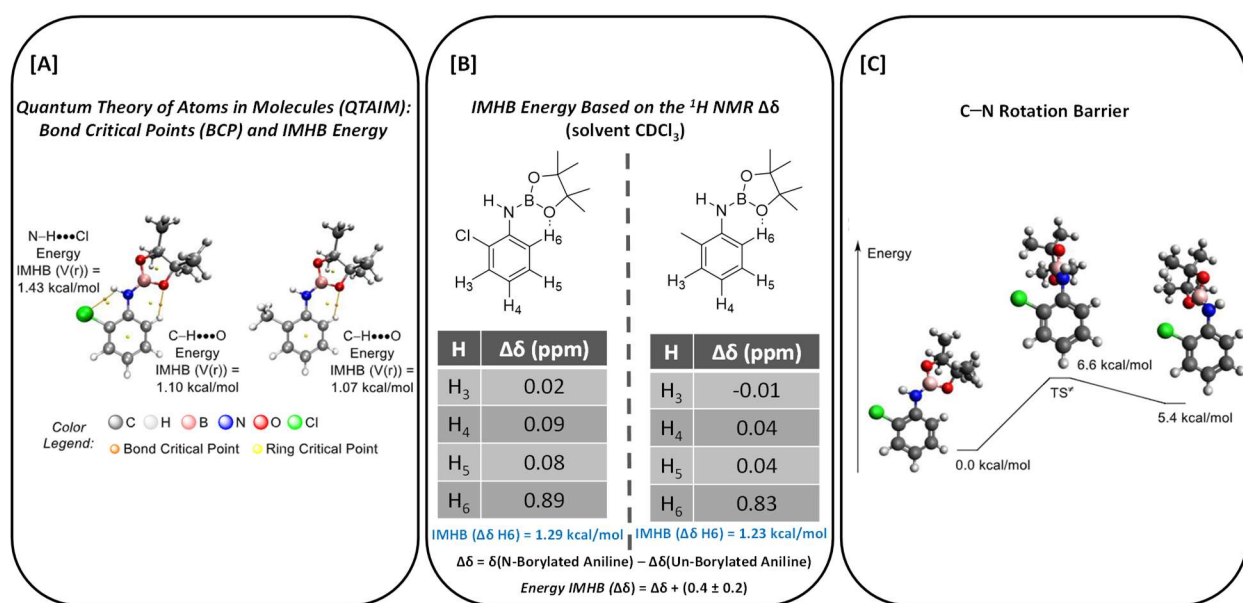


Figure 4-11 Energies of Intramolecular Hydrogen Bonding

Seeking further evidence of intramolecular hydrogen bonding involvement, we examined N-borylated anilines with the Quantum Theory of Atoms in Molecules (QTAIM) developed by Bader using the multiwfn program.<sup>43–45</sup> QTAIM is used to identify intramolecular hydrogen bonding based on a topological analysis of the electronic distribution. Bond critical points (BCP) are defined as the position between two atoms where the electron density reaches a minimum. QTAIM identifies bond critical points when two atoms are connected by any type of bond including intramolecular hydrogen bonding interactions. The QTAIM analysis of both N-borylated anilines shows a bond critical points between the oxygen of the N-Bpin group and the nearest *ortho* hydrogen of the aromatic ring supporting the existence of a C–H...O intramolecular hydrogen bond. An additional bond critical point is found in N-borylated 2-chloroaniline between the

chloride and the N-H. This additional N-H...Cl intramolecular hydrogen bond may be one contributor to the greater para C-H borylation selectivity of 2-chloroaniline vs 2-methylaniline.

The energy of hydrogen bonds can be estimated by multiplying the potential energy density ( $V(r)$ ) at the bond critical point found with QTAIM by a scaling factor determined from plotting  $V(r)$  vs experimentally determined hydrogen bonding energies. The linear relationship initially found by Espinosa et al. has been adapted by Afonin et al. for the case of intramolecular hydrogen bonding including cases with C-H...O interactions.<sup>41-46</sup> Afonin's corrected equation to calculate the C-H...O intramolecular hydrogen bond energy of N-borylated 2-chloro and 2-methylaniline gave comparable energies corresponding to 1.10 and 1.07 kcal/mol, respectively (Figure 4-11 Entry [A]). Intramolecular hydrogen Bond energies can also be estimated using NMR spectroscopy. Typically, there is a linear relationship between the intramolecular hydrogen bond stabilization energy and the  $^1\text{H}$  chemical shift difference,  $\Delta\delta$ , of the hydrogen involved in the intramolecular hydrogen bond in the target molecule vs a reference in which no intramolecular hydrogen bond occurs (Figure 4-11 entry [B]).<sup>41,47</sup> We used  $\text{CDCl}_3$  for these experiments since the relationship was established from  $^1\text{H}$  NMR spectra of  $\text{CDCl}_3$  solutions. We chose non-borylated anilines as references and found energies of 1.29 and 1.23 kcal/mol for the intramolecular hydrogen bond of 2-chloro and 2-methylaniline, respectively, in excellent agreement to the energy predictions from QTAIM.

One potential pitfall in attributing para selectivity to IMHB Bpin shielding is the assumption that there is only one energy minimum on the conformational energy surface. For example, the presence of a second local minimum where the plane of the N-Bpin is orthogonal to the plane containing the aryl ring could erode selectivity if (i) the second local minimum has a comparable or lower Gibbs' energy than the IMHB local minimum and (ii) the barrier connecting the local minima is small. Indeed, theory predicts that there are local minima similar to the aforementioned scenario for N-borylated 2-chloroaniline and 2-methylaniline at 5.4 and 3.1 kcal/mol relative to their respective IMHB local minima (Figure 4-11 [C]), and the corresponding transition states that connect these local minima are 6.6 and 4.6 kcal/mol above the IMHB local minima. Based on the energies of the higher-energy local minima, theory predicts that more than 99% of N-borylated anilines adopt IMHB structures. These findings support the hypothesis that IMHB between the Bpin O and the C6 proton creates a steric shield that accounts for the para selectivity.

We next asked if similar relationships could be found in other scaffolds with and without intramolecular hydrogen bonding (Figure 4-12). Accordingly, good C-H borylation selectivities are seen for substrates when protons proximal to Bpin substituents have the largest  $^1\text{H}$  NMR chemical shift displacement, as well as a bond critical points between that proton and the Bpin O from QTAIM analysis. Specific examples are described below.



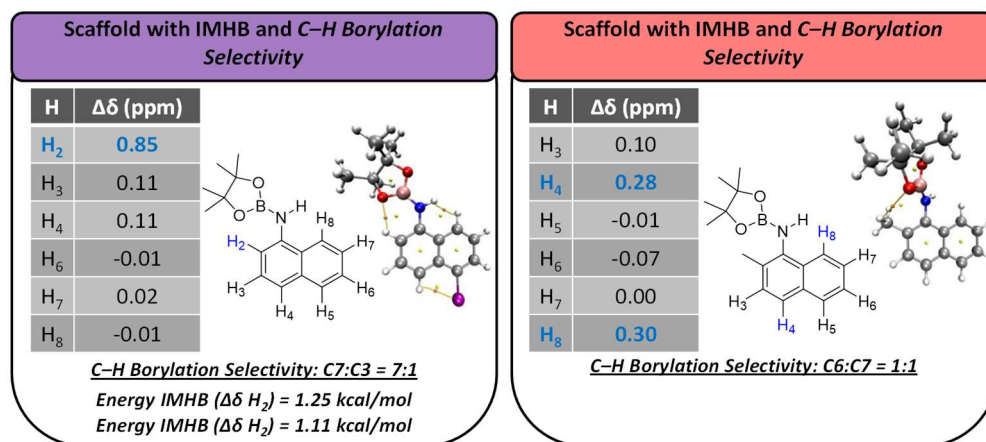


Figure 4-12 Naphthalenes with and Without IMHB

The H<sub>2</sub> of N-borylated 5-bromo-1-aminonaphthalene **13m\*** shows a 0.85 ppm difference from the reference 5-bromo-1-aminonaphthalene. By comparison, all of the other protons deviate by <0.2 ppm. QTAIM shows a BCP that supports an IMHB with an energy of 1.11 kcal/mol, which is close to 1.25 kcal/mol calculated based on the spectroscopically observed <sup>1</sup>H NMR chemical shift displacement. As expected, 5-bromo-1-aminonaphthalene (**13m**) undergoes a C7-selective borylation by blocking the C3 position (Figure 4-5).

In contrast, N-borylated 2-methylnaphthalene **13o\*** show no evidence of C–H···O IMHB with naphthalene as the hydrogen bond donor. H<sub>8</sub> might be available for IMHB, but its  $\Delta\delta$  is only 0.30 ppm, which is close to the  $\Delta\delta$  of H<sub>4</sub> (0.28 ppm), suggesting that chemical shift displacement results from electronic effects after N-borylation. No BCP is detected with arene as the hydrogen bond donor, but a BCP corresponding to a C–H···O IMHB between the N–Bpin and the methyl group is found. The lack of IMHB with the naphthalene ring might be due to steric effects that disrupt any seven-membered ring IMHB from happening. Accordingly, no selectivity was found under CHB reaction conditions.

Similar <sup>1</sup>H NMR and QTAIM studies were done in N-borylated N-methyl-2-aminopyridine (**15b\***), 1,2,3,4-tetrahydro-quinoline (**15d\***), 3-methylindole (**17a\***), and in 1-borylated naphthalenes **18c** and **18f**, which show the presence of an IMHB and CHB remote selectivity accordingly. N-Borylated 2-chloro-N-methylaniline (**15a\***) did not show C–H borylation as shown in Figure 4-6, and there is no presence of an IMHB based on NMR and QTAIM.

Seven-Membered Ring IMHB and Pyrimidines as Directing Groups. Inspired by literature precedent,<sup>37,38,41</sup> we sought to see if a seven-membered ring can be created with IMHB to N–Bpin groups. As explained in the previous section, steric effects can disrupt IMHB. Hence, seven-membered ring IMHB with arenes as hydrogen bond donors are uncommon. However, exceptions appear when a hydrogen bond donor

contains a bicyclic moiety with five- and six- membered fused rings.<sup>37,38,41</sup> We expected that 3-amino-indazoles would form a seven-membered IMHB after N-borylation.

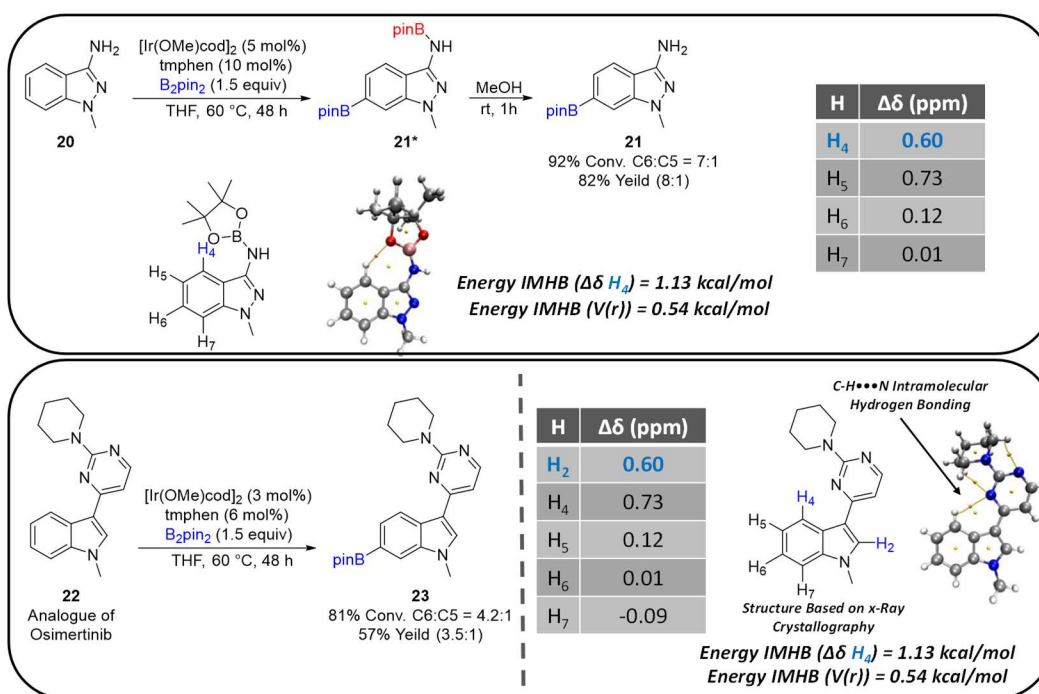


Figure 4-13 7 Member IMHB Rings Guiding Regioselectivity

We were pleased to find that N-methyl-3-aminoindazole **20** undergoes a C6-selective CHB (Figure 4-13).  $^1\text{H}$  NMR comparison of the N-borylated indazole vs the unborylated version shows a significant movement of the chemical shift of the C4 proton, as expected with an IMHB. QTAIM provides more support to this conclusion by recognizing a C-H...O BCP between the C4 proton and the oxygen in the Bpin group. The calculated energies by QTAIM and  $\Delta\delta$  are comparable: 1.19 and 0.85 kcal/mol, respectively.

Certainly, Bpin is not the first IMHB acceptor found in molecules. Nitrogen heterocycles have appeared as part of IMHB networks including C-H...N interactions within heteroarenes.<sup>48-50</sup>

Pyridines, pyrimidines, and triazines are key motifs of biologically active pharmaceuticals, and therefore, their potential use as steric shields via IMHB drew our attention.<sup>51-58</sup> In particular, we became interested in osimertinib, an epidermal growth factor receptor tyrosine kinase inhibitor, which presents a pyrimidine group attached to produced, although with moderate selectivity. We were fortunate to crystallize **22** and the crystal structure showed the C-H...N that we had proposed with the pyrimidine groups as the hydrogen bond acceptor and the C4 hydrogen of the indole being the hydrogen bond donor. We used X-ray coordinates to evaluate the QTAIM topology of **22** and found a BCP that supports the IMHB C-H...N. Next, changes in  $^1\text{H}$  NMR of **22** taking N-methylindole as the reference were calculated. Surprisingly, we

found that both C2 and C4 hydrogens showed a significant chemical shift displacement. We propose that in solution the pyrimidine ring may equilibrate between two conformations involving IMHB with H2 and H4. The IMHB energy for H4 calculated from  $\Delta \delta$  is 1.13 kcal/mol, which is higher than that calculated by QTAIM. This difference might be due to the different conformations found in the solution in contrast to the solid state.

A diverse array of regioselective remote C–H borylations can be driven by intramolecular steric shields created via IMHB. The previously inexplicable para CHB found with 2-chloro and 2-methoxyaniline now is explained by a Bpin steric shield generated after in situ N-borylation. Furthermore, N–Bpin steric shields can lead to para CHB of other *ortho*-substituted anilines, 7-borylation of 1-naphthylamines, para CHB of certain N-alkylated anilines, and to the elusive 5-borylation of indoles. Bpin steric shielding can be extended to motifs without nitrogen, such as 1-borylated naphthalenes, which undergo C6-selective CHB. The wide variety of scaffolds that can be selectively borylated at remote positions due to a Bpin group highlights the versatility of intramolecular steric shields.

We traced back the remote CHB selectivity to the presence of a C–H $\cdots$ O IMHB in N-borylated intermediates with the Bpin as the hydrogen bond acceptor. A BCP found by QTAIM and a characteristic  $^1\text{H}$  NMR chemical shift displacement of the hydrogen bond donor, the *ortho* aniline hydrogen after N-borylation here, is support for an IMHB. The energetic cost to disrupt the planarity of N-borylated anilines and the necessity of oxygen in the boryl group to achieve a para CHB also support the observed selectivity to involve IMHB. A seven-membered ring IMHB can also produce the steric as shown in the C6-selective borylation of N-methyl-3-aminoindazole. Furthermore, a C5 borylation of the indole ring in an osimertinib analogue where a pyrimidine forms the steric shield via a C–H $\cdots$ N IMHB further expands this means of remote regiocontrol. The most significant outcome of our study is that the IMHB Bpin steric shielding explains regioselectivities in catalytic C–H borylations, where standard steric models and correlations with NMR chemical shifts fail. We anticipate that our efforts presented here will be used to design other methods for remote functionalization driven by intramolecular interactions.

## Experimental Procedures

### General Information

All available reagents were used as received unless otherwise indicated. Bis(pinacolato)diboron ( $\text{B}_2\text{pin}_2$ ) was generously supplied by BoroPharm. THF was refluxed over Na/benzophenone ketyl and distilled. Anhydrous 1,4-dioxane was obtained through Sigma-Aldrich and used as received. 3,4,7,8-tetramethyl-1,10-phenanthroline (tmphen) and neocuproine were purchased from Combi-blocks and recrystallized from ethanol. 2-chloroaniline, 2-methoxyaniline, 2-methylaniline, 2-ethylaniline, 2-tertbutylaniline and

tetrahydroquinoline were distilled over molecular sieves prior to use. Column chromatography was done using 240-400 mesh silica P-Flash silica gel. TLC was done on 0.25 mm thick aluminum backed silica gel plates and visualized with UV light ( $\lambda = 254$  nm) with alizarin stain.<sup>58</sup>

$^1\text{H}$ ,  $^{13}\text{C}$ ,  $^{11}\text{B}$  and  $^{19}\text{F}$  NMR spectra were recorded on a Varian 500 MHz DD2 Spectrometer equipped with a  $^1\text{H}$ - $^{19}\text{F}/^{15}\text{N}$ - $^{31}\text{P}$  5 mm Pulsed Field Gradient (PFG) Probe. Spectra taken in  $\text{CDCl}_3$  were referenced to 7.26 ppm in  $^1\text{H}$  NMR and 77.2 ppm in  $^{13}\text{C}$  NMR. Spectra taken in  $\text{C}_6\text{D}_6$  were referenced to 7.16 ppm in  $^1\text{H}$  NMR and 128.1 ppm in  $^{13}\text{C}$ .  $^{11}\text{B}$  NMR spectra were referenced to neat  $\text{BF}_3\cdot\text{Et}_2\text{O}$  as the external standard. NMR spectra were processed for display using the MNova software program with only phasing and baseline corrections applied. High-resolution mass spectra (HRMS) were obtained at the Molecular Metabolism and Disease Mass Spectrometry Core facility and at the Mass Spectrometry Service Center at Michigan State University using electrospray ionization (ESI+ or ESI-) on quadrupole time-of-flight (Q-TOF) instruments.

Parts of this chapter were reprinted with permission from Montero Bastidas, J. R.; Chhabra, A.; Feng, Y.; Oleskey, T. J.; Smith, M. R.; Maleczka, R. E. Steric Shielding Effects Induced by Intramolecular C–H $\cdots$ O Hydrogen Bonding: Remote Borylation Directed by Bpin Groups *ACS. Catal.* **2022**, *12*, 2694-2705.

Copyright 2022 American Chemical Society.

The work presented in this chapter was not all conducted by Thomas Oleskey. Substrate exploration was a team effort with Montero Bastidas, J. R.; Chhabra, A.; Feng, Y.

#### Unselective Borylation of 2-chloro-N-methylaniline (14a)

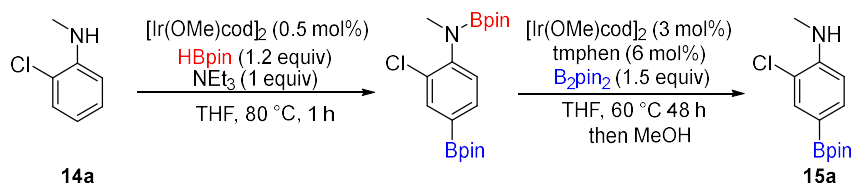


Figure 4-14 Unselective Borylation of 2-chloro-N-methylaniline (14a)

In a glove box, a 5.0 mL Wheaton microreactor was charged with 2-chloro-N-methyl aniline (71 mg, 0.5 mmol, 1 equiv),  $[\text{Ir}(\text{cod})(\text{OMe})]_2$  (1.7mg, 0.5 mol %), HBpin (77 mg, 0.6 mmol, 1.2 equiv),  $\text{NEt}_3$  (0.08 mL, 0.5 mmol), and THF (0.5 mL). The microreactor was capped with a teflon pressure cap and placed into an aluminum block pre-heated to 80 °C. After 1 h, the microreactor was brought back to the glove box. The microreactor was charged  $[\text{Ir}(\text{cod})(\text{OMe})]_2$  (10 mg, 3 mol %),  $\text{B}_2\text{pin}_2$  (190 mg, 0.75 mmol), and THF (0.5 mL). The reaction was then stirred for 5 minutes over which the reaction turned a dark golden color. tmphen (3.6 mg, 6.0 mol %) and THF (0.5 mL) was then added causing the reaction to turn

a dark green color. The microreactor was capped with a teflon pressure cap and placed into an aluminum block pre-heated to 40 °C. After 48 h, an aliquot of the reaction mixture was taken and analyzed directly by <sup>1</sup>H NMR showing complete conversion and a 1:1 *para* : *meta* borylation ratio. MeOH (2.25 mL) was added resulting in vigorous bubbling, and the mixture was stirred for 1 h at room temperature. The mixture was concentrated and passed through a plug of silica gel (2 cm x 5 cm) (chloroform as eluent). The fractions containing product were collected and concentrated to give a first fraction containing 1.4 mg of *para* borylated 2-chloro-N-methylaniline **15a** (1% yield). The fraction was too small to take an accurate <sup>13</sup>C{<sup>1</sup>H} NMR but the peaks could be obtained by subtracting the *meta* carbon peaks from the *para:meta* mixture isolated previously. The NMR data of the *para* isomer were consistent with previously reported NMR values. Three more fractions were collected corresponding to 17.3 mg of *meta* borylated 2-chloro-N-methylaniline **15a** (13% yield), 19.8 mg, and 7.9 mg.

**Data for 2-chloro-N-methyl-4-(4,4,5,5-tetramethyl-1,3,2-dioxaborolan-2-yl)aniline (15a)**

**Para:**

<sup>1</sup>H NMR (500 MHz, CDCl<sub>3</sub>) δ 7.69 (d, J = 1.4 Hz, 1H), 7.60 (dd, J = 8.1, 1.4 Hz, 1H), 6.61 (d, J = 8.1 Hz, 1H), 4.60 (bs, 1H), 2.92 (d, J = 5.2 Hz, 3H), 1.32 (s, 12H).

<sup>13</sup>C NMR (126 MHz, CDCl<sub>3</sub>) δ 147.4, 135.4, 134.9, 118.7, 109.8, 83.6, 30.3, 25.0.

<sup>11</sup>B NMR (160 MHz, CDCl<sub>3</sub>) δ 30.9.

HRMS (ESI) m/z calcd for C<sub>13</sub>H<sub>20</sub>BClNO<sub>2</sub> [M+H]<sup>+</sup> 268.1276, found 268.1273

**Data for 2-chloro-N-methyl-5-(4,4,5,5-tetramethyl-1,3,2-dioxaborolan-2-yl)aniline (15a)**

**Meta:**

<sup>1</sup>H NMR (500 MHz, CDCl<sub>3</sub>) δ 7.25 (d, J = 7.7 Hz, 1H), 7.08 (dd, J = 7.7, 1.4 Hz, 1H), 7.07 (d, J = 1.4 Hz, 1H), 4.32 (bs, 1H), 2.95 (s, 3H), 1.34 (s, 12H).

<sup>13</sup>C NMR (126 MHz, CDCl<sub>3</sub>) δ 144.5, 128.6, 123.8, 122.5, 116.5, 84.0, 30.7, 25.0. <sup>11</sup>B{<sup>1</sup>H} NMR (160 MHz, CDCl<sub>3</sub>) δ 30.8.

HRMS (ESI) m/z calcd for C<sub>13</sub>H<sub>20</sub>BClNO<sub>2</sub> [M+H]<sup>+</sup> 268.1276, found 268.1271

### Para Borylation of 1,2,3,4-tetrahydroquinoline (14d)

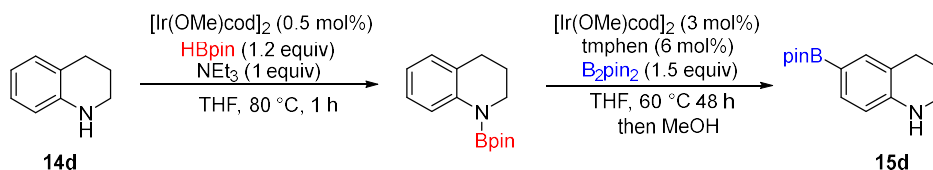


Figure 4-15 Para Borylation of 1,2,3,4-tetrahydroquinoline (14d)

In a glove box, a 5.0 mL Wheaton microreactor was charged with 1,2,3,4-tetrahydroquinoline (60 mg, 0.5 mmol, 1 equiv), [Ir(cod)(OMe)]<sub>2</sub> (1.7 mg, 0.5 mol %), HBpin (77 mg, 0.6 mmol, 1.2 equiv), NEt<sub>3</sub> (0.08 mL, 0.5 mmol), and THF (0.5 mL). The microreactor was capped with a teflon pressure cap and placed into an aluminum block pre-heated to 80 °C. After 1 h, the microreactor was brought back to the glove box. The microreactor was charged [Ir(cod)(OMe)]<sub>2</sub> (10 mg, 3 mol %), B<sub>2</sub>pin<sub>2</sub> (190 mg, 0.75 mmol), and THF (0.5 mL). The reaction was then stirred for 5 minutes over which the reaction turned a dark golden color. tmphen (3.6 mg, 6.0 mol %) and THF (0.5 mL) was then added causing the reaction to turn a dark green color. The microreactor was capped with a teflon pressure cap and placed into an aluminum block pre-heated to 60 °C. After 48 h, an aliquot of the reaction mixture was taken and analyzed directly by <sup>1</sup>H NMR showing complete conversion and a 9:1 *para* : *meta* borylation ratio. MeOH (2.25 mL) was added resulting in vigorous bubbling, and the mixture was stirred for 1 h at room temperature. The mixture was concentrated and passed through a plug of silica gel (chloroform/hexane/ethyl acetate 7:2:1 as eluent). The fractions containing product were collected as two groups and concentrated to give 46.7 mg of a *para* borylated 1,2,3,4-tetrahydroquinoline **15d** as a colorless oil (36% yield) with the *meta* isomer as a minor byproduct being collected as a white solid at 4.3 mg (3% yield).

### Data for 6-(4,4,5,5-tetramethyl-1,3,2-dioxaborolan-2-yl)-1,2,3,4-tetrahydroquinoline (15d)

#### Para:

<sup>1</sup>H NMR (500 MHz, CDCl<sub>3</sub>) δ 7.45-7.39 (m, 2H), 6.45-6.40 (m, 1H), 4.09 (bs, 1H), 3.31 (t, J=5.5, 2H), 2.76 (t, J = 6.3, 2H), 1.95-1.87 (m, 2H), 1.32 (s, 12H).

<sup>13</sup>C NMR (126 MHz, CDCl<sub>3</sub>) δ 147.6, 136.4, 133.9, 120.3, 113.2, 83.2, 41.9, 26.9, 24.9, 22.0.

<sup>11</sup>B NMR (160 MHz, CDCl<sub>3</sub>) δ 30.6.

HRMS (ESI) m/z calcd for C<sub>15</sub>H<sub>23</sub>BNO<sub>2</sub> [M+H]<sup>+</sup> 260.1822, found 260.1814.

**Data for 7-(4,4,5,5-tetramethyl-1,3,2-dioxaborolan-2-yl)-1,2,3,4-tetrahydroquinoline (15d)**

**Meta:**

$^1\text{H}$  NMR (500 MHz,  $\text{CDCl}_3$ )  $\delta$  7.05 (d,  $J$  = 7.4 Hz, 1H), 6.96 (d,  $J$  = 7.4 Hz, 1H), 6.91 (s, 1H), 3.81 (bs, 1H), 3.34 – 3.21 (m, 2H), 2.77 (t,  $J$  = 6.3 Hz, 2H), 1.93 (p,  $J$  = 6.5 Hz, 2H), 1.32 (s, 12H).

$^{13}\text{C}$  NMR (126 MHz,  $\text{CDCl}_3$ )  $\delta$  144.5, 129.2, 125.1, 123.5, 120.5, 83.6, 42.2, 27.3, 25.0, 22.2.

$^{11}\text{B}$  NMR (160 MHz,  $\text{CDCl}_3$ )  $\delta$  30.6.

HRMS (ESI)  $m/z$  calcd for  $\text{C}_{15}\text{H}_{23}\text{BNO}_2$   $[\text{M}+\text{H}]^+$  260.1822, found 260.1814

**Para Borylation of 8-fluoro-3,4-dihydro-2H-benzo[b][1,4]oxazine (14i)**

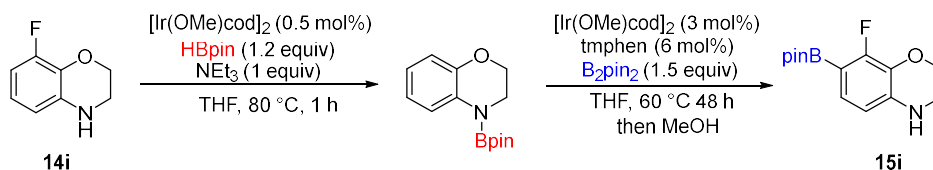


*Figure 4-16 Para Borylation of 8-fluoro-3,4-dihydro-2H-benzo[b][1,4]oxazine (14i)*

In a glove box, a 5.0 mL Wheaton microreactor was charged with 8-fluoro-3,4-dihydro-2H-benzo[b][1,4]oxazine (77 mg, 0.5 mmol),  $[\text{Ir}(\text{cod})(\text{OMe})]_2$  (1.7 mg, 0.5 mol %), HBpin (77 mg, 0.6 mmol, 1.2 equiv),  $\text{NEt}_3$  (0.08 mL, 0.5 mmol), and THF (0.5 mL). The microreactor was capped with a teflon pressure cap and placed into an aluminum block pre-heated to 80 °C. After 1 h, the microreactor was brought back to the glove box. The microreactor was charged  $[\text{Ir}(\text{cod})(\text{OMe})]_2$  (10 mg, 3 mol %),  $\text{B}_2\text{pin}_2$  (190 mg, 0.75 mmol), and THF (0.5 mL). The reaction was then stirred for 5 minutes over which the reaction turned a dark golden color. tmphen (3.6 mg, 6.0 mol %) and THF (0.5 mL) was then added causing the reaction to turn a dark green color. The microreactor was capped with a teflon pressure cap and placed into an aluminum block pre-heated to 60 °C. After 24 h, an aliquot of the reaction mixture was taken and analyzed directly by  $^1\text{H}$  NMR showing complete conversion and a 8:1 para : meta borylation ratio. The mixture was concentrated and passed through a plug of silica gel (2 cm x 5 cm) (hexane/ethyl acetate 7:3 as eluent). The fractions containing product were collected, concentrated and washed with water (2 mL). The water layer was decanted, and the residue was dried to yield 68 mg of a para borylated 4i with the meta isomer as a minor byproduct (para:meta = 10:1) as a tan solid that darkened over time (89% yield).

**Data for 8-fluoro-7-(4,4,5,5-tetramethyl-1,3,2-dioxaborolan-2-yl)-3,4-dihydro-2H-benzo[b][1,4]oxazine (15i)**

**Para:**

$^1\text{H}$  NMR (500 MHz,  $\text{CDCl}_3$ )  $\delta$  7.07 (dd,  $J$  = 8.1, 5.9 Hz, 1H), 6.33 (dd,  $J$  = 8.1, 0.9), 4.28-4.22 (m, 2H), 4.14-4.05 (m, 1H), 3.54-3.39 (m, 2H), 1.32 (s, 12H).

$^{19}\text{F}$  NMR (470 MHz,  $\text{CDCl}_3$ )  $\delta$  -127.4 (d,  $J$  = 6.7 Hz).

$^{13}\text{C}$  NMR (126 MHz,  $\text{CDCl}_3$ )  $\delta$  156.5 (d,  $J$  = 248.1 Hz), 138.8 (dd,  $J$  = 5.3, 3.3 Hz), 131.4 (d,  $J$  = 15.3 Hz), 128.0 (d,  $J$  = 9.6 Hz), 110.0 (d,  $J$  = 2.4 Hz), 83.4, 64.9, 40.7, 24.9.

$^{11}\text{B}$  NMR (160 MHz,  $\text{CDCl}_3$ )  $\delta$  30.3.

HRMS (ESI)  $m/z$  calcd for  $\text{C}_{14}\text{H}_{20}\text{BFNO}_3$   $[\text{M}+\text{H}]^+$  280.1520, found 280.1508

**Data for 8-fluoro-6-(4,4,5,5-tetramethyl-1,3,2-dioxaborolan-2-yl)-3,4-dihydro-2H-benzo[b][1,4]oxazine (15i)**

**Meta:**

$^1\text{H}$  NMR (500 MHz,  $\text{CDCl}_3$ )  $\delta$  6.92 (dd,  $J$  = 10.78, 1.16 Hz, 1H), 6.82 (s, 1H), 4.33-4.30 (m, 1H), 4.14-4.05 (m, 1H), 3.54-3.39 (m, H), 1.31 (s, 12H).

$^{19}\text{F}$  NMR (470 MHz,  $\text{CDCl}_3$ )  $\delta$  -138.73 (d,  $J$  = 10.8 Hz).

HRMS (ESI)  $m/z$  calcd for  $\text{C}_{14}\text{H}_{20}\text{BFNO}_3$   $[\text{M}+\text{H}]^+$  280.1520, found 280.1



## REFERENCES

- (1) Boerner, L. K. C –H Bond Breakers Seek Smarter Tools. *Chemical & Engineering News*, 2021.
- (2) Rej, S.; Das, A.; Chatani, N. Strategic Evolution in Transition Metal-Catalyzed Directed C–H Bond Activation and Future Directions. *Coord. Chem. Rev.* **2021**, *431*, 213683
- (3) Mahmudov, K. T.; Gurbanov, A. V.; da Silva, M. F. C. G.; Pombeiro, A.J.L. Noncovalent Interactions in C– H Bond Functionalization. In *Noncovalent Interactions in Catalysis*; Royal Society of Chemistry, 2019; Chapter 1, pp 1–25.
- (4) Haldar, C.; Hoque, E.; Bisht, R.; Chattopadhyay, B. Concept of Ir-Catalyzed CH Bond Activation/Borylation by Noncovalent Interaction. *Tetrahedron Lett.* **2018**, *59*, 1269–1277.
- (5) Kuninobu, Y.; Torigoe, T. Recent Progress of Transition Metal-Catalysed Regioselective C–H Transformations Based on Non- covalent Interactions. *Org. Biomol. Chem.* **2020**, *18*, 4126–4134.
- (6) Trouvé, J.; Gramage-Doria, R. Beyond Hydrogen Bonding : Recent Trends of Outer Sphere Interactions in Transition Metal Catalysis. *Chem. Soc. Rev.* **2021**, *50*, 3565–3584.
- (7) Pandit, S.; Maiti, S.; Maiti, D. Noncovalent Interactions in Ir-Catalyzed Remote C-H Borylation: A Recent Update. *Org. Chem. Front.* **2021**, *8*, 4349–4358.
- (8) Genov, G. R.; Mihai, M. T.; Phipps, R. J. Harnessing Non-covalent Interactions for Distal C(sp<sup>2</sup>)–H Functionalization of Arenes. In *Remote C–H Bond Functionalizations*; Wiley, **2021**; pp 169–189.
- (9) Dutta, U.; Maiti, D. Transition Metal Catalyzed Distal *Para*-selective C– H Functionalization. In *Remote C– H Bond Functionalizations*; Wiley, 2021; pp 221– 251.
- (10) Dutta, U.; Maiti, S.; Bhattacharya, T.; Maiti, D. Arene Diversification through Distal C(sp<sup>2</sup>)–H Functionalization. *Science* **2021**, *372*, No. eabd5992.
- (11) Mihai, M. T.; Phipps, R. J. Ion-Pair-Directed *Meta*-Selective C–H Borylation of Aromatic Quaternary Ammonium Salts. *Synlett* **2017**, *28*, 1011–1017.
- (12) Yang, L.; Semba, K.; Nakao, Y. Para-Selective C-H Borylation of (Hetero)Arenes by Cooperative Iridium/Aluminum Catalysis. *Angew. Chem., Int. Ed.* **2017**, *56*, 4853–4857.
- (13) Okumura, S.; Tang, S.; Saito, T.; Semba, K.; Sakaki, S.; Nakao, Y. Para-Selective Alkylation of Benzamides and Aromatic Ketones by Cooperative Nickel/Aluminum Catalysis. *J. Am. Chem. Soc.* **2016**, *138*, 14699– 14704.
- (14) Nakao, Y.; Okumura, S.; Ebara, T.; Semba, K. Synthesis of N-Heterocyclic Carbene Ligands for Site-Selective C-H Alkylation by Cooperative Nickel/Aluminum Catalysis. *Heterocycles* **2019**, *99*, 1128.
- (15) Okumura, S.; Nakao, Y. Par a-Selective Alkylation of Sulfonylarenes by Cooperative Nickel/Aluminum Catalysis. *Org. Lett.* **2017**, *19*, 584–587.
- (16) Iverson, C. N.; Smith, M. R., III. Stoichiometric and Catalytic B–C Bond Formation from Unactivated Hydrocarbons and Boranes. *J. Am. Chem. Soc.* **1999**, *121*, 7696–7697.
- (17) Cho, J.-Y.; Tse, M. K.; Holmes, D.; Maleczka, R. E., Jr.; Smith, M. R., III. Remarkably Selective Iridium Catalysts for the Elaboration of Aromatic C-H Bonds. *Science* **2002**, *295*, 305– 308.

- (18) Mkhalid, I. A. I.; Barnard, J. H.; Marder, T. B.; Murphy, J. M.; Hartwig, J. F. C-H Activation for the Construction of C-B Bonds. *Chem. Rev.* **2010**, *110*, 890– 931.
- (19) Ros, A.; Fernández, R.; Lassaletta, J. M. Functional Group Directed C–H Borylation. *Chem. Soc. Rev.* **2014**, *43*, 3229–3243.
- (20) Preshlock, S. M.; Plattner, D. L.; Maligres, P. E.; Krska, S. W.; Maleczka, R. E., Jr.; Smith, M. R., III. A Traceless Directing Group for C-H Borylation. *Angew. Chem., Int. Ed.* **2013**, *52*, 12915–12919.
- (21) Mihai, M. T.; Williams, B. D.; Phipps, R. J. Para-Selective C-H Borylation of Common Arene Building Blocks Enabled by Ion-Pairing with a Bulky Counteranion. *J. Am. Chem. Soc.* **2019**, *141*, 15477– 15482.
- (22) Montero Bastidas, J. R.; Oleskey, T. J.; Miller, S. L.; Smith, M. R., III; Maleczka, R. E., Jr. Para-Selective, Iridium-Catalyzed C-H Borylations of Sulfated Phenols, Benzyl Alcohols, and Anilines Directed by Ion-Pair Electrostatic Interactions. *J. Am. Chem. Soc.* **2019**, *141*, 15483–15487.
- (23) Esteruelas, M. A.; Martínez, A.; Oliván, M.; Onate, E. Direct C- H Borylation of Arenes Catalyzed by Saturated Hydride-Boryl- Iridium-POP Complexes: Kinetic Analysis of the Elemental Steps. *Chem. – Eur. J.* **2020**, *26*, 12632–12644.
- (24) Cho, J.-Y.; Iverson, C. N.; Smith, M. R., III. Steric and Chelate Directing Effects in Aromatic Borylation. *J. Am. Chem. Soc.* **2000**, *122*, 12868– 12869.
- (25) Tajuddin, H.; Harrison, P.; Bitterlich, B.; Collings, J. C.; Sim, N.; Batsanov, A. S.; Cheung, M. S.; Kawamorita, S.; Maxwell, A. C.; Shukla, L.; Morris, J.; Lin, Z.; Marder, T. B.; Steel, P. G. Iridium-Catalyzed C– H Borylation of Quinolines and Unsymmetrical 1,2- Disubstituted Benzenes: Insights into Steric and Electronic Effects on Selectivity. *Chem. Sci.* **2012**, *3*, 3505.
- (26) Hoque, M. E.; Bisht, R.; Haldar, C.; Chattopadhyay, B. Noncovalent Interactions in Ir-Catalyzed C-H Activation: L-Shaped Ligand for Para-Selective Borylation of Aromatic Esters. *J. Am. Chem. Soc.* **2017**, *139*, 7745–7748.
- (27) Chotana, G. A.; Rak, M. A.; Smith, M. R., III. Sterically Directed Functionalization of Aromatic C–H Bonds: Selective Borylation *Ortho* to Cyano Groups in Arenes and Heterocycles. *J. Am. Chem. Soc.* **2005**, *127*, 10539–10544.
- (28) Vanchura, B. A., II; Preshlock, S. M.; Roosen, P. C.; Kallepalli, V. A.; Staples, R. J.; Maleczka, R. E., Jr.; Singleton, D. A.; Smith, M. R., III. Electronic Effects in Iridium C-H Borylations: Insights from Unencumbered Substrates and Variation of Boryl Ligand Substituents. *Chem. Commun.* **2010**, *46*, 7724– 7726.
- (29) Zhang, G.; Rominger, F.; Mastalerz, M. Fused  $\pi$ -Extended Truxenes via a Threefold Borylation as the Key Step. *Chem. – Eur. J.* **2016**, *22*, 3084–3093.
- (30) Smith, M. R., III; Bisht, R.; Haldar, C.; Pandey, G.; Dannatt, J. E.; Ghaffari, B.; Maleczka, R. E., Jr.; Chattopadhyay, B. Achieving High *Ortho* Selectivity in Aniline C-H Borylations by Modifying Boron Substituents. *ACS Catal.* **2018**, *8*, 6216– 6223.
- (31) Feng, Y.; Holte, D.; Zoller, J.; Umemiya, S.; Simke, L. R.; Baran, P. S. Total Synthesis of Verruculogen and Fumitremorgin A Enabled by Ligand Controlled C– H Borylation. *J. Am. Chem. Soc.* **2015**, *137*, 10160– 10163.

- (32) Del Grosso, A.; Singleton, P. J.; Muryn, C. A.; Ingleson, M. J. Pinacol Boronates by Direct Arene Borylation with Borenium Cations. *Angew. Chem., Int. Ed.* **2011**, *50*, 2102–2106.
- (33) Iqbal, S. A.; Cid, J.; Procter, R. J.; Uzelac, M.; Yuan, K.; Ingleson, M. J. Acyl-Directed *Ortho*-Borylation of Anilines and C7 Borylation of Indoles Using Just BBr<sub>3</sub>. *Angew. Chem., Int. Ed.* **2019**, *58*, 15381–15385.
- (34) Zhang, S.; Han, Y.; He, J.; Zhang, Y. B(C<sub>6</sub>F<sub>5</sub>)<sub>3</sub>-Catalyzed C3- Selective C-H Borylation of Indoles: Synthesis, Intermediates, and Reaction Mechanism. *J. Org. Chem.* **2018**, *83*, 1377–1386.
- (35) Prévost, S. Regioselective C-H Functionalization of Naphthalenes: Reactivity and Mechanistic Insights. *ChemPlusChem* **2020**, *85*, 476–486.
- (36) Charisiadis, P.; Kontogianni, V. G.; Tsiafoulis, C. G.; Tzakos, A. G.; Siskos, M.; Gerothanassis, I. P. <sup>1</sup>H-NMR as a Structural and Analytical Tool of Intra- and Intermolecular Hydrogen Bonds of Phenol-Containing Natural Products and Model Compounds. *Molecules* **2014**, *19*, 13643–13682.
- (37) Sigalov, M. V.; Doronina, E. P.; Sidorkin, V. F. C(Ar)-H ...O Hydrogen Bonds in Substituted Isobenzofuranone Derivatives: Geometric, Topological, and NMR Characterization. *J. Phys. Chem. A* **2012**, *116*, 7718–7725.
- (38) Sigalov, M.; Vashchenko, A.; Khodorkovsky, V. Aromatic C-H...O Interactions in a Series of Bindone Analogues. NMR and Quantum Mechanical Study. *J. Org. Chem.* **2005**, *70*, 92–100.
- (39) Kelly, B.; O'Donovan, D. H.; O'Brien, J.; McCabe, T.; Blanco, F.; Rozas, I. Pyridin-2-yl Guanidine Derivatives: Conformational Control Induced by Intramolecular Hydrogen-Bonding Interactions. *J. Org. Chem.* **2011**, *76*, 9216–9227.
- (40) Hartwig, J.; Liskey, C. Borylation of Arenes with Bis(Hexylene Glycolato)Diboron. *Synthesis* **2013**, *45*, 1837–1842.
- (41) Afonin, A. V.; Vashchenko, A. V.; Sigalov, M. V. Estimating the Energy of Intramolecular Hydrogen Bonds from <sup>1</sup>H NMR and QTAIM Calculations. *Org. Biomol. Chem.* **2016**, *14*, 11199–11211.
- (42) Guzei, I. A.; Wendt, M. An Improved Method for the Computation of Ligand Steric Effects Based on Solid Angles. *Dalton Trans.* **2006**, *128*, 3991–3999.
- (43) Bader, R. F. W. *Atoms in Molecules; International Series of Monographs on Chemistry*; Clarendon Press: Oxford, England, 1994.
- (44) Lu, T.; Chen, F. Multiwfn: A Multifunctional Wavefunction Analyzer. *J. Comput. Chem.* **2012**, *33*, 580–592.
- (45) Emamian, S.; Lu, T.; Kruse, H.; Emamian, H. Exploring Nature and Predicting Strength of Hydrogen Bonds: A Correlation Analysis between Atoms in-Molecules Descriptors, Binding Energies, and Energy Components of Symmetry-Adapted Perturbation Theory. *J. Comput. Chem.* **2019**, *40*, 2868–2881.
- (46) Espinosa, E.; Molins, E.; Lecomte, C. Hydrogen Bond Strengths Revealed by Topological Analyses of Experimentally Observed Electron Densities. *Chem. Phys. Lett.* **1998**, *285*, 170–173.
- (47) Schaefer, T. Relation between Hydroxyl Proton Chemical Shifts and Torsional Frequencies in Some *Ortho*-Substituted Phenol Derivatives. *J. Phys. Chem. A* **1975**, *79*, 1888–1890.

- (48) Constable, E. C.; Ward, M. D. Synthesis and Co-Ordination Behavior of 6',6''-Bis(2-Pyridyl)-2,2':4,4'':2'',2'''-Quaterpyridine; 'Back-to-Back' 2,2':6',2''-Terpyridine. *J. Chem. Soc., Dalton Trans.* **1990**, 1405– 1409.
- (49) Avendaño, C.; Espada, M.; Ocaña, B.; García-Granda, S.; Díaz, M. del R.; Tejerina, B.; Gómez-Beltrán, F.; Martínez, A.; Elguero, J. The Problem of the Existence of C(Ar)–H...N Intramolecular Hydrogen Bonds in a Family of 9-Azaphenyl-9H-Carbazoles. *J. Chem. Soc., Perkin Trans. 2* **1993**, 104, 1547–1555.
- (50) Castellanos, M. L.; Olivella, S.; Roca, N.; Mendoza, J. D.; Elguero, J. N,N-Linked Biazoles. III. MNDO Calculations on the Conformation of N,N Linked Biazoles and Their Quaternary Salts. *Can. J. Chem.* **1984**, 62, 687–695.
- (51) Shinde, R. S.; Salunke, S. D. Synthesis of Novel Substituted 4,6-Dimethoxy-N-Phenyl-1,3,5-Triazin-2-Amine Derivatives and Their Antibacterial and Antifungal Activities. *Asian J. Chem.* **2015**, 27, 4130– 4134.
- (52) Sharma, A.; Sheyi, R.; de la Torre, B. G.; El-Faham, A.; Albericio, F. S-Triazine: A Privileged Structure for Drug Discovery and Bioconjugation. *Molecules* **2021**, 26, No. 864.
- (53) Shah, D. R.; Modh, R. P.; Chikhalia, K. H. Privileged S-Triazines: Structure and Pharmacological Applications. *Future Med. Chem.* **2014**, 6, 463–477.
- (54) Al-Zaydi, K. M.; Khalil, H. H.; El-Faham, A.; Khattab, S. N. Synthesis, Characterization and Evaluation of 1,3,5-Triazine Amino- benzoic Acid Derivatives for Their Antimicrobial Activity. *Chem. Cent. J.* **2017**, 11, No. 39.
- (55) Palanki, M. S. S.; Erdman, P. E.; Gayo-Fung, L. M.; Shevlin, G. I.; Sullivan, R. W.; Goldman, M. E.; Ransone, L. J.; Bennett, B. L.; Manning, A. M.; Suto, M. J. Inhibitors of NF-KB and AP-1 Gene Expression: SAR Studies on the Pyrimidine Portion of 2-Chloro-4-Trifluoromethylpyrimidine-5-[N (3',5'-Bis(Trifluoromethyl)Phenyl) Carboxamide]. *J. Med. Chem.* **2000**, 43, 3995– 4004.
- (56) Yang, R.; Timofte, R.; Liu, J.; Xu, Y.; Zhang, X.; Zhao, M.; Zhou, S.; Chan, K. C. K.; Zhou, S.; Xu, X.; Loy, C. C.; Li, X.; Liu, F.; Zheng, H.; Jiang, L.; Zhang, Q.; He, D.; Li, F.; Dang, Q.; Huang, Y.; Maggioni, M.; Fu, Z.; Xiao, S.; Li, C.; Tanay, T.; Song, F.; Chao, W.; Guo, Q.; Liu, Y.; Li, J.; Qu, X.; Hou, D.; Yang, J.; Jiang, L.; You, D.; Zhang, Z.; Mou, C.; Koshelev, I.; Ostyakov, P.; Somov, A.; Hao, J.; Zou, X.; Zhao, S.; Sun, X.; Liao, Y.; Zhang, Y.; Wang, Q.; Zhan, G.; Guo, M.; Li, J.; Lu, M.; Ma, Z.; Michelini, P. N.; Wang, H.; Chen, Y.; Guo, J.; Zhang, L.; Yang, W.; Kim, S.; Oh, S.; Wang, Y.; Cai, M.; Hao, W.; Shi, K.; Li, L.; Chen, J.; Gao, W.; Liu, W.; Zhang, X.; Zhou, L.; Lin, S.; Wang, R. NTIRE 2021 Challenge on Quality Enhancement of Compressed Video: Methods and Results. *arXiv.org* 2021, 2104.10781.
- (57) Lawrence, H. R.; Martin, M. P.; Luo, Y.; Pireddu, R.; Yang, H.; Gevariya, H.; Ozcan, S.; Zhu, J.-Y.; Kendig, R.; Rodriguez, M.; Elias, R.; Cheng, J. Q.; Sebt, S. M.; Schonbrunn, E.; Lawrence, N. J. Development of O-Chlorophenyl Substituted Pyrimidines as Exceptionally Potent Aurora Kinase Inhibitors. *J. Med. Chem.* **2012**, 55, 7392– 7416.
- (58) Patel, H.; Pawara, R.; Ansari, A.; Surana, S. Recent Updates on Third Generation EGFR Inhibitors and Emergence of Fourth Generation EGFR Inhibitors to Combat C797S Resistance. *Eur. J. Med. Chem.* **2017**, 142, 32–47.

## Chapter 5: Measurement of Isotopic Distribution of Boron

Not all atoms of an element are created equal. While isotopes are predominately seen as the interest of physicists, in the world of chemistry they do find ample use. Contrary to simplified teaching, isotopes do react differently, although this difference in reactivity lies in reaction rate. This difference in reaction rate is in turn dependent on the mass of the two atoms sharing the chemical bond. This is called the kinetic isotope effect. The kinetic isotope effect is often seen used in mechanistic studies of chemical reactions and is often encountered as protium and deuterium isotope effects. This is for three reasons. First because deuterium is widely available and easy to incorporate into molecules. Second, because it is extremely easy to observe via NMR. And third is due to the relative difference masses between hydrogen isotopes. This difference in mass is important as the relative mass difference is proportional to the size of the KIE able to be observed. Hydrogen isotopes have the largest relative difference in mass of all the atoms as they are the lightest element known. This intrinsically causes measured KIE effects for hydrogen to be the largest of all atoms.

Although hydrogen is undisputedly the main atom of interest for KIE studies, other atomic nuclei can be used to measure kinetic isotope effects. These are most often referred to as heavy atom isotope effects. The main difference between hydrogen kinetic isotope effects and heavy atom isotope effects is simply the size of the values. Typically, hydrogen isotope effects ( $K_H/K_D$ ) are between 1 and 8, whereas heavy atom isotope effects typically have a value of 0.975 to 1.075.<sup>1,2</sup> The smaller value of heavy atom kinetic isotope effects makes the practicality of measuring these much harder. Additionally, non-hydrogen isotopically labeled compounds are much harder to obtain, and sometimes prohibitively expensive. Ideally heavy atom kinetic isotope effects could be carried out simply with natural abundance of a compound of interest. This was demonstrated to be possible by Singleton who was able to utilize naturally abundant  $^2\text{H}$  and  $^{13}\text{C}$  to measure isotopic perturbation under reaction conditions.<sup>3,4</sup>

A good candidate for measuring kinetic isotope effects at natural abundance is boron with a natural abundance of about 20 %  $^{10}\text{B}$  and 80 %  $^{11}\text{B}$ . The problem with boron however is the difficulty in measuring the concentration of each isotope. A few methods have been utilized to do this. The simplest method is the use of mass spectroscopy; however, other methods have also been used such as emission spectroscopy, IR, and neutron absorption.<sup>5,6</sup>

NMR has also been used; however, boron was paired with a reporter that is able to differentiate between boron isotopes. In a published report measuring a boron kinetic isotope effect, the authors utilized fluorine to report the isotopic distribution of the boron by NMR shift as shown in Figure 5-1. They however, utilized incorporated deuterium labeling to differentiate between the boron isotopic

labels through shifting of the fluorine signal.<sup>7,8</sup> This presents the same problem associated with having to incorporate labeled boron as well as potential for secondary kinetic isotopic effects.<sup>9</sup>

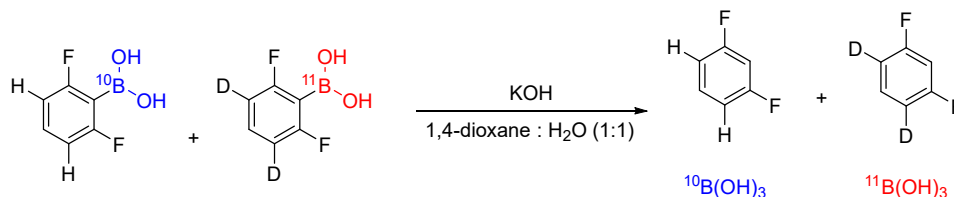


Figure 5-1 Measurement of the Boron KIE for Proto-deborylation as Described by Llyod-Jones

Through our previous studies we realized that we could differentiate between  $^{10}\text{B}$  and  $^{11}\text{B}$  in compounds containing fluorine by  $^{19}\text{F}$  NMR. This effect is most pronounced in molecules where the boron is directly fluorinated such as in tetrafluoroborate salts as shown in Figure 5-2. This was reported in 2017 by the university of Ottawa NMR facility in a blog post.<sup>10</sup> The two Isotopes of boron can be differentiated from each other by their shift as well as by their splitting pattern.  $^{10}\text{B}$  will show up as a septet due to  $^{10}\text{B}$  having a spin of 3 and  $^{11}\text{B}$  will show up as a quartet due to its spin of  $3/2$ .

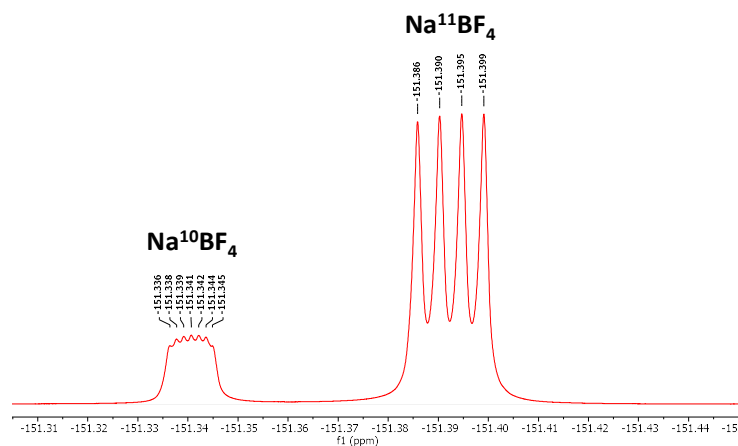


Figure 5-2  $^{19}\text{F}$  NMR of  $\text{NaBF}_4$  in  $\text{D}_2\text{O}$  Showing Both the  $^{10}\text{B}$  and  $^{11}\text{B}$  Isotopic Peaks

We immediately saw potential of this observation in the fact it could be used to directly measure boron isotopic distribution and therefore boron heavy atom isotope effects. Essentially, we desired to utilize  $^{19}\text{F}$  NMR to measure the concentration of each boron isotope in a sample to directly measure boron heavy isotope effects in a reaction as outlined in Figure 5-3. By taking the reaction to high, but not complete conversion, the heavy isotope should be enriched in the leftover starting material while the product should be depleted in the heavy isotope. To study this effect, we elected to investigate the oxidation of 2-fluoro-phenyl boronic acid pinacol ester.

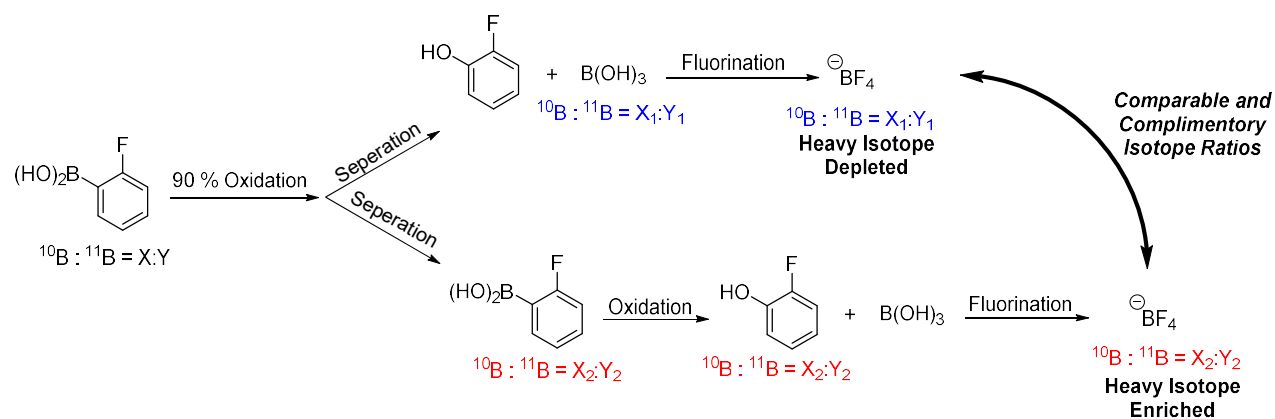


Figure 5-3 Outline of Our Plan to Measure the Boron KIE for Hydrogen Peroxide Oxidation of 2-Fluorophenylboronic Acid

The project first started by looking at conditions for running oxidations of aryl boronic acids. We elected to utilize **23** as a test substrate as our group had prior work with this compound. Initially we started by oxidation of **23** acid following typical oxidation conditions as shown in Figure 5-4.

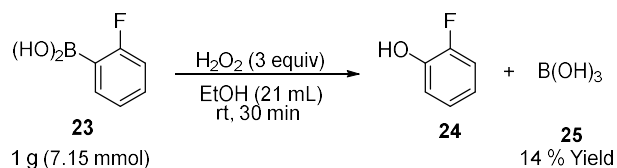
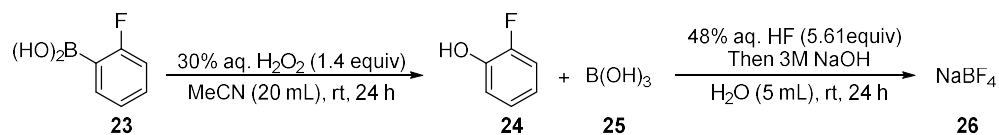


Figure 5-4 Our Initial Attempt at oxidation of a Boronic Acid with Recovery of the Produced Boric Acid

We quickly found that using ethanol as a solvent for hydrogen peroxide oxidations of **23** was not optimal as it led to the loss of a significant amount of the resulting boric acid byproduct thus invalidation results. This was due to the formation and evaporation of triethyl borate, which while advantageous for synthetic applications resulted in the loss of the product of interest. We alleviated this problem by utilizing ethereal solvents, particularly 1,4-dioxane as reaction solvents. While changing solvents did work well in eliminating loss of boron, use of 1,4-dioxane was not pursued due to safety concerns, especially since the first step in the work up is evaporation to dryness. Oxidation of boronic acids in 1,4-dioxane was a serious safety hazard as it is a known peroxide former, and treatment with hydrogen peroxide led to charring of some reaction mixtures upon evaporation. This led us to believe that we were forming organic peroxides to some extent and thus we abandoned ethereal solvents. Despite this, it was evident that by using non-alcoholic solvents boron evaporation could be eliminated. Acetonitrile was then used as a replacement solvent as it has ideal properties as a solvent for oxidation of aryl boronic acids (Figure 5-5). It easily

solvates aryl boronic acids, is non-reactive with hydrogen peroxide solutions while also being volatile enough to be easily removed.



*Figure 5-5 Reaction Conditions for Oxidation of 2-Fluoro-Phenylboronic Acid in Acetonitrile*

After treatment of **23** with hydrogen peroxide, the product was removed from the unreacted starting material by aqueous extraction with chloroform. This was successful in separating the synthesized boric acid from the unreacted **23**.

From here we converted the isolated boric acid to the boron tetrafluoride anion. We found that the best way of accomplishing this was with hydrofluoric acid. Initially we found that 28% aq. HF added to the boric acid was able to produce the desired fluoroboric acid. This was a serendipitous discovery as the original HF concentration that we planned to use was concentrated HF or 48% in accordance with preparation described for tetrafluoro borate by Brauer (Figure: 5-5).<sup>11</sup>

While fluoroboric acid can be directly analyzed by  $^{19}\text{F}$  NMR for isotope ratios, this is undesirable for a few reasons. Like HF, fluoroboric acid etches glass and therefore can be vulnerable to reactive changes in the concentration of labeled boron. This of course will also damage equipment used for characterization. It cannot simply be fixed by adding a commercial NMR tube protective insert as they are usually made from perfluorinated plastics which becomes evident in the  $^{19}\text{F}$  NMR spectra. What is most undesirable though, is the toxicity of fluoroboric acid. As an acidic fluoride source, it shares the same hazards as HF.

Nearly all these issues can simply be avoided by quenching the fluoroboric acid with a base to give a far less hazardous tetrafluoroborate salt. We chose to pursue sodium tetrafluoroborate as initial studies showed us that sodium tetrafluoroborate gave superior solubility and resolution of the isotopic peaks. To convert fluoroboric acid to sodium tetrafluoro borate, the fluorination solution merely needs to be brought to a neutral pH with a sodium base.

In early trials nearly every attempt failed due to imprecise pH control. While sodium tetrafluoroborate is a stable salt, it is prone to hydrolysis. In the case of hydrolysis, sodium tetrafluoroborate will hydrolyze slowly back to boric acid and HF. This process is accelerated greatly by basic conditions. In our case due to the imprecise quenching of the fluoroboric acid with base, we often had excess base in solution which caused reversion of the sodium tetrafluoro borate back to boric acid. We were able to easily identify this by boron NMR in which we were able to observe the characteristic peak for boric acid as opposed to the



tetrafluoroborate anion. This was an issue for quenching with sodium hydroxide and sodium carbonate. We initially thought by measuring the concentration of our solutions of hydrofluoric acid and sodium carbonate by titration with KHP and phenolphthalein we could dial in our quenching, however, we found we could more exactly neutralize the fluoroboric acid by simply adding a small quantity of phenolphthalein to the fluoroboric acid and simply titrating with sodium carbonate. This was successful in precisely forming sodium tetrafluoroborate without addition of excess base. This alleviated our problem with hydrolysis of the tetrafluoroborate anion. The problem with adding phenolphthalein became evident when this mixture was observed by  $^{19}\text{F}$  NMR. As shown below, an additional peak was observed forming in the fluorine spectra. It was evident that this was due to an interaction between the sodium tetrafluoroborate and phenolphthalein as addition of additional phenolphthalein caused this peak to grow. We theorized that the fluorine of the sodium tetrafluoroborate was able to bind to the arenes of the phenolphthalein via fluorine – pi orbital interactions, the theorized adduct. This was further supported by the fact that when sodium chloride was added this additional peak disappeared however, additional fluoroborate peaks appeared due to fluorine chlorine scrambling as shown in Figure 5-6.<sup>12</sup> It was theorized that by replacement of one or more fluorides of the tetrafluoroborate anion with chlorine was able to disrupt the fluorine-arene interaction and thus separate the adduct that was formed.

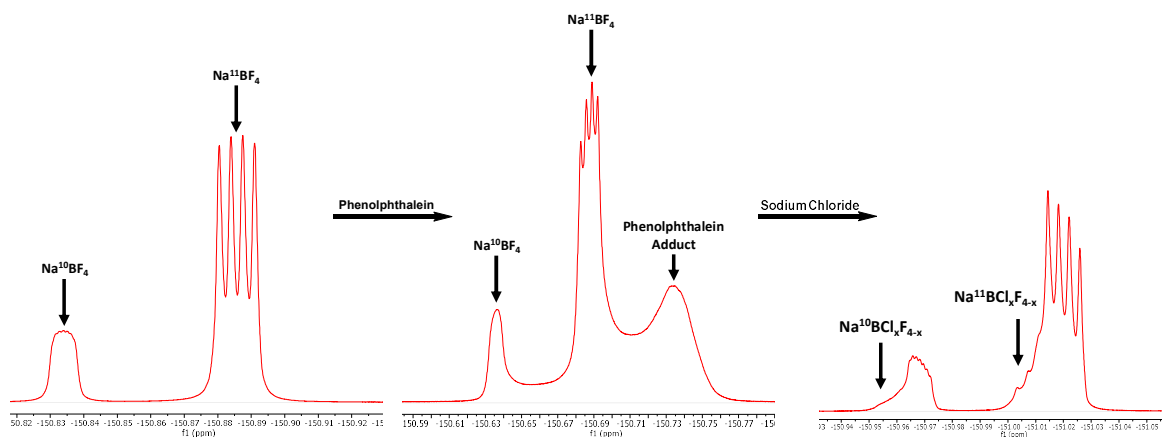


*Figure 5-6 Formation of the  $\text{NaBF}_4$  Phenolphthalein Adduct and Treatment with Sodium Chloride*

It was hypothesized that the three-dimensional shape of the phenolphthalein was responsible for this interaction as the shape of phenolphthalein would be expected to change with protonation state as demonstrated below in Figure 5-7. By deprotonating phenolphthalein, the lactone will open resulting in flattening of the molecule.<sup>12</sup> Once opened, it was theorized that this molecule can undergo fluorine arene electronic interactions to form an unidentified adduct. If this theory is correct by retaining the

based on the three-dimensional structure of the phenolphthalein, we can eliminate the proposed fluorine-arene interaction. The problem with this is of course, is that the geometry is entirely dependent on the pH of the solution and therefore to reform the desired geometry, the phenolphthalein would have to be reprotonated.

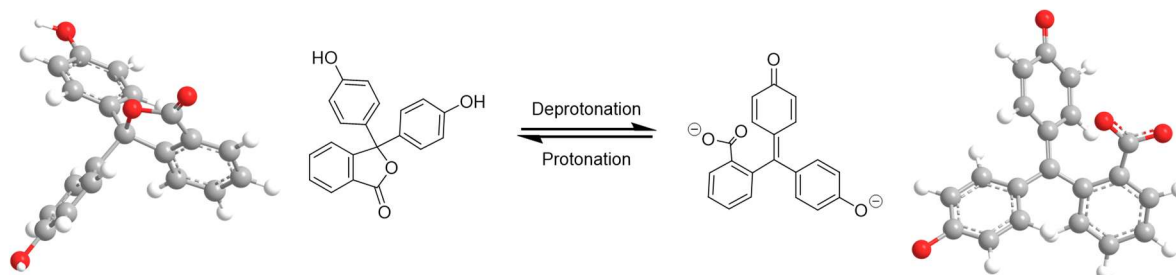


*Figure 5-7 Approximate Three-Dimensional Geometries of Phenolphthalein*

We tried reprotonating the phenolphthalein by adding a small amount of acetic acid. Acetic acid was chosen due to its pKa. As fluoroboric acid is a strong acid with a pKa of approximately -0.4, and acetic acid is a weak acid with a pKa of approximately 5, we postulated that the acetic acid would reprotonate the phenolphthalein without reprotonating the sodium tetrafluoroborate. To our pleasure this worked and eliminated the fluorine peak caused by the addition of the phenolphthalein as shown in Figure 5-8. This concluded our initial method development work on designing a process to oxidize **23**, separate the produced **25** from residual starting material, and install a reporter allowing us to directly measure the boron isotopic distribution by  $^{19}\text{F}$  NMR.

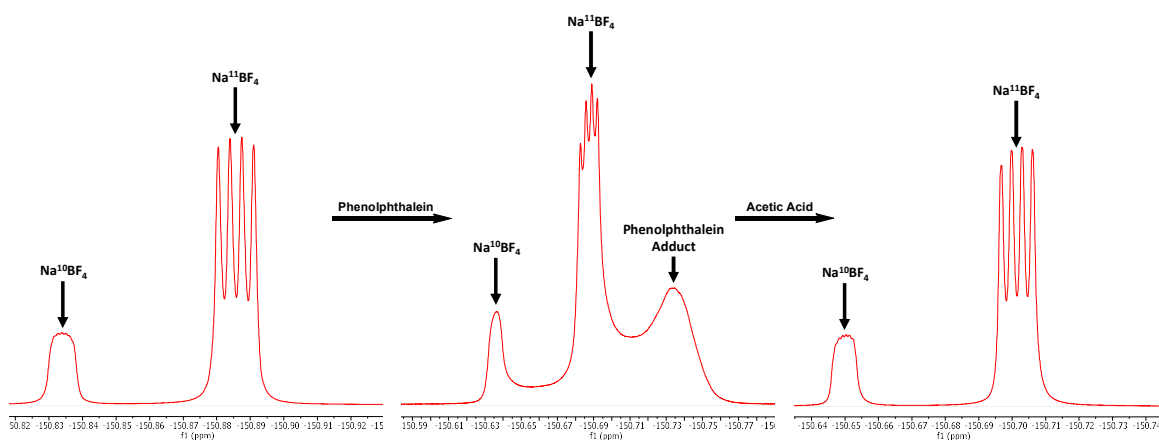


*Figure 5-8 Formation of the  $\text{NaBF}_4$  Phenolphthalein Adduct and Treatment with Acetic Acid*

With this method in hand, we started working on how to spectroscopically measure the boronic isotopic distribution. The crux of this project is to be able to accurately measure the boron isotopic distribution in a sample. To do this we need to measure two values, total weight of the sample and boron isotopic distribution. Weighing the sample is simple enough, however measuring the concentration of each boron isotope is not as simple due to the presence of impurities. The fluorinated sample is inherently not pure due to the presence of additives namely phenolphthalein, however this impurity pales in comparison to the amount of NaF that was produced due to the quenching of excess HF leftover from the fluorination of boric acid. This leaves us with only one option and that is to use an internal standard. Due to the inherent solubility of sodium tetrafluoro borate or rather its insolubility in everything save water or for NMR deuterium oxide, the internal standard must be soluble in water. The obvious standard would simply be a fluoride salt, however due to the sodium fluoride impurity no fluoride salts can be utilized. Additionally, if a salt is to be used as a standard it must have the same counter ions as the tetrafluoroborate, which in this case is balanced by sodium. A different counter ion would interchange with the sodium tetrafluoroborate. Because of this we elected to use dried sodium trifluoroacetate as a standard as this seemed to be the simplest and cleanest.

The final complication we observed was simply the difficulty in accurately measuring masses and integration values. As most modern reactions are often done on sub-gram scales, the masses that are measured are often quite small. As scales have a standard deviation, usually a tenth of a milligram for most common analytical balances, the error in any given measurement is usually around a percent or two at most although, this rises significantly with smaller and smaller masses being measured. Despite this being a reported accuracy, true accuracy is often far worse, which can be illustrated by measuring the same object multiple times on the same scale. As the anticipated perturbation of boron isotopic ratios is expected to be small, accurate measurements are a necessity placing practical limits on the scale of the reactions. To minimize error, we envision doing reactions on the largest reasonable scale and maximizing the mass of products being measured while also averaging multiple mass measurements. Additionally accurate integration of the resulting peaks is imperative. While the  $\text{Na}^{10}\text{BF}_4$  and the  $\text{Na}^{11}\text{BF}_4$  are resolved peaks, they must be carefully integrated. We accomplished this by utilizing two different NMR spectra. First a  $^{19}\text{F}$  NMR spectra was run with a wide spectral window in which we integrated the entirety of the  $\text{NaBF}_4$  as a singular peak. This allowed us to compare it to our internal standard to measure the moles of  $\text{NaBF}_4$  in solution. Second, we collected a spectrum of the  $\text{NaBF}_4$  utilizing a small spectral window of only about 5 ppm. This allows us to have a spectrum of the  $\text{NaBF}_4$  that contains far more critical points in the region of interest resulting in a more resolute peak allowing for more accurate

integration. From here careful integration of the  $\text{Na}^{10}\text{BF}_4$  and the  $\text{Na}^{11}\text{BF}_4$  peaks is possible. As the peaks are very close to each other, integration can be done by integrating from the center of each peak to the mathematical center of between the two isotopic peaks and an equal distance in the opposite direction. Additionally, we collected each of these spectra five times using the same NMR sample so that each integration could be averaged.

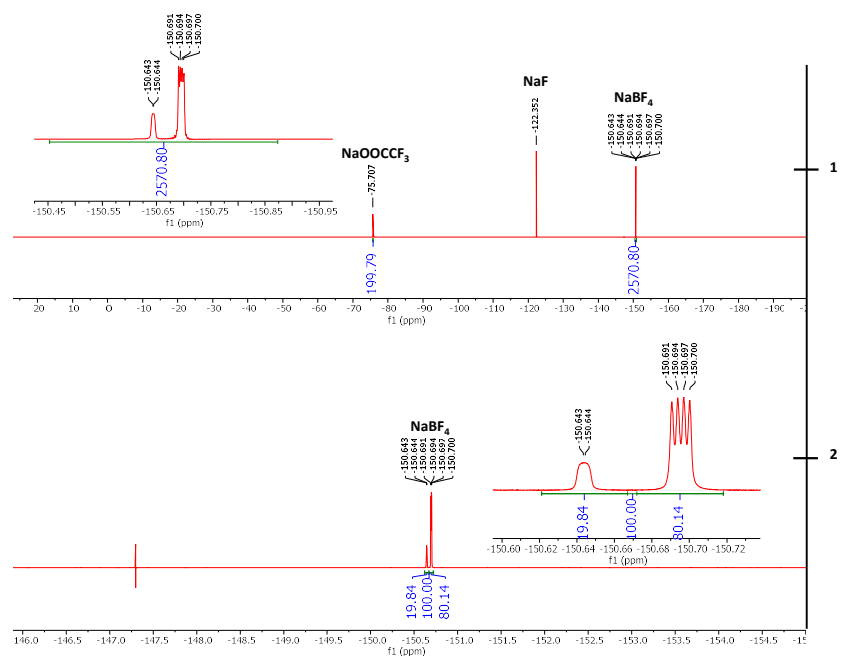


*Figure 5-9 NMR 1 Shows a Full Fluorine Spectral Window with  $\text{NaOCCF}_3$  Internal Standard,  $\text{NaF}$  Biproduct, and  $\text{NaBF}_4$ . NMR 2 Shows the  $\text{NaBF}_4$  Spectrum Taken with a Small Spectral Window*

We are confident that utilizing the method outlined within this chapter the heavy atom kinetic isotope effect can be directly measured for boron related reactions. As of now the method has been developed but not validated and thus future work should start with validation. This method however gives the ability to directly measure boron KIEs though NMR which is accessible to practically all synthetic organic chemists. The biggest benefit is this can be utilized at natural abundance which will avoid costly labeled reagents and the necessity to label starting materials. While we emphasized its use in calculating boron KIE's this method is feasible to any application requiring the measurement or boron isotopic ratios.

## Experimental Procedures

### General Information

All available reagents were used as received unless otherwise indicated. THF was refluxed over Na/benzophenone ketyl and distilled. Anhydrous 1,4-dioxane was obtained through Sigma-Aldrich and used as received.

$^1\text{H}$ ,  $^{13}\text{C}$ ,  $^{11}\text{B}$  and  $^{19}\text{F}$  NMR spectra were recorded on a Varian 500 MHz DD2 Spectrometer equipped with a  $^1\text{H}$ - $^{19}\text{F}/^{15}\text{N}$ - $^{31}\text{P}$  5 mm Pulsed Field Gradient (PFG) Probe. Spectra taken in  $\text{CDCl}_3$  were referenced to 7.26 ppm in  $^1\text{H}$  NMR and 77.2 ppm in  $^{13}\text{C}$  NMR. Spectra taken in  $\text{C}_6\text{D}_6$  were referenced to 7.16 ppm in  $^1\text{H}$  NMR and 128.1 ppm in  $^{13}\text{C}$ .  $^{11}\text{B}$  NMR spectra were referenced to neat  $\text{BF}_3\cdot\text{Et}_2\text{O}$  as the external standard. NMR spectra were processed for display using the MNova software program with only phasing and baseline corrections applied. High-resolution mass spectra (HRMS) were obtained at the Molecular Metabolism and Disease Mass Spectrometry Core facility and at the Mass Spectrometry Service Center at Michigan State University using electrospray ionization (ESI+ or ESI-) on quadrupole time-of-flight (Q-TOF) instruments.

### Oxidation of 1 with $\text{H}_2\text{O}_2$ in Ethanol

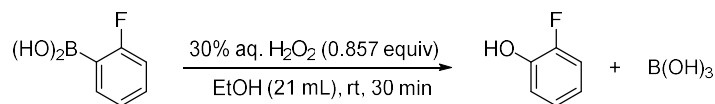


Figure 5-10 Oxidation of 1 with  $\text{H}_2\text{O}_2$  in Ethanol

In a 125 mL Erlenmeyer flask, (2-fluorophenyl)boronic acid (1 g, 7.15 mmol) was dissolved in ethanol (21 mL, 16.57 g, 0.36 mol) with the help of magnetic stirring utilizing a Teflon coated stir bar. To this solution 30% aq.  $\text{H}_2\text{O}_2$  (0.66 mL, 6.46 mmol) was then added. The reaction was stirred for 30 mins at room temperature. The reaction mixture was then evaporated under reduced pressure on a rotavap yielding a white solid. This mass (0.1008 g) was collected and presumed to be boric acid. With this assumption, the total yield of  $\text{B(OH)}_3$  is 14%. Due to the low yield this product was not spectroscopically investigated.

### Addition of Phenolphthalein and Sodium Chloride to Sodium Tetrafluoroborate (Reaction 1)

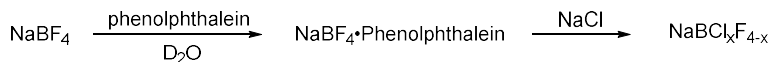
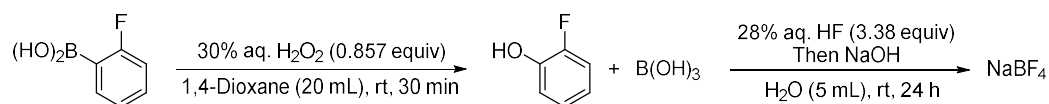


Figure 5-11 Addition of Phenolphthalein and Sodium Chloride to Sodium Tetrafluoroborate (Reaction 1)

A solution of phenolphthalein was made in 1 mL of water by addition of approximately 0.05 g of phenolphthalein and enough sodium hydroxide to allow the phenolphthalein to dissolve. In a quartz

NMR tube, approximately 10 mg of NaBF<sub>4</sub>. Enough of the phenolphthalein solution was then added to cause the phenolphthalein NaBF<sub>4</sub> adduct peak to appear. The addition of the phenolphthalein caused the red color of the phenolphthalein solution to immediately turn colorless. When the adduct peak was clearly observable by <sup>19</sup>F NMR a drop of brine was then added to the solution and the sample was observed via <sup>19</sup>F NMR.

#### Oxidation of (2-fluorophenyl)boronic acid in 1,4-Dioxane (Reaction 2)



*Figure 5-12 Oxidation of (2-fluorophenyl)boronic acid in 1,4-Dioxane (Reaction 2)*

In a new 100 mL round bottom flask, (2-fluorophenyl)boronic acid (1 g, 7.15 mmol) was added with a net Teflon coated stir bar and dissolved in 1,4-dioxane (20 mL, 0.234 mol). 30% aq. H<sub>2</sub>O<sub>2</sub> (2.2 mL, 0.733 g, 0.022 mmol) was added and the reaction stirred at room temperature for 1 h. The 1,4-dioxane was then evaporated under a stream of nitrogen. The resulting white solid was then transferred into a 50 mL plastic conical bottom centrifuge tube with a small stir bar using 5 mL of water. 28% aq. HF (1.5 mL, 0.48 g, 0.024 mmol) was then added and the reaction stirred at room temperature for 24 h. The solution was then neutralized with 3M aq. NaOH while following the neutralization process with pH paper. The water was then evaporated by leaving the container uncovered resulting in 1.3698 g of a white solid consisting predominately of NaBF<sub>4</sub> and NaF. This solid was transferred to a plastic bag and homogenized by grinding to a fine powder by rolling a vial over the bag and mixing the resulting powder. 4.7 mg of this powder was mixed with 0.295 mg of sodium trifluoro acetate and dissolved into 0.6 mL of D<sub>2</sub>O in a quartz NMR tube.

#### Synthesis of sodium tetrafluoroborate from boric acid (Reaction 3)

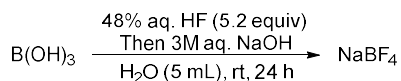


*Figure 5-13 Synthesis of sodium tetrafluoroborate from boric acid (Reaction 3)*

In a 50 mL plastic conical bottom centrifuge tube with a small stir bar boric acid (1g, 0.016 mmol) using 5 mL of water. 28% aq. HF (2.5 mL, 1.38 g, 0.069 mmol) was then added and the reaction stirred at room temperature for 24 h. The solution was then neutralized with 3M aq. NaOH while following the neutralization with pH paper. The water was then evaporated from the reaction mixture to yield 3.0952 g of a white solid. This solid was transferred to a plastic bag and homogenized by grinding to a fine powder

by rolling a vial over the bag and mixing the resulting powder. 51.8 mg of this powder was mixed with 0.38 mg of sodium trifluoro acetate and dissolved into 0.6 mL of D<sub>2</sub>O in a quartz NMR tube.

#### Oxidation of 1 using acetonitrile as a solvent (Reaction 5)

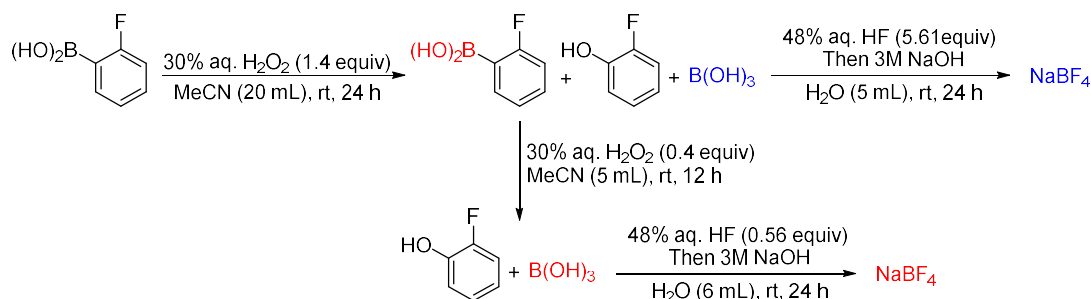


Figure 5-14 Oxidation of 1 using acetonitrile as a solvent (Reaction 5)

In a 100 mL round bottom flask, (2-fluorophenyl)boronic acid (1 g, 7.15 mmol) was dissolved in acetonitrile (20 mL, 15.72 g, 383 mmol) using a stir bar. 30% aq. H<sub>2</sub>O<sub>2</sub> (1 mL, 0.33 g, 10 mmol) was then added and the reaction flask sealed with a glass stopper. The reaction was stirred for 24 hours. The reaction flask was then opened, and the acetonitrile evaporated under a stream of nitrogen. The remaining white solid was then dissolved in H<sub>2</sub>O (20 mL) and extracted into CHCl<sub>3</sub> (50 mL, 3x). The two layers were separated. The water layer containing boric acid was designated as the primary oxidation. The CHCl<sub>3</sub> layer was collected and evaporated to yield the remaining (2-fluorophenyl)boronic acid. The remaining (2-fluorophenyl)boronic acid was then dissolved in acetonitrile (5 mL, g, mmol) and 30% aq. H<sub>2</sub>O<sub>2</sub> (0.25 mL, 0.08325 g, 2.5 mmol) added. This reaction was stirred at room temperature for 12 hours. This reaction was then evaporated to yield boric acid as a white powder designated secondary oxidation. The primary oxidation products were then dissolved in H<sub>2</sub>O (5 mL) and 48% aq. HF (1.5 mL, 0.828 g, 41.39 mmol) added after which the reaction was stirred at room temperature for 24 hours. To the secondary oxidation, the boric acid was dissolved in H<sub>2</sub>O (6 mL) and 48% aq. (0.15 mL, 0.0828 g, 4.139 mmol) added after which the reaction was stirred for 24 hours. After reacting with HF, both oxidation reactions were neutralized by first adding a drop of a phenolphthalein indicator solution (0.2g phenolphthalein in 2 mL of H<sub>2</sub>O with enough NaOH to make it soluble), then adding a 1M Na<sub>2</sub>C<sub>2</sub>O<sub>3</sub> until a slight pink color appeared after which the reactions were evaporated to dryness.

#### Study of Additive effects on the <sup>19</sup>F NMR peak of NaBF<sub>4</sub> (Reaction 6)

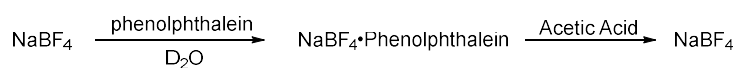


Figure 5-15 Study of Additive effects on the <sup>19</sup>F peak of NaBF<sub>4</sub> (Reaction 6)

A quartz NMR tube was charged with  $\text{NaBF}_4$  (5.8 mg, 0.0528 mmol) and  $\text{D}_2\text{O}$  (0.5 mL). The mixture was then analyzed by NMR. After analysis, 0.1 mL of a sodium trifluoroacetate solution (463 mg per 10 mL  $\text{D}_2\text{O}$ ) was added and the solution analyzed by NMR. Then a drop of a phenolphthalein solution in  $\text{D}_2\text{O}$  with enough  $\text{Na}_2\text{CO}_3$  added to keep the phenolphthalein soluble. The solution was analyzed by NMR. After analysis, 1 drop of glacial acetic acid was added to the solution and the solution analyzed by NMR.



## REFERENCES

- (1) Paneth, P. Some Analytical Aspects of the Measurement of heavy-Atom Kinetic Isotope Effects *Talanta* **1987**, *34*, 877-883.
- (2) Kinetic Isotope Effects,  
[https://chem.libretexts.org/Bookshelves/Physical\\_and\\_Theoretical\\_Chemistry\\_Textbook\\_Maps/Supplemental\\_Modules\\_\(Physical\\_and\\_Theoretical\\_Chemistry\)/Quantum\\_Mechanics/06.\\_One\\_Dimensional\\_Harmonic\\_Oscillator/Kinetic\\_Isotope\\_Effects](https://chem.libretexts.org/Bookshelves/Physical_and_Theoretical_Chemistry_Textbook_Maps/Supplemental_Modules_(Physical_and_Theoretical_Chemistry)/Quantum_Mechanics/06._One_Dimensional_Harmonic_Oscillator/Kinetic_Isotope_Effects), Accessed 12-5-2023.
- (3) Singleton, D. A.; Szymanski, M. J. Simultaneous Determination of Intermolecular and Intramolecular <sup>13</sup>C and <sup>2</sup>H Kinetic Isotope Effects at Natural Abundance *J. Am. Chem. Soc.* **1999**, *121*, 9455- 9456.
- (4) Singleton, D. A.; Thomas, A. A. High-Precision Simultaneous Determination of Multiple Small Kinetic Isotope Effects at Natural Abundance *J. Am. Chem. Soc.* **1995**, *117*, 9357-9358.
- (5) Chkhartishvili, L. Isotopic Effects of Boron. *Trends Inorg. Chem* **2009**, *11*, 105–167.
- (6) Matteson, D. S.; Waldbilling, J. O.; Peterson, S. W. Isotope Effects in Mercurideboronations Measured by Neutron Absorption **1964**, *86*, 3781-3783.
- (7) Cox, P. A.; Reid, R.; Leach, A. G., Campbell, A. D.; King, E. J.; Lloyd-Jones, G. C. Base-Catalyzed Aryl-B(OH)<sub>2</sub> Protodeboronation Revisited: From Concerted Proton Transfer to Liberation of a Transient Aryl Anion *J. Am. Chem. Soc.* **2017**, *139*, 13156-13165.
- (8) Gonzalez, J. A.; Ogba, O. M.; Morehouse, G. F.; Rosson, N.; Houk, K. N.; Leach, A. G.; Cheong, P. H.-Y.; Burke, M. D.; Lloyd-Jones, G. C. MIDA Boronates Are Hydrolysed Fast and Slow by Two Different Mechanisms. *Nat. Chem.* **2016**, *8*, 1067–1075.
- (9) Perrin, C. L.; Dong, Y. Secondary Deuterium Isotope Effects on the Acidity of Carboxylic Acids and Phenols. *J. Am. Chem. Soc.* **2007**, *129*, 4490–4497.
- (10) <https://u-of-o-nmr-facility.blogspot.com/2017/08/boron-isotope-effects-in-fluorine-nmr.html>, Accessed 12-5-2023.
- (11) Brauer, G. Brauer, G. HANDBOOK OF PREPARATIVE INORGANIC CHEMISTRY Vol. I, 2nd ed. 1963. Academic Press INC. **1963**.
- (12) Hartman, J. S.; Schrobilgen, G. J. Mixed Tetrahaloborate Ions. Detection and Study by Nuclear Magnetic Resonance *Inorg. Chem.* **1972**, *11*, 940-951.
- (13) Tamura, Z.; Abe, S.; Ito, K.; Maeda, M. Spectrophotometric Analysis of the Relationship between Dissociation and Coloration, and of the Structural Formulas of Phenolphthalein in Aqueous Solution *Anal. Sci.* **1996**, *12*, 927–930.

# APPENDIX A: NMR SPECTRA

## Chapter 2 NMR Spectra <sup>1</sup>H NMR Spectra of [Ir(OMe)cod]<sub>2</sub>

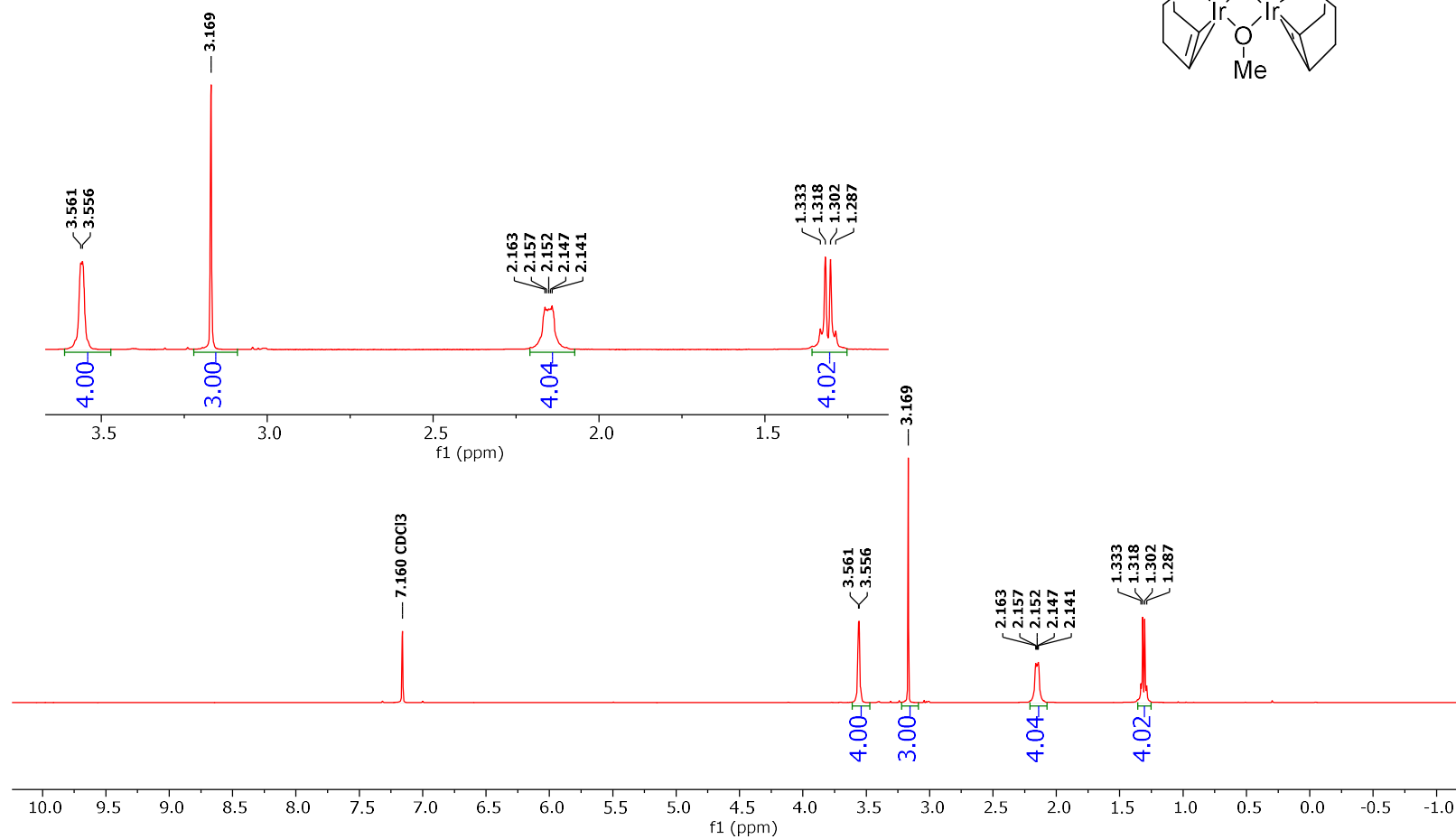
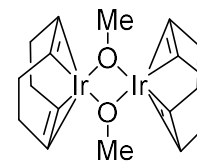


Figure 6-1 Conditions: 25 °C, 500 MHz, CDCl<sub>3</sub>

<sup>13</sup>C NMR Spectra of [Ir(OMe)cod]<sub>2</sub>

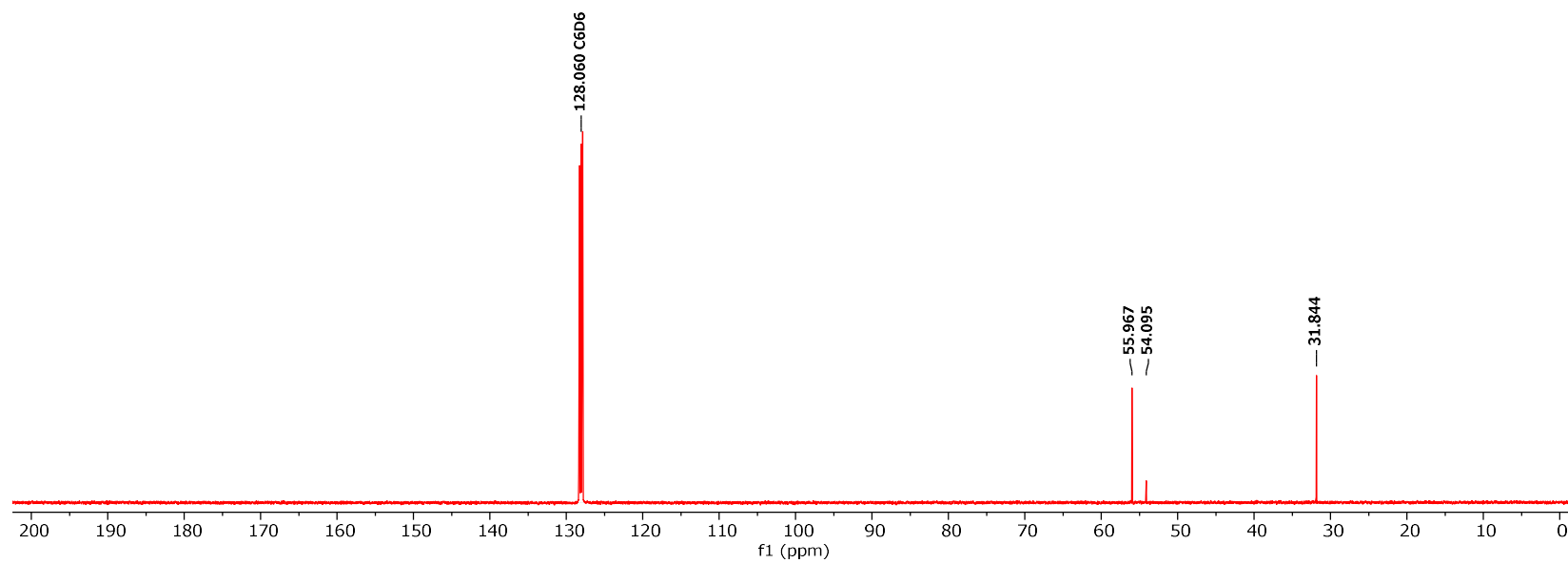
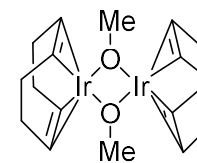


Figure 6-2 Conditions: 25 °C, 500 MHz, CDCl<sub>3</sub>

<sup>1</sup>H NMR Spectra of Bipyrazine

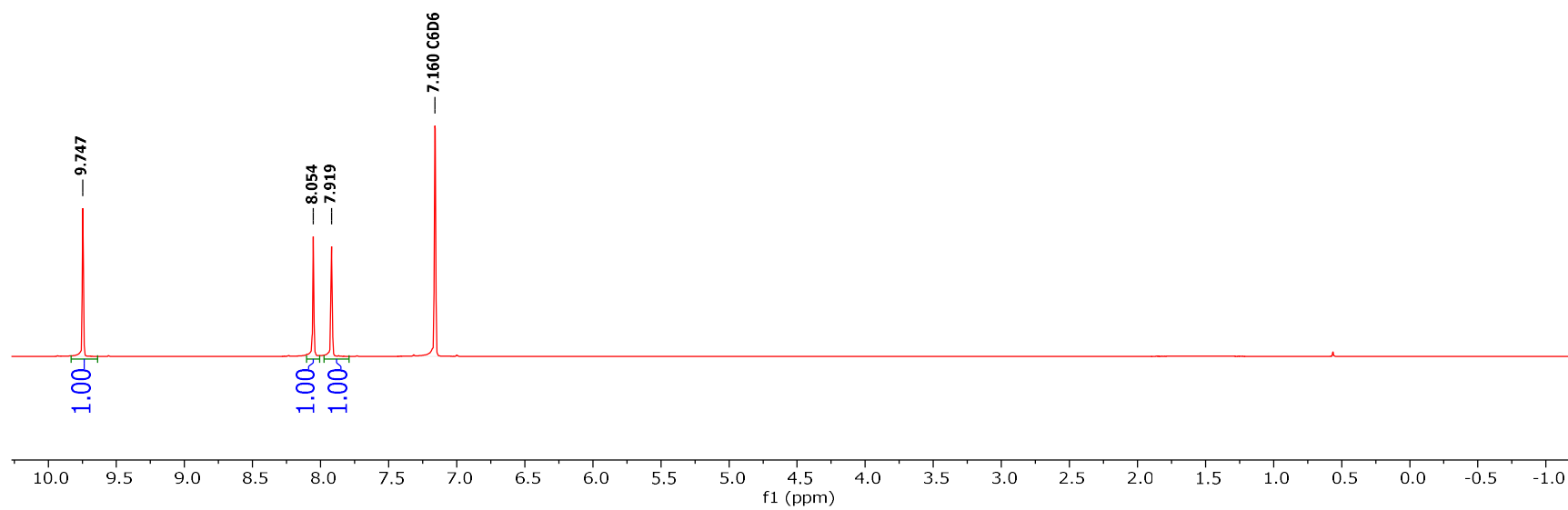
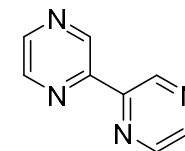


Figure 6-3 Conditions: 25 °C, 500 MHz, CDCl<sub>3</sub>

# <sup>1</sup>H NMR Spectra of Bipyrazine

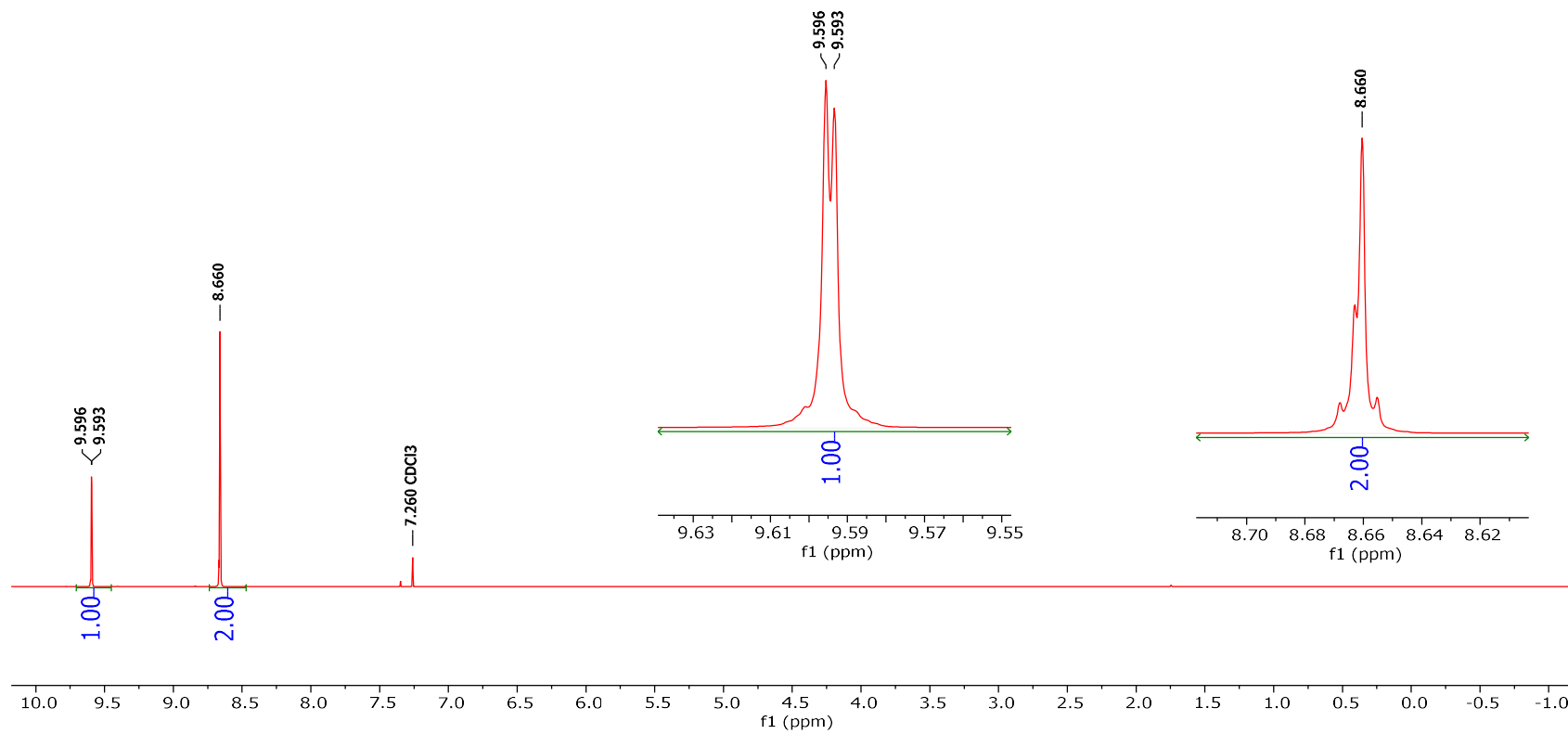
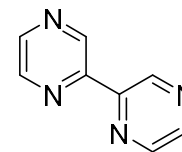


Figure 6-4 Conditions: 25 °C, 500 MHz, C<sub>6</sub>D<sub>6</sub>

<sup>13</sup>C NMR Spectra of Bipyrazine

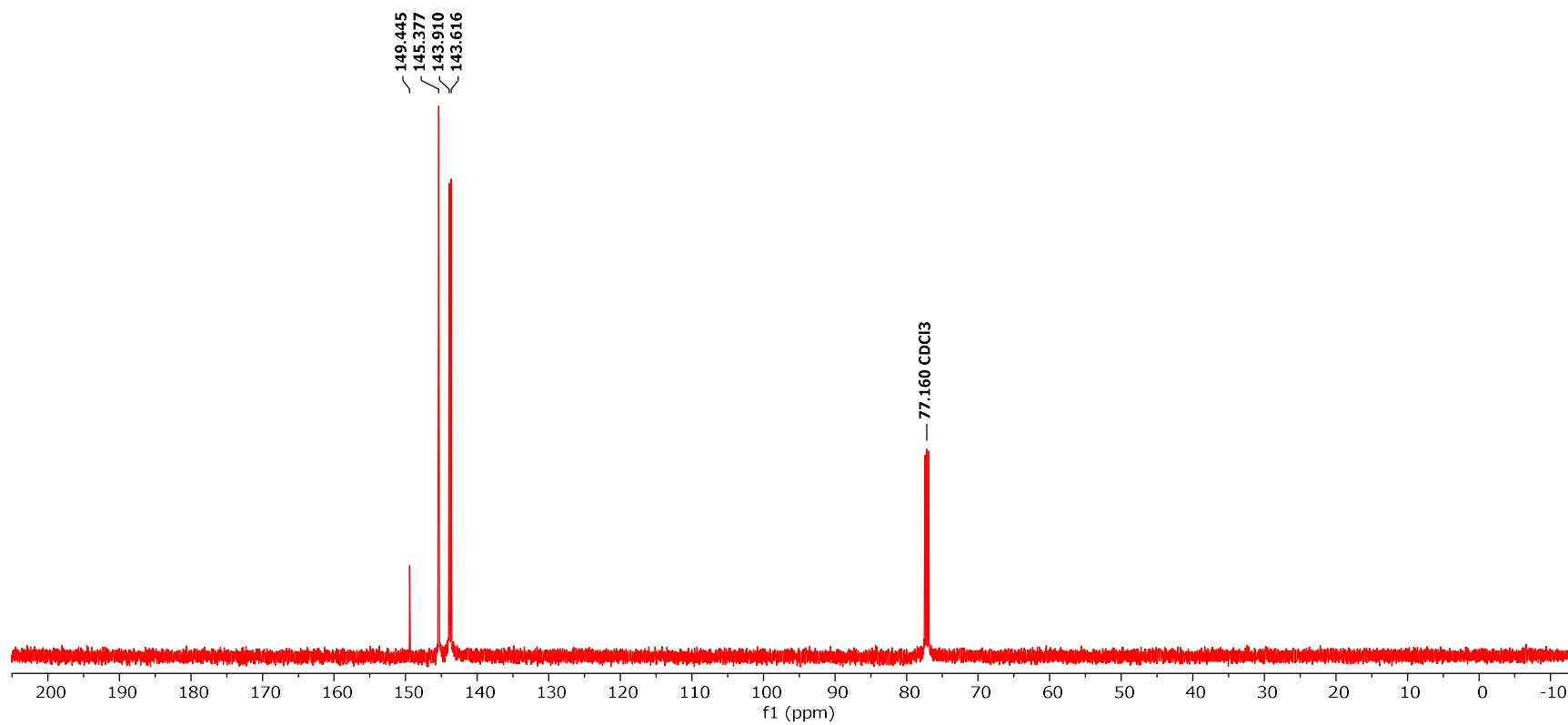
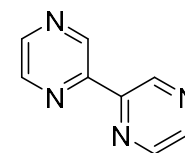


Figure 6-5 Conditions: 25 °C, 126 MHz, CDCl<sub>3</sub>

<sup>1</sup>H NMR of Ligand-213

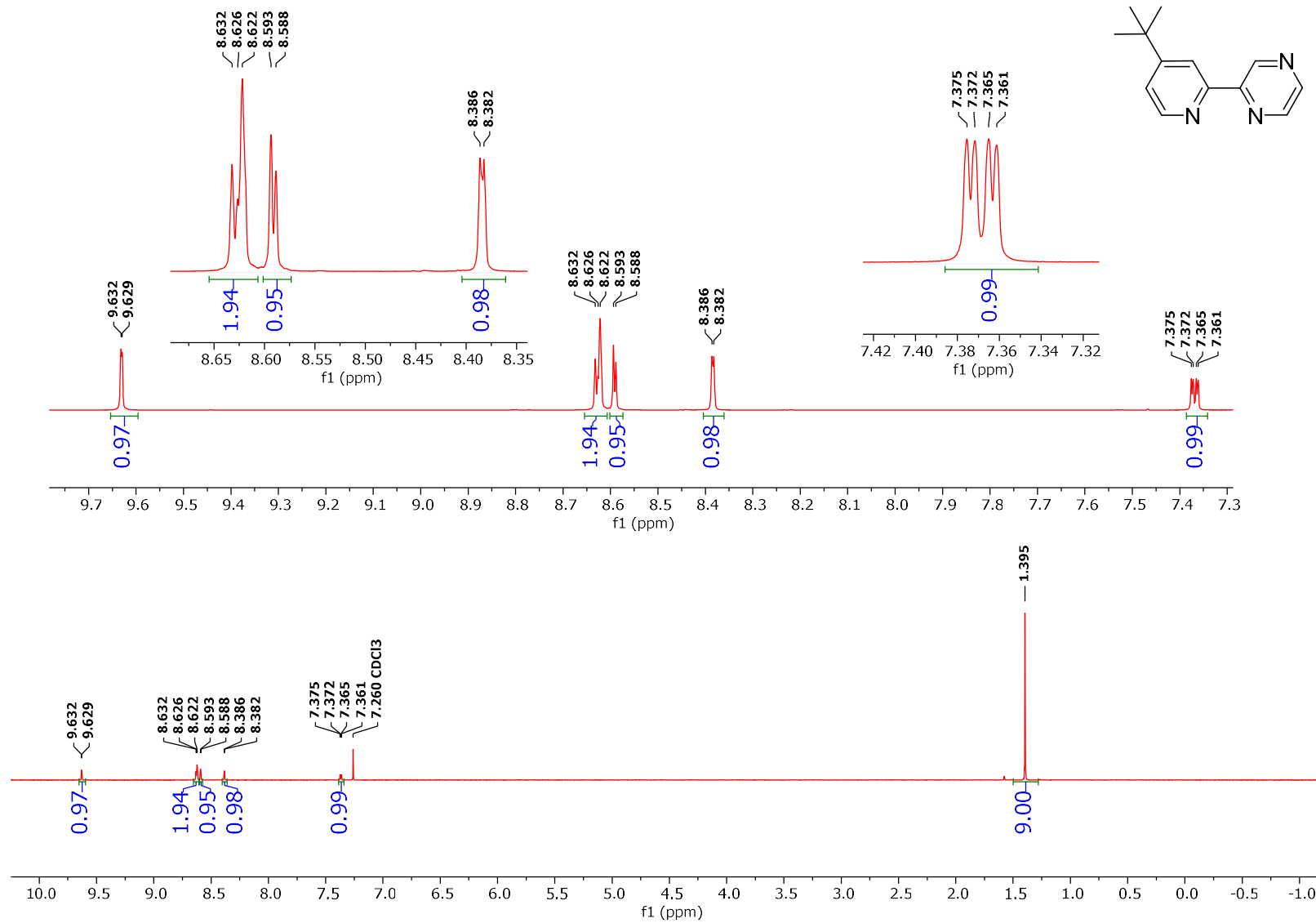


Figure 6-6 Conditions: 25 °C, 500 MHz, CDCl<sub>3</sub>

**$^{13}\text{C}$  NMR Spectra of Ligand-213**

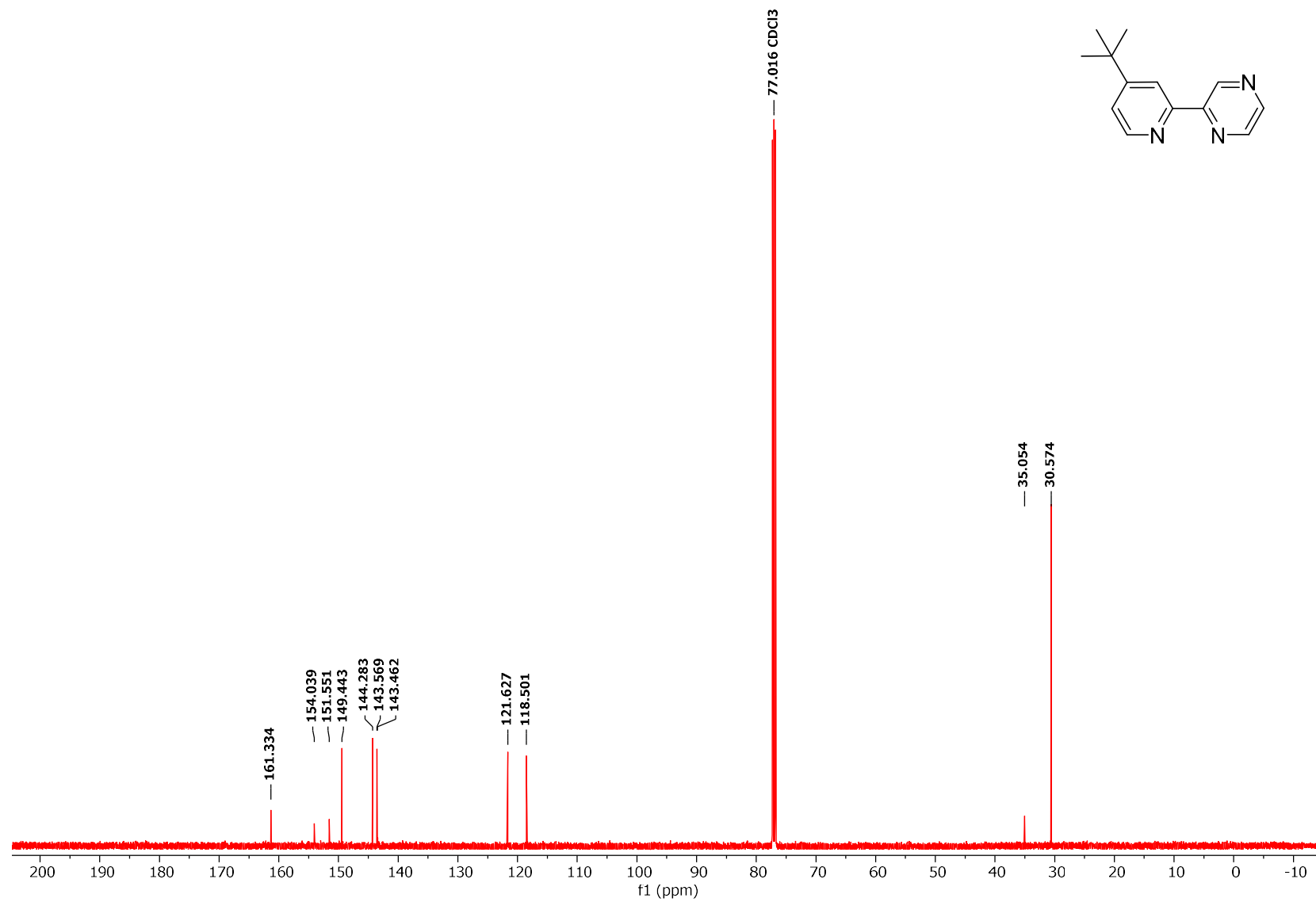


Figure 6-7 Conditions: 25 °C, 126 MHz, CDCl<sub>3</sub>



<sup>1</sup>H NMR of 4,4,5,5-tetramethyl-2-(4-(trifluoromethyl)phenyl)-1,3,2-dioxaborolane (1b)

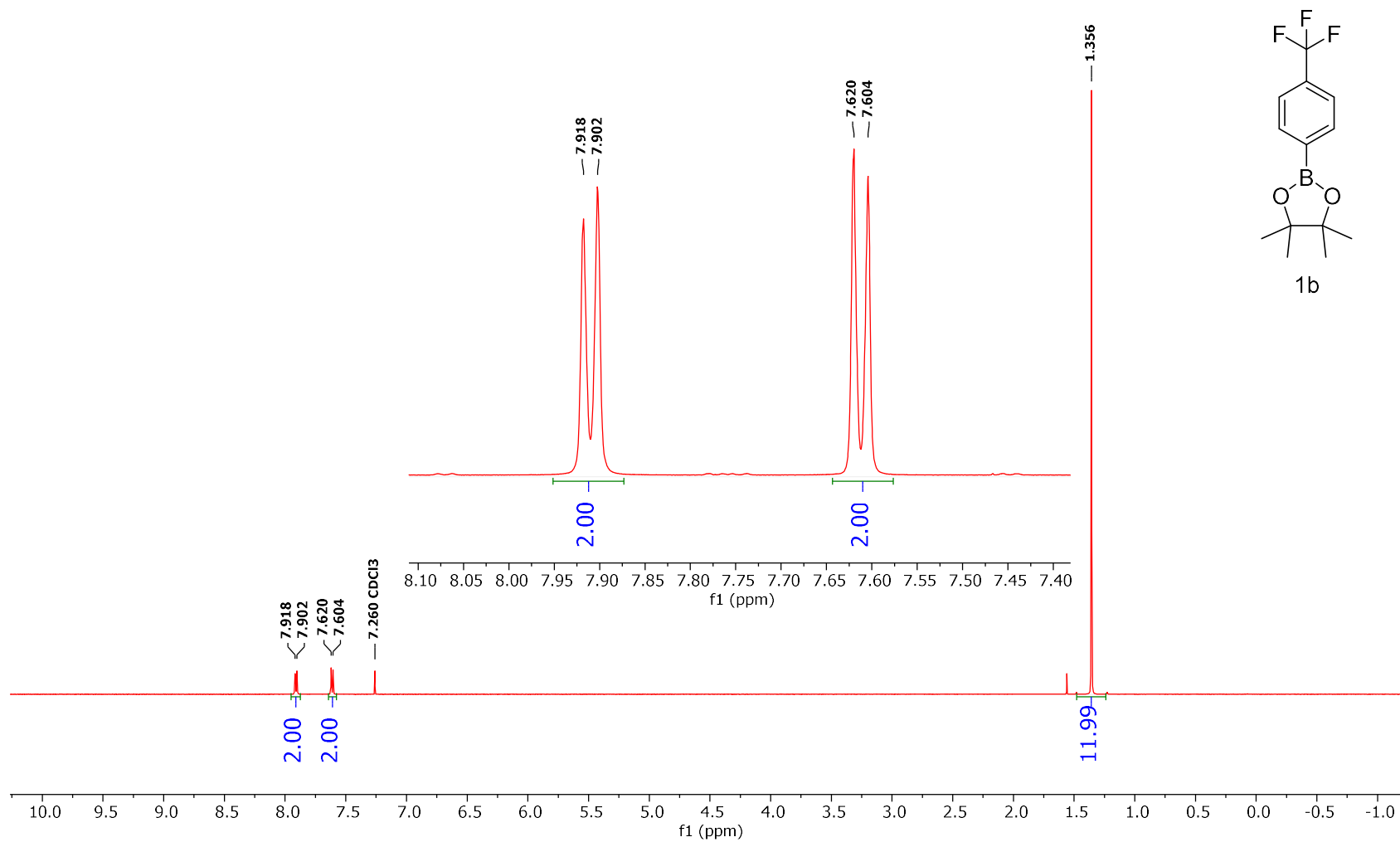


Figure 6-8 Conditions: 25 °C, 500 MHz, CDCl<sub>3</sub>

**$^{19}\text{F}$  NMR of 4,4,5,5-tetramethyl-2-(4-(trifluoromethyl)phenyl)-1,3,2-dioxaborolane (1b)**

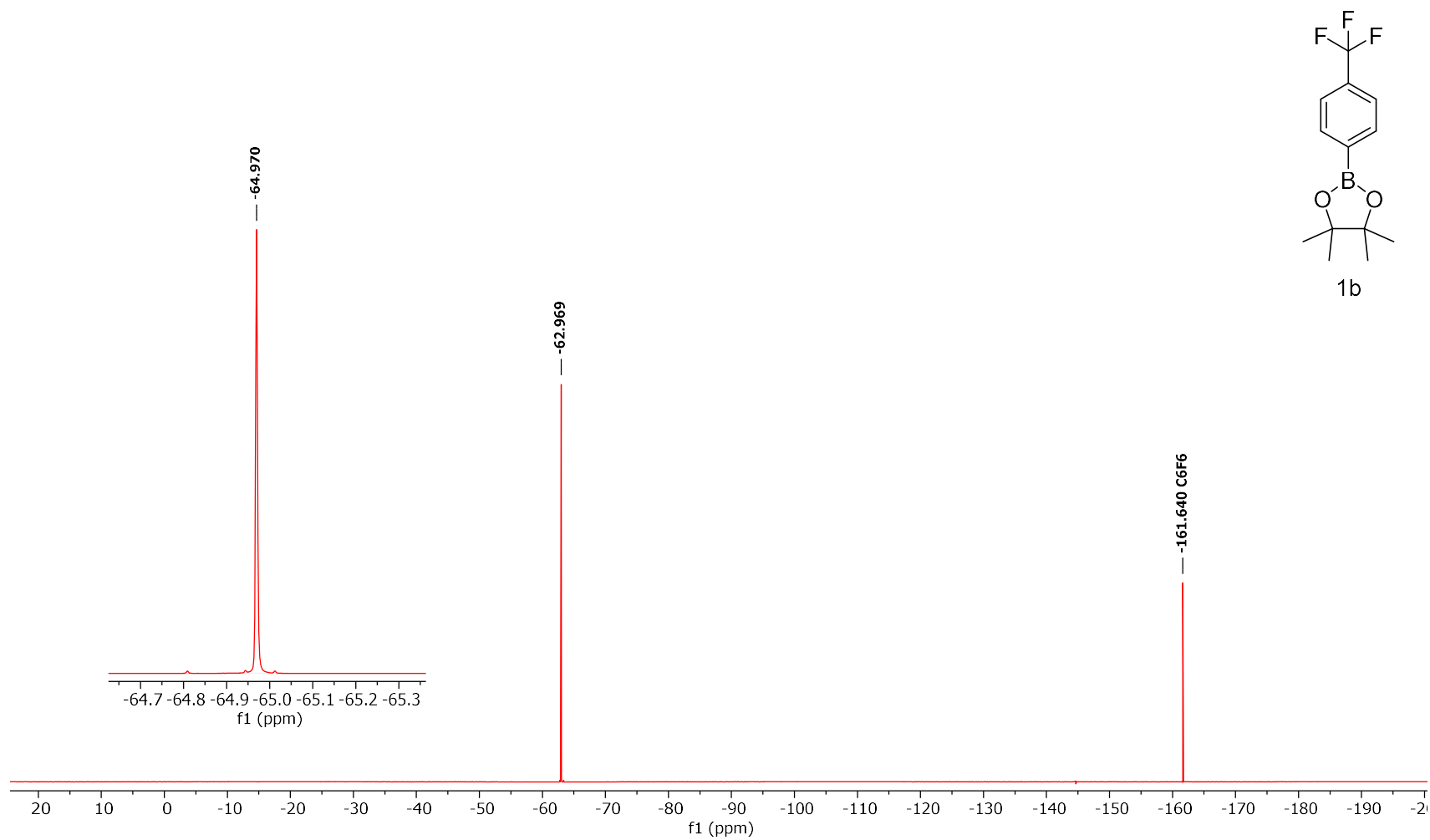


Figure 6-9 Conditions: 25 °C, 470 MHz, CDCl<sub>3</sub>, Referenced with C<sub>6</sub>F<sub>6</sub> at -161.64

<sup>13</sup>C NMR of 4,4,5,5-tetramethyl-2-(4-(trifluoromethyl)phenyl)-1,3,2-dioxaborolane (1b)

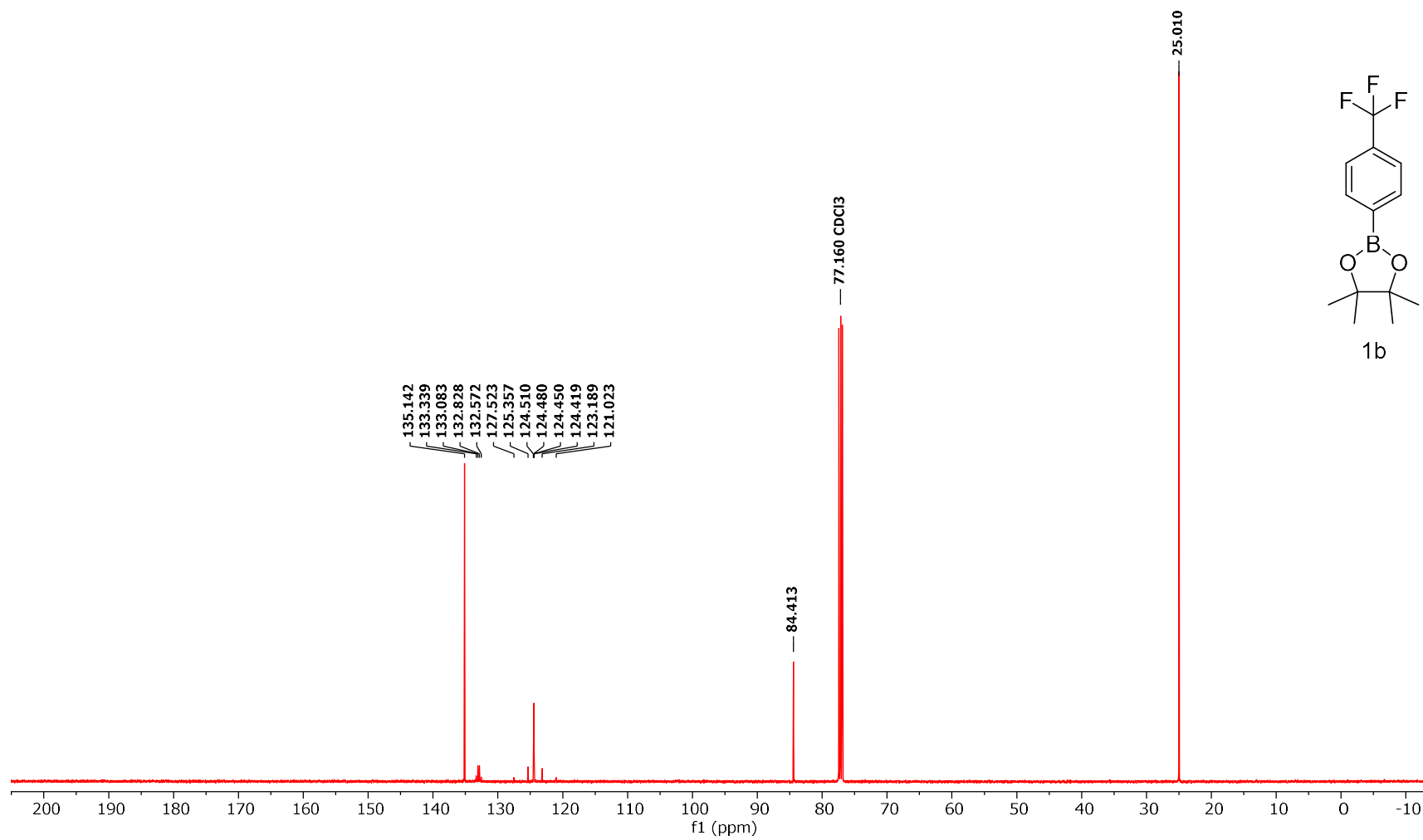


Figure 6-10 Conditions: 25 °C, 126 MHz, CDCl<sub>3</sub>

<sup>11</sup>B NMR of 4,4,5,5-tetramethyl-2-(4-(trifluoromethyl)phenyl)-1,3,2-dioxaborolane (1b)

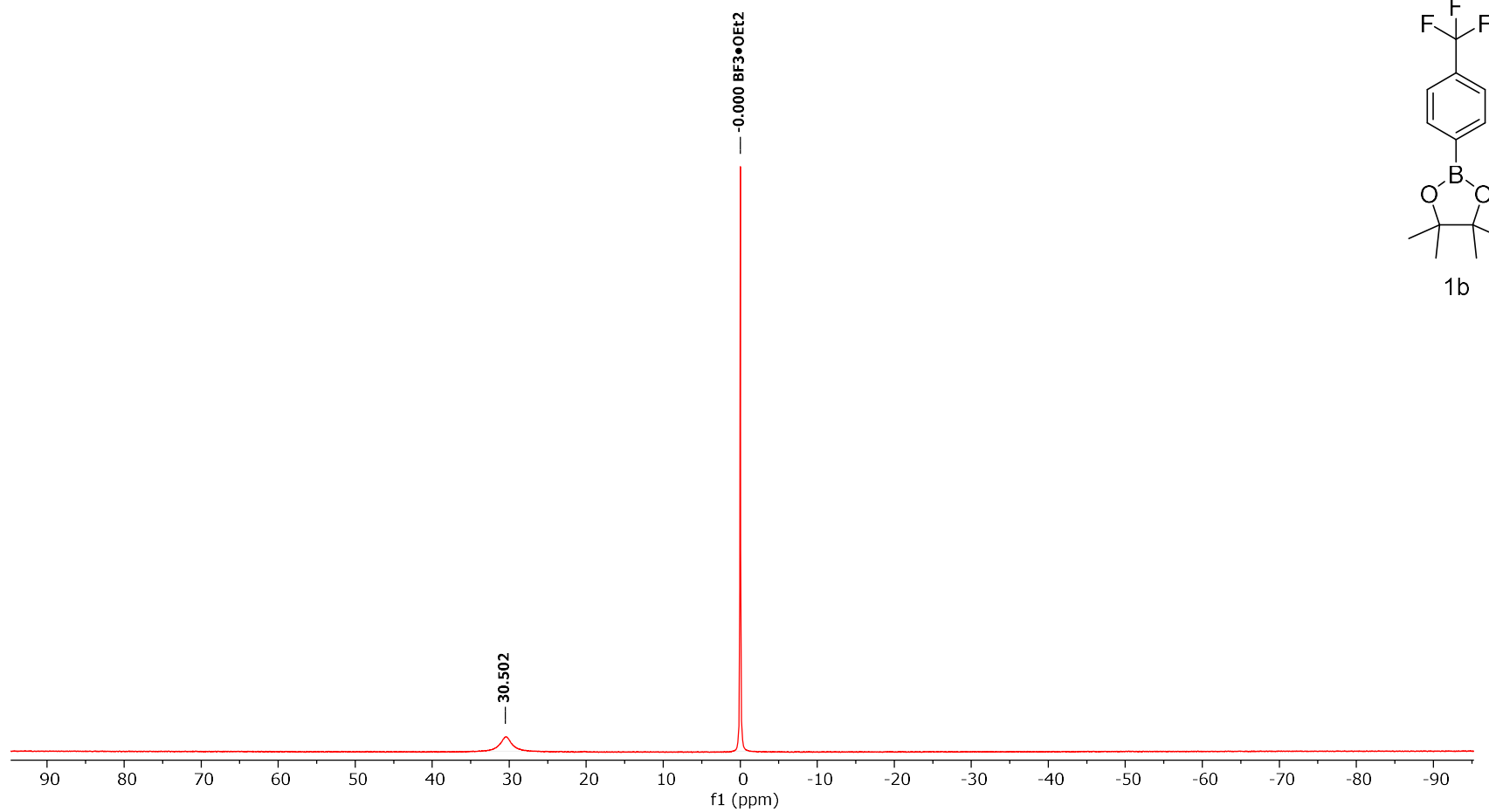


Figure 6-11 Conditions: 25 °C, 160 MHz, CDCl<sub>3</sub>, Referenced with BF<sub>3</sub>•OEt<sub>2</sub> at 0.00

<sup>1</sup>H NMR Spectra of 4,4,5,5-tetramethyl-2-(4-(trifluoromethoxy)phenyl)-1,3,2-dioxaborolane (1c)

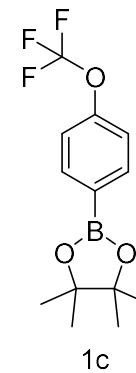
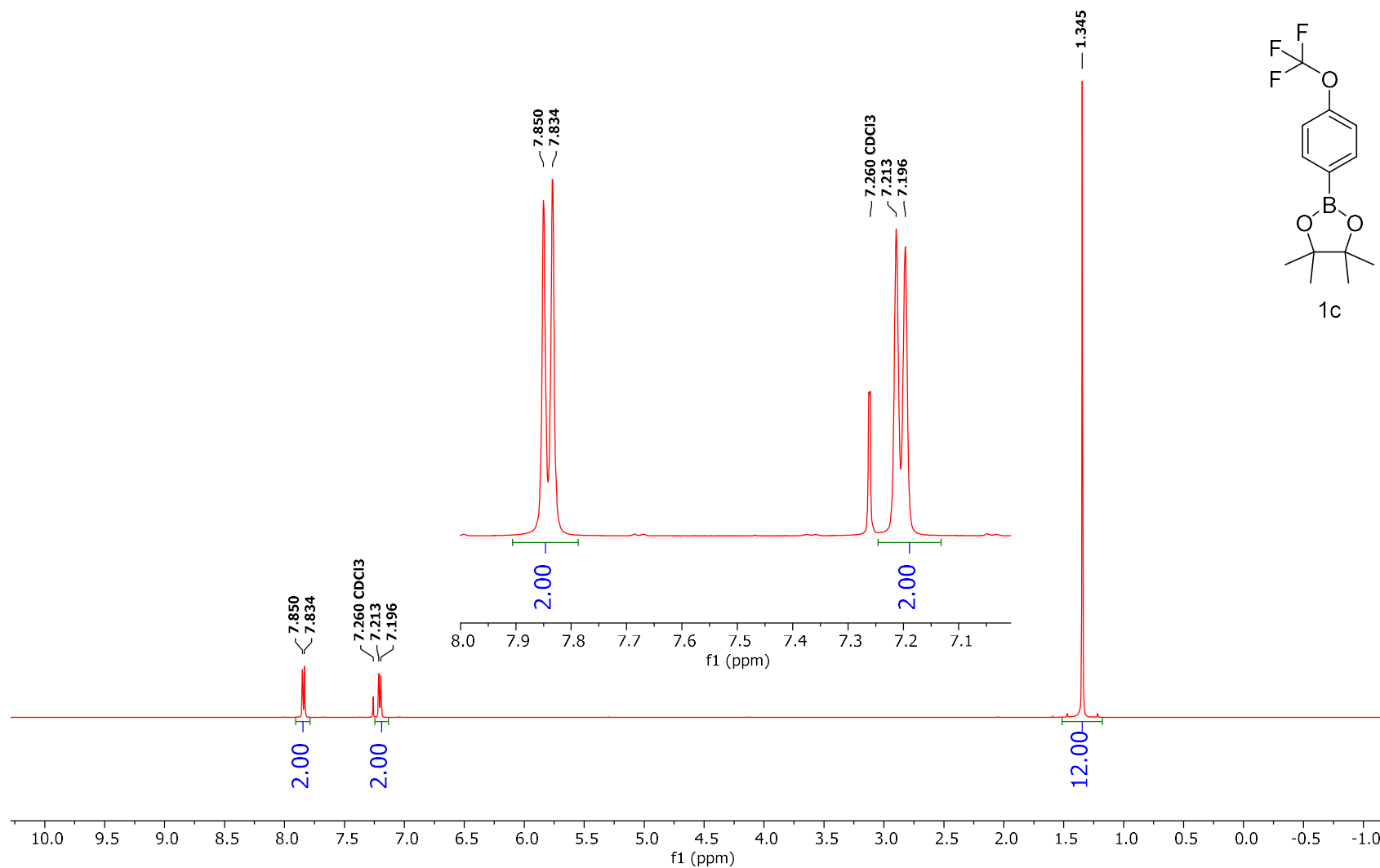


Figure 6-12 Conditions: 25 °C, 500 MHz, CDCl<sub>3</sub>

**$^{19}\text{F}$  NMR Spectra of 4,4,5,5-tetramethyl-2-(4-(trifluoromethoxy)phenyl)-1,3,2-dioxaborolane (1c)**

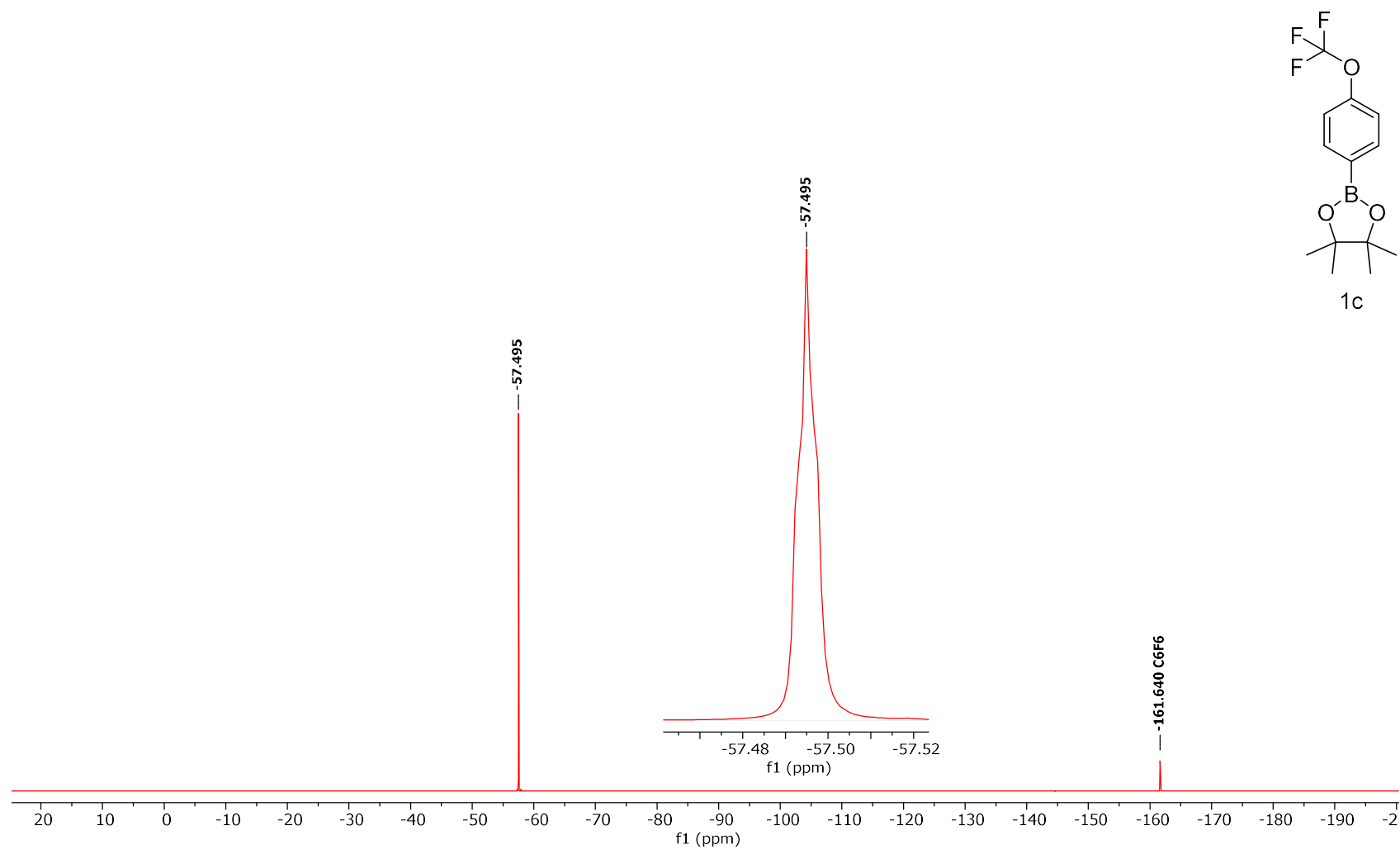


Figure 6-13 Conditions: 25 °C, 470 MHz,  $\text{CDCl}_3$ , Referenced with  $\text{C}_6\text{F}_6$  at -161.64

<sup>13</sup>C NMR Spectra of 4,4,5,5-tetramethyl-2-(4-(trifluoromethoxy)phenyl)-1,3,2-dioxaborolane (1c)

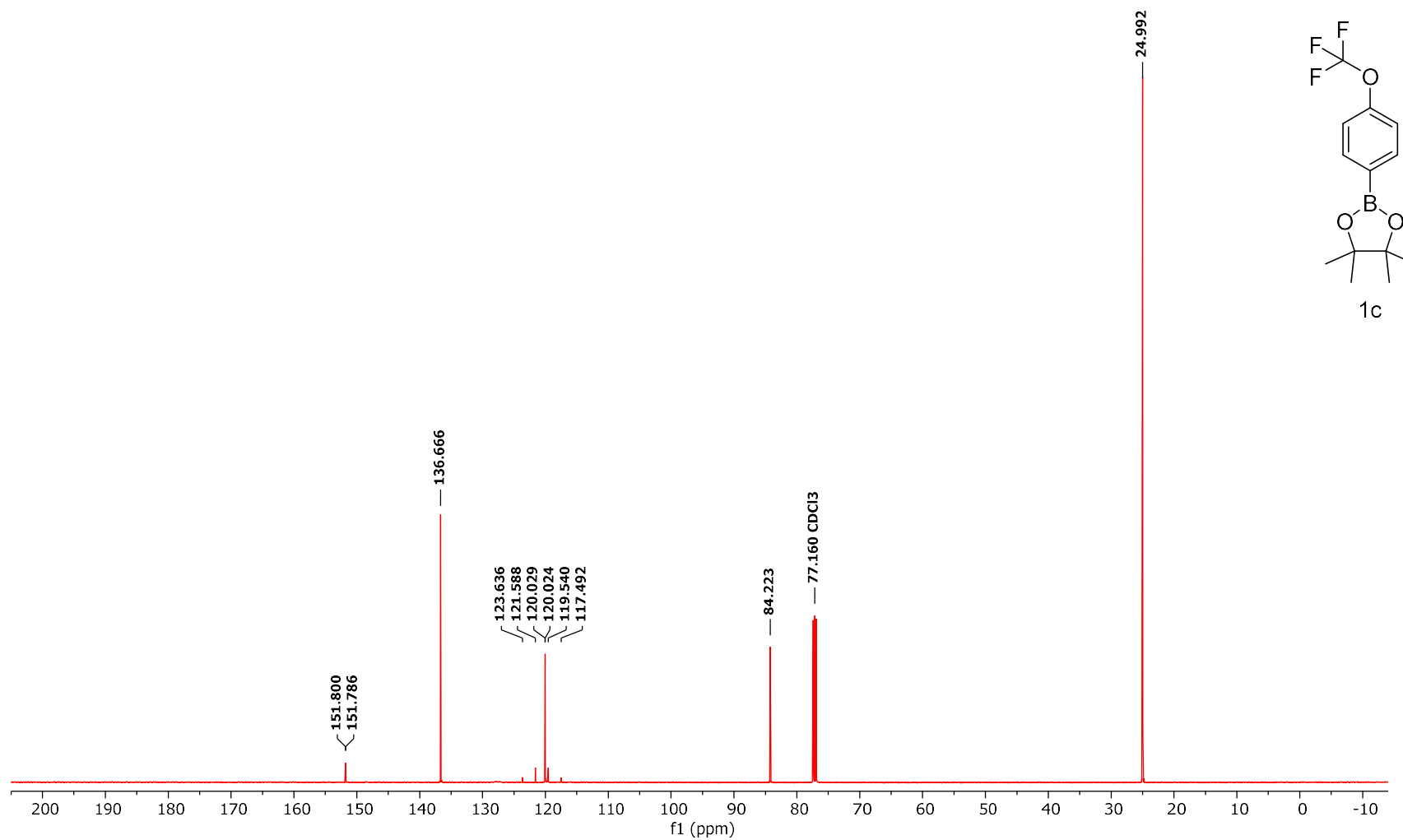


Figure 6-14 Conditions: 25 °C, 126 MHz, CDCl<sub>3</sub>

**$^{11}\text{B}$  NMR Spectra of 4,4,5,5-tetramethyl-2-(4-(trifluoromethoxy)phenyl)-1,3,2-dioxaborolane (1c)**

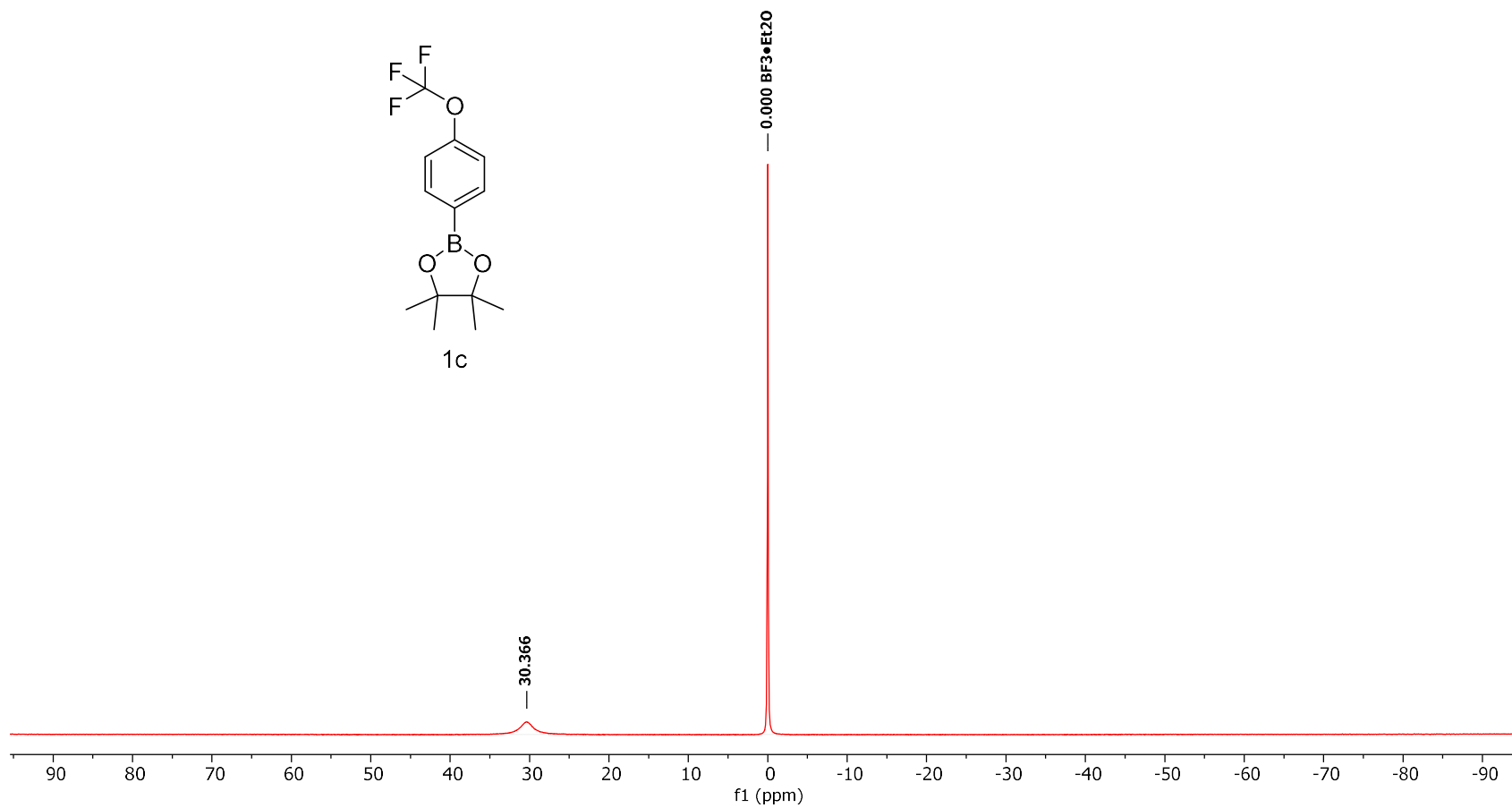


Figure 6-15 Conditions: 25 °C, 160 MHz,  $\text{CDCl}_3$ , Referenced with  $\text{BF}_3 \cdot \text{OEt}_2$  at 0.00



**<sup>1</sup>H NMR Spectra of 2-(4-chloro-2-fluoro-3-methoxyphenyl)-4,4,5,5-tetramethyl-1,3,2-dioxaborolane (1d)**

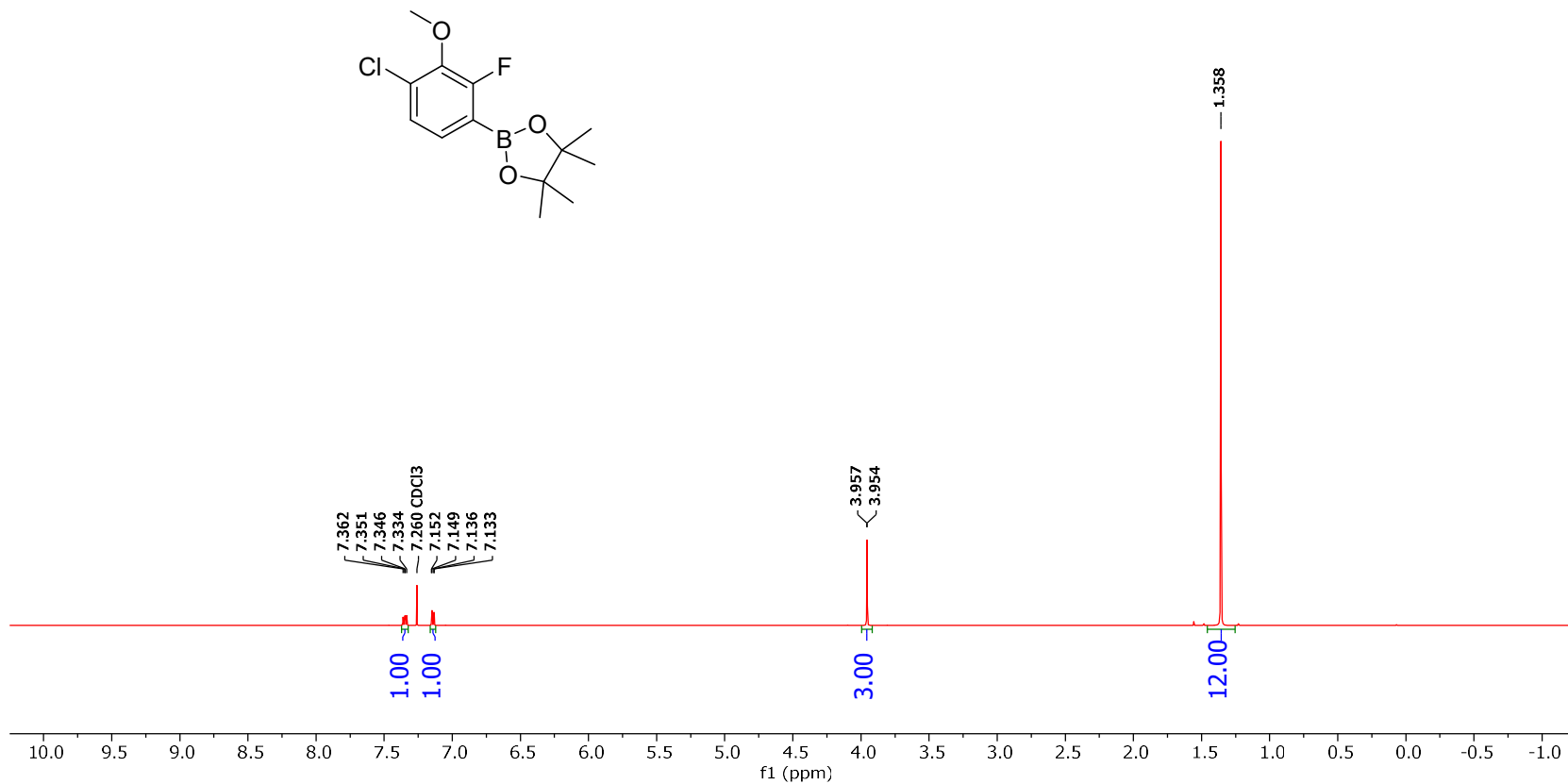


Figure 6-16 Conditions: 25 °C, 500 MHz, CDCl<sub>3</sub>

**$^{19}\text{F}$  NMR Spectra of 2-(4-chloro-2-fluoro-3-methoxyphenyl)-4,4,5,5-tetramethyl-1,3,2-dioxaborolane (1d)**

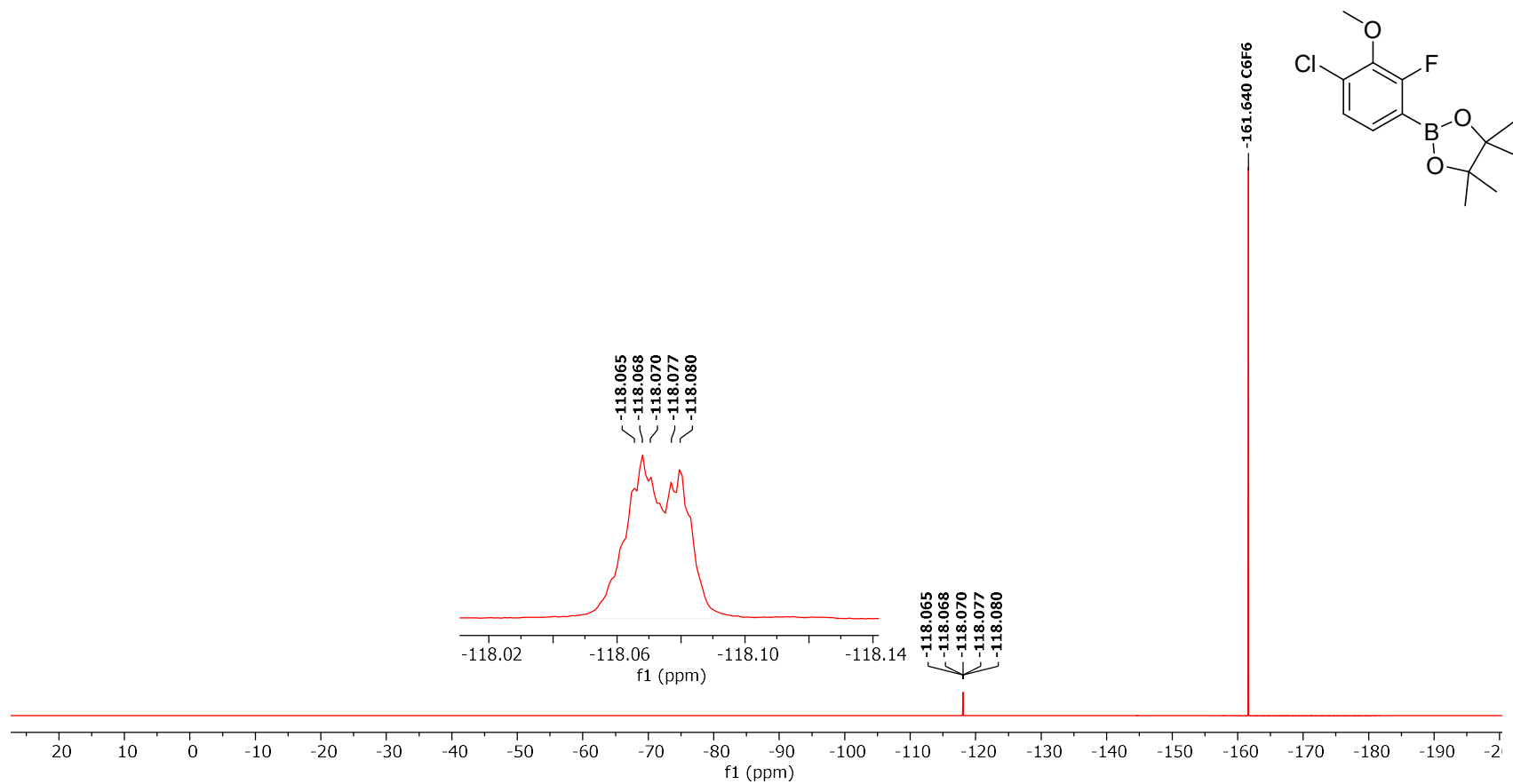


Figure 6-17 Conditions: Conditions: 25 °C, 470 MHz,  $\text{CDCl}_3$ , Referenced with  $\text{C}_6\text{F}_6$  at -161.64

**$^{13}\text{C}$  NMR Spectra of 2-(4-chloro-2-fluoro-3-methoxyphenyl)-4,4,5,5-tetramethyl-1,3,2-dioxaborolane (1d)**

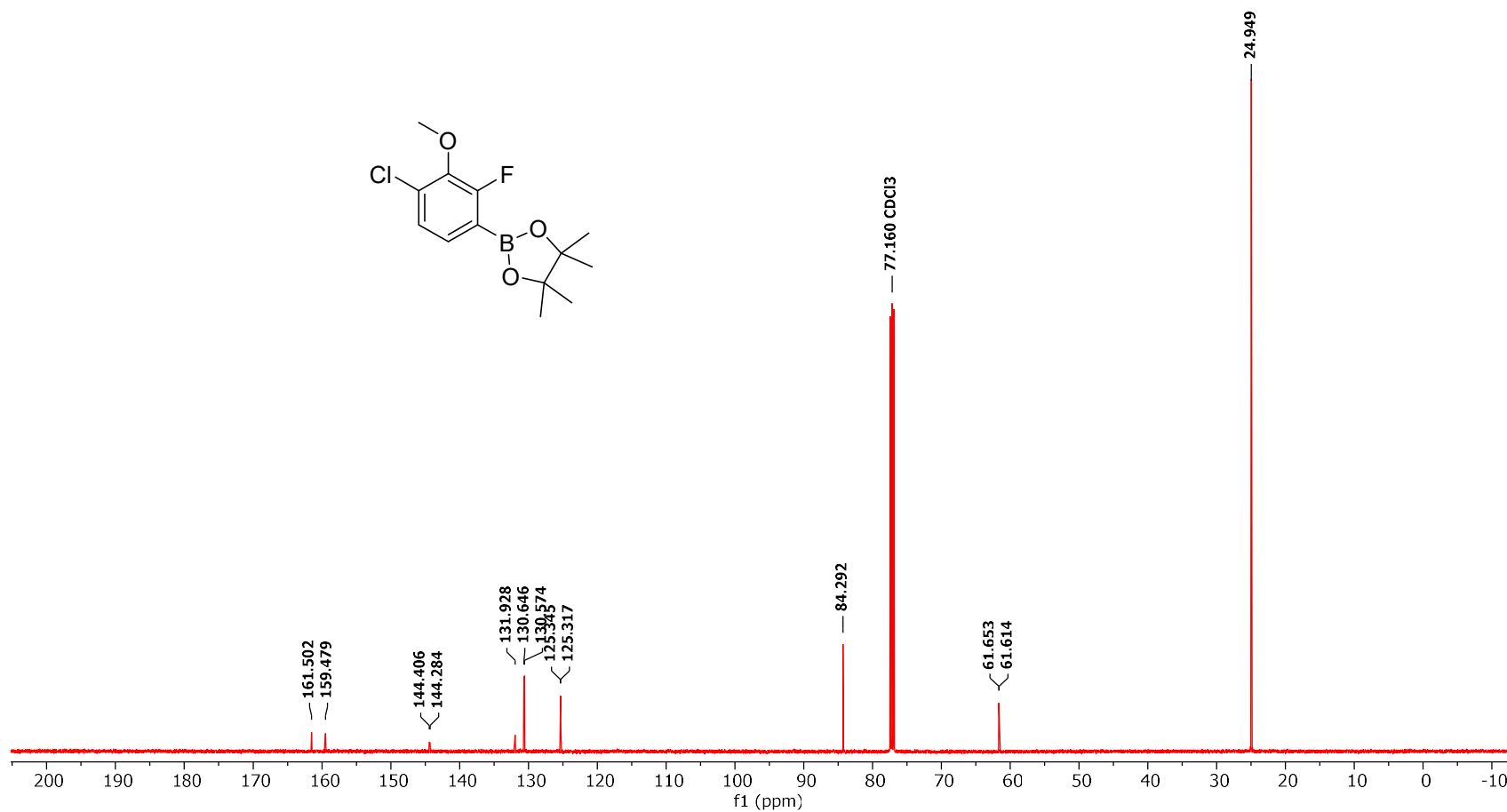


Figure 6-18 Conditions: 25 °C, 126 MHz, CDCl<sub>3</sub>

11B NMR Spectra of 2-(4-chloro-2-fluoro-3-methoxyphenyl)-4,4,5,5-tetramethyl-1,3,2-dioxaborolane (1d)

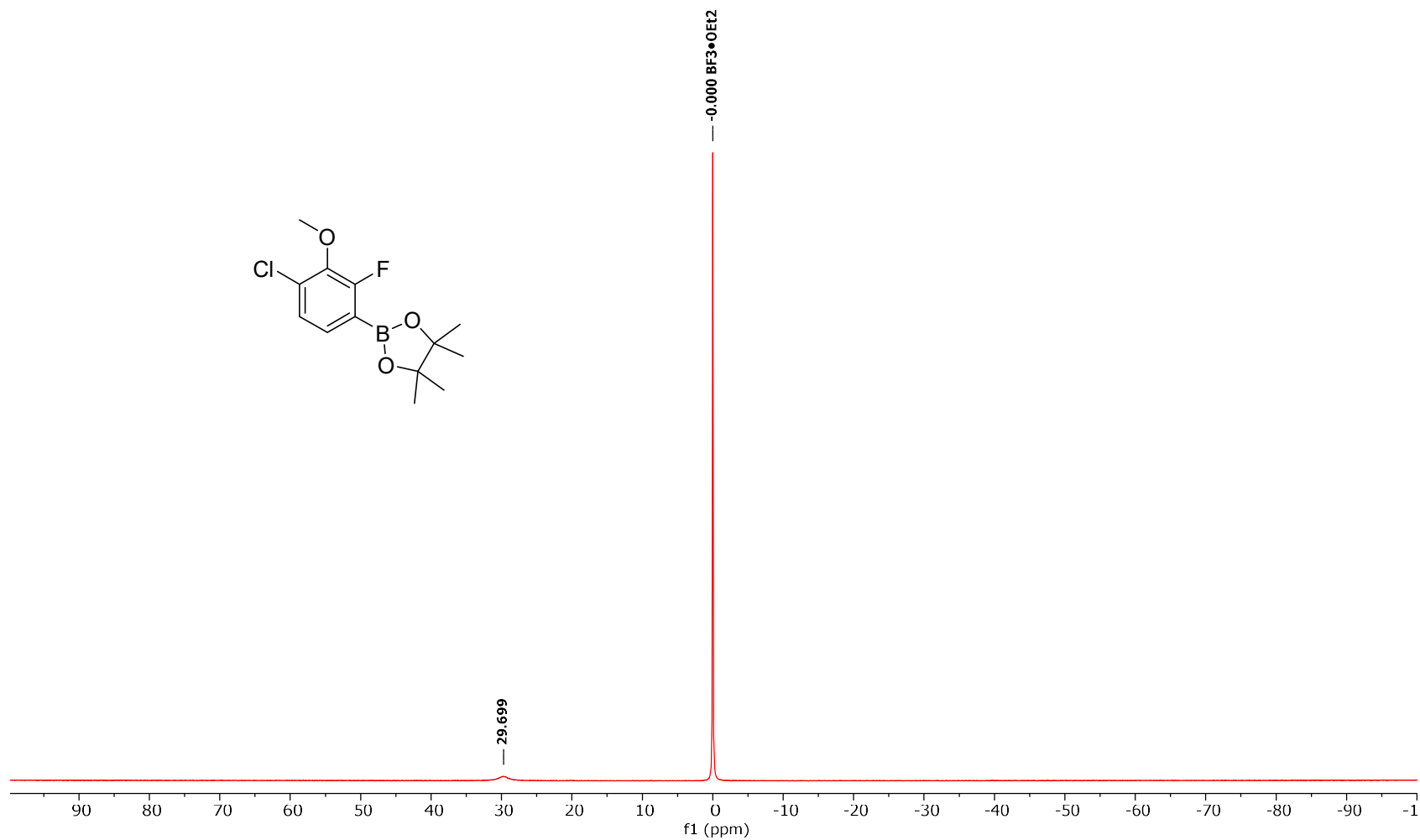


Figure 6-19 Conditions: 25 °C, 160 MHz, CDCl<sub>3</sub>, Referenced with BF<sub>3</sub>•OEt<sub>2</sub> at 0.00

**<sup>1</sup>H NMR Spectra of Independently Synthesized 2,2',2''-(2-fluorobenzene-1,3,5-triyl)tris(4,4,5,5-tetramethyl-1,3,2-dioxaborolane) (3a'')**

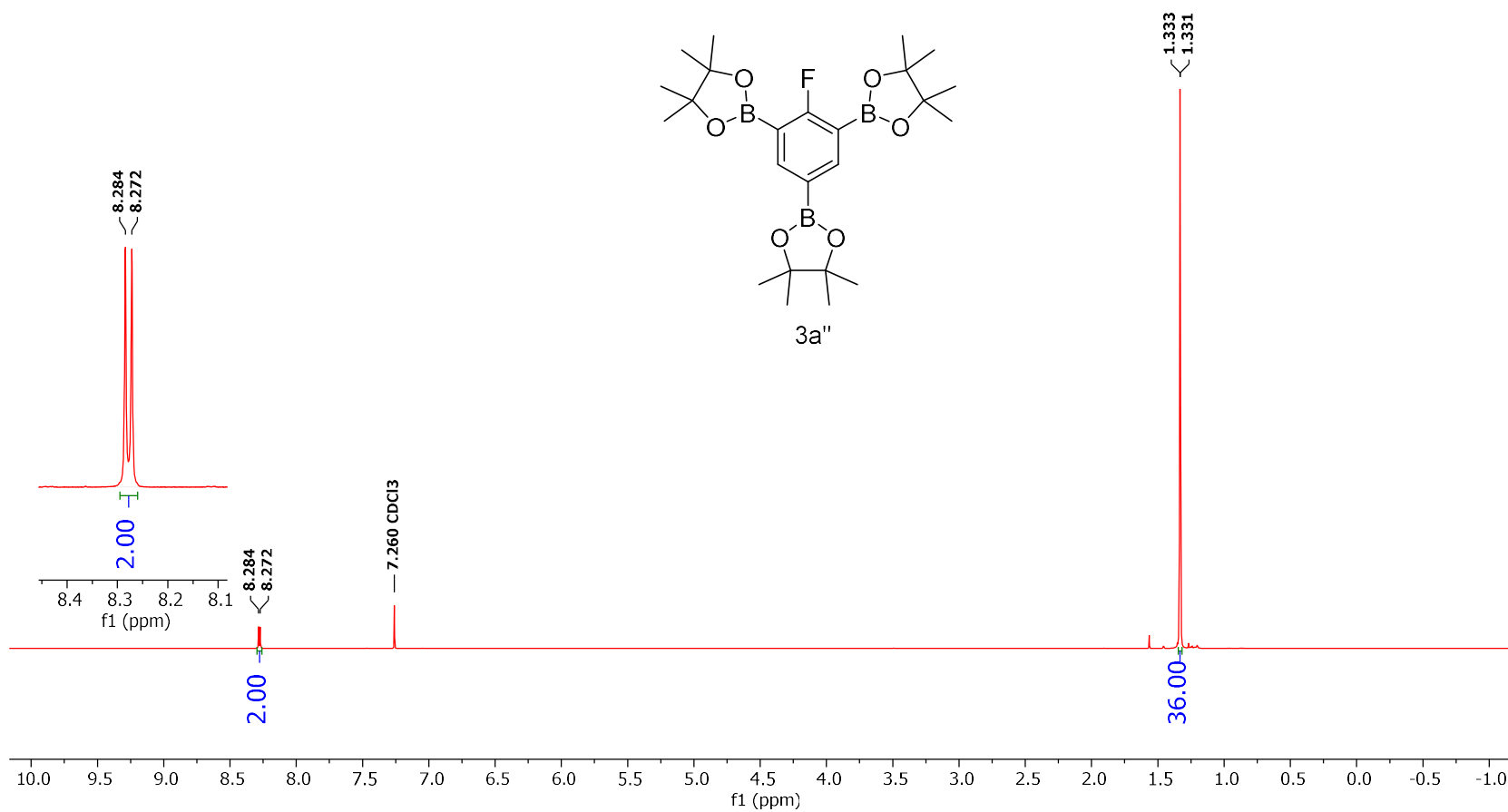


Figure 6-20 Conditions: 25 °C, 500 MHz, CDCl<sub>3</sub>

**$^{19}\text{F}$  NMR Spectra of Independently Synthesized 2,2',2''-(2-fluorobenzene-1,3,5-triyl)tris(4,4,5,5-tetramethyl-1,3,2-dioxaborolane) (3a'')**

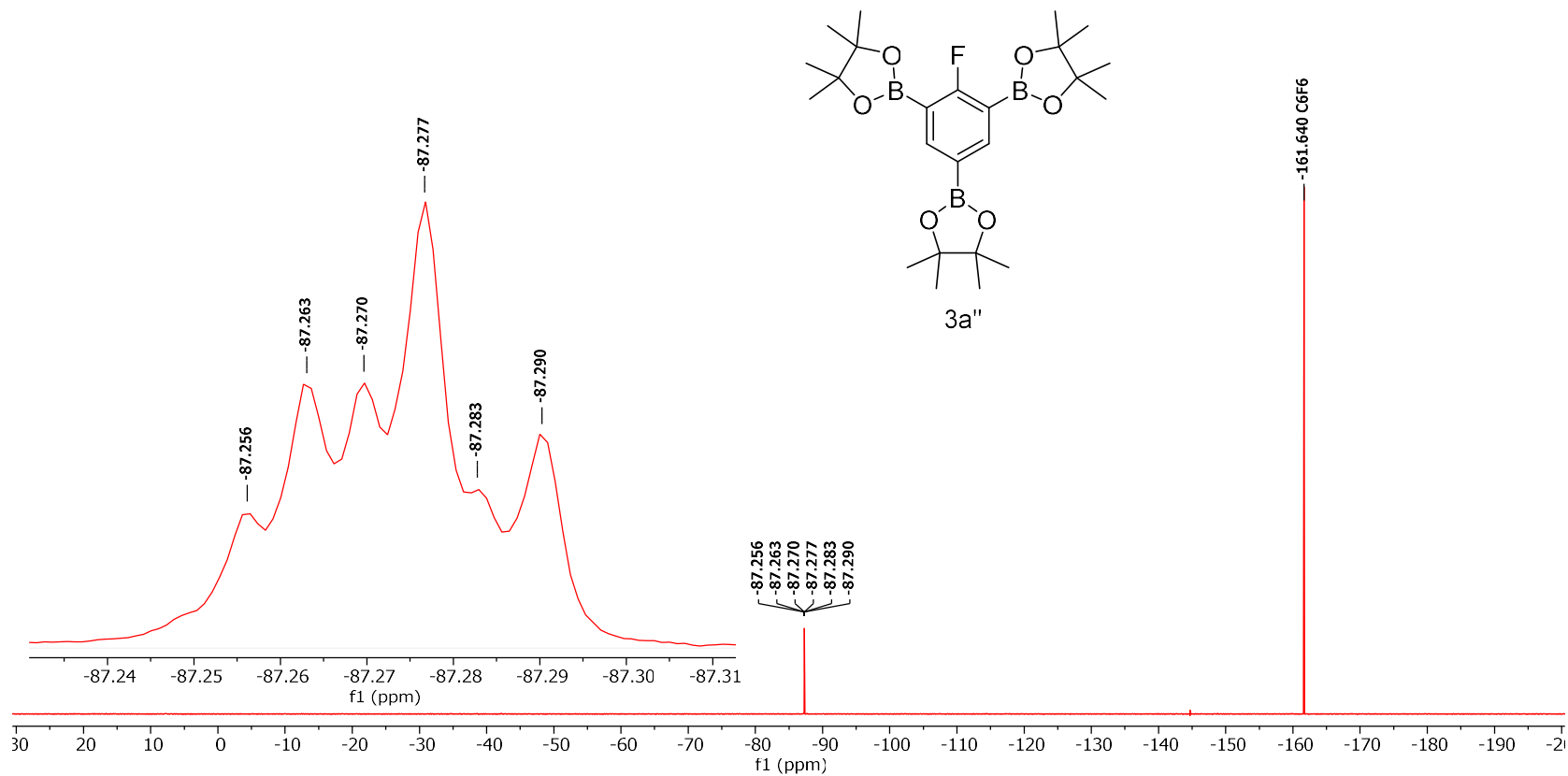


Figure 6-21 Conditions: 25 °C, 470 MHz,  $\text{CDCl}_3$ , Referenced with  $\text{C}_6\text{F}_6$  at -161.64

**<sup>13</sup>C NMR Spectra of Independently Synthesized 2,2',2''-(2-fluorobenzene-1,3,5-triyl)tris(4,4,5,5-tetramethyl-1,3,2-dioxaborolane) (3a'')**

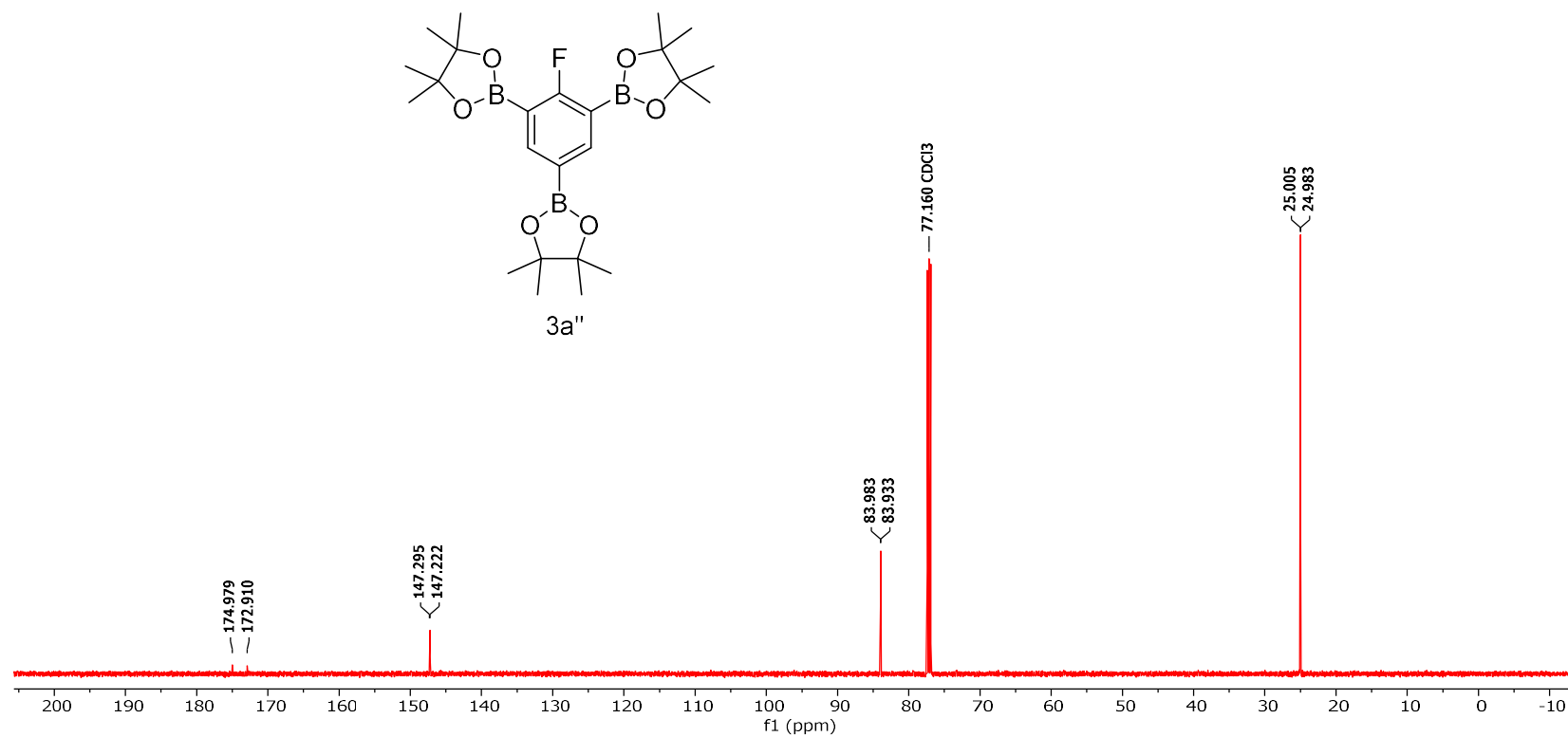


Figure 6-22 Conditions: 25 °C, 126 MHz, CDCl<sub>3</sub>

<sup>1</sup>H NMR Spectra of the crude reaction mixture of Table 1 Entry 1 Trial 1

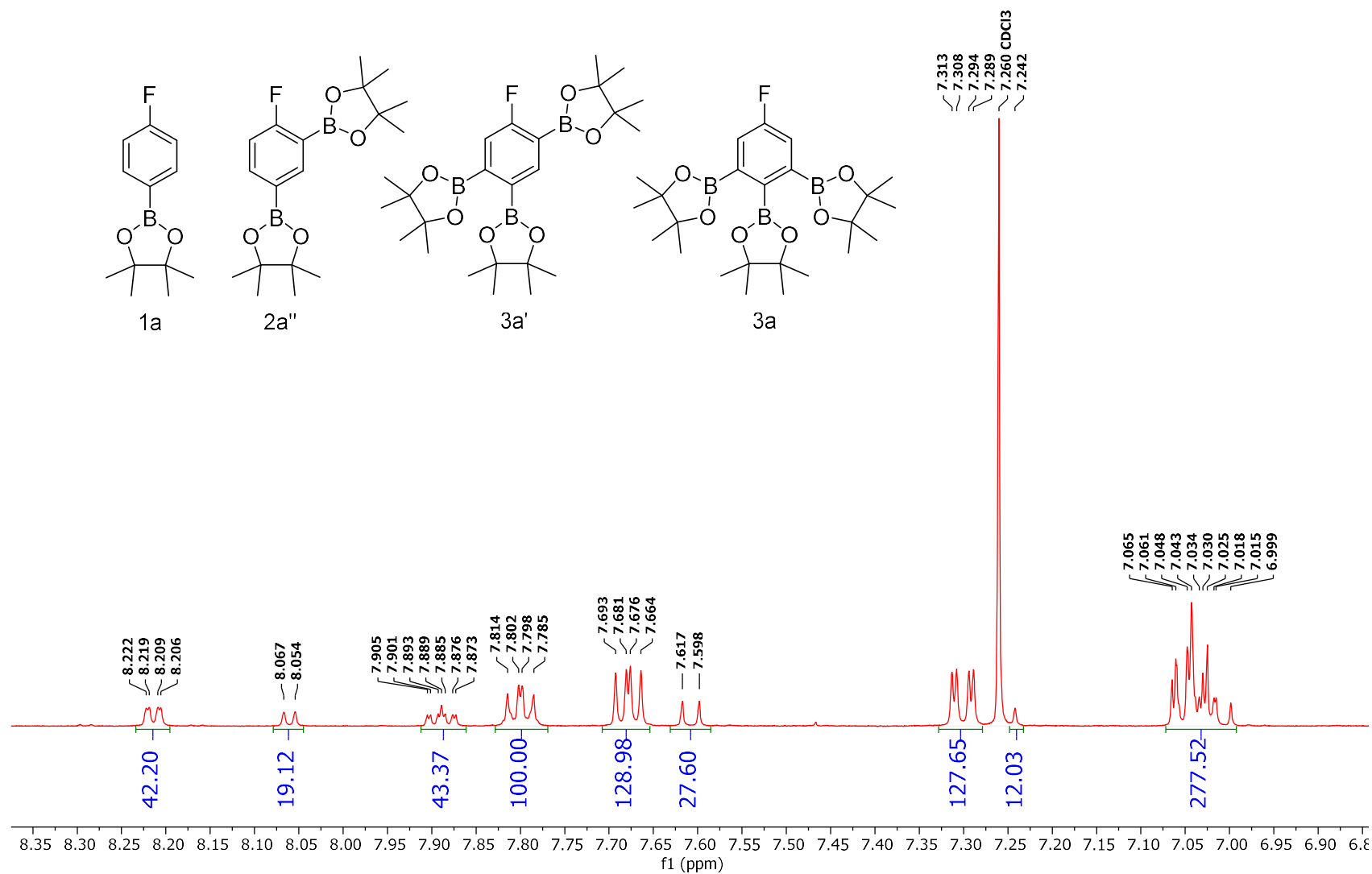


Figure 6-23 Conditions: 25 °C, 500 MHz, CDCl<sub>3</sub>



**<sup>19</sup>F NMR Spectra of the crude reaction mixture of Table 1 Entry 1 Trial 1**

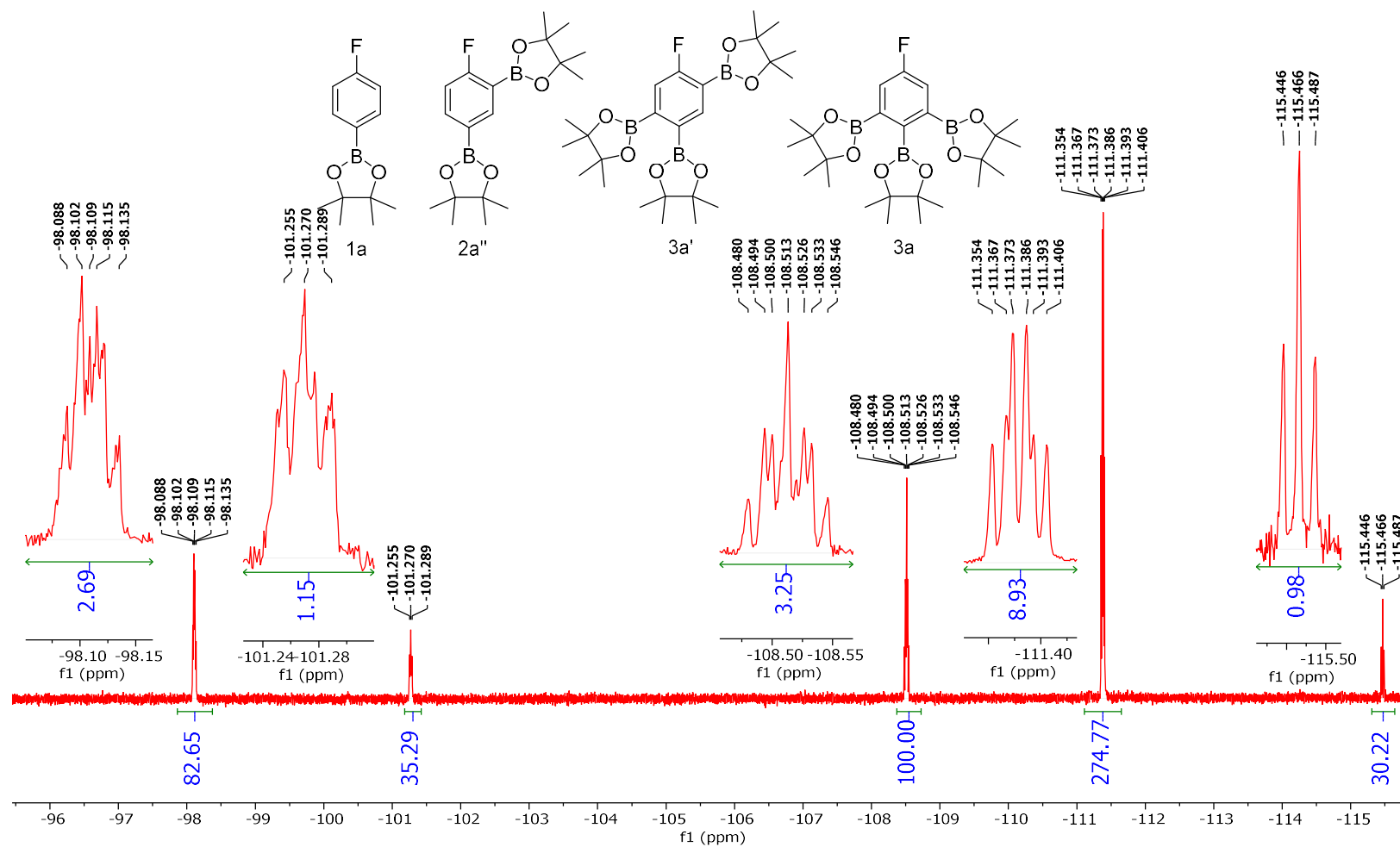


Figure 6-24 Conditions: 25 °C, 470 MHz, CDCl<sub>3</sub>

<sup>1</sup>H NMR Spectra of the purified reaction mixture of Table 1 Entry 1 Trial 1

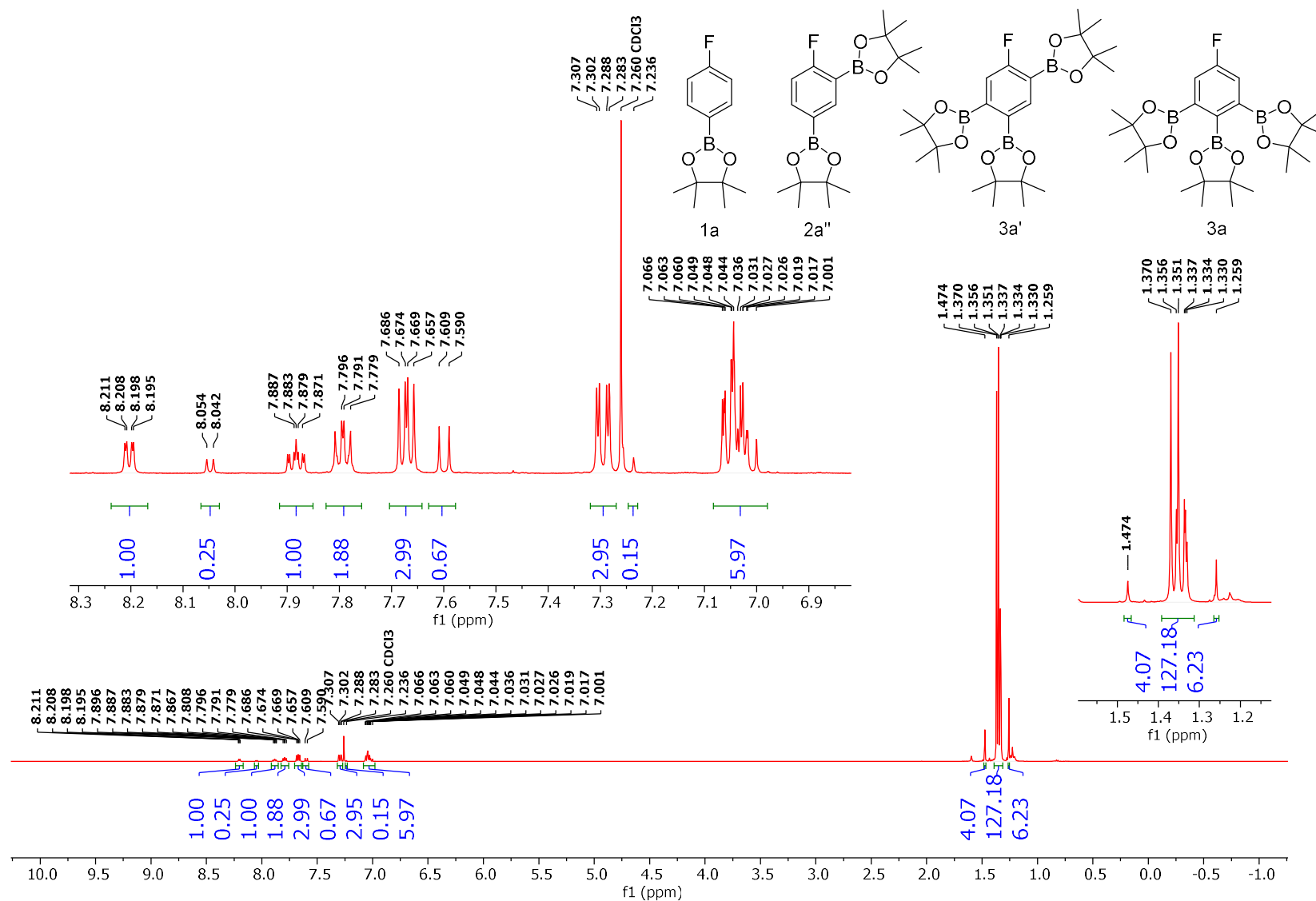


Figure 6-25 Conditions: 25 °C, 500 MHz, CDCl<sub>3</sub>

**$^{19}\text{F}$  NMR Spectra of the purified reaction mixture of Table 1 Entry 1 Trial 1**

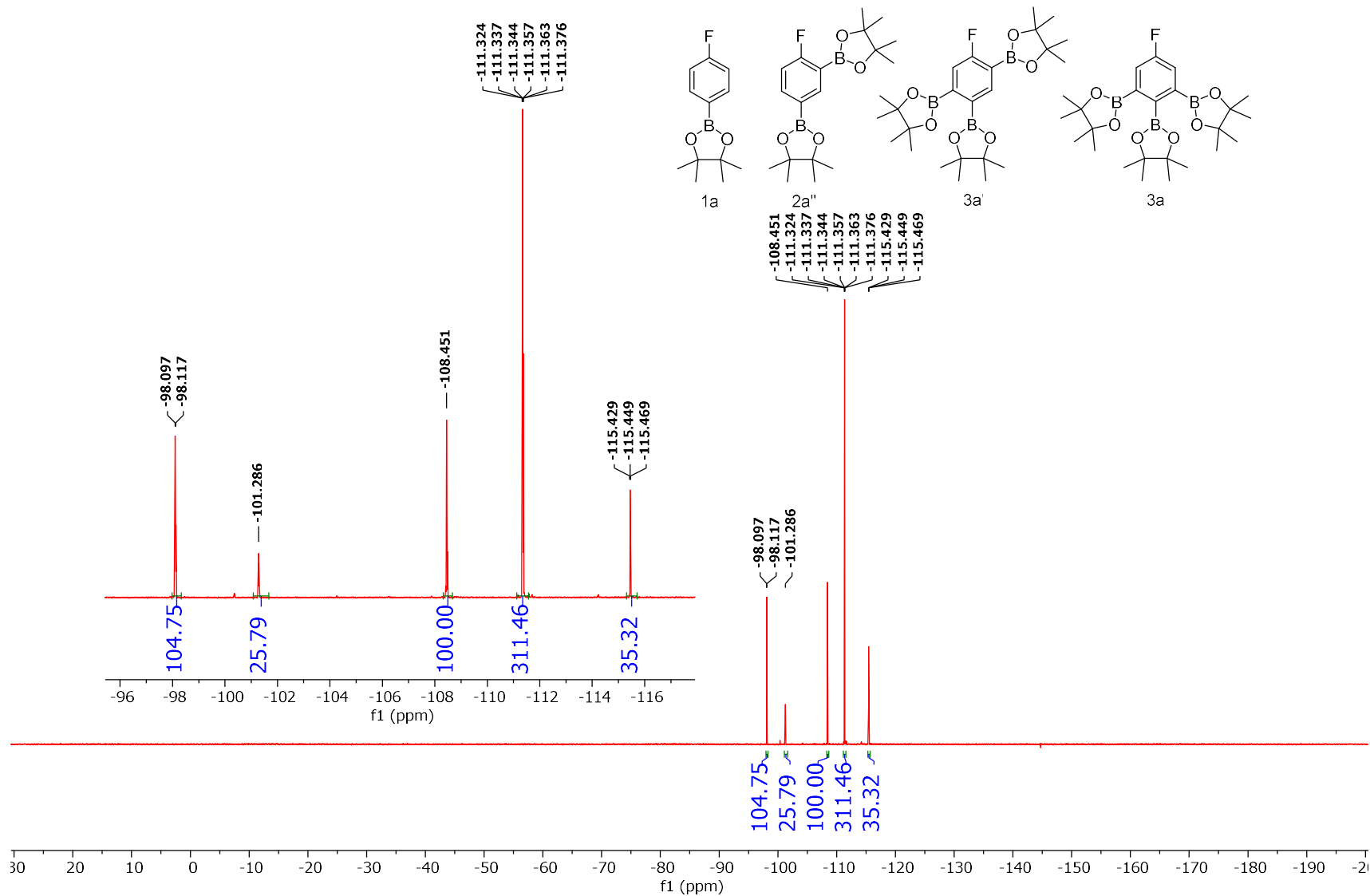


Figure 6-26 Conditions: 25 °C, 470 MHz,  $\text{CDCl}_3$

**<sup>13</sup>C NMR Spectra of the purified reaction mixture of Table 1 Entry 1 Trial 1**

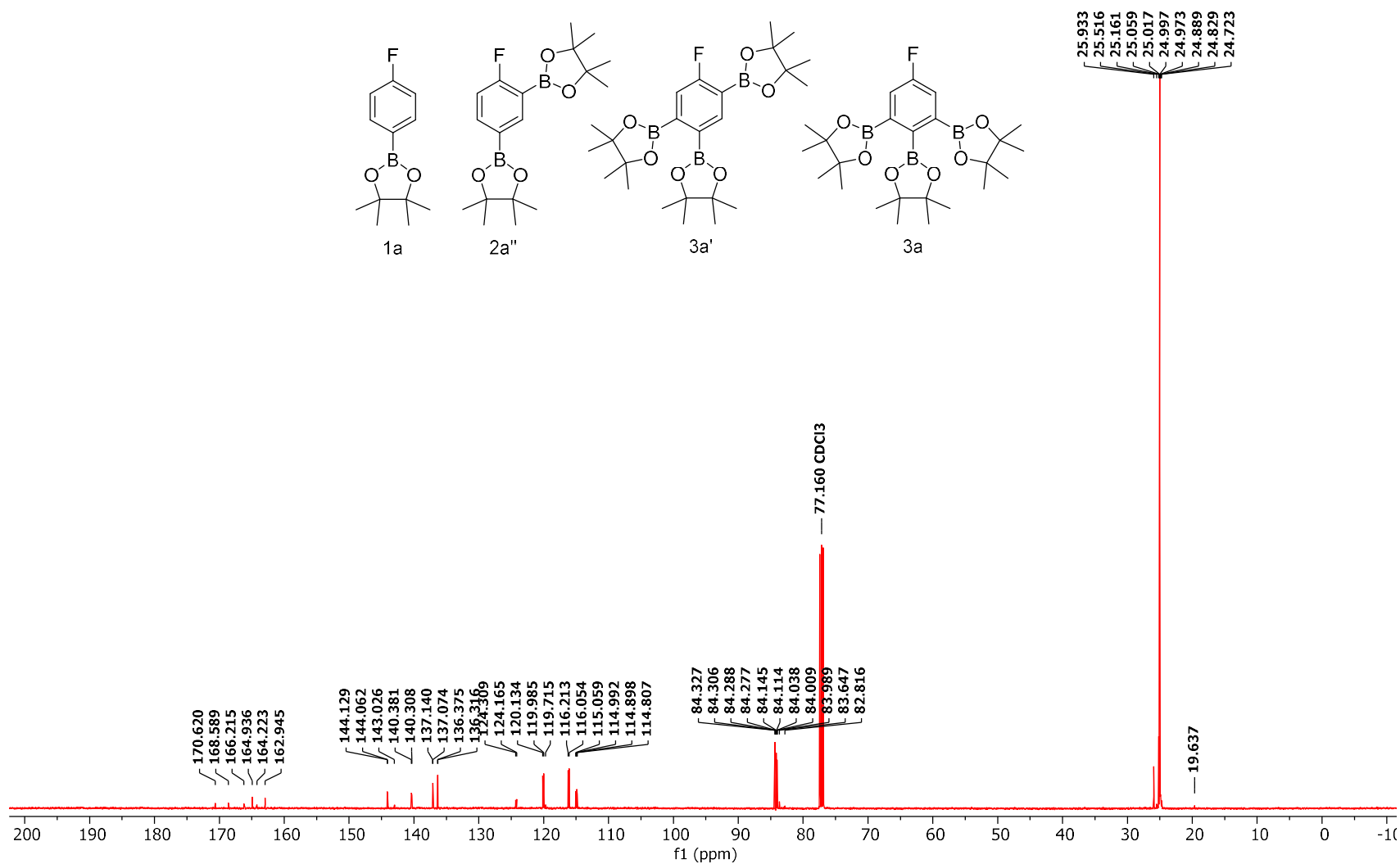


Figure 6-27 Conditions: 25 °C, 126 MHz, CDCl<sub>3</sub>

**$^{11}\text{B}$  NMR Spectra of the purified reaction mixture of Table 1 Entry 1 Trial 1**

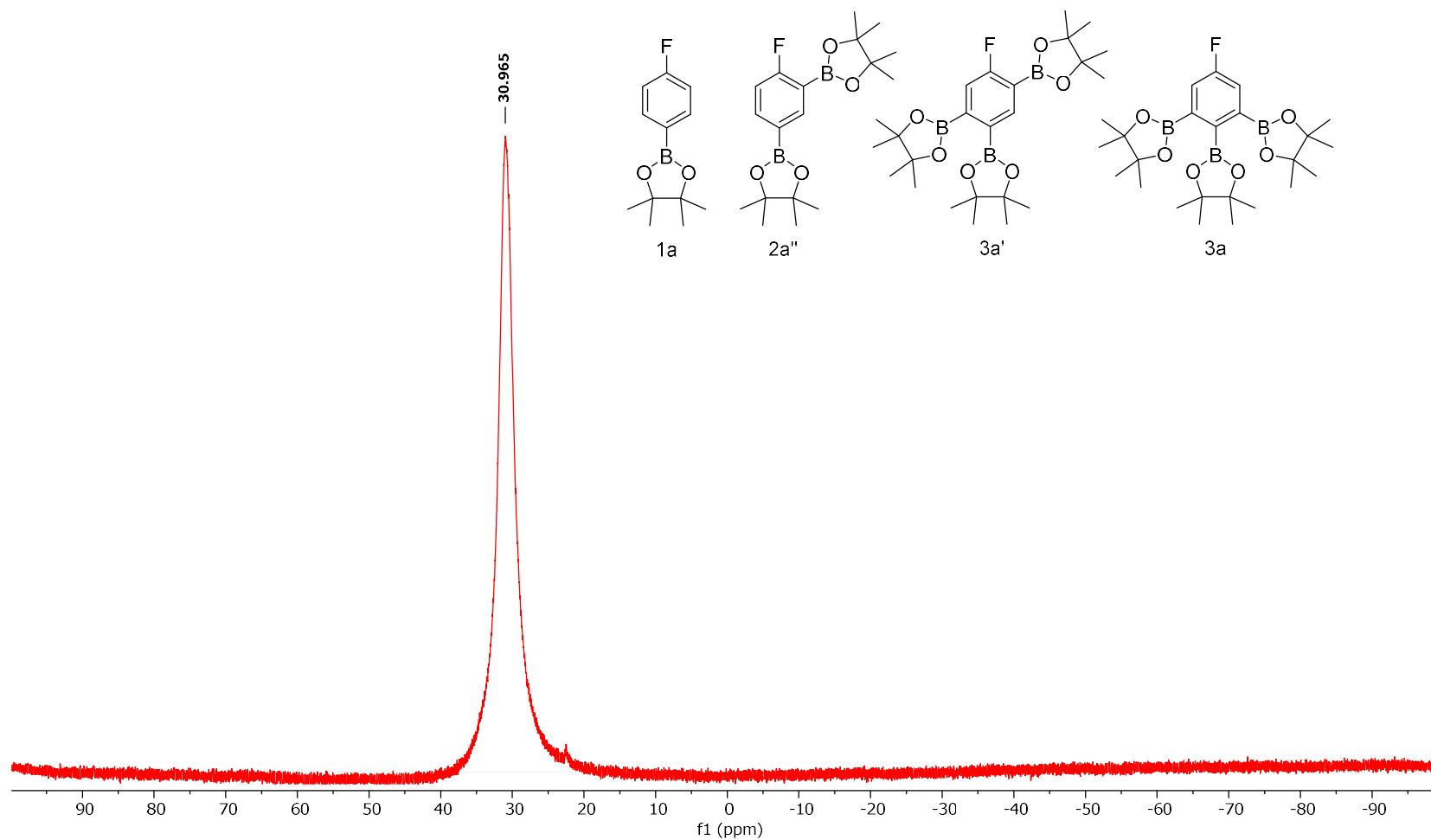


Figure 6-28 Conditions: 25 °C, 160 MHz,  $\text{CDCl}_3$

**$^1\text{H}$  NMR Spectra of the Isolated 2,2',2''-(5-fluorobenzene-1,2,3-triyl)tris(4,4,5,5-tetramethyl-1,3,2-dioxaborolane) (3a)**

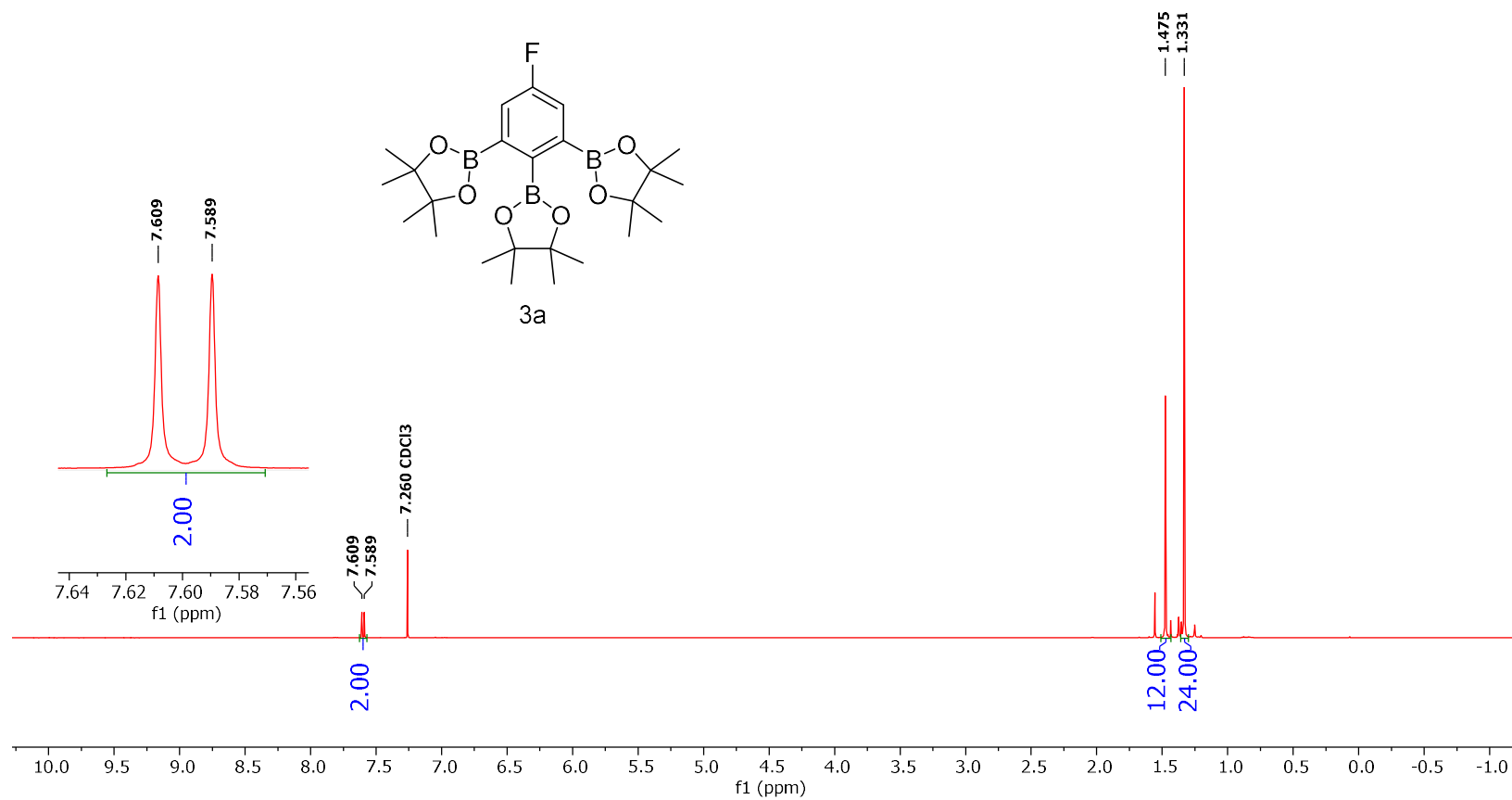


Figure 2-29 Conditions: 25  $^\circ\text{C}$ , 500 MHz,  $\text{CDCl}_3$

**$^{19}\text{F}$  NMR Spectra of the Isolated 2,2',2''-(5-fluorobenzene-1,2,3-triyl)tris(4,4,5,5-tetramethyl-1,3,2-dioxaborolane) (3a)**

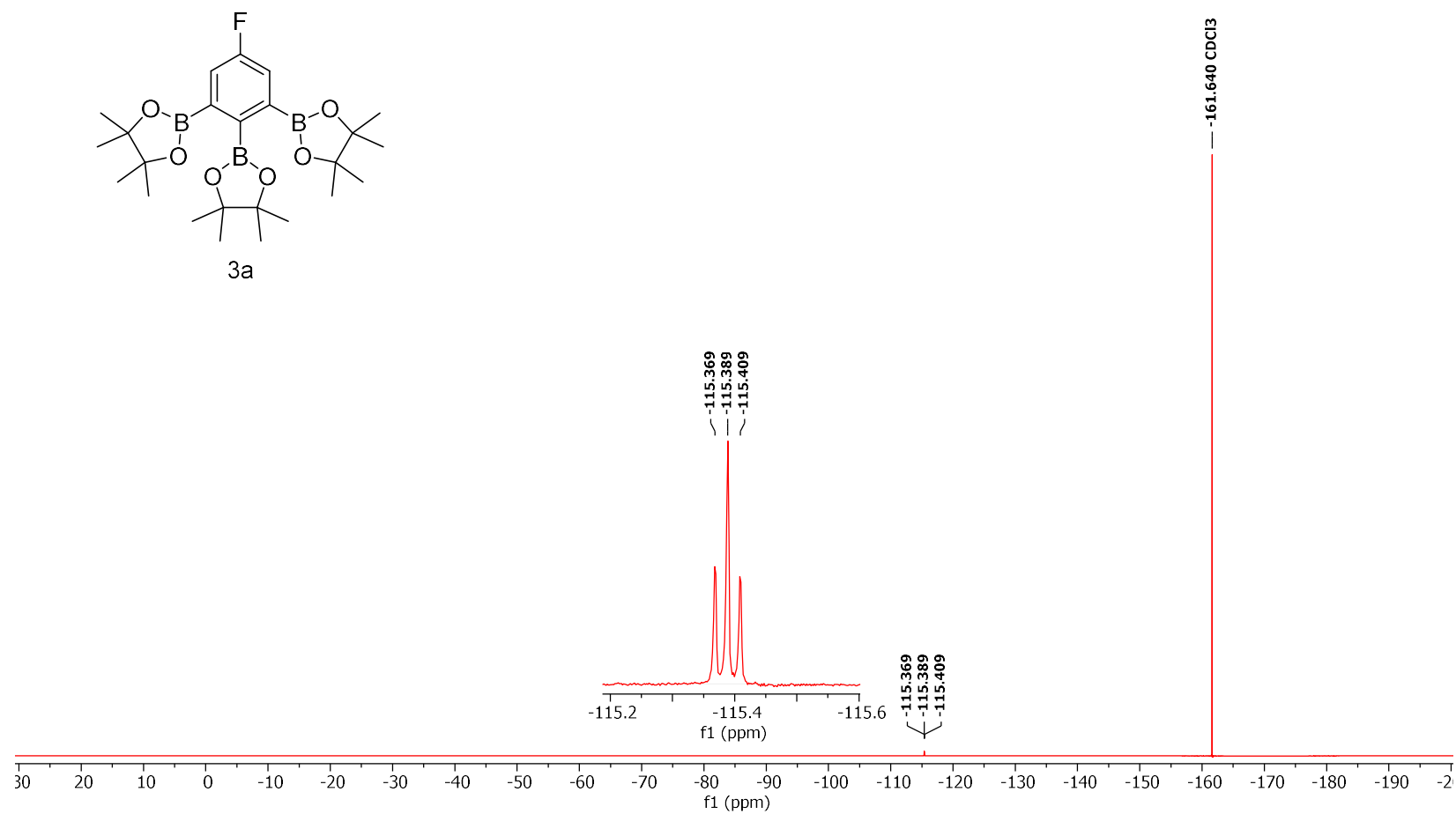


Figure 6-30 Conditions: 25 °C, 470 MHz, CDCl<sub>3</sub>

**<sup>13</sup>C NMR Spectra of the Isolated 2,2',2''-(5-fluorobenzene-1,2,3-triyl)tris(4,4,5,5-tetramethyl-1,3,2-dioxaborolane) (3a)**

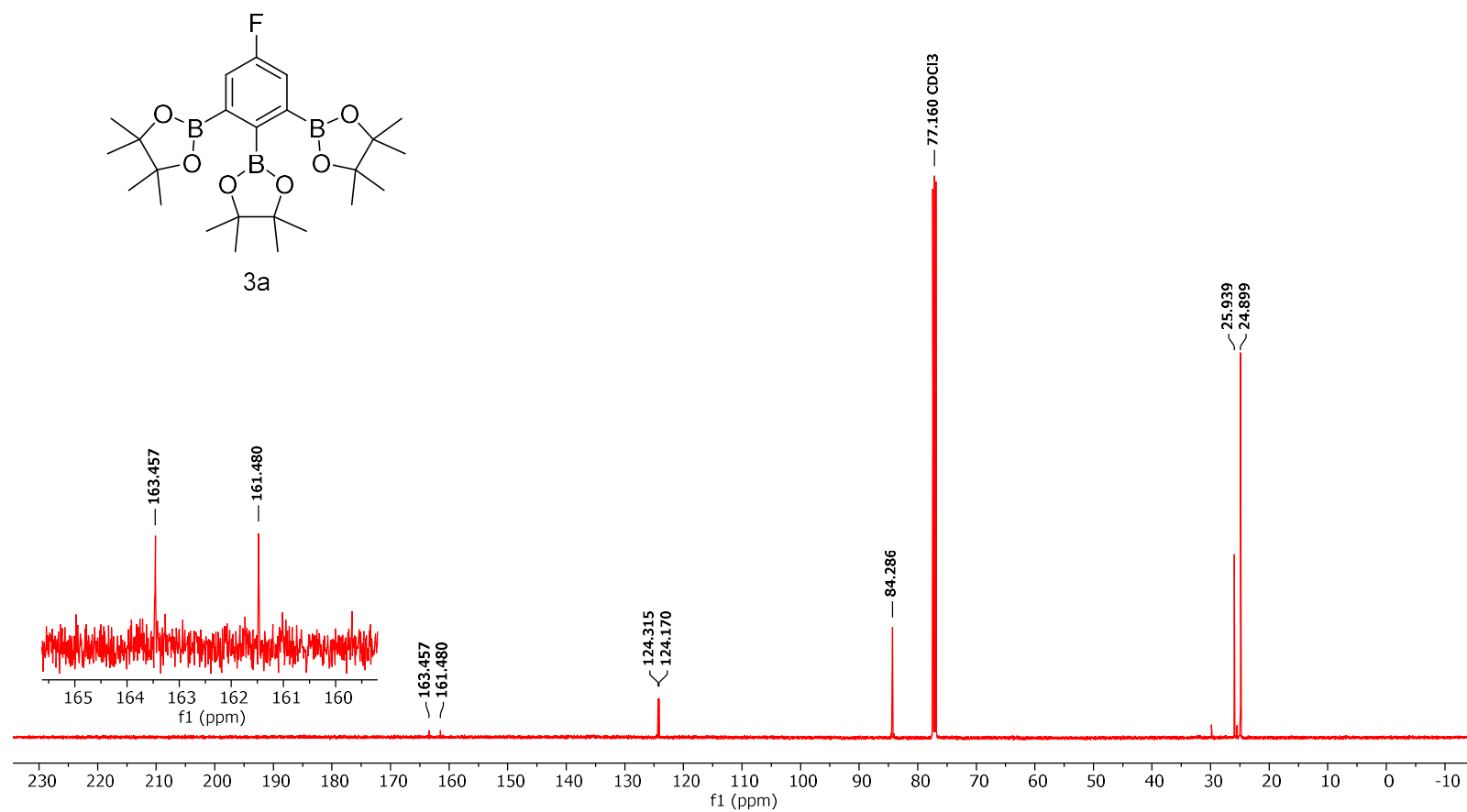


Figure 6-31 Conditions: 25 °C, 126 MHz, CDCl<sub>3</sub>



**$^{11}\text{B}$  NMR Spectra of the Isolated 2,2',2''-(5-fluorobenzene-1,2,3-triyl)tris(4,4,5,5-tetramethyl-1,3,2-dioxaborolane) (3a)**

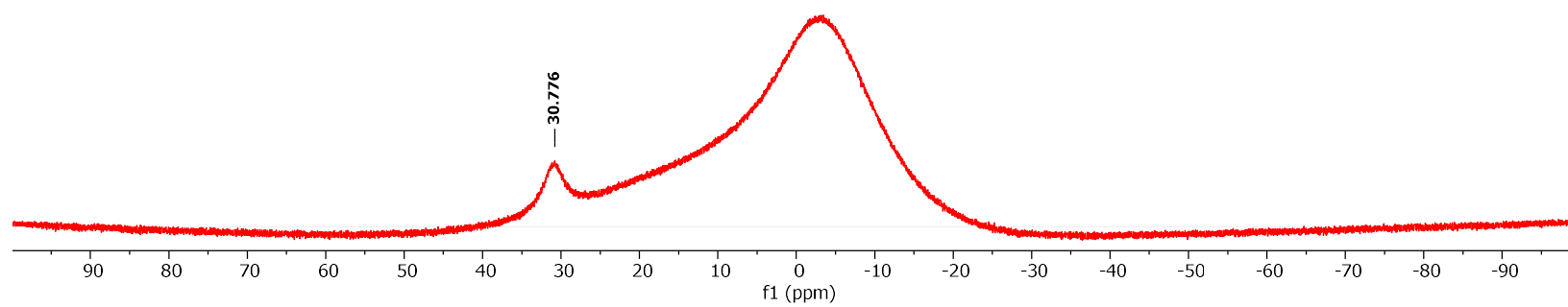
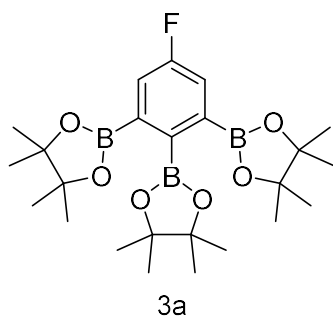


Figure 6-32 Conditions: 25 °C, 160 MHz,  $\text{CDCl}_3$

<sup>1</sup>H NMR Spectra of the crude reaction mixture of Table 1 Entry 1 Trial 2

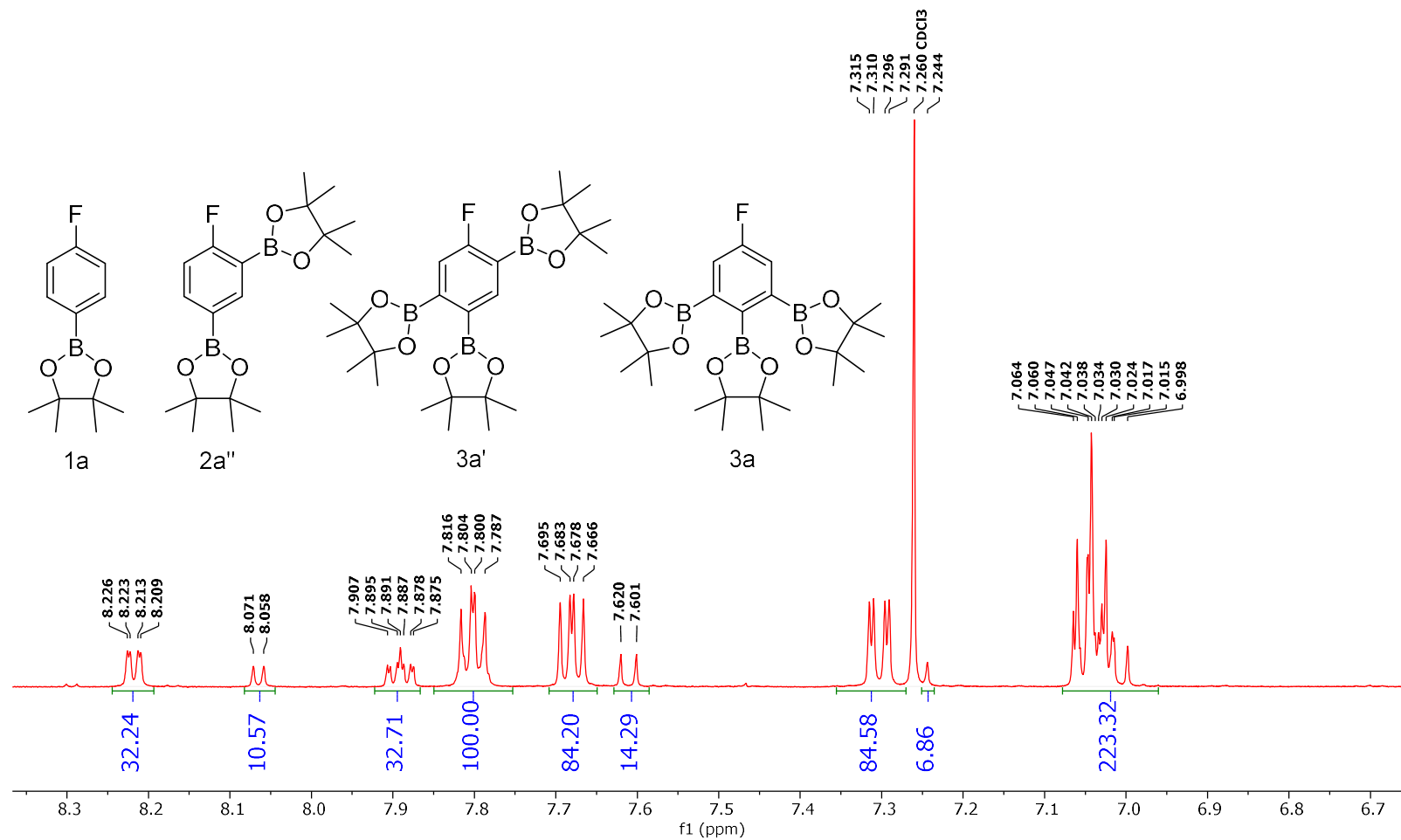


Figure 6-33 Conditions: 25 °C, 500 MHz, CDCl<sub>3</sub>

**<sup>19</sup>F NMR Spectra of the crude reaction mixture of Table 1 Entry 1 Trial 2**

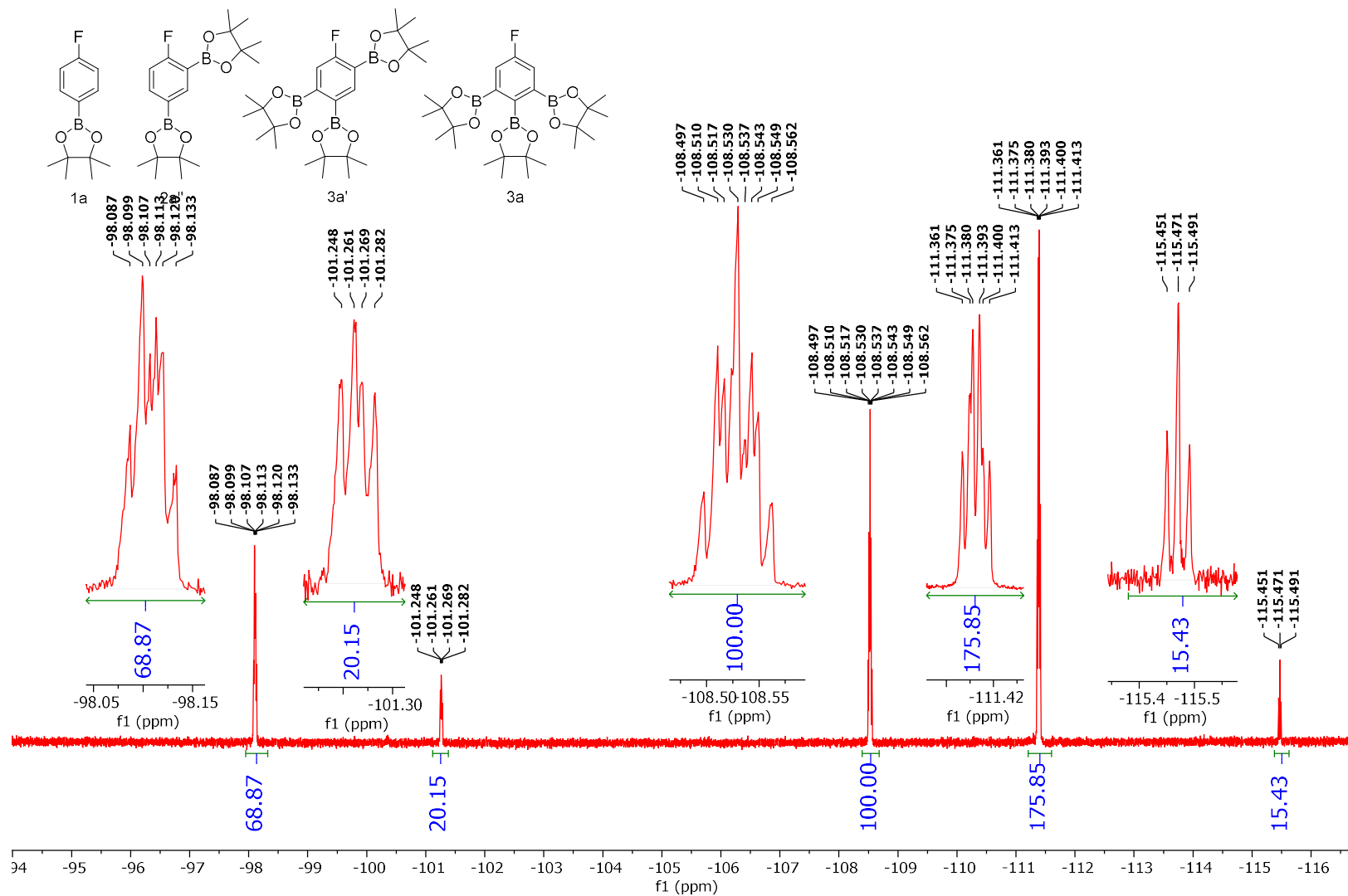


Figure 6-34 Conditions: 25 °C, 470 MHz, CDCl<sub>3</sub>

<sup>1</sup>H NMR Spectra of the crude reaction mixture of Table 1 Entry 1 Trial 3

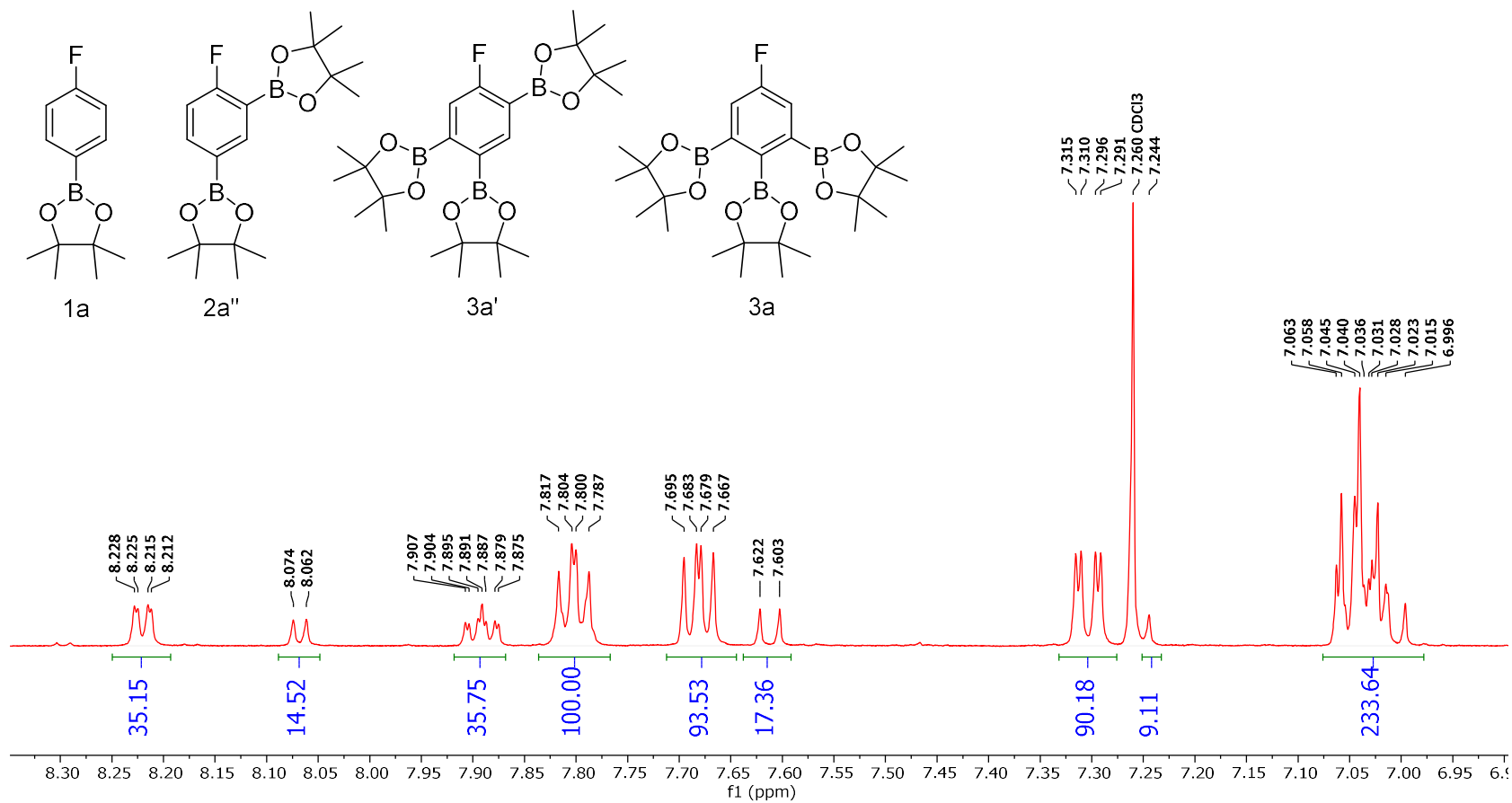


Figure 6-35 Conditions: 25 °C, 500 MHz, CDCl<sub>3</sub>

<sup>19</sup>F NMR Spectra of the crude reaction mixture of Table 1 Entry 1 Trial 3

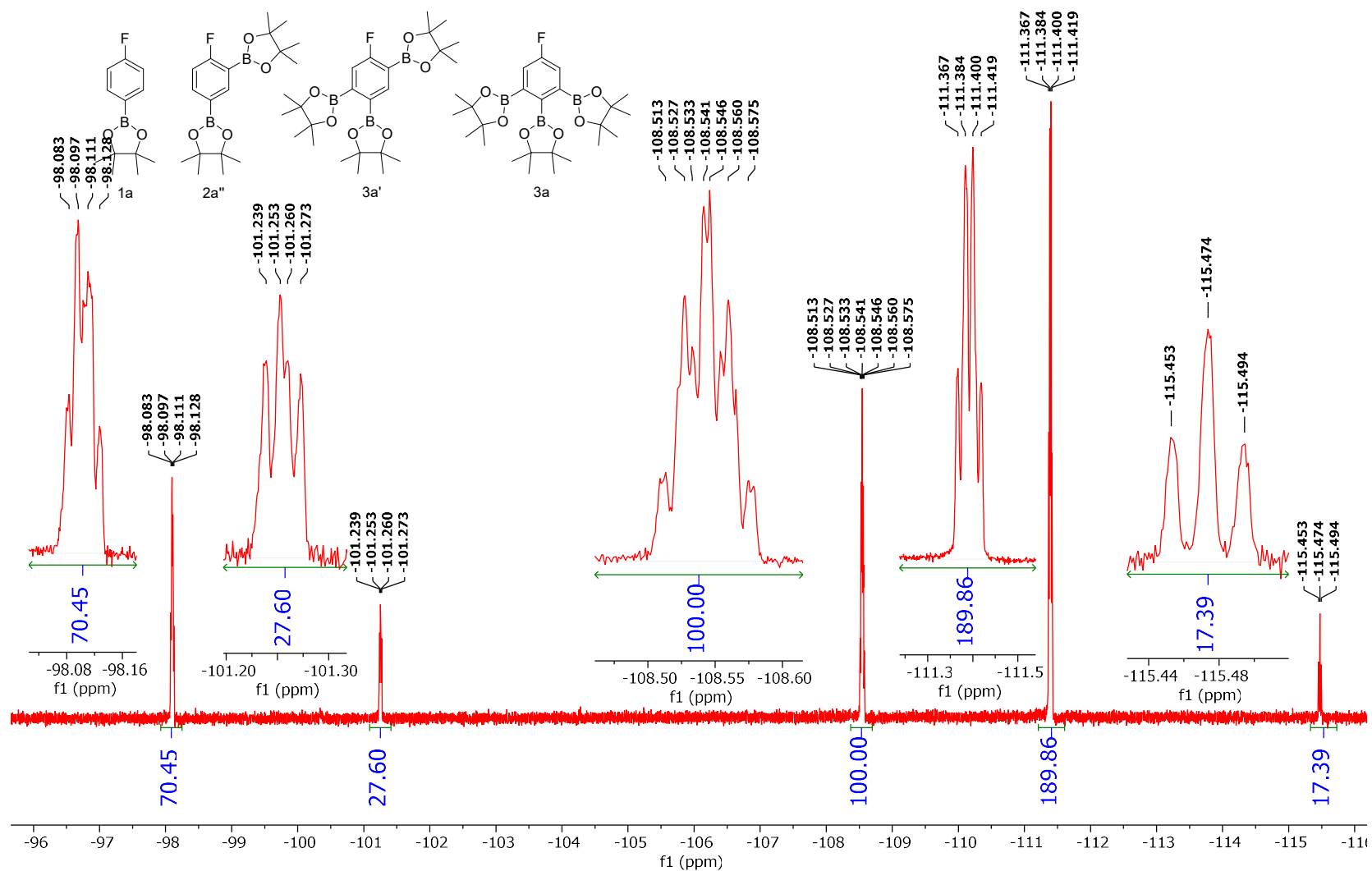


Figure 6-36 Conditions: 25 °C, 470 MHz, CDCl<sub>3</sub>

**<sup>1</sup>H NMR Spectra of the Crude reaction mixture of Table 1 Entry 2 Trial 1**

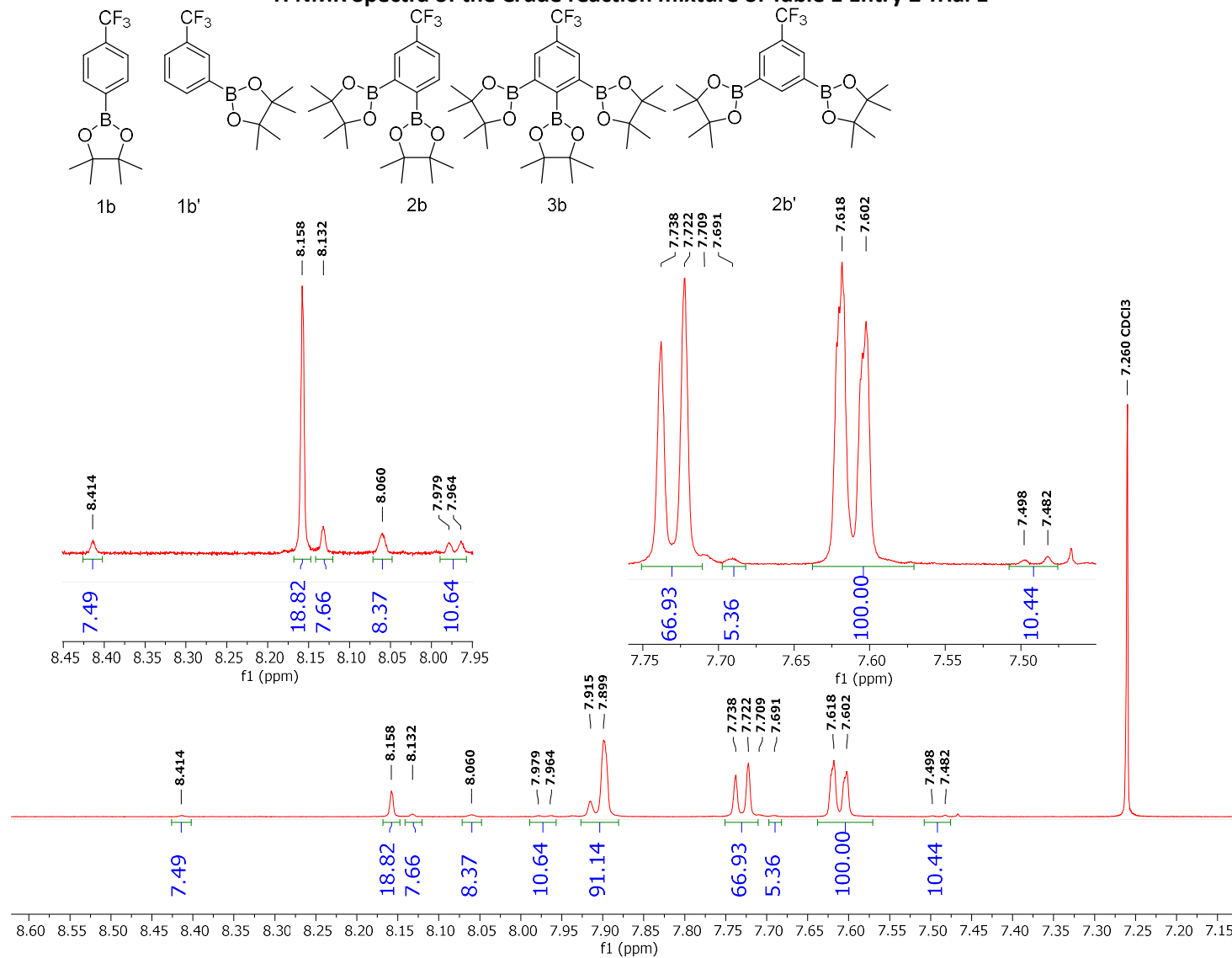


Figure 6-37 Conditions: 25 °C, 500 MHz, CDCl<sub>3</sub>

**<sup>19</sup>F NMR Spectra of the Crude reaction mixture of Table 1 Entry 2 Trial 1**

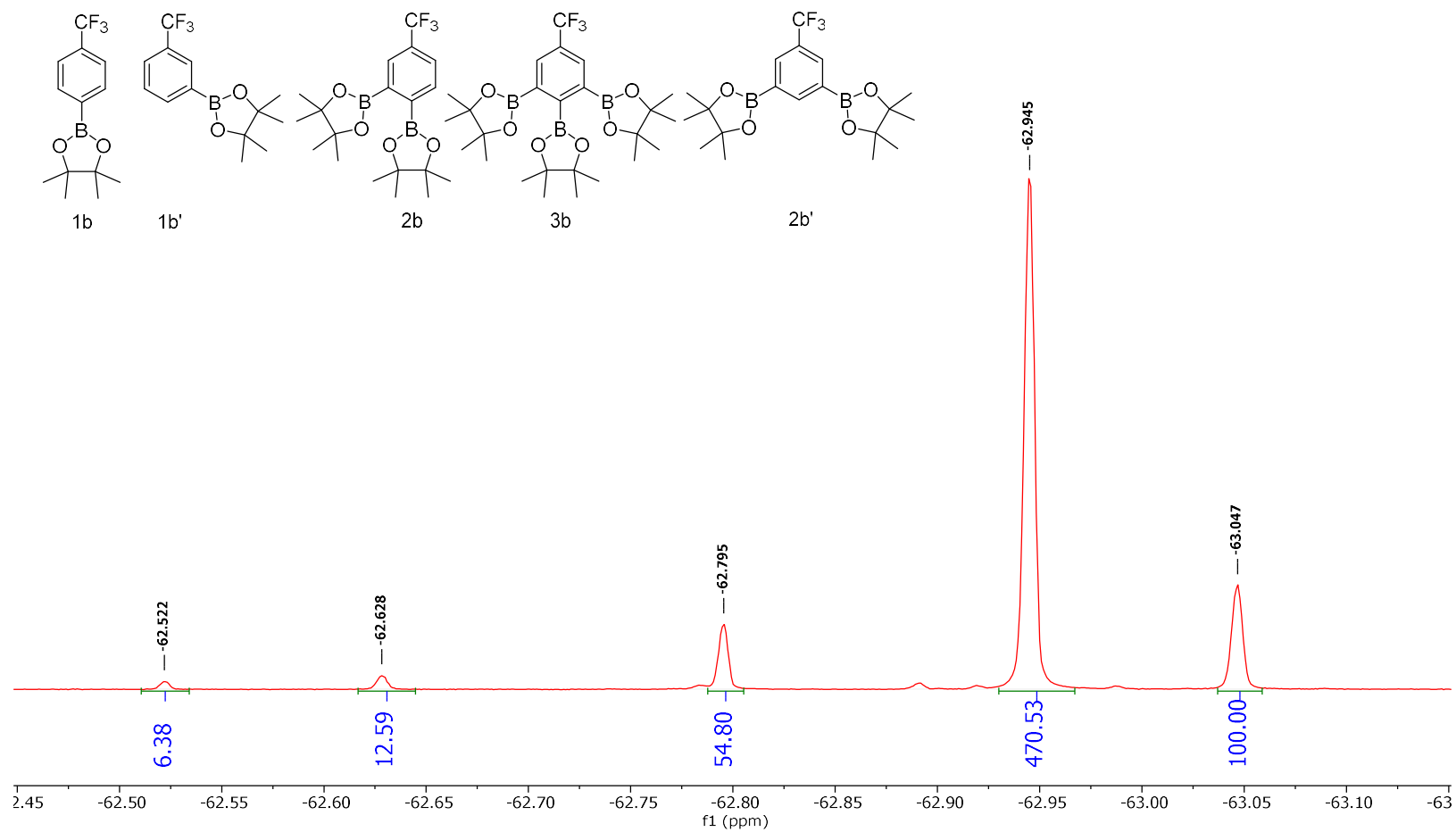


Figure 6-38 Conditions: 25 °C, 470 MHz, CDCl<sub>3</sub>

**<sup>1</sup>H NMR Spectra of the first purified fraction of the reaction mixture of Table 1 Entry 2 Trial 1**

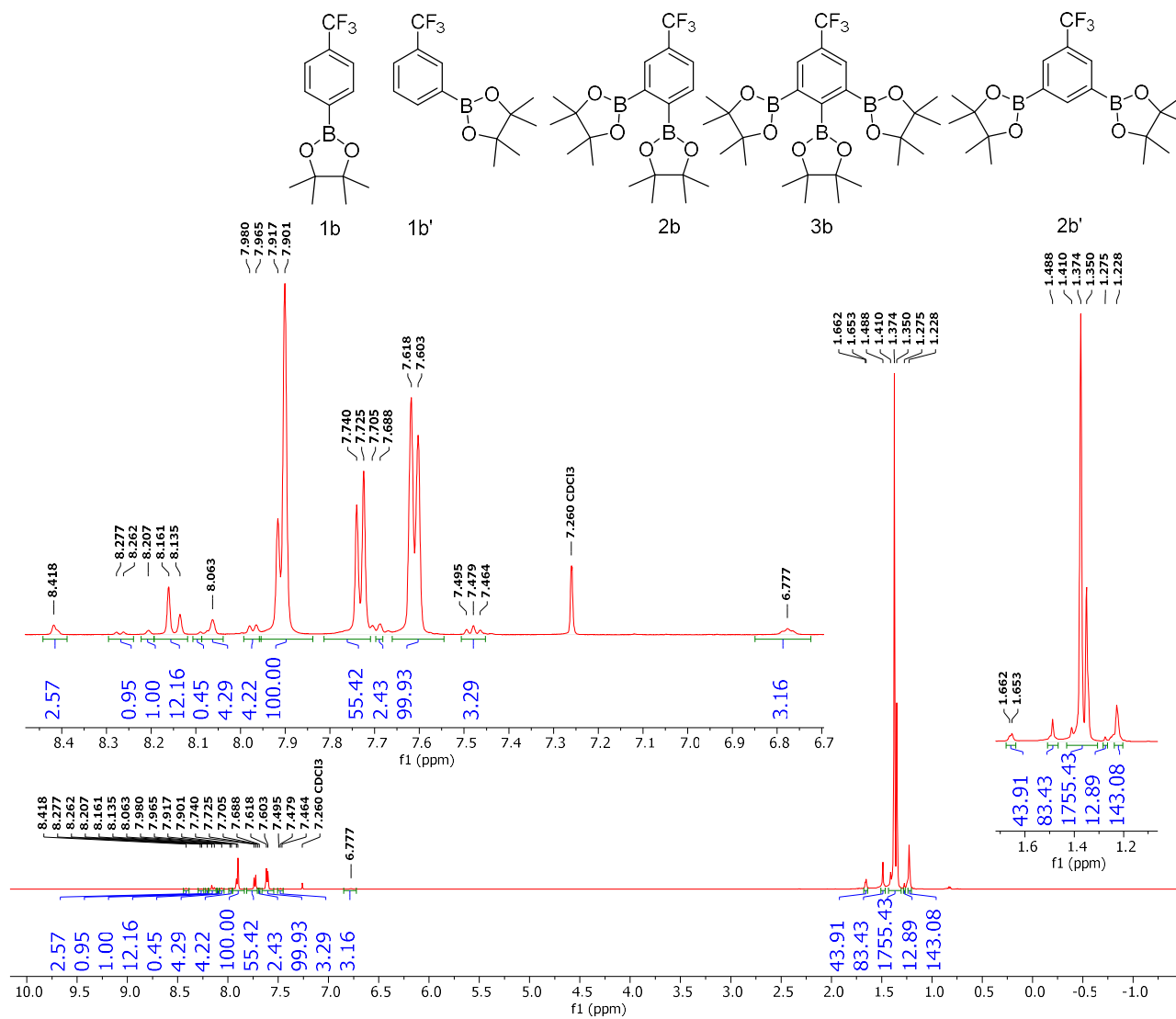


Figure 6-39 Conditions: 25 °C, 500 MHz, CDCl<sub>3</sub>



**<sup>19</sup>F NMR Spectra of the first purified fraction of the reaction mixture of Table 1 Entry 2 Trial 1**

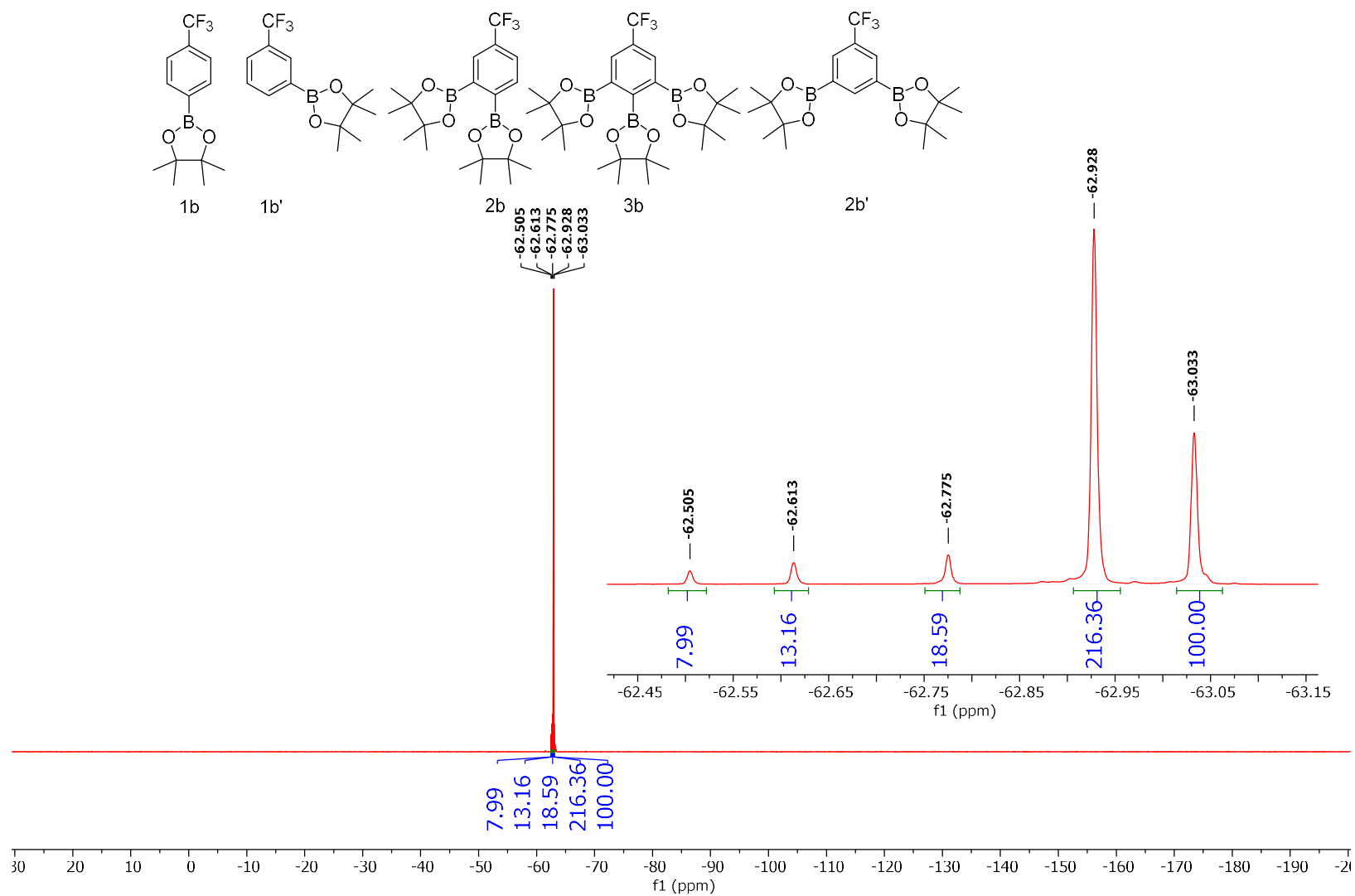


Figure 6-40 Conditions: 25 °C, 470 MHz, CDCl<sub>3</sub>

**$^{13}\text{C}$  NMR Spectra of the first purified fraction of the reaction mixture of Table 1 Entry 2 Trial 1**

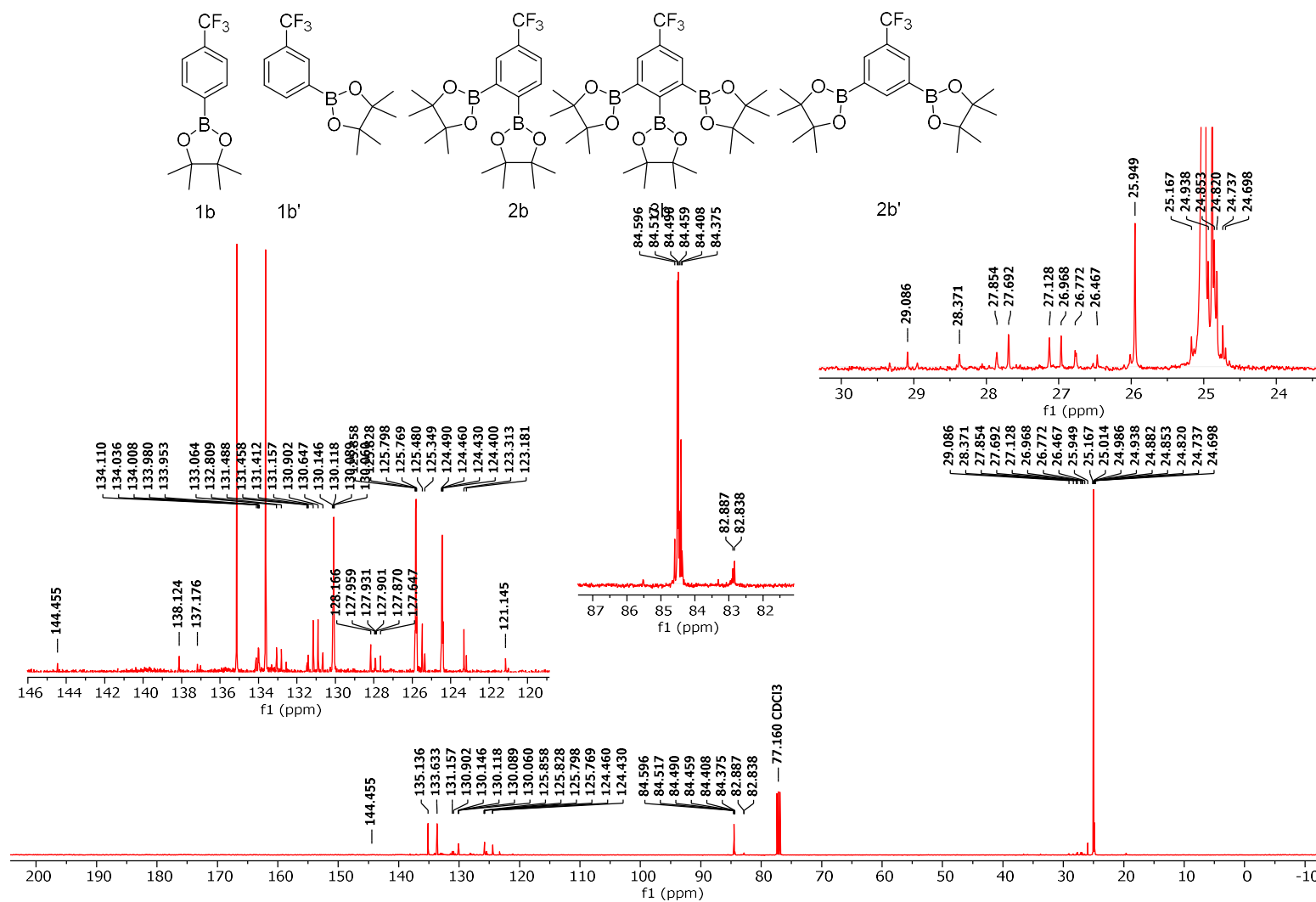


Figure 6-41 Conditions: 25 °C, 126 MHz, CDCl<sub>3</sub>

**<sup>11</sup>B NMR Spectra of the first purified fraction of the reaction mixture of Table 1 Entry 2 Trial 1**

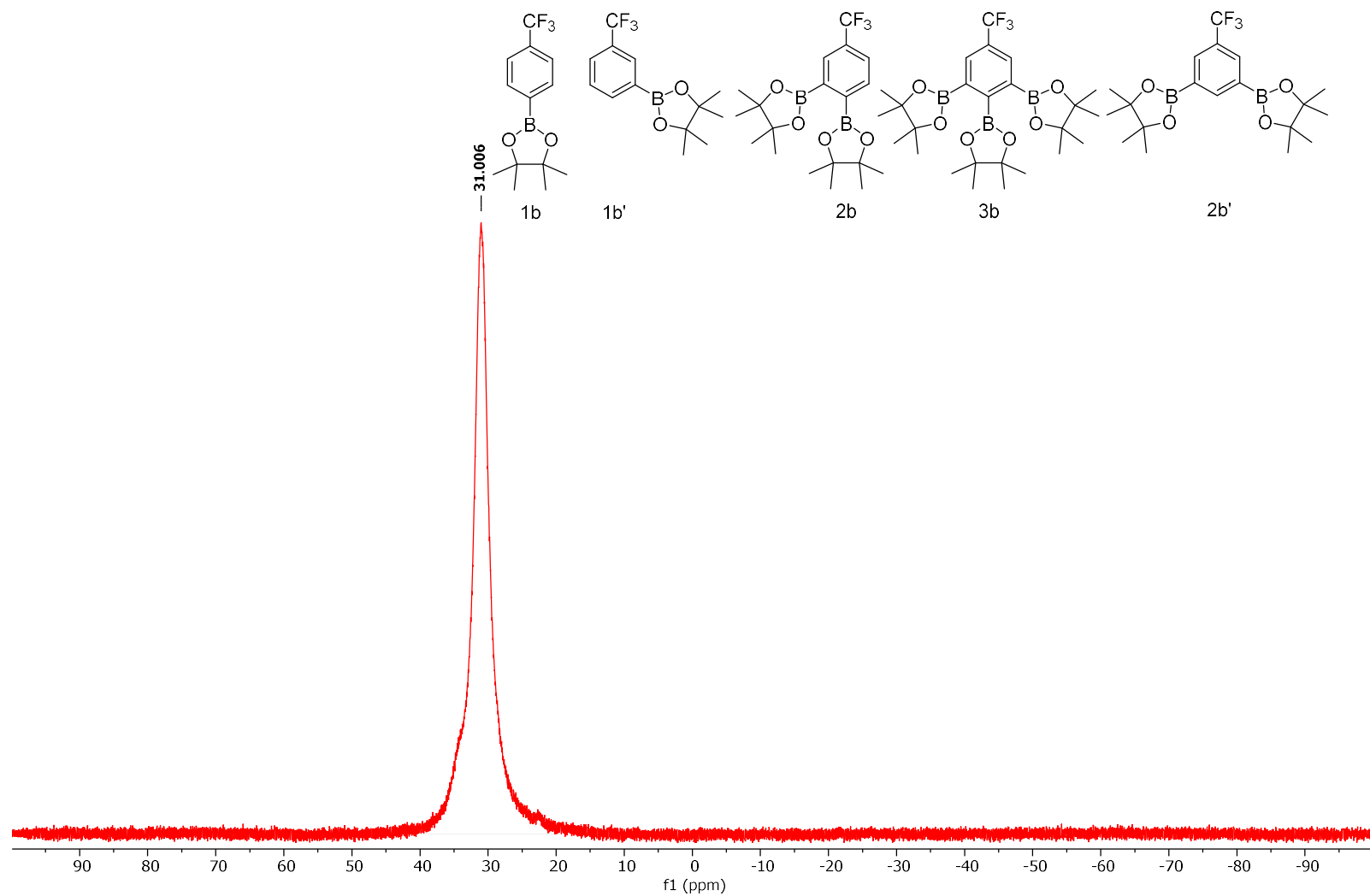


Figure 6-42 Conditions: 25 °C, 160 MHz, CDCl<sub>3</sub>

**<sup>1</sup>H NMR Spectra of the second purified fraction of the reaction mixture of Table 1 Entry 2 Trial 1**

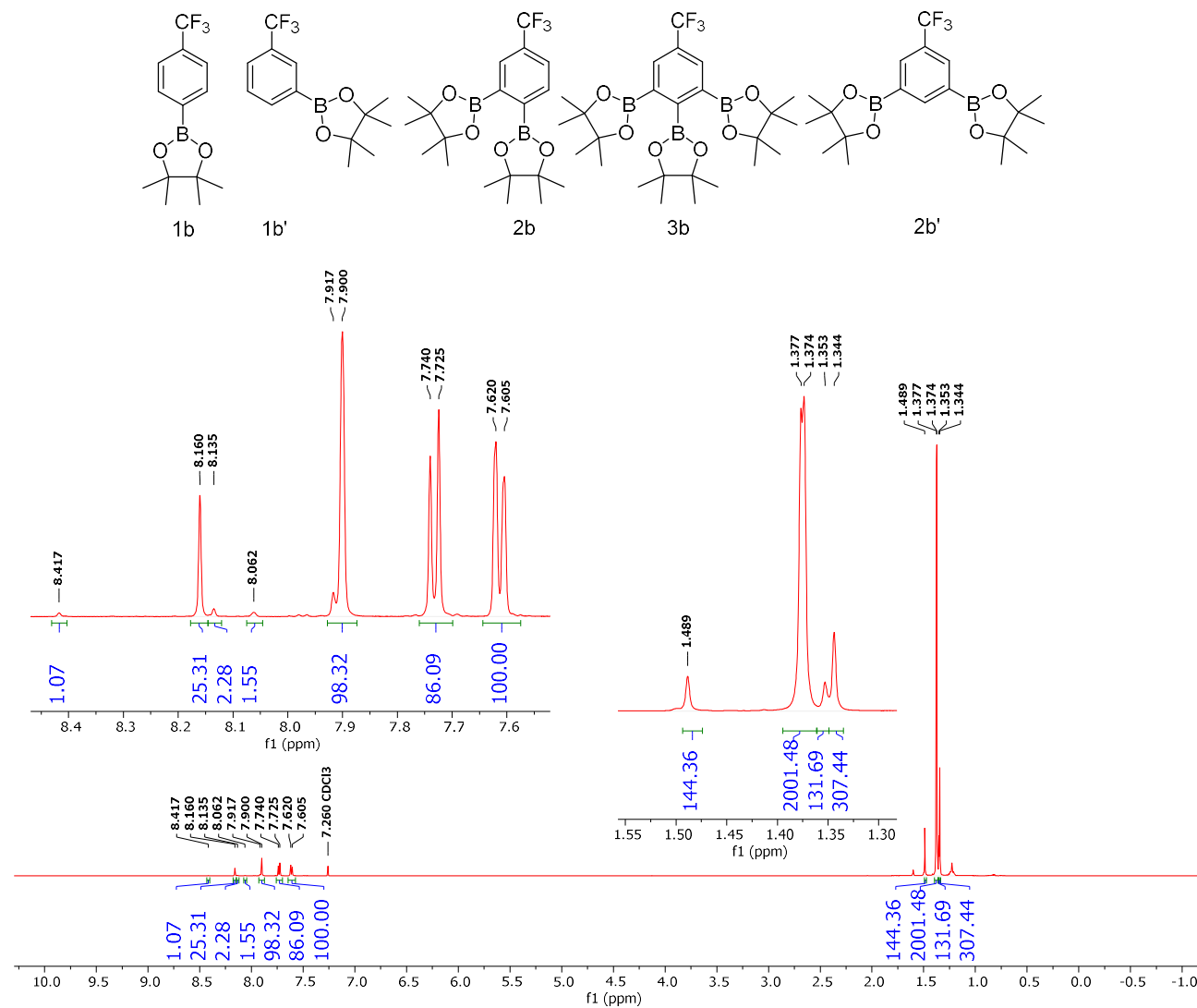


Figure 6-43 Conditions: 25 °C, 500 MHz, CDCl<sub>3</sub>

**$^{19}\text{F}$  NMR Spectra of the second purified fraction of the reaction mixture of Table 1 Entry 2 Trial 1**

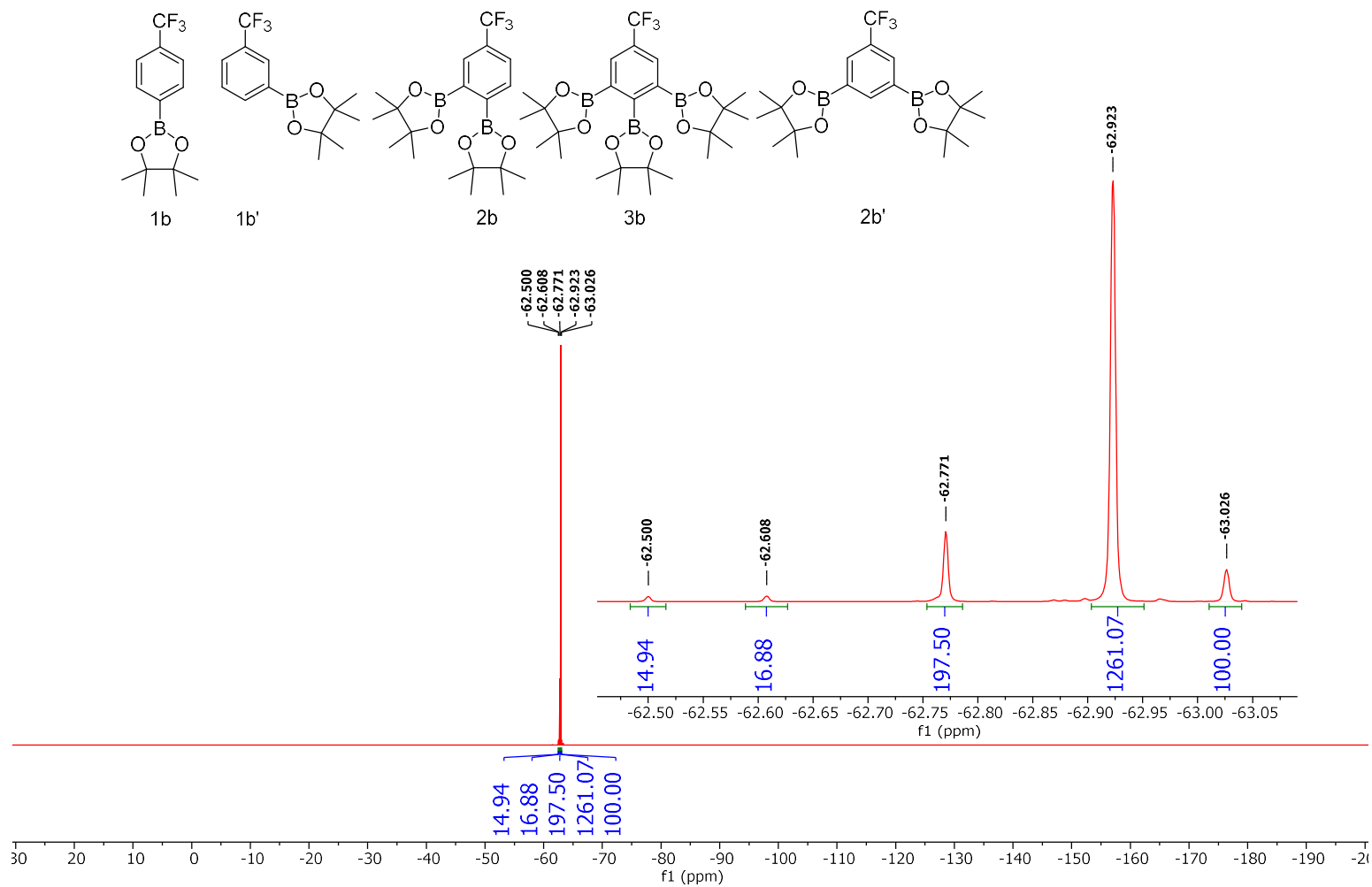


Figure 6-44 Conditions: 25 °C, 470 MHz,  $\text{CDCl}_3$

**<sup>13</sup>C NMR Spectra of the second purified fraction of the reaction mixture of Table 1 Entry 2 Trial 1**

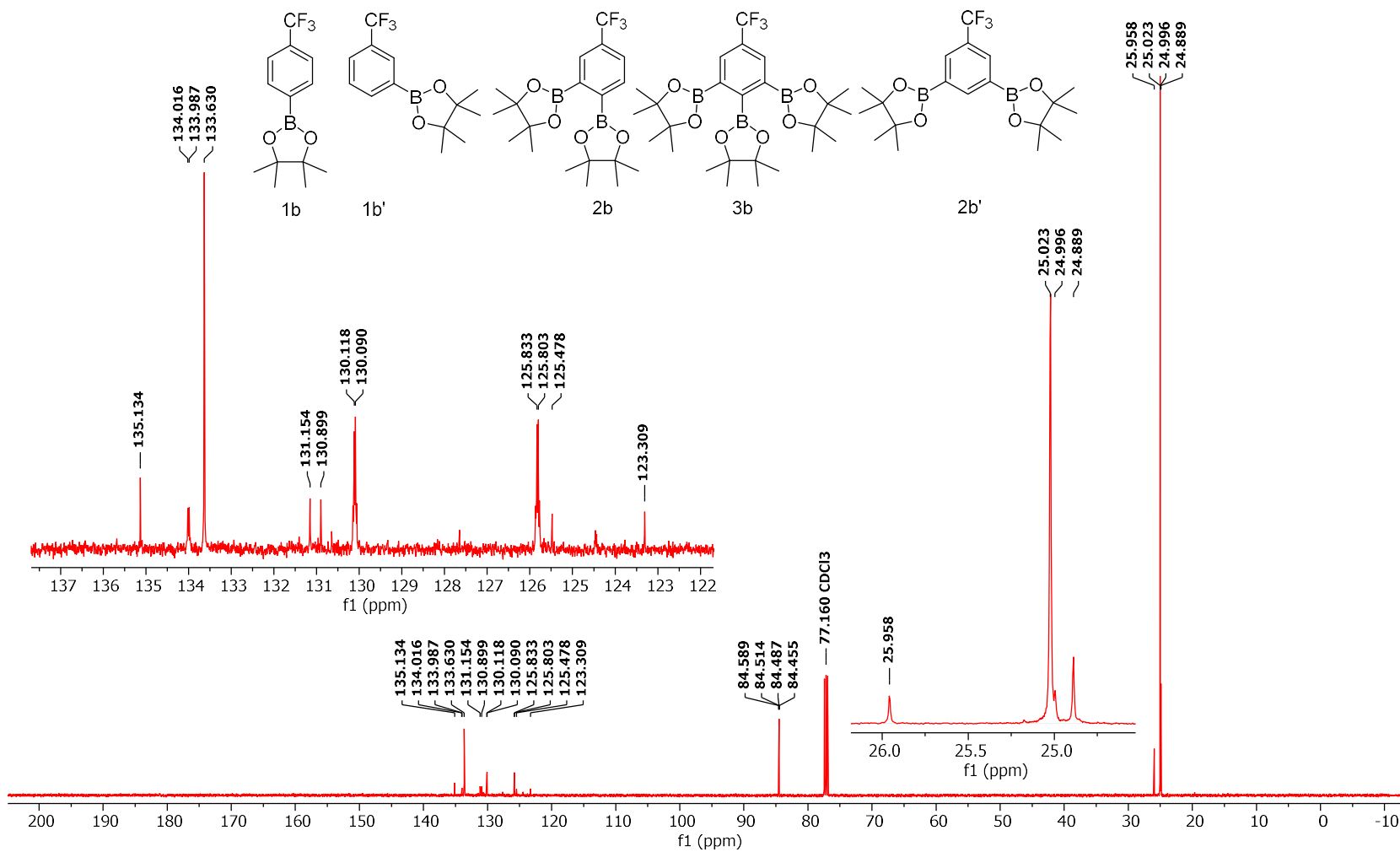


Figure 6-45 Conditions: 25 °C, 126 MHz, CDCl<sub>3</sub>

**$^{11}\text{B}$  NMR Spectra of the second purified fraction of the reaction mixture of Table 1 Entry 2 Trial 1**

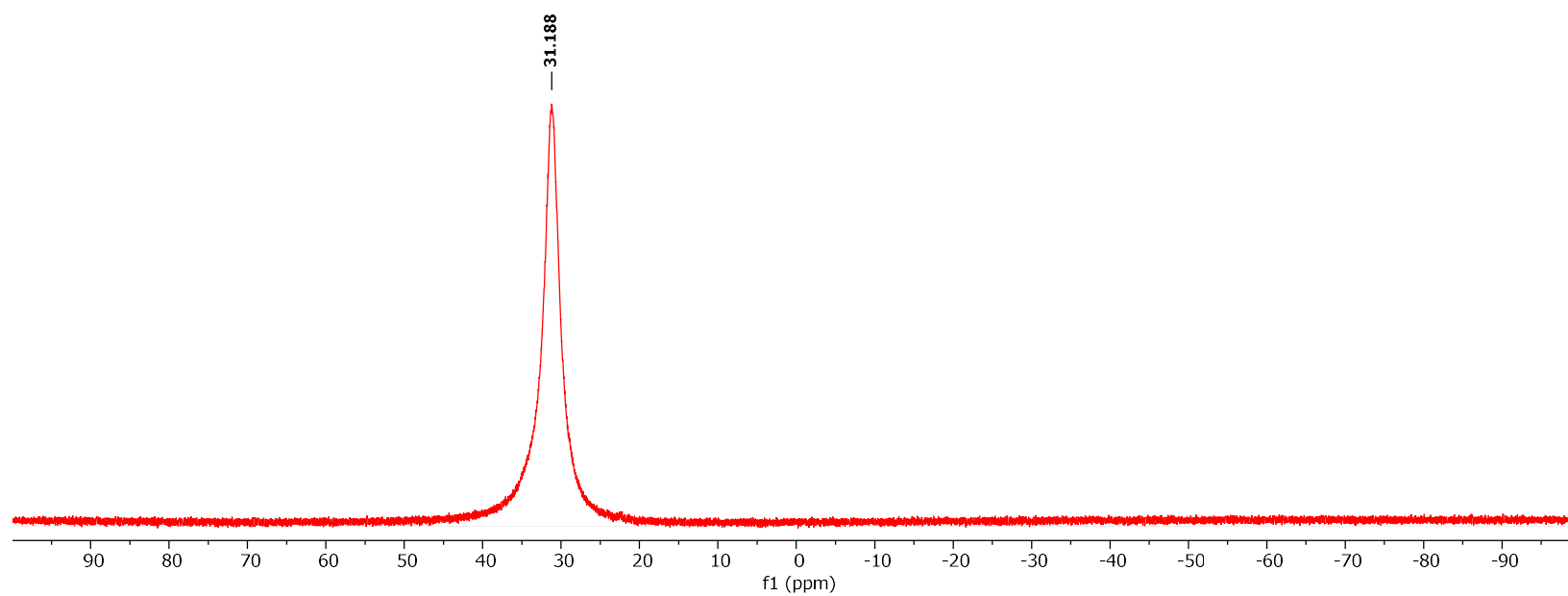
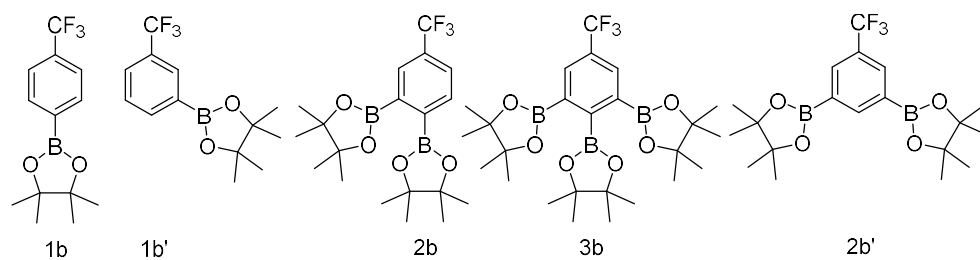


Figure 6-46 Conditions: 25 °C, 160 MHz,  $\text{CDCl}_3$

<sup>1</sup>H NMR Spectra of the third purified fraction of the reaction mixture of Table 1 Entry 2 Trial 1

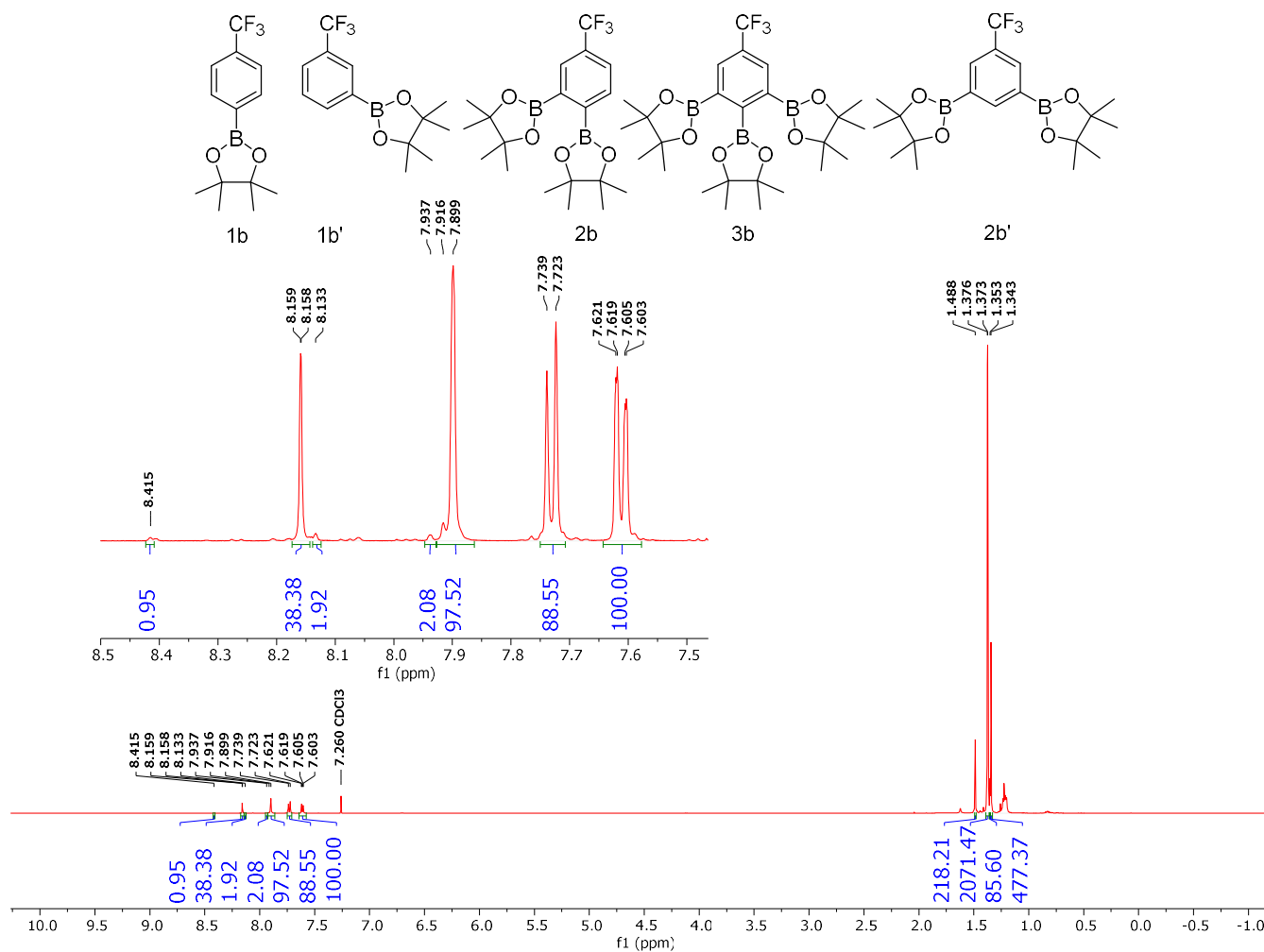


Figure 6-47 Conditions: 25 °C, 500 MHz, CDCl<sub>3</sub>



**$^{19}\text{F}$  NMR Spectra of the third purified fraction of the reaction mixture of Table 1 Entry 2 Trial 1**

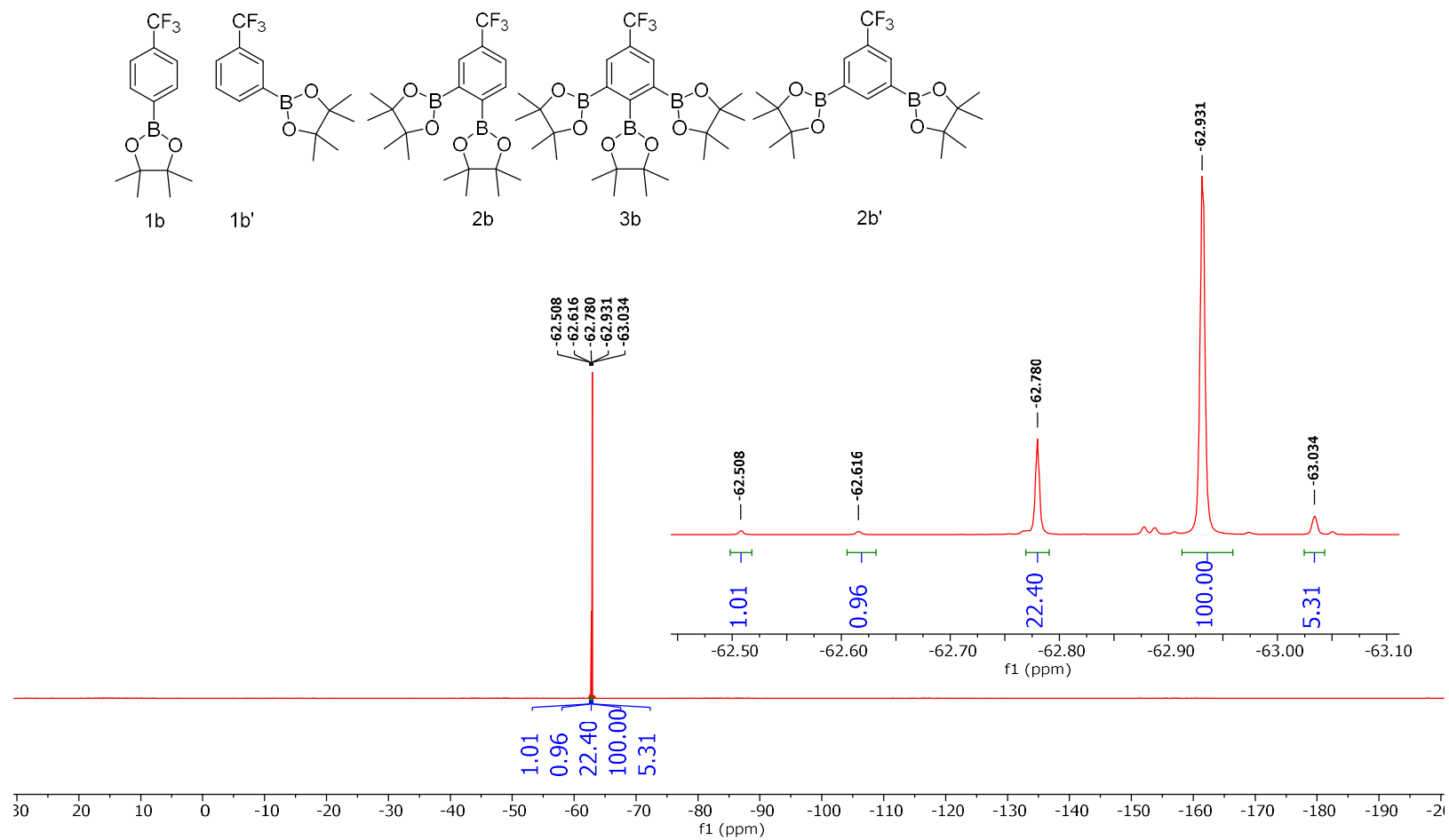


Figure 6-48 Conditions: 25 °C, 470 MHz,  $\text{CDCl}_3$

**<sup>13</sup>C NMR Spectra of the third purified fraction of the reaction mixture of Table 1 Entry 2 Trial 1**

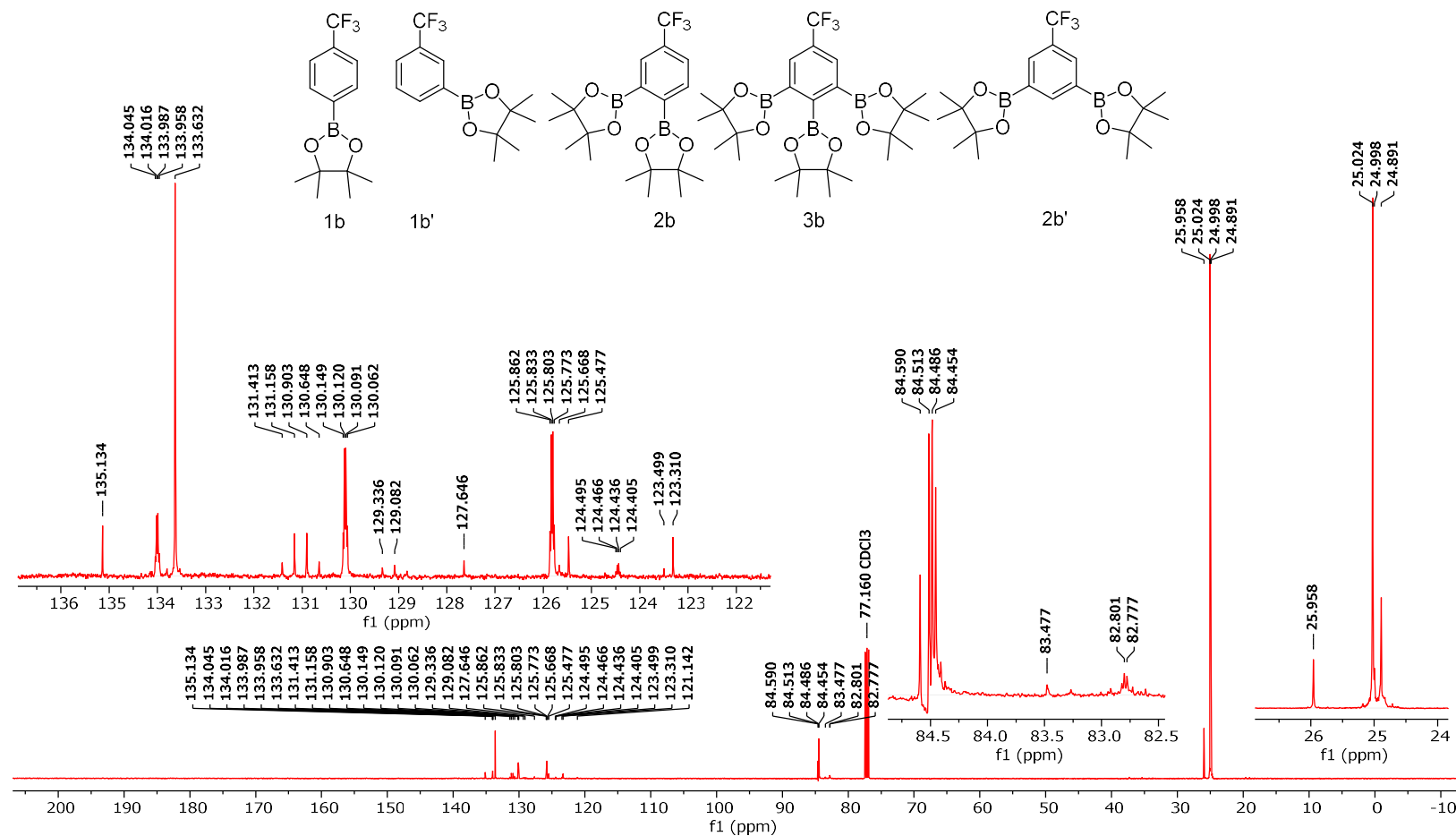


Figure 6-49 Conditions: 25 °C, 126 MHz, CDCl<sub>3</sub>

**$^{11}\text{B}$  NMR Spectra of the third purified fraction of the reaction mixture of Table 1 Entry 2 Trial 1**

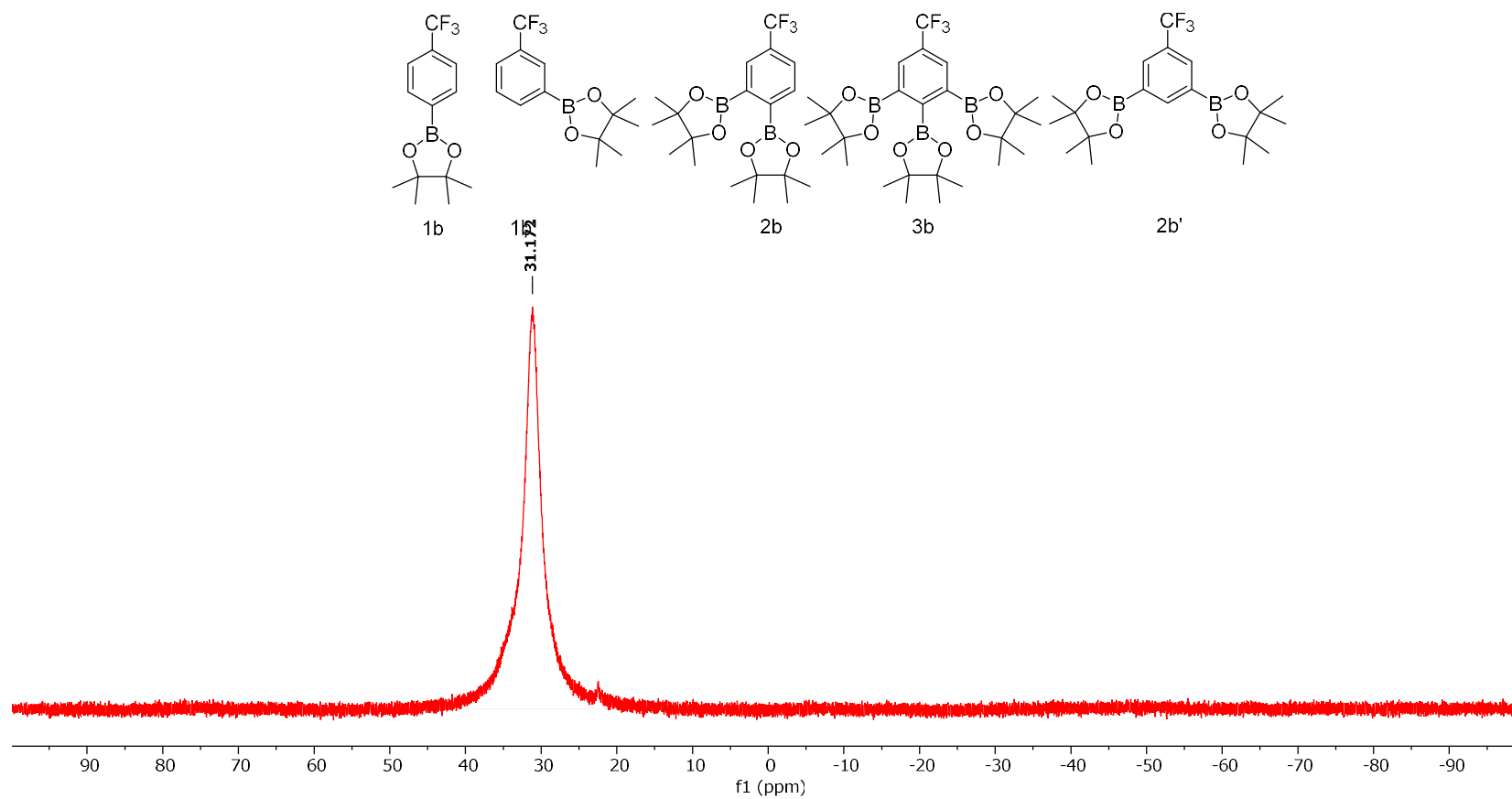


Figure 6-50 Conditions: 25 °C, 160 MHz,  $\text{CDCl}_3$

**<sup>1</sup>H NMR Spectra of the crude reaction mixture of Table 1 Entry 2 Trial 2**

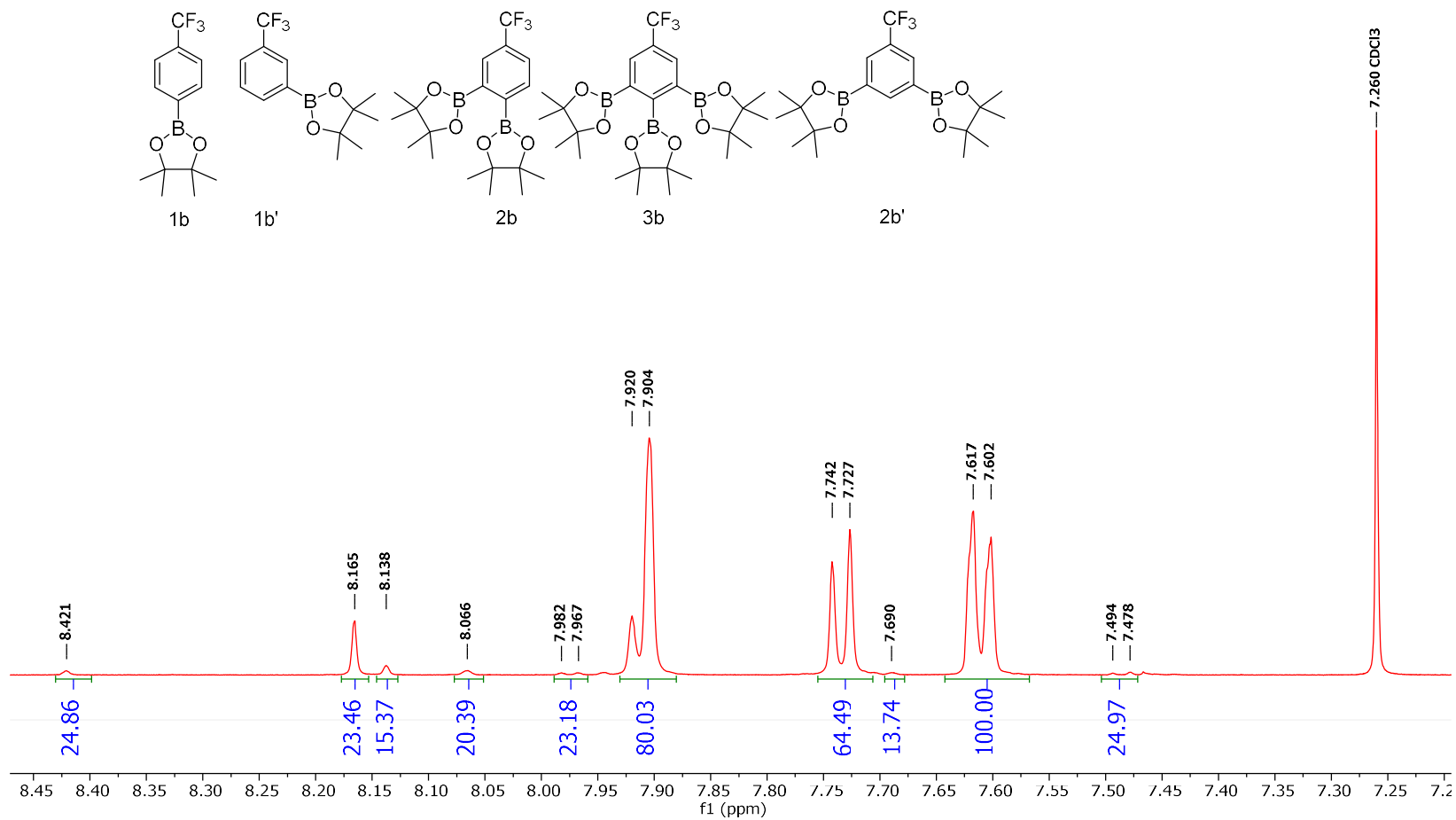


Figure 6-51 Conditions: 25 °C, 500 MHz, CDCl<sub>3</sub>

**$^{19}\text{F}$  NMR Spectra of the crude reaction mixture of Table 1 Entry 2 Trial 2**

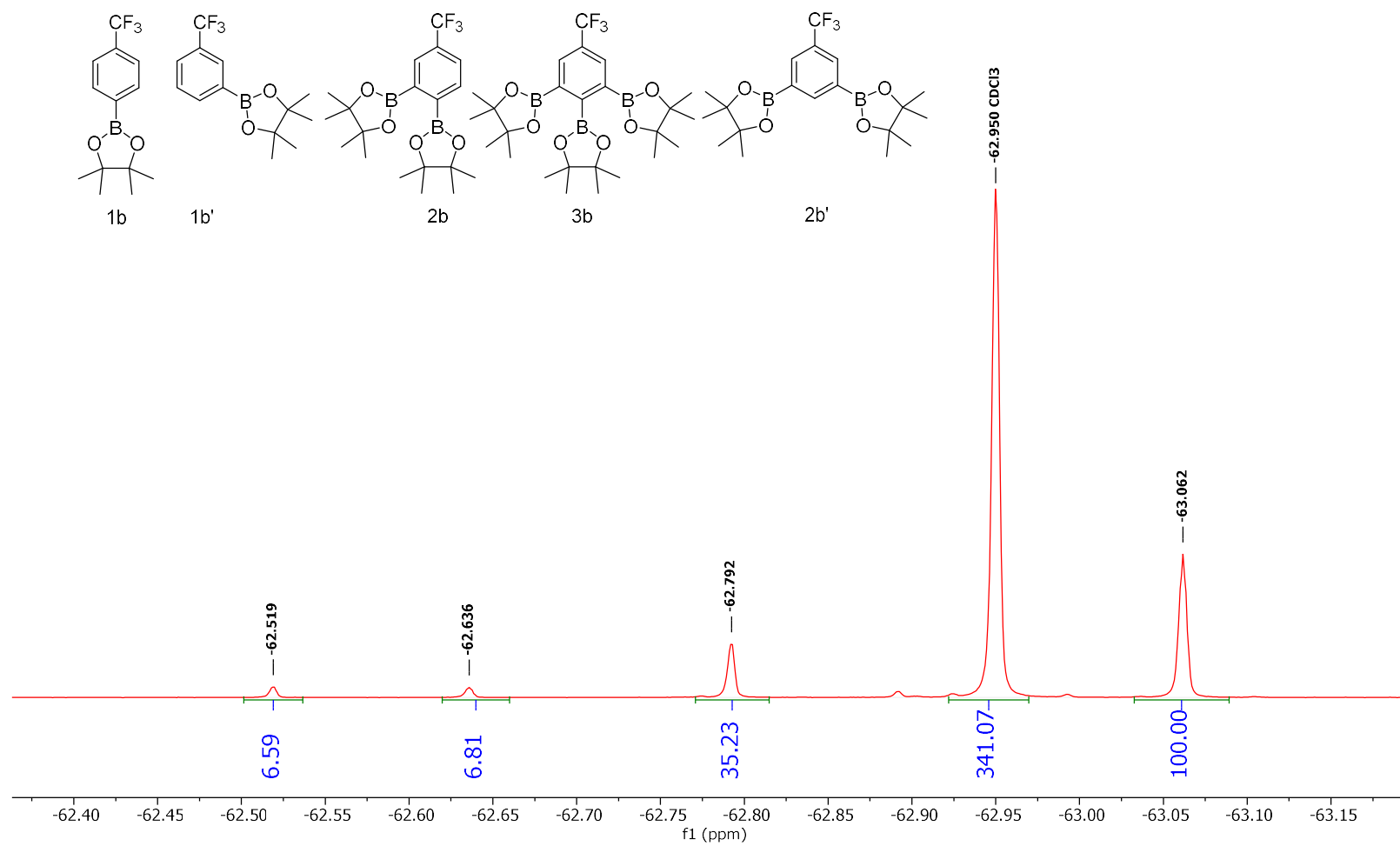


Figure 6-52 Conditions: 25 °C, 470 MHz, CDCl<sub>3</sub>

**<sup>1</sup>H NMR Spectra of the crude reaction mixture of Table 1 Entry 2 Trial 3**

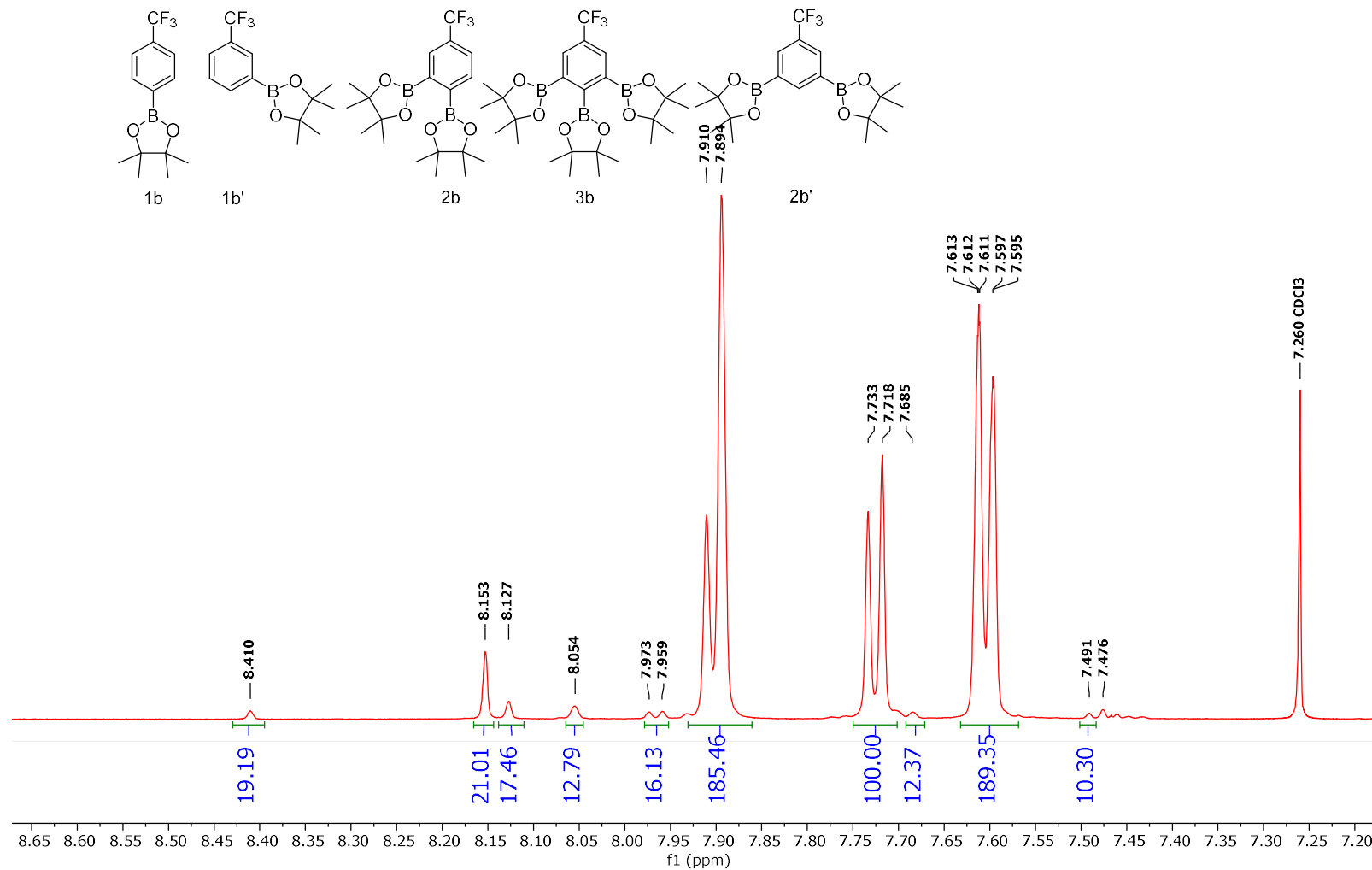


Figure 6-53 Conditions: 25 °C, 500 MHz, CDCl<sub>3</sub>

**<sup>1</sup>H NMR Spectra of the crude reaction mixture of Table 1 Entry 3 Trial 1**

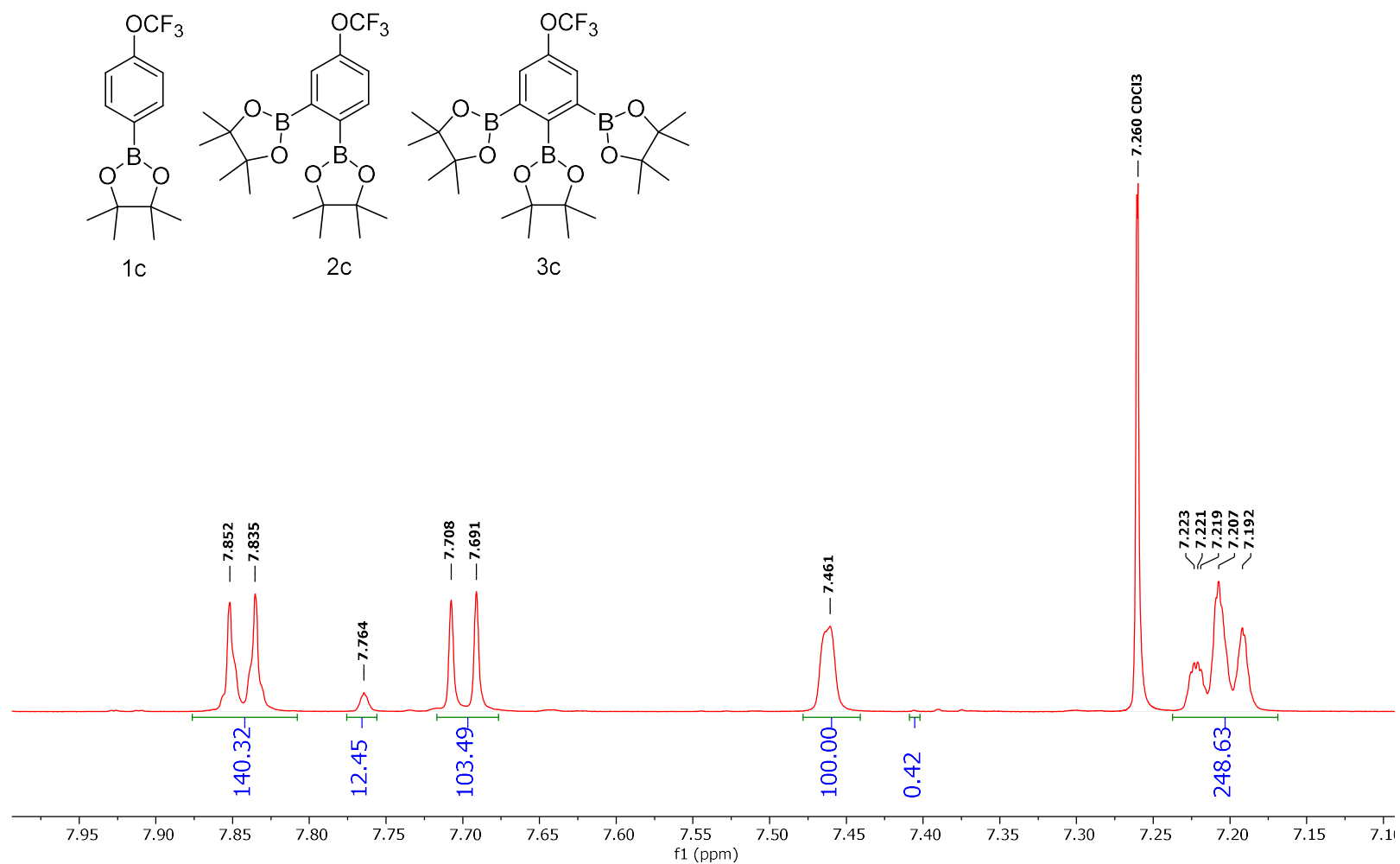


Figure 6-54 Conditions: 25 °C, 500 MHz, CDCl<sub>3</sub>

**$^{19}\text{F}$  NMR Spectra of the crude reaction mixture of Table 1 Entry 3 Trial 1**

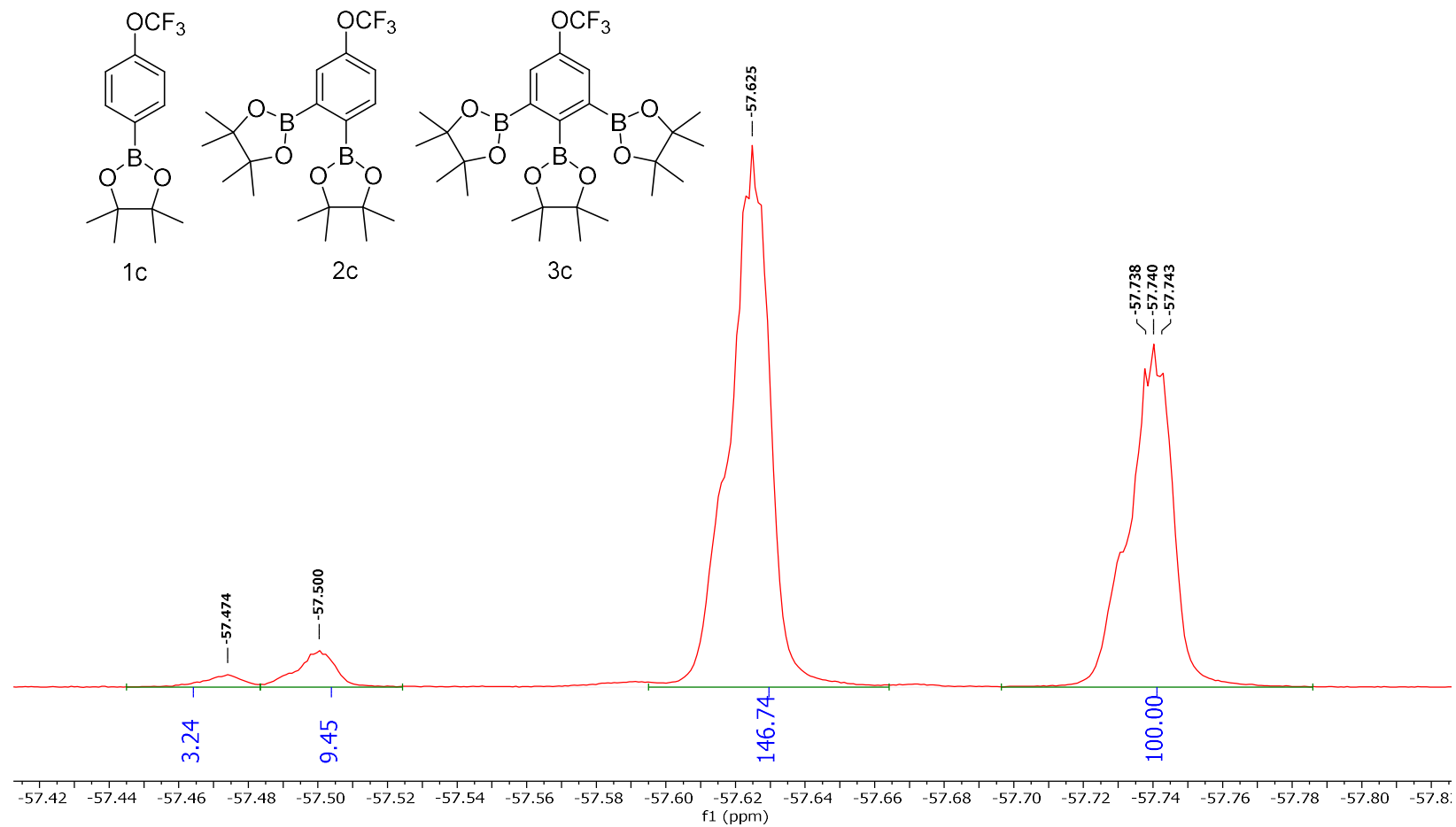


Figure 6-55 Conditions: 25 °C, 470 MHz, CDCl<sub>3</sub>



<sup>1</sup>H NMR Spectra of the Isolated reaction mixture of Table 1 Entry 3 Trial 1

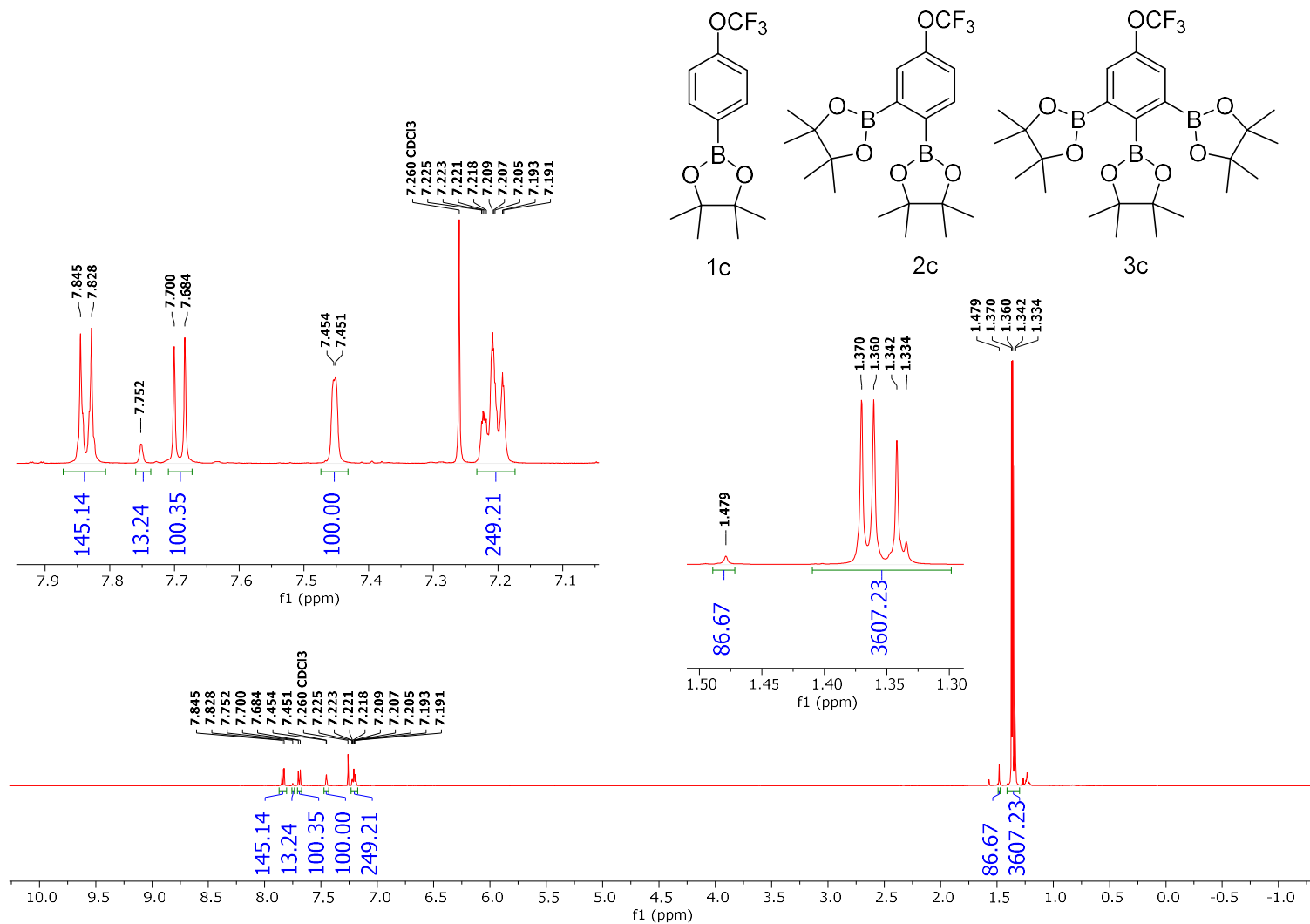


Figure 6-56 Conditions: 25 °C, 500 MHz, CDCl<sub>3</sub>

**$^{19}\text{F}$  NMR Spectra of the Isolated reaction mixture of Table 1 Entry 3 Trial 1**

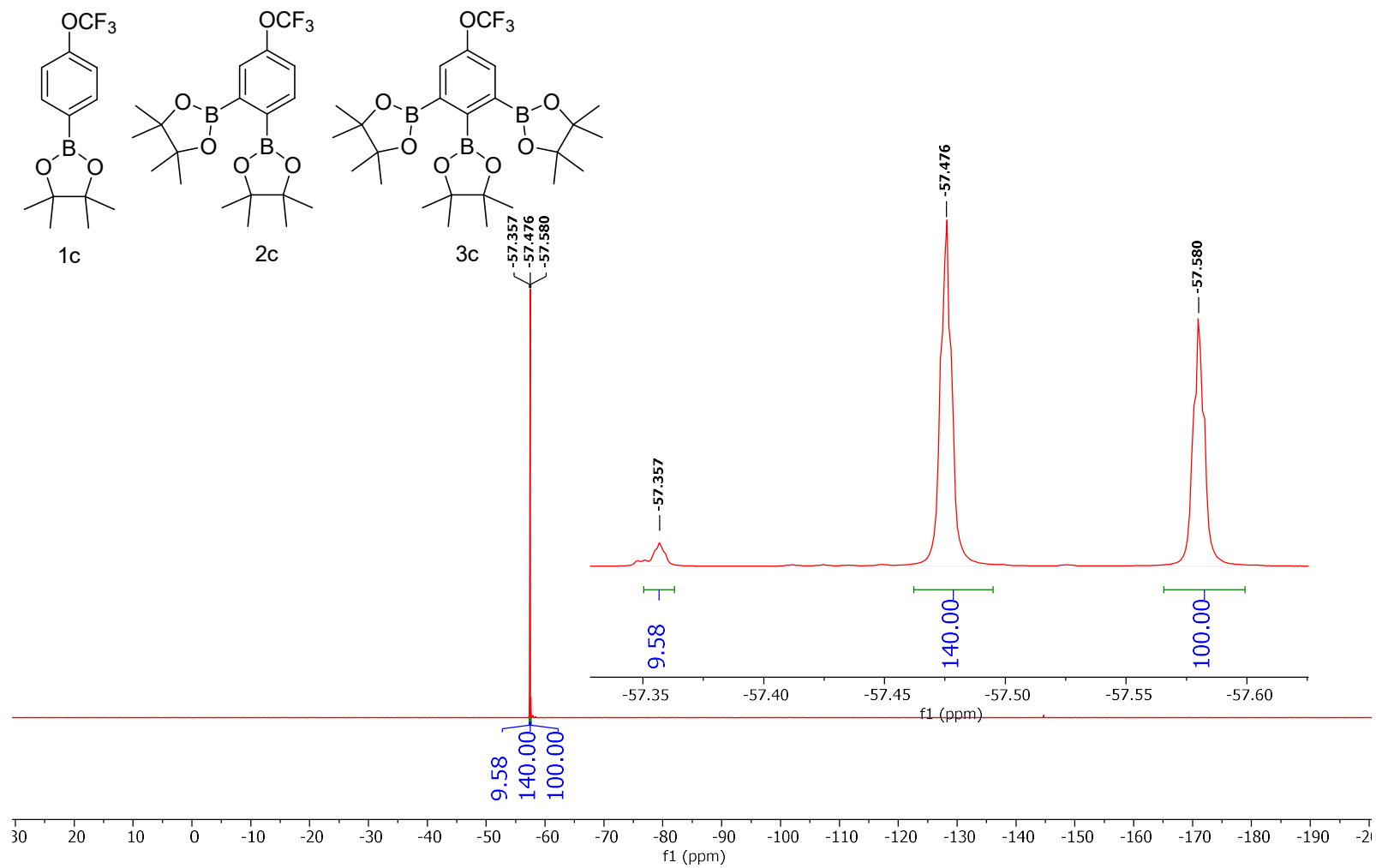


Figure 6-57 Conditions: 25 °C, 470 MHz,  $\text{CDCl}_3$

**<sup>13</sup>C NMR Spectra of the Isolated reaction mixture of Table 1 Entry 3 Trial 1**

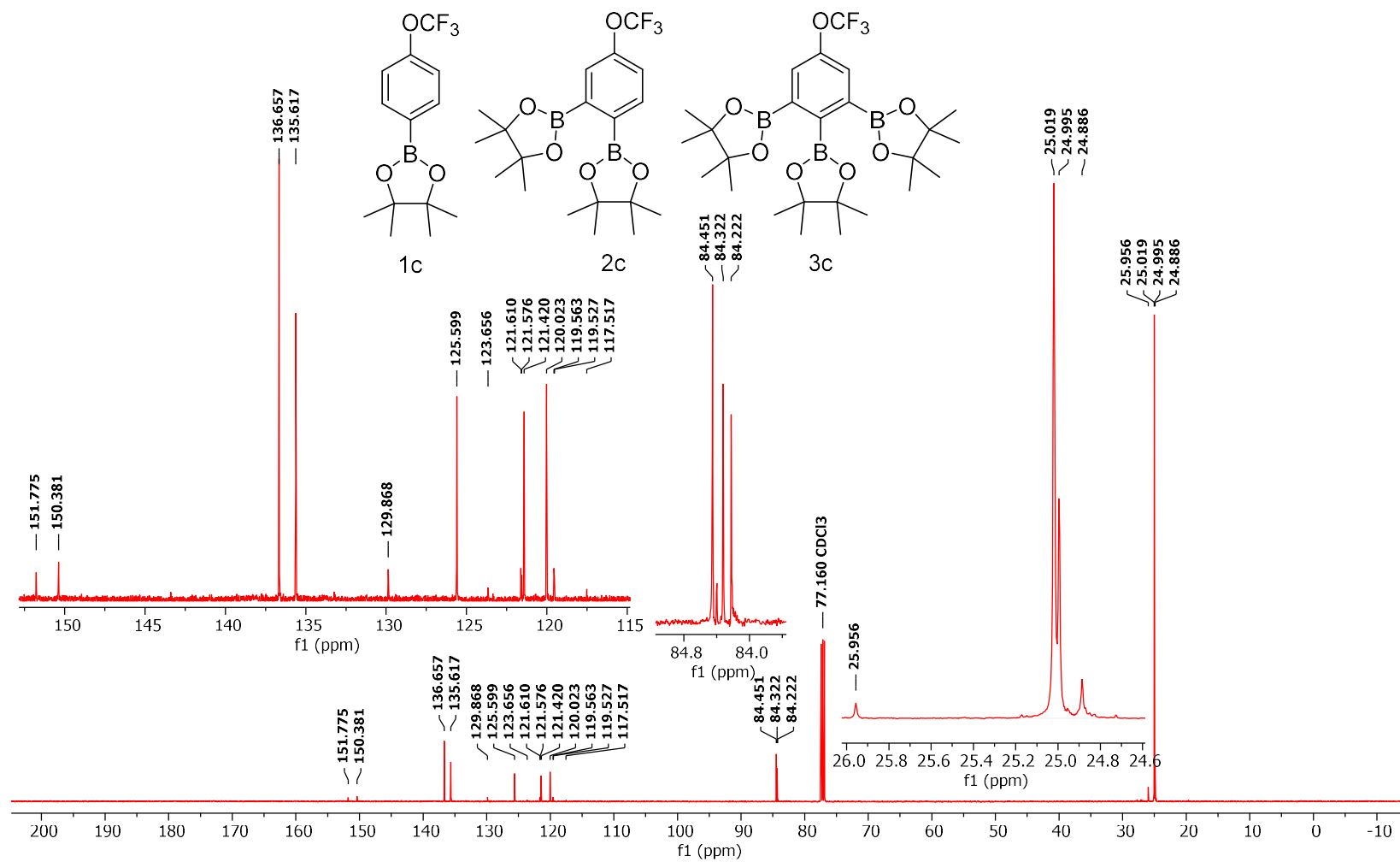


Figure 6-58 Conditions: 25 °C, 126 MHz, CDCl<sub>3</sub>

**$^{11}\text{B}$  NMR Spectra of the Isolated reaction mixture of Table 1 Entry 3 Trial 1**

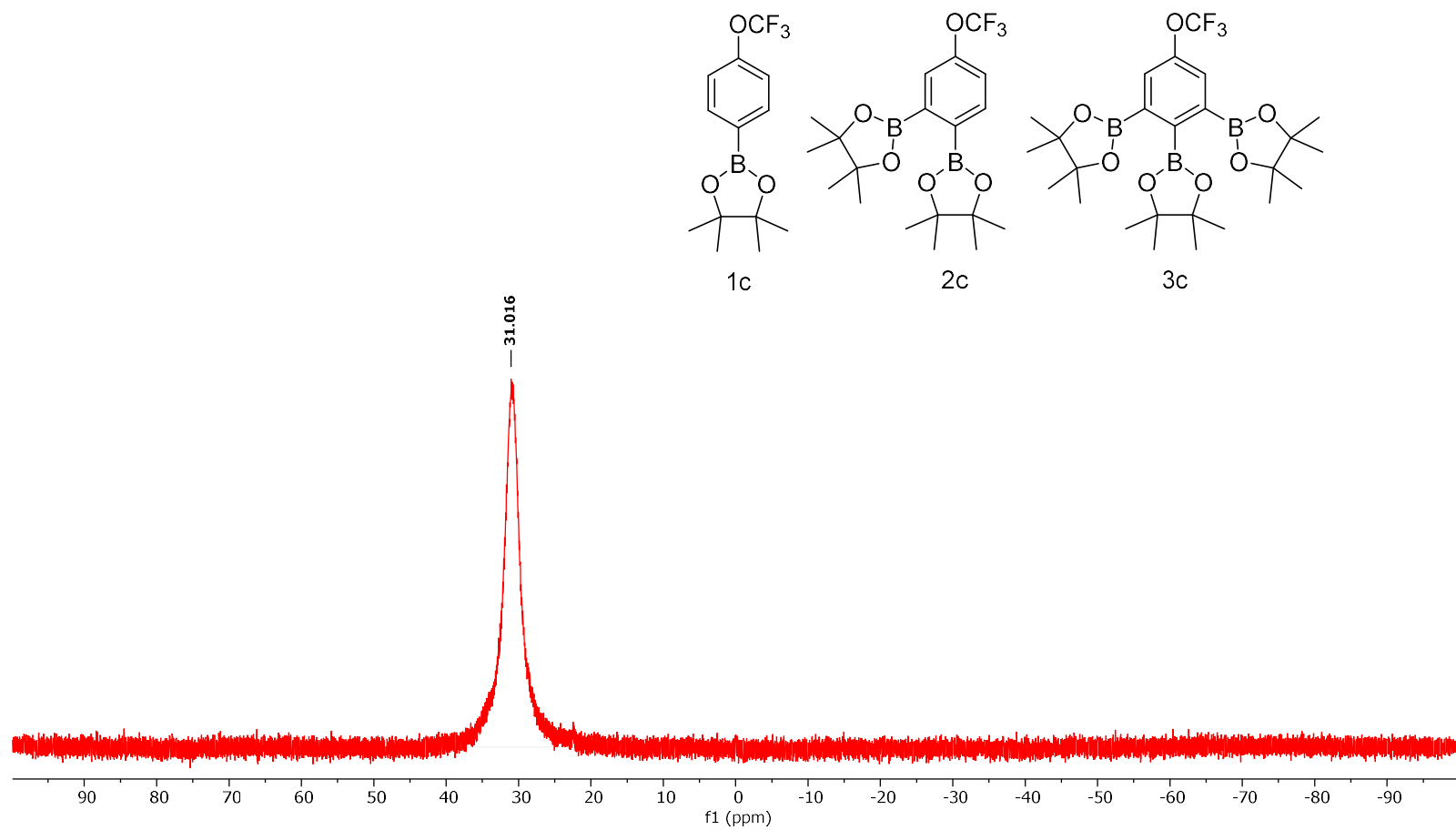


Figure 6-59 Conditions: 25 °C, 160 MHz,  $\text{CDCl}_3$

**<sup>1</sup>H NMR Spectra of the Isolated reaction mixture of Table 1 Entry 3 Trial 2**

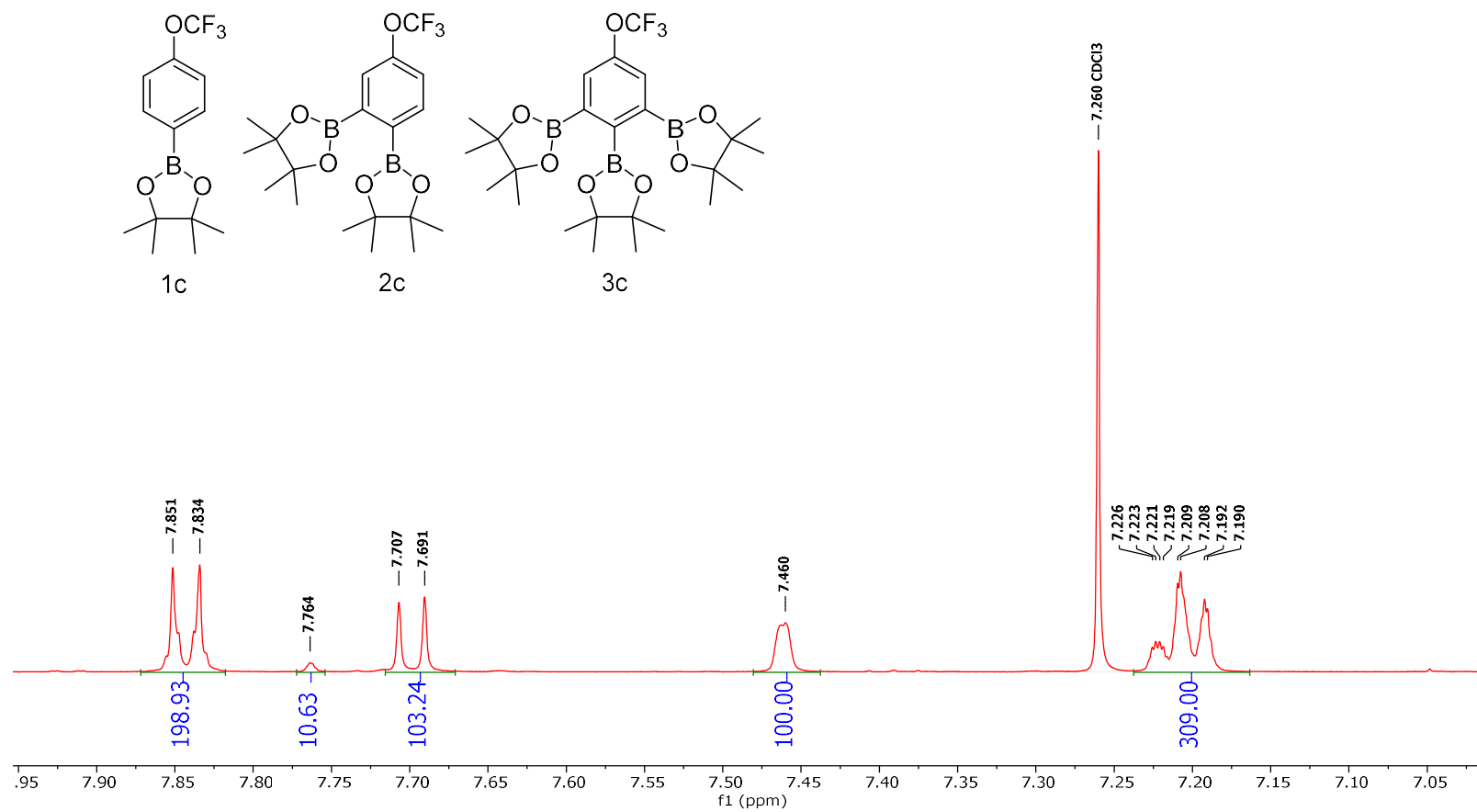


Figure 6-60 Conditions: 25 °C, 500 MHz, CDCl<sub>3</sub>

<sup>19</sup>F NMR Spectra of the Crude Reaction mixture of Table 1 Entry 3 Trial 2

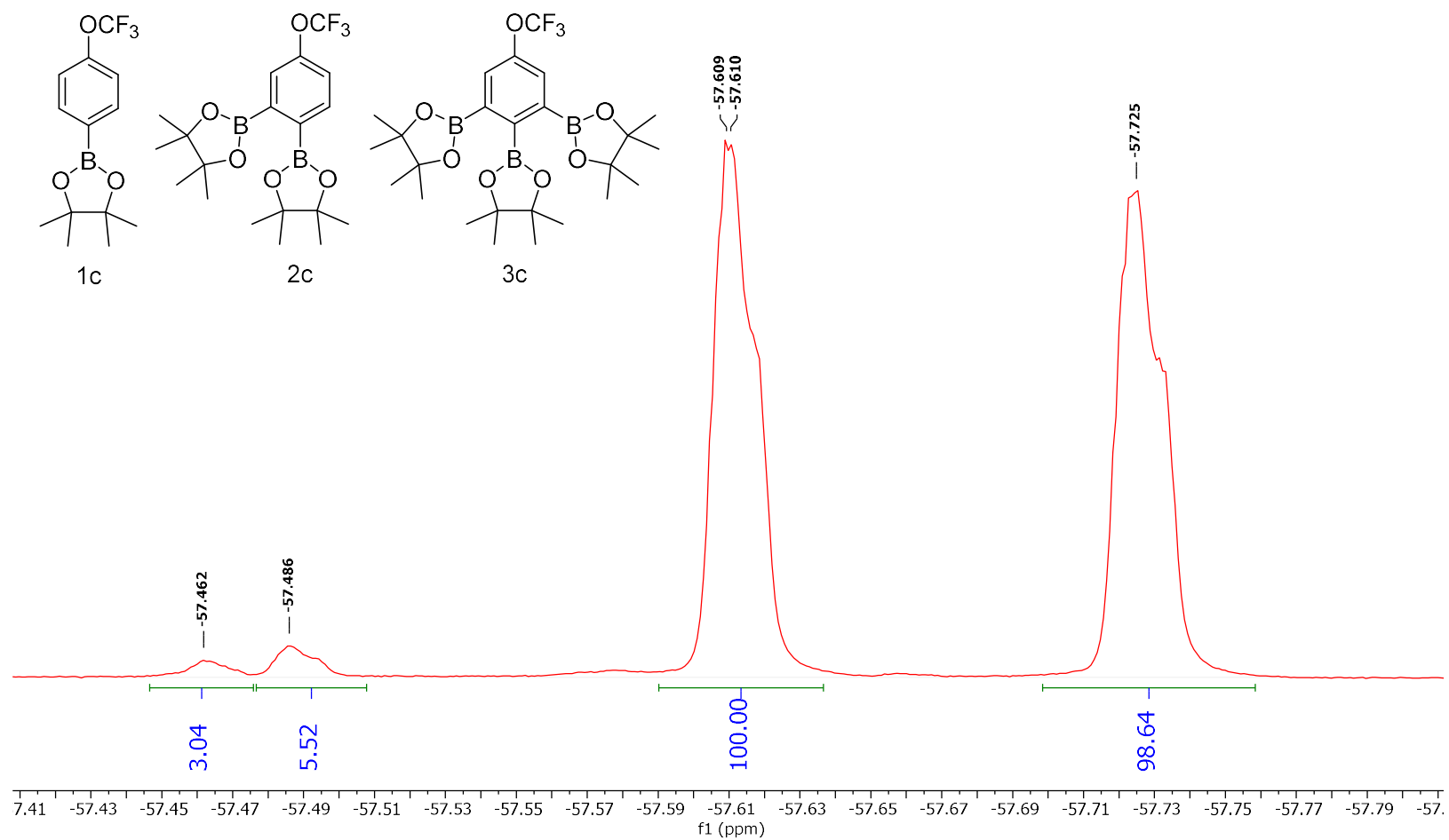


Figure 6-61 Conditions: 25 °C, 470 MHz, CDCl<sub>3</sub>

<sup>1</sup>H NMR Spectra of the Crude Reaction Mixture of Table 1 Entry 4 Trial 1

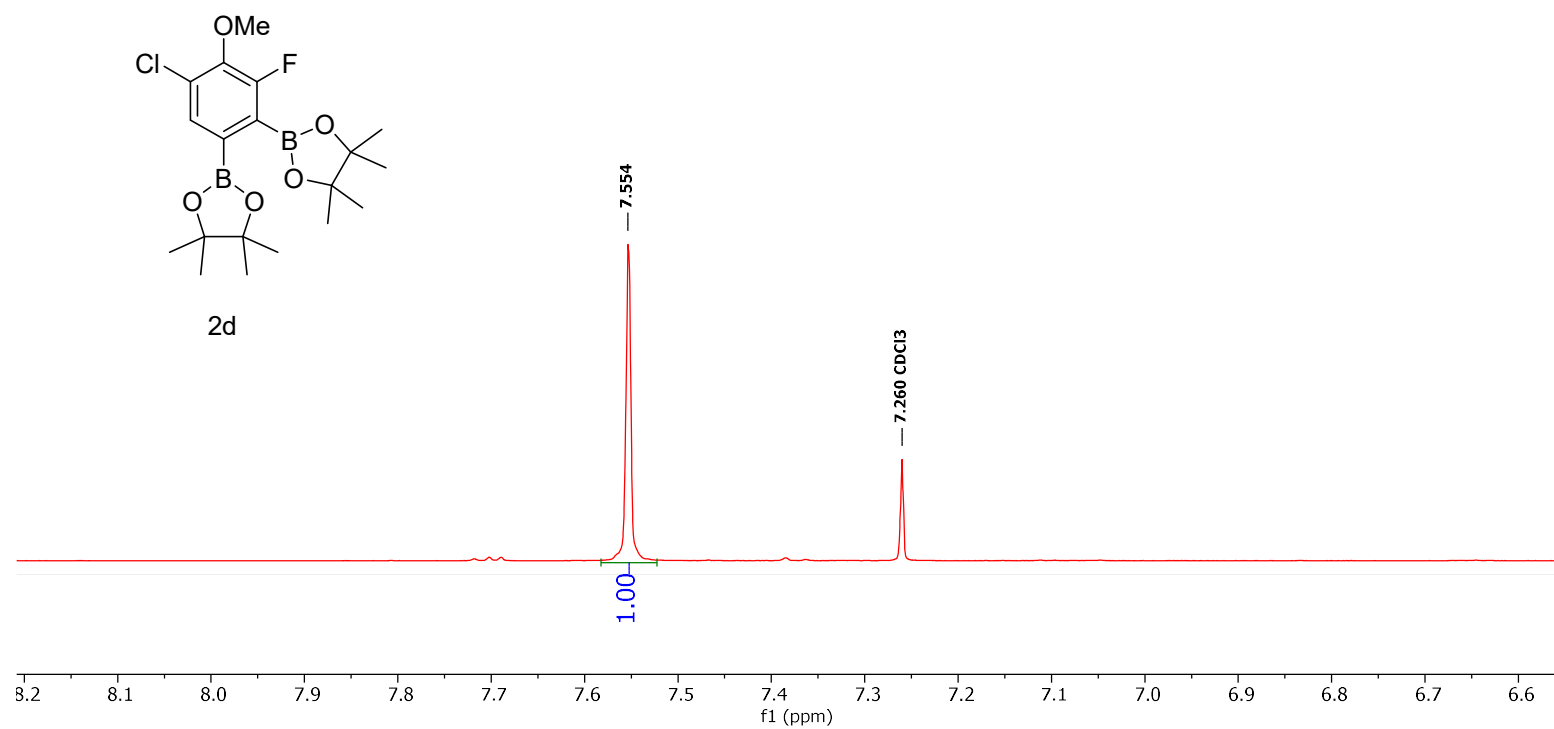


Figure 6-62 Conditions: 25 °C, 500 MHz, CDCl<sub>3</sub>

**<sup>1</sup>H NMR Spectra of the Isolated Reaction Mixture of Table 1 Entry 4 Trial 1**

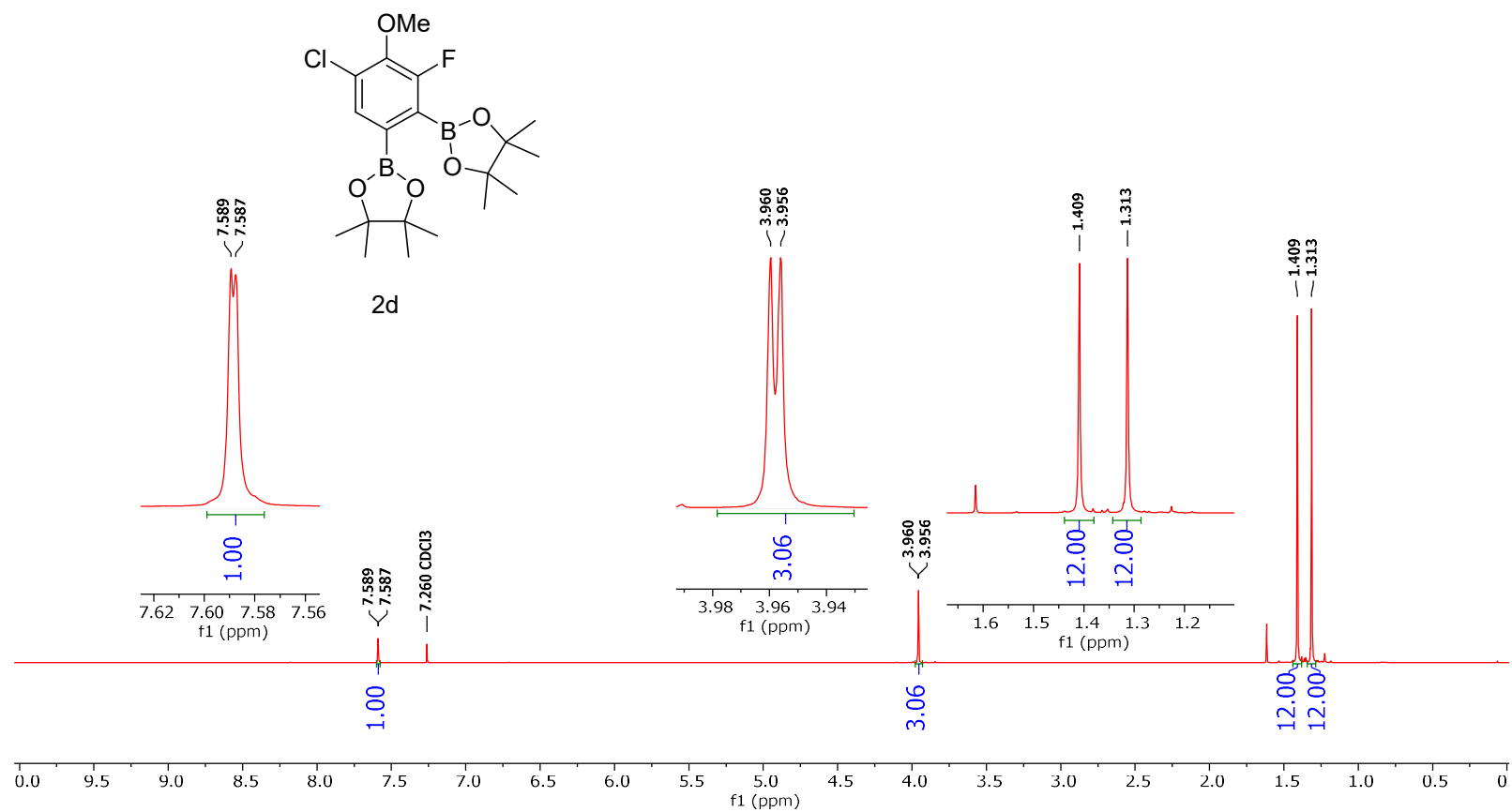


Figure 6-63 Conditions: 25 °C, 500 MHz, CDCl<sub>3</sub>



**$^{19}\text{F}$  NMR Spectra of the isolated reaction mixture of Table 1 Entry 4 Trial 1**

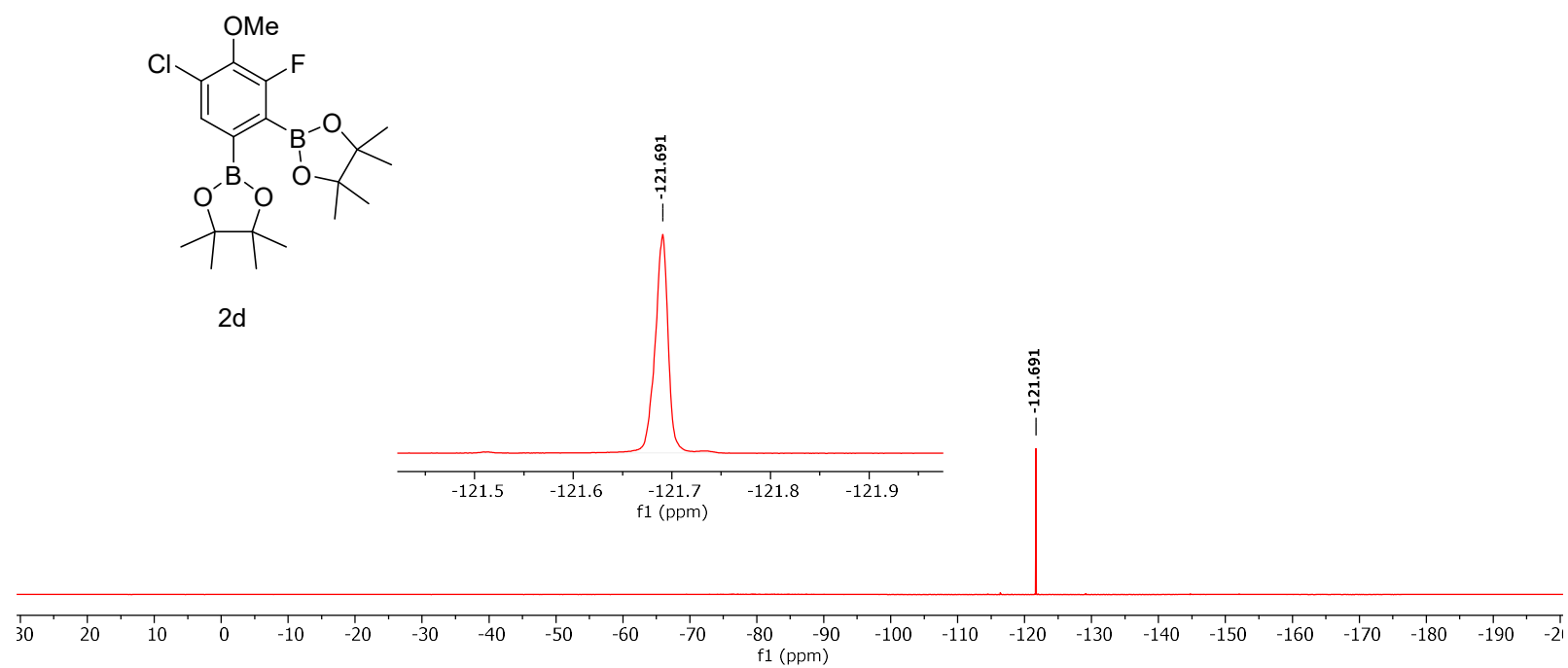


Figure 6-64 Conditions: 25 °C, 470 MHz, CDCl<sub>3</sub>

**<sup>13</sup>C NMR Spectra of the isolated reaction mixture of Table 1 Entry 4 Trial 1**

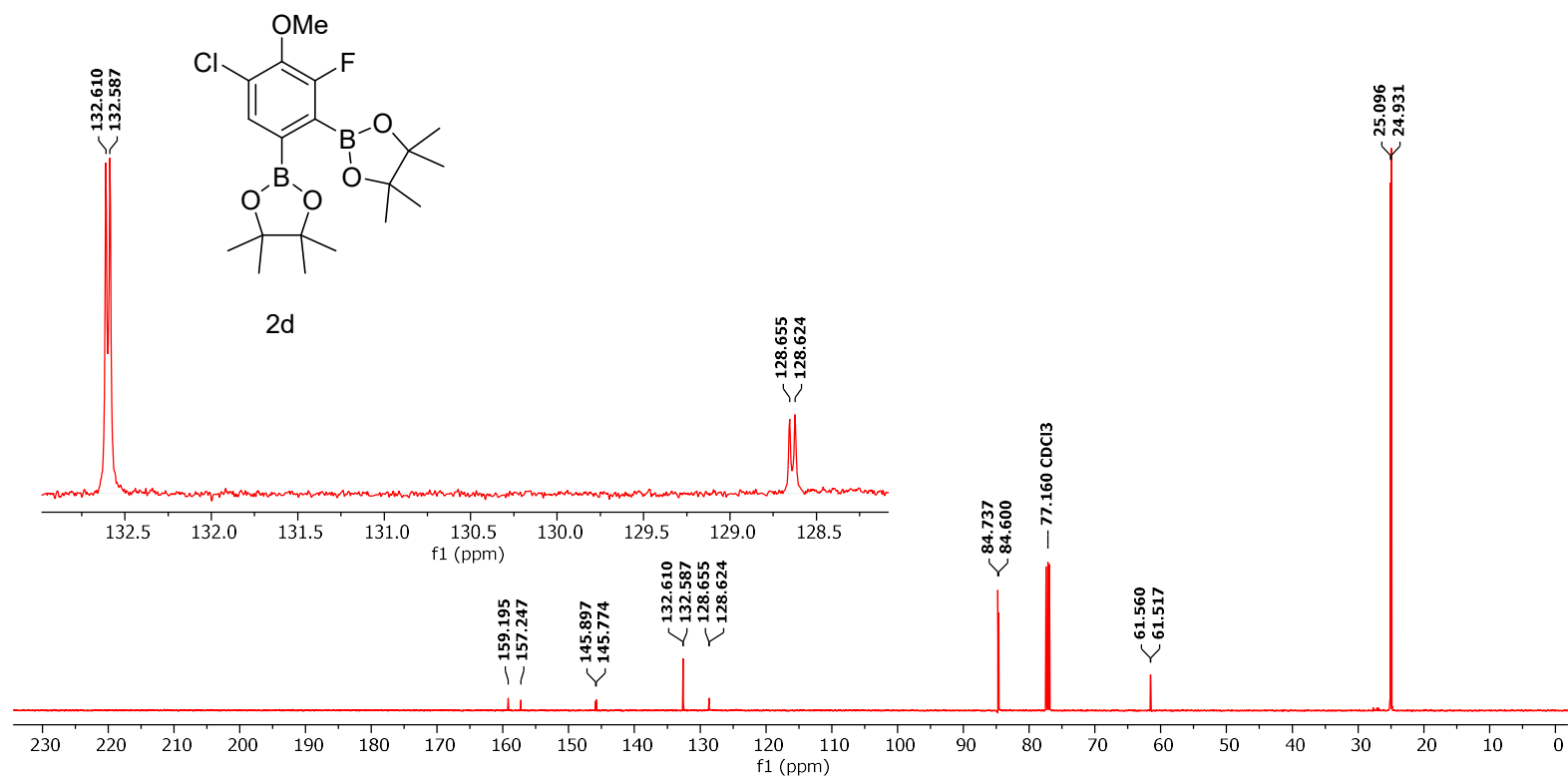


Figure 6-65 Conditions: 25 °C, 126 MHz, CDCl<sub>3</sub>

**$^{11}\text{B}$  NMR Spectra of the isolated reaction mixture of Table 1 Entry 4 Trial 1**

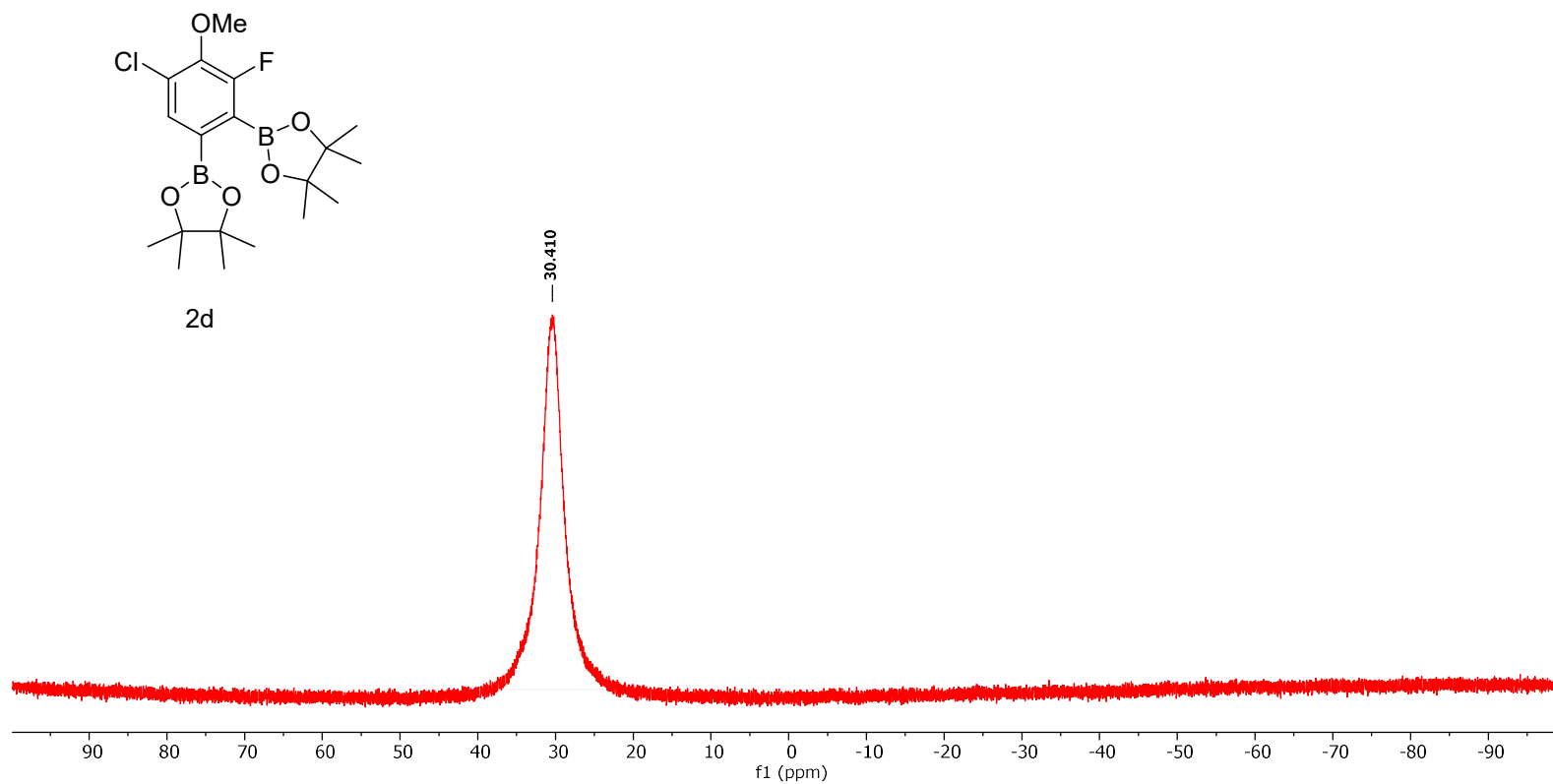


Figure 6-66 Conditions: 25 °C, 160 MHz,  $\text{CDCl}_3$

<sup>1</sup>H NMR Spectra of the crude reaction mixture of Table 1 Entry 5 Trial 1

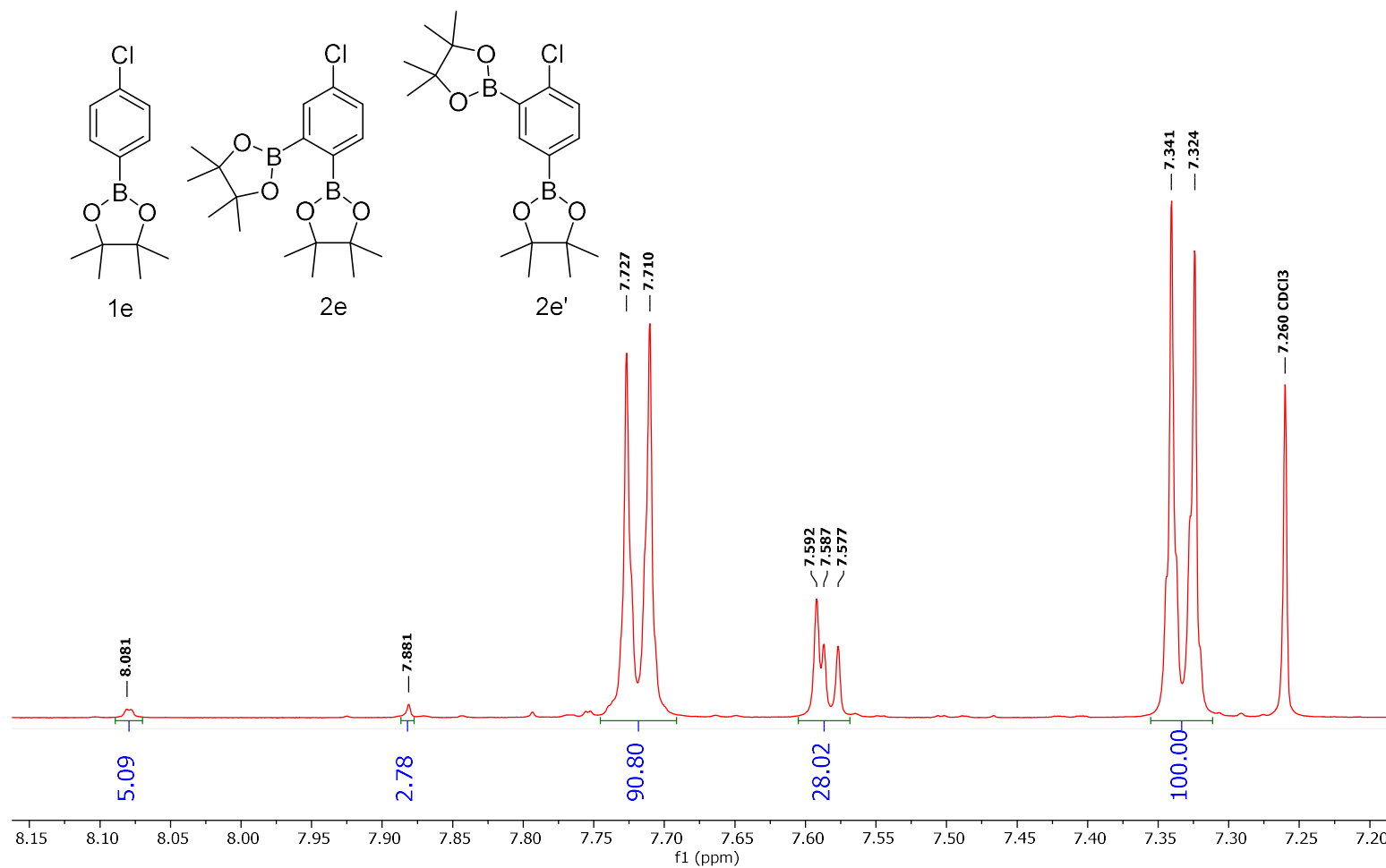


Figure 6-67 Conditions: 25 °C, 500 MHz, CDCl<sub>3</sub>

<sup>1</sup>H NMR Spectra of the isolated reaction mixture of Table 1 Entry 5 Trial 1

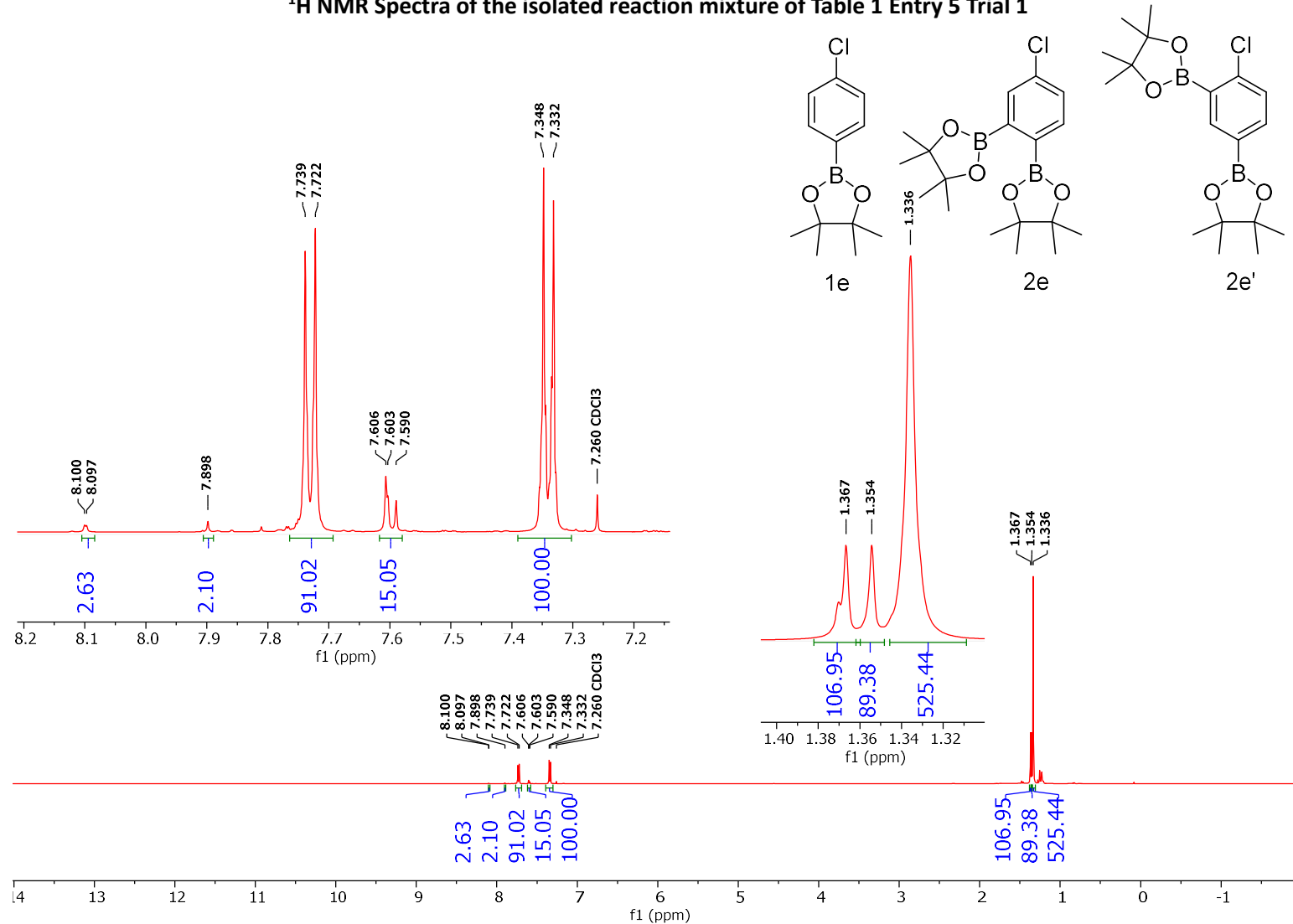


Figure 6-68 Conditions: 25 °C, 500 MHz, CDCl<sub>3</sub>

**<sup>13</sup>C NMR Spectra of the isolated reaction mixture of Table 1 Entry 5 Trial 1**

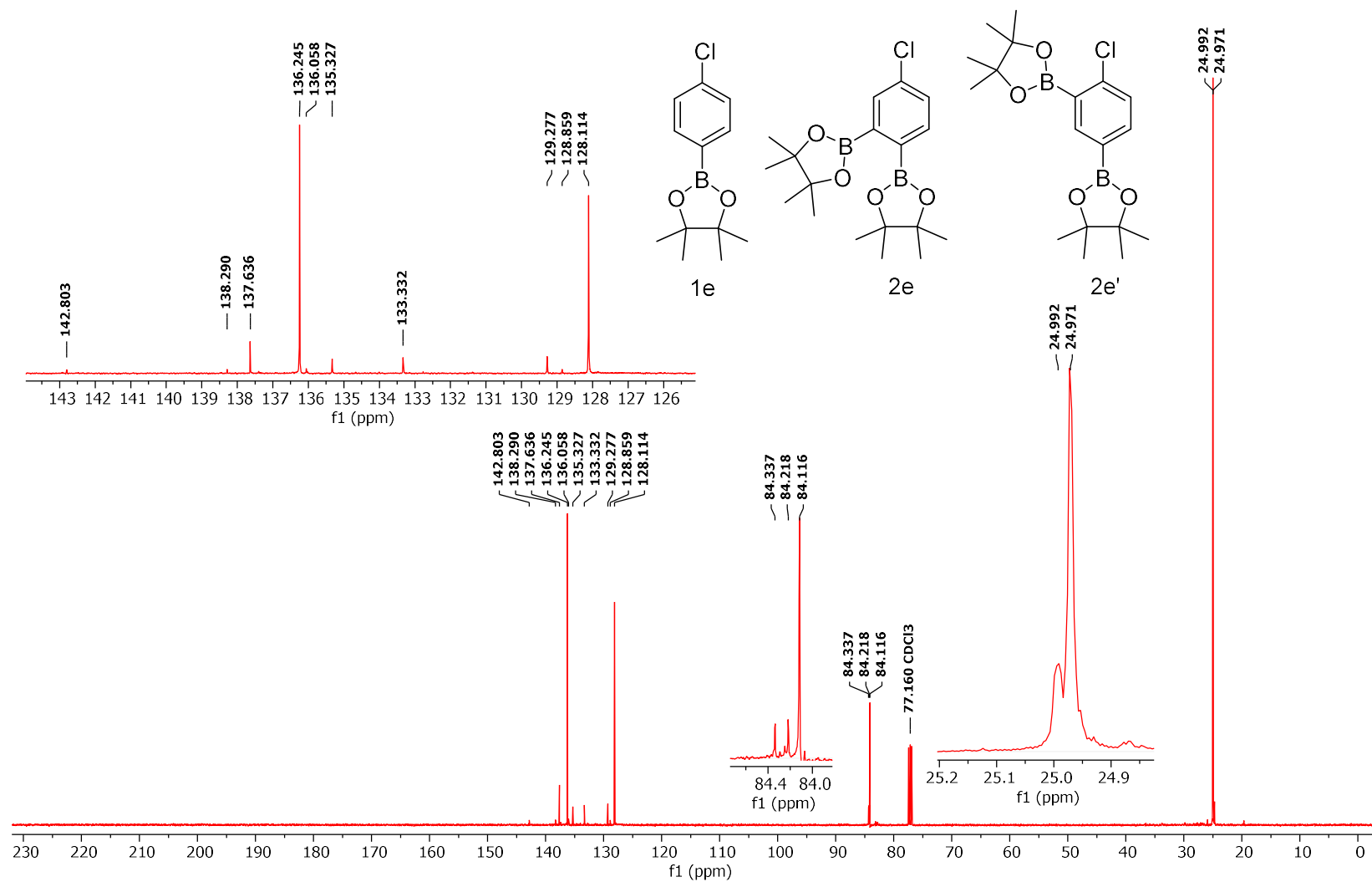


Figure 6-69 Conditions: 25 °C, 126 MHz, CDCl<sub>3</sub>

**$^{11}\text{B}$  NMR Spectra of the isolated reaction mixture of Table 1 Entry 5 Trial 1**

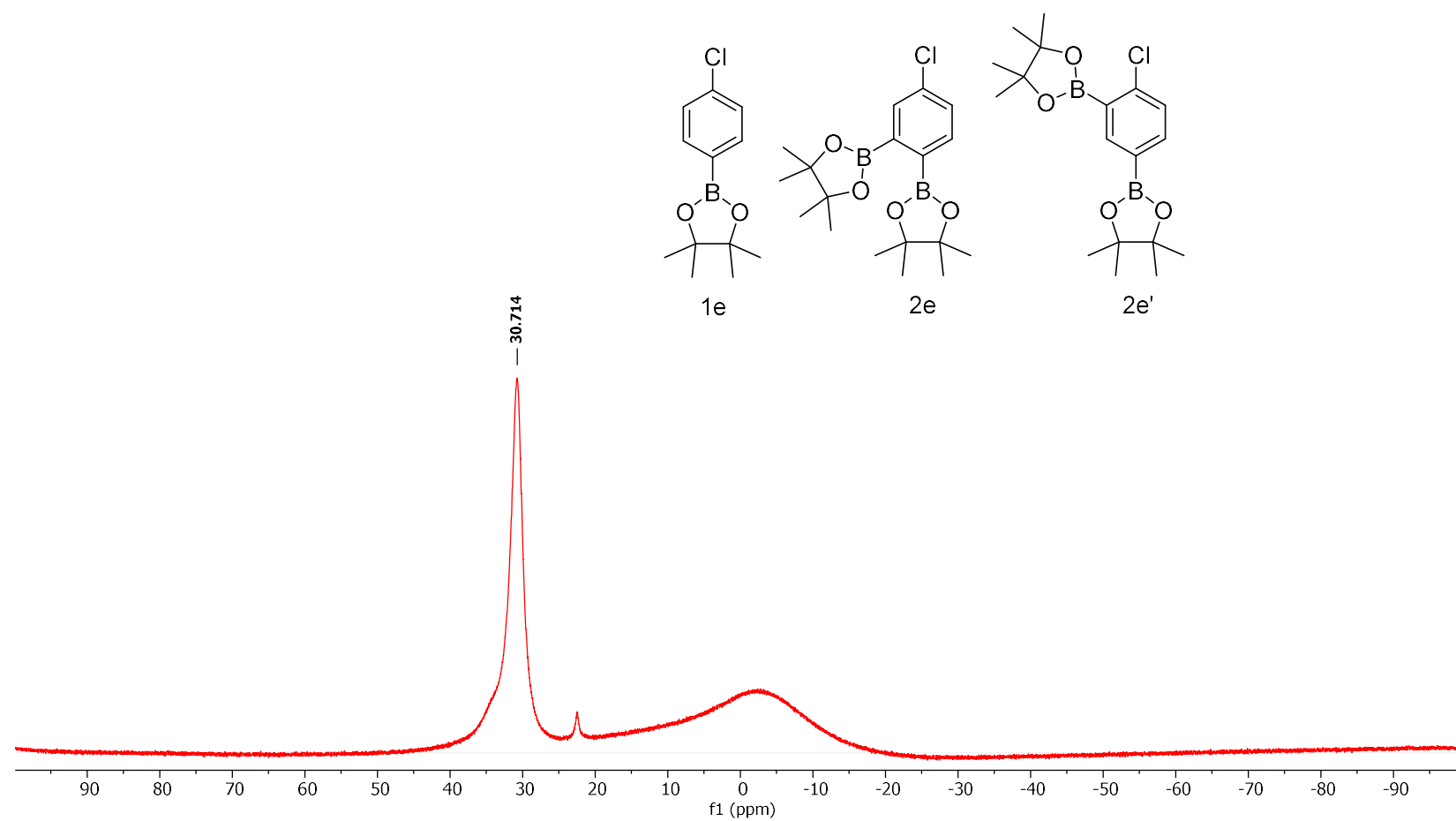


Figure 6-70 Conditions: 25 °C, 160 MHz,  $\text{CDCl}_3$

<sup>1</sup>H NMR Spectra of the Crude reaction mixture of Table 2 Entry 1 Trial 1

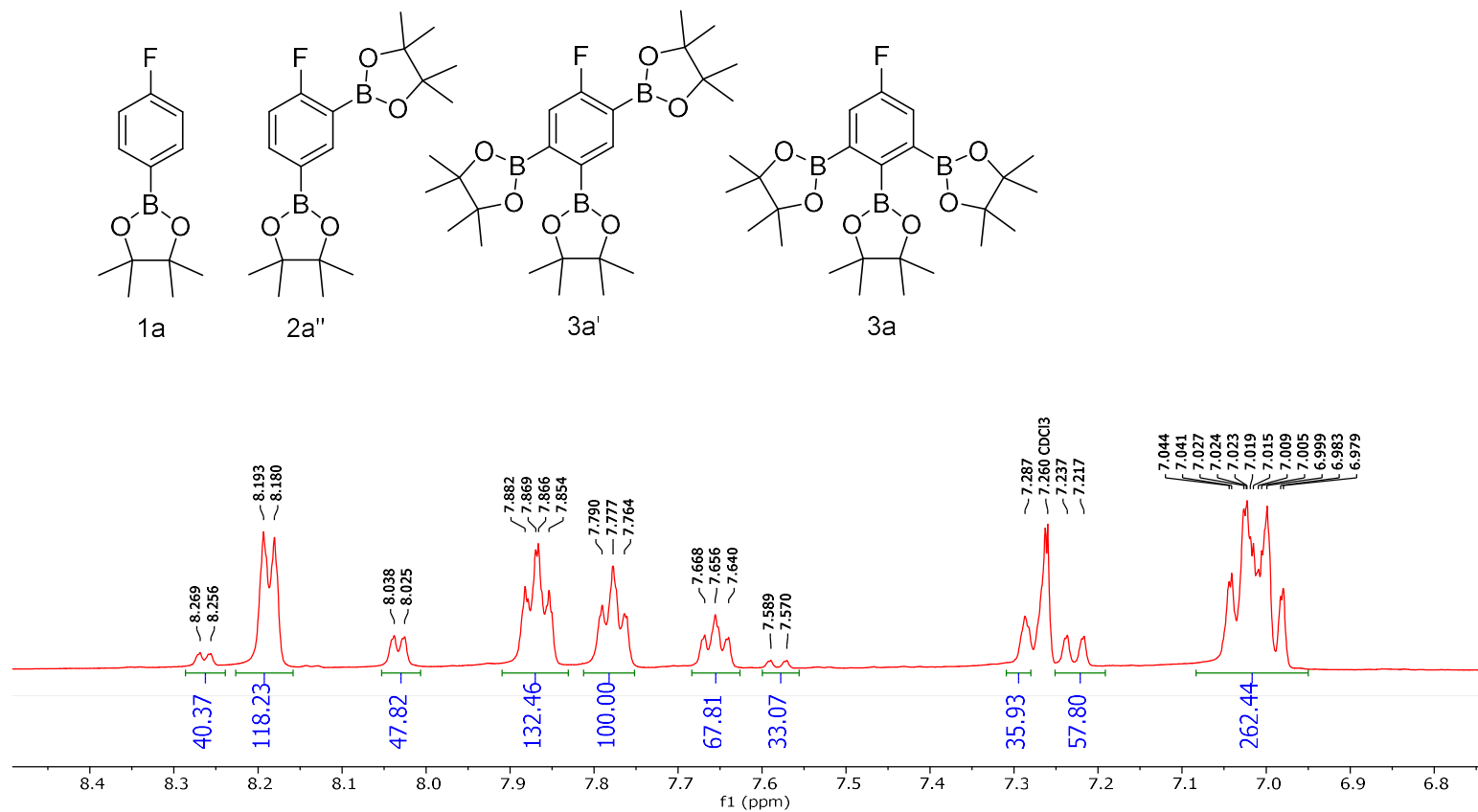


Figure 6-71 Conditions: 25 °C, 500 MHz, CDCl<sub>3</sub>



**<sup>19</sup>F NMR Spectra of the Crude reaction mixture of Table 2 Entry 1 Trial 1**

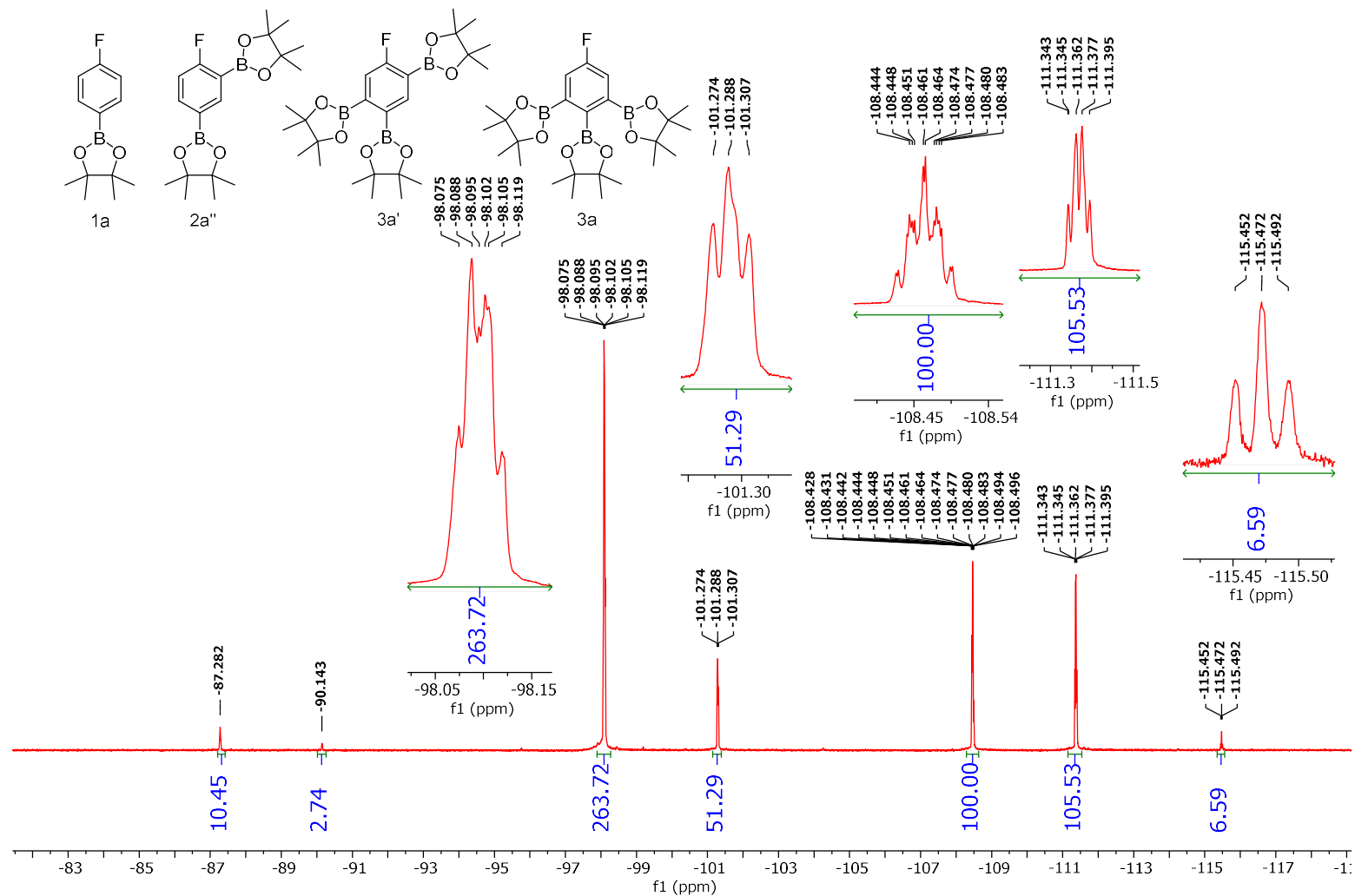


Figure 6-72 Conditions: 25 °C, 470 MHz, CDCl<sub>3</sub>

<sup>1</sup>H NMR Spectra of Fraction 1 of the Purified Reaction Mixture of Table 2 Entry 1 Trial 1

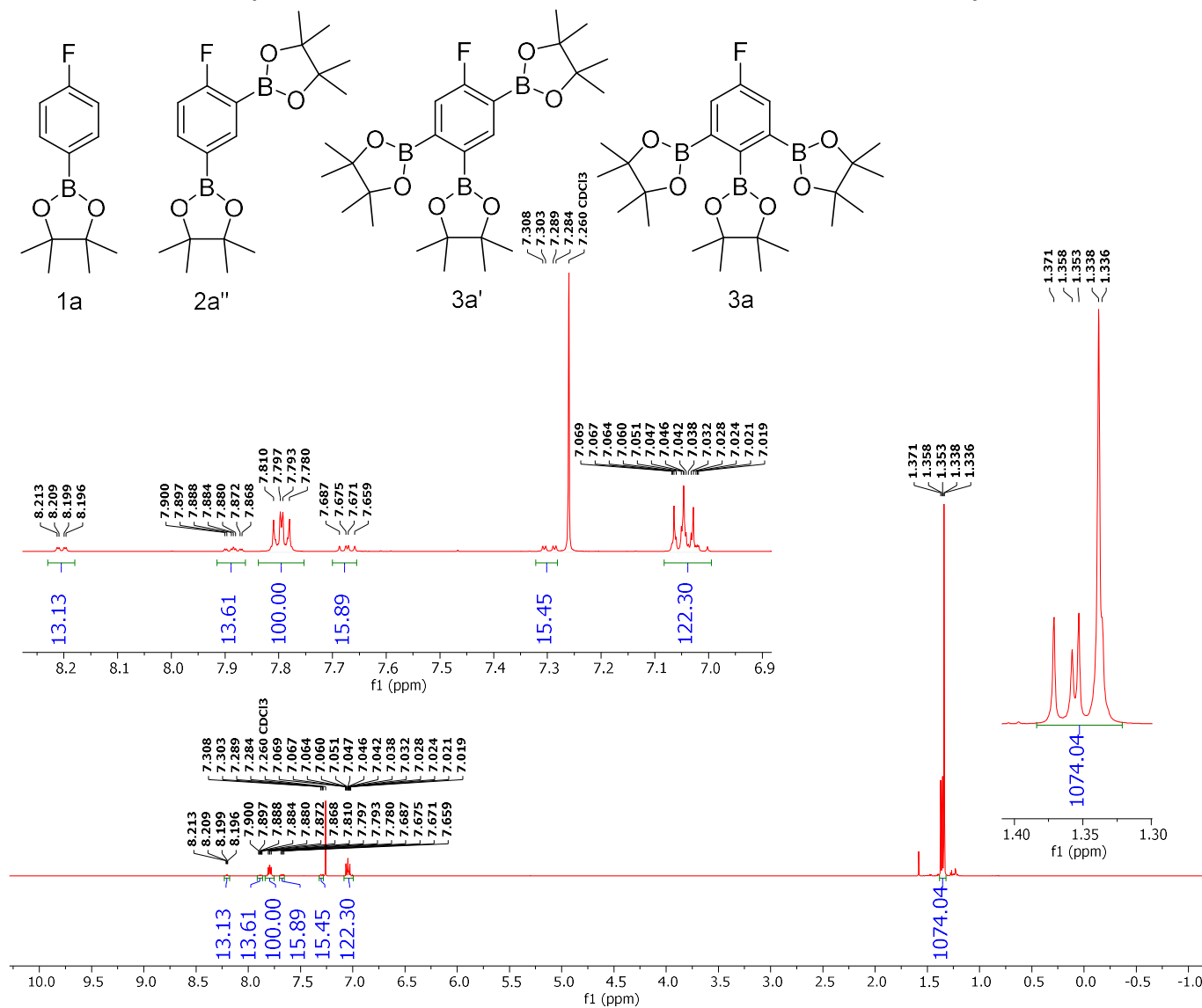


Figure 6-73 Conditions: 25 °C, 500 MHz, CDCl<sub>3</sub>

<sup>19</sup>F NMR Spectra of Fraction 1 of the Purified Reaction Mixture of Table 2 Entry 1 Trial 1

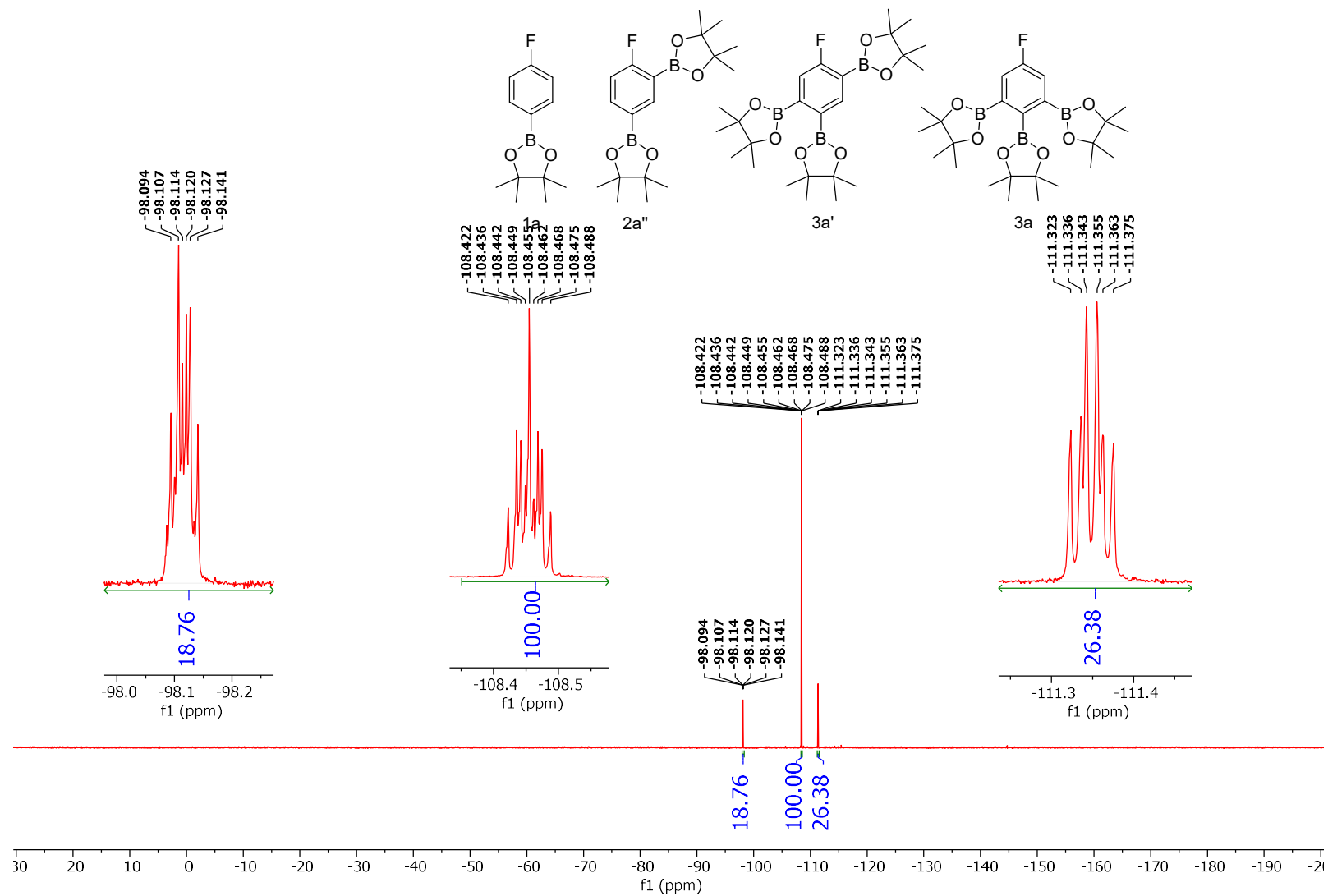


Figure 6-74 Conditions: 25 °C, 470 MHz, CDCl<sub>3</sub>

**$^{11}\text{B}$  NMR Spectra of Fraction 1 of the Purified Reaction Mixture of Table 2 Entry 1 Trial 1**

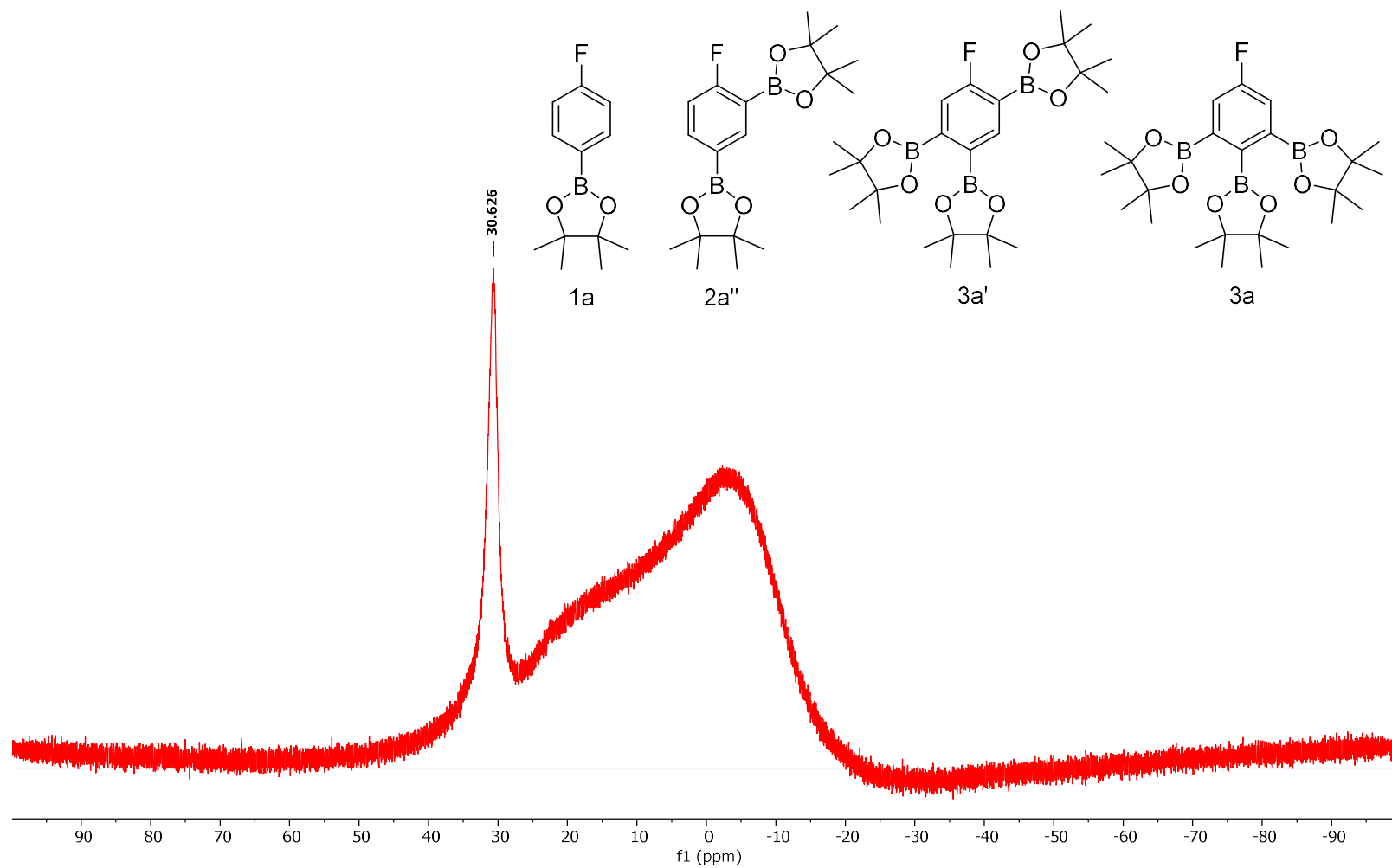


Figure 6-75 Conditions: 25 °C, 160 MHz,  $\text{CDCl}_3$

**<sup>1</sup>H NMR Spectra of Fraction 2 of the Purified Reaction Mixture of Table 2 Entry 1 Trial 1**

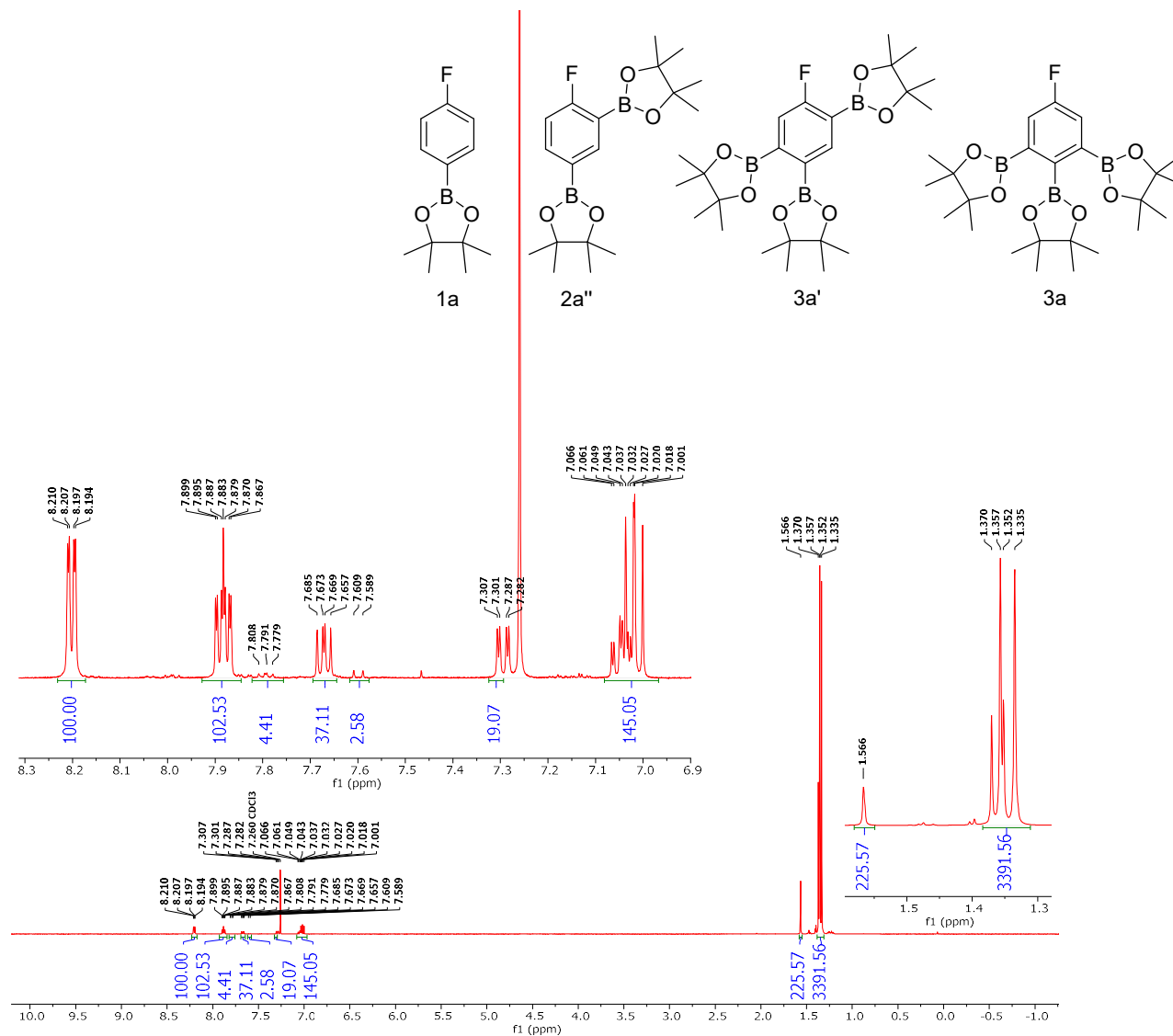


Figure 6-76 Conditions: 25 °C, 160 MHz, CDCl<sub>3</sub>

**<sup>19</sup>F NMR Spectra of Fraction 2 of the Purified Reaction Mixture of Table 2 Entry 1 Trial 1**

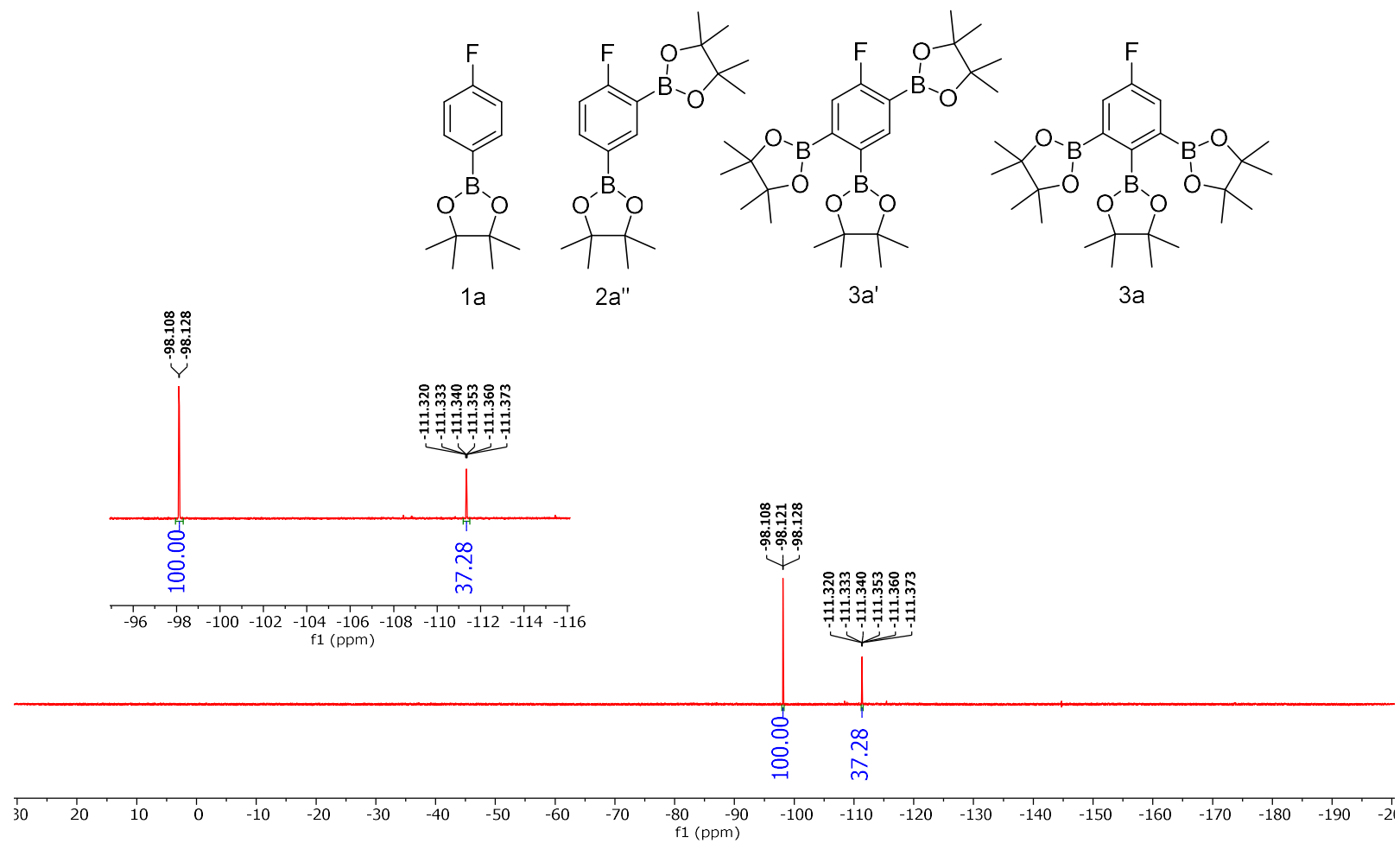


Figure 6-77 Conditions: 25 °C, 470 MHz, CDCl<sub>3</sub>

**<sup>13</sup>C NMR Spectra of Fraction 2 of the Purified Reaction Mixture of Table 2 Entry 1 Trial 1**

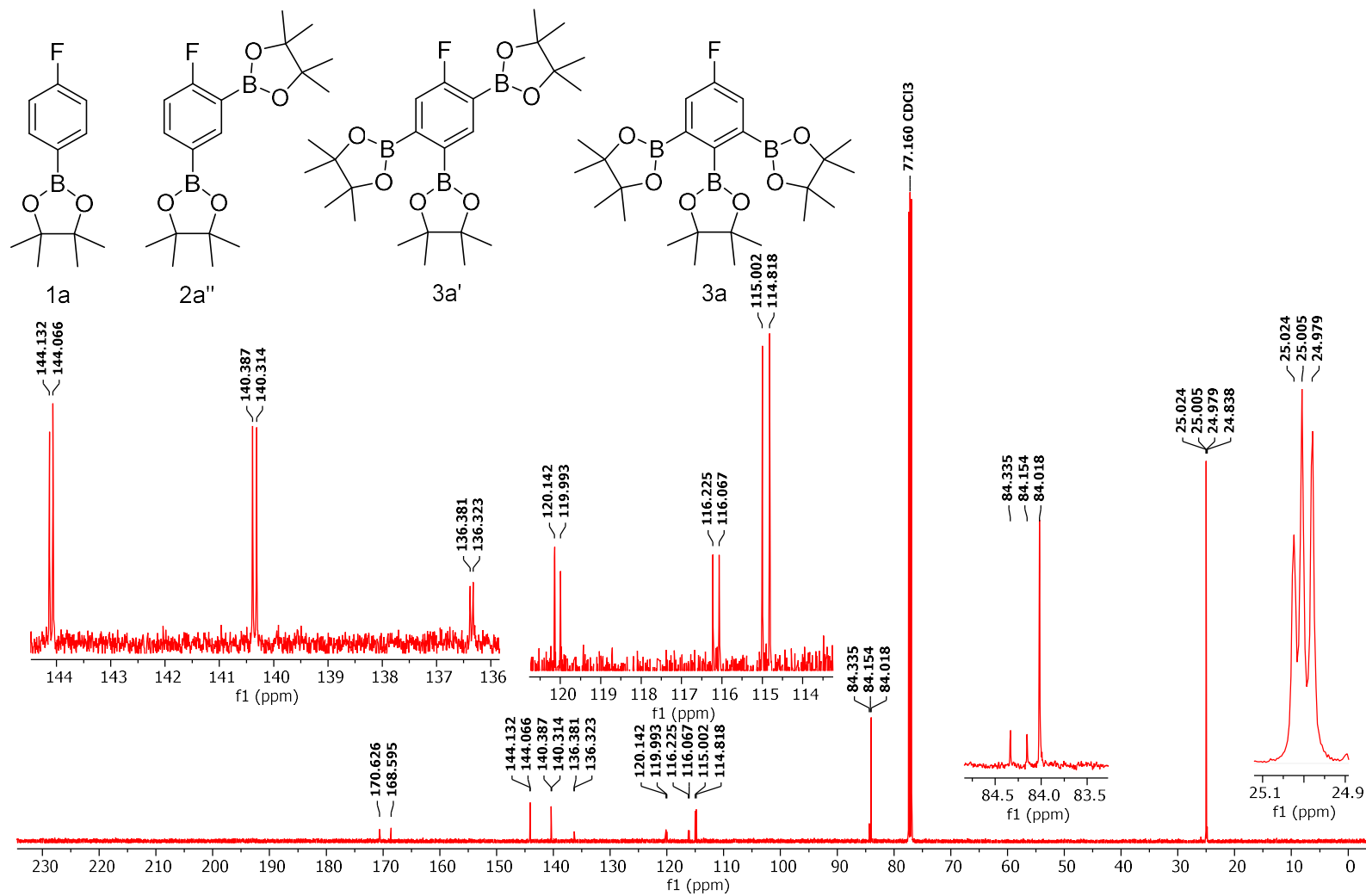


Figure 6-78 Conditions: 25 °C, 126 MHz, CDCl<sub>3</sub>

**$^{11}\text{B}$  NMR Spectra of Fraction 2 of the Purified Reaction Mixture of Table 2 Entry 1 Trial 1**

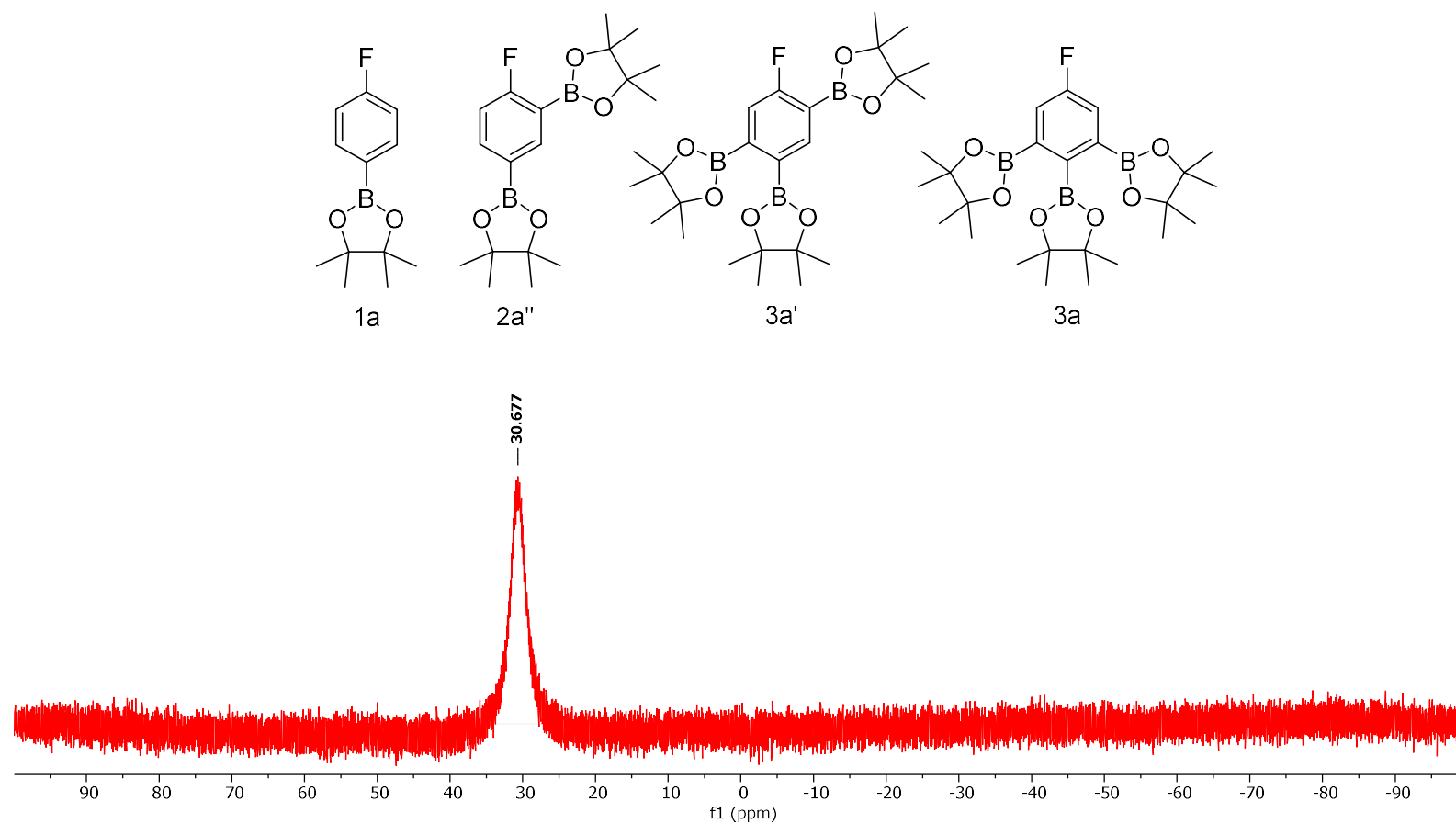


Figure 6-79 Conditions: 25 °C, 160 MHz,  $\text{CDCl}_3$



**<sup>1</sup>H NMR Spectra of Fraction 3 of the Purified Reaction Mixture of Table 2 Entry 1 Trial 1**

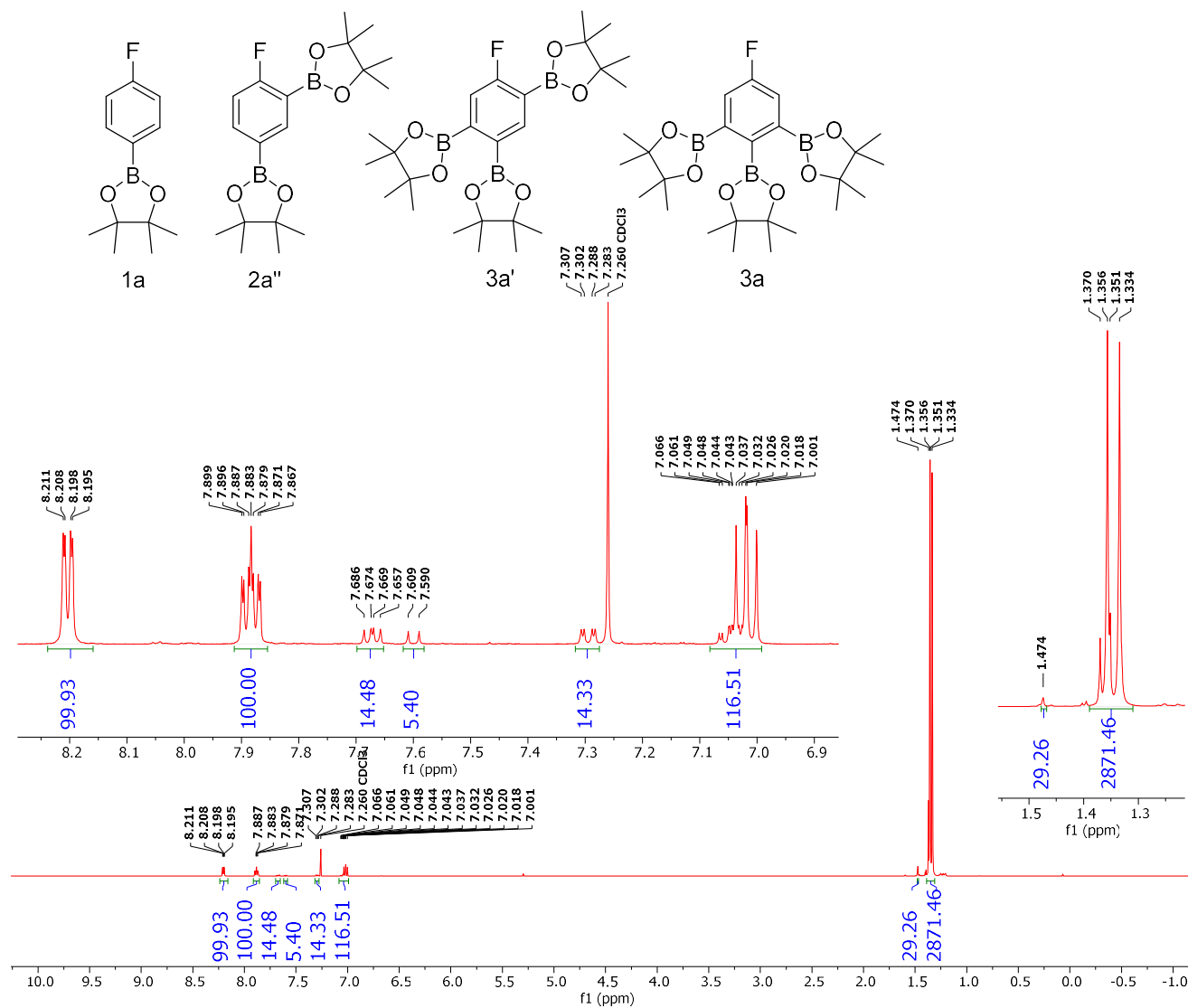


Figure 6-80 Conditions: 25 °C, 160 MHz, CDCl<sub>3</sub>

**<sup>19</sup>F NMR Spectra of Fraction 3 of the Purified Reaction Mixture of Table 2 Entry 1 Trial 1**

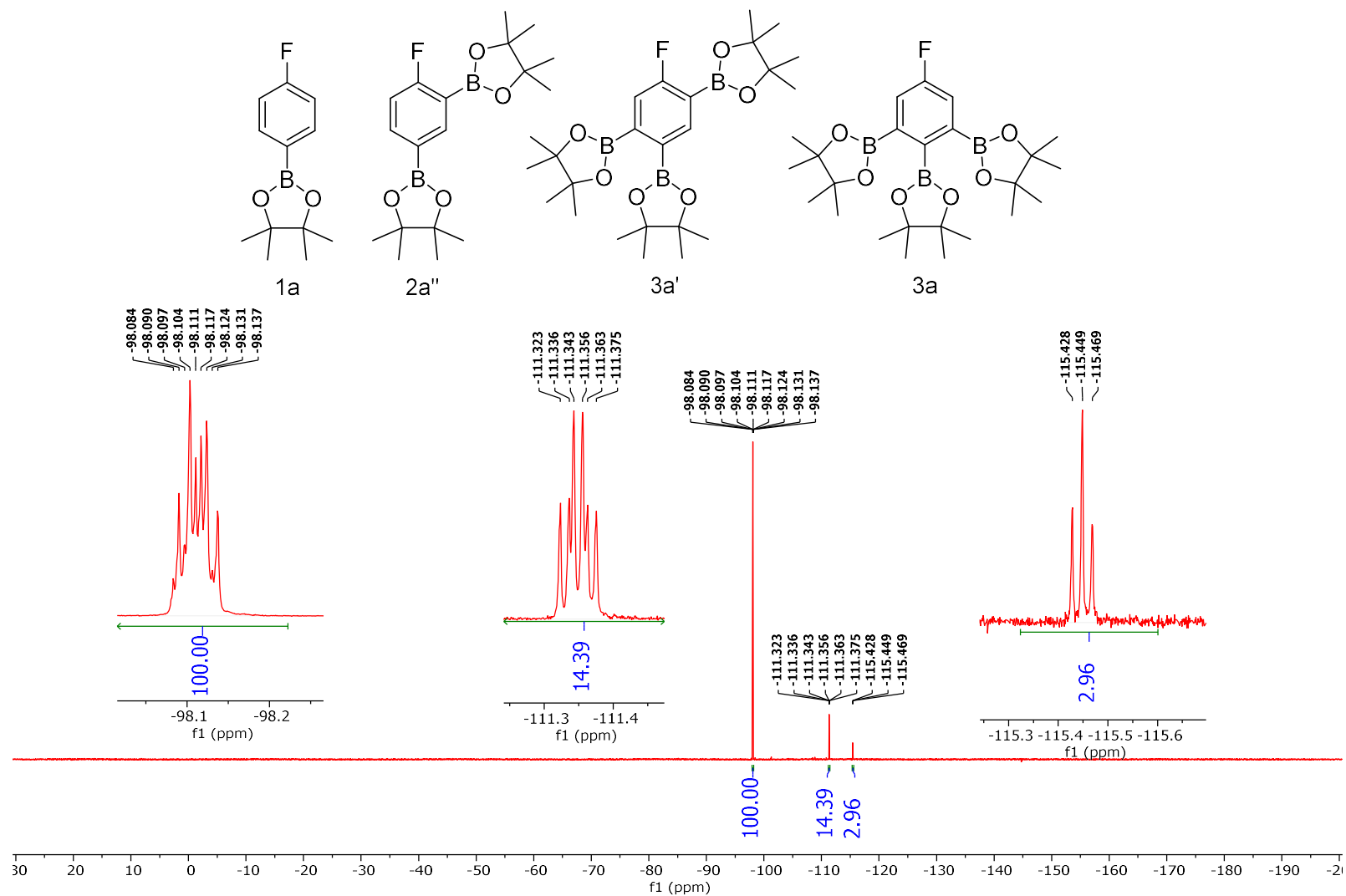


Figure 6-81 Conditions: 25 °C, 470 MHz, CDCl<sub>3</sub>

**<sup>13</sup>C NMR Spectra of Fraction 3 of the Purified Reaction Mixture of Table 2 Entry 1 Trial 1**

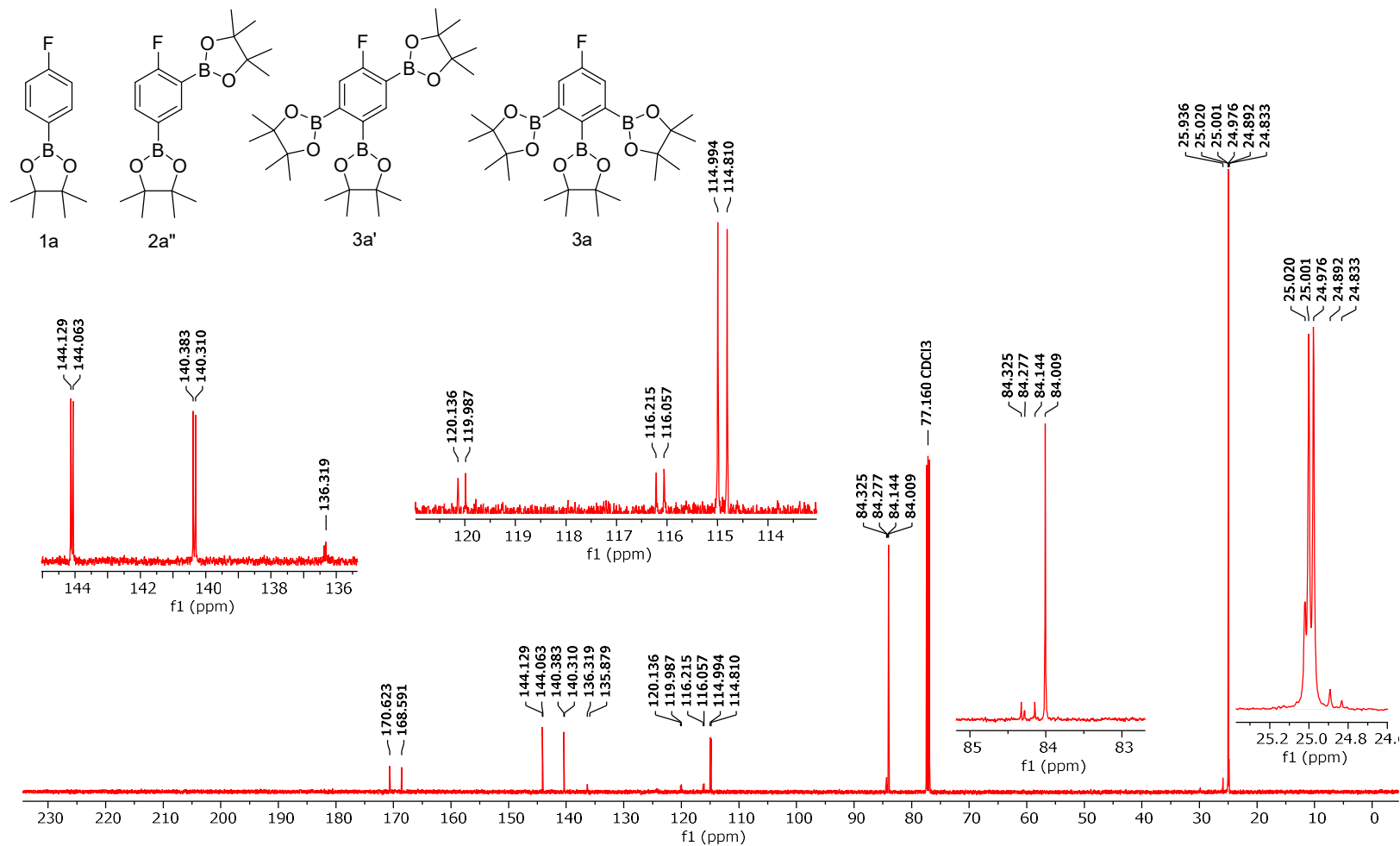


Figure 6-82 Conditions: 25 °C, 126 MHz, CDCl<sub>3</sub>

**<sup>11</sup>B NMR Spectra of Fraction 3 of the Purified Reaction Mixture of Table 2 Entry 1 Trial 1**

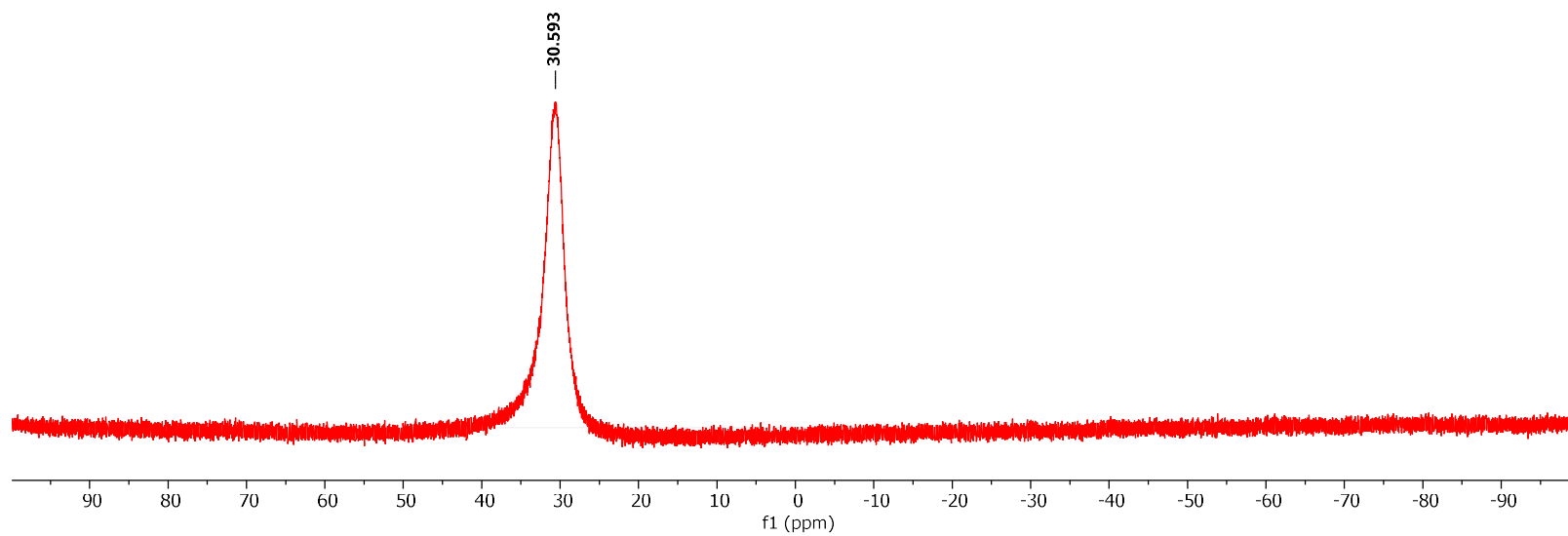
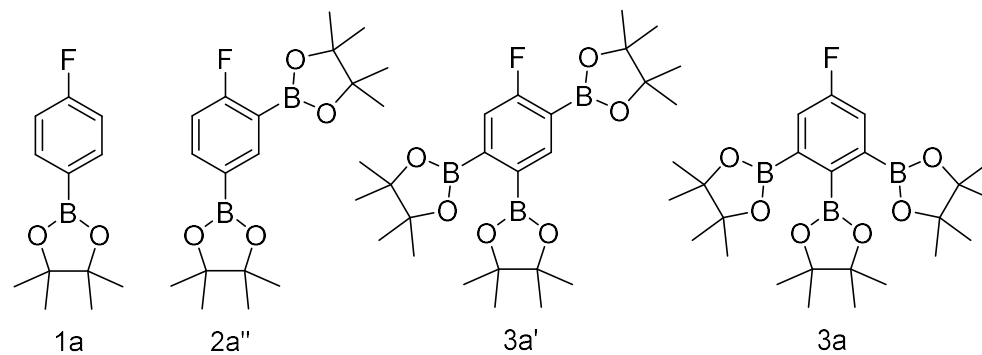


Figure 6-83 Conditions: 25 °C, 160 MHz, CDCl<sub>3</sub>

<sup>1</sup>H NMR Spectra of the Crude reaction mixture of Table 2 Entry 1 Trial 2

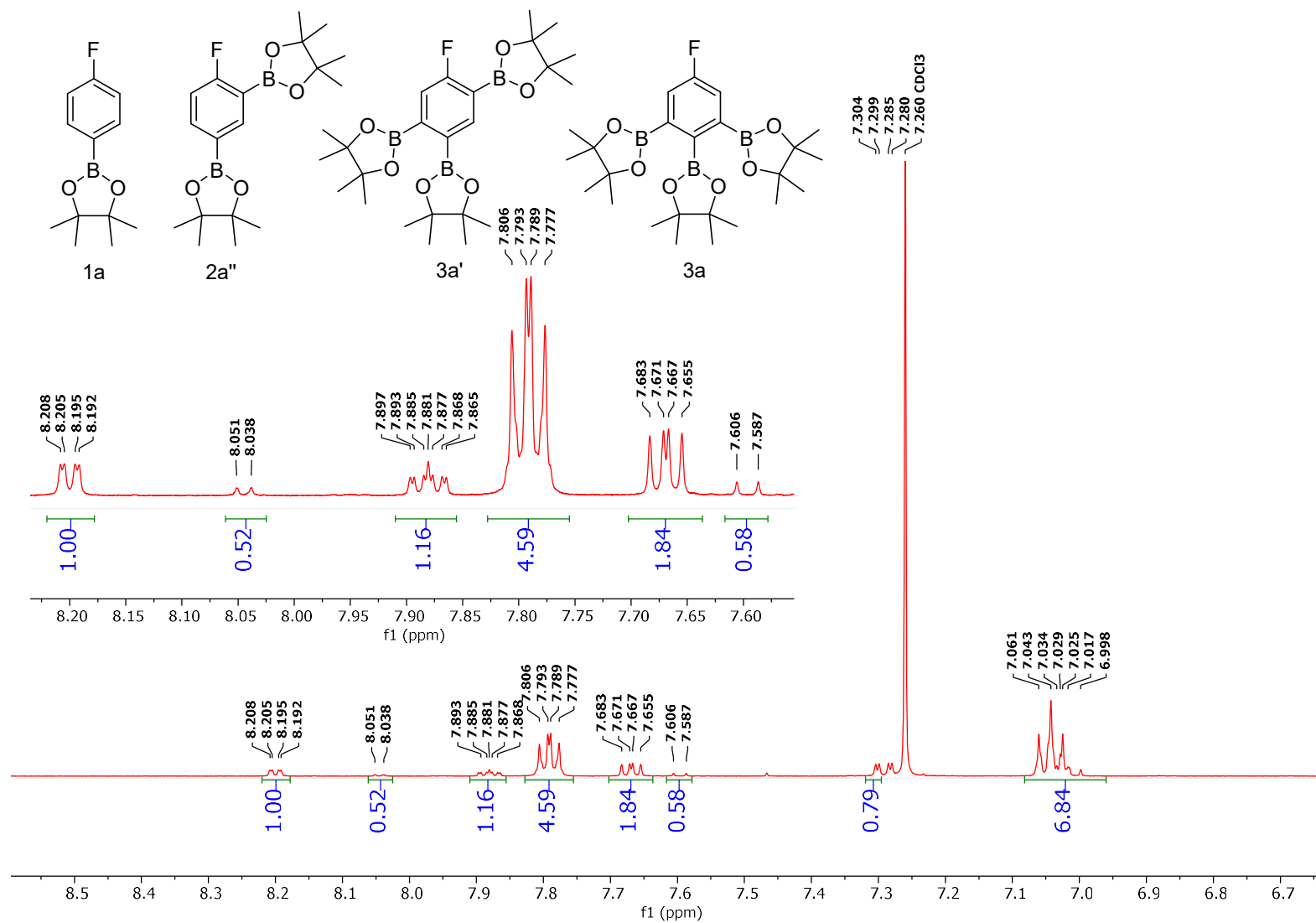


Figure 6-84 Conditions: 25 °C, 500 MHz, CDCl<sub>3</sub>

<sup>19</sup>F NMR Spectra of the Crude reaction mixture of Table 2 Entry 1 Trial 2

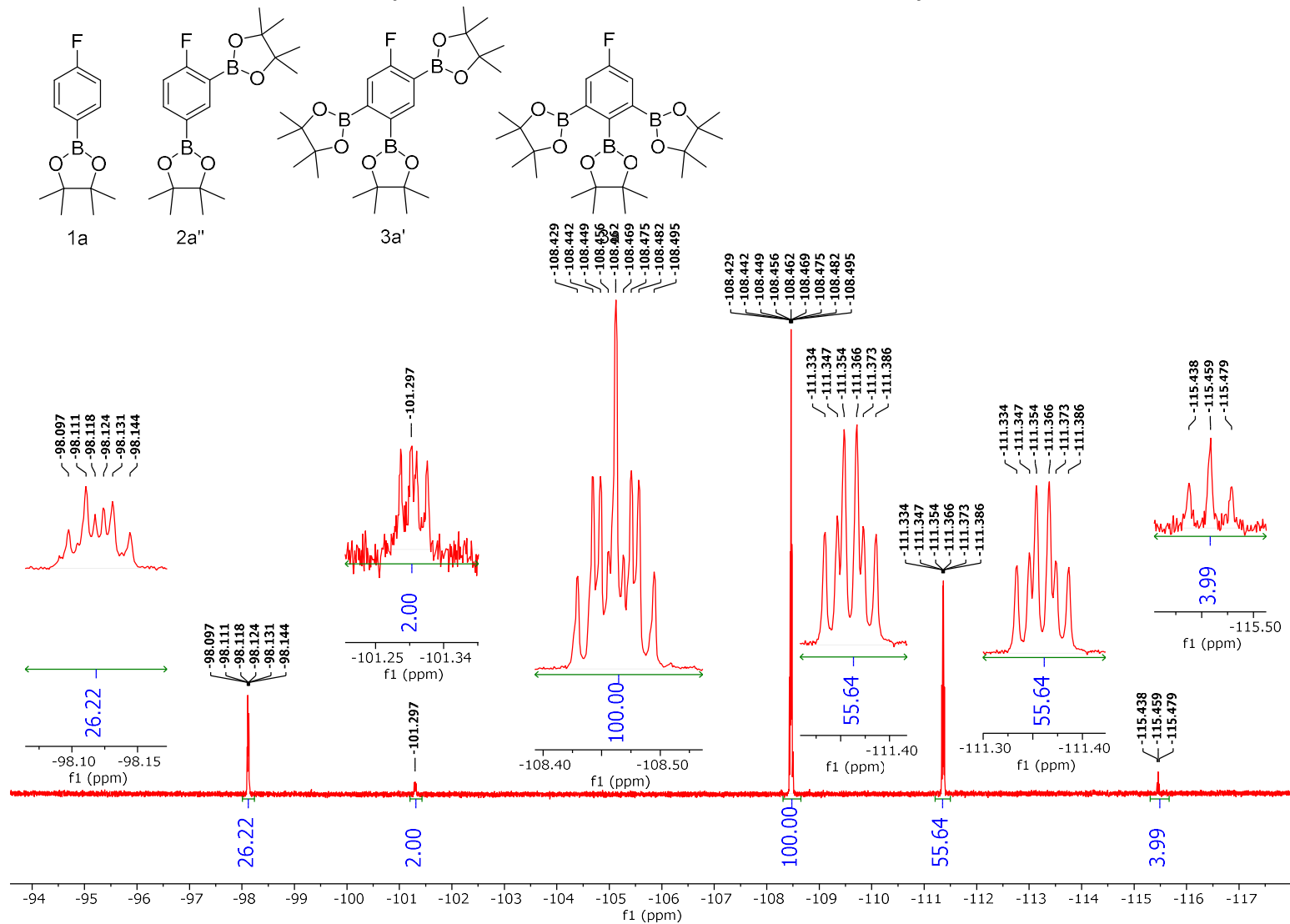


Figure 6-85 Conditions: 25 °C, 470 MHz, CDCl<sub>3</sub>

<sup>1</sup>H NMR Spectra of the Crude reaction mixture of Table 2 Entry 1 Trial 3

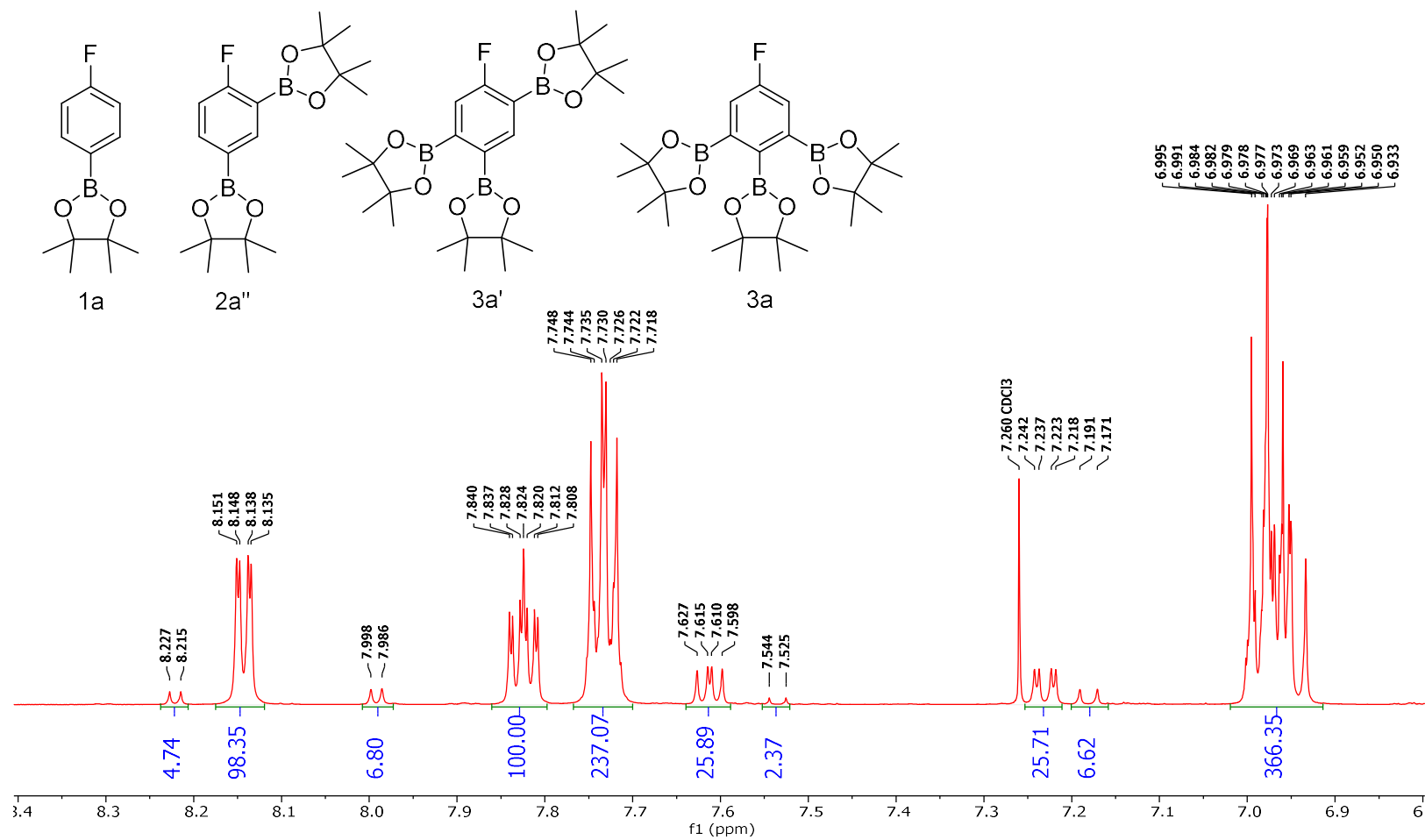


Figure 6-86 Conditions: 25 °C, 500 MHz, CDCl<sub>3</sub>

<sup>19</sup>F NMR Spectra of the Crude reaction mixture of Table 2 Entry 1 Trial 3

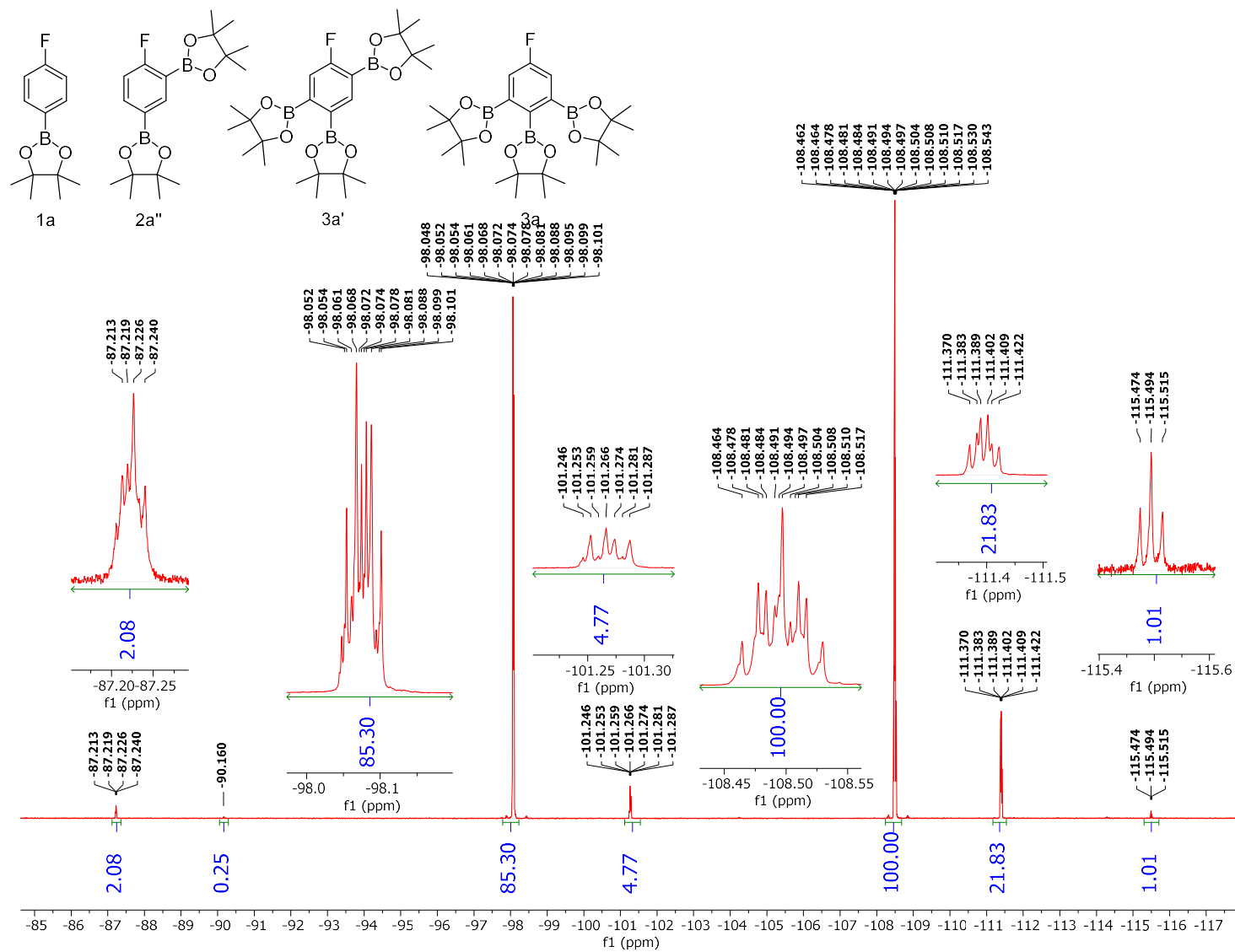


Figure 6-87 Conditions: 25 °C, 470 MHz, CDCl<sub>3</sub>



**<sup>1</sup>H NMR Spectra of the Crude reaction mixture of Table 2 Entry 2 Trial 1**

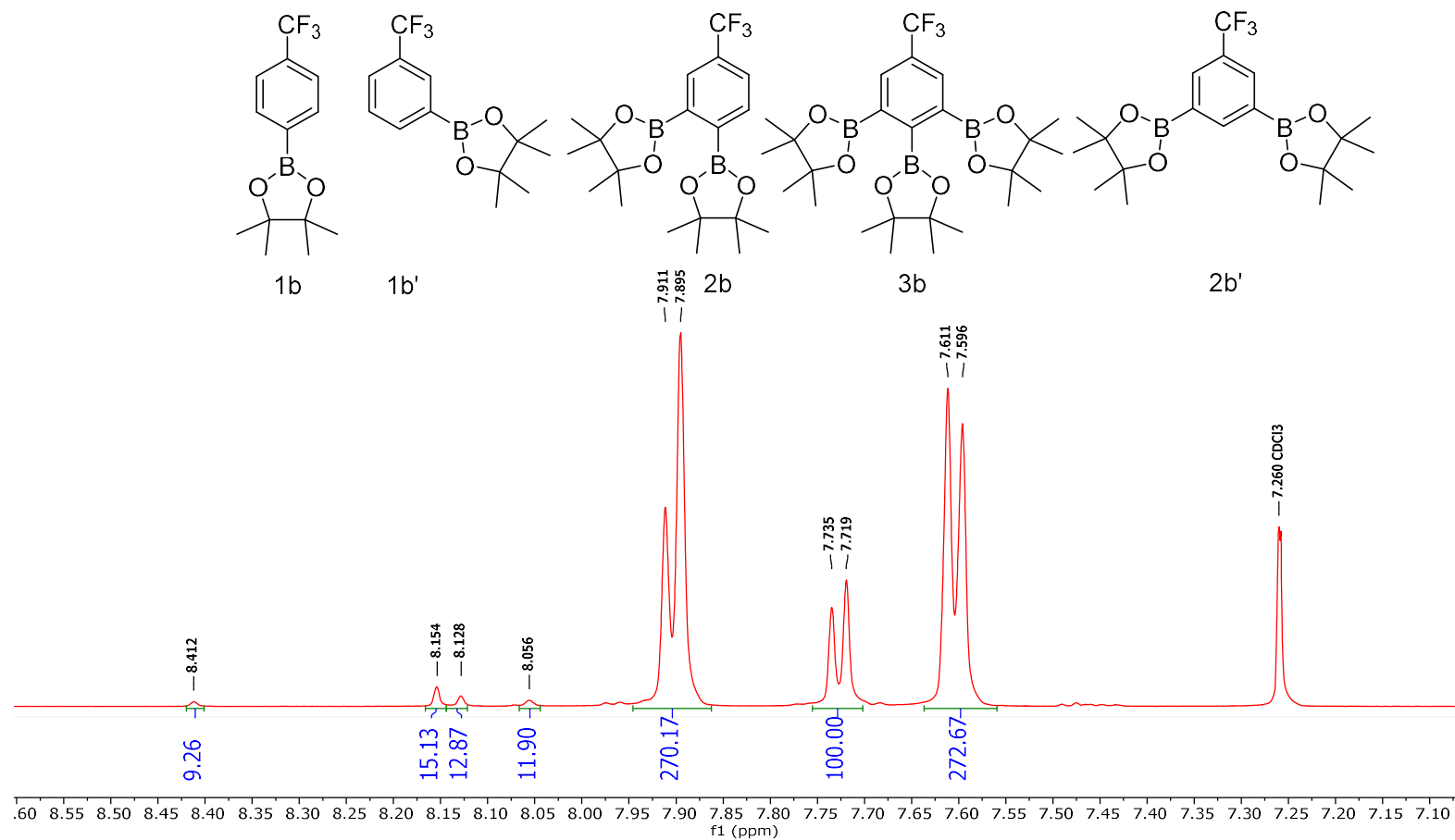


Figure 6-88 Conditions: 25 °C, 500 MHz, CDCl<sub>3</sub>

**<sup>19</sup>F NMR Spectra of the Crude reaction mixture of Table 2 Entry 2 Trial 1**

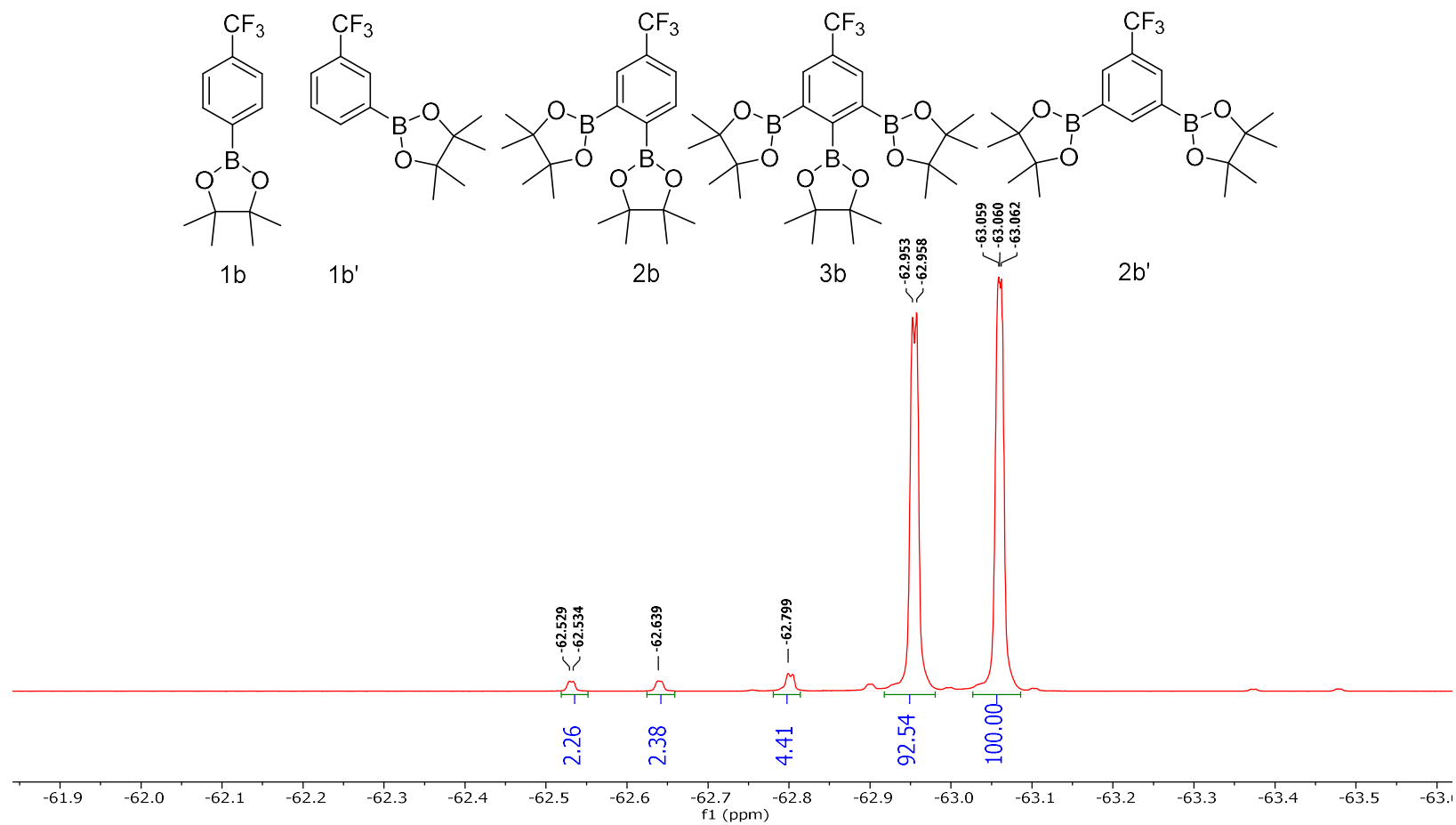


Figure 6-89 Conditions: 25 °C, 470 MHz, CDCl<sub>3</sub>

<sup>1</sup>H NMR Spectra of Fraction 1 of the purified reaction mixture of Table 2 Entry 2 Trial 1

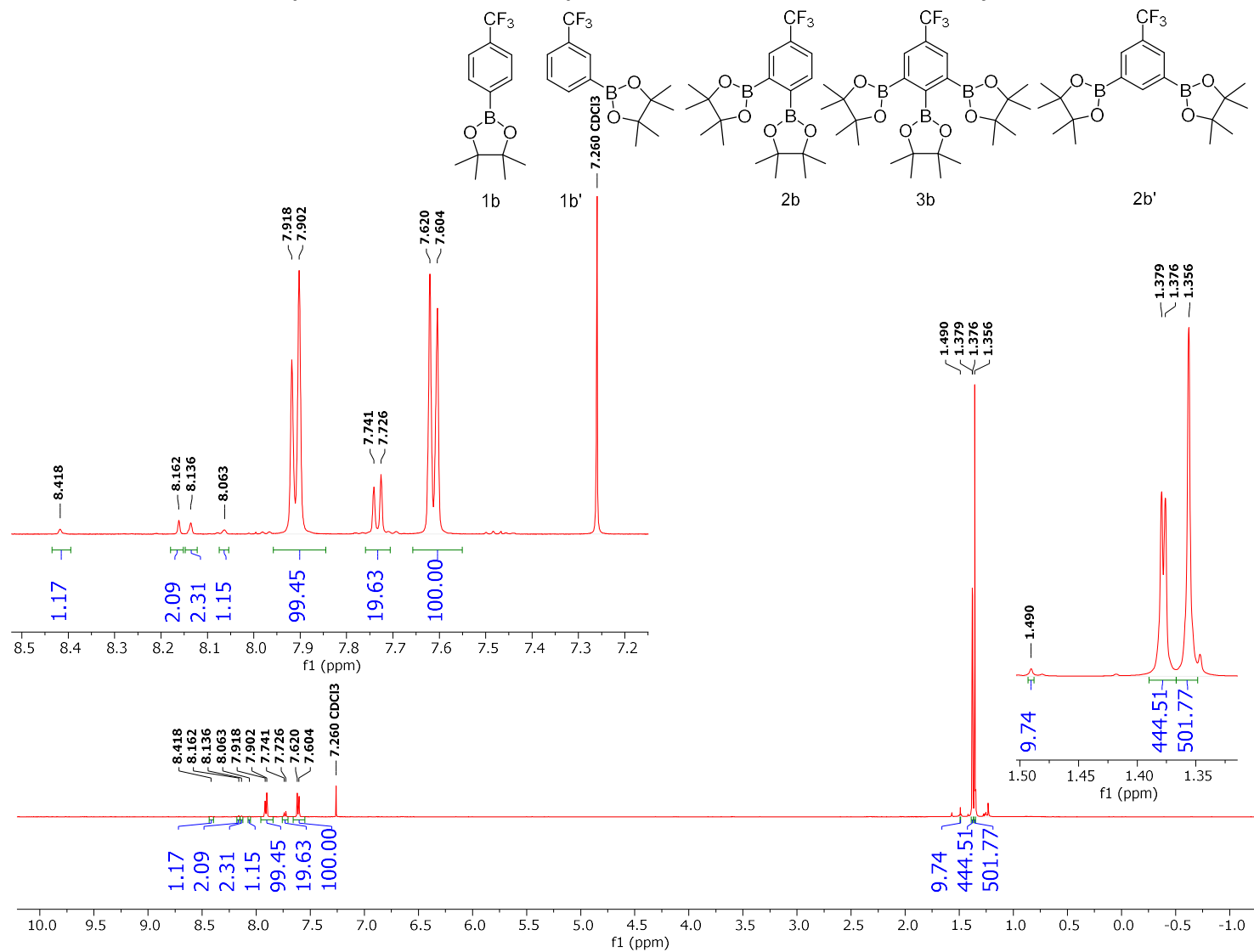


Figure 6-90 Conditions: 25 °C, 500 MHz, CDCl<sub>3</sub>

**$^{19}\text{F}$  NMR Spectra of Fraction 1 of the purified reaction mixture of Table 2 Entry 2 Trial 1**

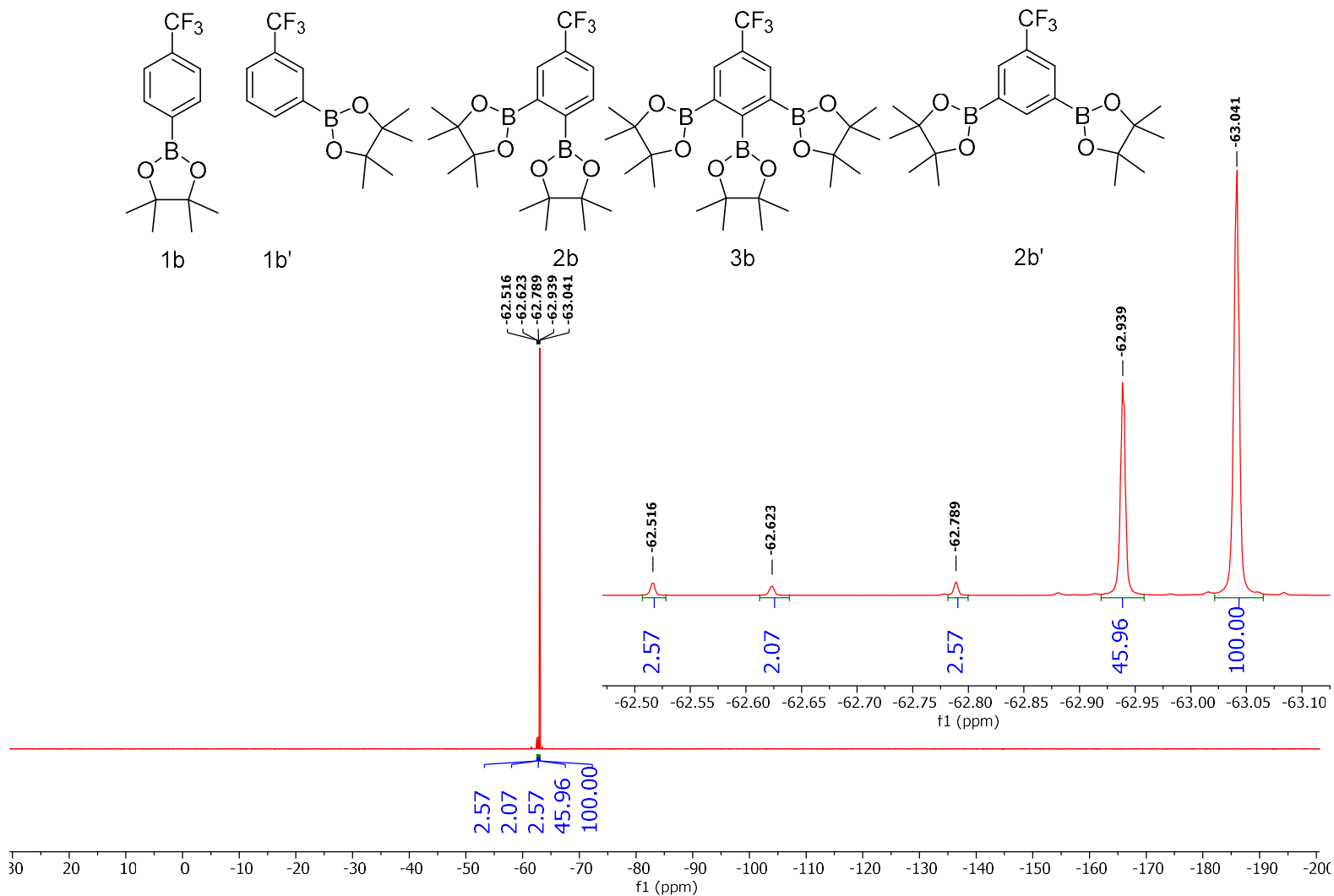


Figure 6-91 Conditions: 25 °C, 470 MHz,  $\text{CDCl}_3$

**<sup>13</sup>C NMR Spectra of Fraction 1 of the purified reaction mixture of Table 2 Entry 2 Trial 1**

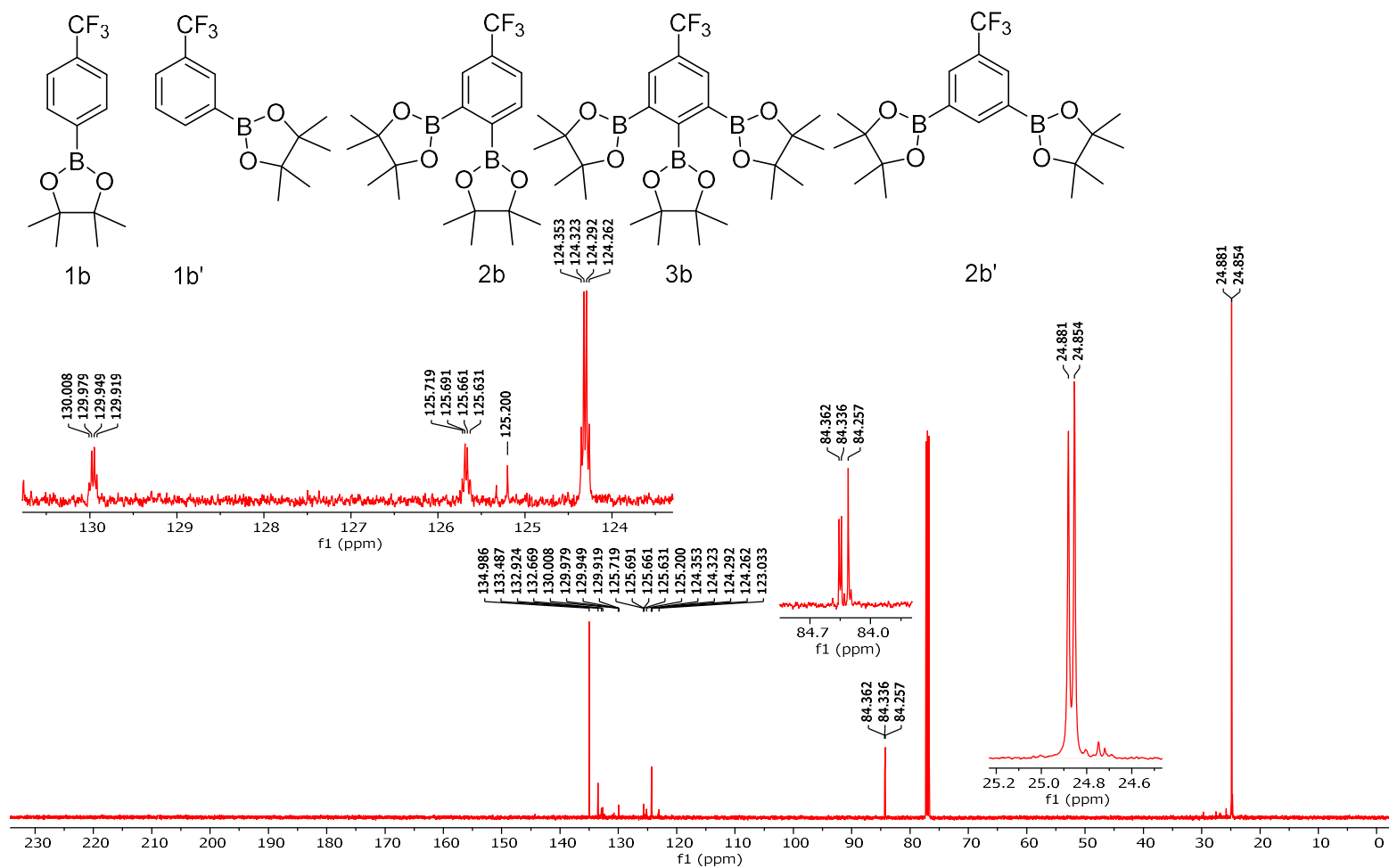


Figure 6-92 Conditions: 25 °C, 126 MHz, CDCl<sub>3</sub>

**<sup>11</sup>B NMR Spectra of Fraction 1 of the purified reaction mixture of Table 2 Entry 2 Trial 1**

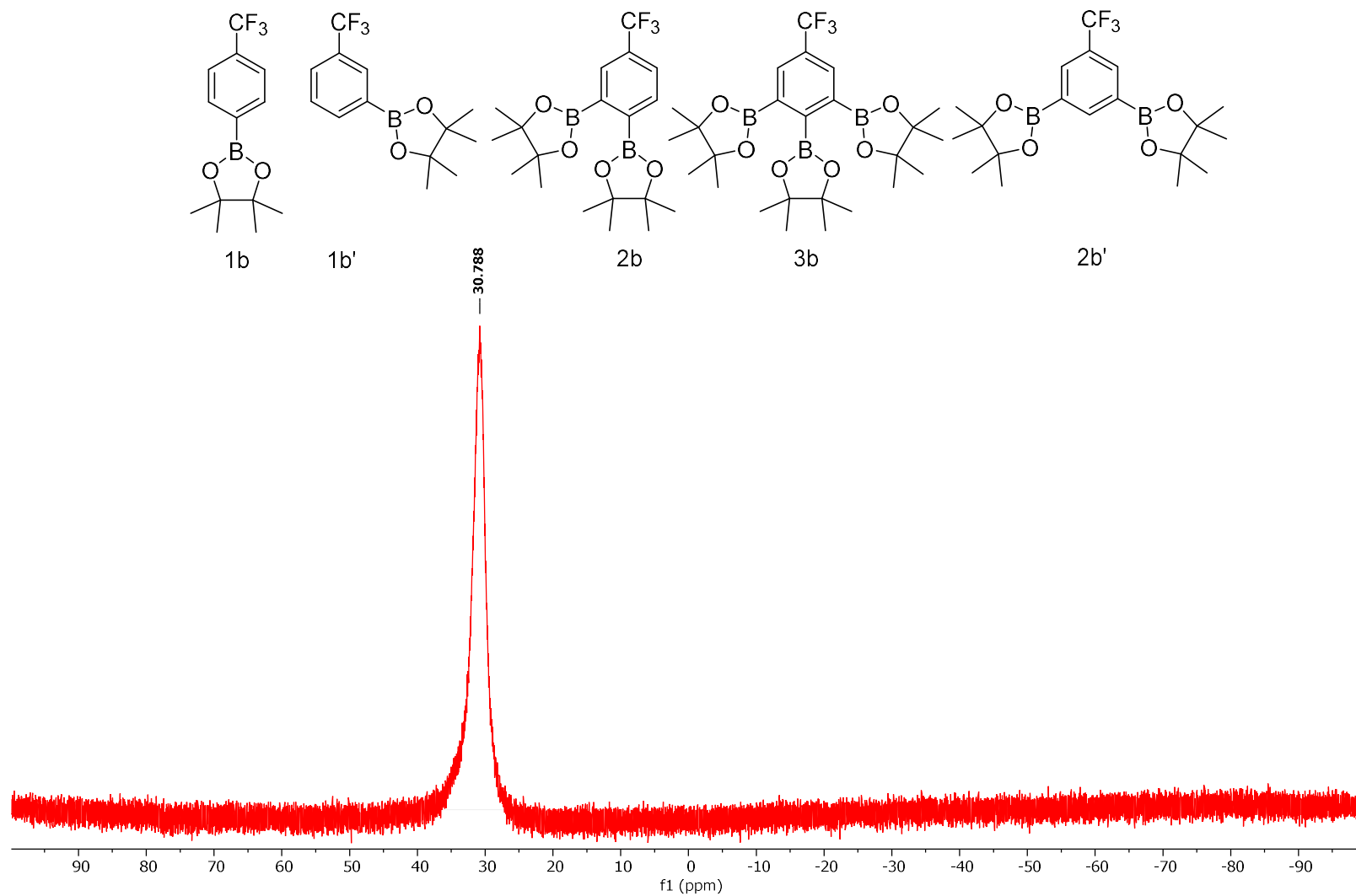


Figure 6-93 Conditions: 25 °C, 160 MHz, CDCl<sub>3</sub>

<sup>1</sup>H NMR Spectra of Fraction 2 of the purified reaction mixture of Table 2 Entry 2 Trial 1

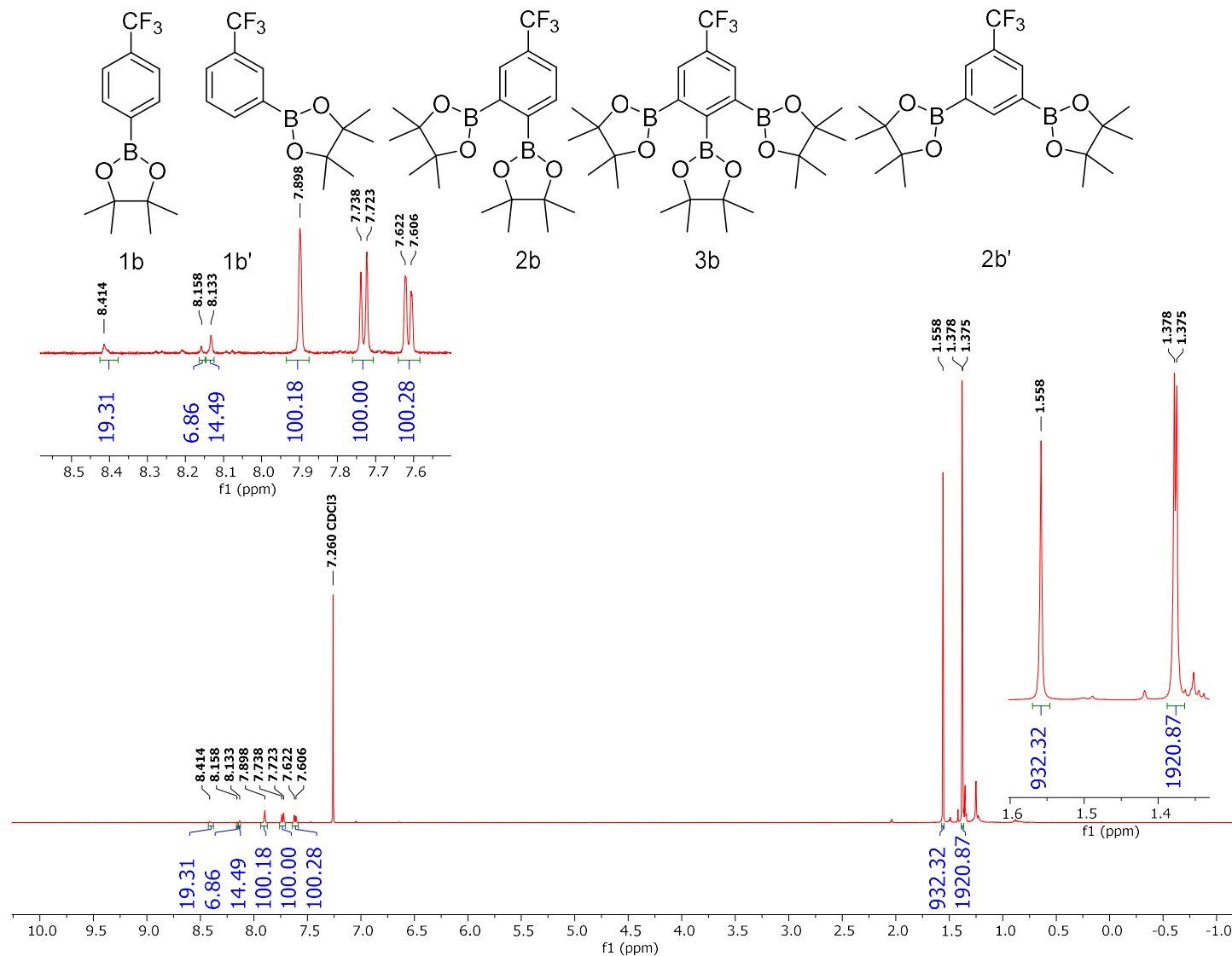


Figure 6-94 Conditions: 25 °C, 500 MHz, CDCl<sub>3</sub>

**<sup>19</sup>F NMR Spectra of Fraction 2 of the purified reaction mixture of Table 2 Entry 2 Trial 1**

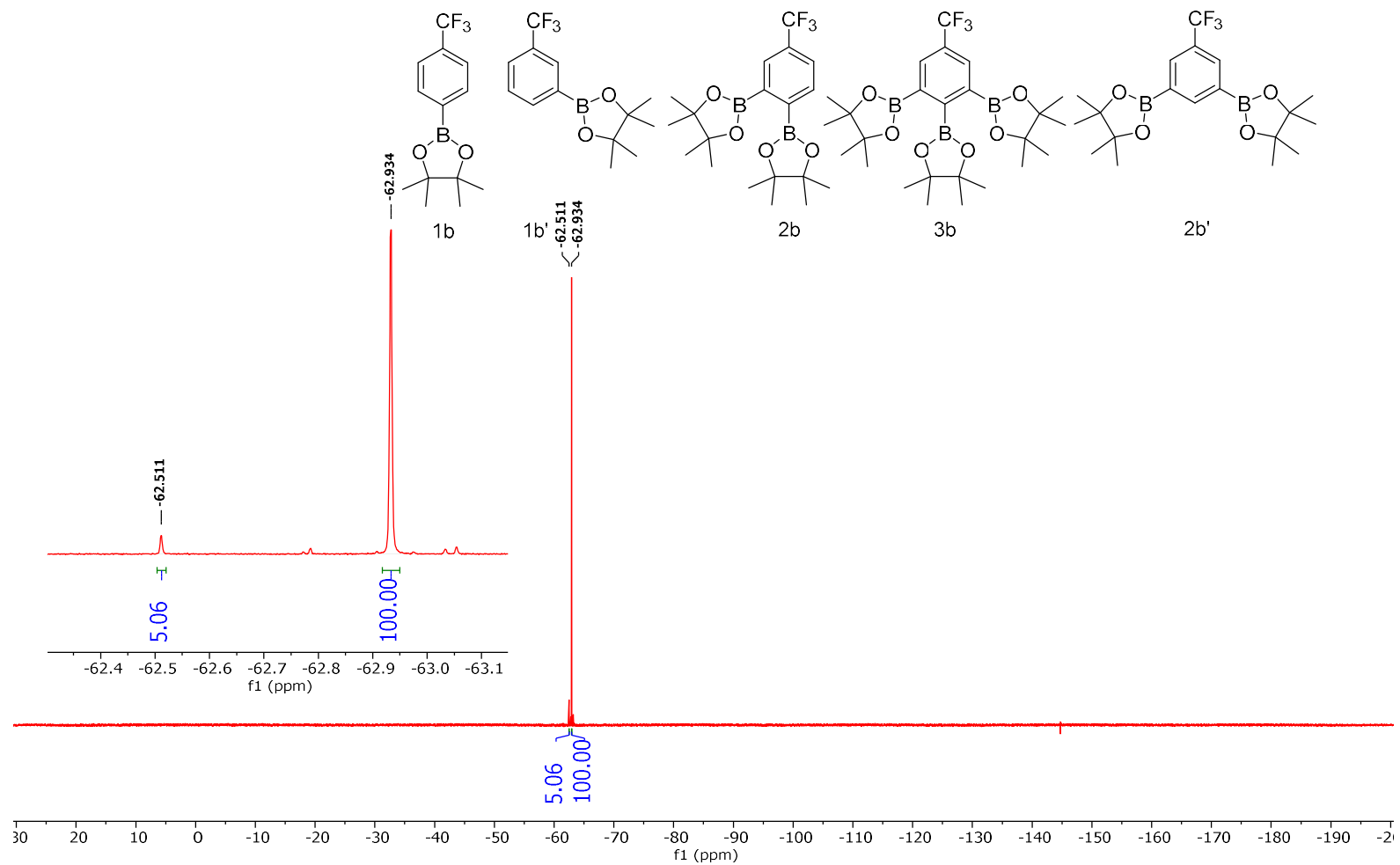


Figure 6-95 Conditions: 25 °C, 470 MHz, CDCl<sub>3</sub>



**<sup>13</sup>C NMR Spectra of Fraction 2 of the purified reaction mixture of Table 2 Entry 2 Trial 1**

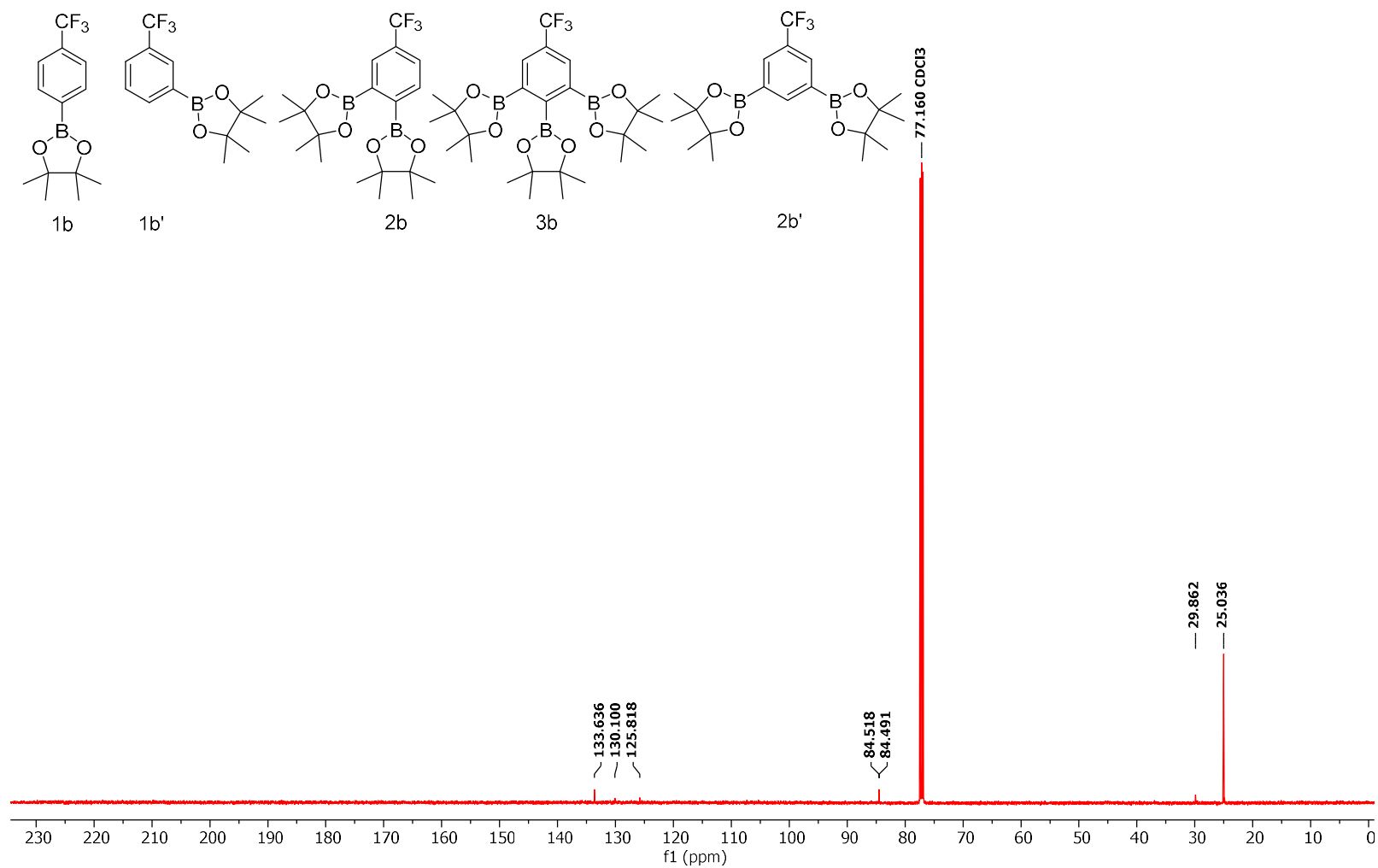


Figure 6-96 Conditions: 25 °C, 126 MHz, CDCl<sub>3</sub>

**$^{11}\text{B}$  NMR Spectra of Fraction 2 of the purified reaction mixture of Table 2 Entry 2 Trial 1**

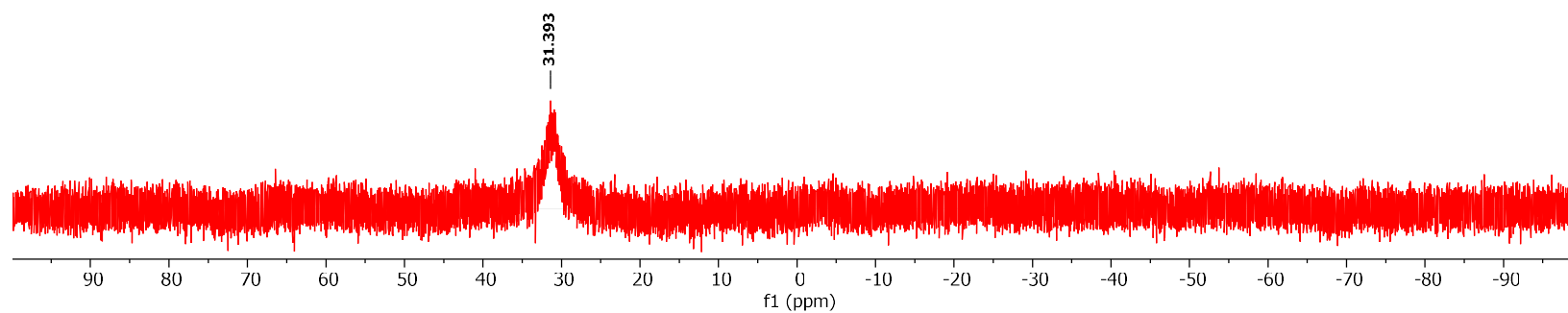
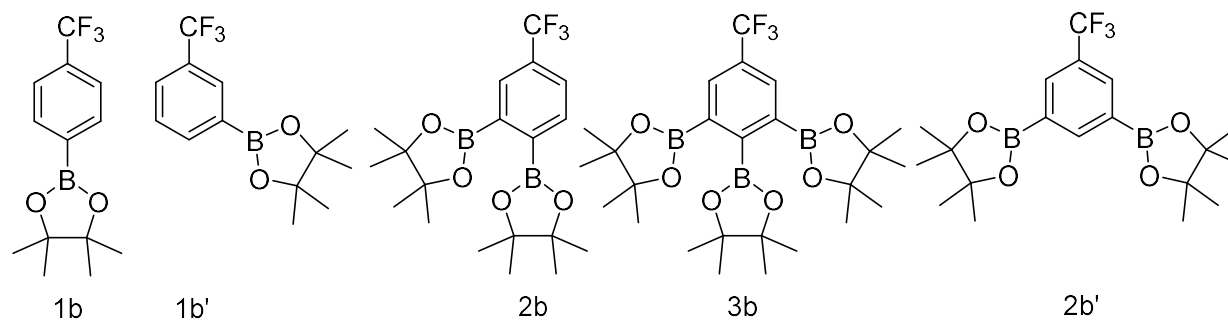


Figure 6-97 Conditions: 25 °C, 160 MHz,  $\text{CDCl}_3$

**<sup>1</sup>H NMR Spectra of Fraction 3 of the purified reaction mixture of Table 2 Entry 2 Trial 1**

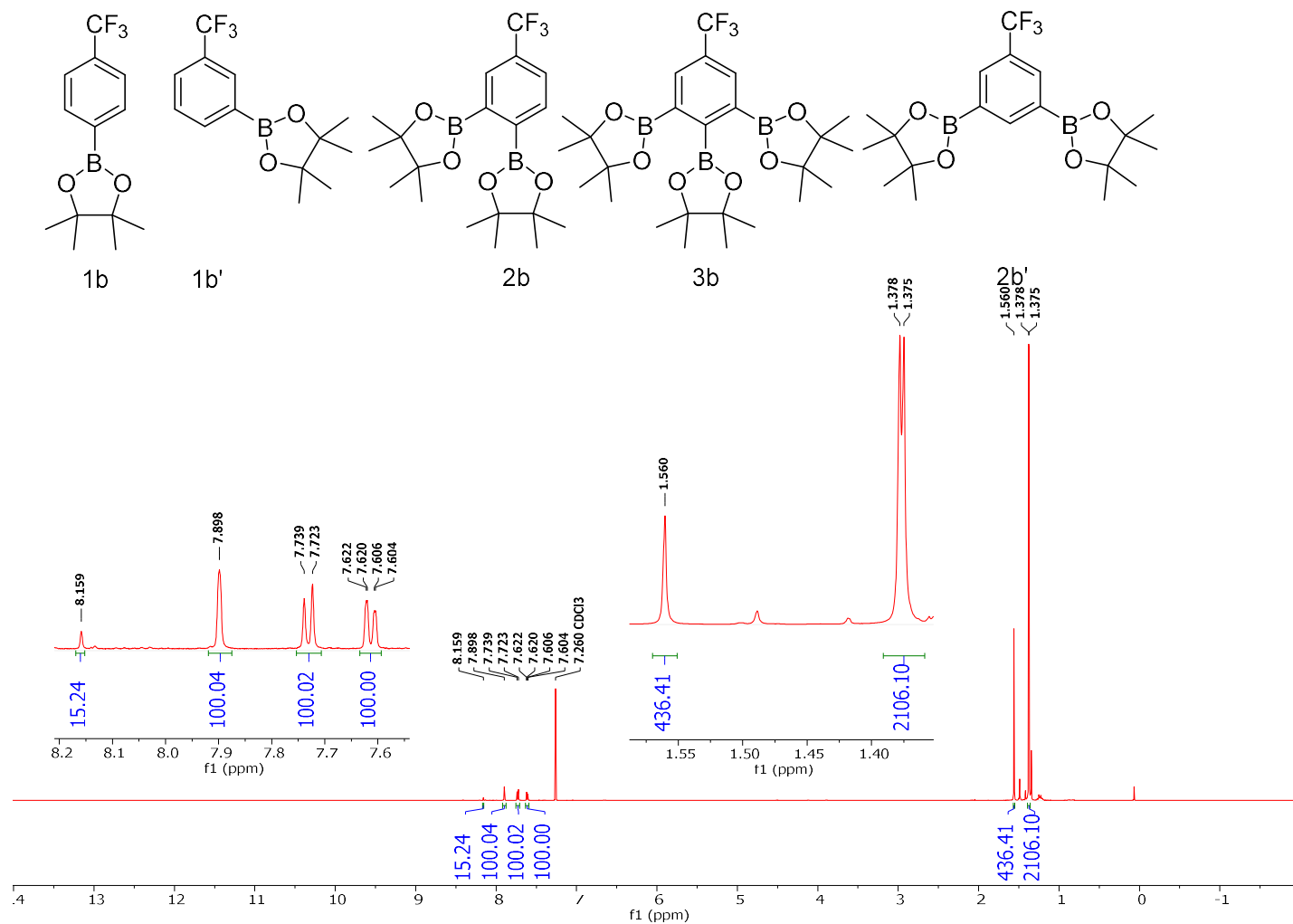


Figure 6-98 Conditions: 25 °C, 500 MHz, CDCl<sub>3</sub>

**$^{19}\text{F}$  NMR Spectra of Fraction 3 of the purified reaction mixture of Table 2 Entry 2 Trial 1**

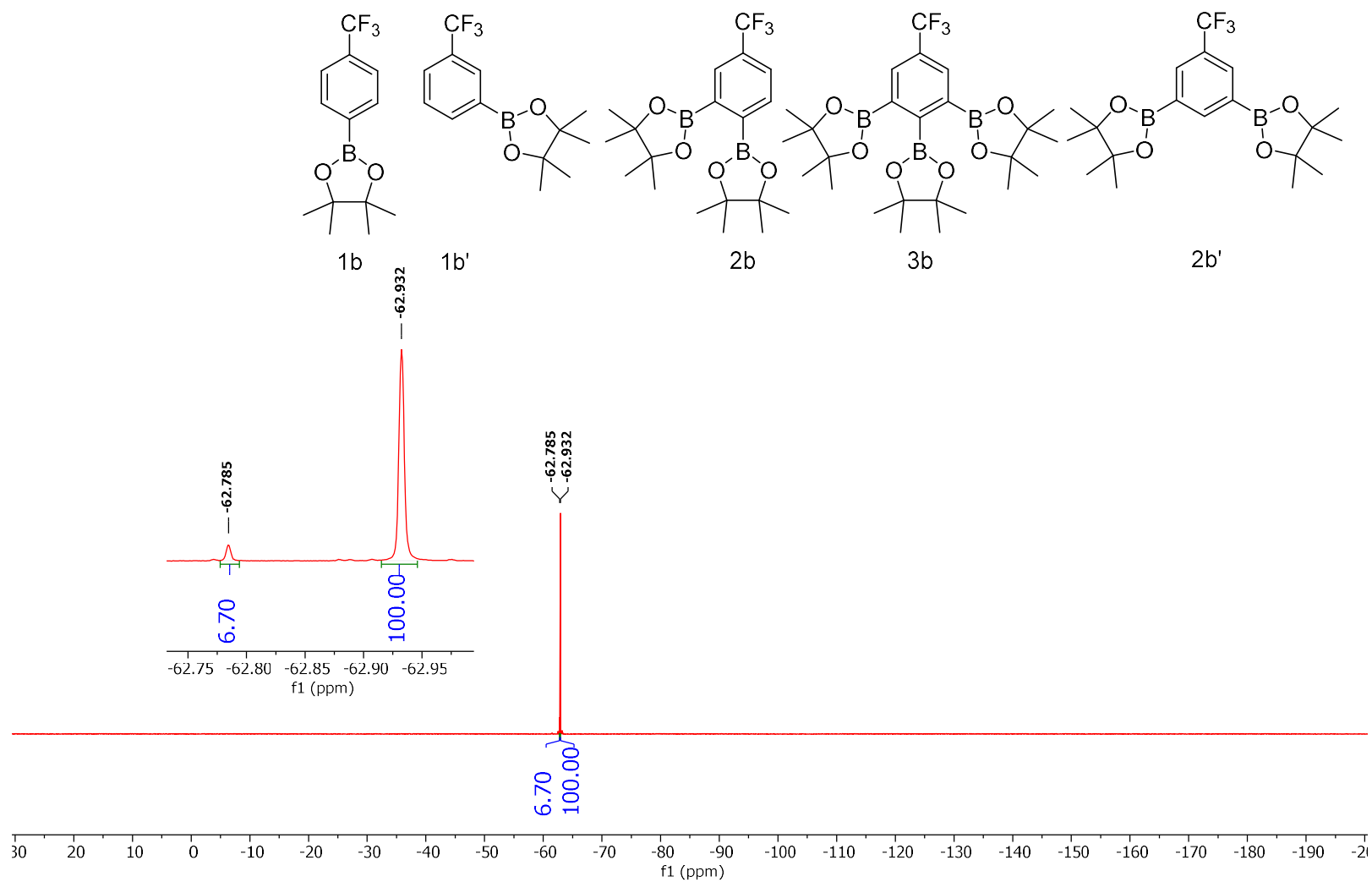


Figure 6-99 Conditions: 25 °C, 470 MHz,  $\text{CDCl}_3$

**<sup>13</sup>C NMR Spectra of Fraction 3 of the purified reaction mixture of Table 2 Entry 2 Trial 1**

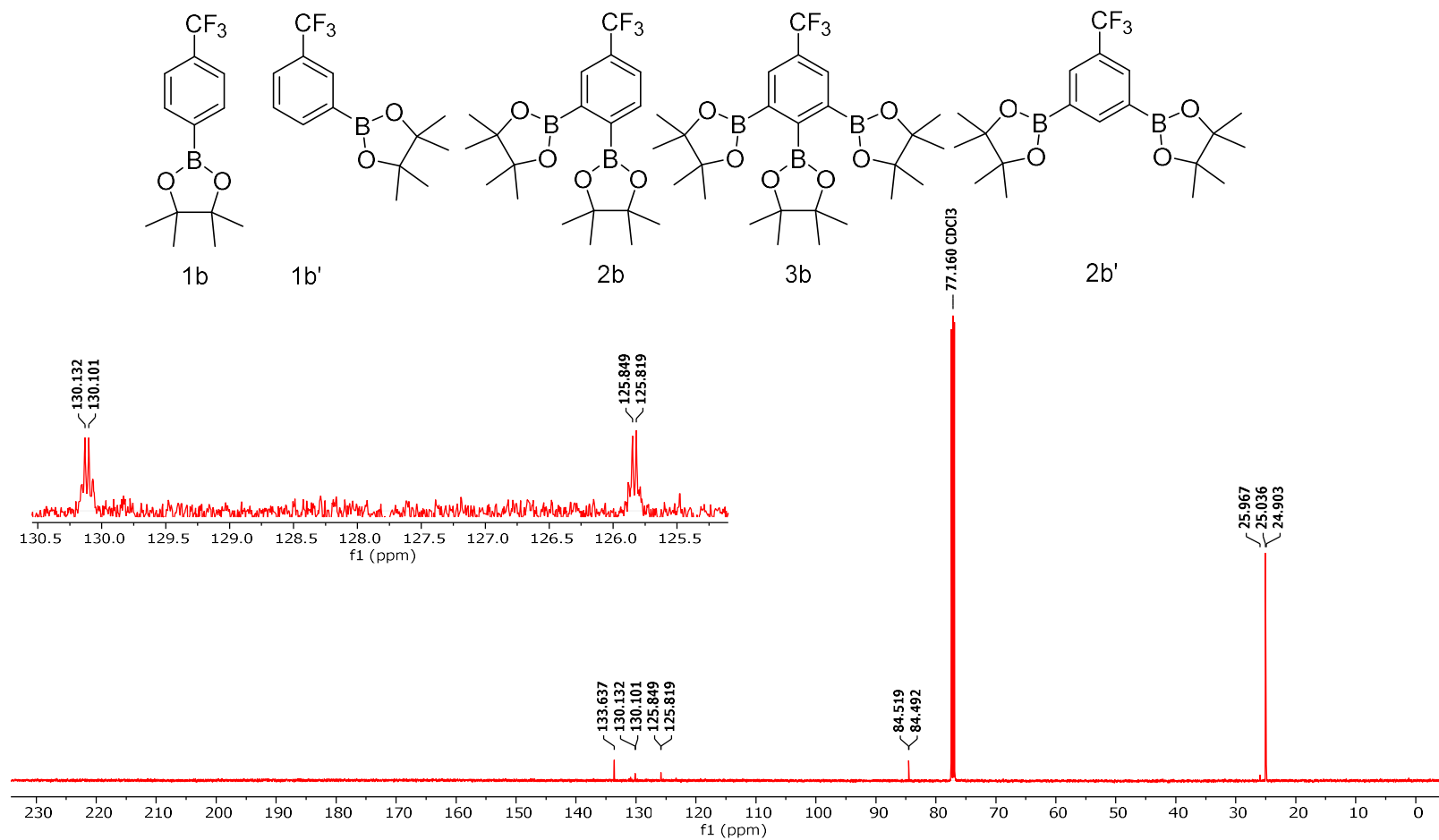


Figure 6-100 Conditions: 25 °C, 126 MHz, CDCl<sub>3</sub>

**$^{11}\text{B}$  NMR Spectra of Fraction 3 of the purified reaction mixture of Table 2 Entry 2 Trial 1**

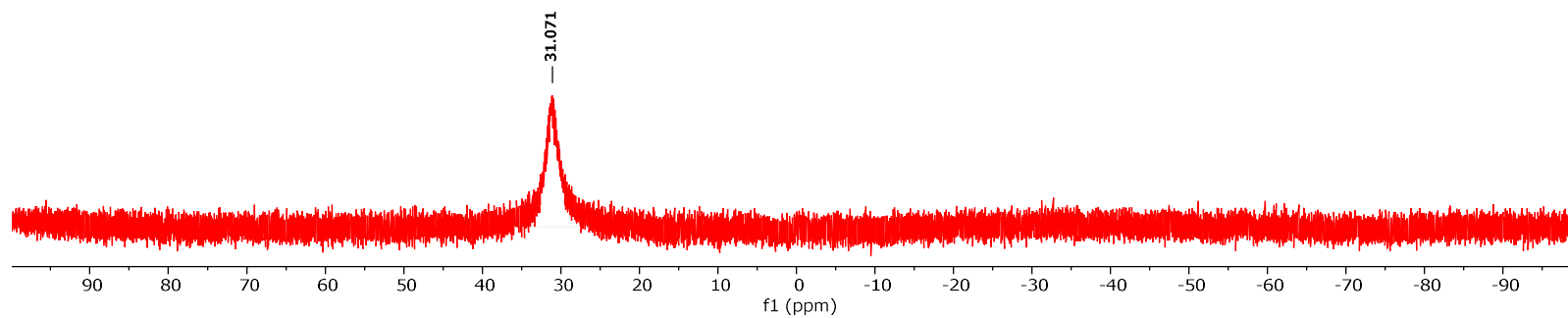
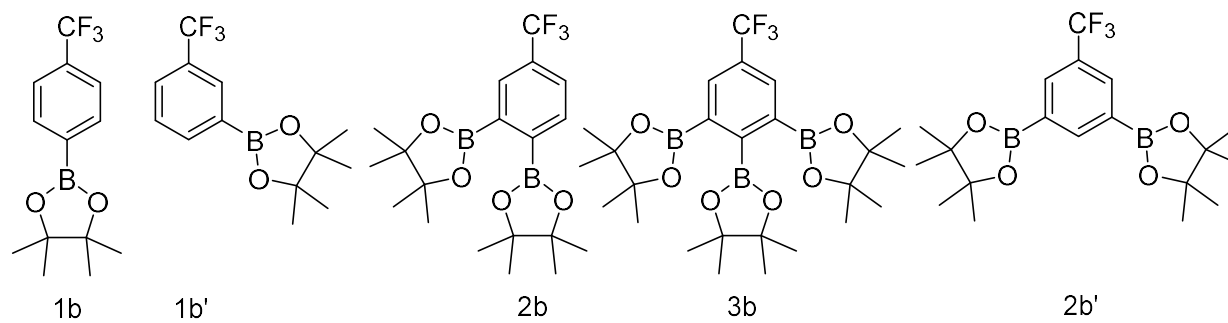


Figure 6-101 Conditions: 25 °C, 160 MHz,  $\text{CDCl}_3$

<sup>1</sup>H NMR Spectra of the crude reaction mixture of Table 2 Entry 2 Trial 2

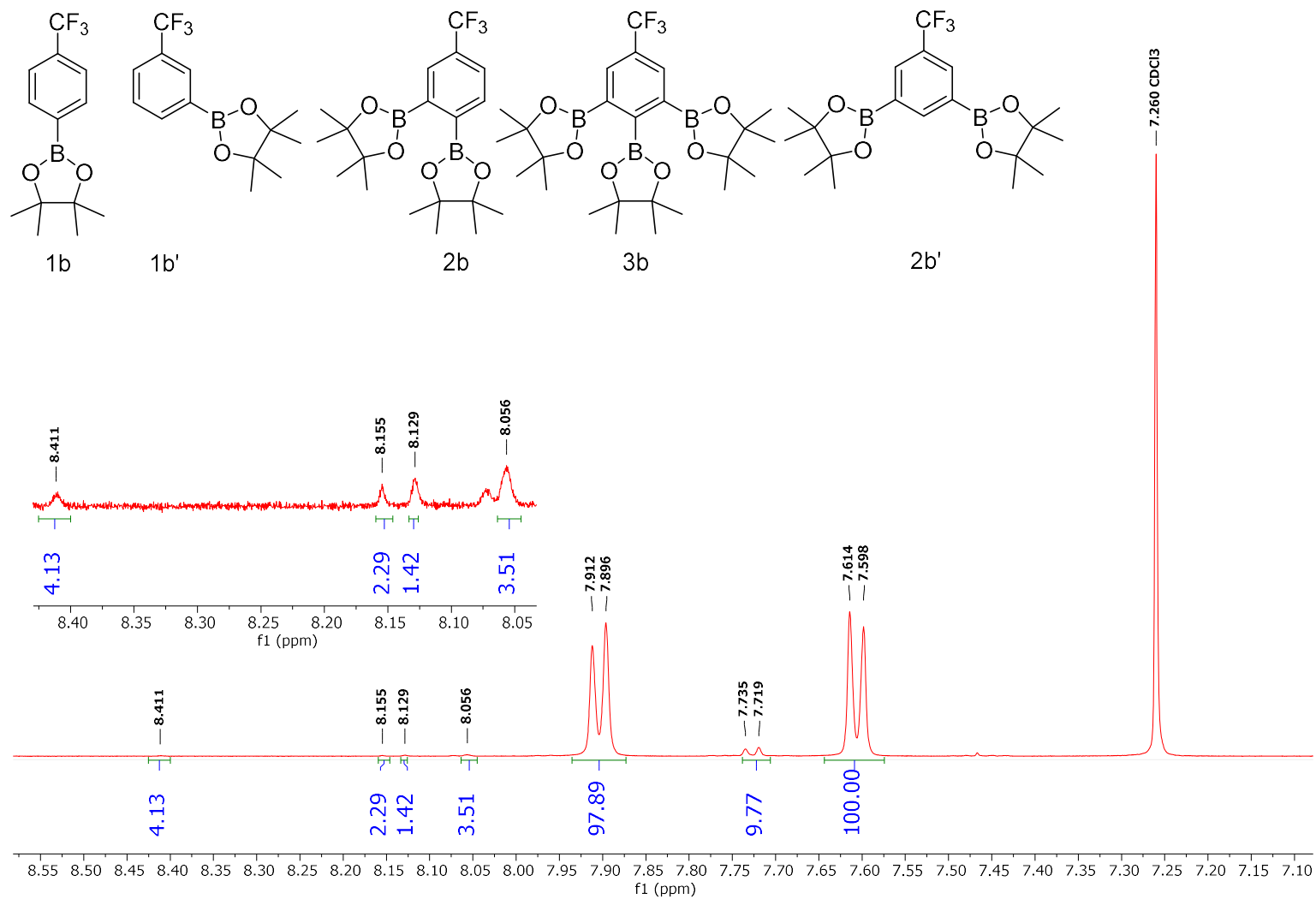


Figure 6-102 Conditions: 25 °C, 500 MHz, CDCl<sub>3</sub>

**$^{19}\text{F}$  NMR Spectra of the crude reaction mixture of Table 2 Entry 2 Trial 2**

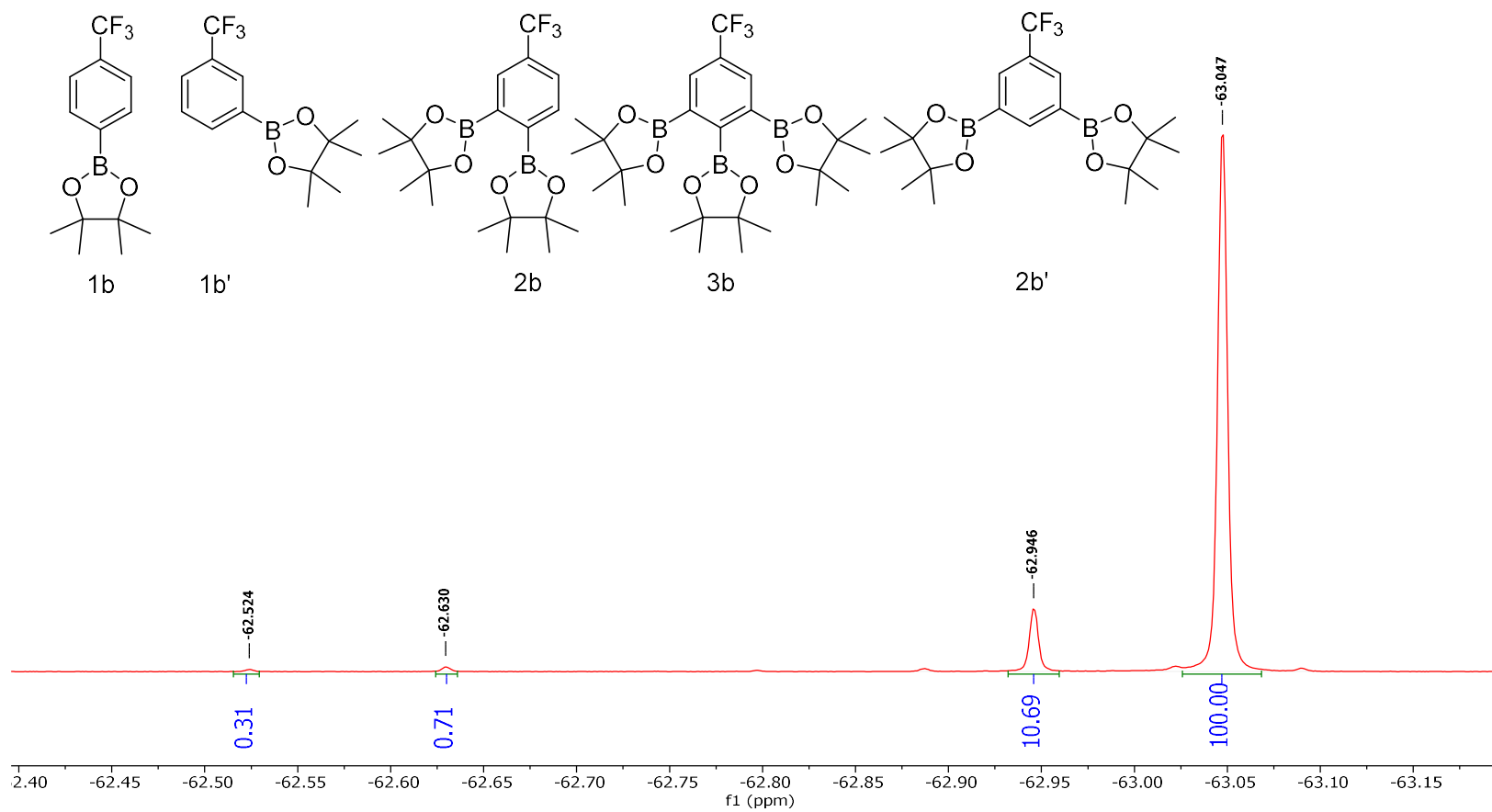


Figure 6-103 Conditions: 25 °C, 470 MHz,  $\text{CDCl}_3$



**<sup>1</sup>H NMR Spectra of the crude reaction mixture of Table 2 Entry 2 Trial 3**

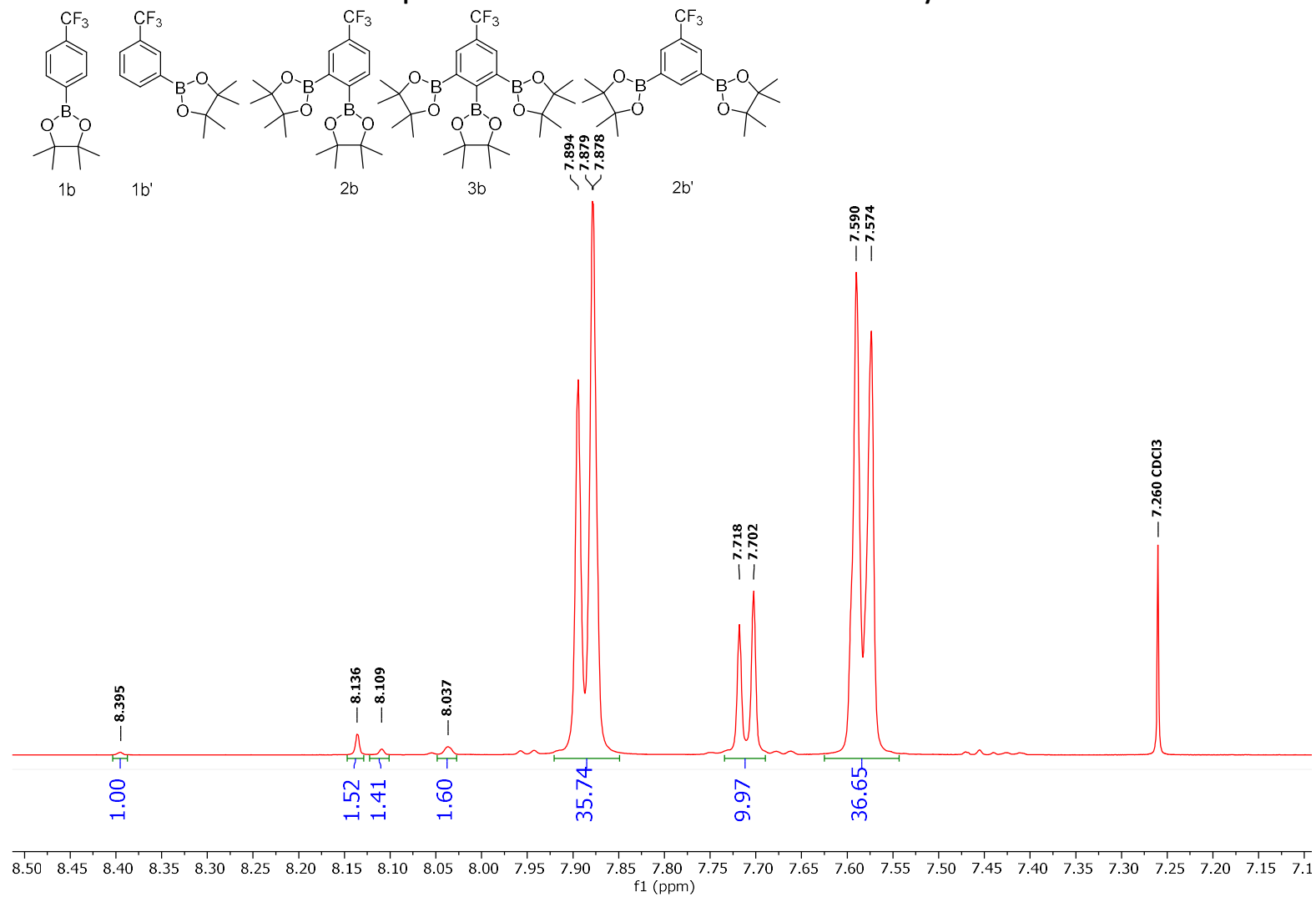


Figure 6-104 Conditions: 25 °C, 500 MHz, CDCl<sub>3</sub>

**$^{19}\text{F}$  NMR Spectra of the crude reaction mixture of Table 2 Entry 2 Trial 3**

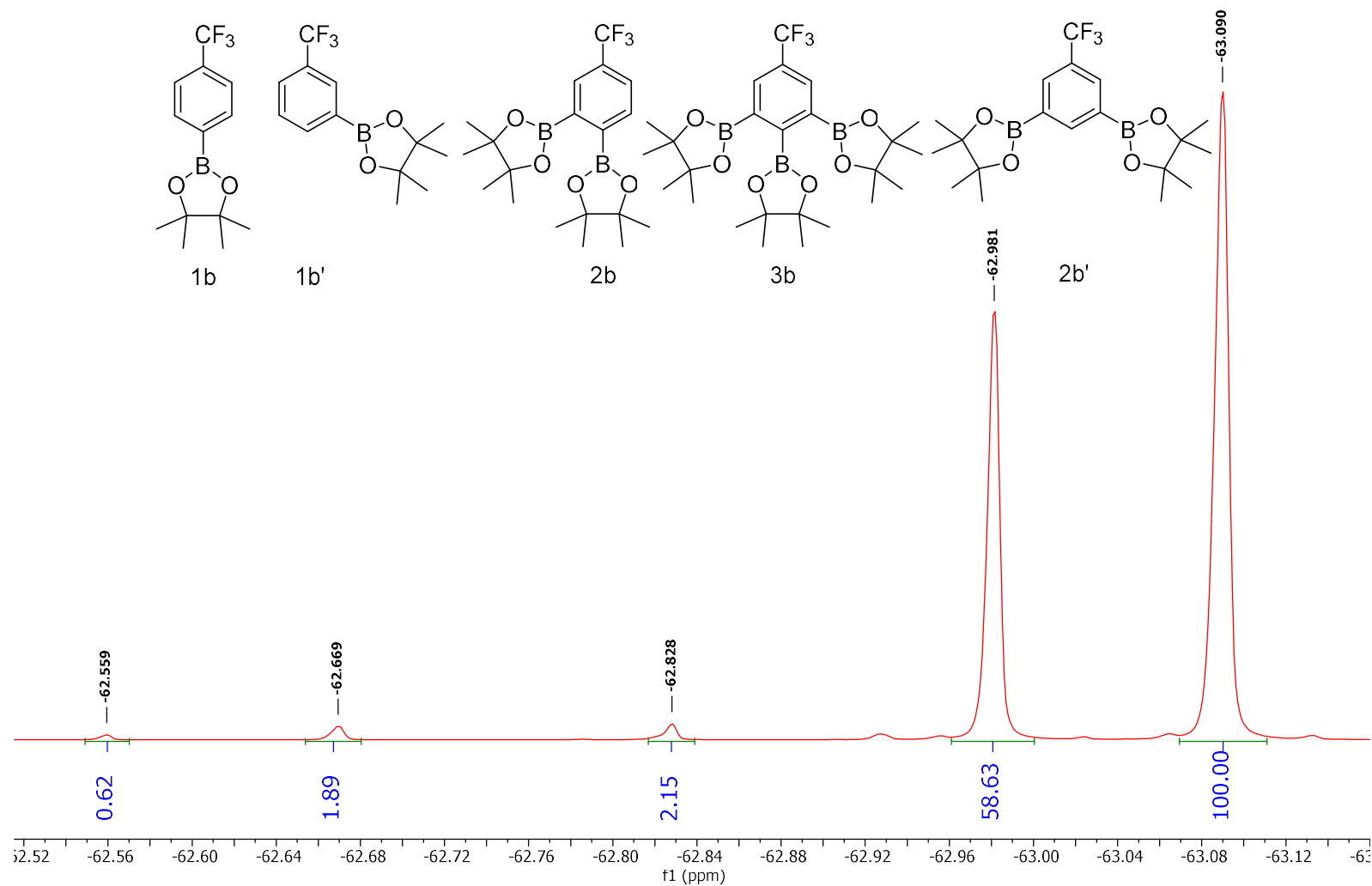


Figure 6-105 Conditions: 25 °C, 470 MHz,  $\text{CDCl}_3$

**<sup>1</sup>H NMR Spectra of the crude reaction mixture of Table 2 Entry 3 Trial 1**

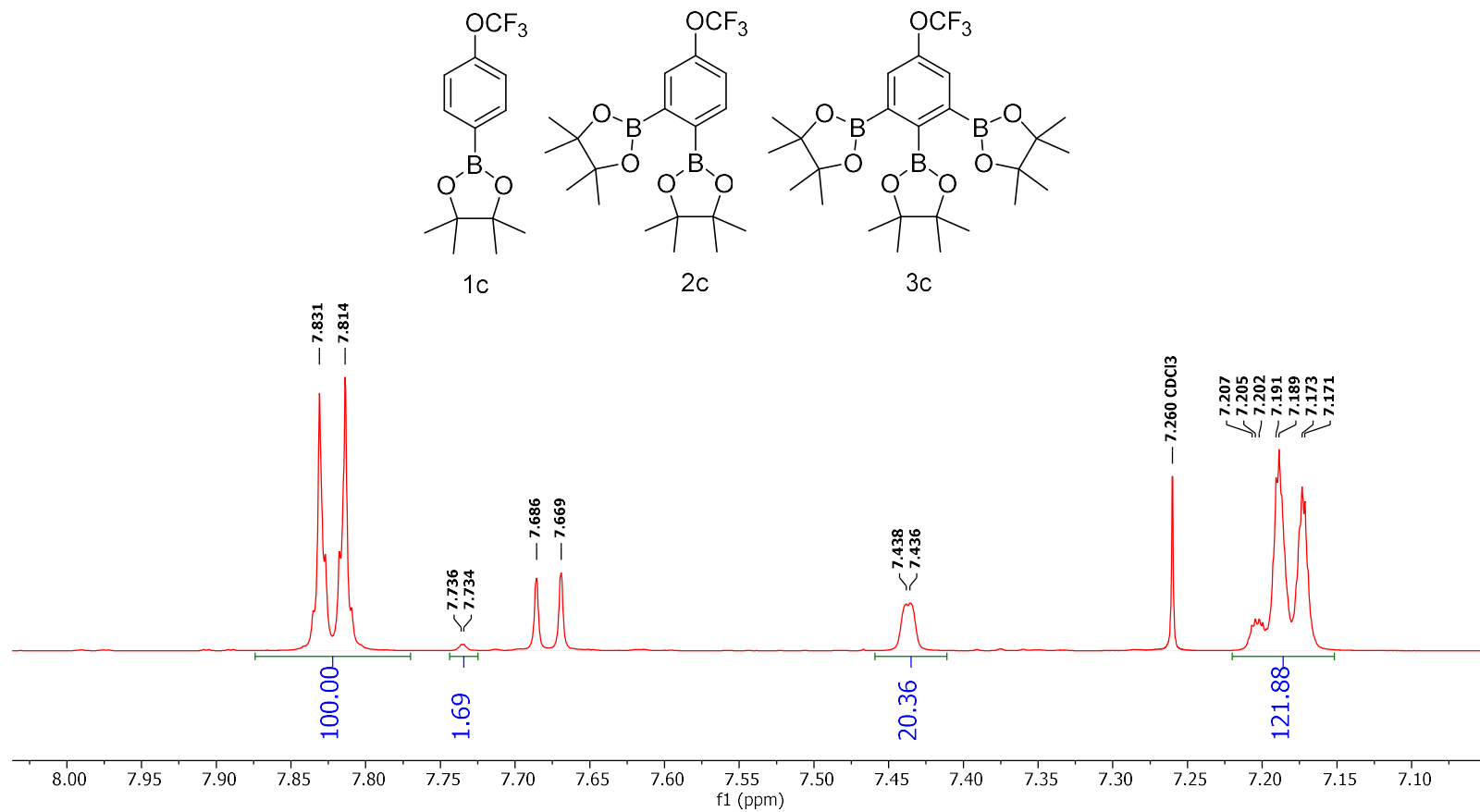


Figure 6-106 Conditions: 25 °C, 500 MHz, CDCl<sub>3</sub>

**$^{19}\text{F}$  NMR Spectra of the crude reaction mixture of Table 2 Entry 3 Trial 1**

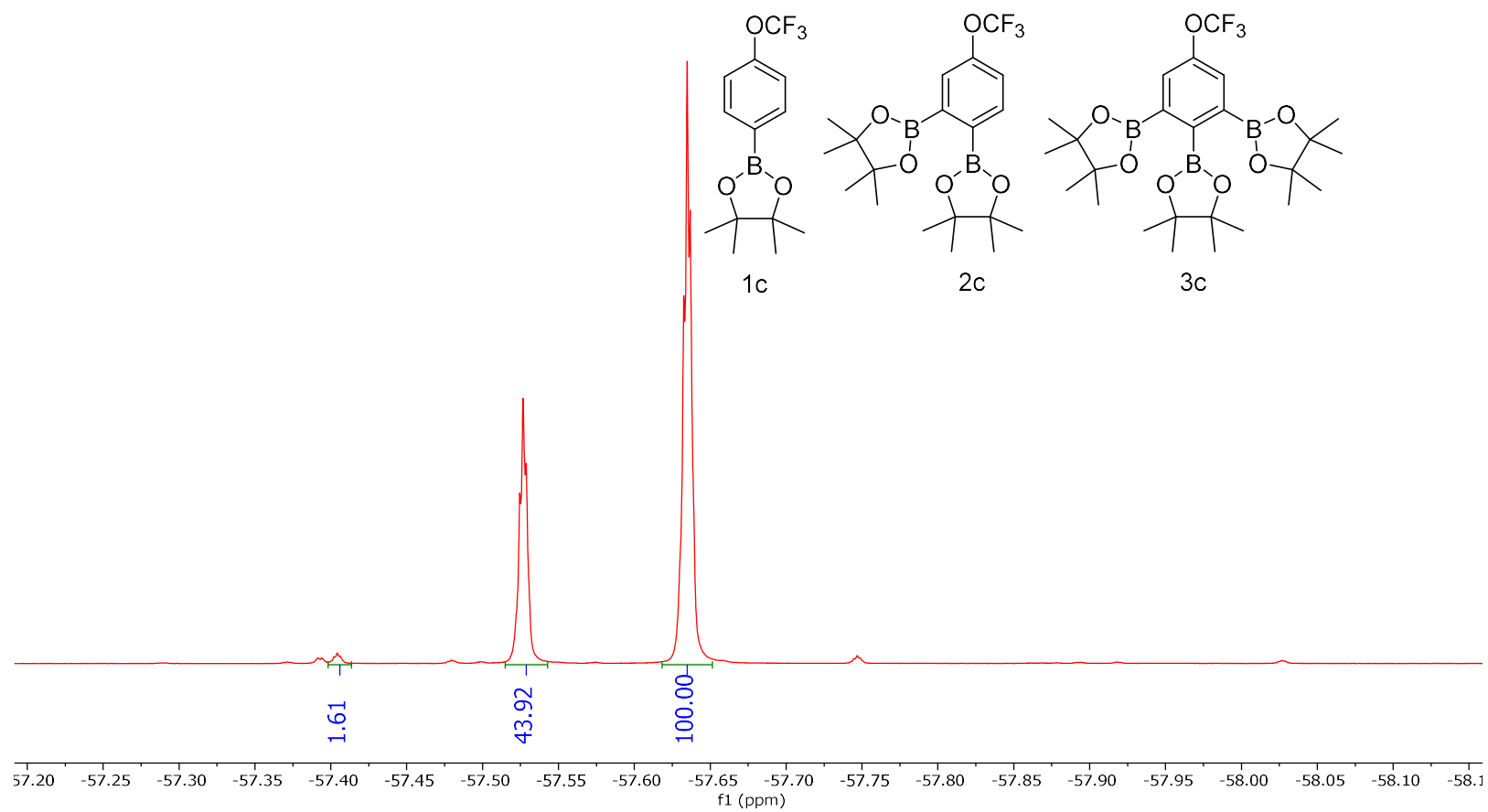


Figure 6-107 Conditions: 25 °C, 470 MHz,  $\text{CDCl}_3$

**<sup>1</sup>H NMR Spectra of the Isolated Reaction Mixture of Table 2 Entry 3 Trial 1**



Figure 6-108 Conditions: 25 °C, 500 MHz, CDCl<sub>3</sub>

**$^{19}\text{F}$  NMR Spectra of the Isolated Reaction Mixture of Table 2 Entry 3 Trial 1**

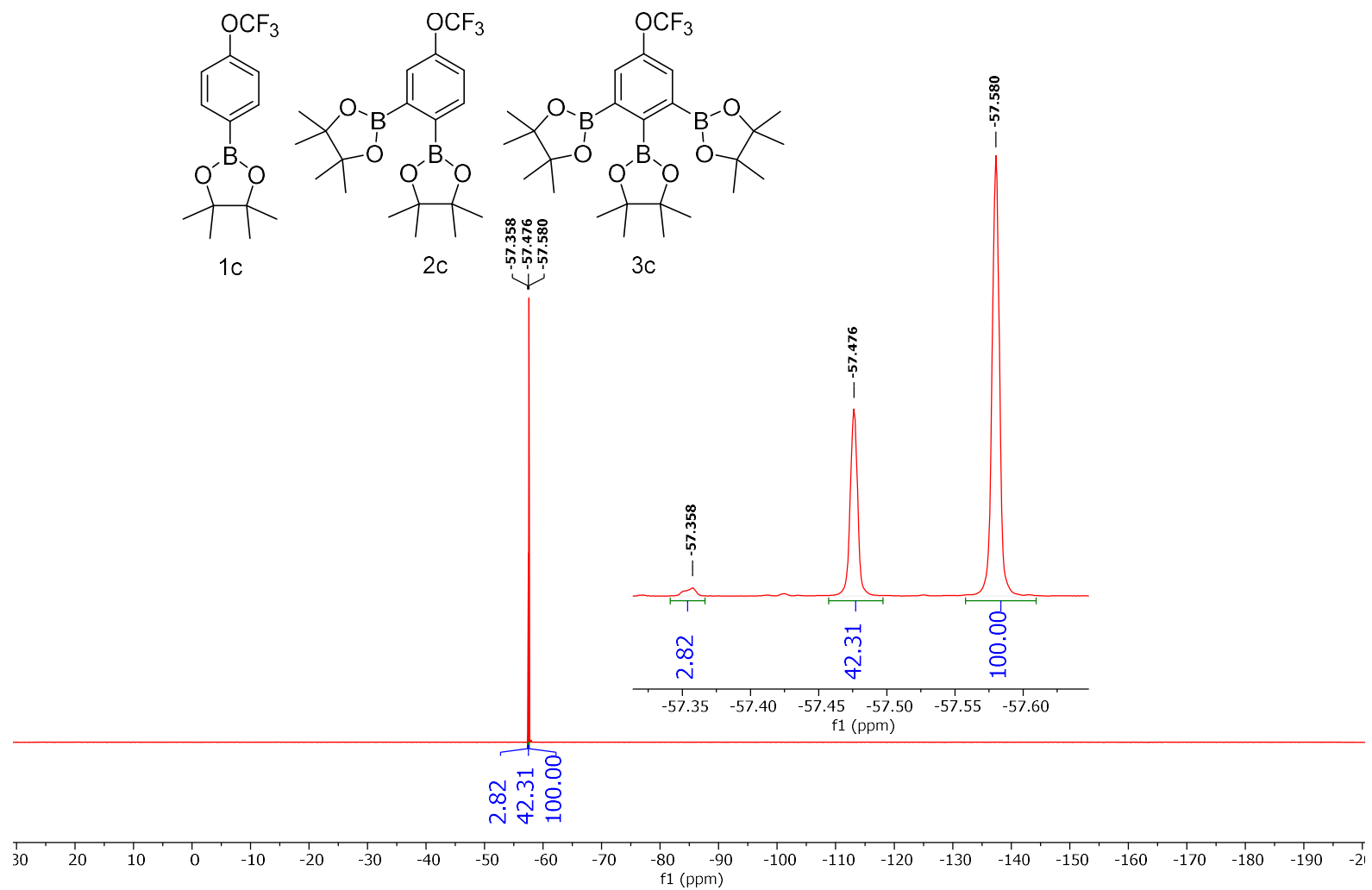


Figure 6-109 Conditions: 25 °C, 470 MHz,  $\text{CDCl}_3$

<sup>13</sup>C NMR Spectra of the Isolated Reaction Mixture of Table 2 Entry 3 Trial 1

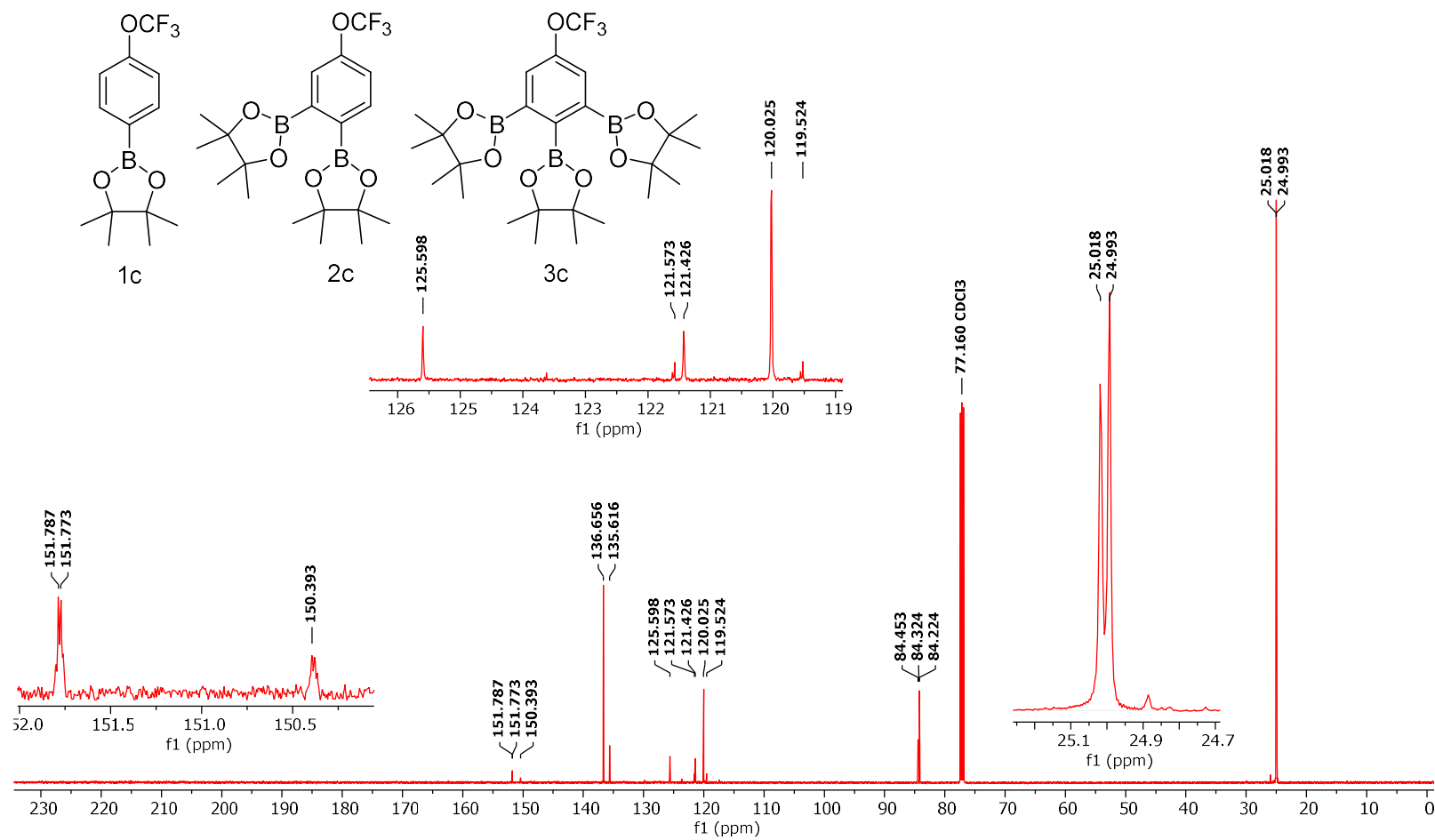


Figure 6-110 Conditions: 25 °C, 126 MHz, CDCl<sub>3</sub>

**$^{11}\text{B}$  NMR Spectra of the Isolated Reaction Mixture of Table 2 Entry 3 Trial 1**

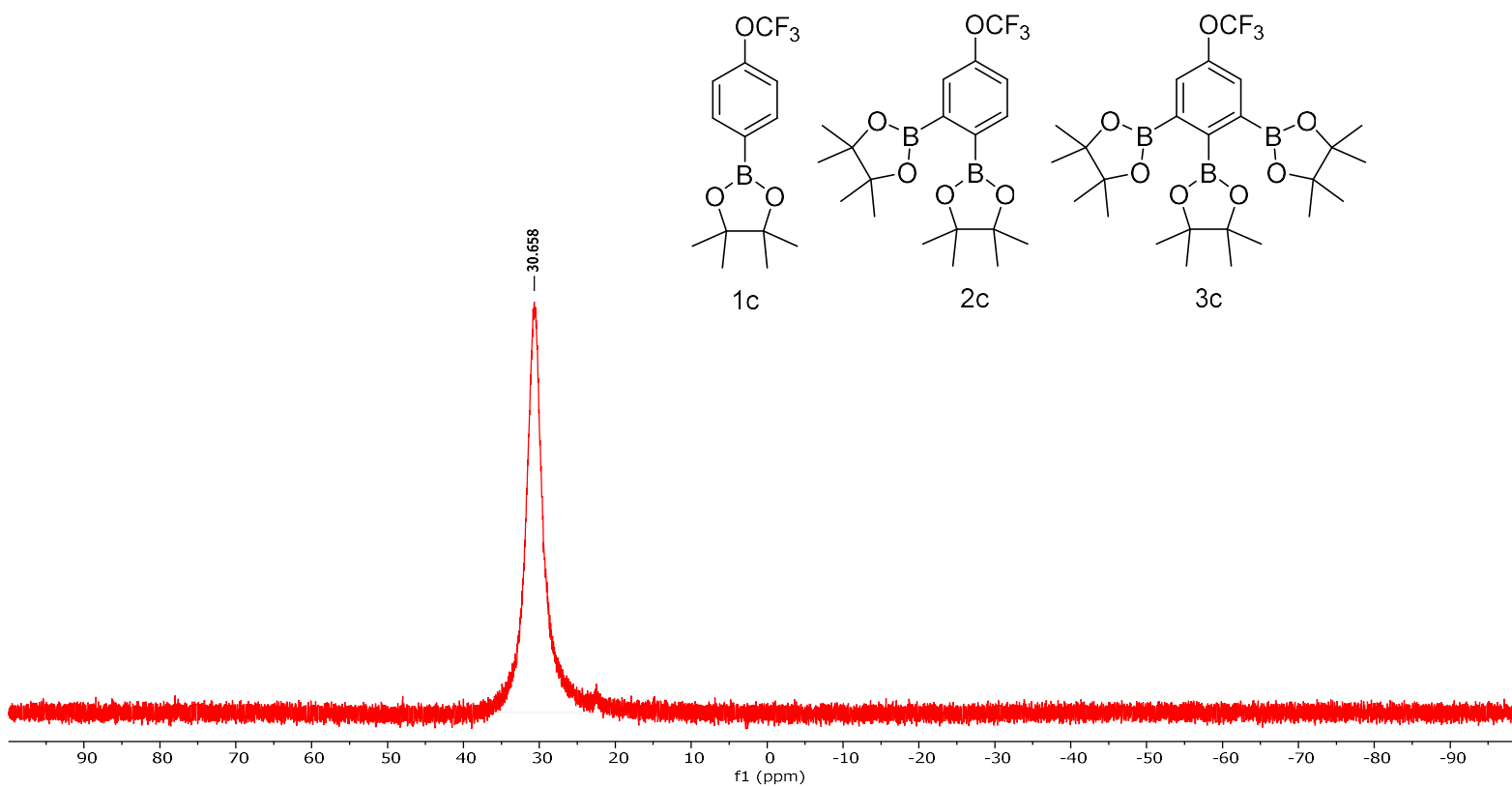


Figure 6-111 Conditions: 25 °C, 160 MHz,  $\text{CDCl}_3$



**<sup>1</sup>H NMR Spectra of the Crude reaction mixture of Table 2 Entry 3 Trial 2**

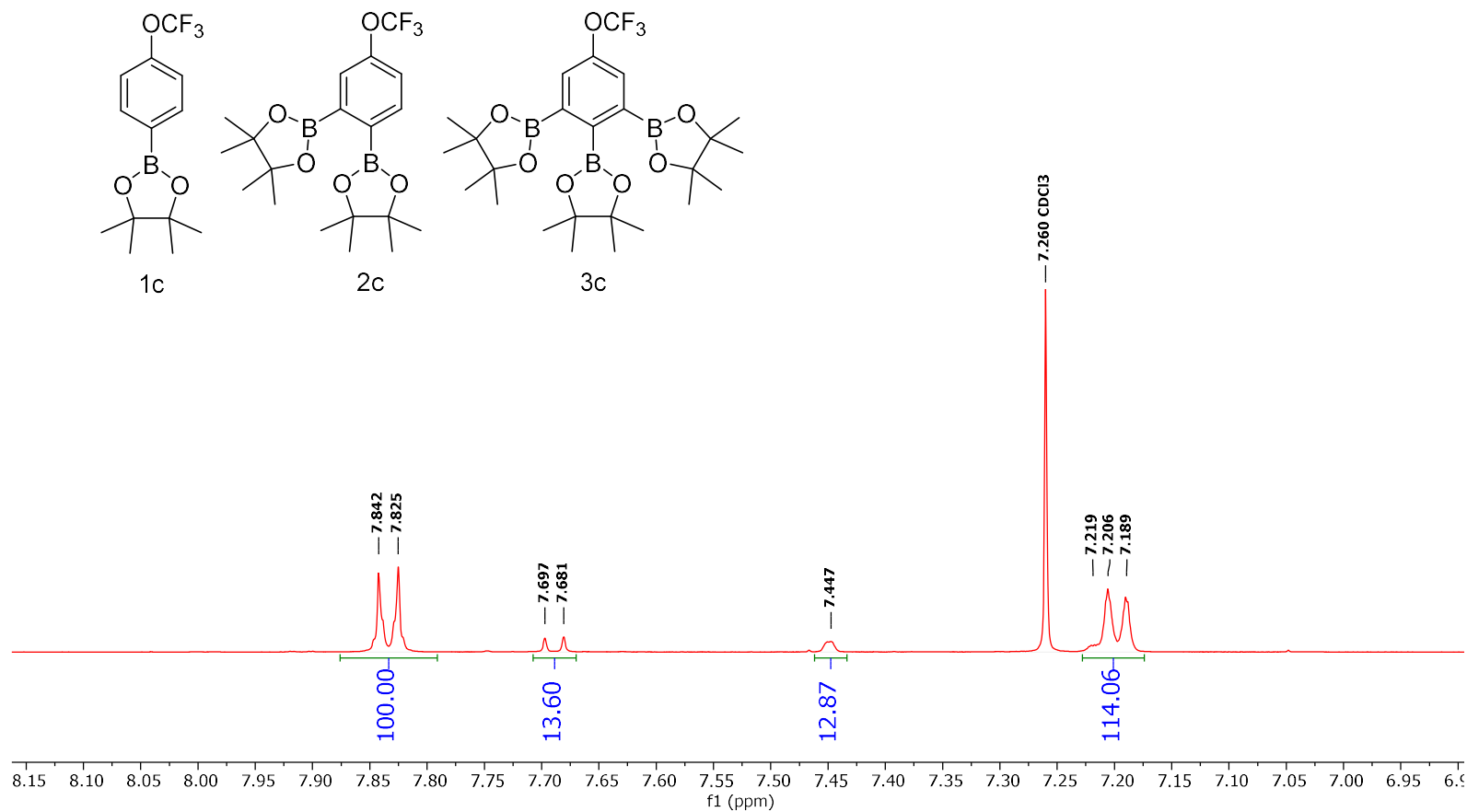


Figure 6-112 Conditions: 25 °C, 500 MHz, CDCl<sub>3</sub>

**<sup>19</sup>F NMR Spectra of the Crude reaction mixture of Table 2 Entry 3 Trial 2**

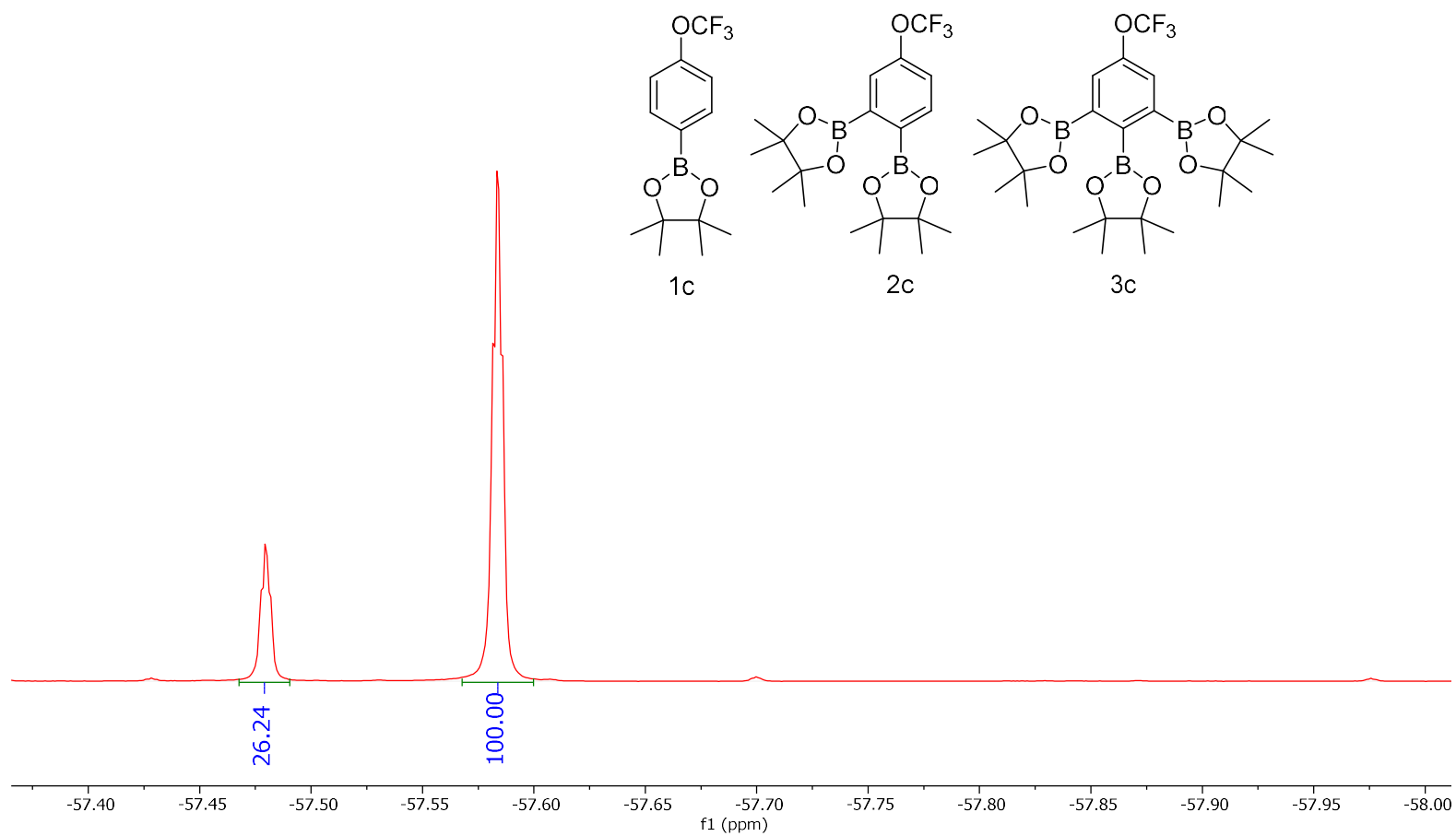


Figure 6-113 Conditions: 25 °C, 470 MHz, CDCl<sub>3</sub>

**<sup>1</sup>H NMR Spectra of the Crude reaction mixture of Table 2 Entry 3 Trial 3**

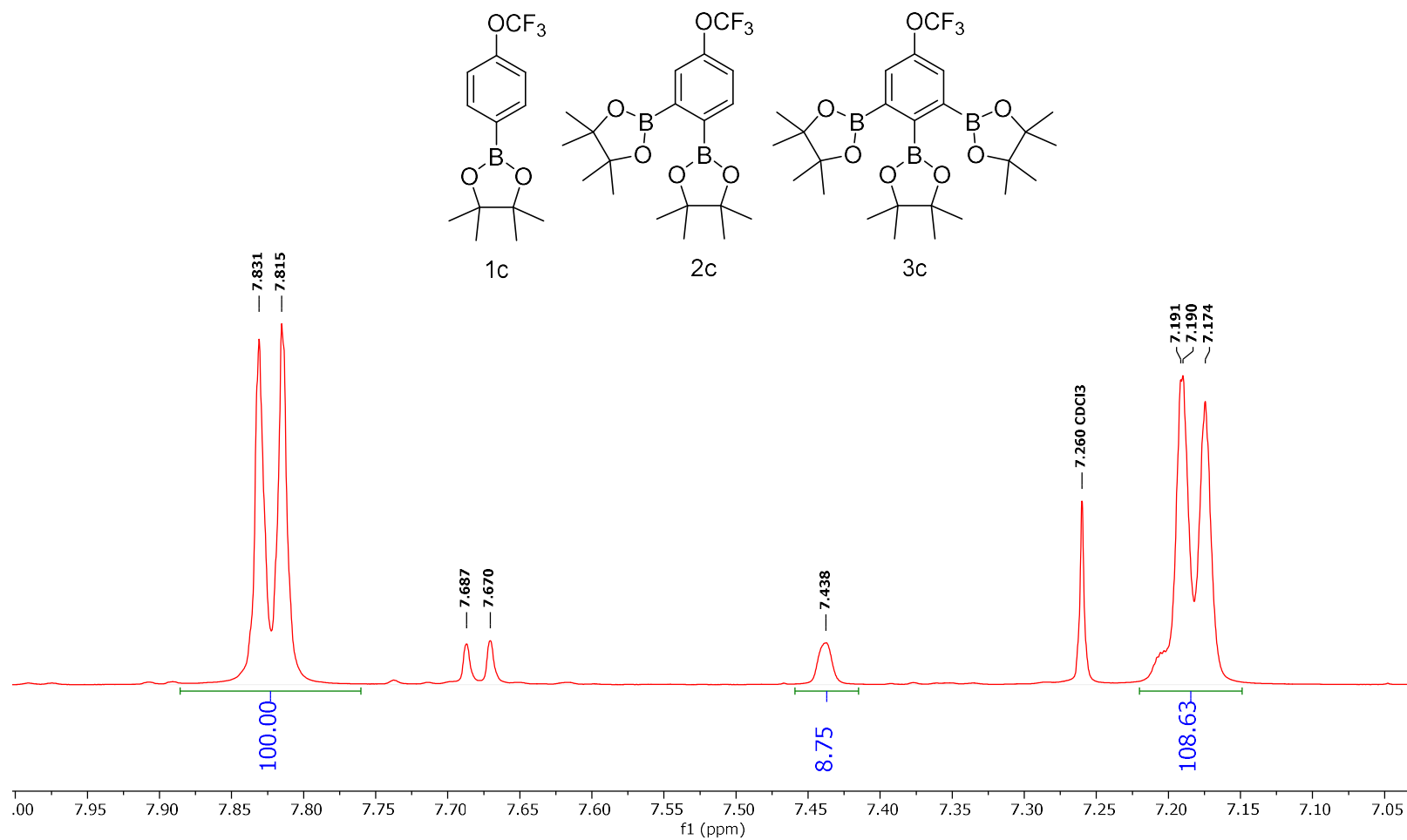


Figure 6-114 Conditions: 25 °C, 500 MHz, CDCl<sub>3</sub>

**$^{19}\text{F}$  NMR Spectra of the Crude reaction mixture of Table 2 Entry 3 Trial 3**

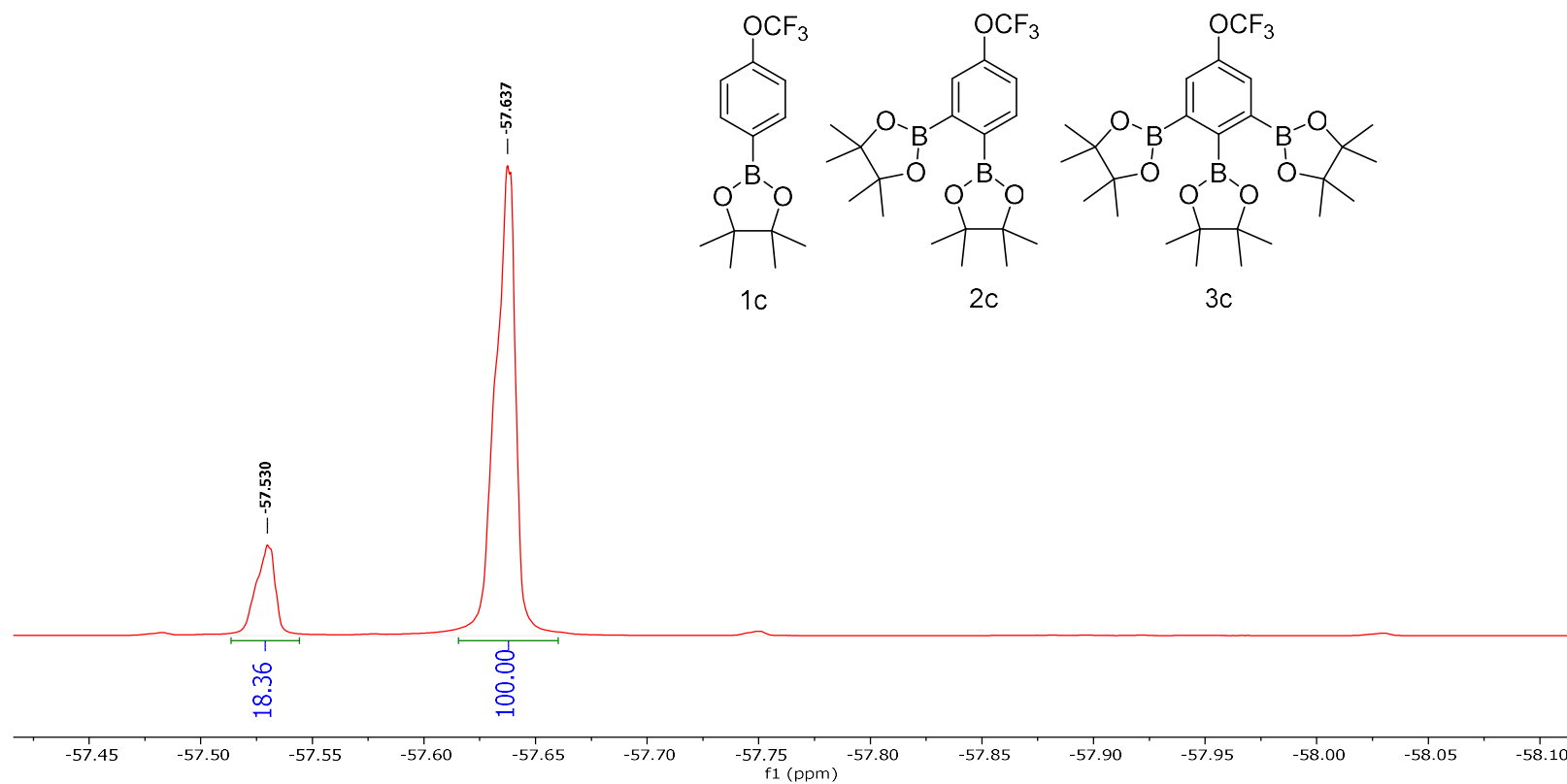


Figure 6-115 Conditions: 25 °C, 470 MHz,  $\text{CDCl}_3$

<sup>1</sup>H NMR Spectra of the Crude reaction mixture of Table 2 Entry 4 Trial 1

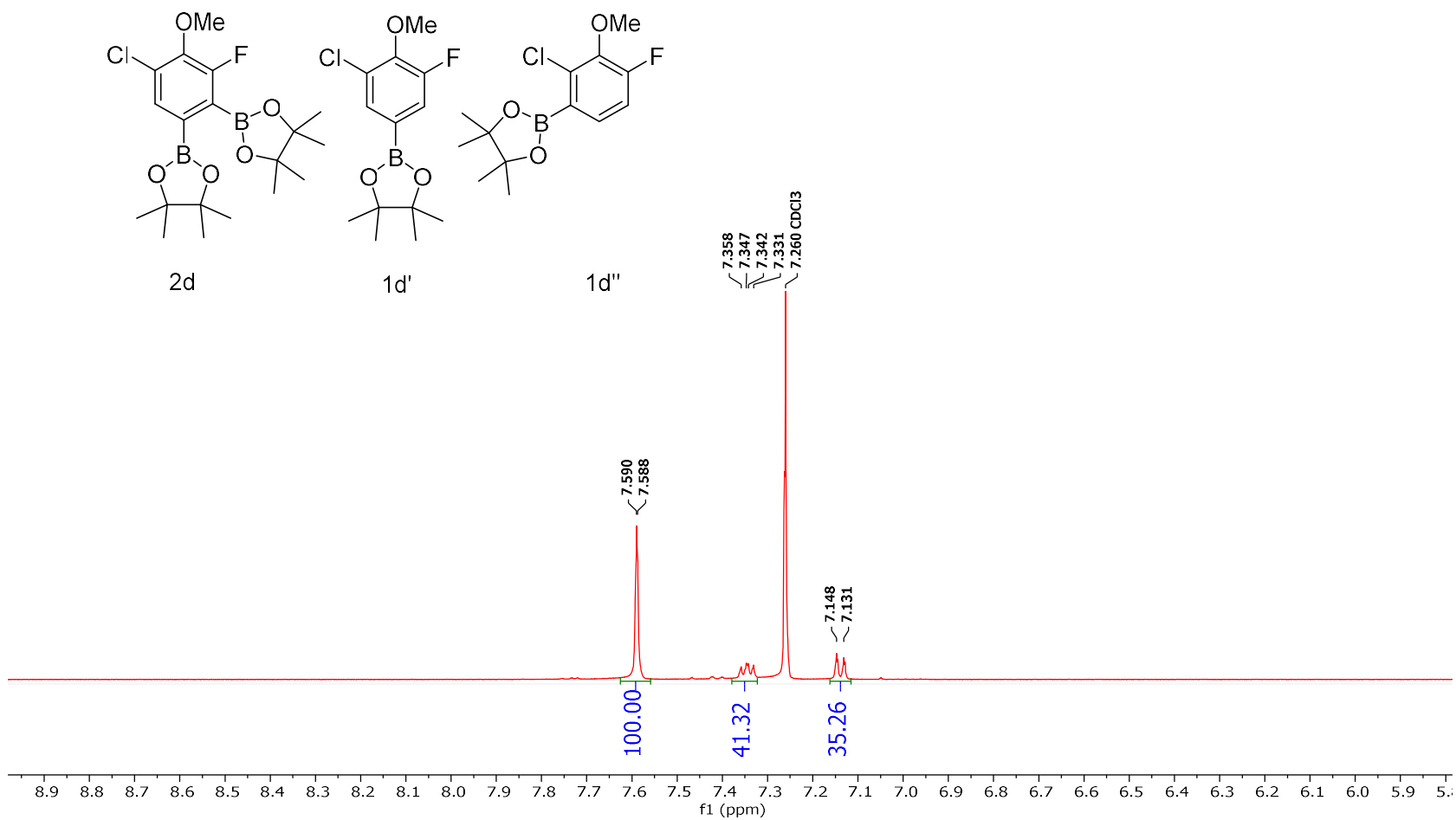


Figure 6-116 Conditions: 25 °C, 500 MHz, CDCl<sub>3</sub>

**$^{19}\text{F}$  NMR Spectra of the Crude reaction mixture of Table 2 Entry 4 Trial 1**

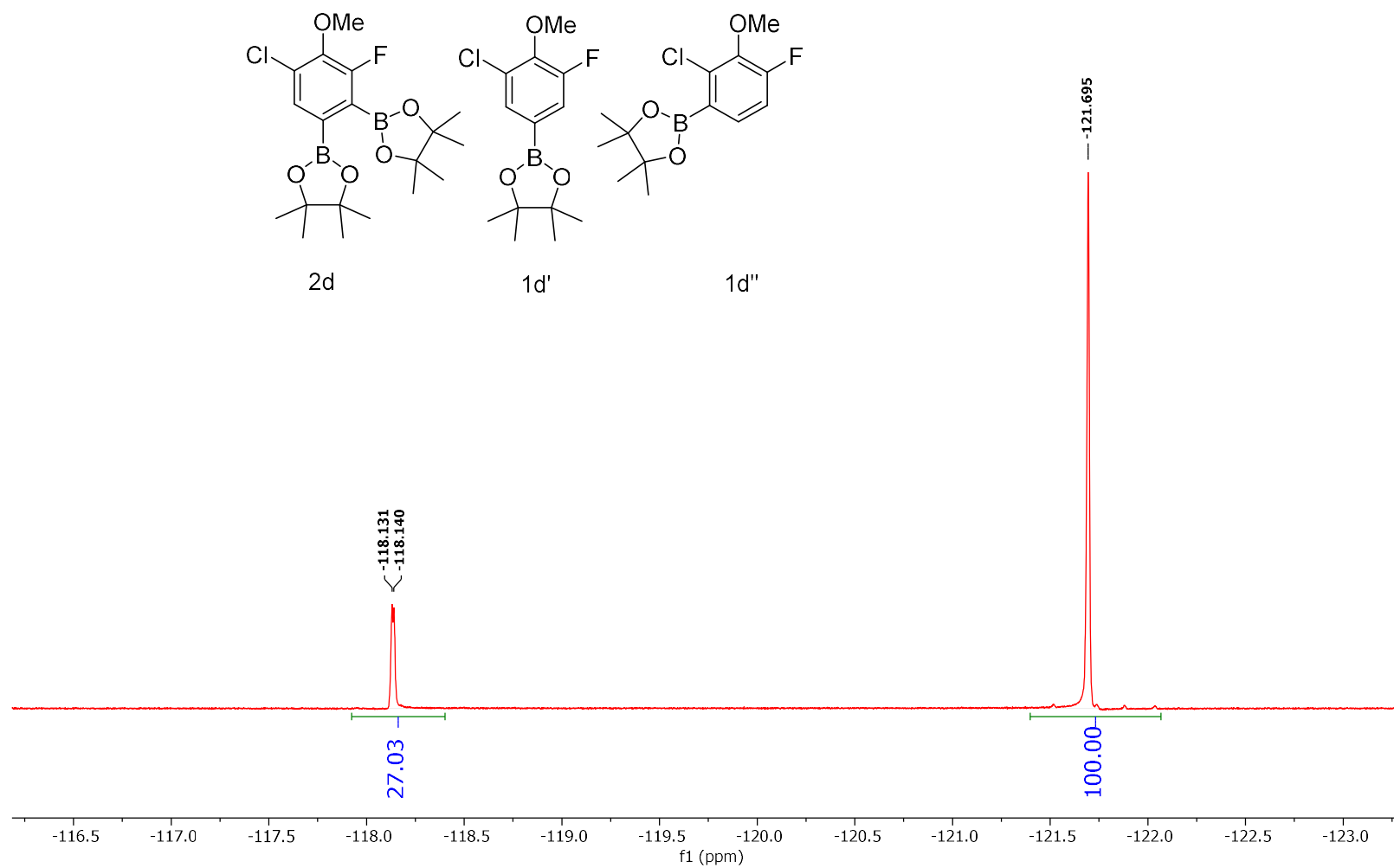


Figure 6-117 Conditions: 25 °C, 470 MHz,  $\text{CDCl}_3$

<sup>1</sup>H NMR Spectra of Fraction 1 of the Isolated Reaction Mixture of Table 2 Entry 4 Trial 1

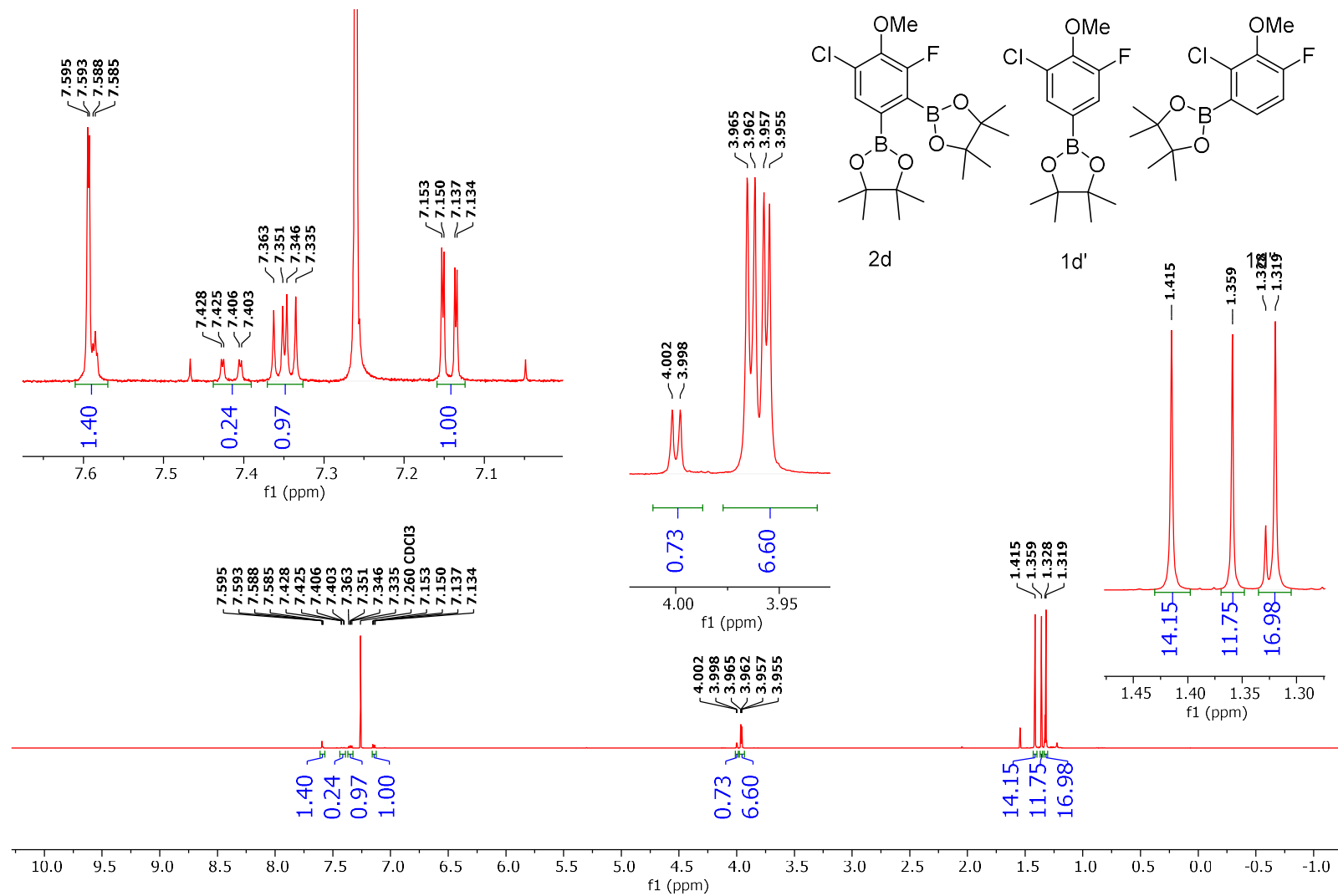


Figure 6-118 Conditions: 25 °C, 500 MHz, CDCl<sub>3</sub>

<sup>19</sup>F NMR Spectra of Fraction 1 of the Isolated Reaction Mixture of Table 2 Entry 4 Trial 1

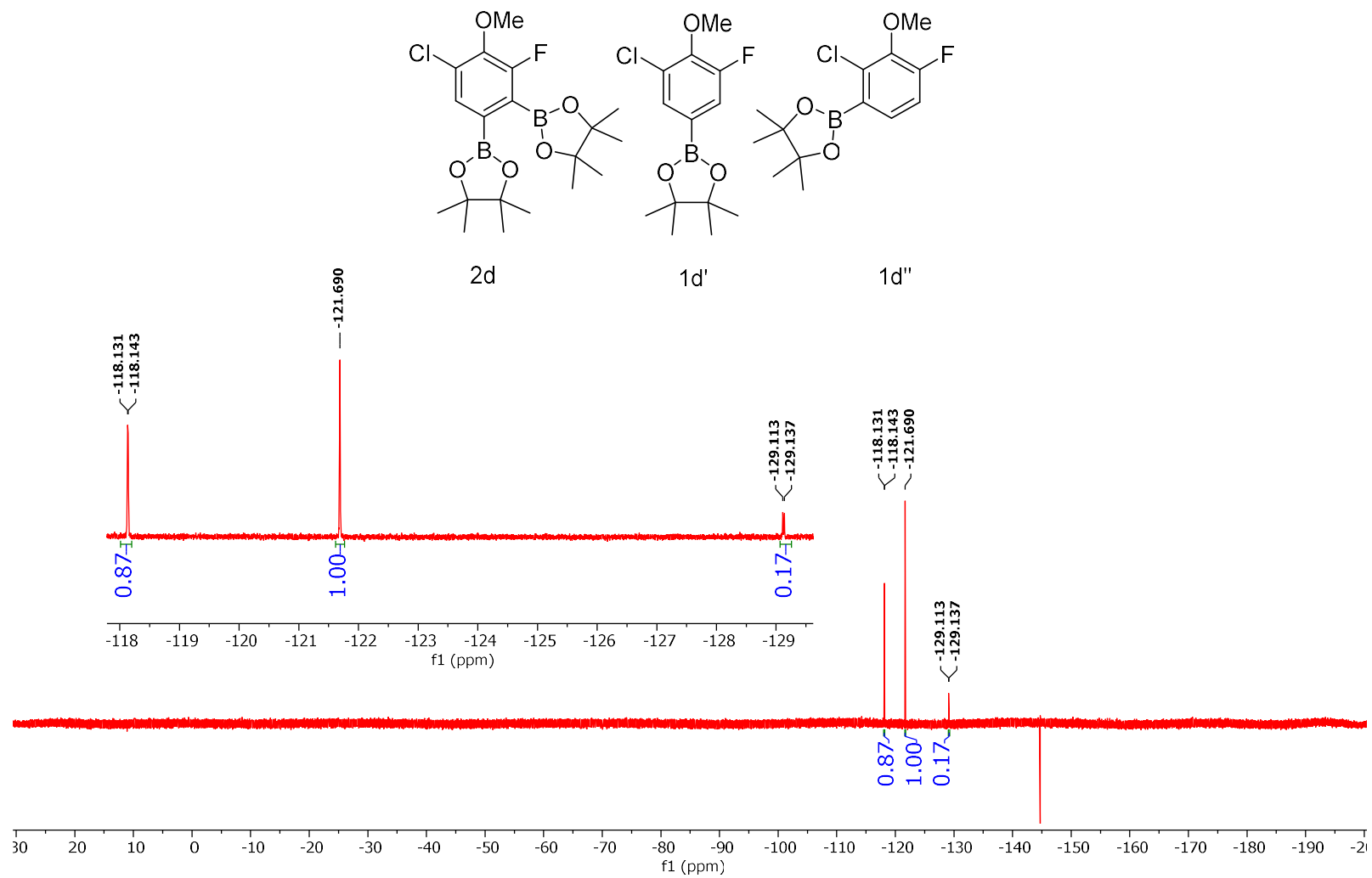


Figure 6-119 Conditions: 25 °C, 470 MHz, CDCl<sub>3</sub>



**<sup>13</sup>C NMR Spectra of Fraction 1 of the Isolated Reaction Mixture of Table 2 Entry 4 Trial 1**

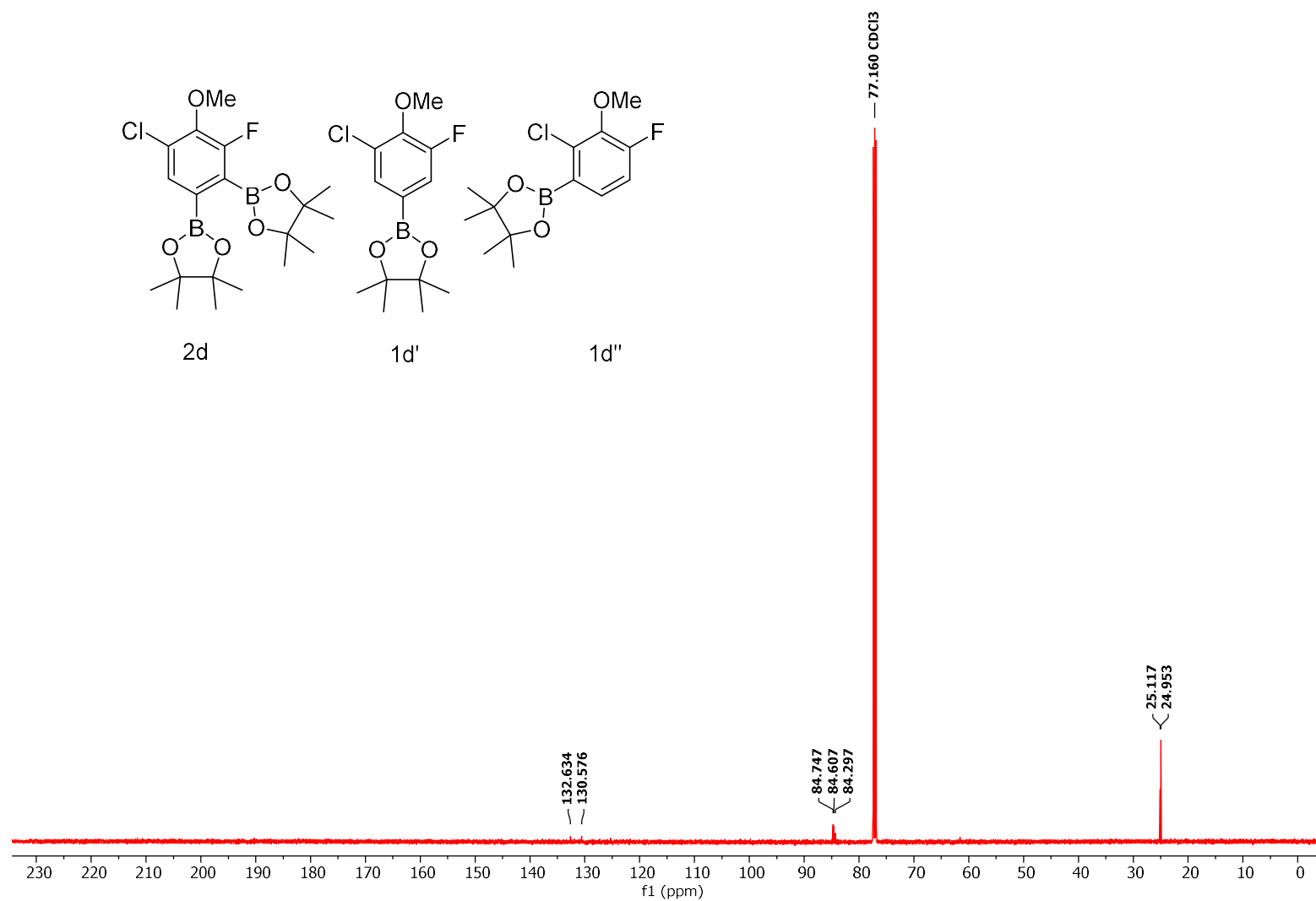


Figure 6-120 Conditions: 25 °C, 126 MHz, CDCl<sub>3</sub>

**$^{11}\text{B}$  NMR Spectra of Fraction 1 of the Isolated Reaction Mixture of Table 2 Entry 4 Trial 1**

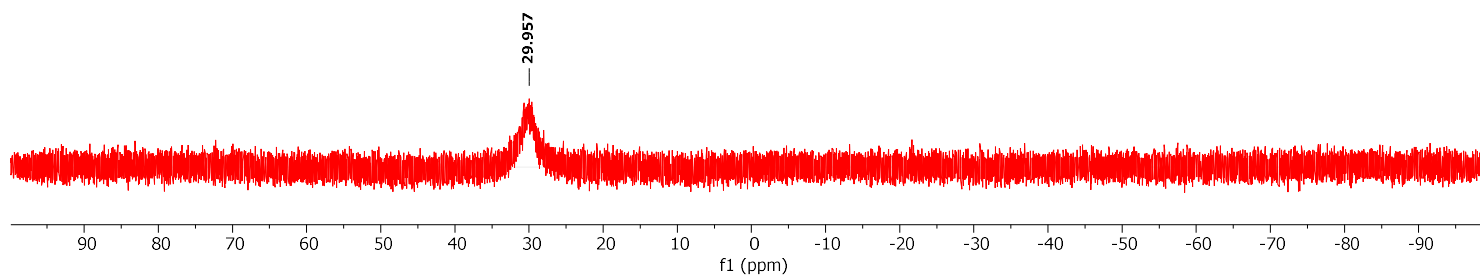
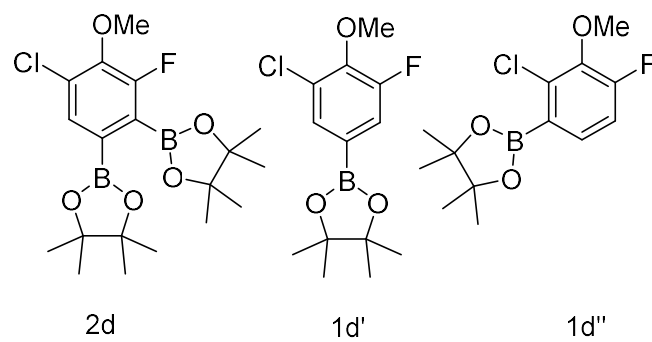


Figure 6-121 Conditions: 25 °C, 160 MHz,  $\text{CDCl}_3$

**<sup>1</sup>H NMR Spectra of Fraction 2 of the Isolated Reaction Mixture of Table 2 Entry 4 Trial 1**

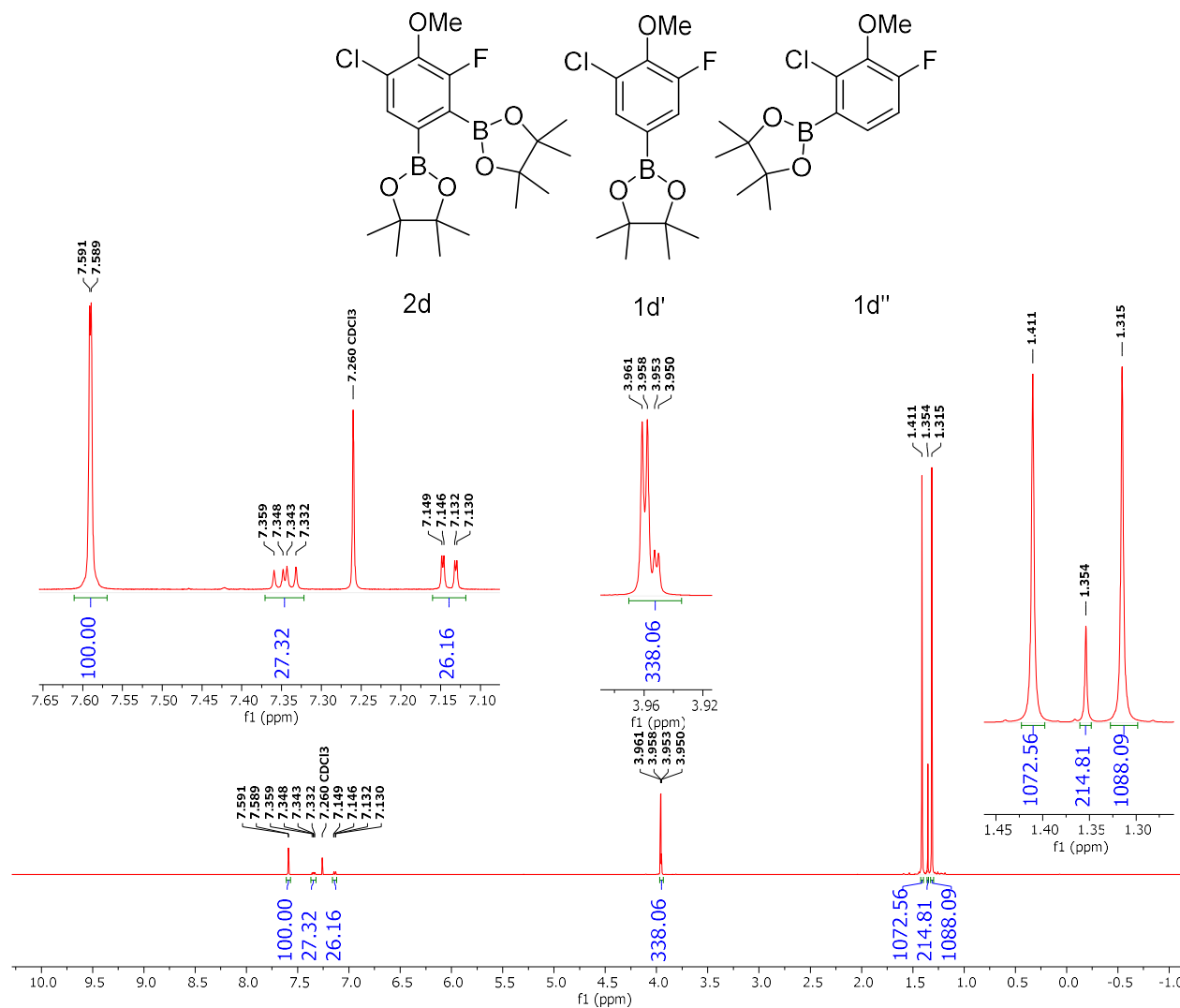


Figure 6-122 Conditions: 25 °C, 500 MHz, CDCl<sub>3</sub>

<sup>19</sup>F NMR Spectra of Fraction 2 of the Isolated Reaction Mixture of Table 2 Entry 4 Trial 1

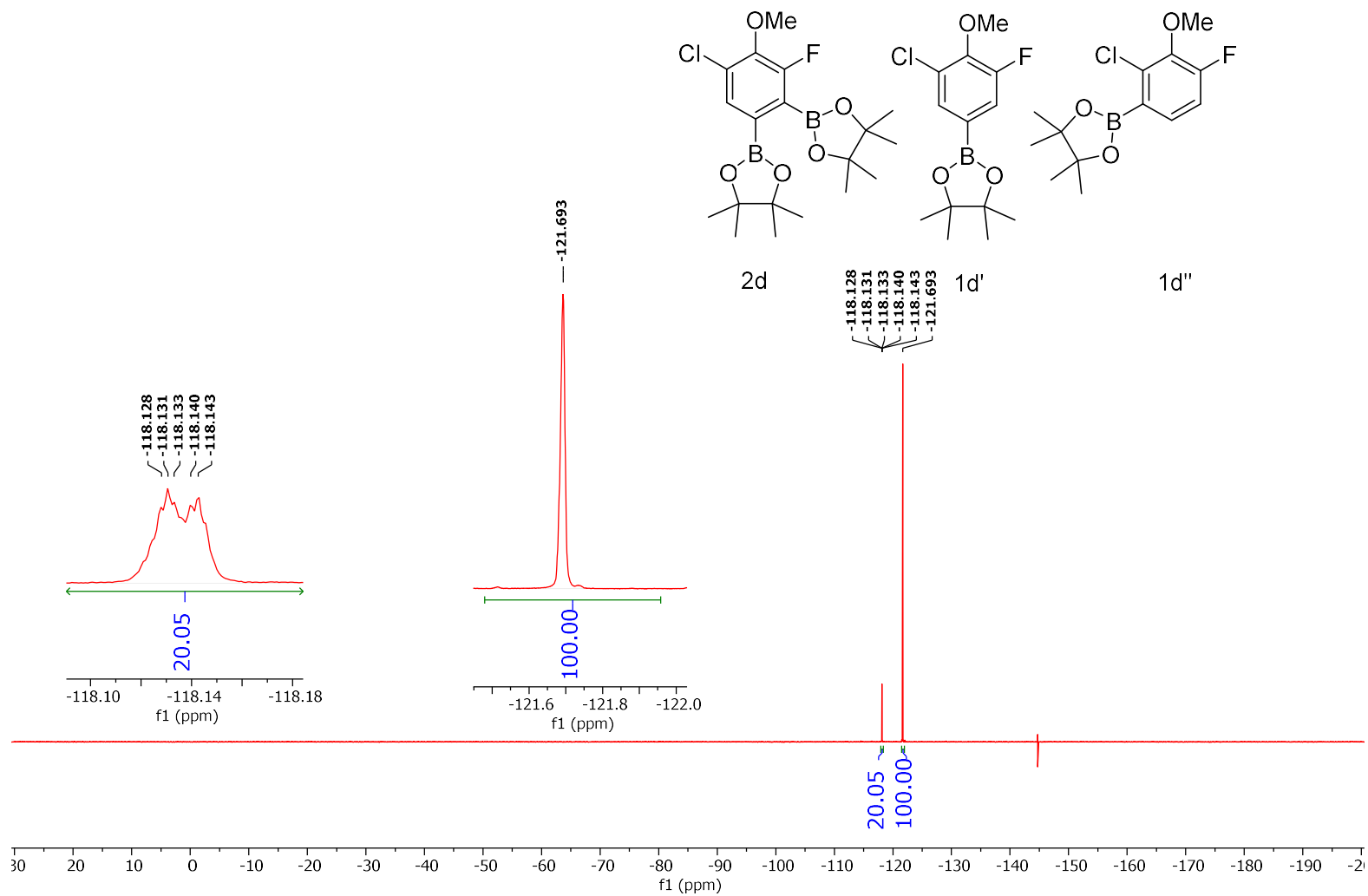


Figure 6-123 Conditions: 25 °C, 470 MHz, CDCl<sub>3</sub>

<sup>13</sup>C NMR Spectra of Fraction 2 of the Isolated Reaction Mixture of Table 2 Entry 4 Trial 1

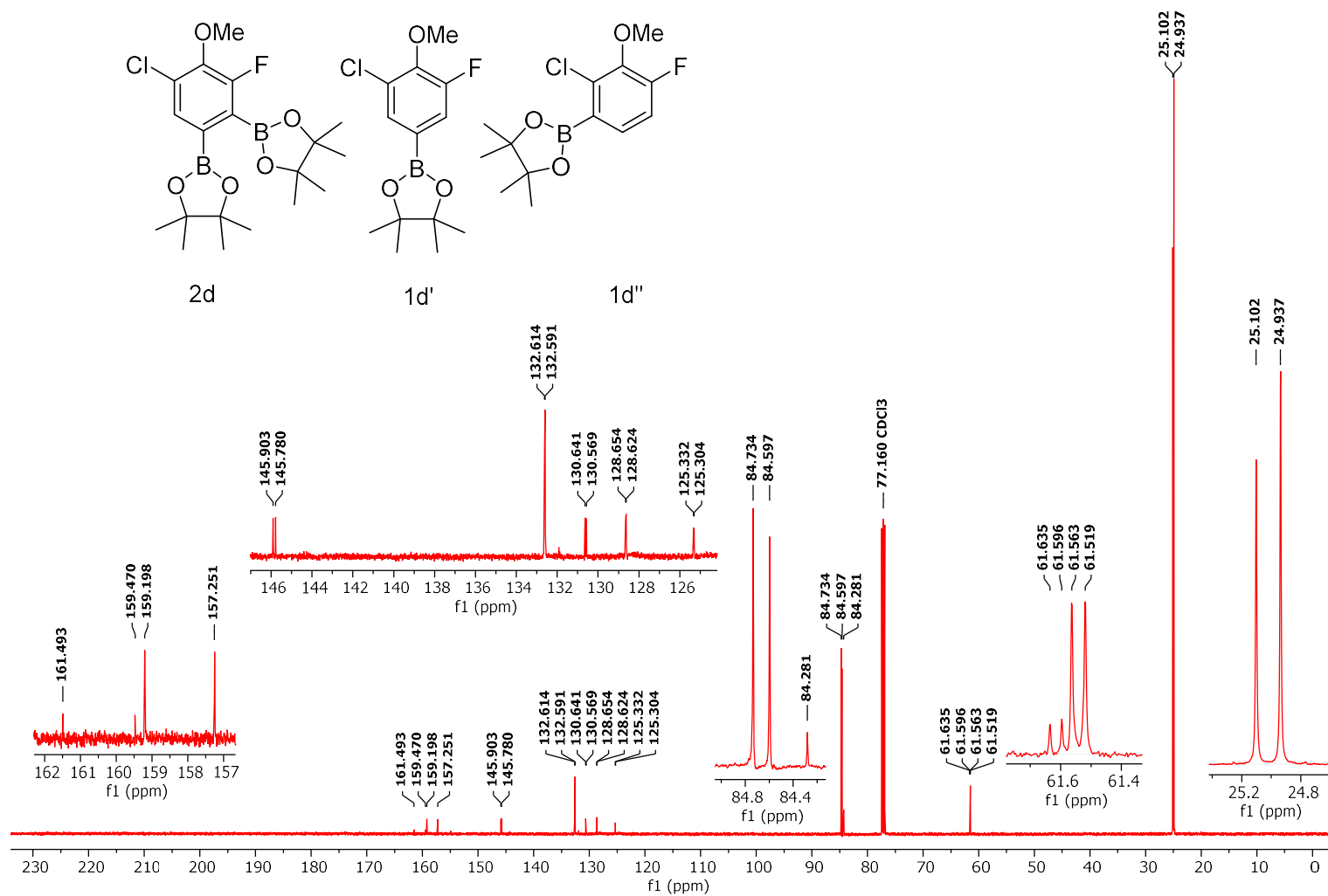


Figure 6-124 Conditions: 25 °C, 126 MHz, CDCl<sub>3</sub>

**$^{11}\text{B}$  NMR Spectra of Fraction 2 of the Isolated Reaction Mixture of Table 2 Entry 4 Trial 1**

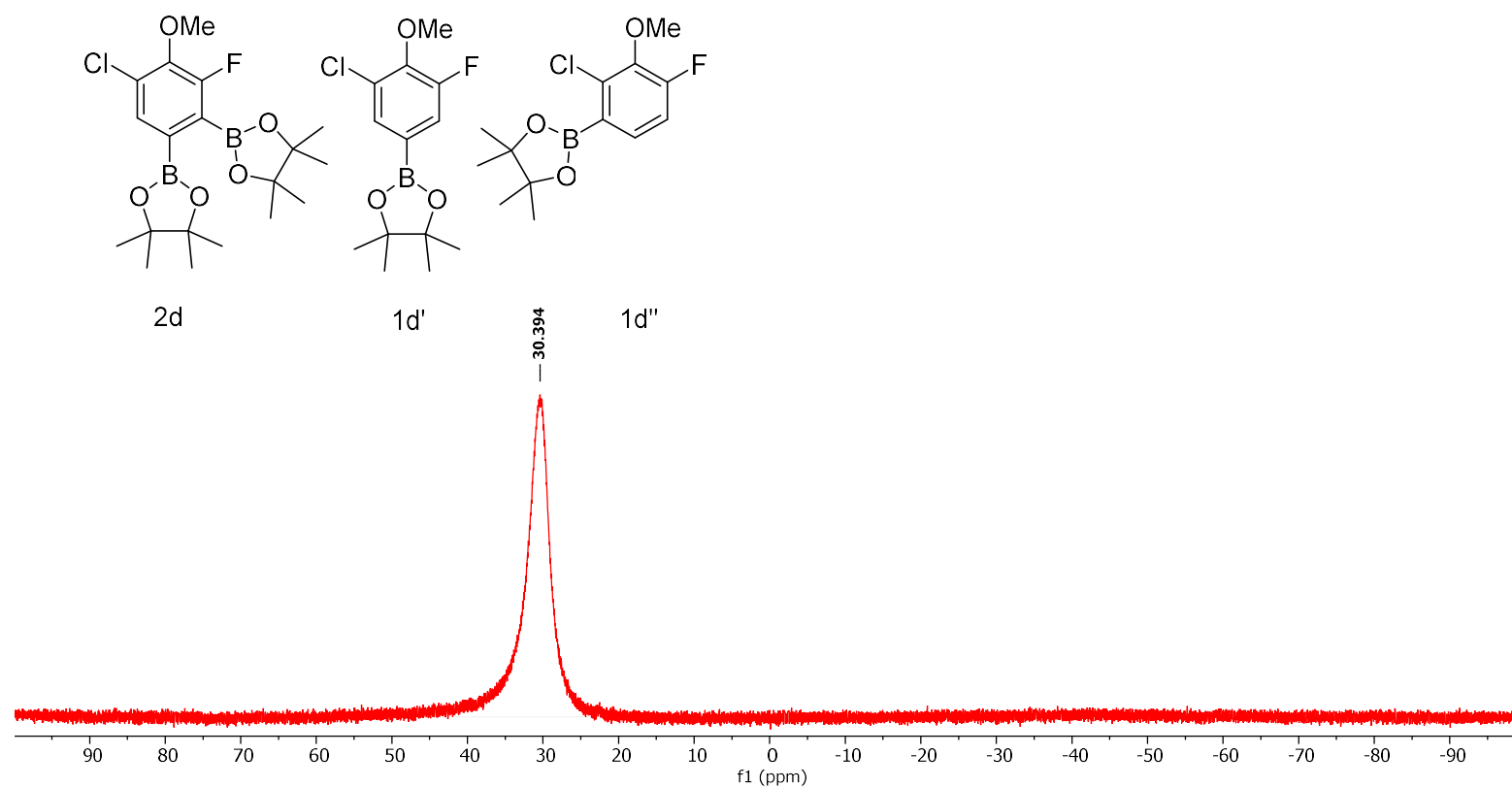


Figure 6-125 Conditions: 25 °C, 160 MHz,  $\text{CDCl}_3$

**<sup>1</sup>H NMR Spectra of Fraction 3 of the Isolated Reaction Mixture of Table 2 Entry 4 Trial 1**

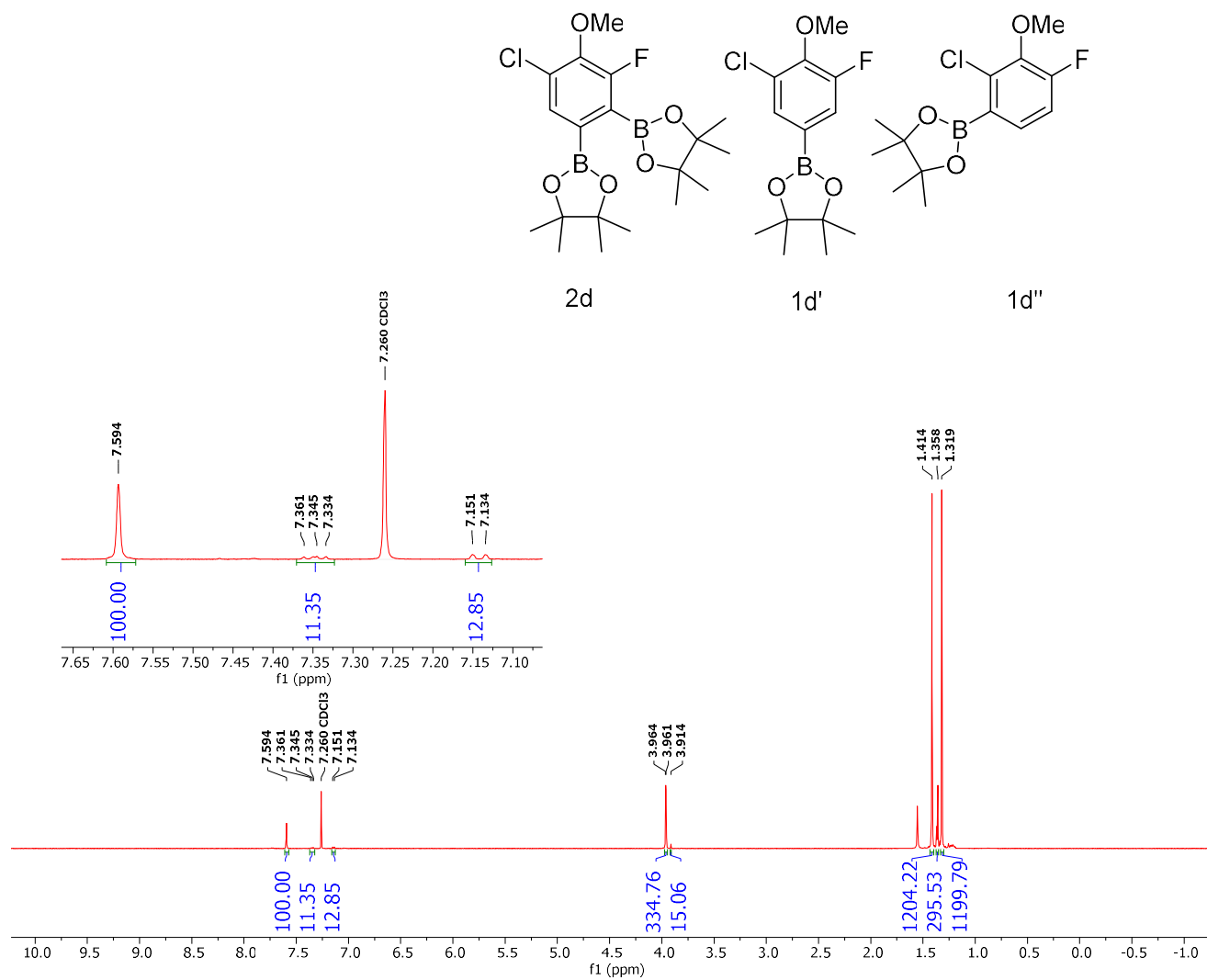


Figure 6-126 Conditions: 25 °C, 500 MHz, CDCl<sub>3</sub>

**$^{19}\text{F}$  NMR Spectra of Fraction 3 of the Isolated Reaction Mixture of Table 2 Entry 4 Trial 1**

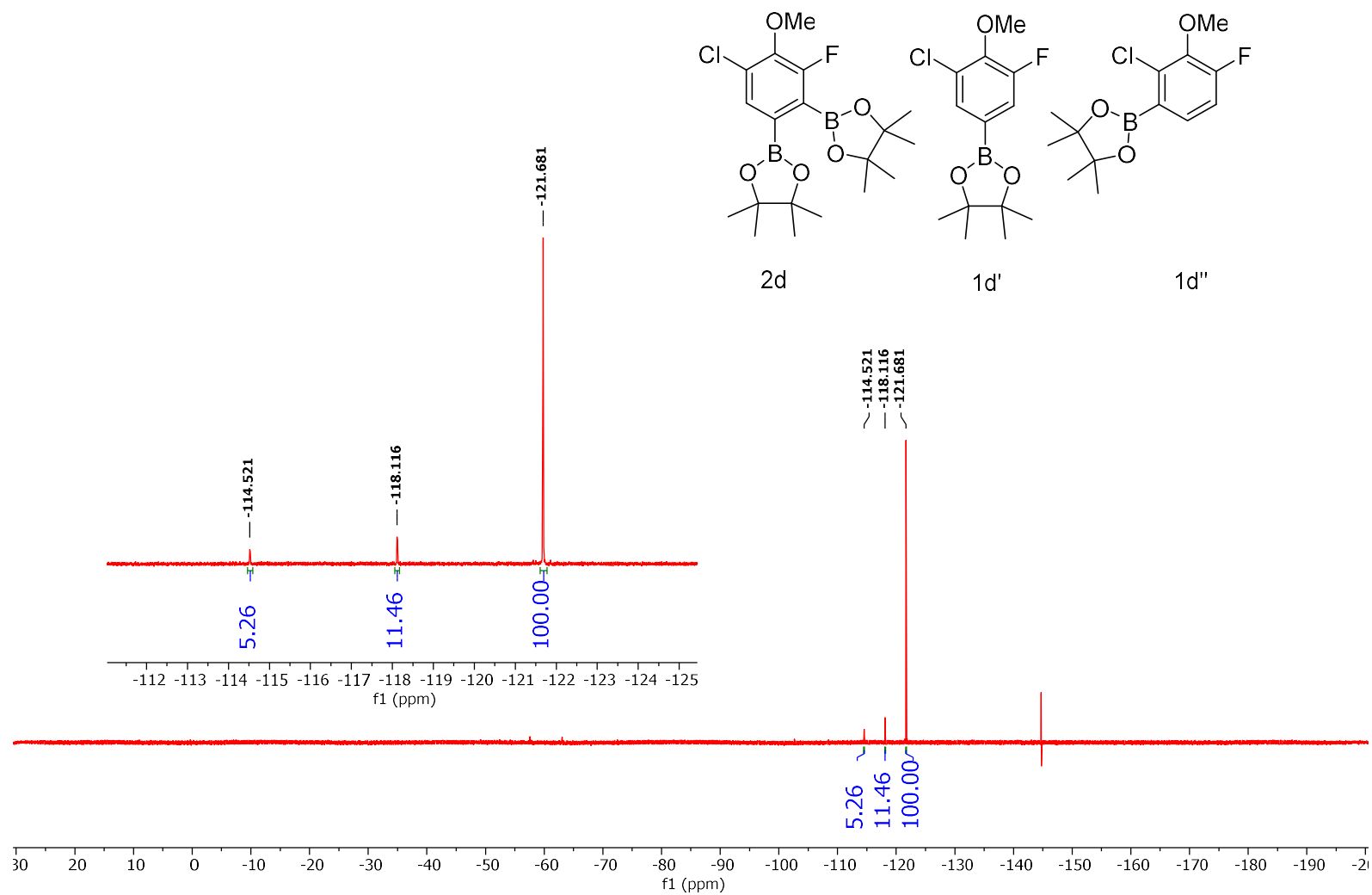


Figure 6-127 Conditions: 25 °C, 470 MHz,  $\text{CDCl}_3$



**<sup>13</sup>C NMR Spectra of Fraction 3 of the Isolated Reaction Mixture of Table 2 Entry 4 Trial 1**

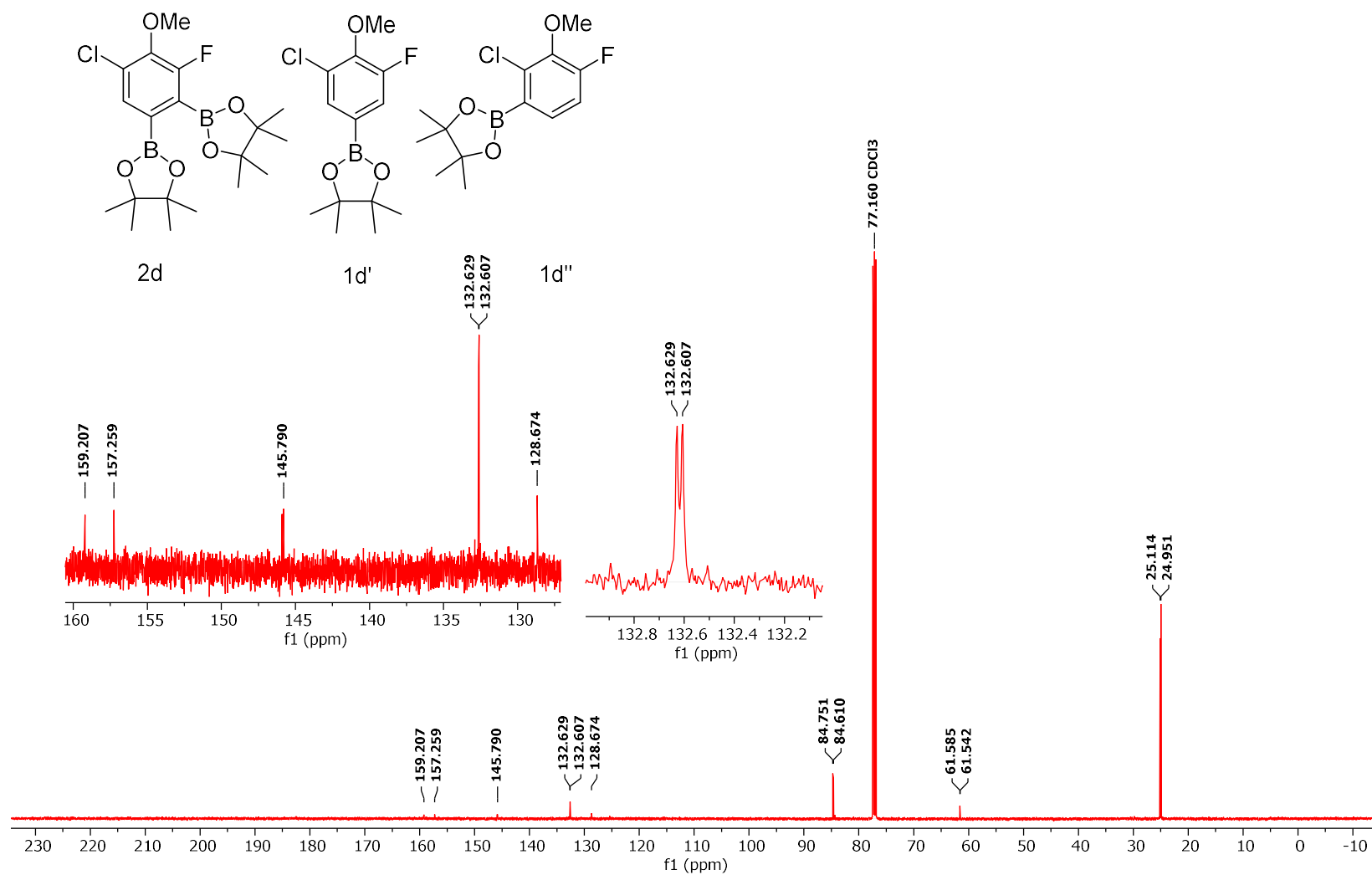


Figure 6-128 Conditions: 25 °C, 126 MHz, CDCl<sub>3</sub>

**<sup>11</sup>B NMR Spectra of Fraction 3 of the Isolated Reaction Mixture of Table 2 Entry 4 Trial 1**

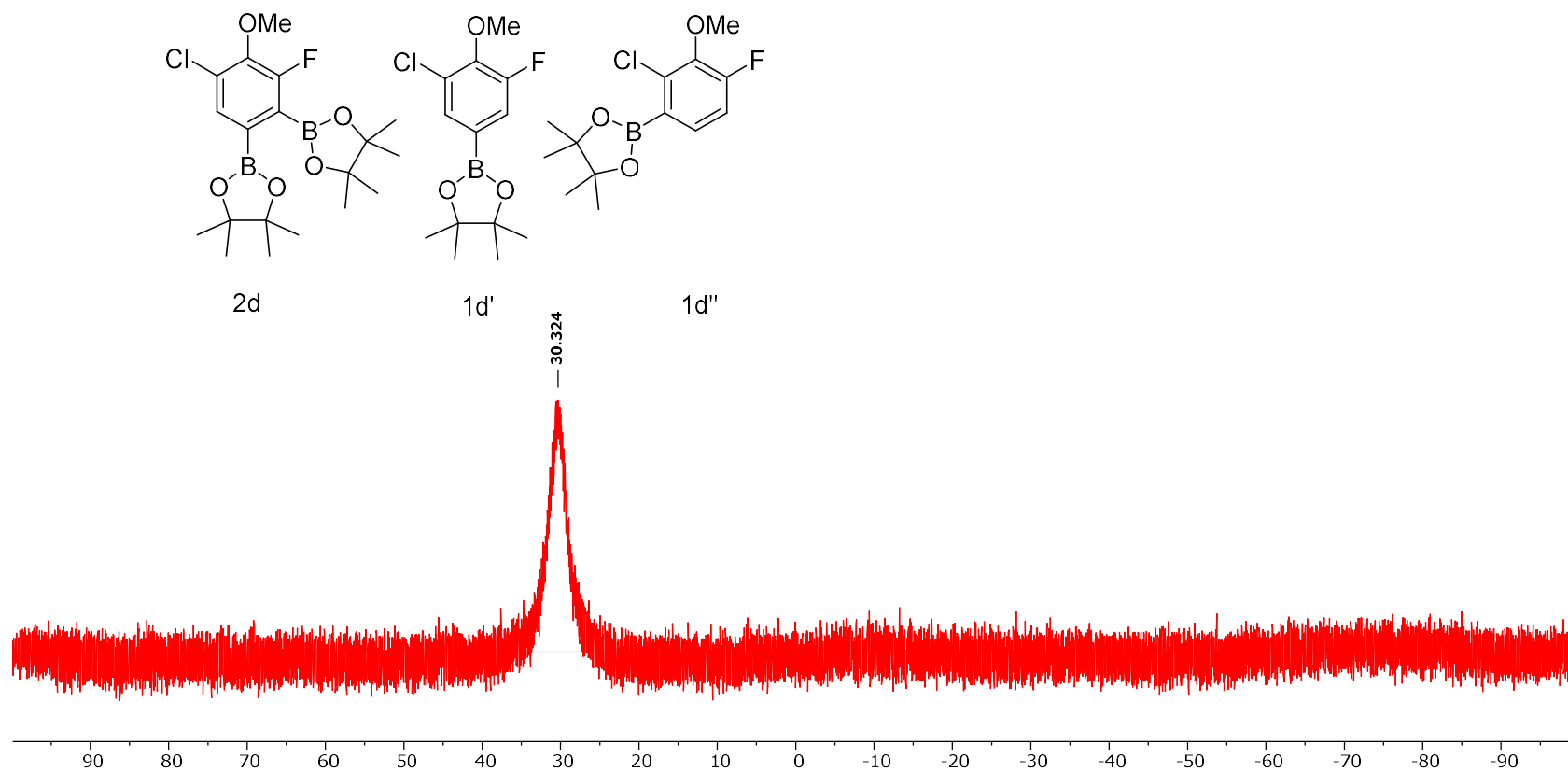


Figure 6-129 Conditions: 25 °C, 160 MHz, CDCl<sub>3</sub>

**<sup>1</sup>H NMR Spectra of Fraction 4 of the Isolated Reaction Mixture of Table 2 Entry 4 Trial 1**

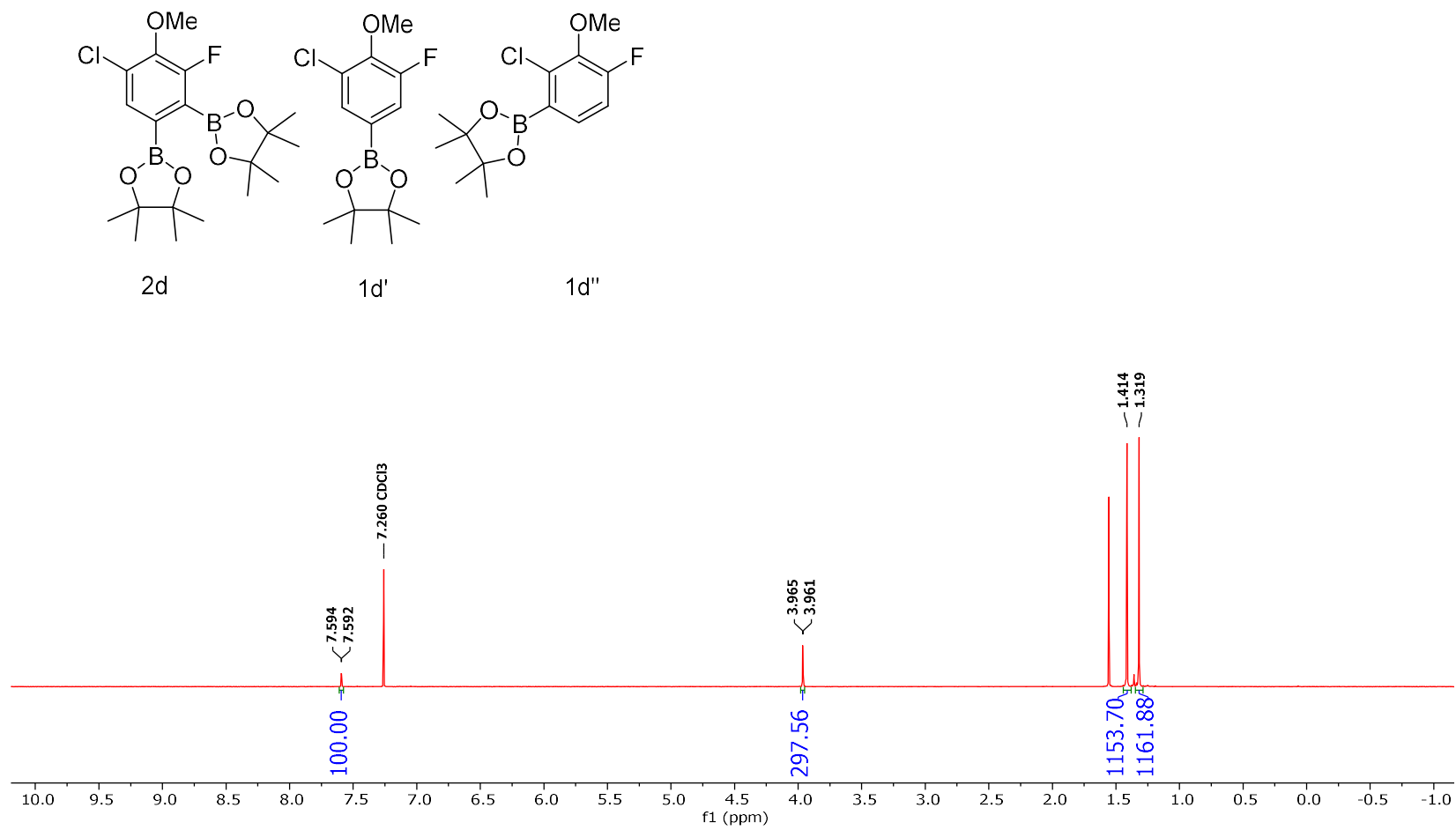


Figure 6-130 Conditions: 25 °C, 500 MHz, CDCl<sub>3</sub>

**<sup>19</sup>F NMR Spectra of Fraction 4 of the Isolated Reaction Mixture of Table 2 Entry 4 Trial 1**

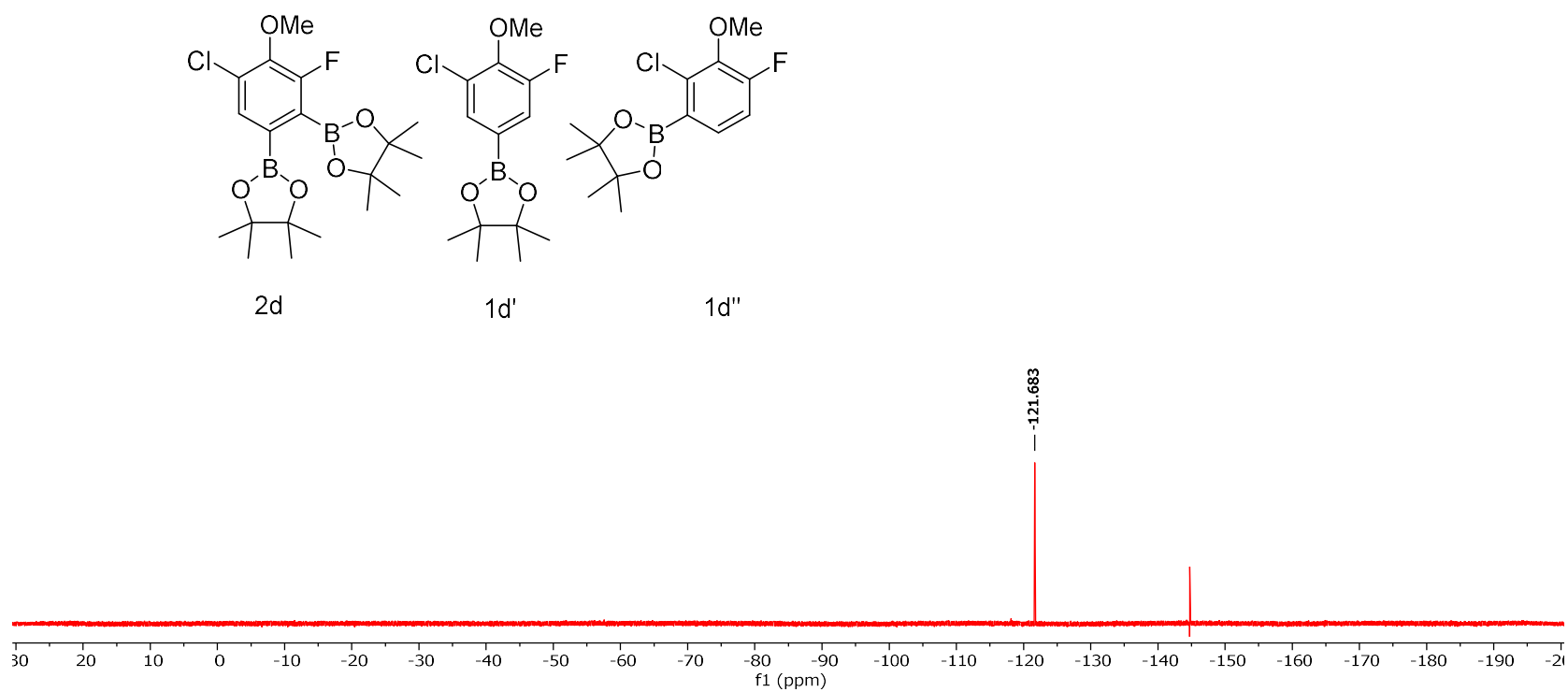


Figure 6-131 Conditions: 25 °C, 470 MHz, CDCl<sub>3</sub>

**$^{13}\text{C}$  NMR Spectra of Fraction 4 of the Isolated Reaction Mixture of Table 2 Entry 4 Trial 1**

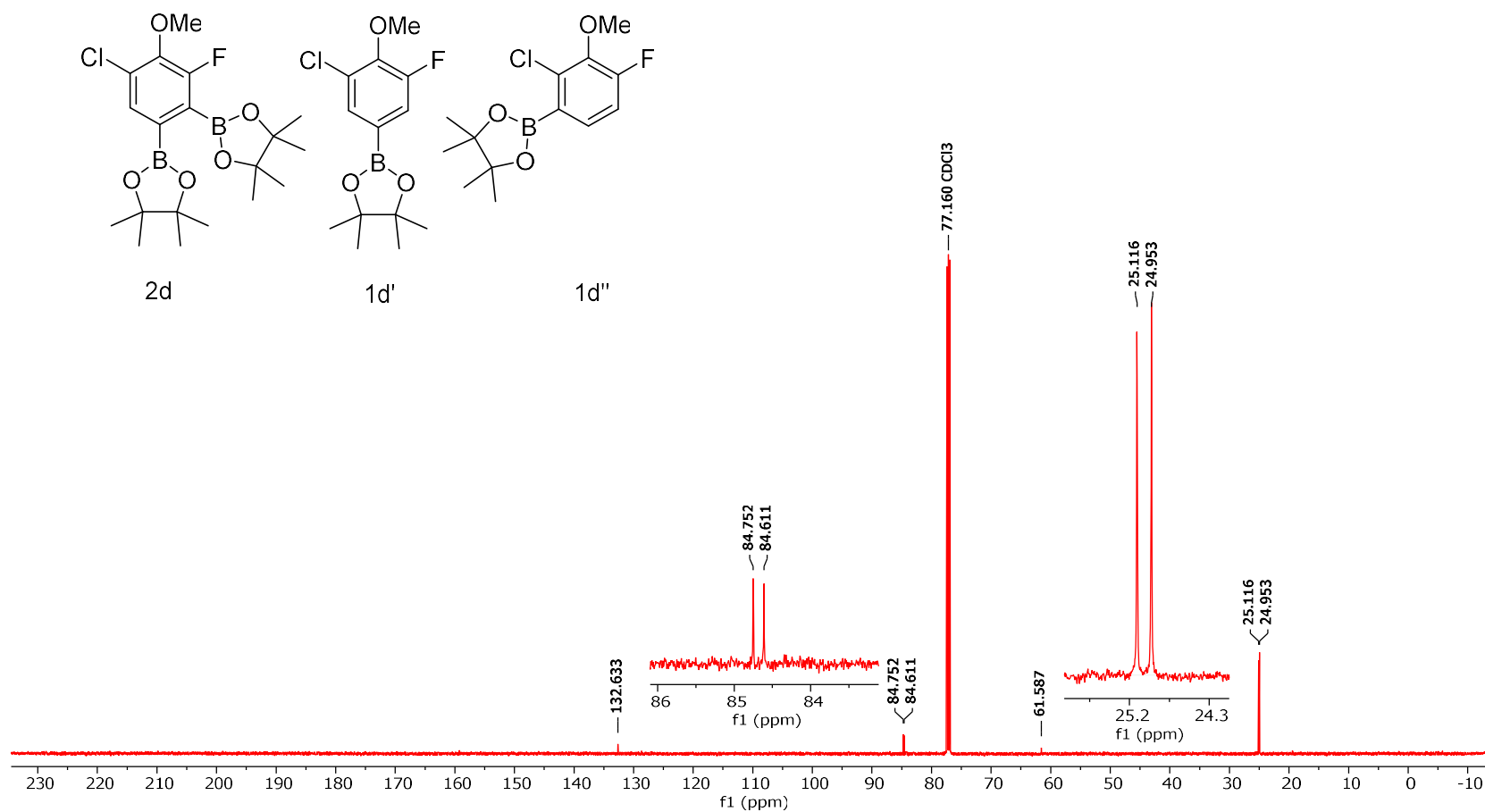


Figure 6-132 Conditions: 25 °C, 126 MHz, CDCl<sub>3</sub>

**<sup>11</sup>B NMR Spectra of Fraction 4 of the Isolated Reaction Mixture of Table 2 Entry 4 Trial 1**

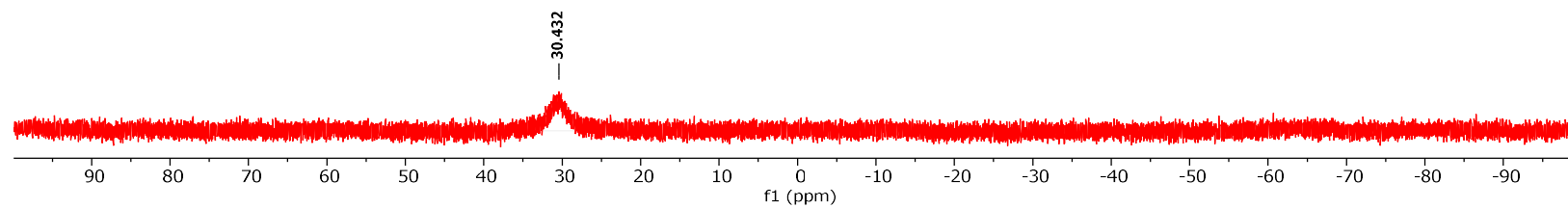
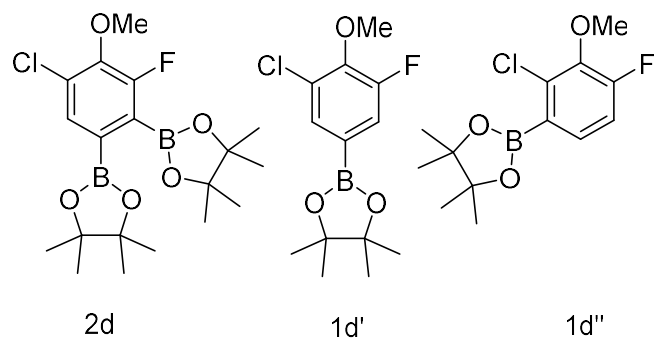


Figure 6-133 Conditions: 25 °C, 160 MHz, CDCl<sub>3</sub>

**<sup>1</sup>H NMR Spectra of the Isolated Reaction Mixture of Table 2 Entry 4 Trial 2**

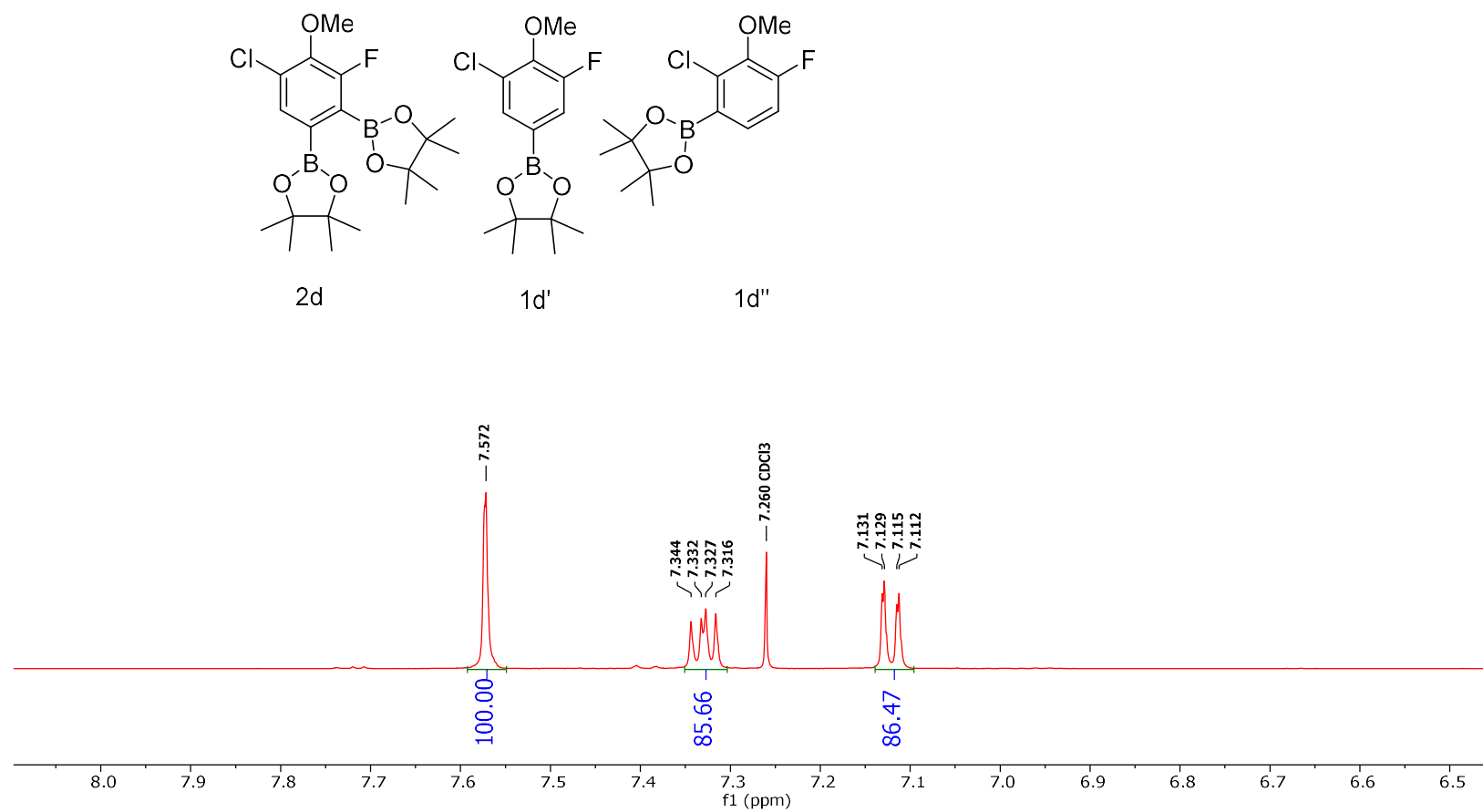
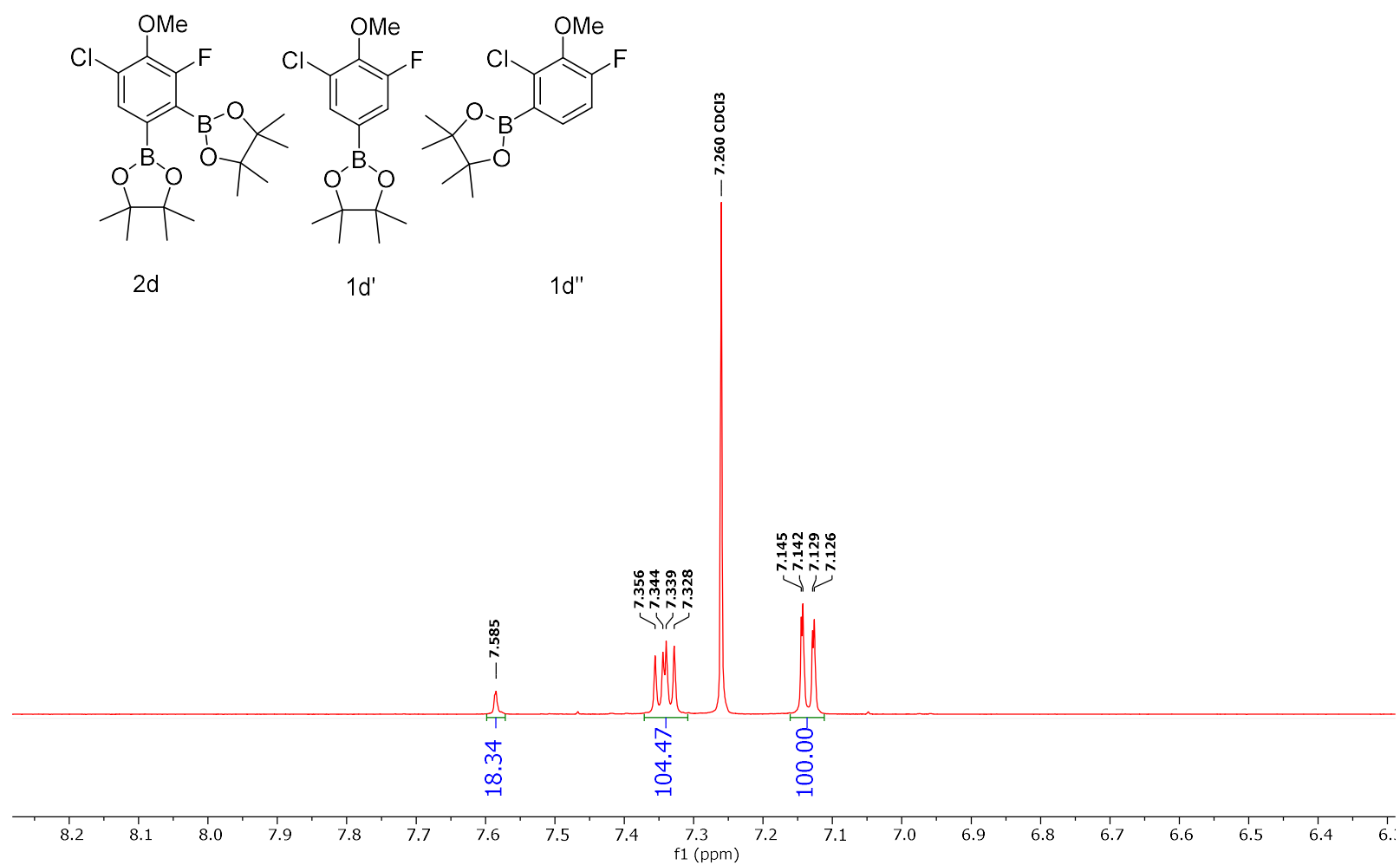


Figure 6-134 Conditions: 25 °C, 500 MHz, CDCl<sub>3</sub>

**<sup>1</sup>H NMR Spectra of the Isolated Reaction Mixture of Table 2 Entry 4 Trial 3**





## Chapter 3 NMR Spectra

<sup>1</sup>H NMR spectrum of tetrapropylammonium 2-iodophenylsulfate (6c)

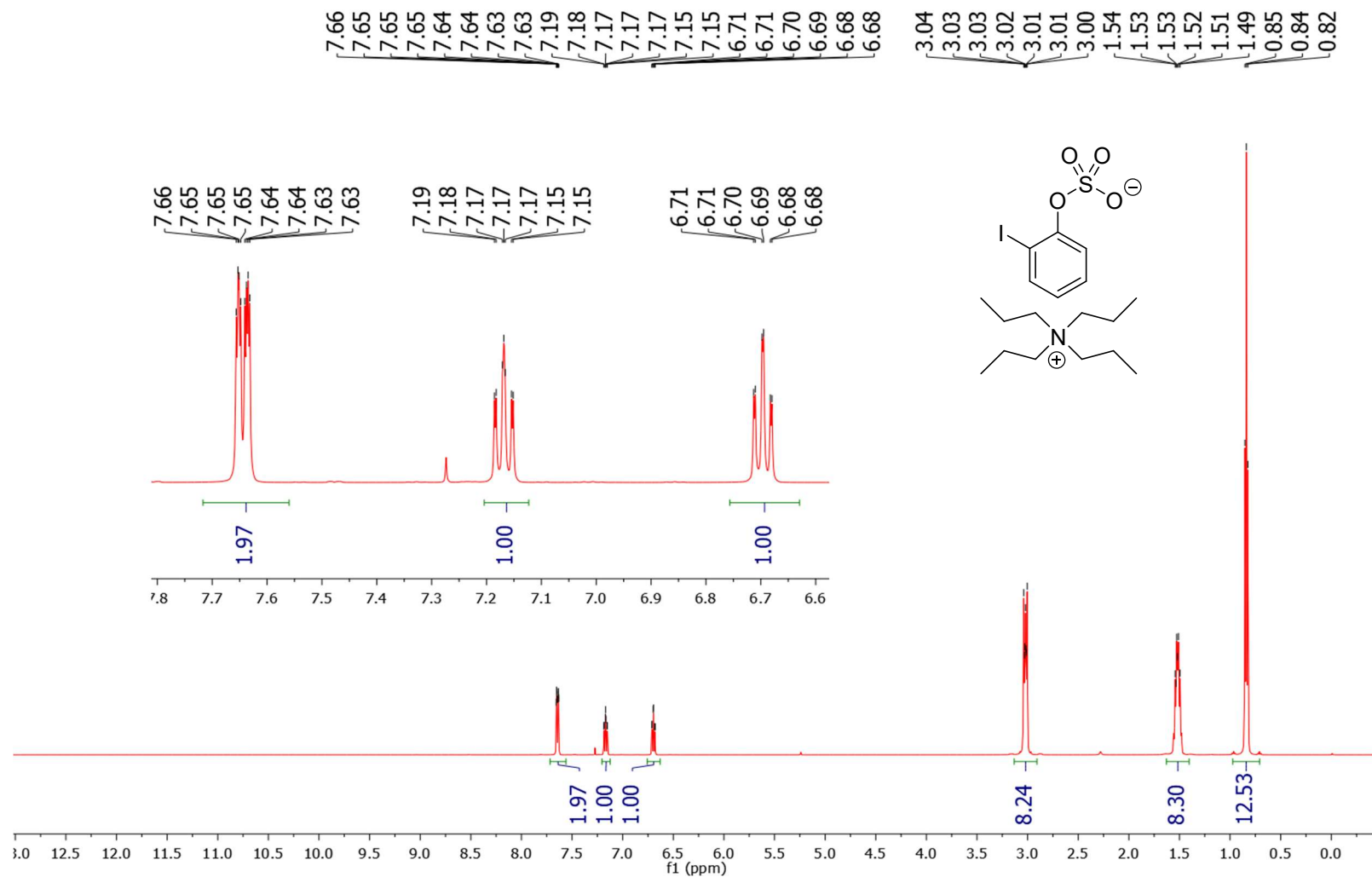
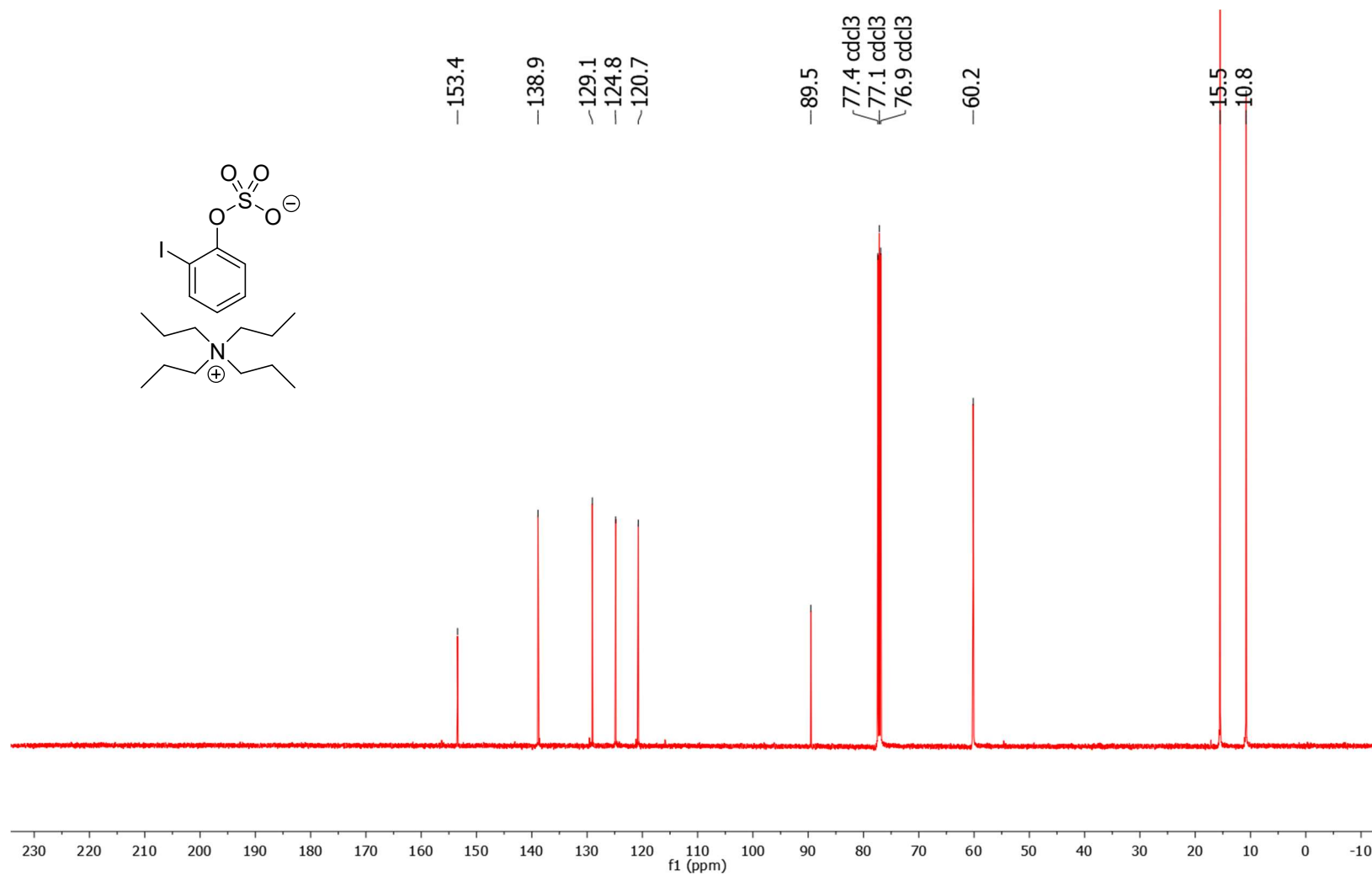


Figure 7-1 Conditions: 25 °C, 500 MHz, CDCl<sub>3</sub>

<sup>13</sup>C NMR spectrum of tetrapropylammonium 2-iodophenylsulfate (6c)



Figure

7-2 Conditions: 25 °C, 126 MHz, CDCl<sub>3</sub>

<sup>1</sup>H NMR spectrum of tetrapropylammonium 3-fluorophenylsulfate (6e)

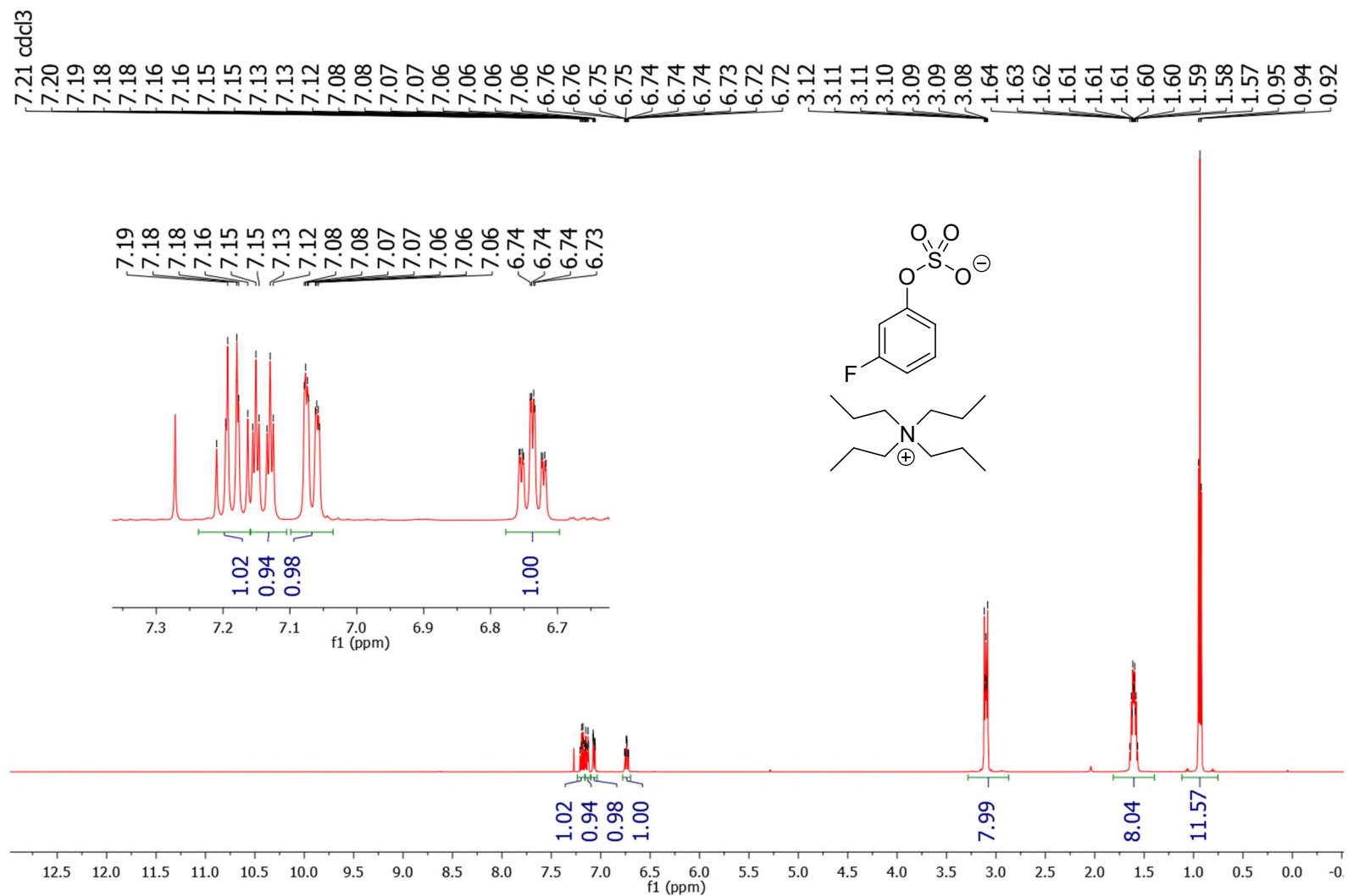


Figure 7-3 Conditions: 25 °C, 500 MHz, CDCl<sub>3</sub>

<sup>13</sup>C NMR spectrum of tetrapropylammonium 3-fluorophenylsulfate (6e)

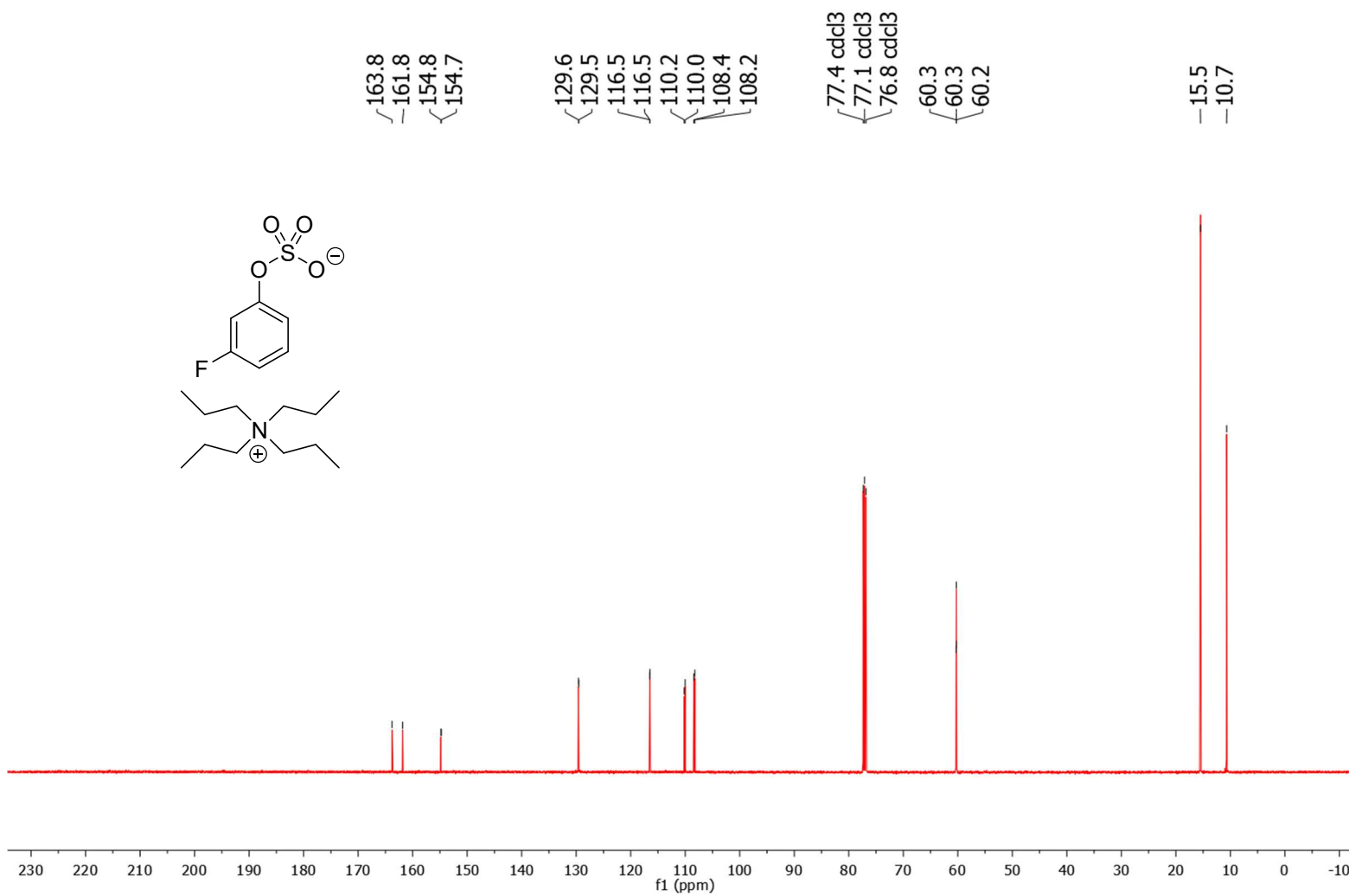


Figure 7-4 Conditions: 25 °C, 126 MHz, CDCl<sub>3</sub>

<sup>19</sup>F NMR spectrum of tetrapropylammonium 3-fluorophenylsulfate (6e)

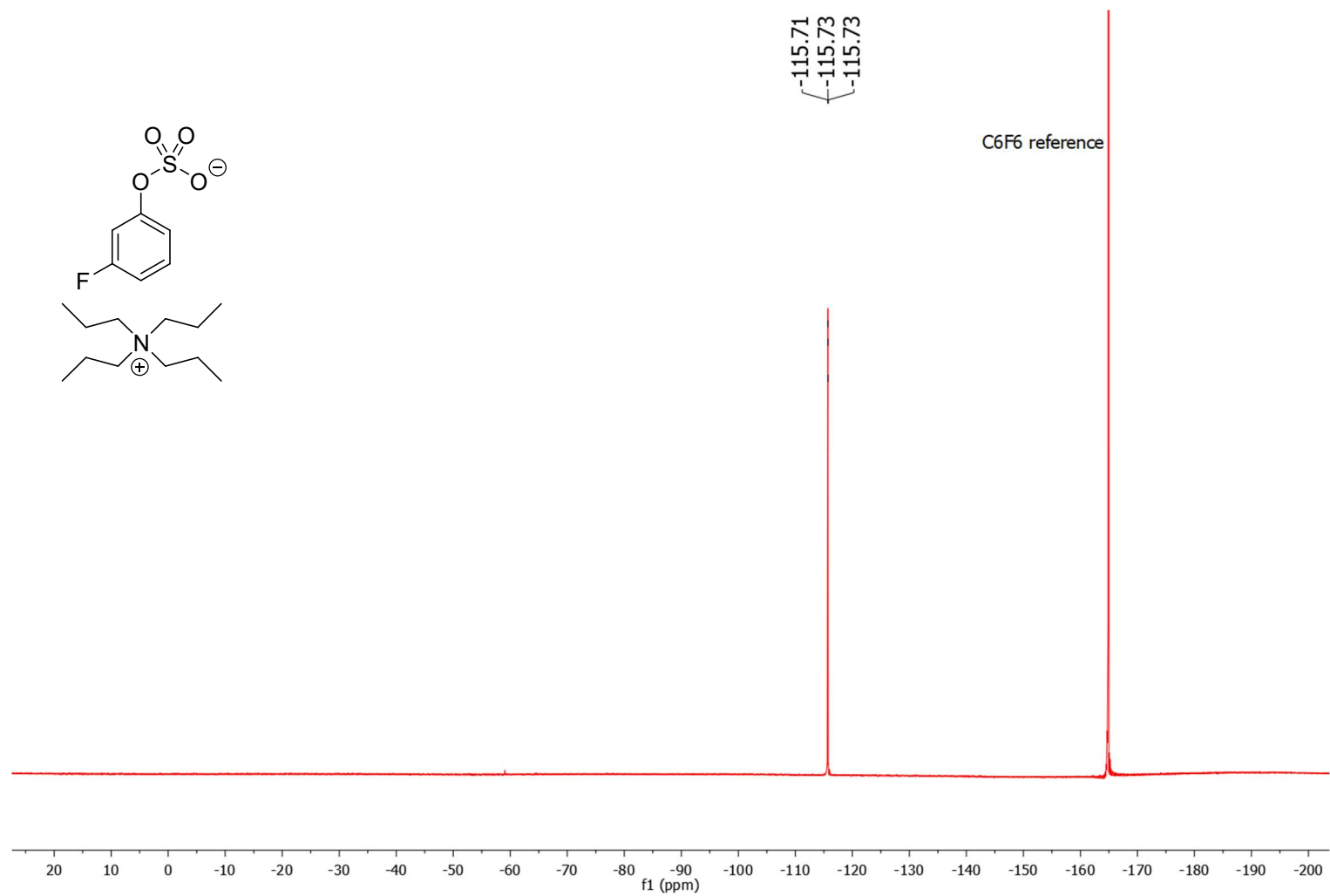


Figure 7-5 Conditions: 25 °C, 470 MHz, CDCl<sub>3</sub>

<sup>1</sup>H NMR spectrum of tetrapropylammonium 2-cyanophenylsulfate (6i)

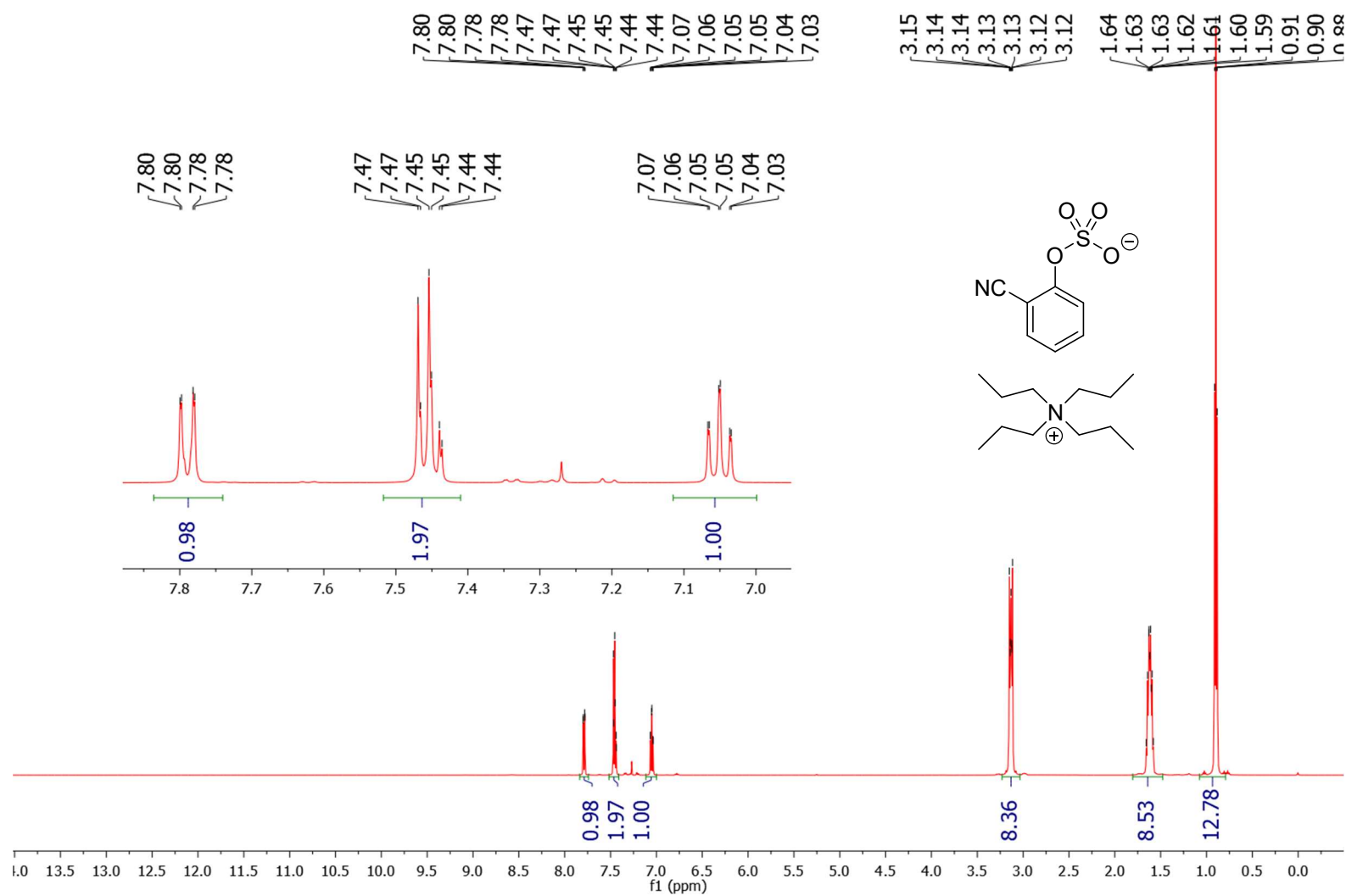


Figure 7-6 Conditions: 25 °C, 500 MHz, CDCl<sub>3</sub>

<sup>13</sup>C NMR spectrum of tetrapropylammonium 2-cyanophenylsulfate (6i)

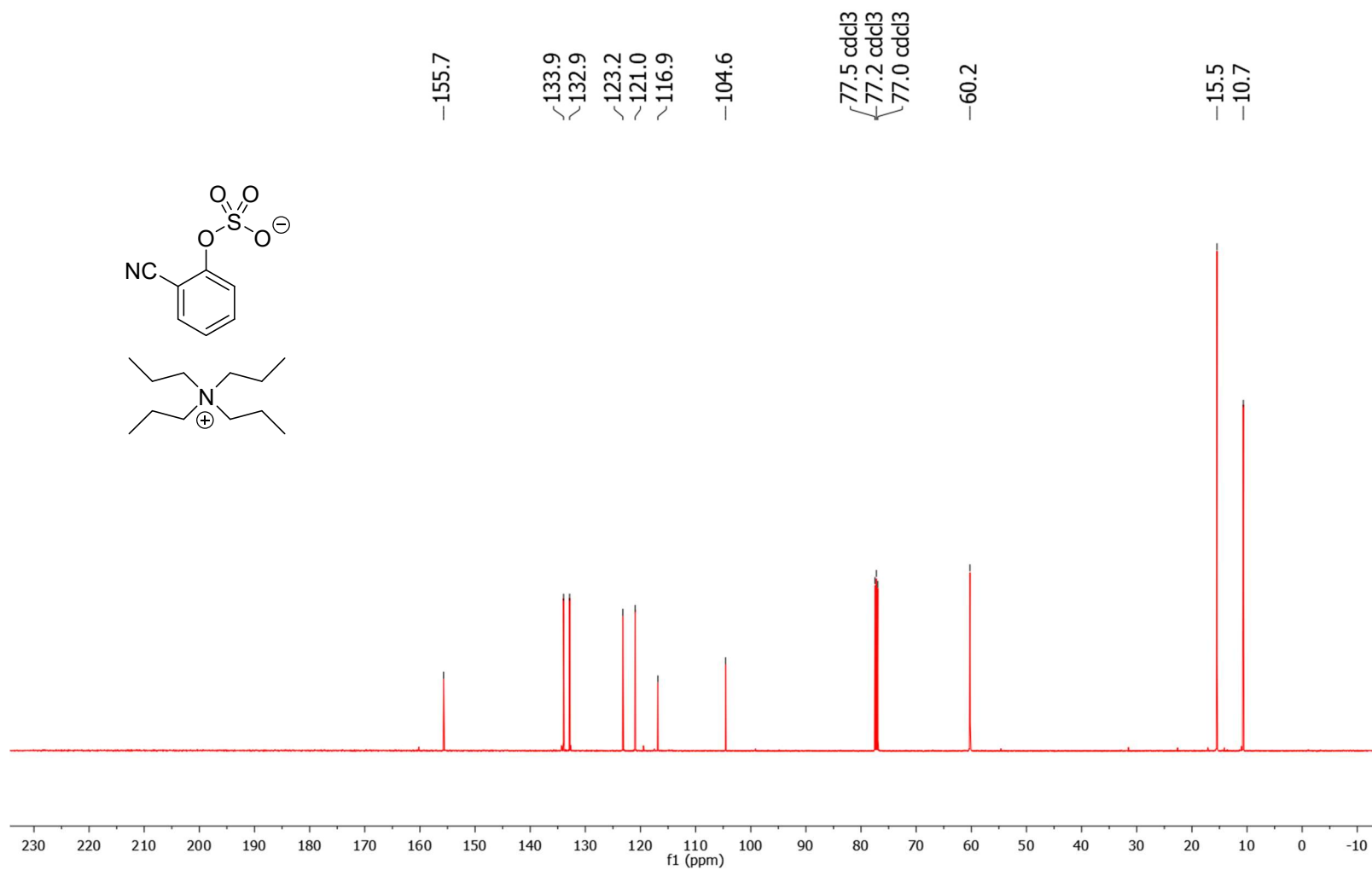
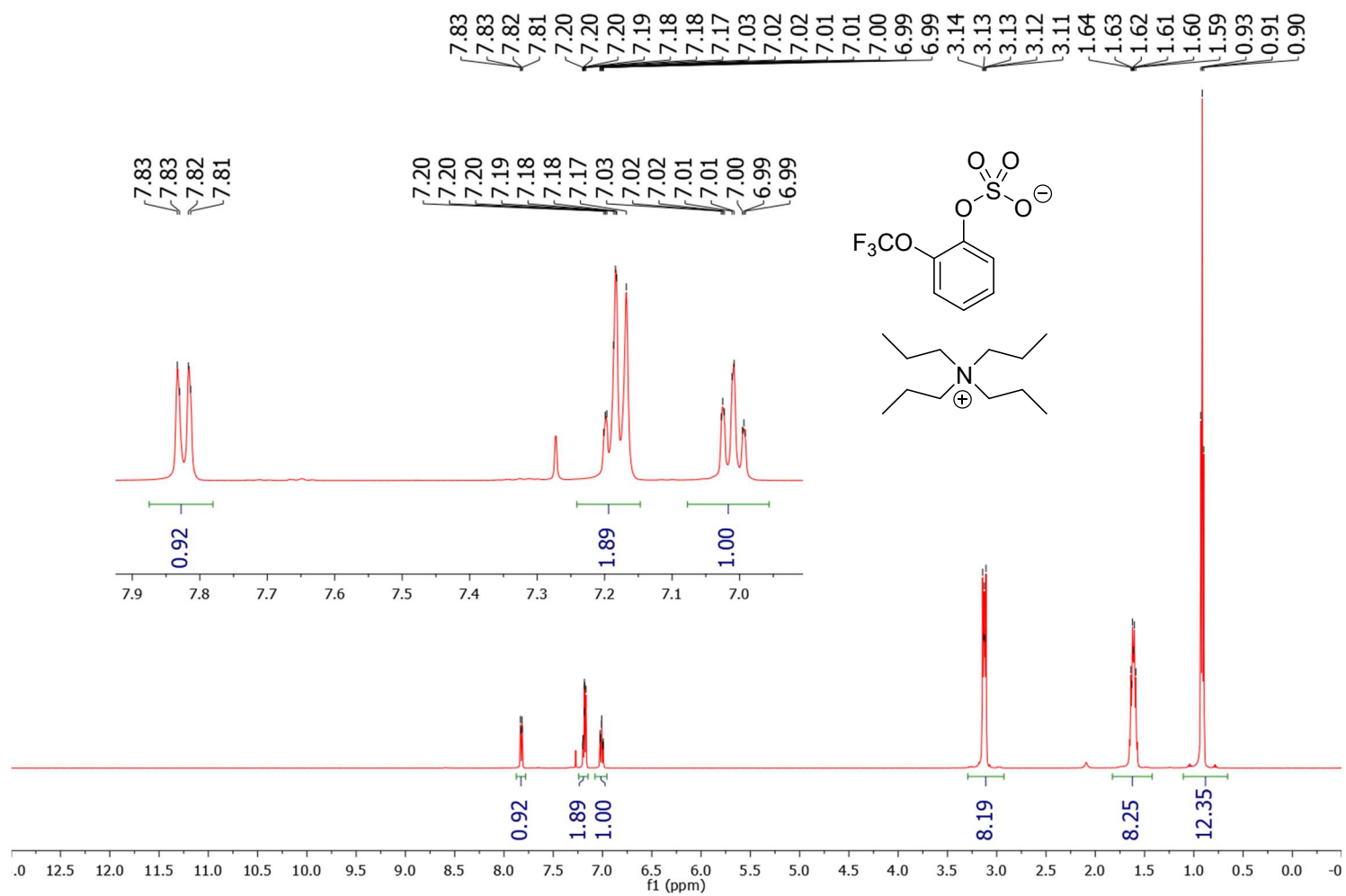


Figure 7-7 Conditions: 25 °C, 126 MHz, CDCl<sub>3</sub>



<sup>1</sup>H NMR spectrum of tetrapropylammonium 2-(trifluoromethoxy)phenylsulfate (6k)



<sup>13</sup>C NMR spectrum of tetrapropylammonium 2-(trifluoromethoxy)phenylsulfate (6k)

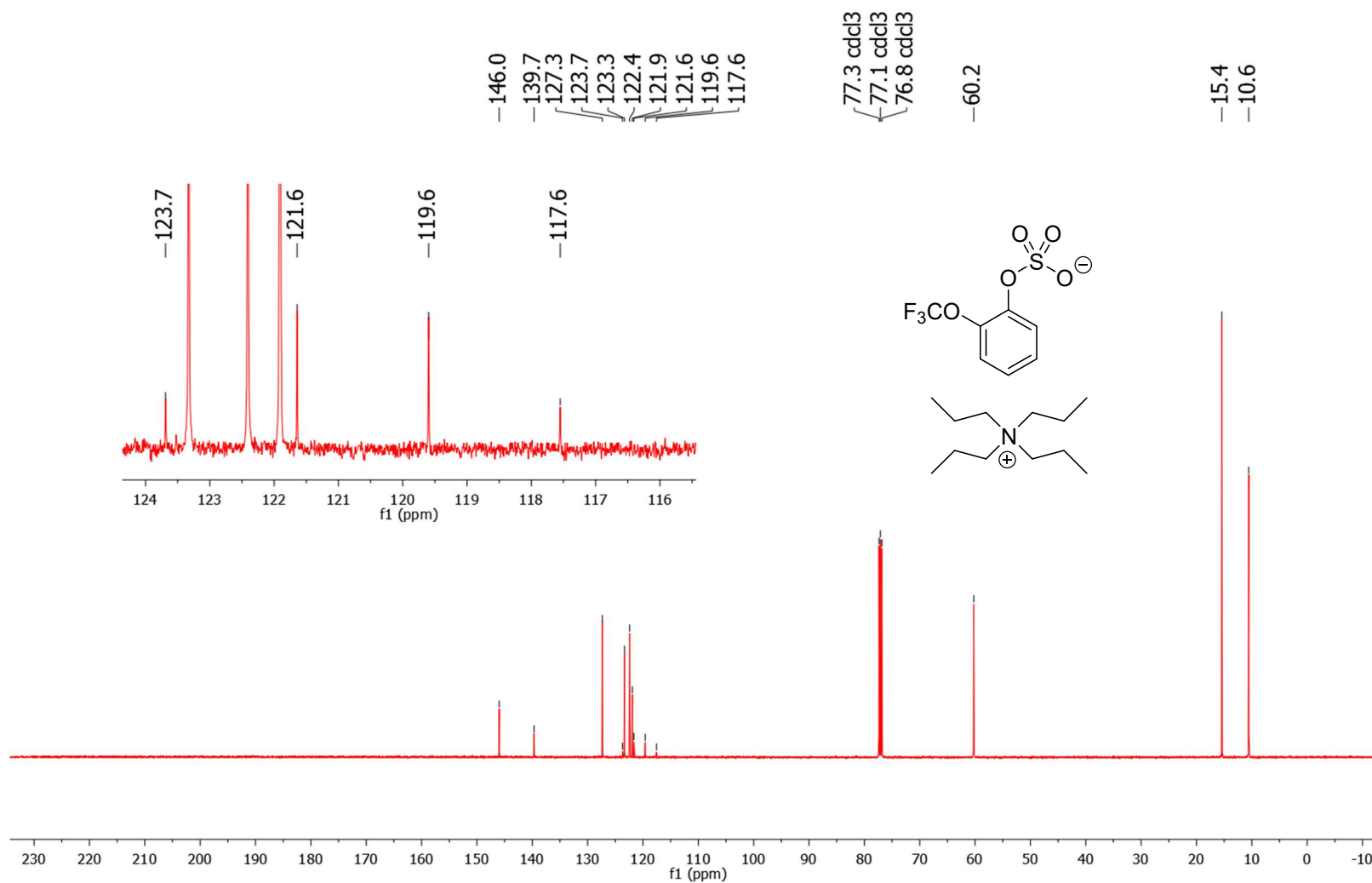


Figure 7-9 Conditions: 25 °C, 126 MHz, CDCl<sub>3</sub>

**$^{19}\text{F}$  NMR spectrum of tetrapropylammonium 2-(trifluoromethoxy)phenylsulfate (6k)**

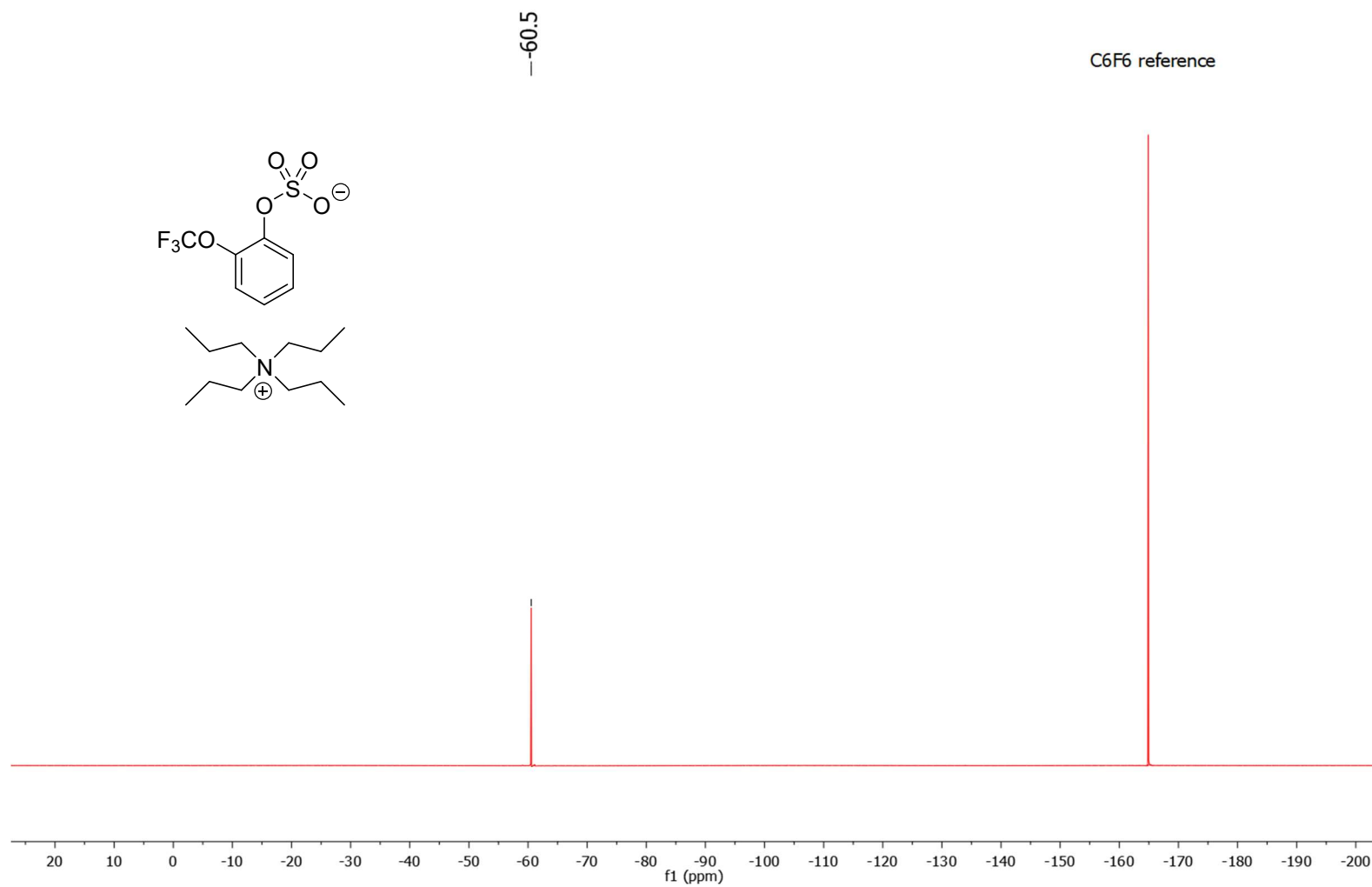


Figure 7-10 Conditions: 25 °C, 470 MHz,  $\text{CDCl}_3$

<sup>1</sup>H NMR spectrum of tetrapropylammonium 2-bromo-6-fluorophenylsulfate (6I)

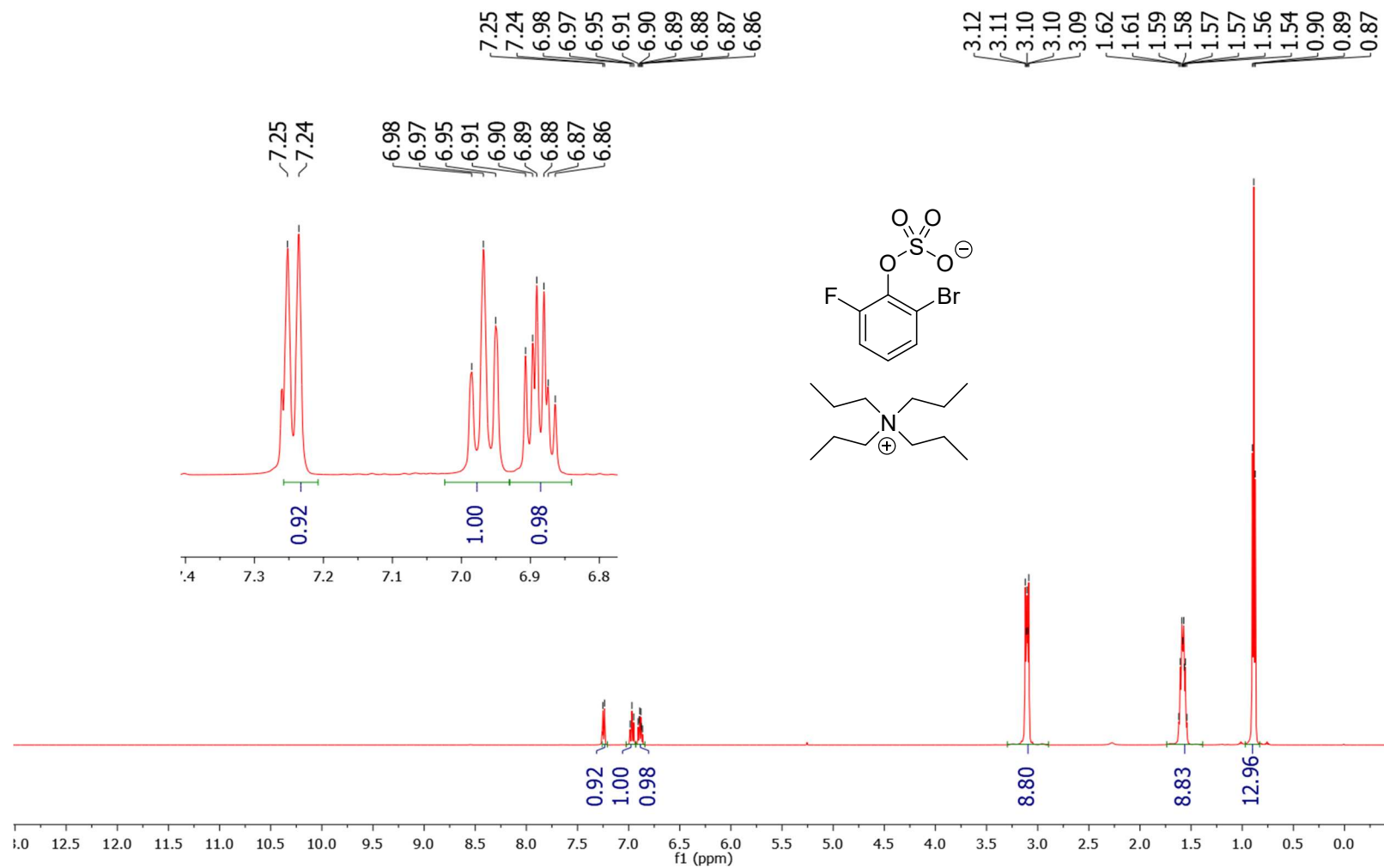


Figure 7-11 Conditions: 25 °C, 500 MHz, CDCl<sub>3</sub>

<sup>13</sup>C NMR spectrum of tetrapropylammonium 2-bromo-6-fluorophenylsulfate (6I)

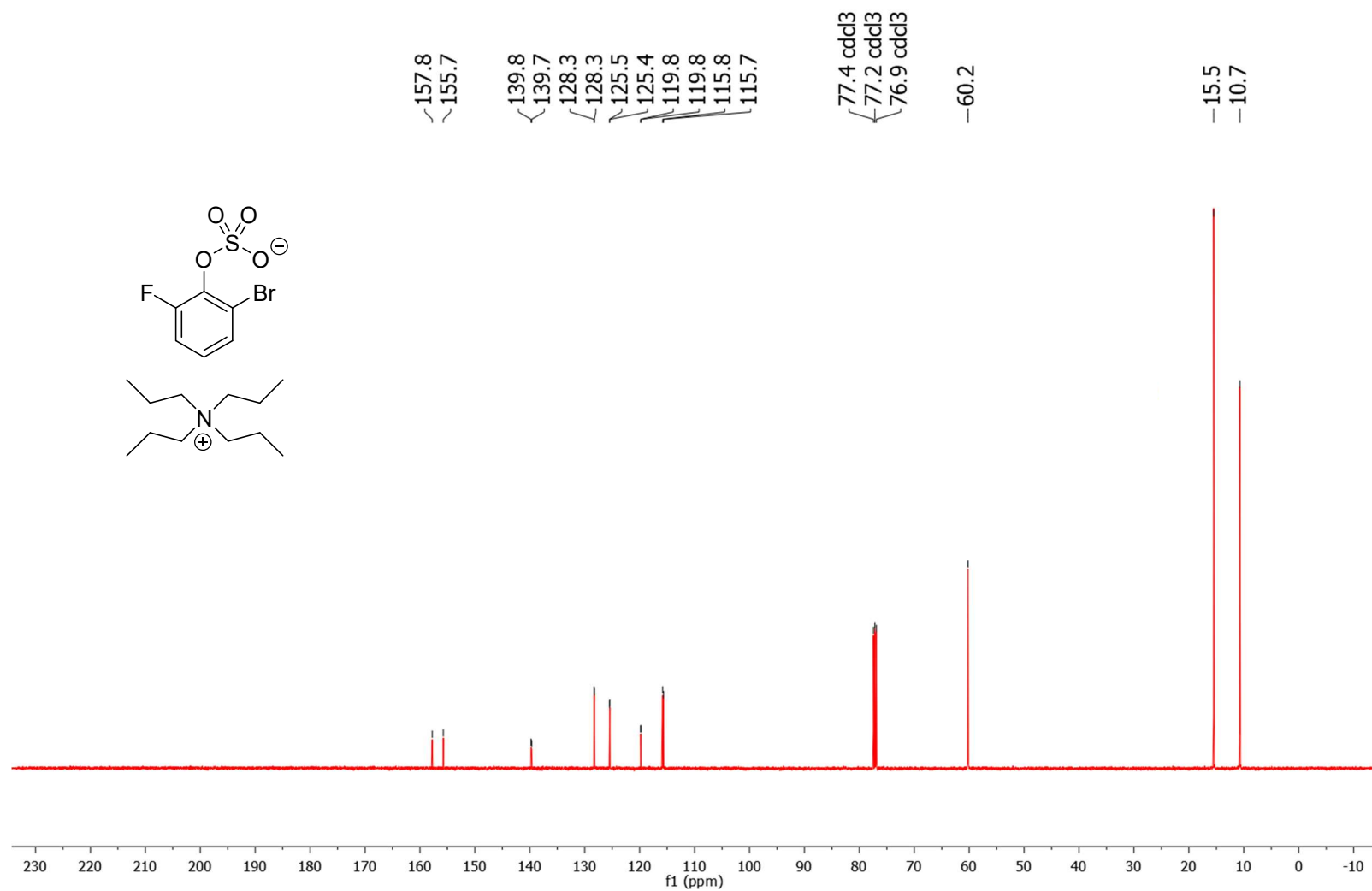


Figure 7-12 Conditions: 25 °C, 126 MHz, CDCl<sub>3</sub>

<sup>19</sup>F NMR spectrum of tetrapropylammonium 2-bromo-6-fluorophenylsulfate (6I)

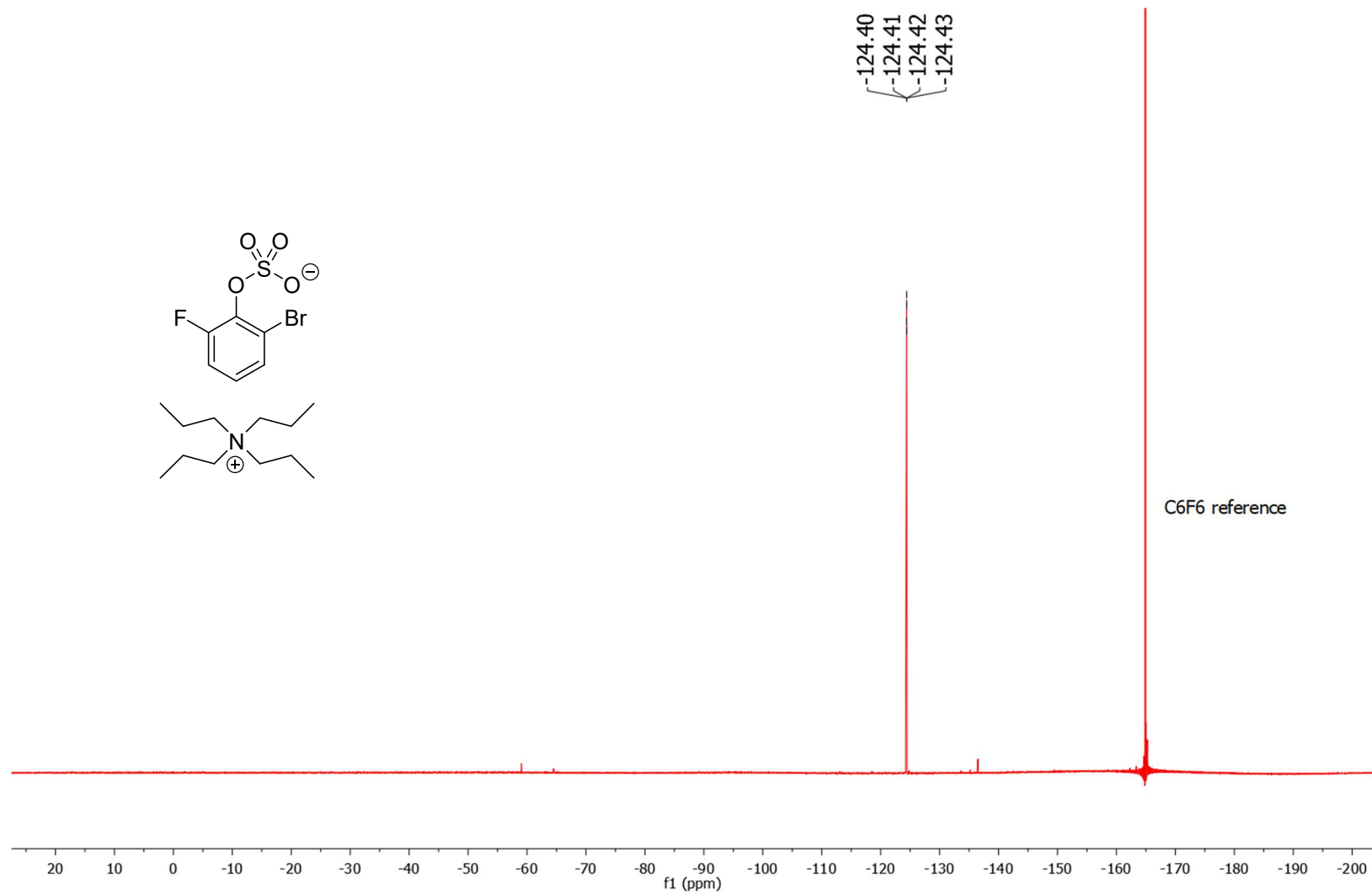


Figure 7-13 Conditions: 25 °C, 470 MHz, CDCl<sub>3</sub>

**<sup>1</sup>H NMR spectrum of tetrapropylammonium 2-phenylsulfate (6p)**

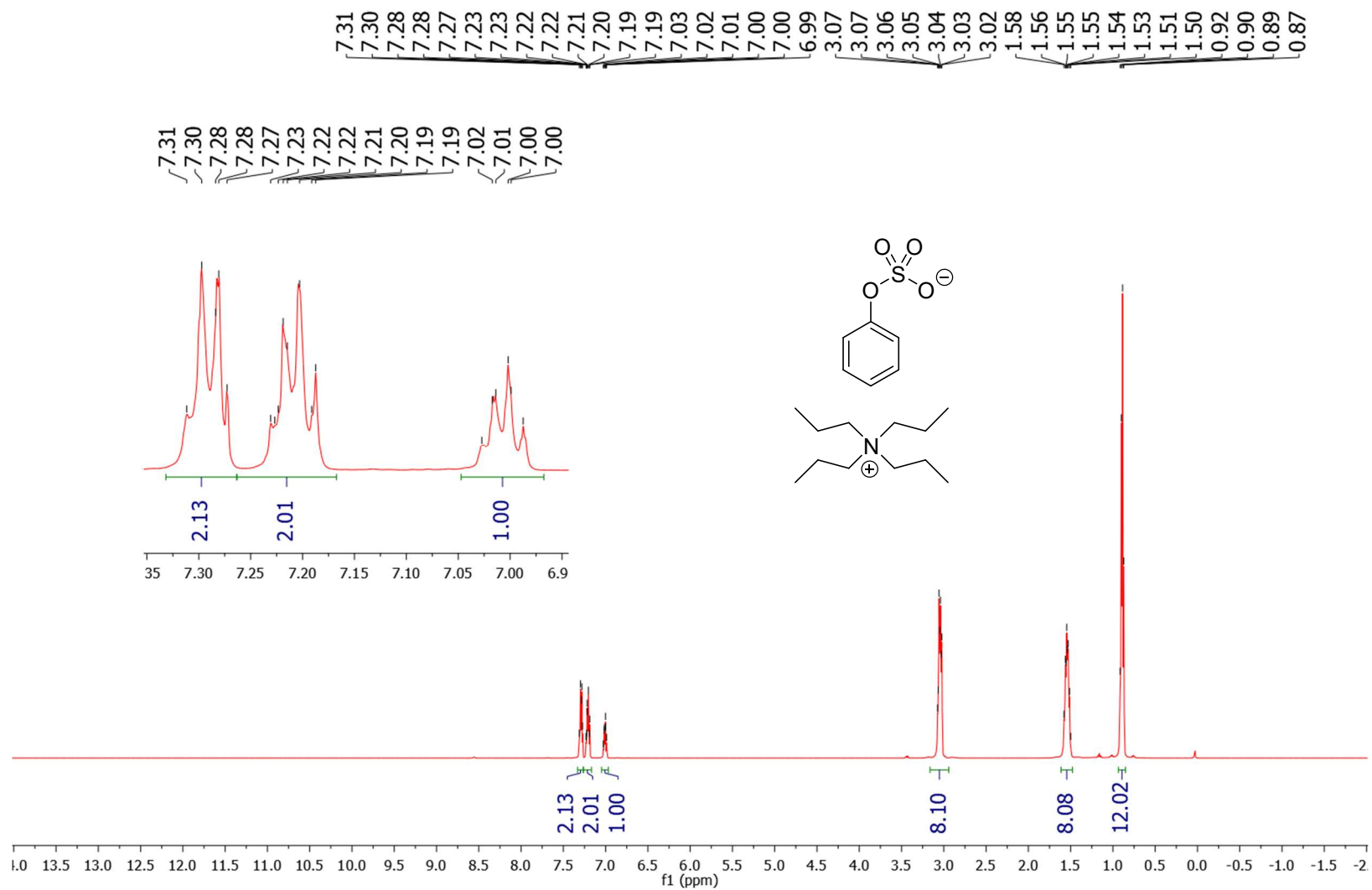
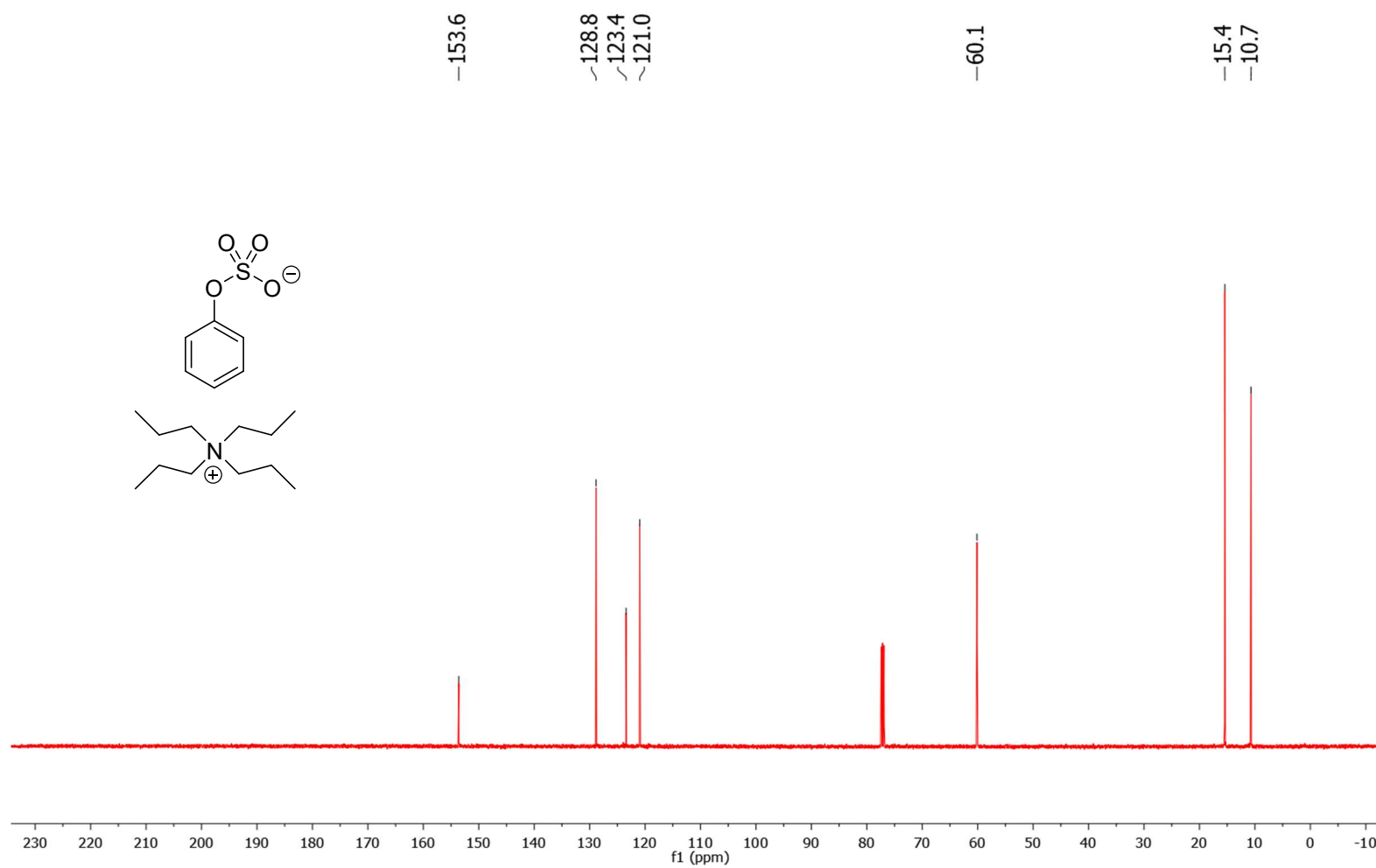


Figure 7-14 Conditions: 25 °C, 500 MHz, CDCl<sub>3</sub>

<sup>13</sup>C NMR spectrum of tetrapropylammonium 2-phenylsulfate (6p)





<sup>1</sup>H NMR spectrum of tetrabutylammonium 2-chlorophenylsulfamate (8a)

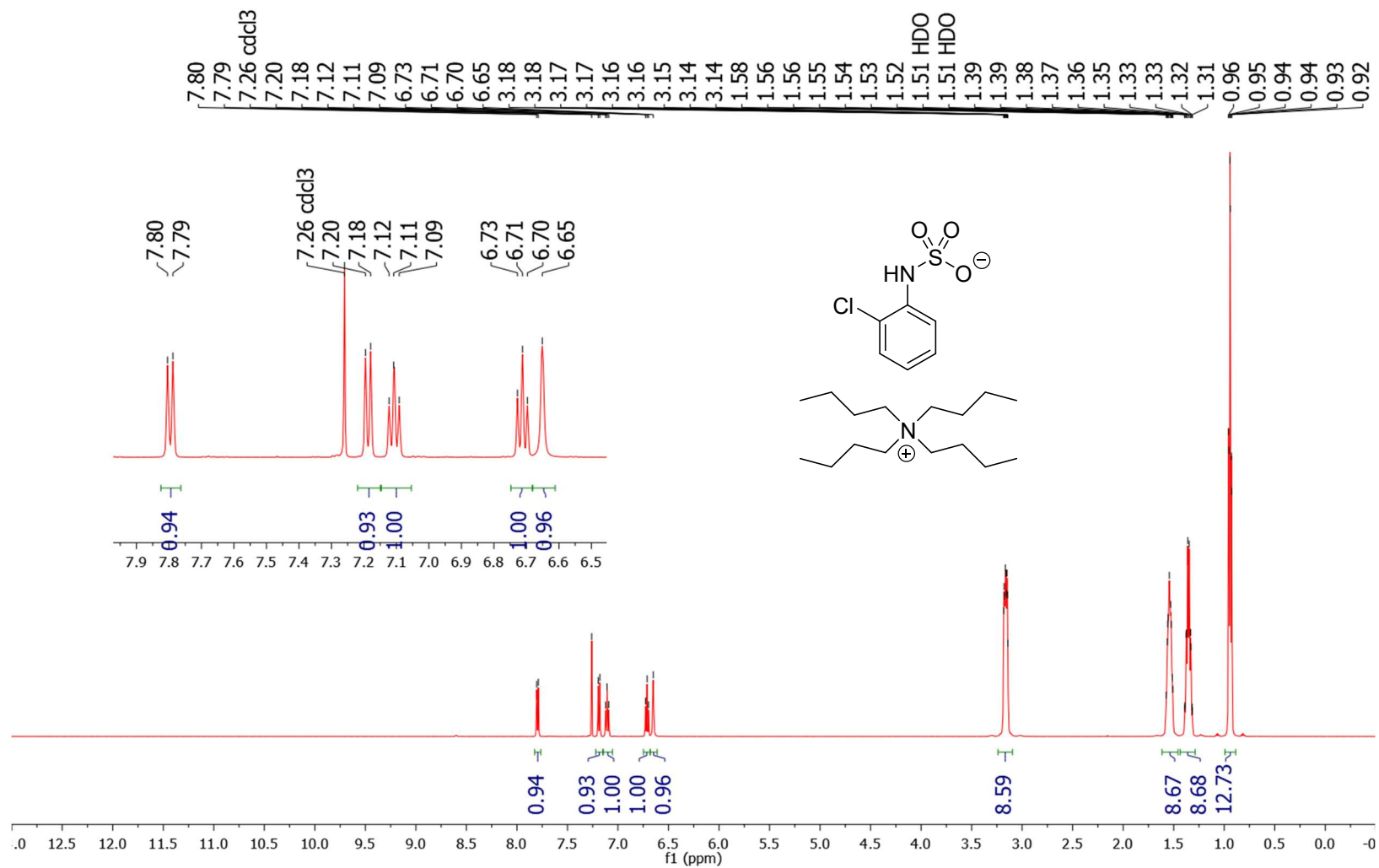


Figure 7-16 Conditions: 25 °C, 500 MHz, CDCl<sub>3</sub>

<sup>13</sup>C NMR spectrum of tetrabutylammonium 2-chlorophenylsulfamate (8a)

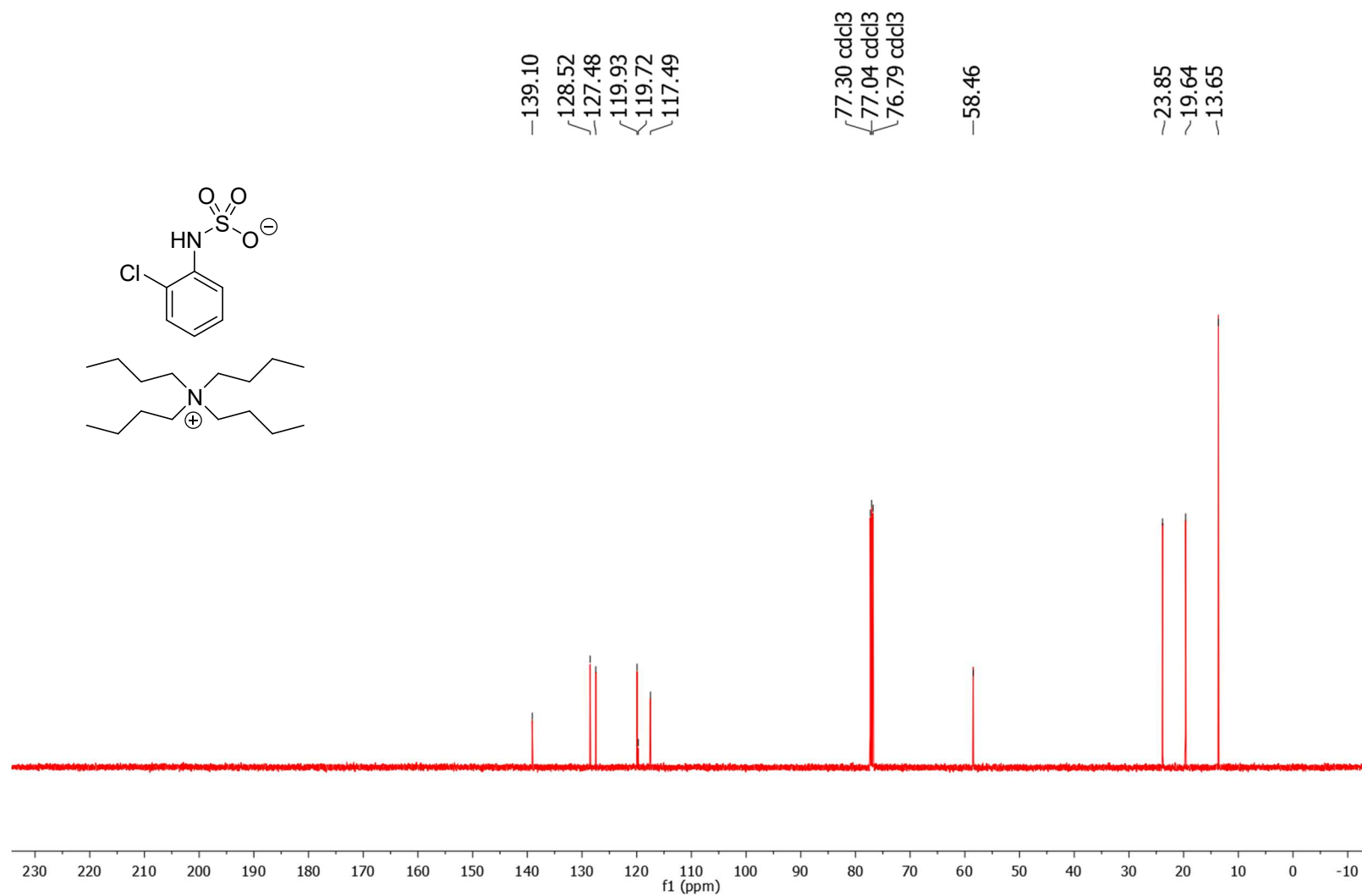


Figure 7-17 Conditions: 25 °C, 126 MHz, CDCl<sub>3</sub>

<sup>1</sup>H NMR spectrum of tetrabutylammonium 2-bromophenylsulfamate (8b)

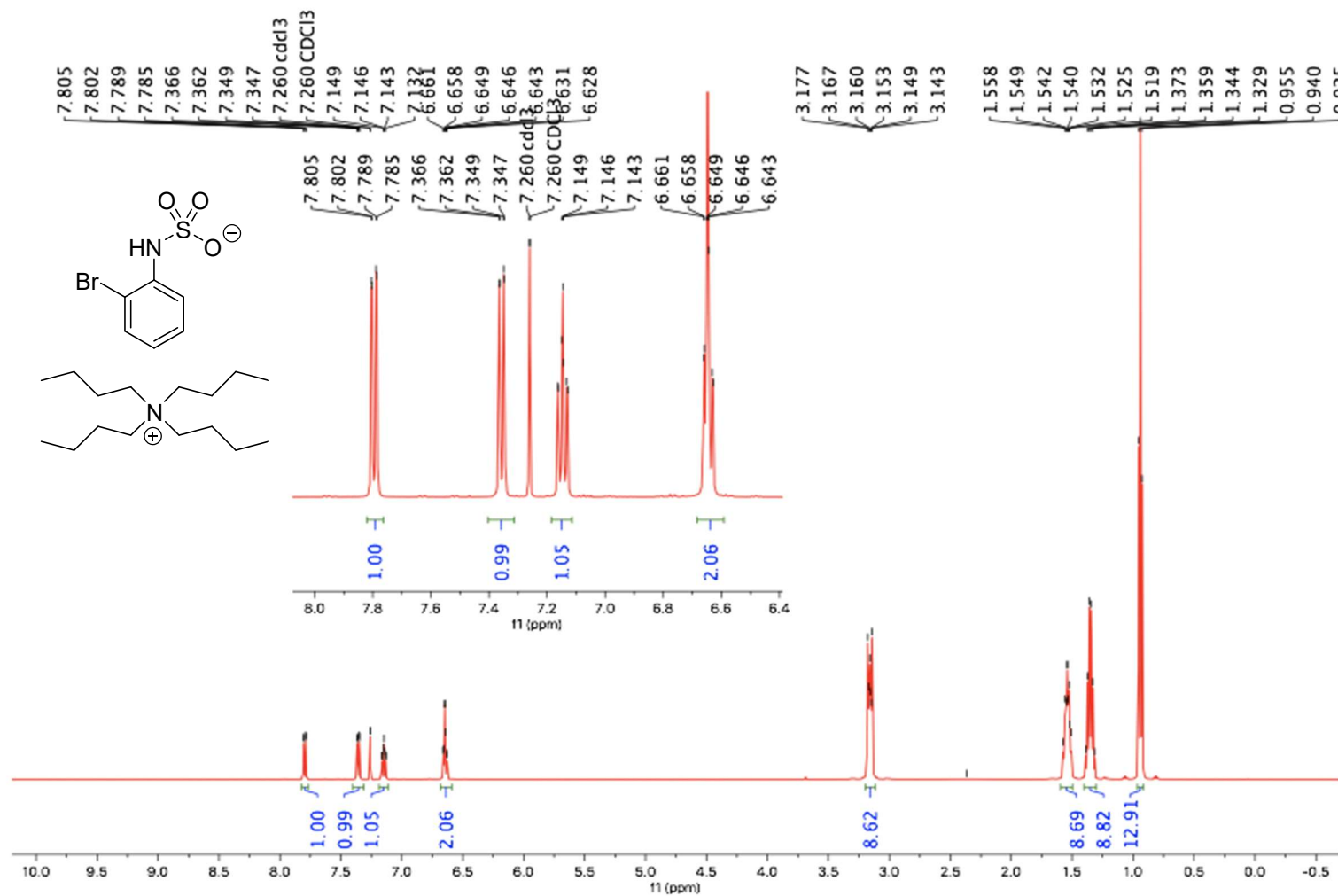


Figure 7-18 Conditions: 25 °C, 500 MHz, CDCl<sub>3</sub>

<sup>13</sup>C NMR spectrum of tetrabutylammonium 2-bromophenylsulfamate (8b)

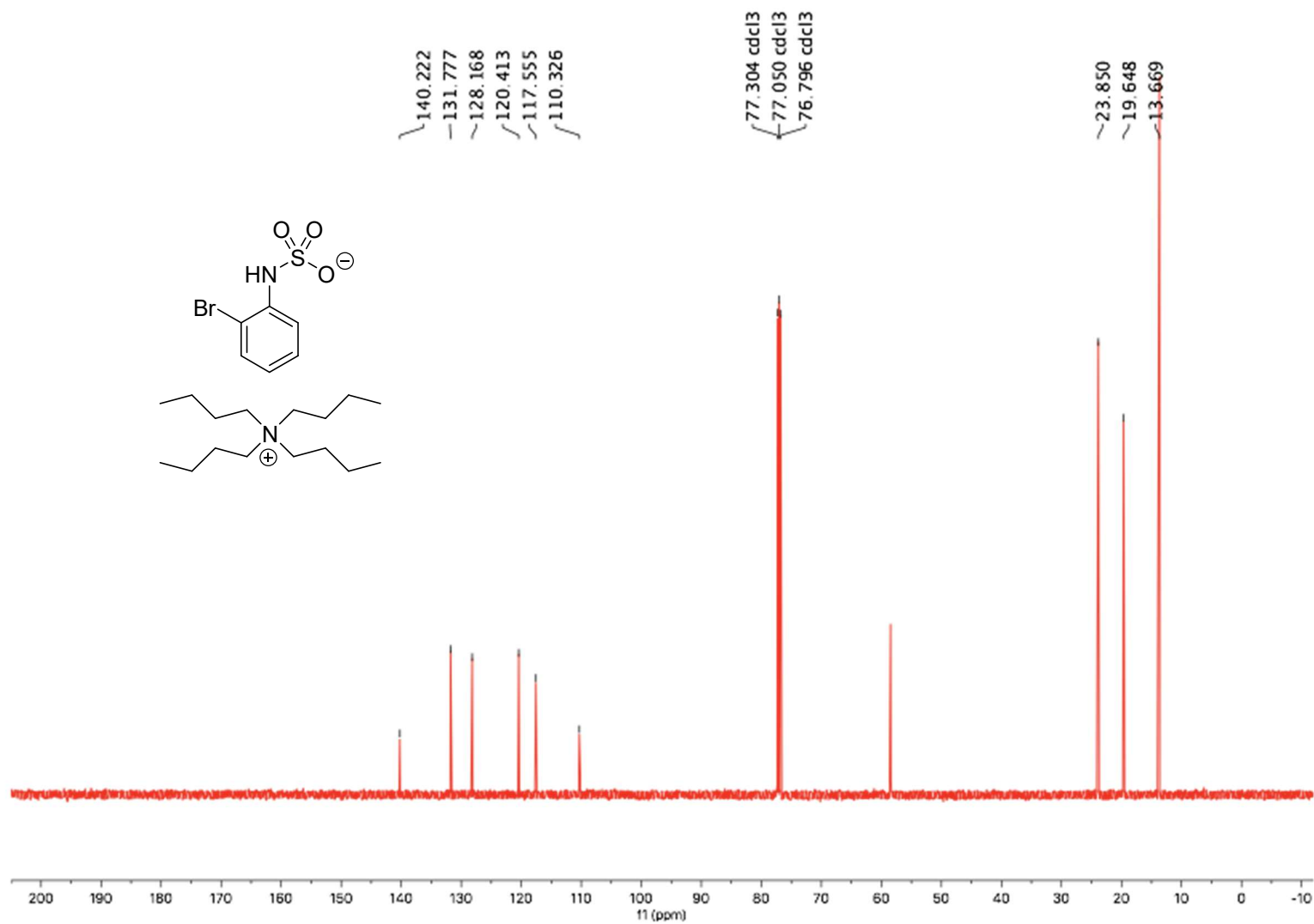
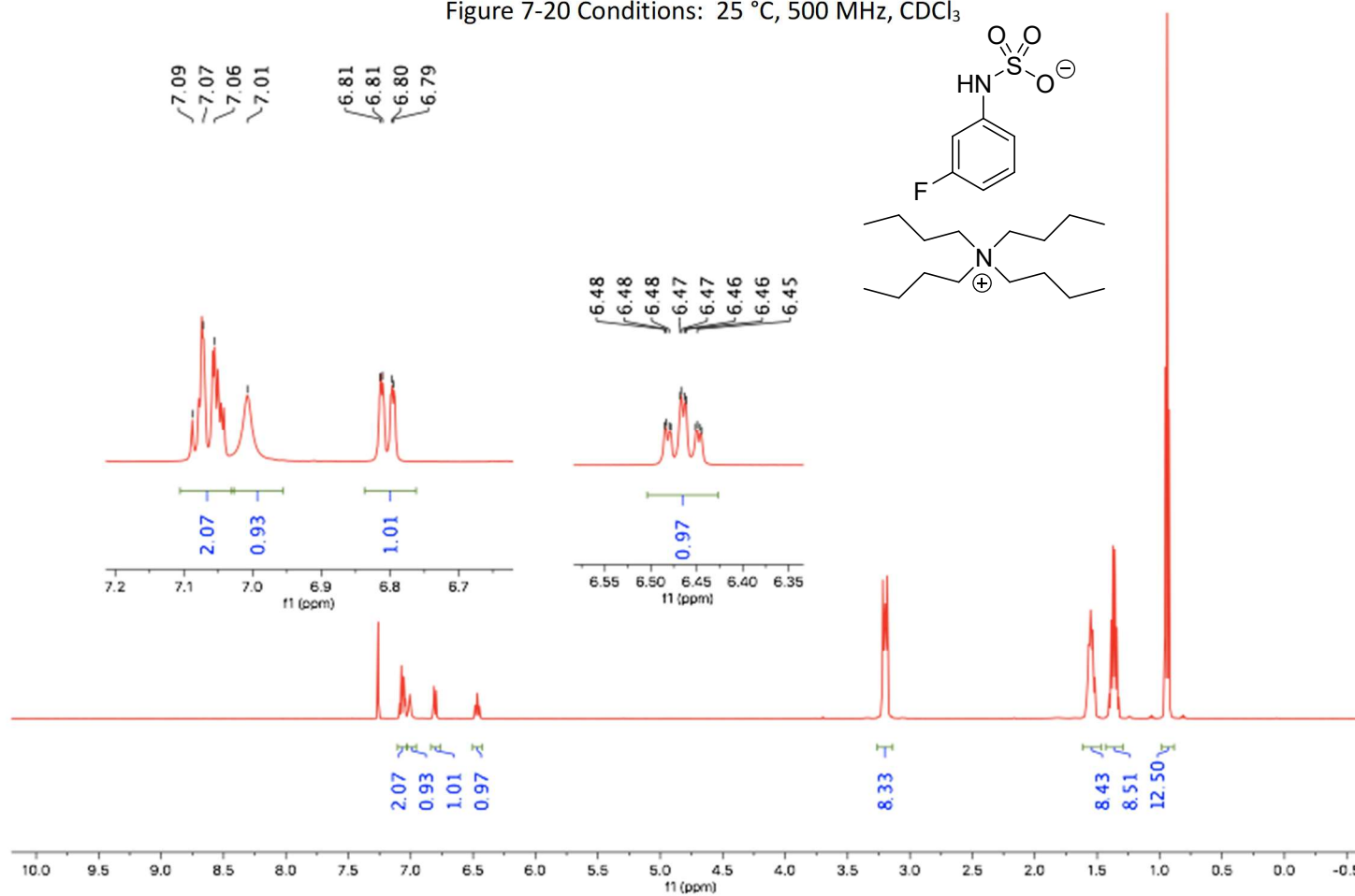


Figure 7-19 Conditions: 25 °C, 126 MHz, CDCl<sub>3</sub>

**<sup>1</sup>H NMR spectrum of tetrabutylammonium 3-fluorophenylsulfamate (8c)**

Figure 7-20 Conditions: 25 °C, 500 MHz, CDCl<sub>3</sub>



<sup>13</sup>C NMR spectrum of tetrabutylammonium 3-fluorophenylsulfamate (8c)

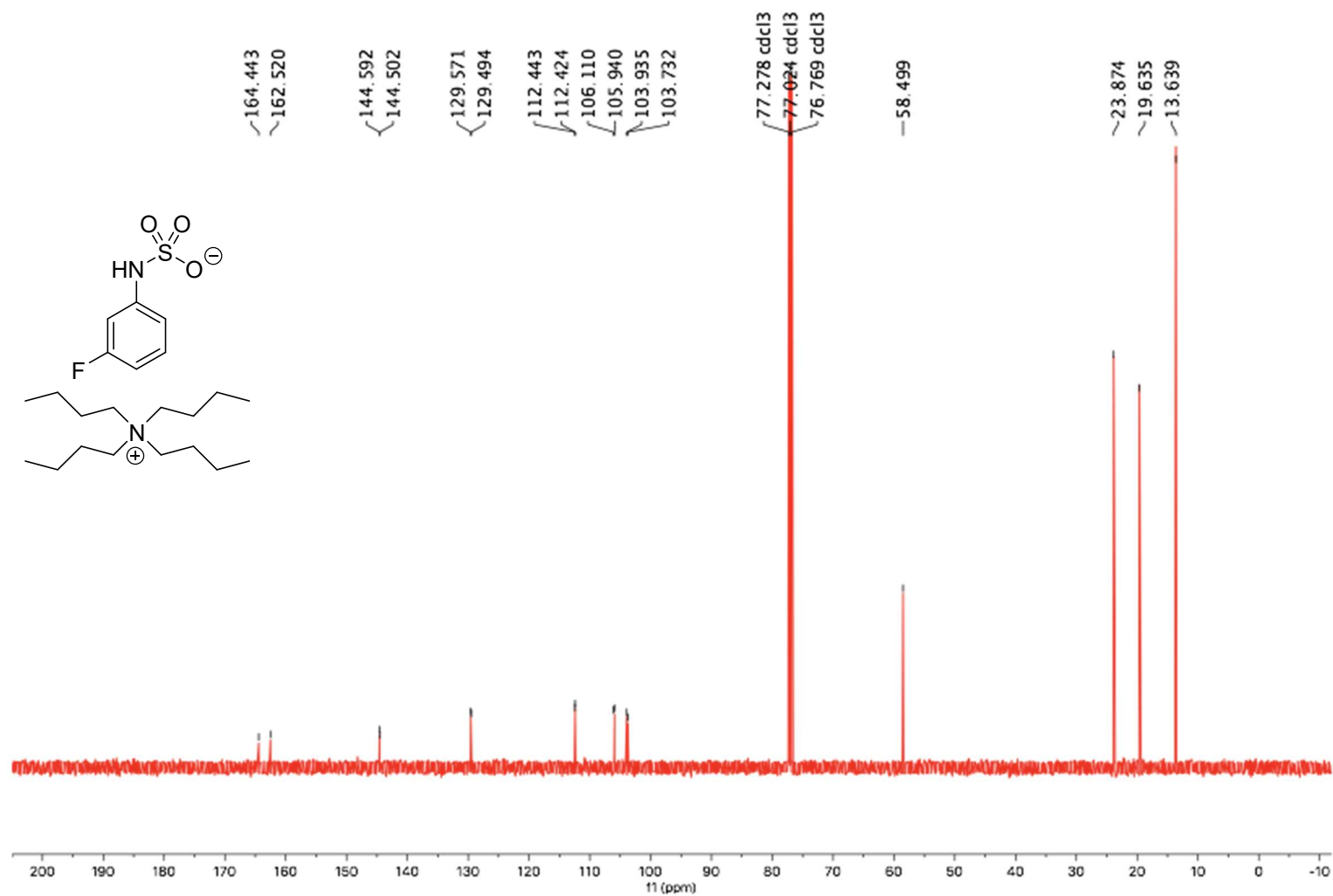


Figure 7-21 Conditions: 25 °C, 126 MHz, CDCl<sub>3</sub>

<sup>19</sup>F NMR spectrum of tetrabutylammonium 3-fluorophenylsulfamate (8c)

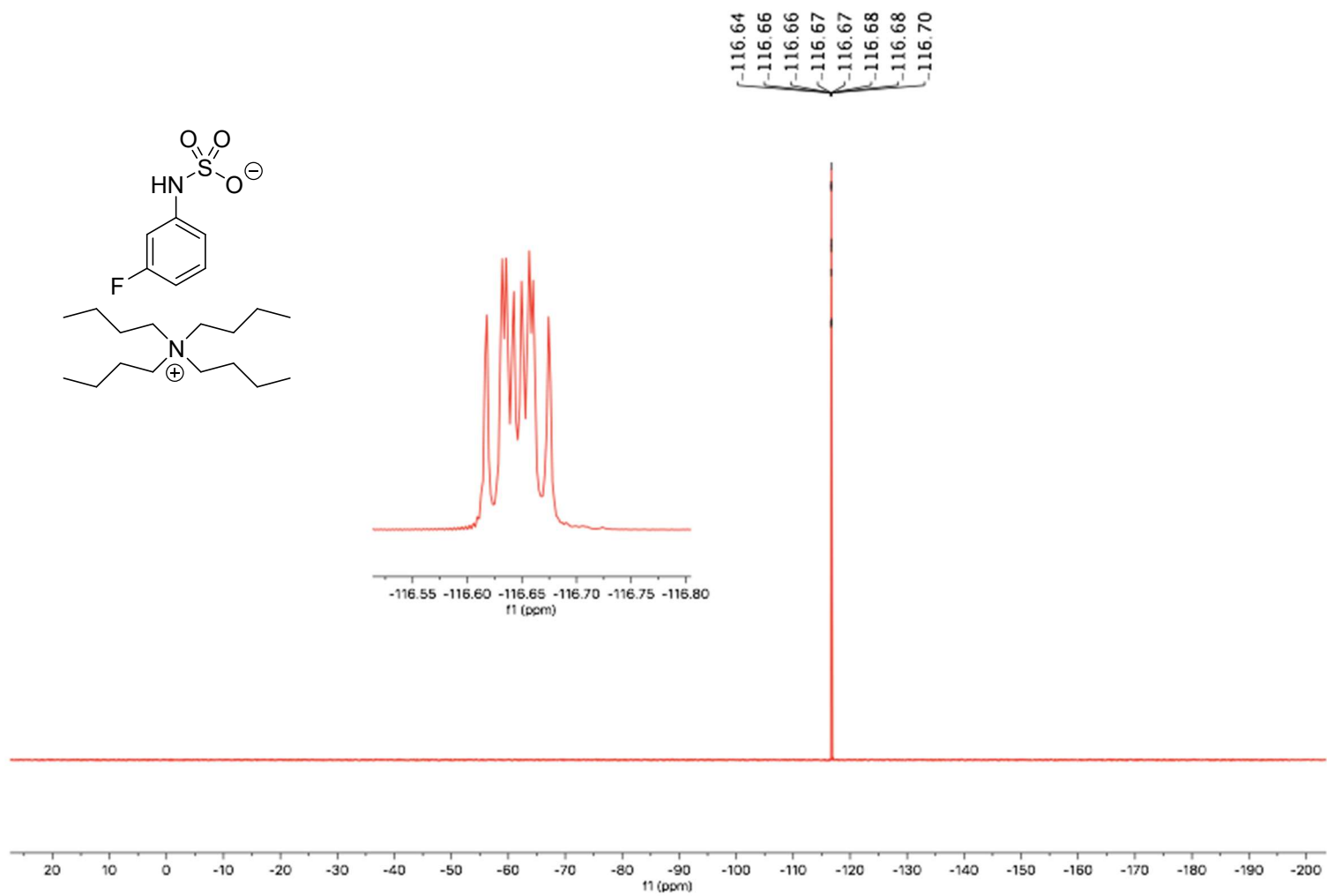


Figure 7-22 Conditions: 25 °C, 470 MHz, CDCl<sub>3</sub>

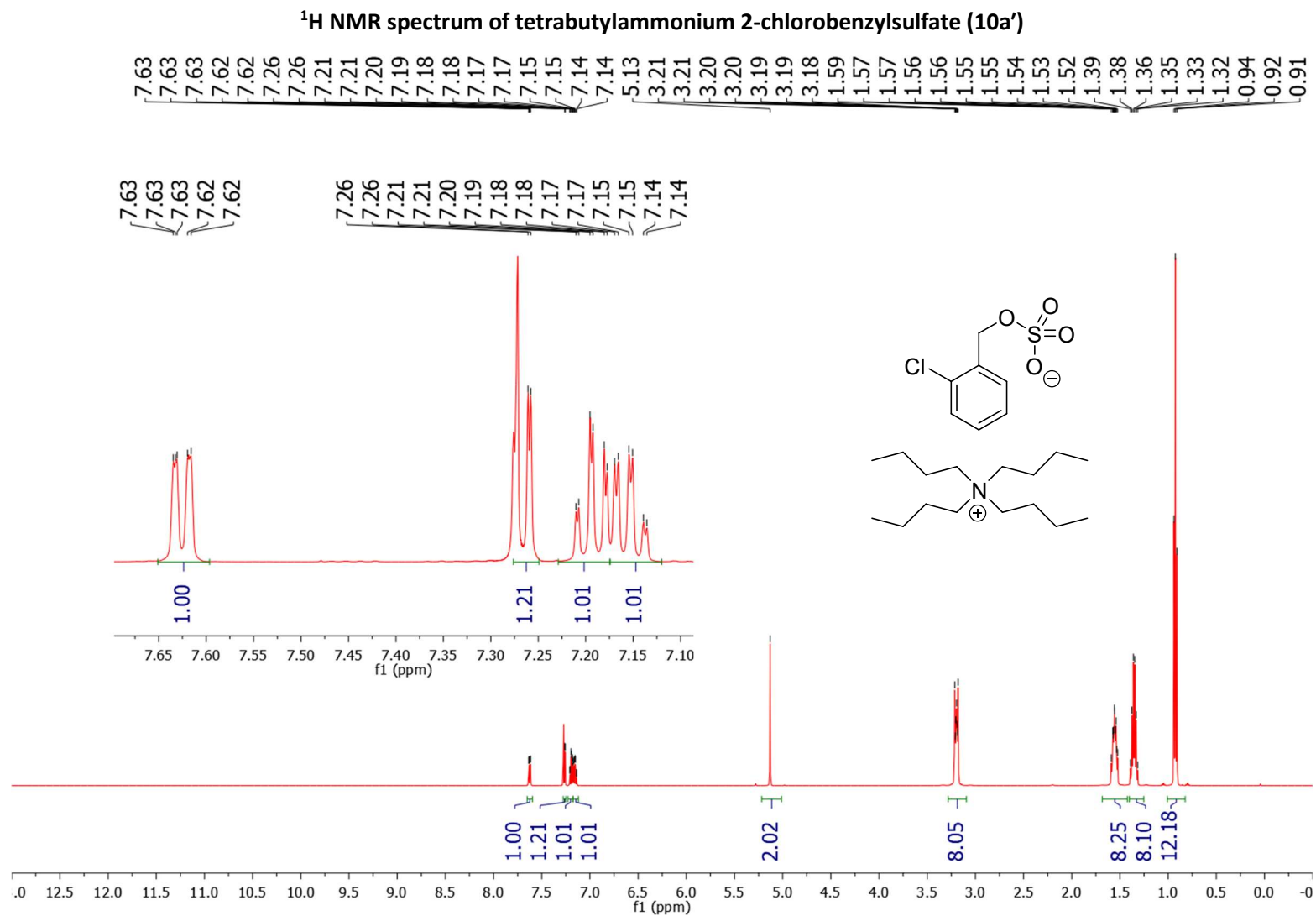


Figure 7-23 Conditions: 25 °C, 500 MHz, CDCl<sub>3</sub>



<sup>13</sup>C NMR spectrum of tetrabutylammonium 2-chlorobenzy sulfate (10a')

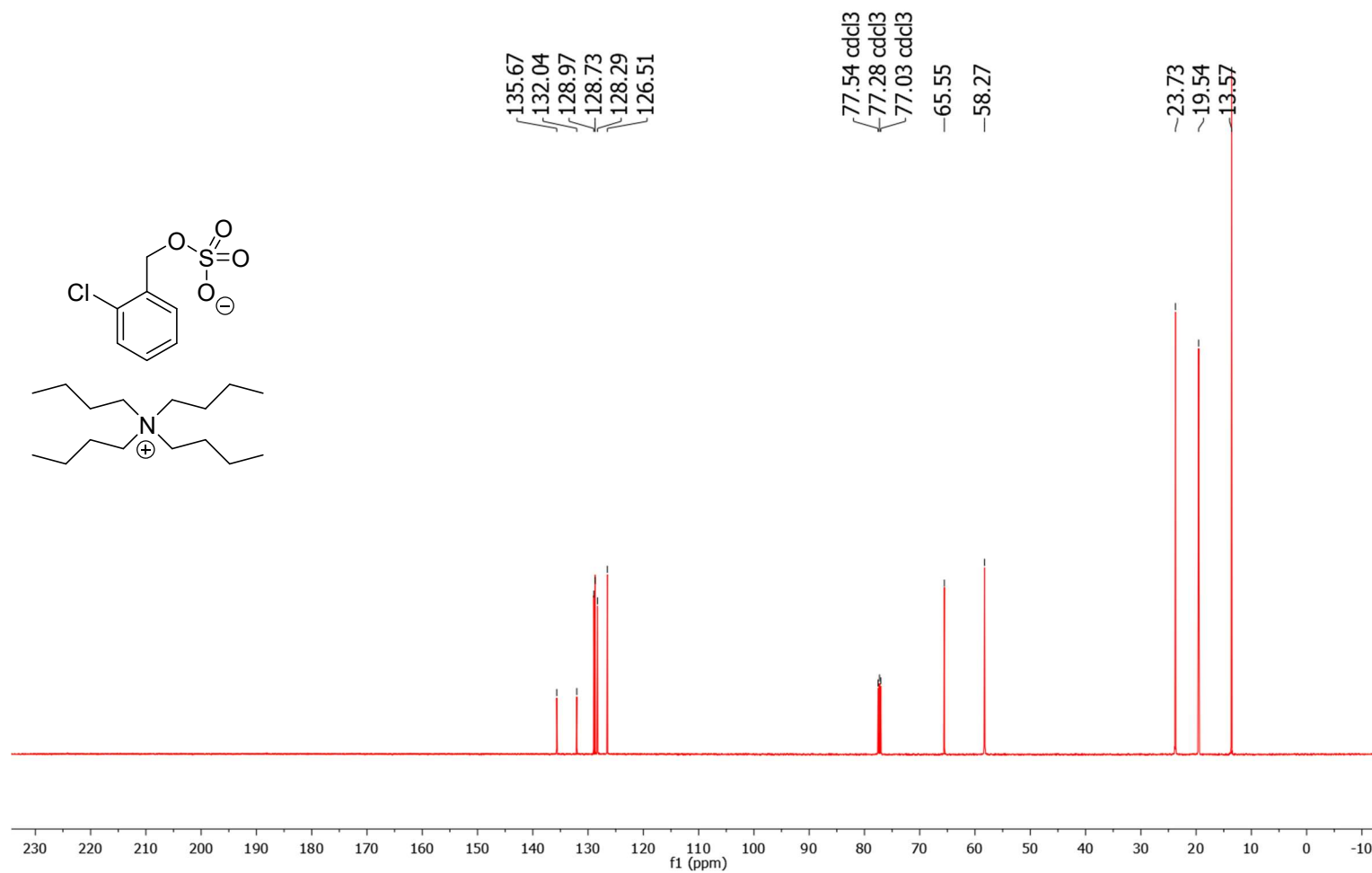


Figure 7-24 Conditions: 25 °C, 126 MHz, CDCl<sub>3</sub>

<sup>1</sup>H NMR spectrum of tetrapropylammonium 2-trifluoromethylbenzylsulfate (10c)

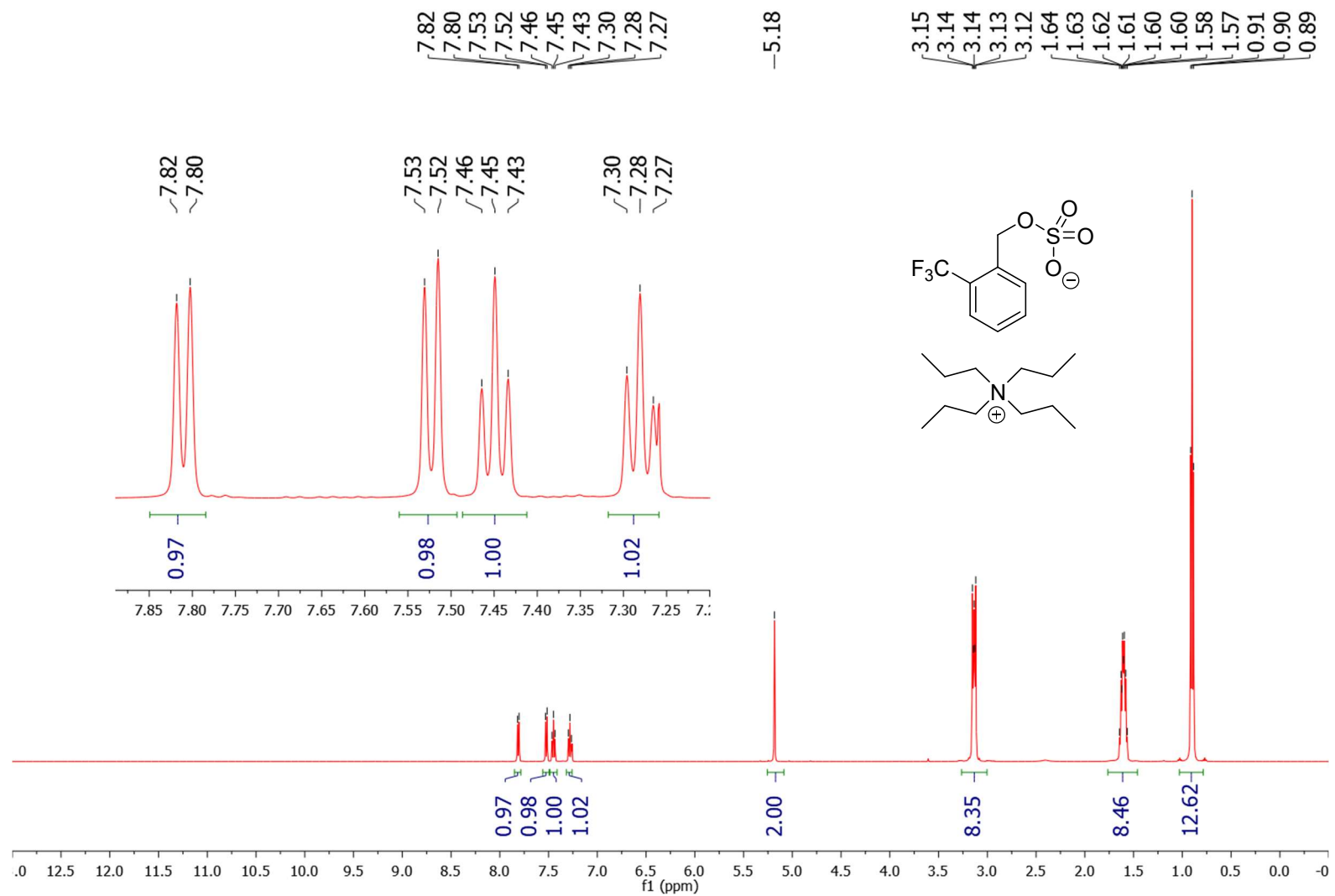


Figure 7-25 Conditions: 25 °C, 500 MHz, CDCl<sub>3</sub>

<sup>13</sup>C NMR spectrum of tetrapropylammonium 2-trifluoromethylbenzylsulfate (10c)

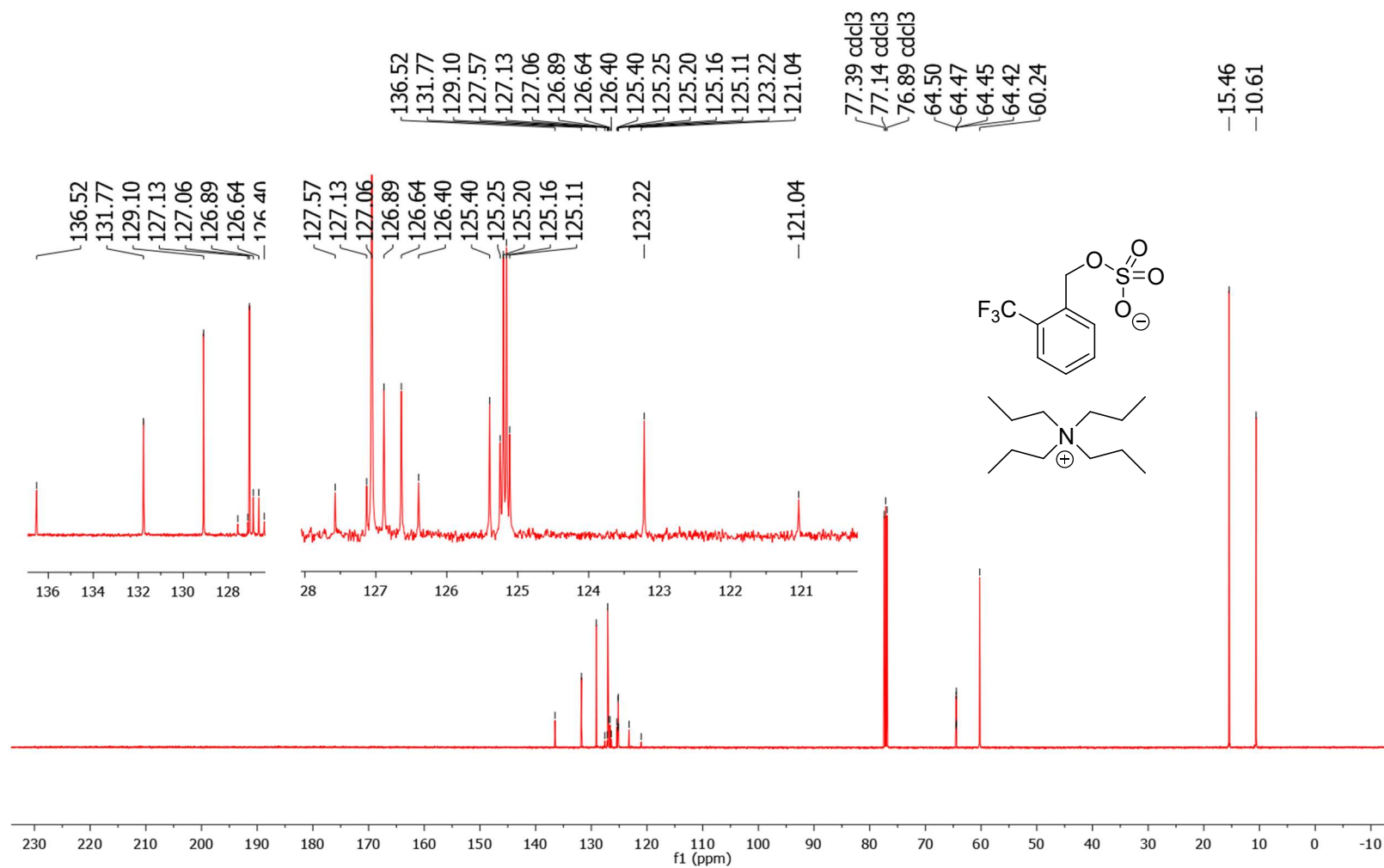


Figure 7-26 Conditions: 25 °C, 126 MHz, CDCl<sub>3</sub>

<sup>19</sup>F NMR spectrum of tetrapropylammonium 2-trifluoromethylbenzylsulfate (10c)

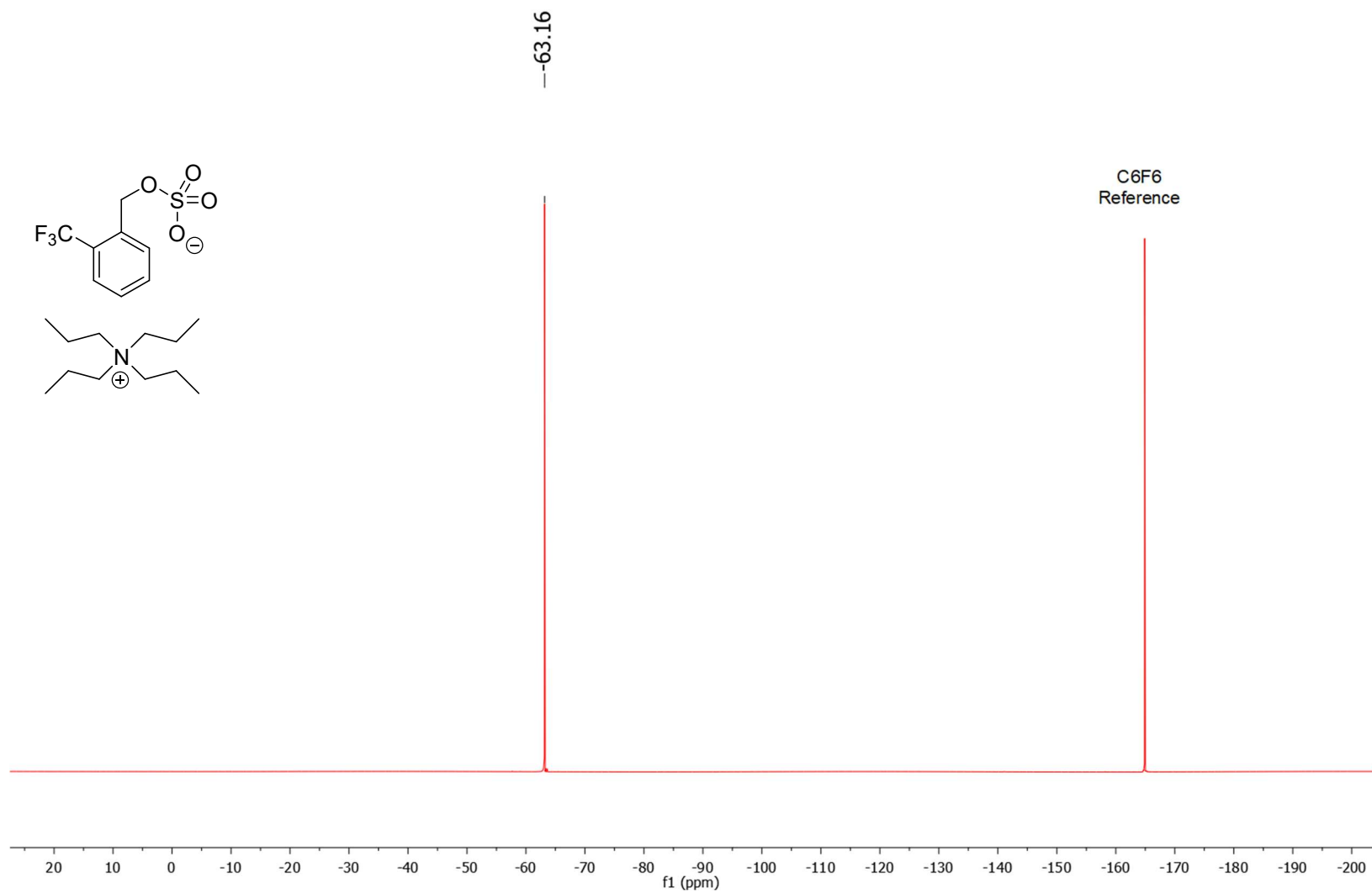


Figure 7-27 Conditions: 25 °C, 470 MHz, CDCl<sub>3</sub>

<sup>1</sup>H NMR spectrum of tetrapropylammonium 2-methylbenzylsulfate (11d)

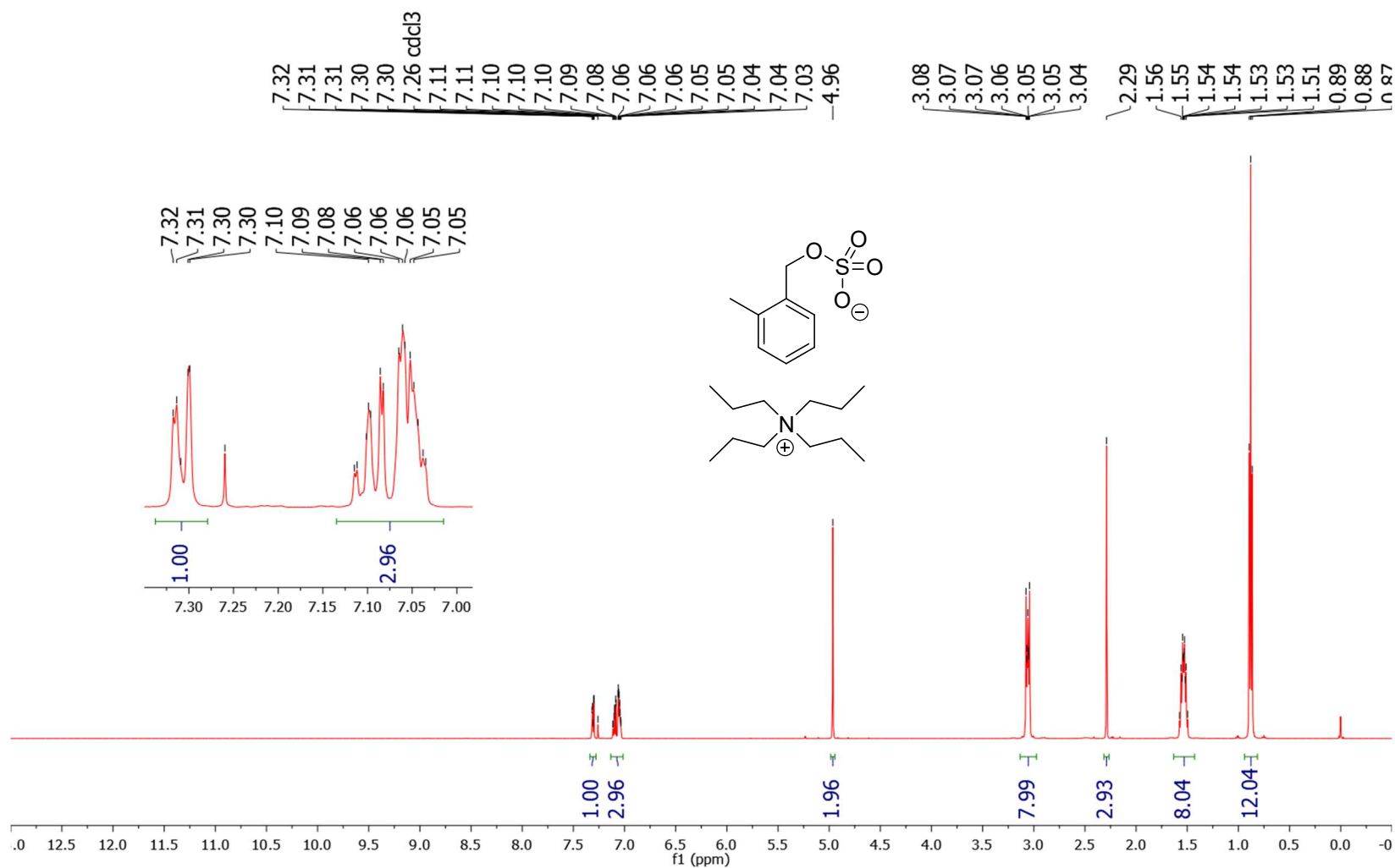


Figure 7-28 Conditions: 25 °C, 500 MHz, CDCl<sub>3</sub>

**$^{13}\text{C}$  NMR spectrum of tetrapropylammonium 2-methylbenzylsulfate (11d)**

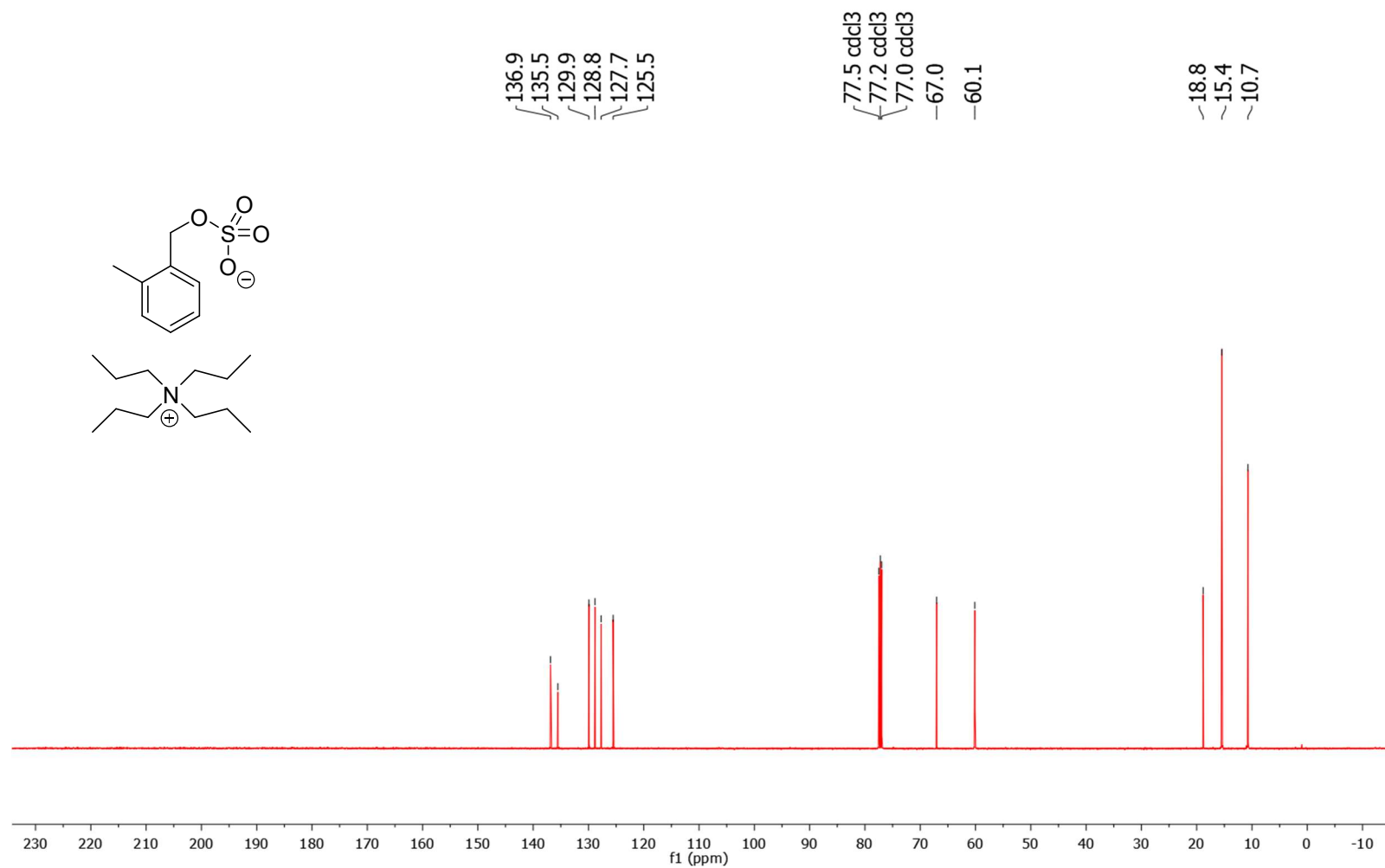


Figure 7-29 Conditions: 25 °C, 126 MHz,  $\text{CDCl}_3$

<sup>1</sup>H NMR spectrum of tetrapropylammonium 2-fluorobenzenesulfate (10g)

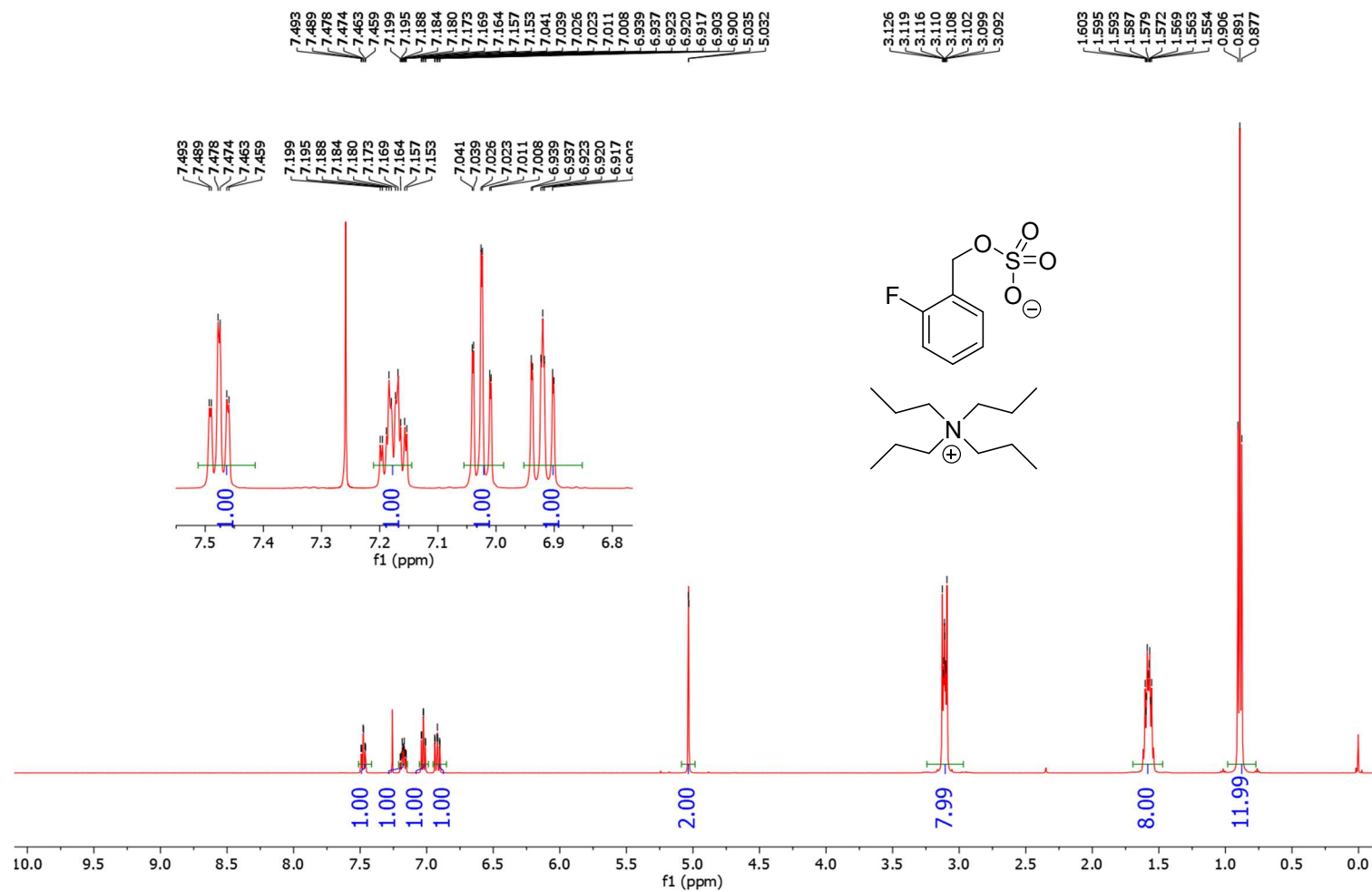
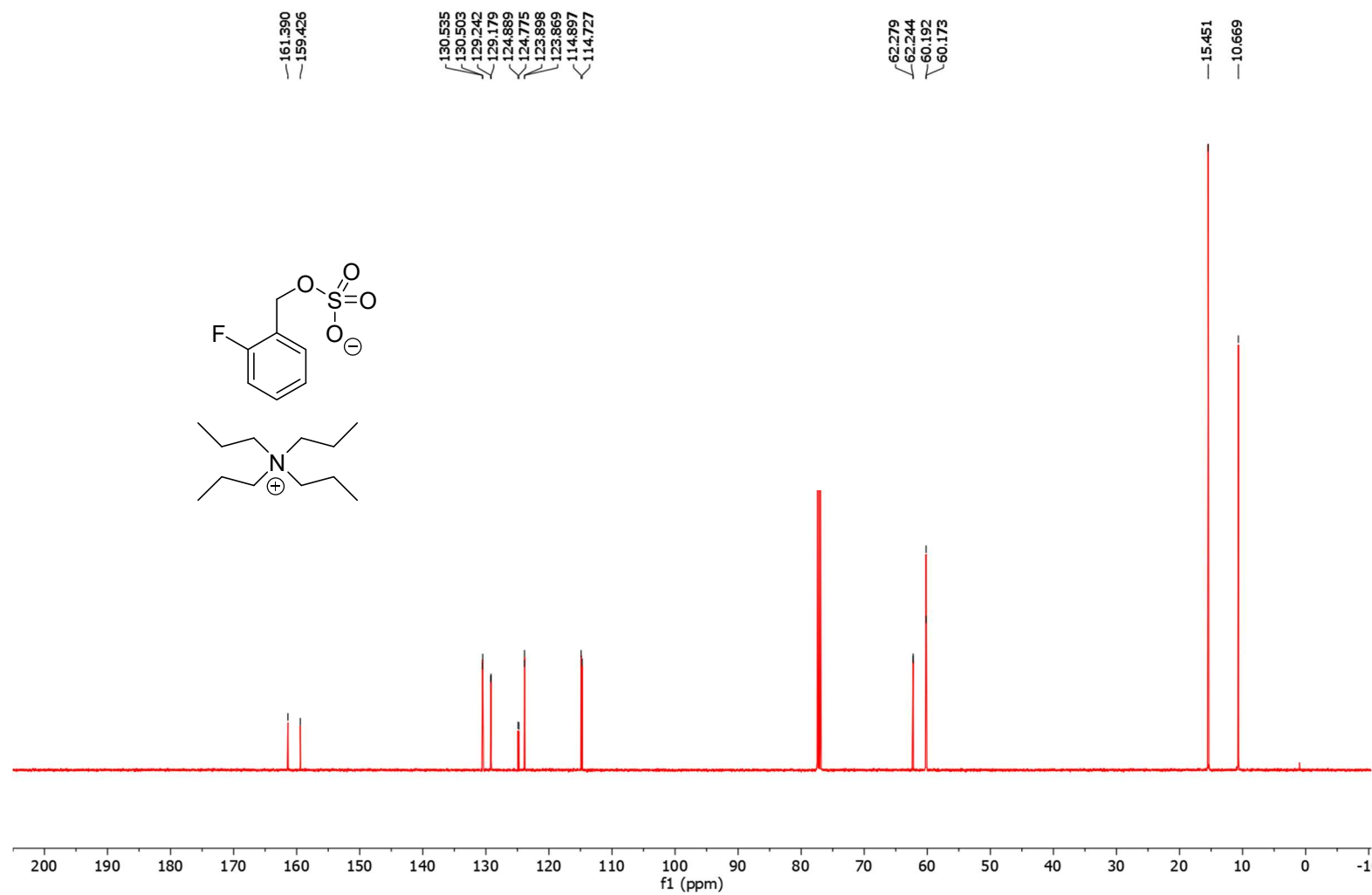


Figure 7-30 Conditions: 25 °C, 500 MHz, CDCl<sub>3</sub>

<sup>13</sup>C NMR spectrum of tetrapropylammonium 2-fluorobenzenesulfate (10g)





**<sup>19</sup>F NMR spectrum of tetrapropylammonium 2-fluorobenzenesulfate (10g)**

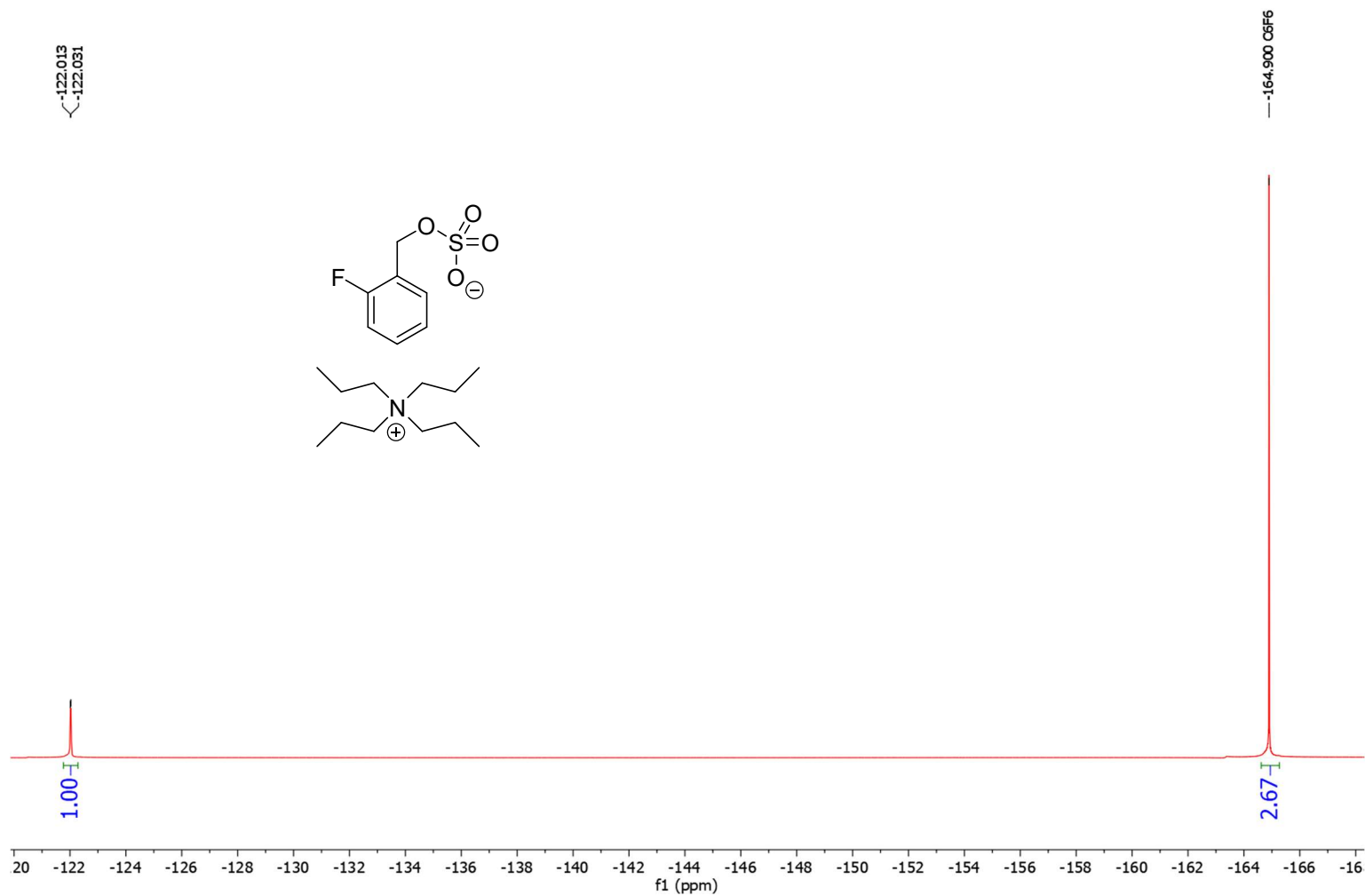


Figure 7-32 Conditions: 25 °C, 470 MHz, CDCl<sub>3</sub>

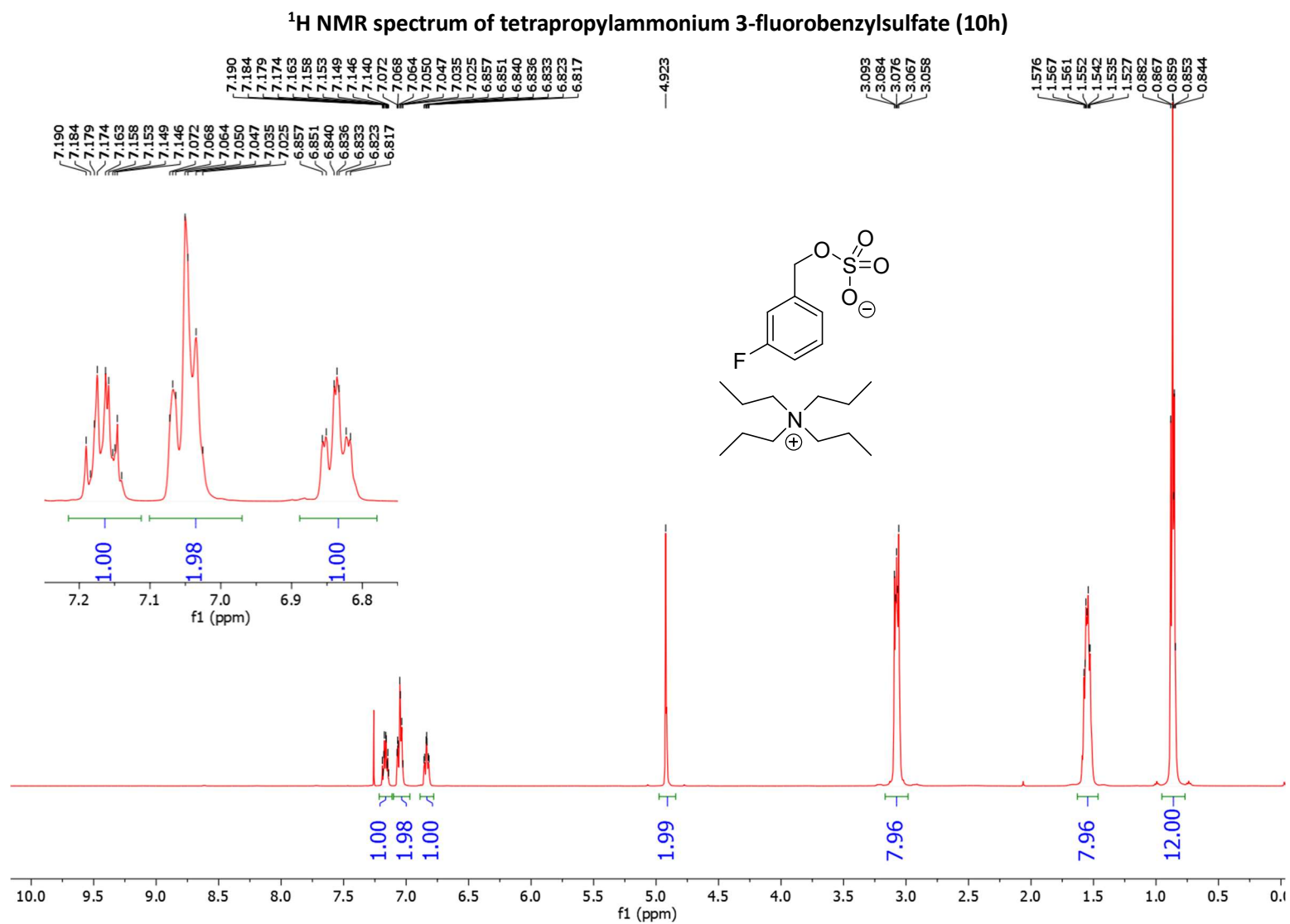
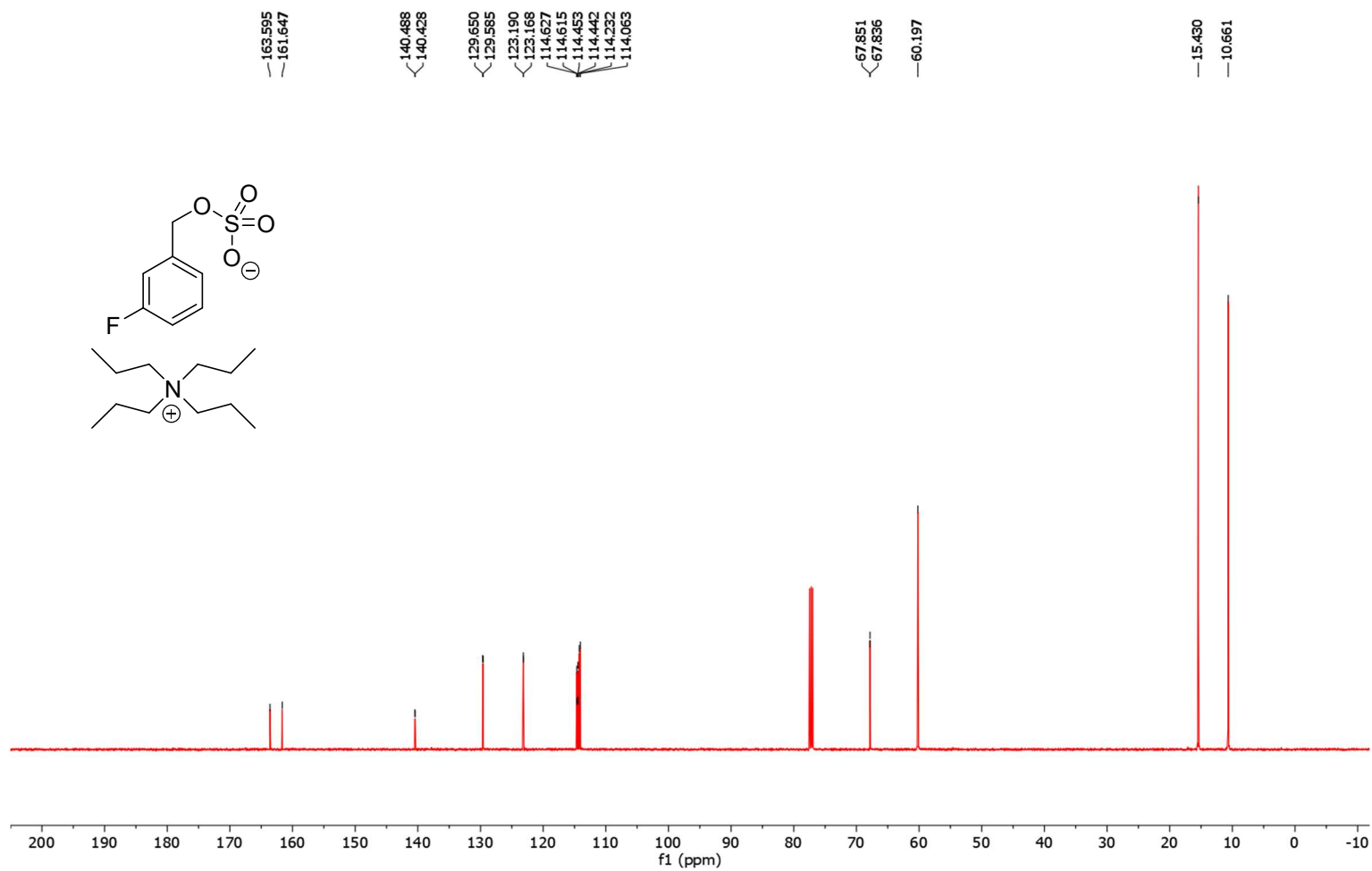


Figure 7-33 Conditions: 25 °C, 500 MHz,  $\text{CDCl}_3$

<sup>13</sup>C NMR spectrum of tetrapropylammonium 3-fluorobenzenesulfate (10h)



7-34 Conditions: 25 °C, 126 MHz, CDCl<sub>3</sub>

<sup>19</sup>F NMR spectrum of tetrapropylammonium 3-fluorobenzyisulfate (10h)

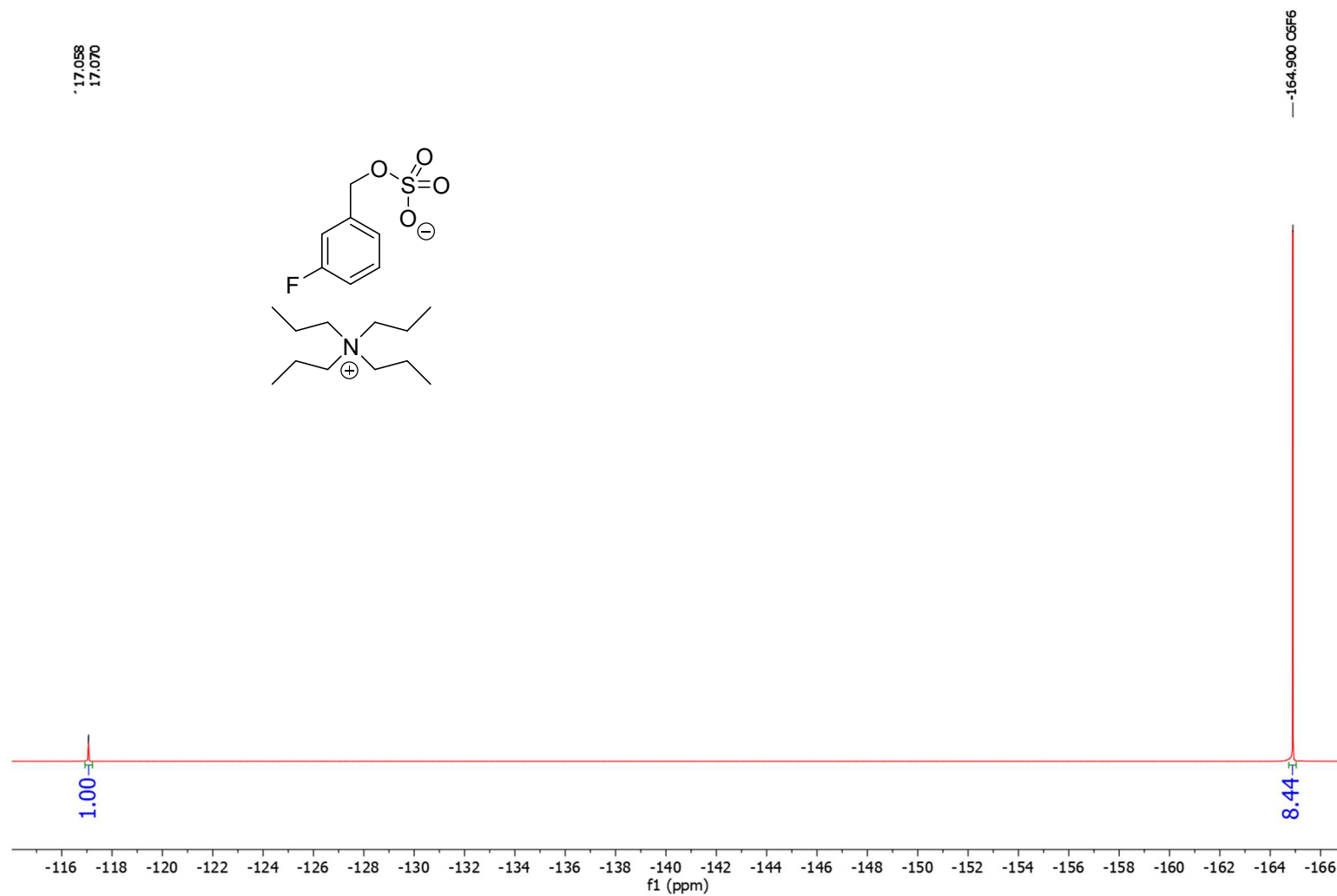


Figure 7-35 Conditions: 25 °C, 470 MHz, CDCl<sub>3</sub>

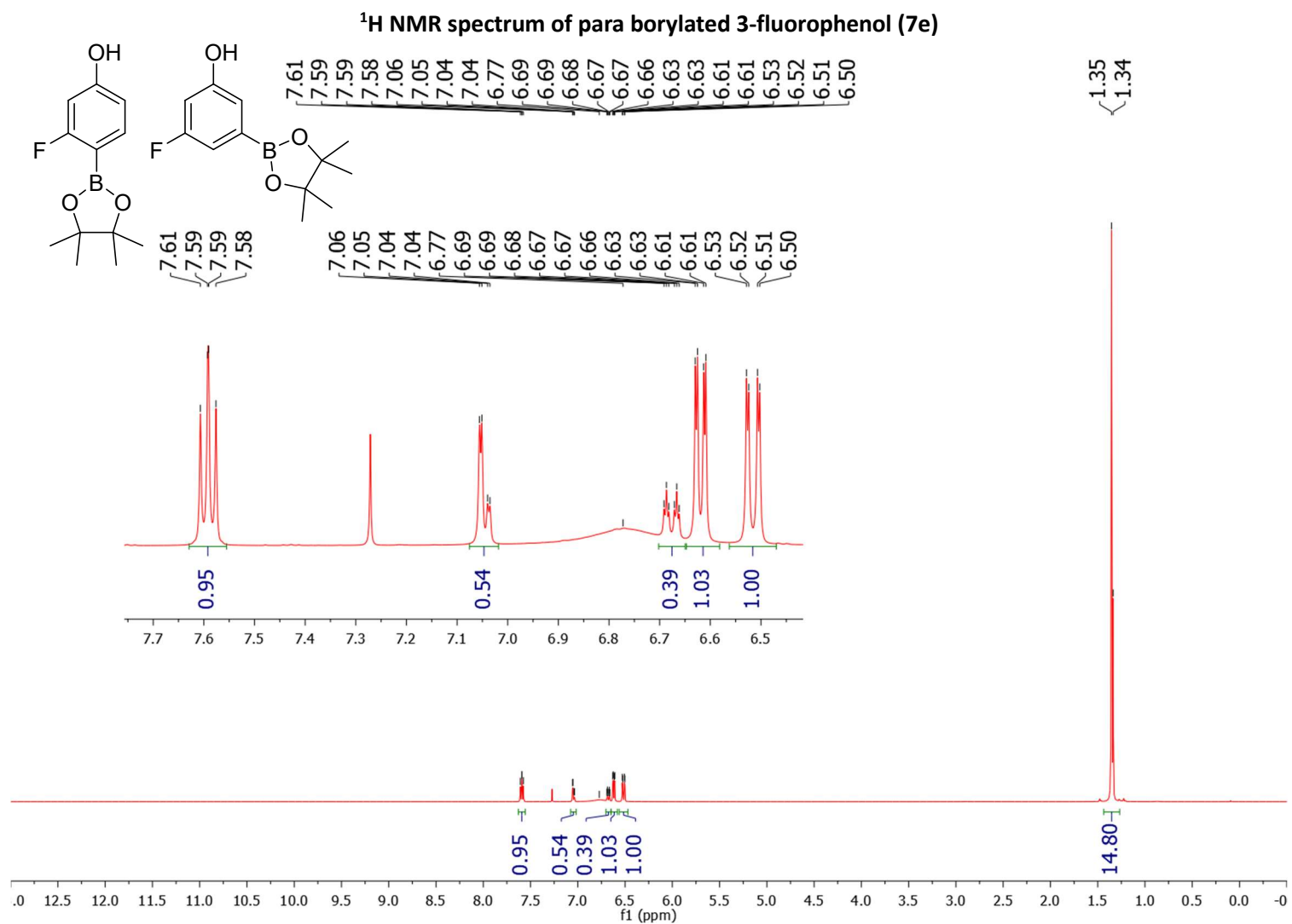


Figure 7-36 Conditions: 25 °C, 500 MHz,  $\text{CDCl}_3$

**$^{13}\text{C}$  NMR spectrum of para borylated 3-fluorophenol (7e)**

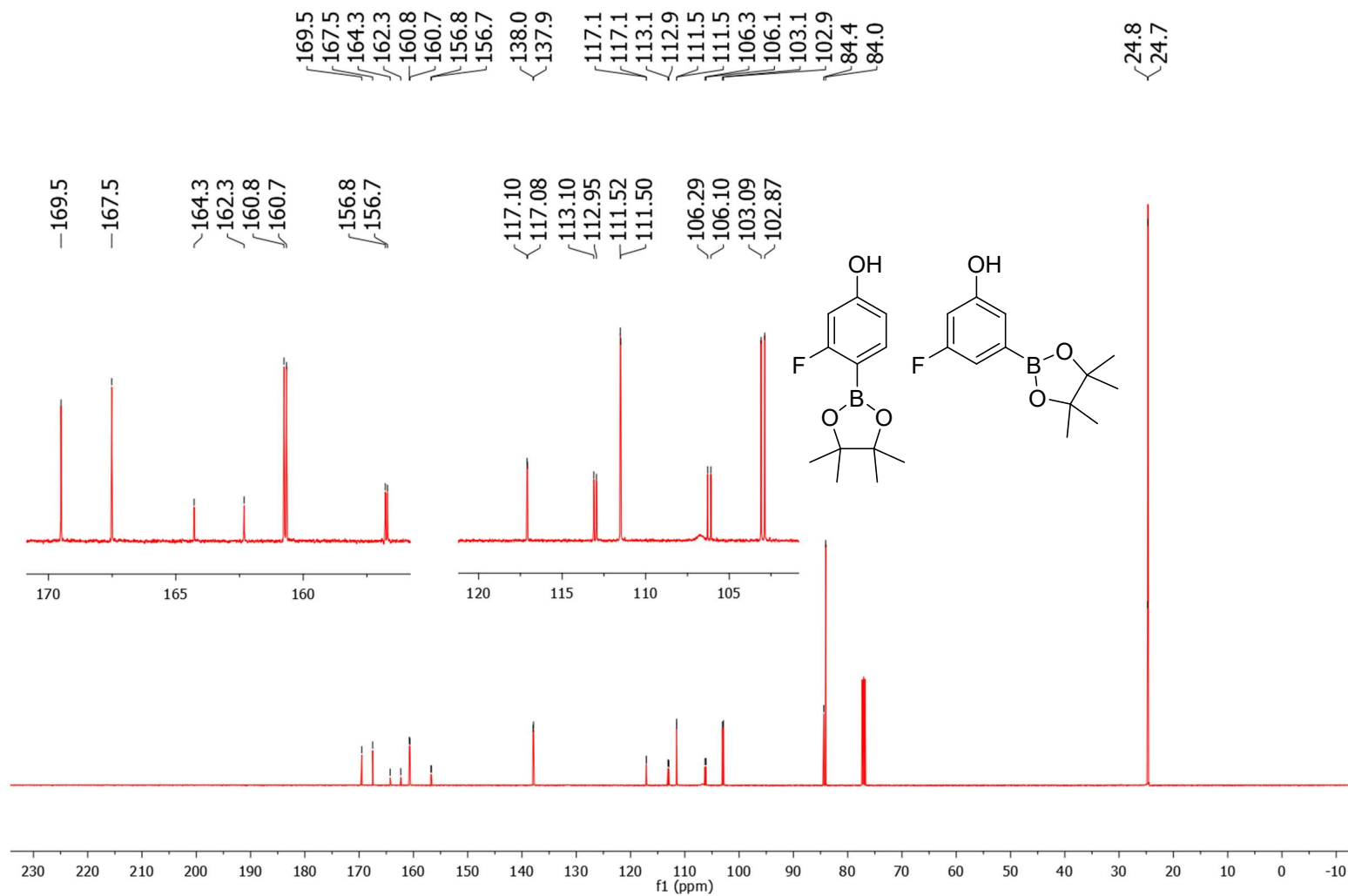
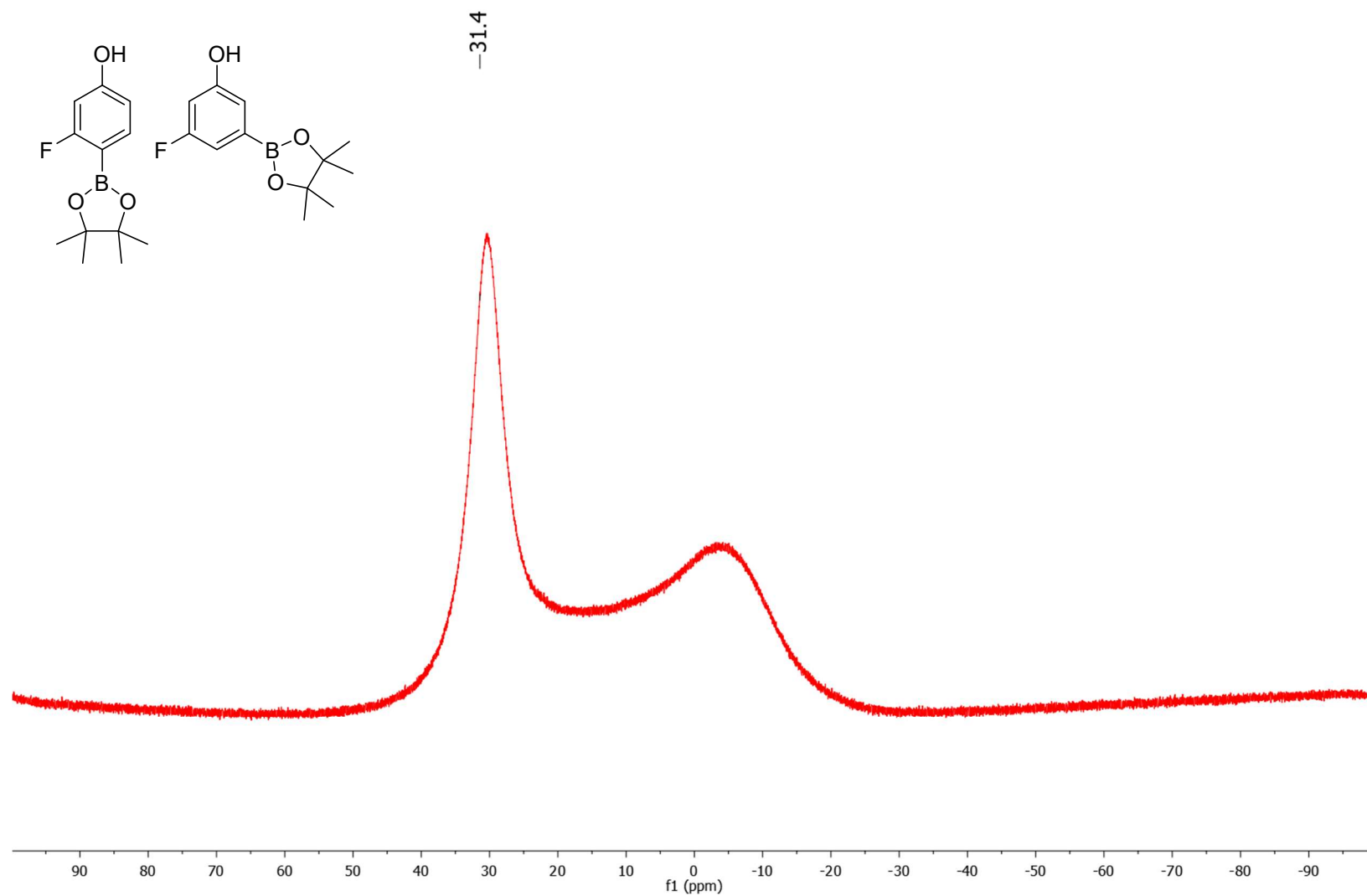


Figure 7-37 Conditions: 25 °C, 126 MHz,  $\text{CDCl}_3$

<sup>11</sup>B NMR spectrum of para borylated 3-fluorophenol (7e)



<sup>19</sup>F NMR spectrum of para borylated 3-fluorophenol (7e)

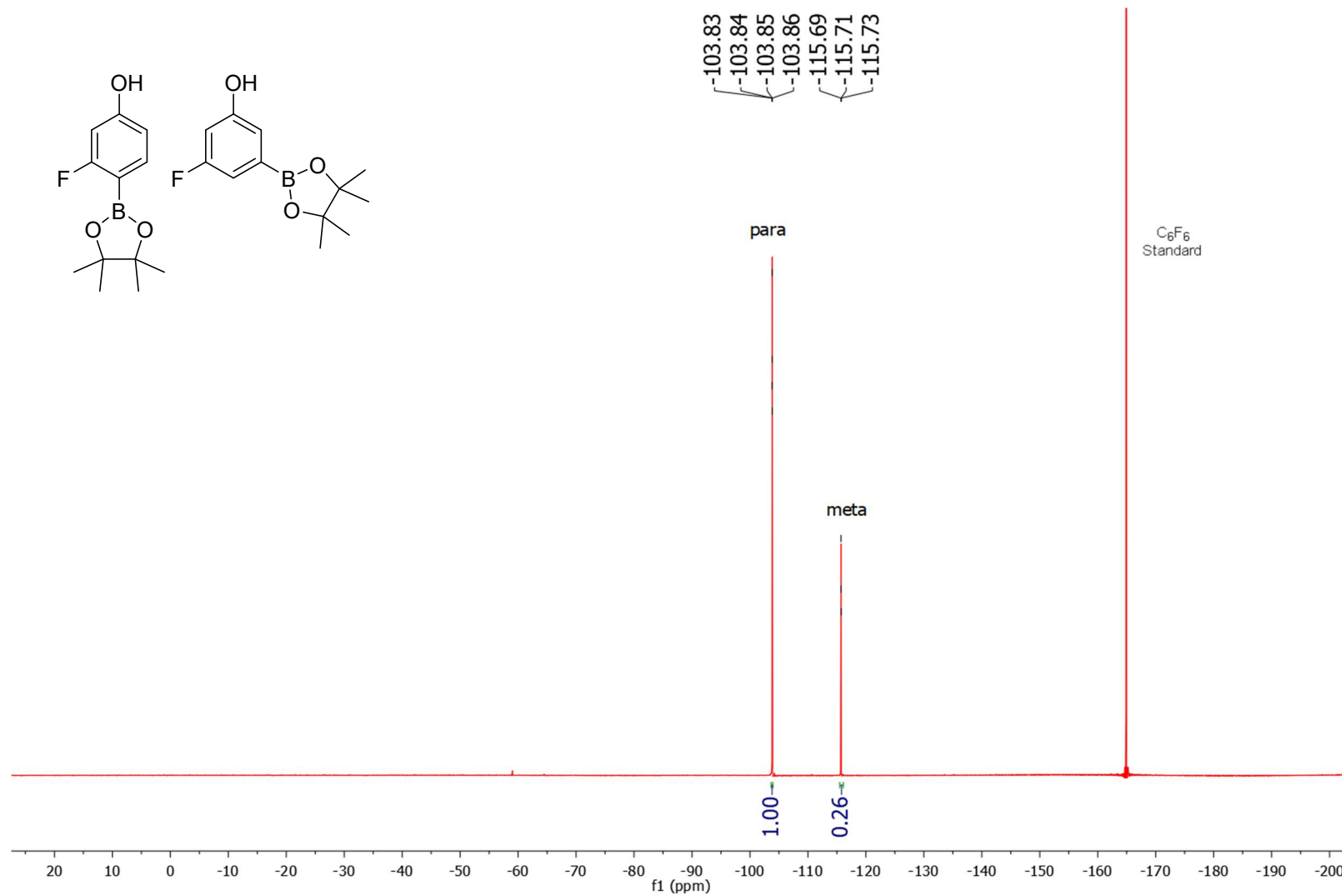


Figure 7-39 Conditions: 25 °C, 470 MHz, CDCl<sub>3</sub>



<sup>1</sup>H NMR spectrum of para borylated 2-methylphenol (7g)

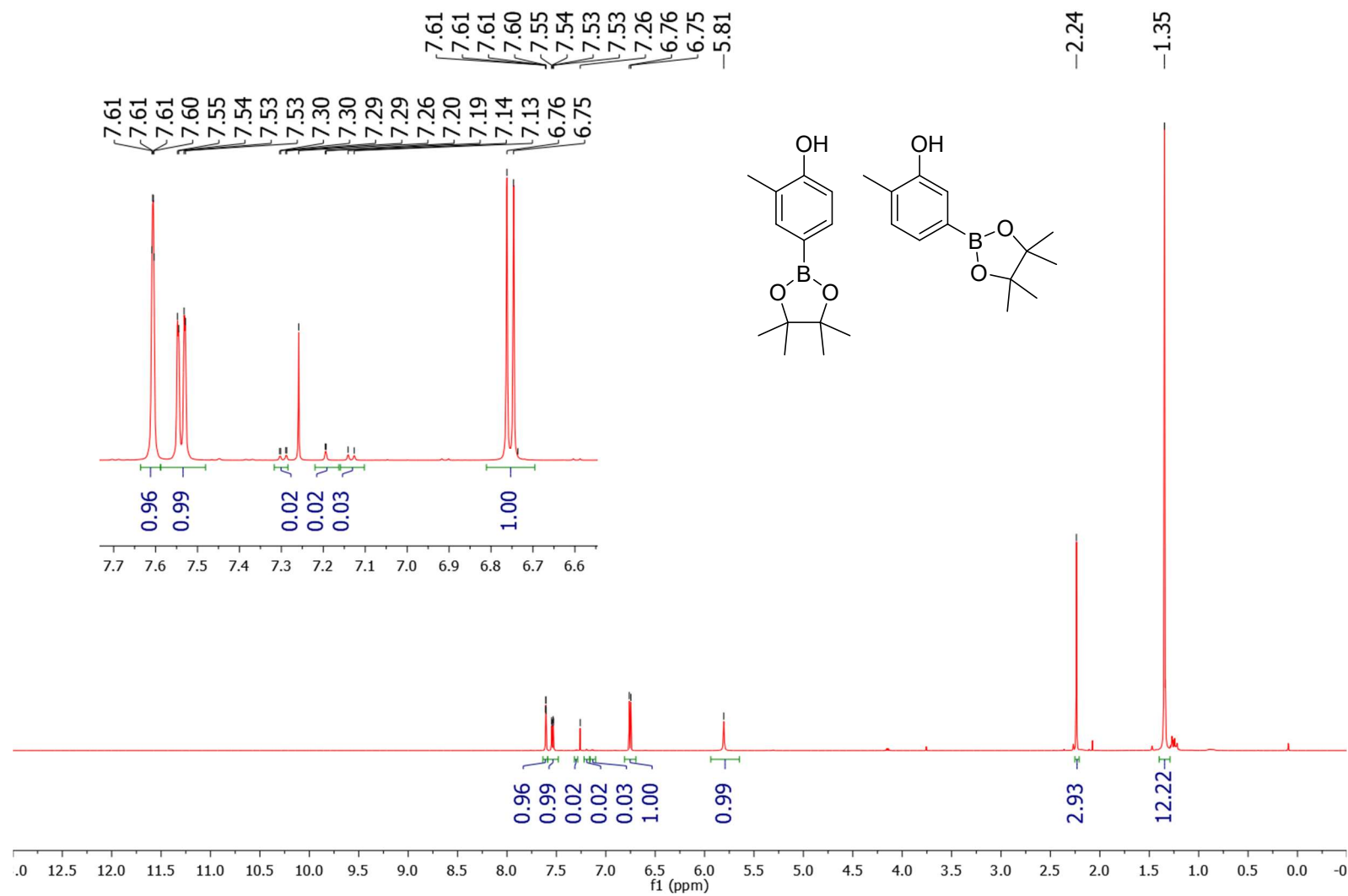


Figure 7-40 Conditions: 25 °C, 500 MHz, CDCl<sub>3</sub>

<sup>13</sup>C NMR spectrum of para borylated 2-methylphenol (7g)

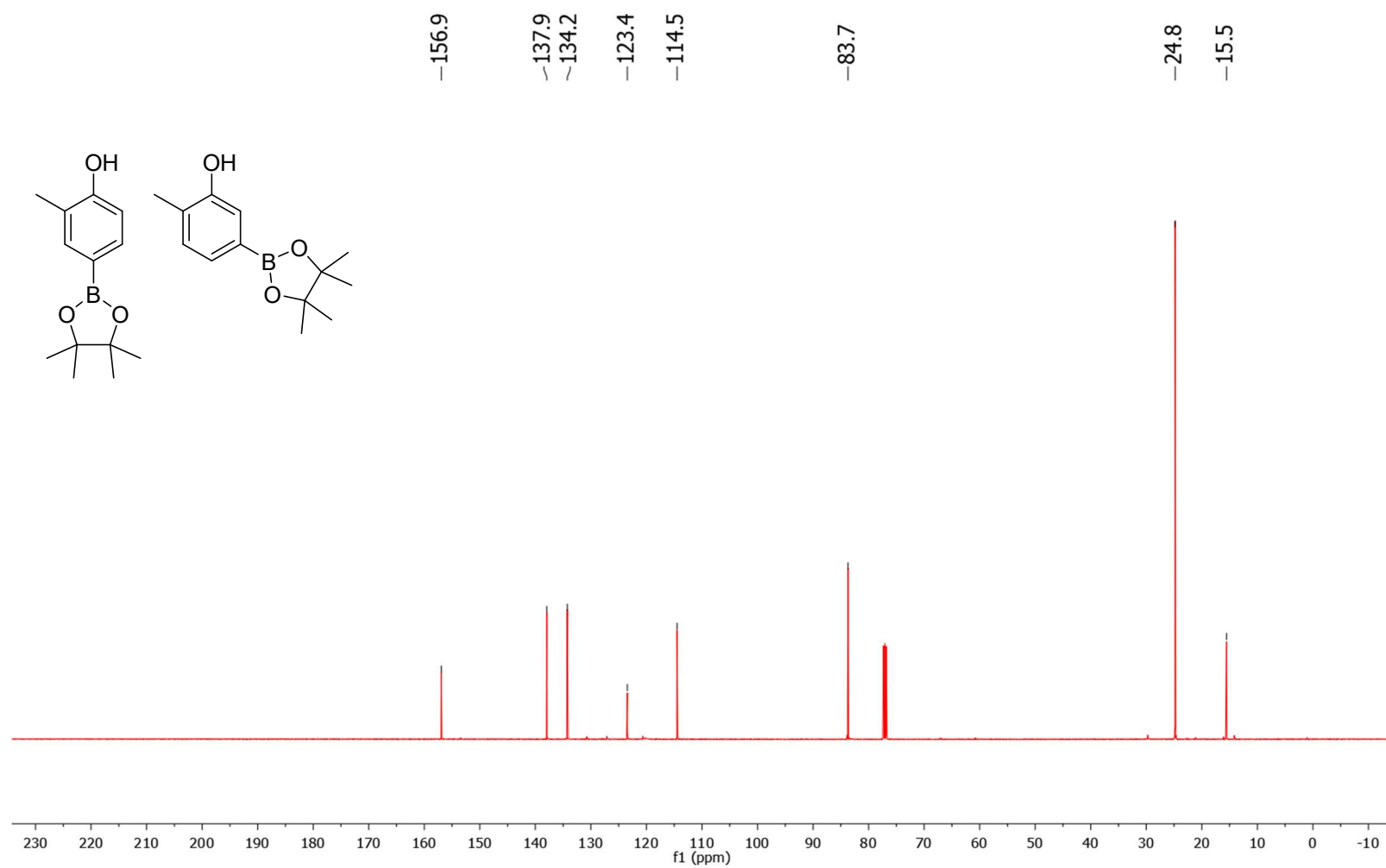


Figure 7-41 Conditions: 25 °C, 126 MHz, CDCl<sub>3</sub>

<sup>11</sup>B NMR spectrum of para borylated 2-methylphenol (7g)

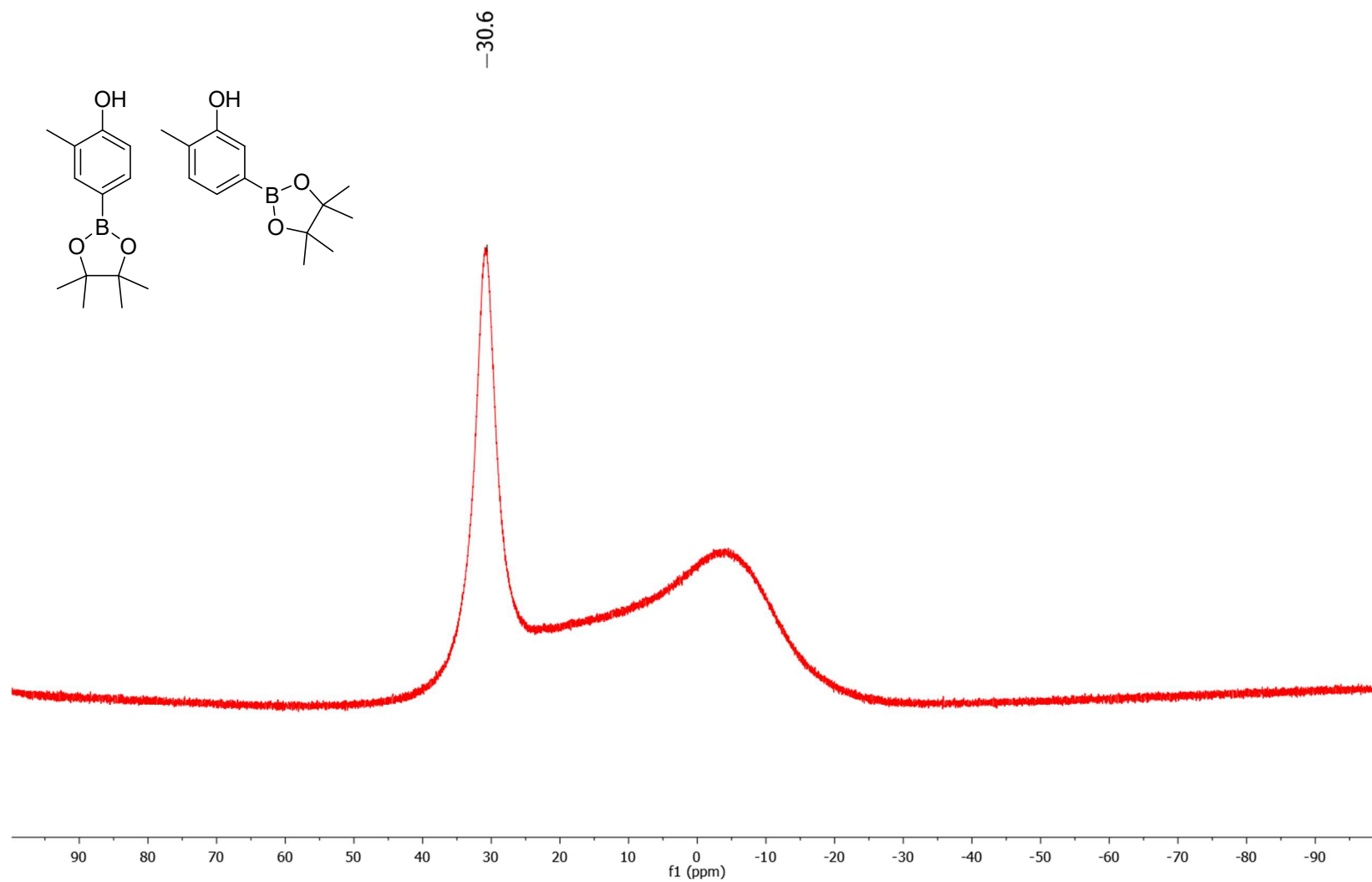


Figure 7-42 Conditions: 25 °C, 160 MHz, CDCl<sub>3</sub>

<sup>1</sup>H NMR spectrum of para borylated 2-isopropylphenol (7h)

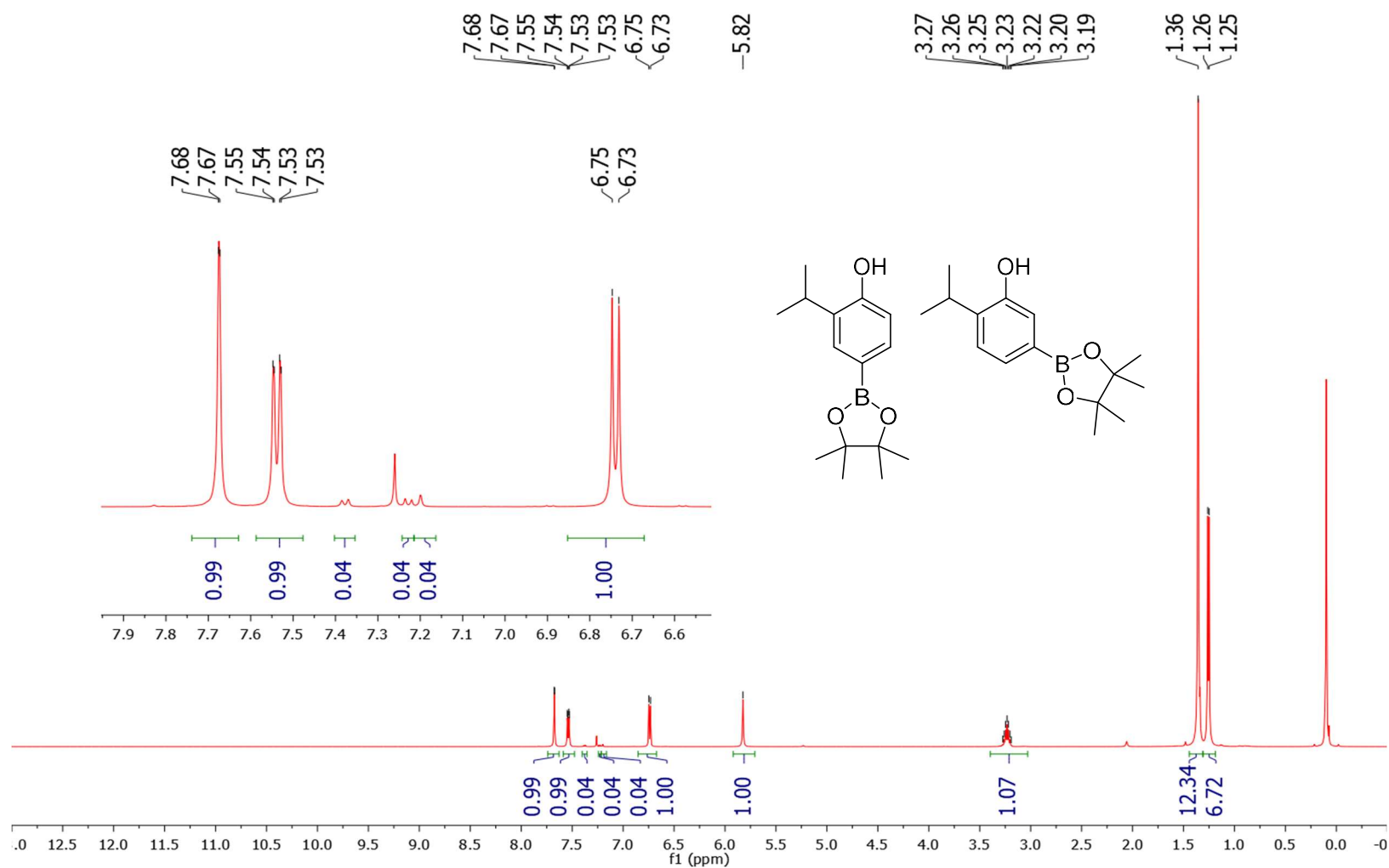


Figure 7-43 Conditions: 25 °C, 500 MHz, CDCl<sub>3</sub>

<sup>13</sup>C NMR spectrum of para borylated 2-isopropylphenol (7h)

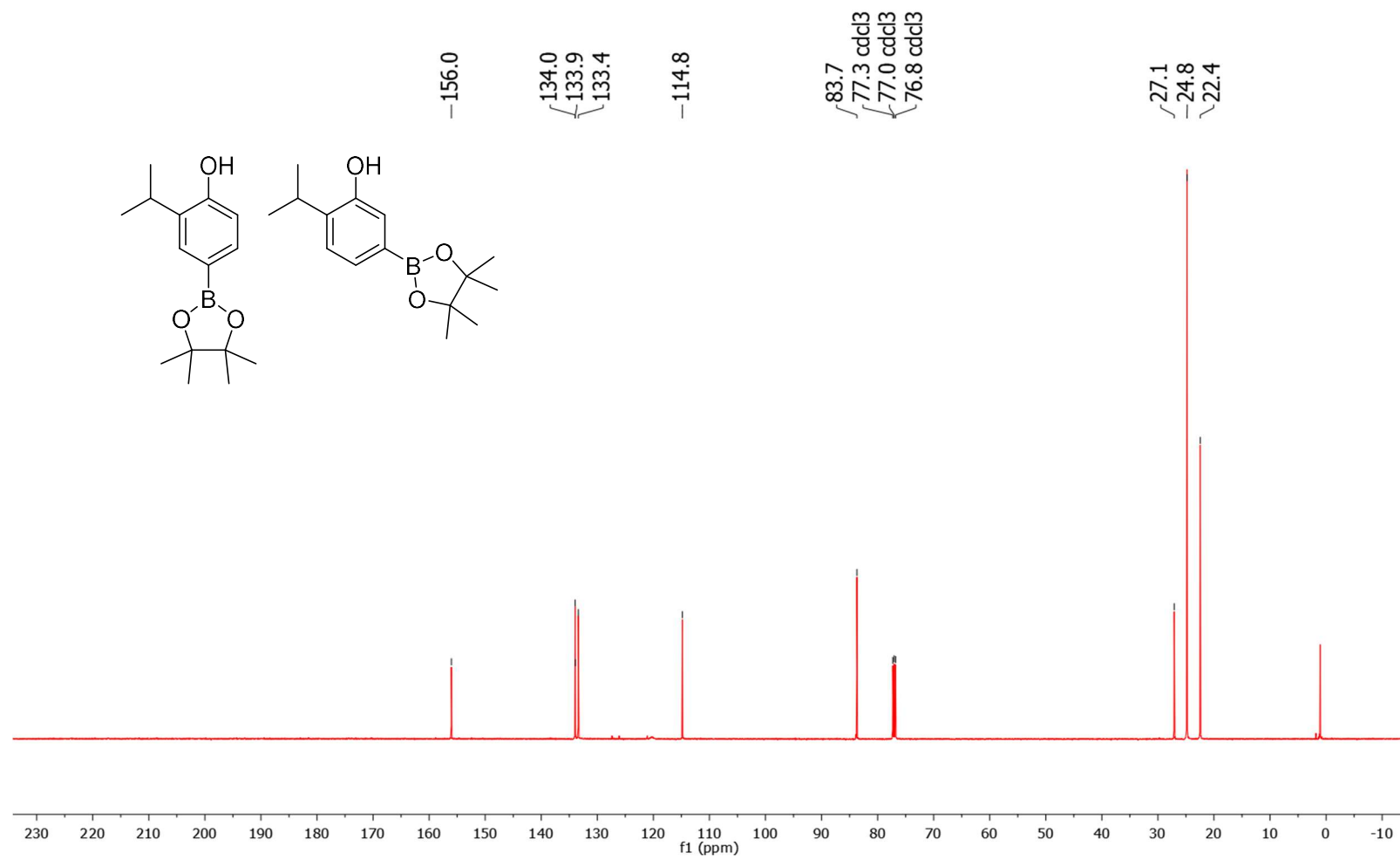


Figure 7-44 Conditions: 25 °C, 126 MHz, CDCl<sub>3</sub>

<sup>11</sup>B NMR spectrum of para borylated 2-isopropylphenol (7h)

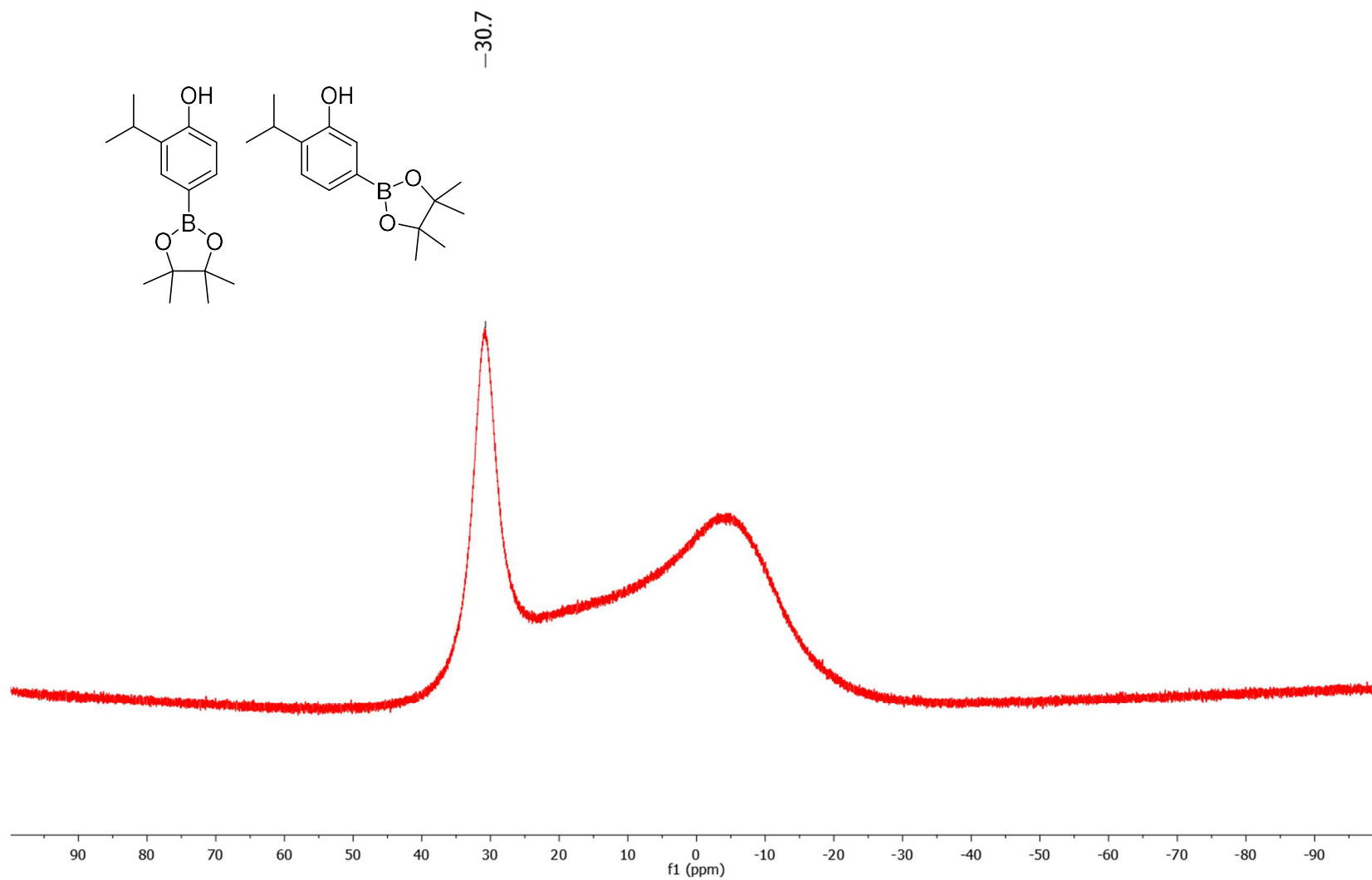


Figure 7-45 Conditions: 25 °C, 160 MHz, CDCl<sub>3</sub>

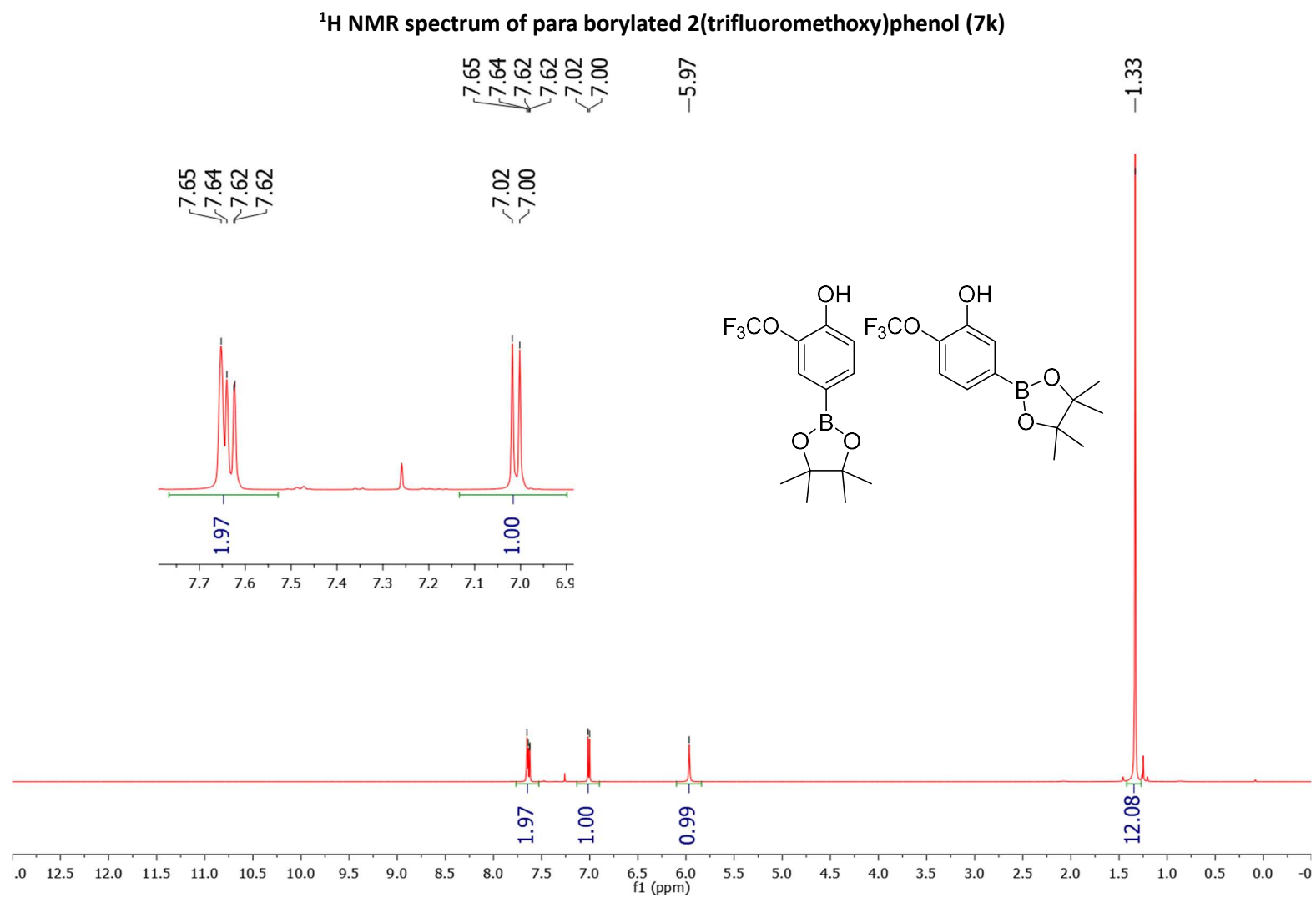


Figure 7-46 Conditions: 25 °C, 500 MHz,  $\text{CDCl}_3$

**$^{13}\text{C}$  NMR spectrum of para borylated 2-(trifluoromethoxy)phenol (7k)**

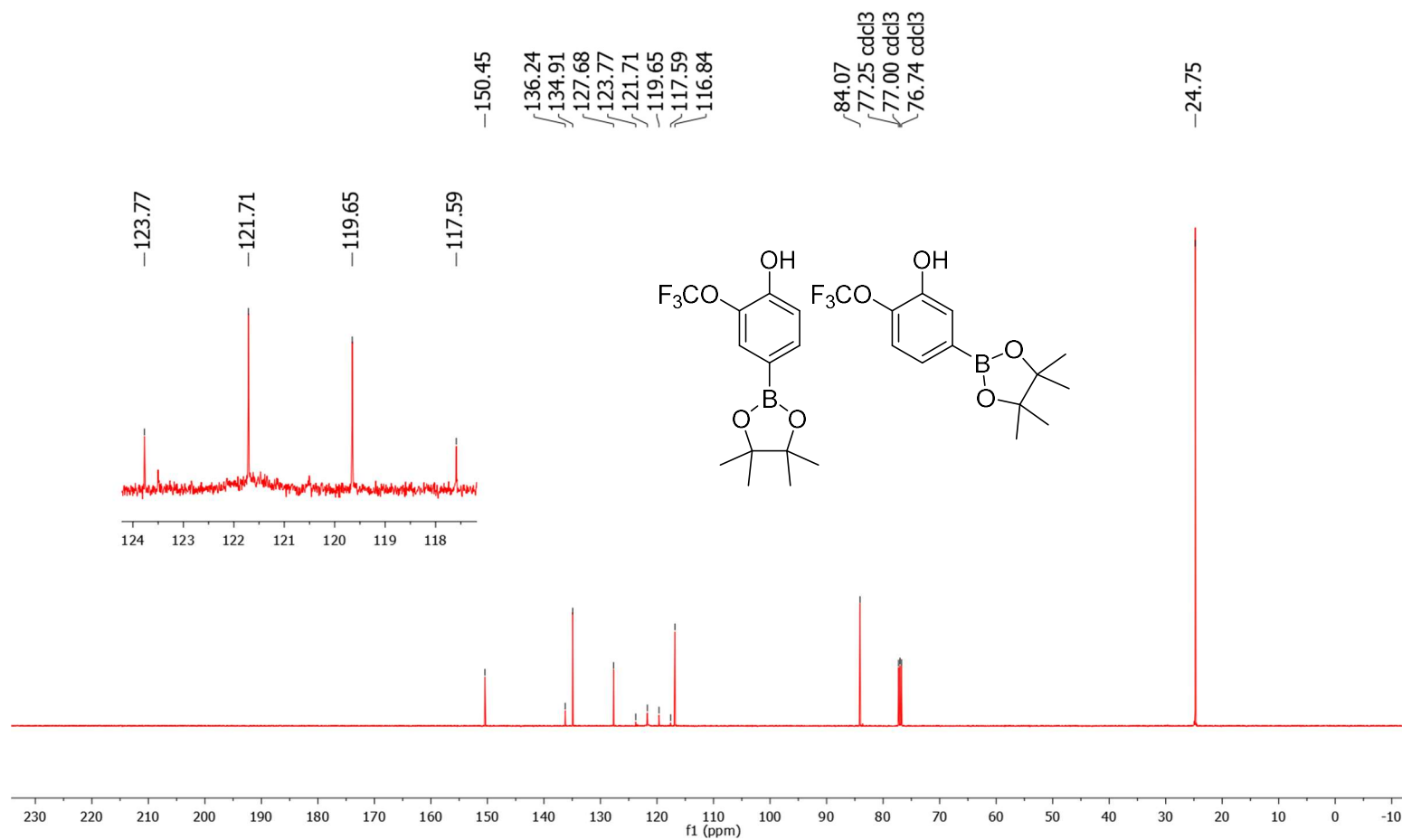


Figure 7-47 Conditions: 25 °C, 126 MHz,  $\text{CDCl}_3$



**$^{11}\text{B}$  NMR spectrum of para borylated 2-(trifluoromethoxy)phenol (7k)**

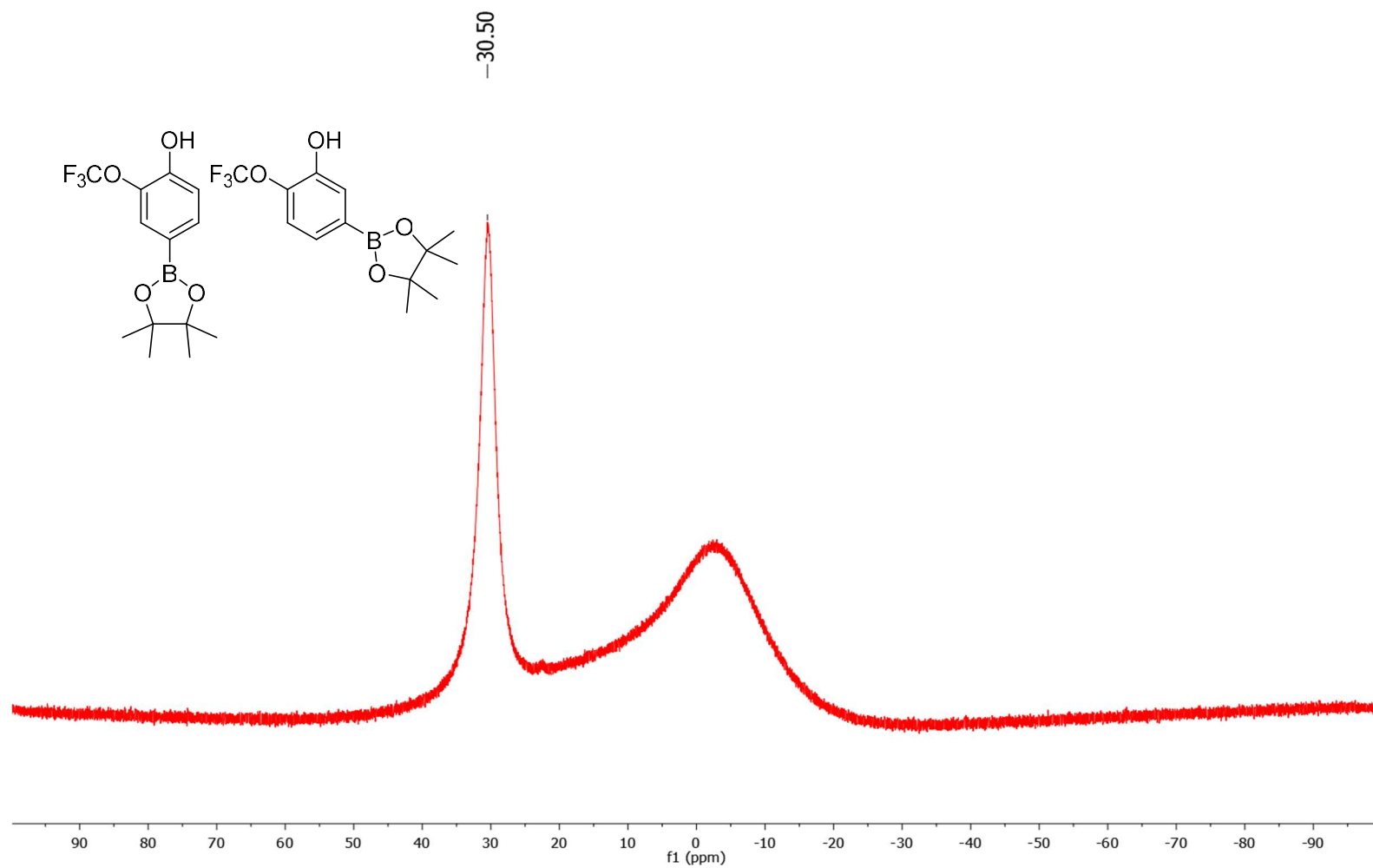


Figure 7-48 Conditions: 25 °C, 160 MHz,  $\text{CDCl}_3$

<sup>19</sup>F NMR spectrum of para borylated 2-(trifluoromethoxy)phenol (7k)

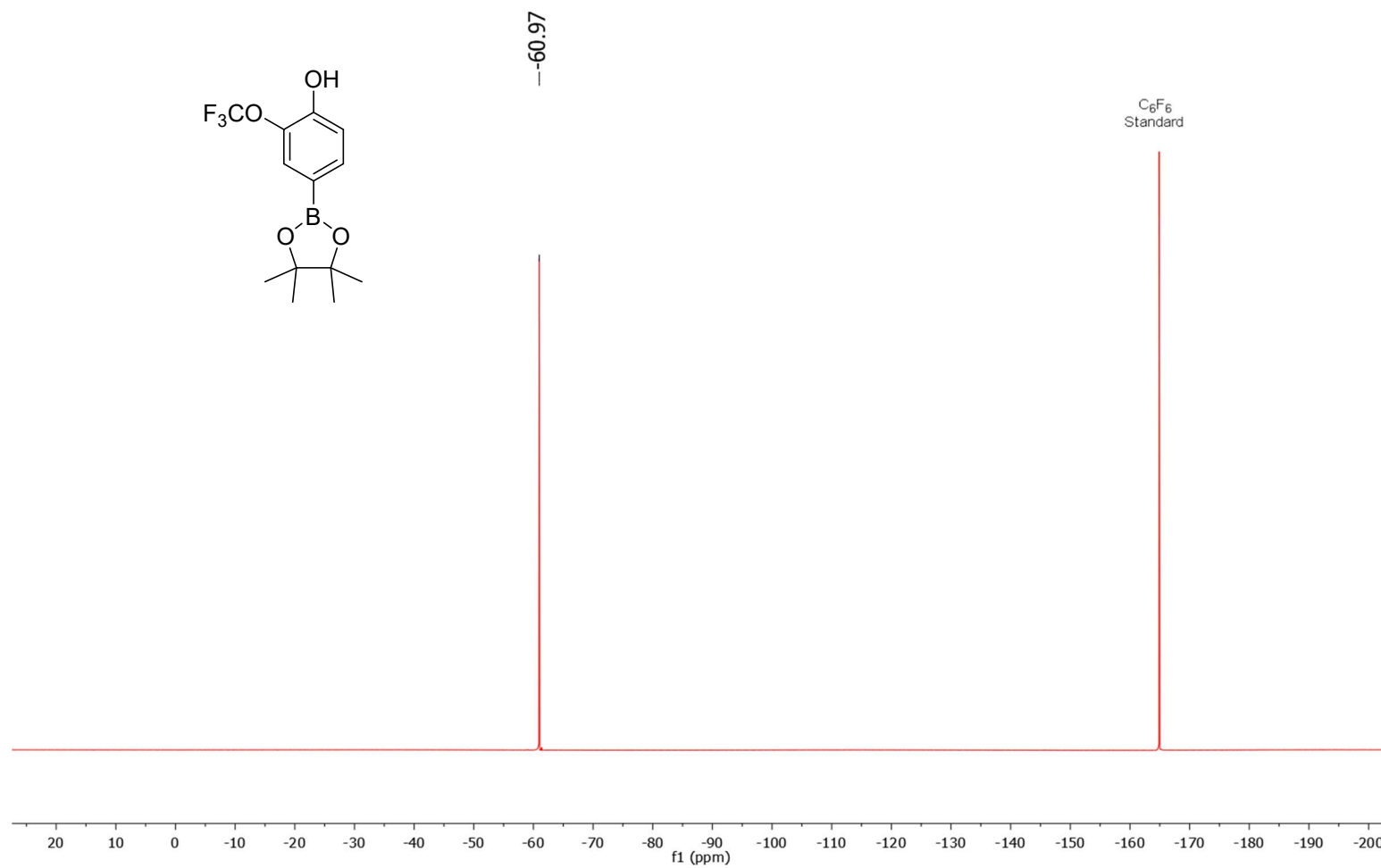


Figure7-49 Conditions: 25 °C, 470 MHz, CDCl<sub>3</sub>

<sup>1</sup>H NMR spectrum of reaction mixture of para borylation of tetrapropylammonium 2-bromobenzy sulfate (crude 10b)

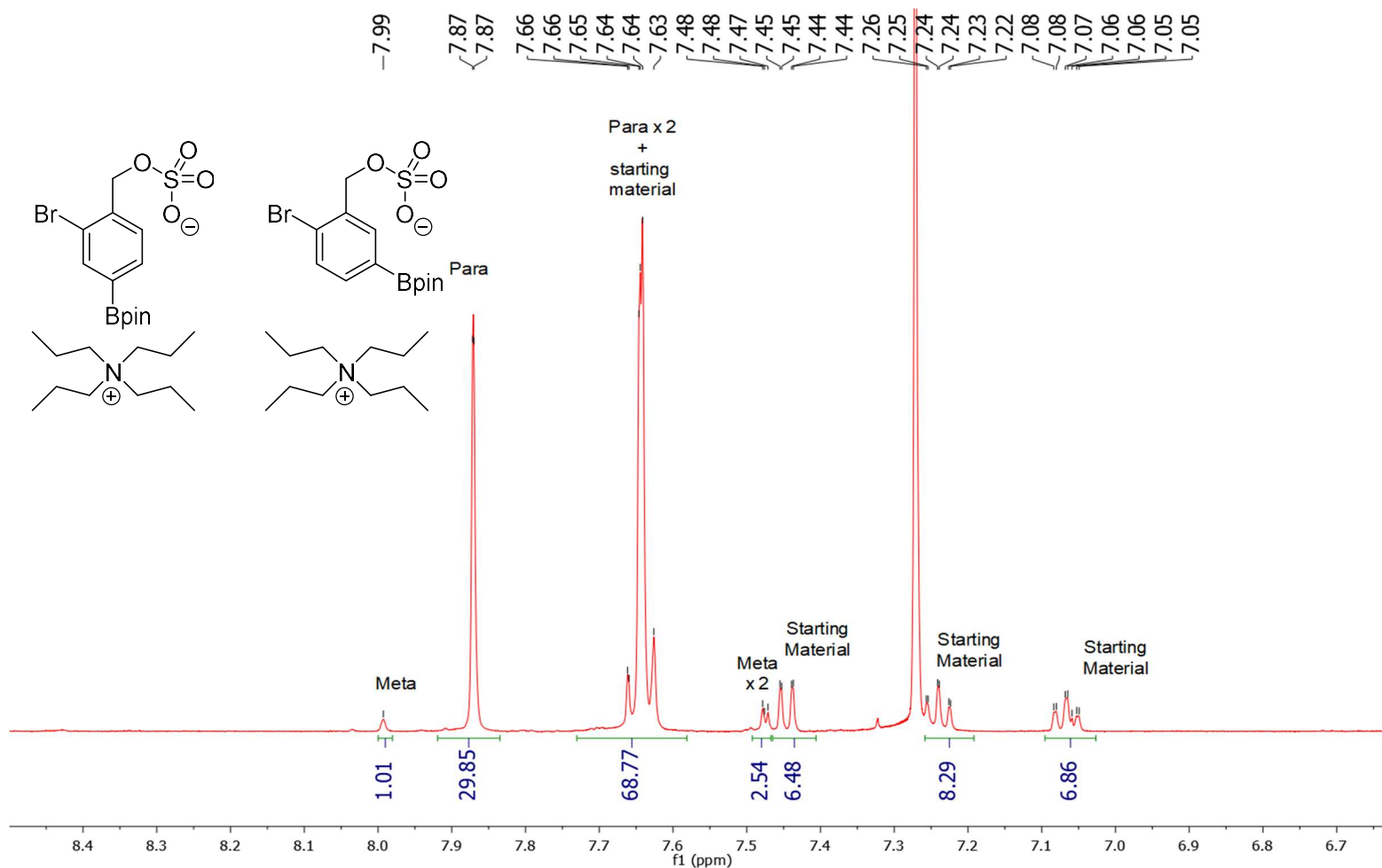


Figure 7-50 Conditions: 25 °C, 500 MHz, CDCl<sub>3</sub>

<sup>1</sup>H NMR spectrum of para borylated of 2-bromobenzylalcohol (11b)

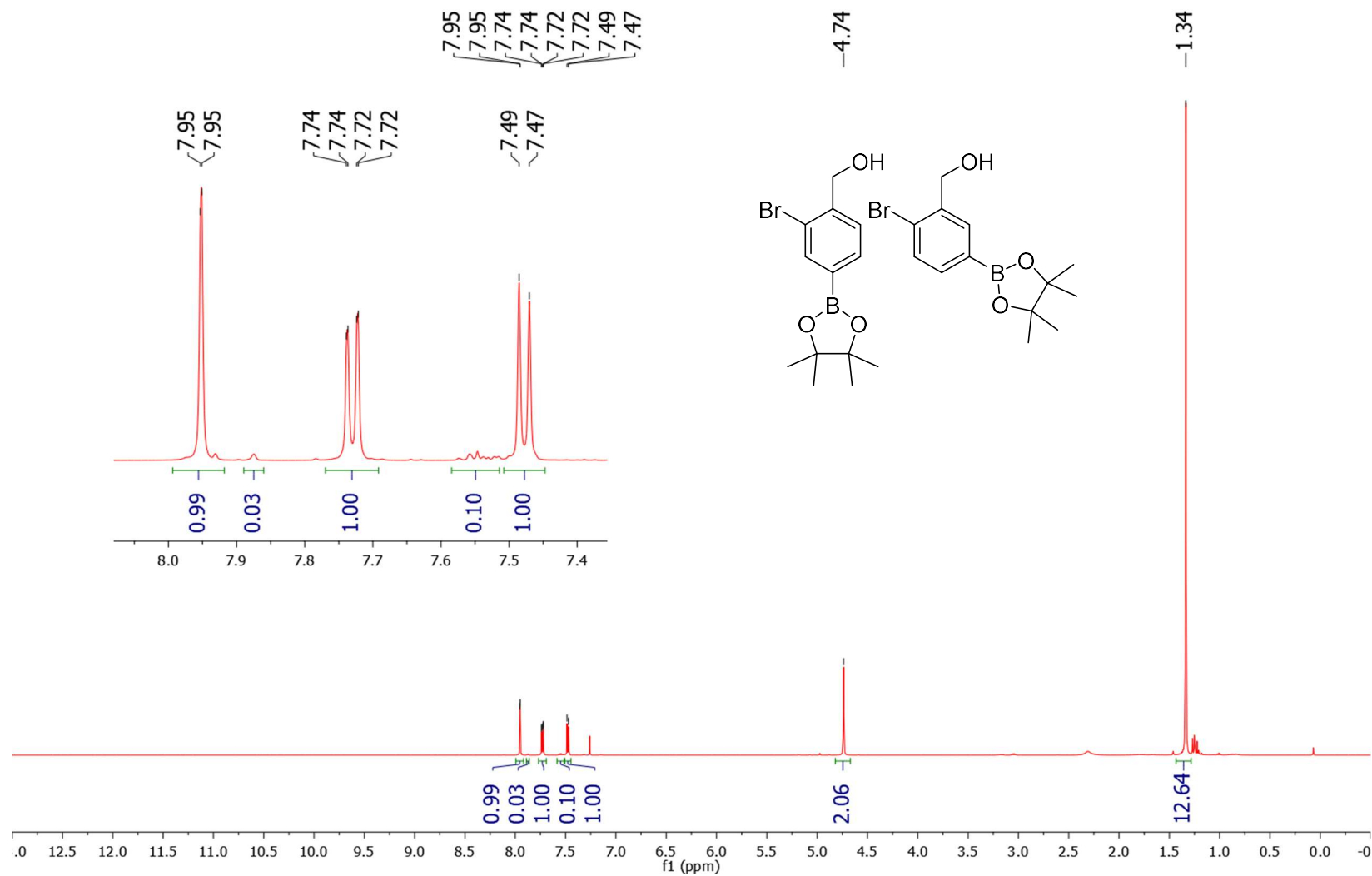


Figure7-51 Conditions: 25 °C, 500 MHz, CDCl<sub>3</sub>

<sup>13</sup>C NMR spectrum of para borylated 2-bromobenzylalcohol (11b)

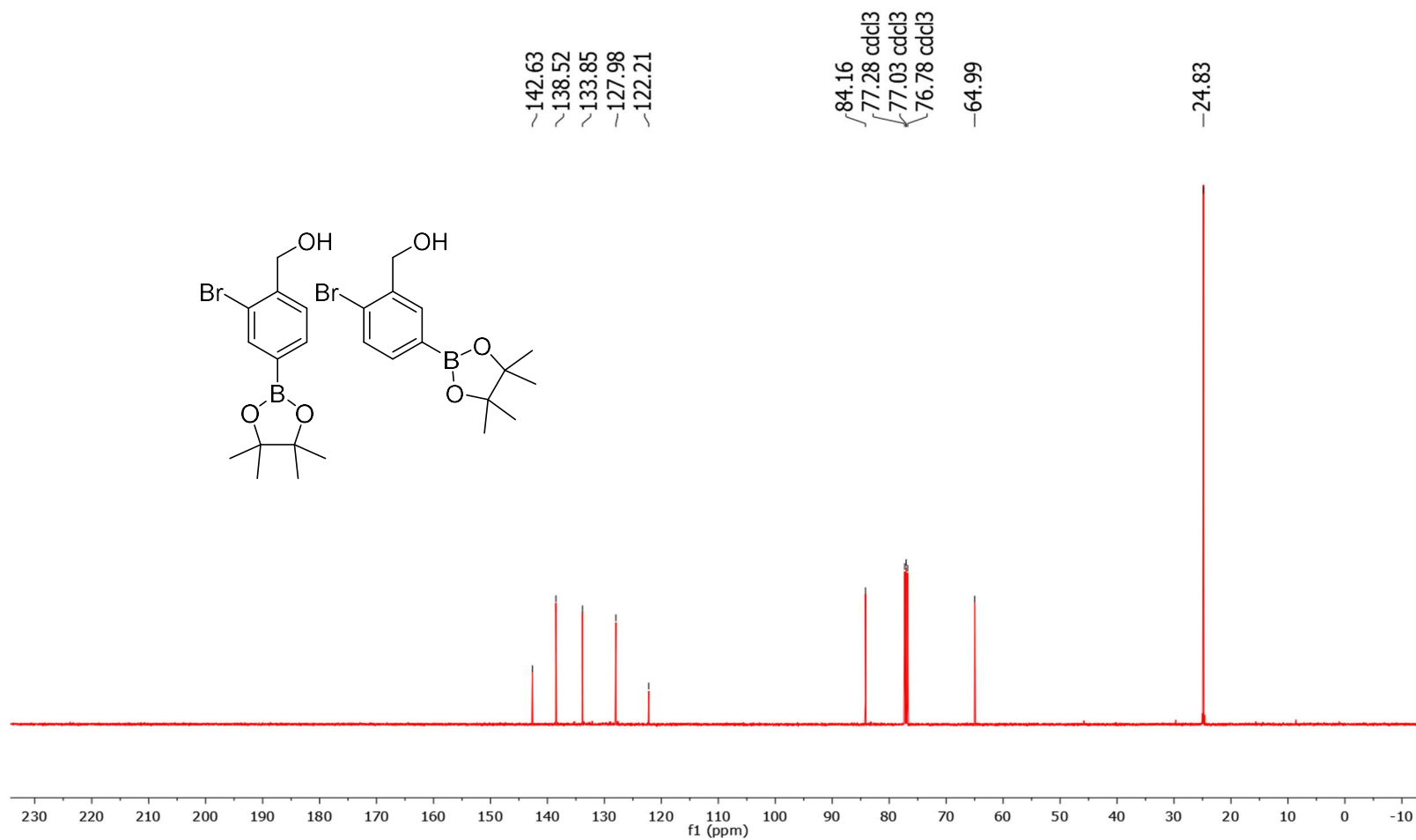


Figure 7-52 Conditions: 25 °C, 126 MHz, CDCl<sub>3</sub>

<sup>11</sup>B NMR spectrum of para borylated 2-bromobenzylalcohol (11b)

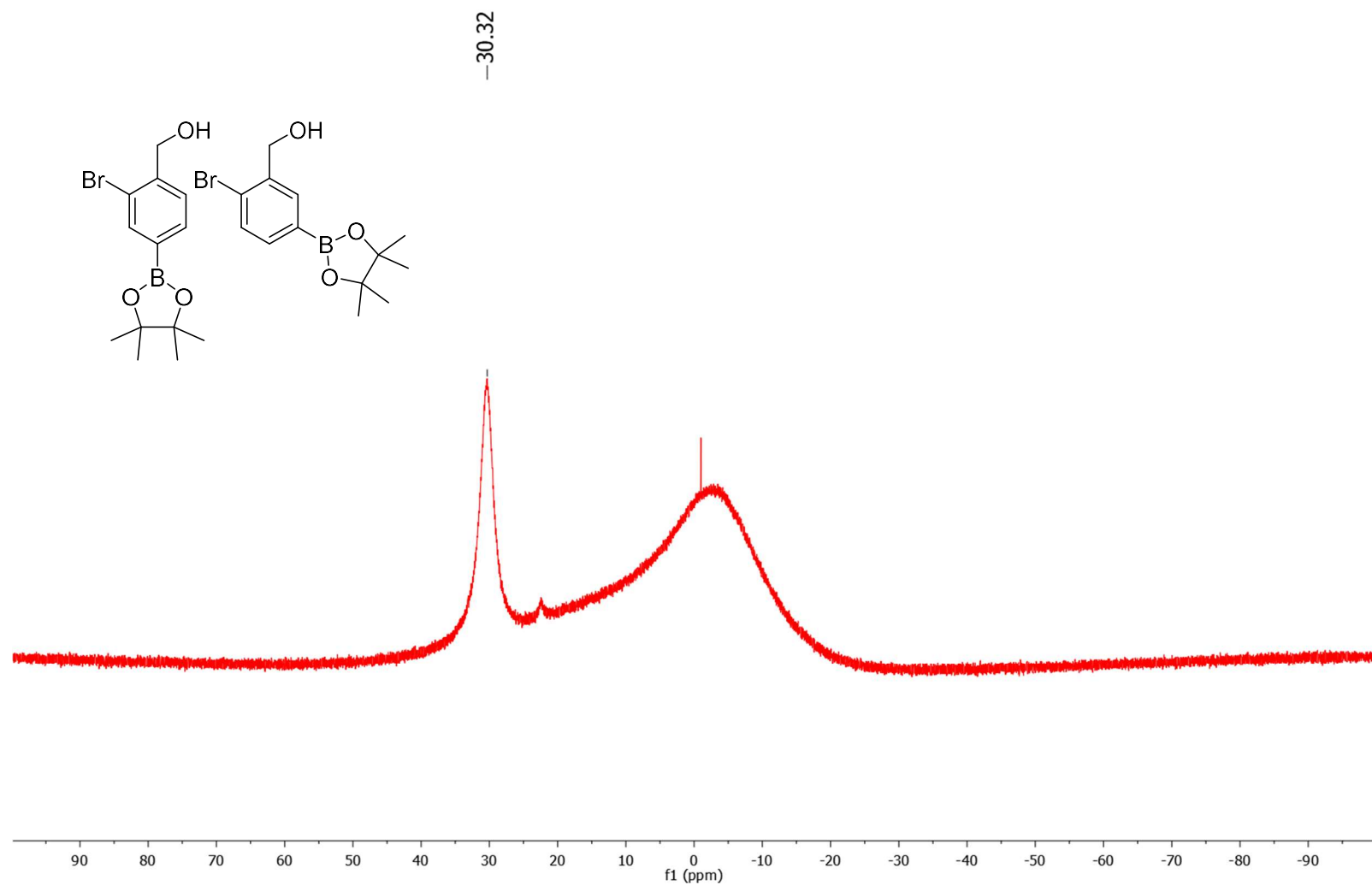


Figure 7-53 Conditions: 25 °C, 160 MHz, CDCl<sub>3</sub>

<sup>1</sup>H NMR spectrum of the reaction mixture of para borylation of 2-fluorobenzylsulfate (10g)

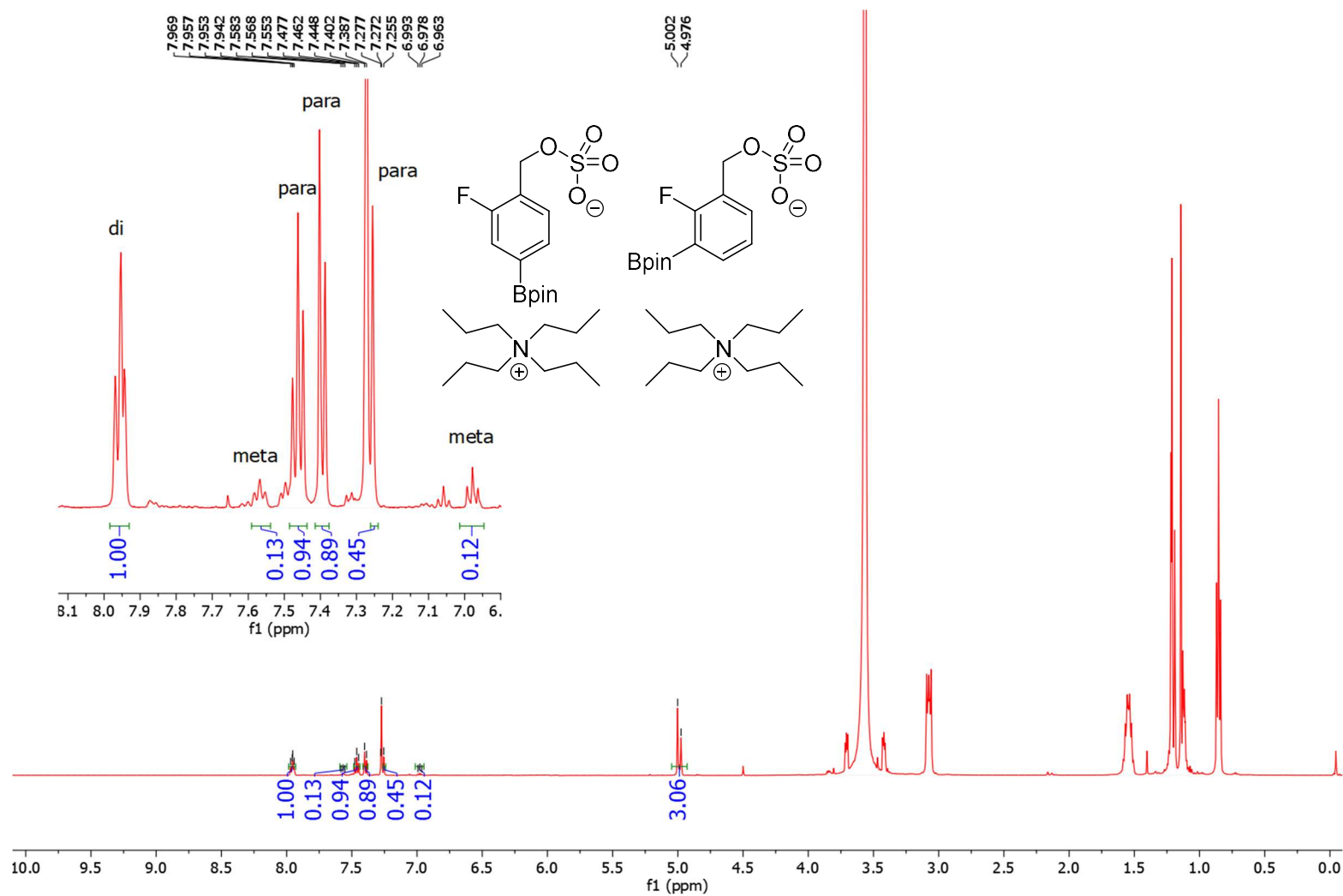


Figure 7-54 Conditions: 25 °C, 500 MHz, CDCl<sub>3</sub>

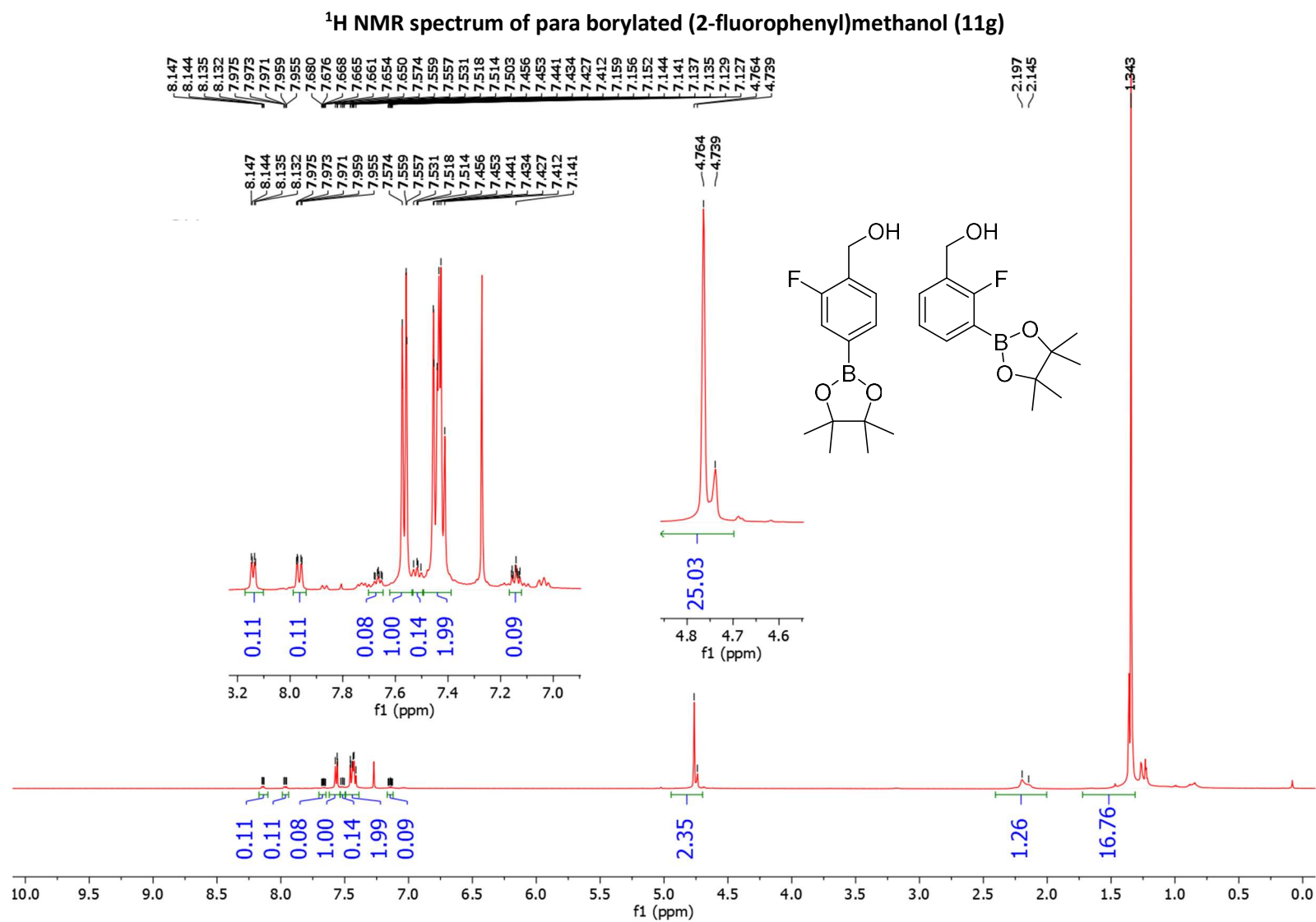


Figure 7-55 Conditions: 25 °C, 500 MHz,  $\text{CDCl}_3$



<sup>13</sup>C NMR spectrum of para borylated (2-fluorophenyl)methanol (11g)

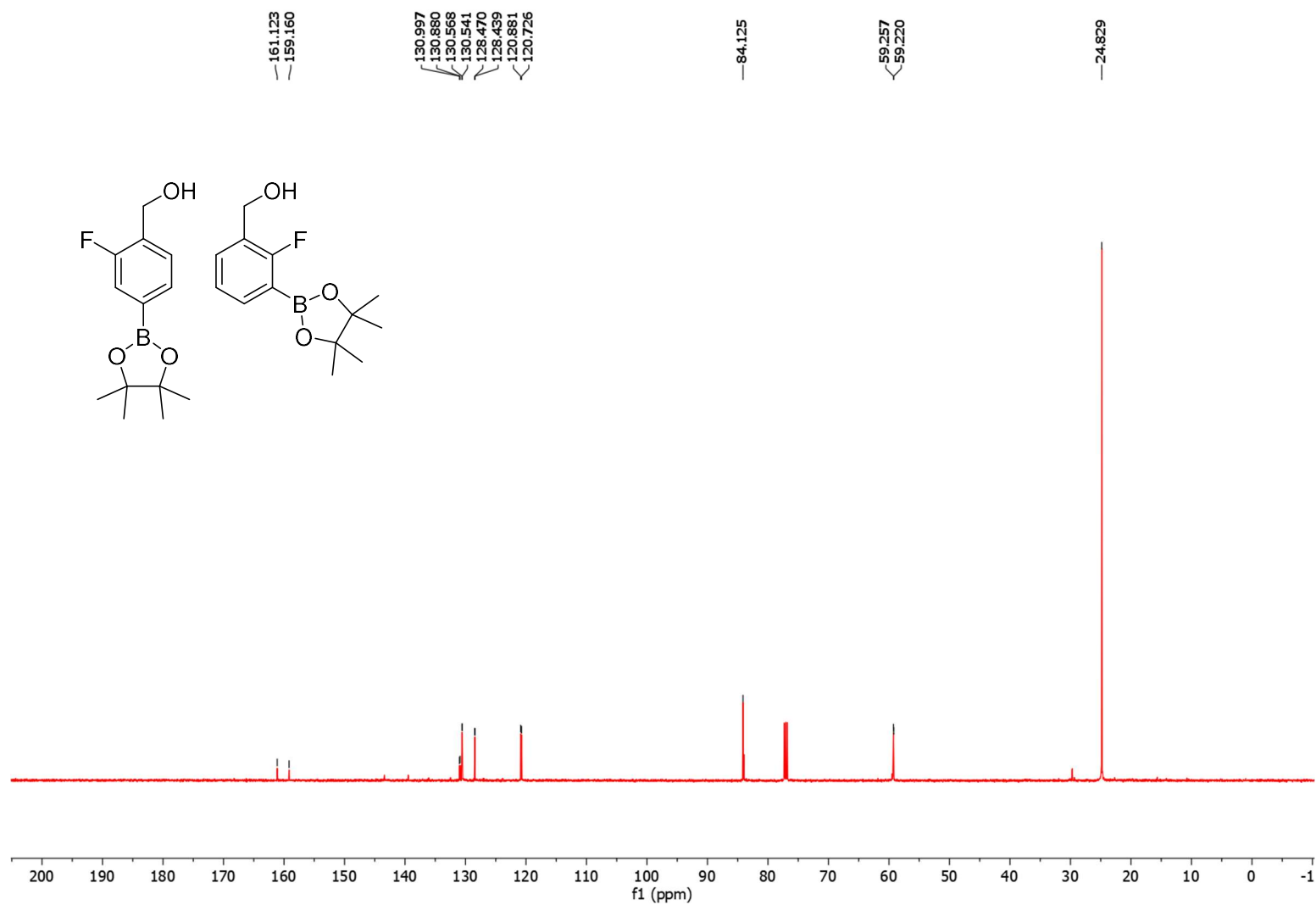


Figure 7-56 Conditions: 25 °C, 126 MHz, CDCl<sub>3</sub>

<sup>11</sup>B NMR spectrum of para borylated (2-fluorophenyl)methanol (11g)

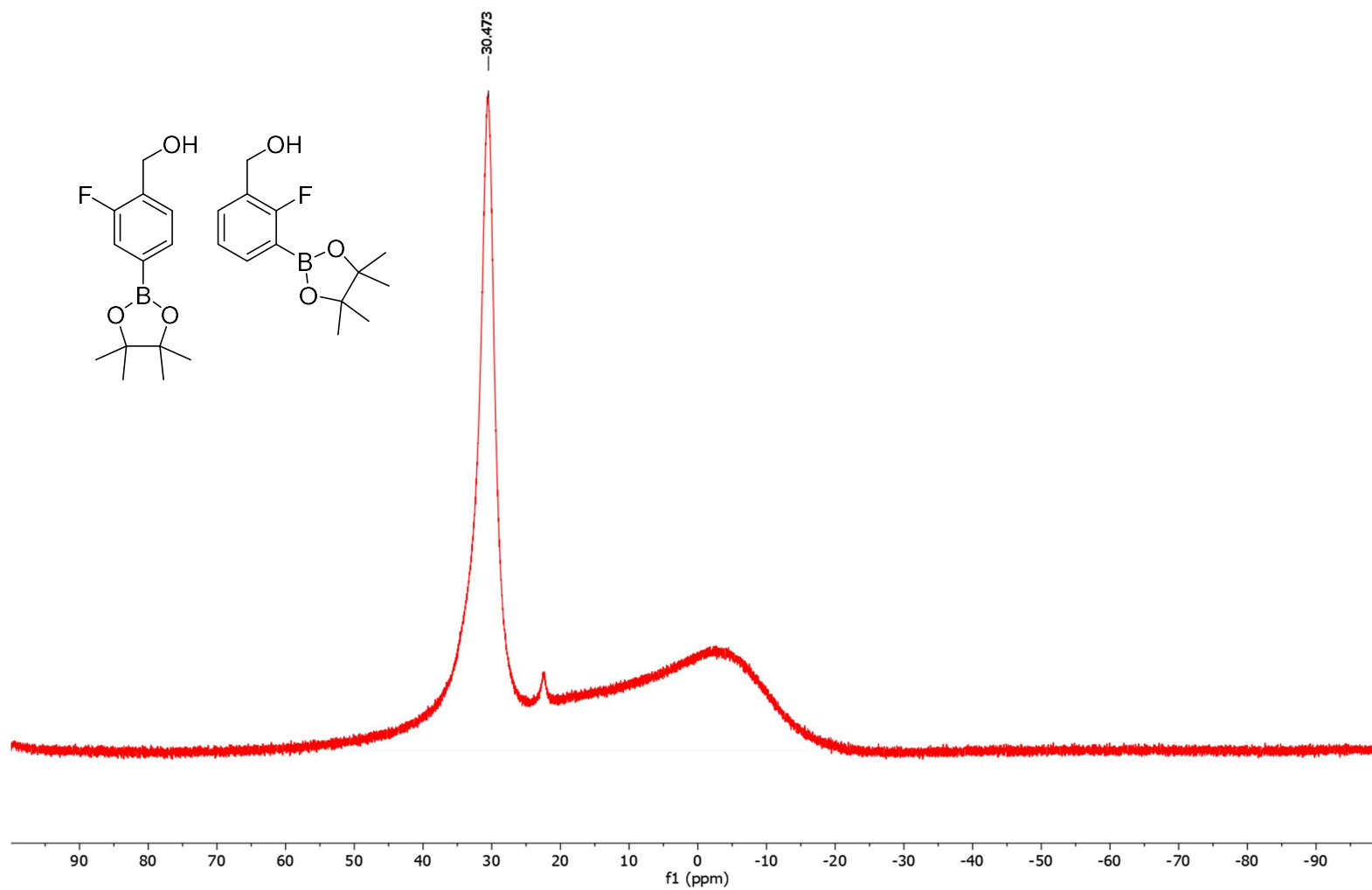


Figure 7-57 Conditions: 25 °C, 160 MHz, CDCl<sub>3</sub>

<sup>19</sup>F NMR spectrum of para borylated (2-fluorophenyl)methanol (11g)

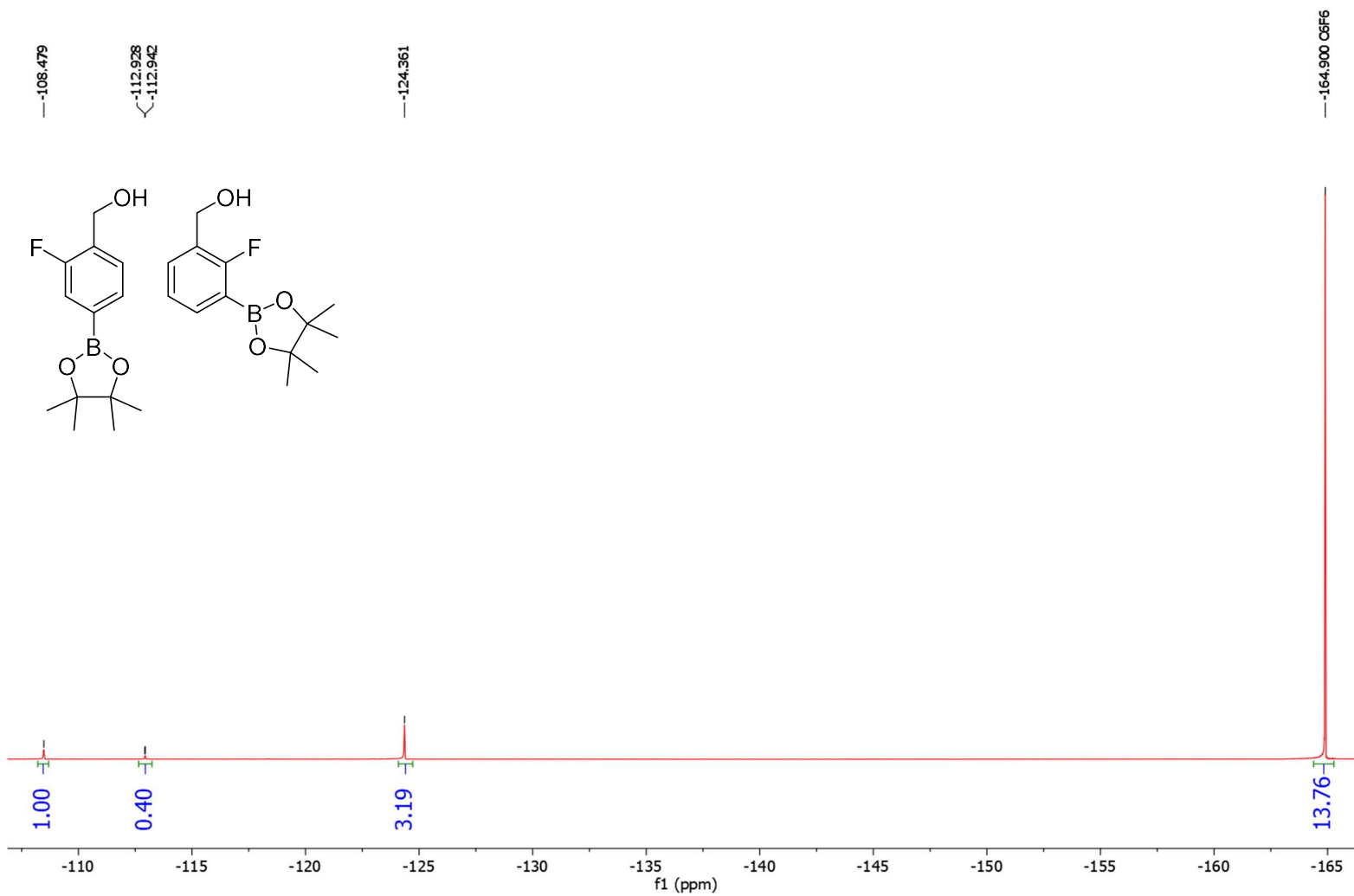


Figure 7-58 Conditions: 25 °C, 470 MHz, CDCl<sub>3</sub>

## Chapter 4 NMR Spectra

<sup>1</sup>H NMR Spectra of the Crude Reaction Mixture of the Borylation of 2-chloro-N-methylaniline (14a)

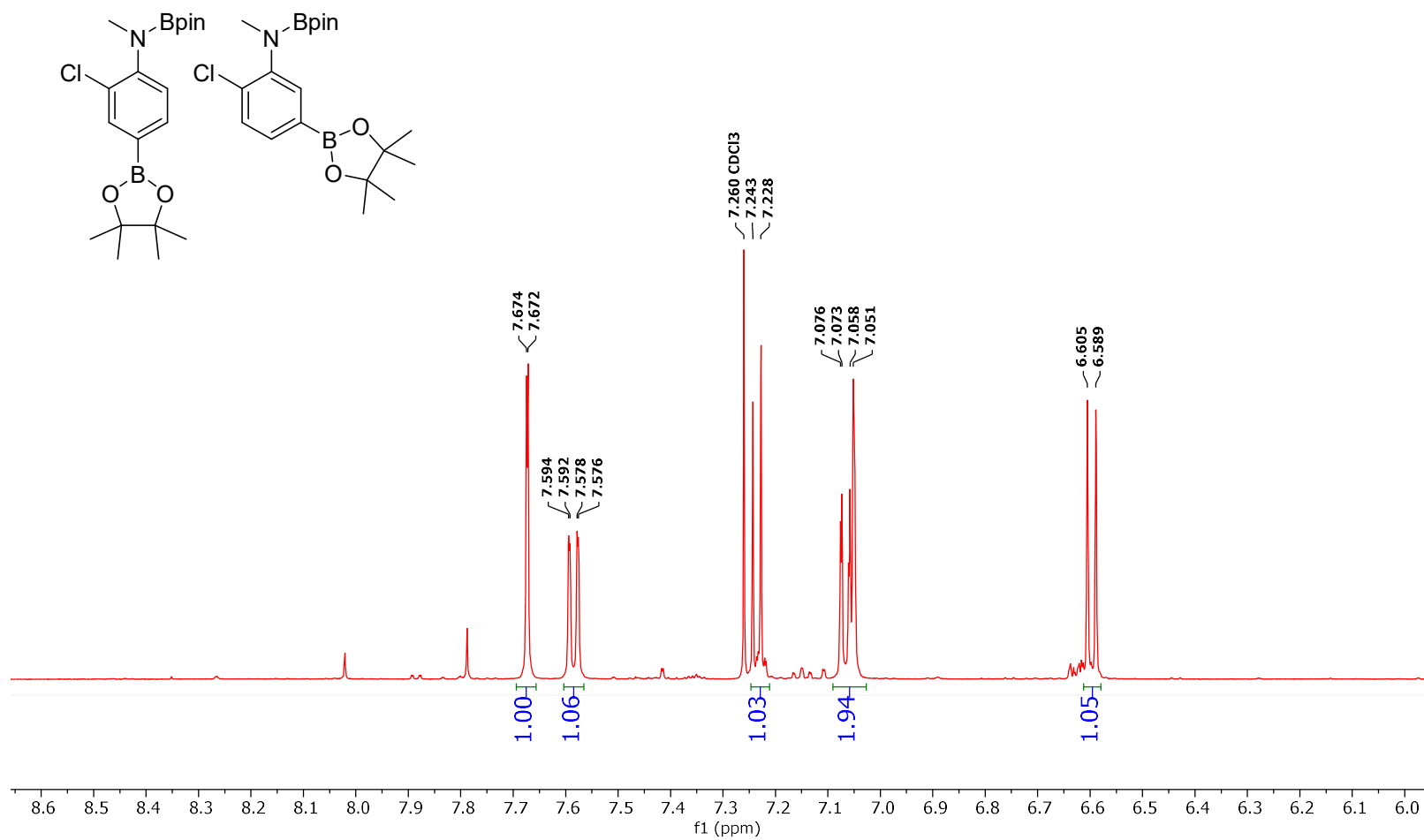


Figure 8-1 Conditions: 25 °C, 500 MHz, CDCl<sub>3</sub>

**<sup>1</sup>H NMR Spectra of the Unselective Borylation of 2-chloro-N-methylaniline (14a) Fraction 1**

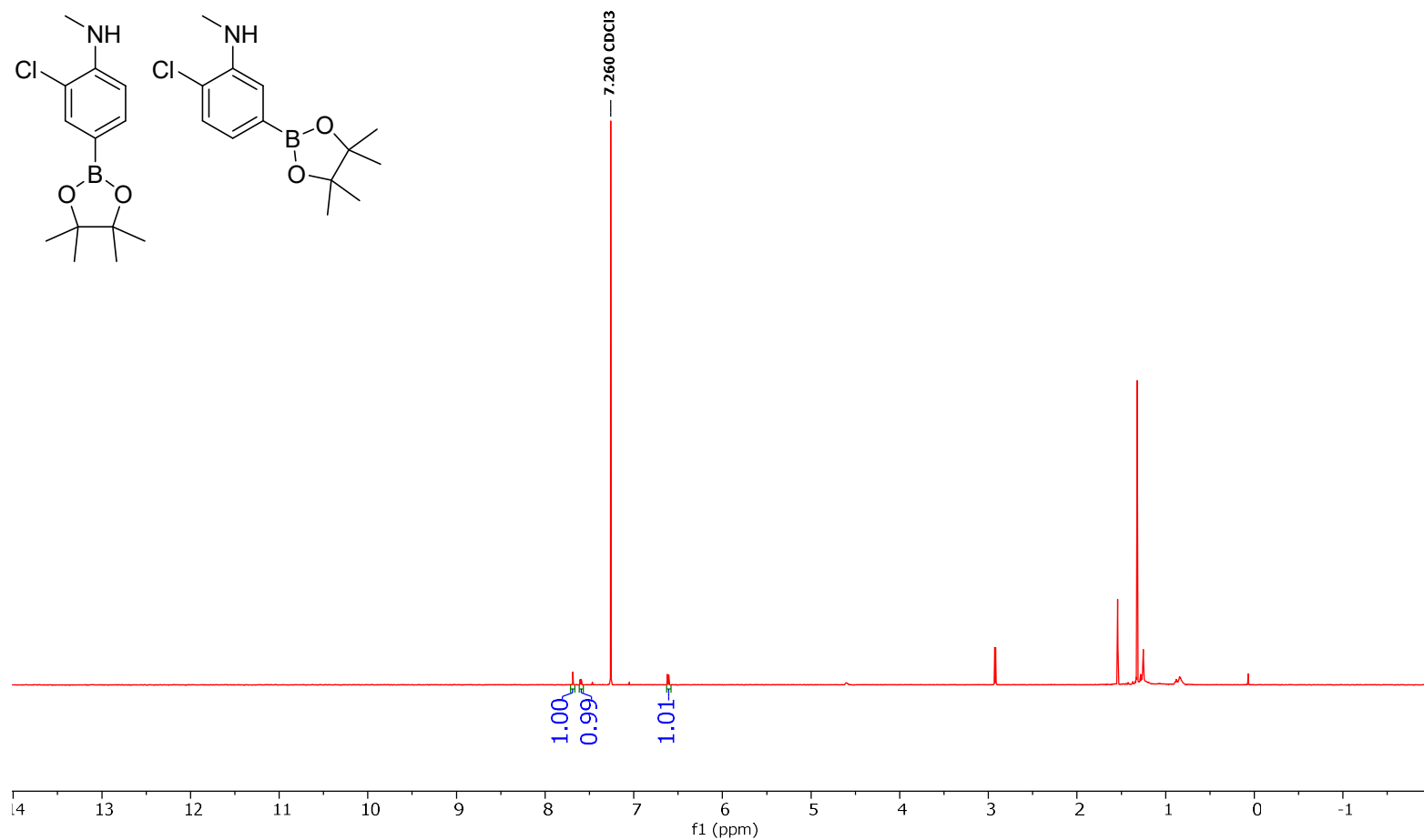


Figure 8-2 Conditions: 25 °C, 500 MHz, CDCl<sub>3</sub>

<sup>1</sup>H NMR Spectra of the Unselective Borylation of 2-chloro-N-methylaniline (14a) Fraction 2

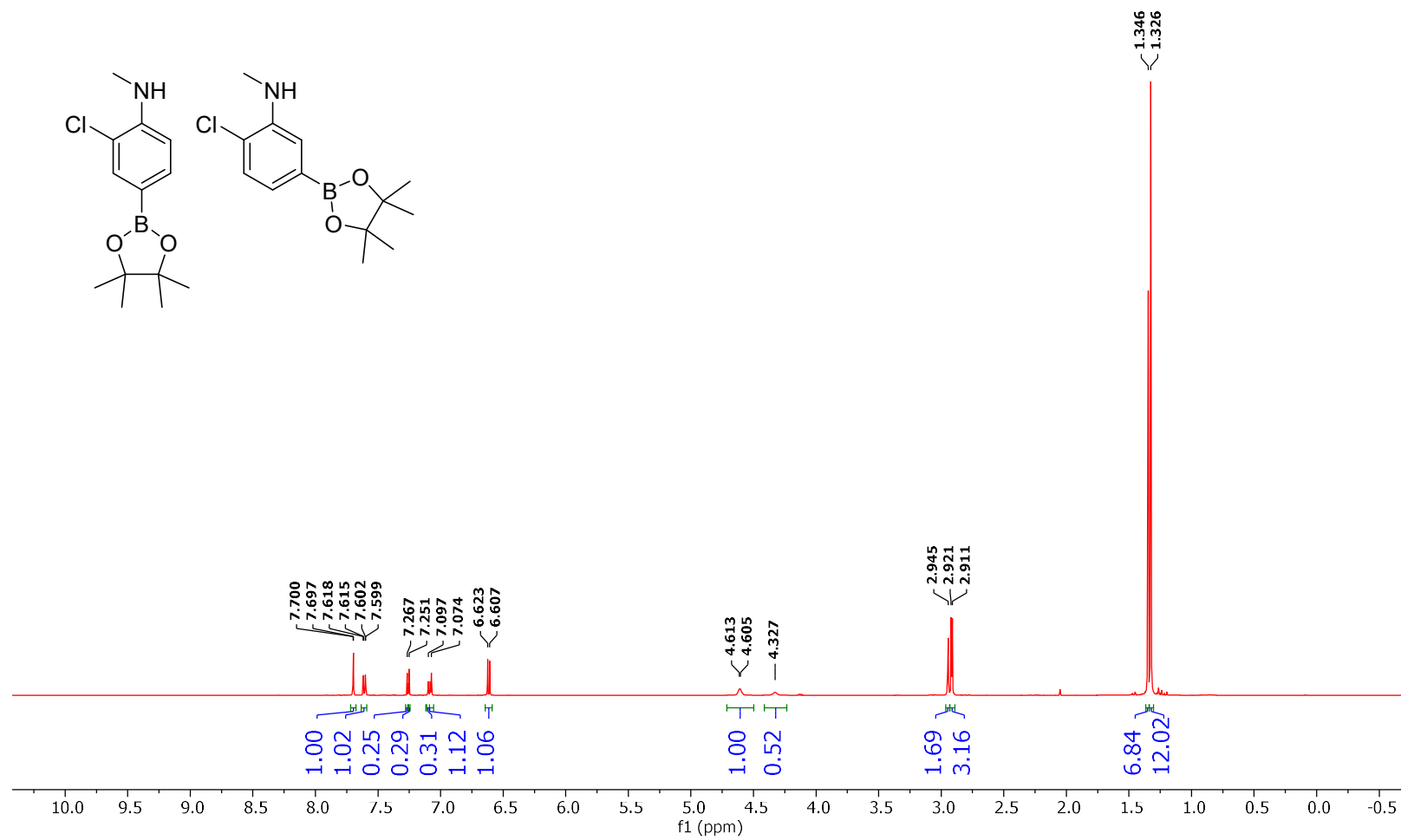


Figure 8-3 Conditions: 25 °C, 500 MHz, CDCl<sub>3</sub>

<sup>13</sup>C NMR Spectra of the Unselective Borylation of 2-chloro-N-methylaniline (14a) Fraction 2

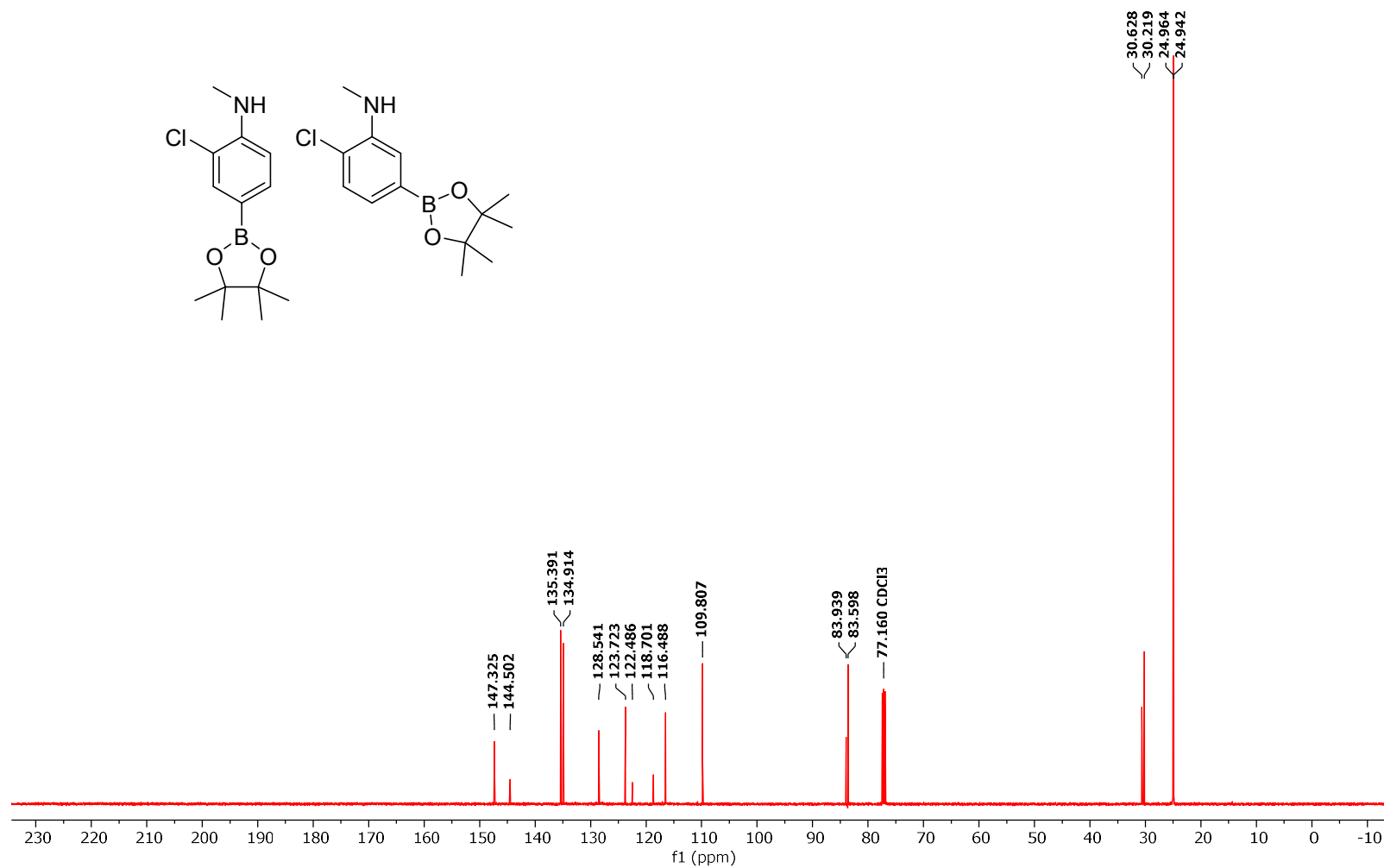


Figure 8-4 Conditions: 25 °C, 126 MHz, CDCl<sub>3</sub>



**$^{11}\text{B}$  NMR Spectra of the Unselective Borylation of 2-chloro-N-methylaniline (14a) Fraction 2**

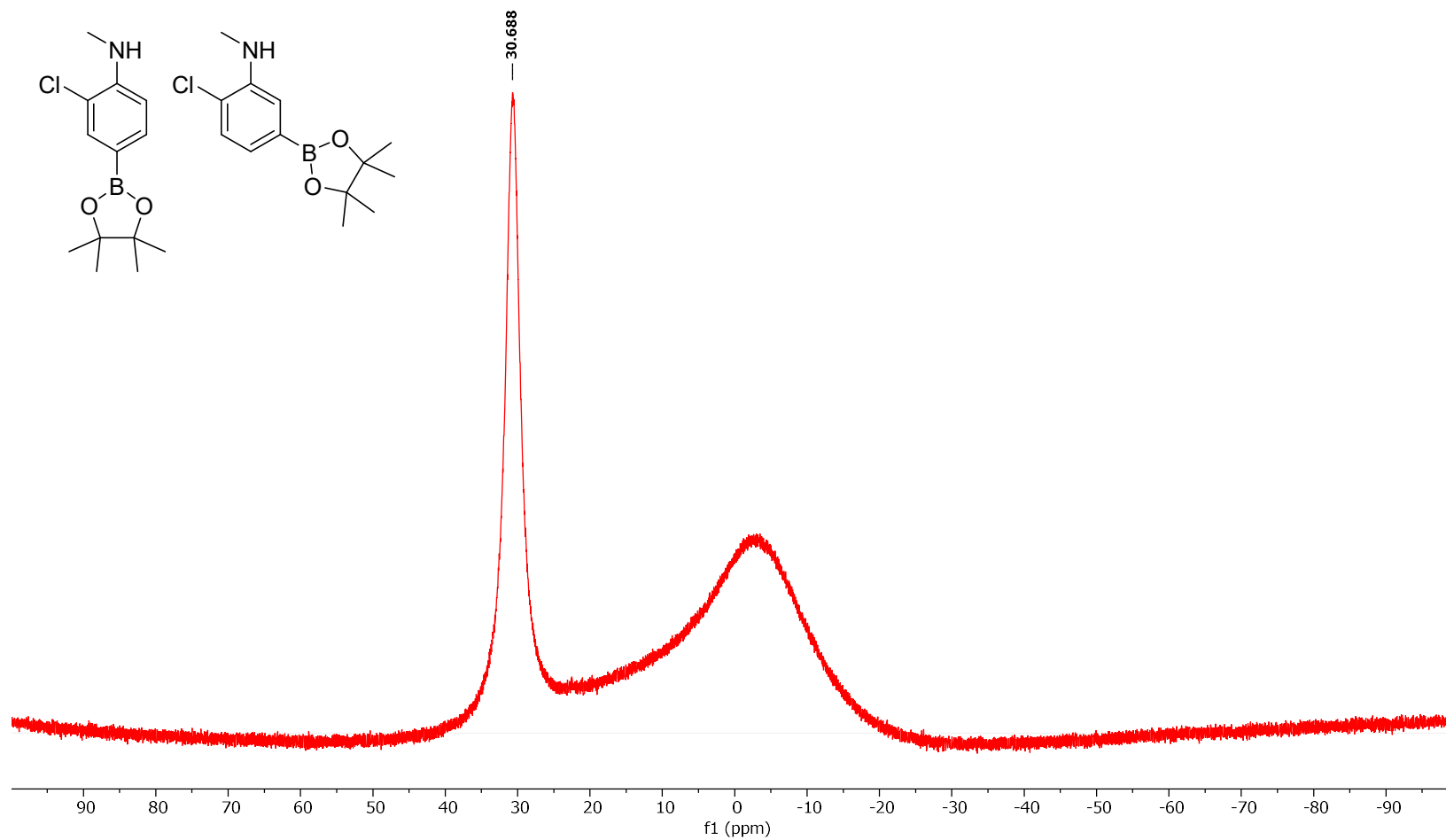


Figure 8-5 Conditions: 25 °C, 160 MHz,  $\text{CDCl}_3$

<sup>1</sup>H NMR Spectra of the Unselective Borylation of 2-chloro-N-methylaniline (14a) Fraction 3

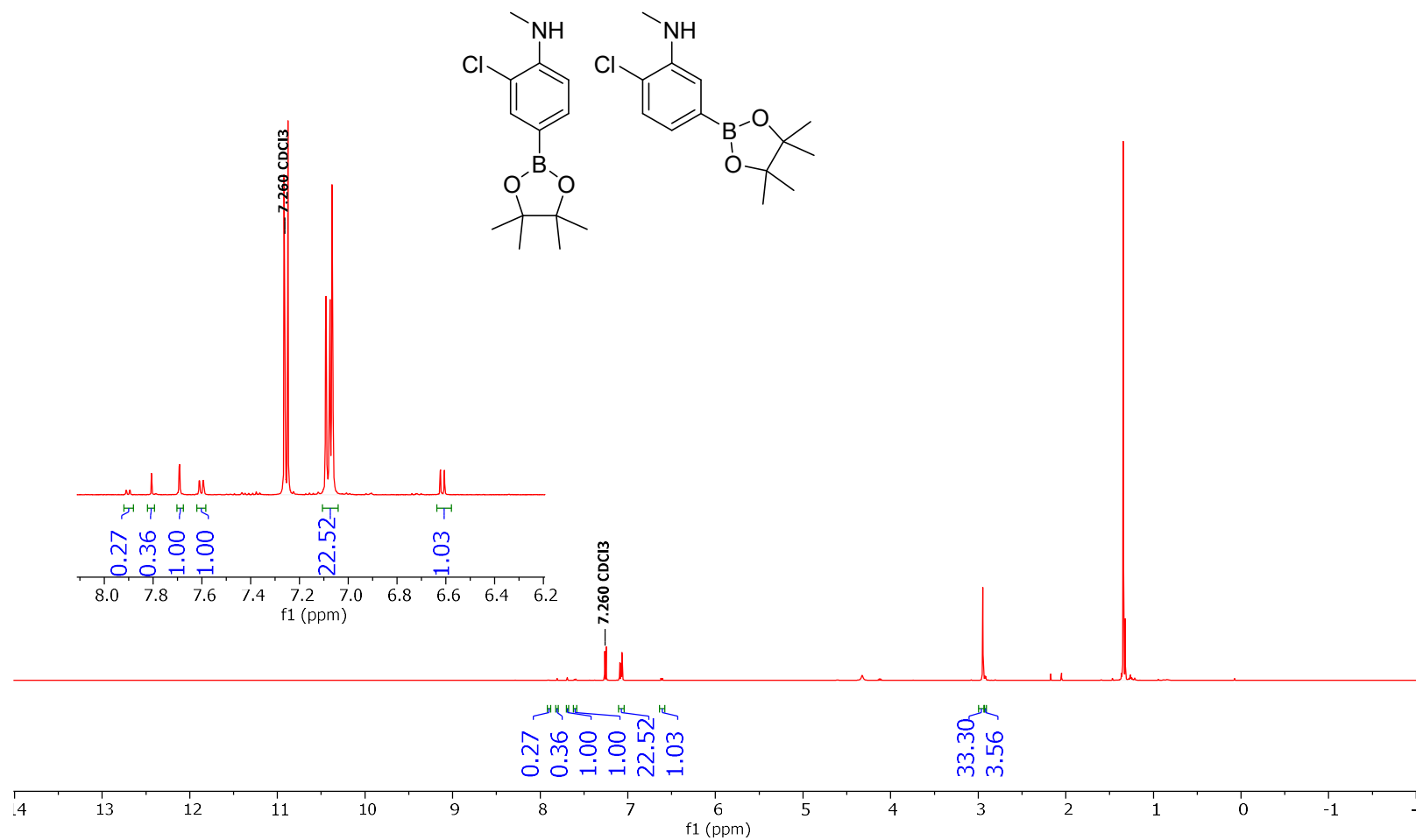


Figure 8-6 Conditions: 25 °C, 500 MHz, CDCl<sub>3</sub>

<sup>13</sup>C NMR Spectra of the Unselective Borylation of 2-chloro-N-methylaniline (14a) Fraction 3

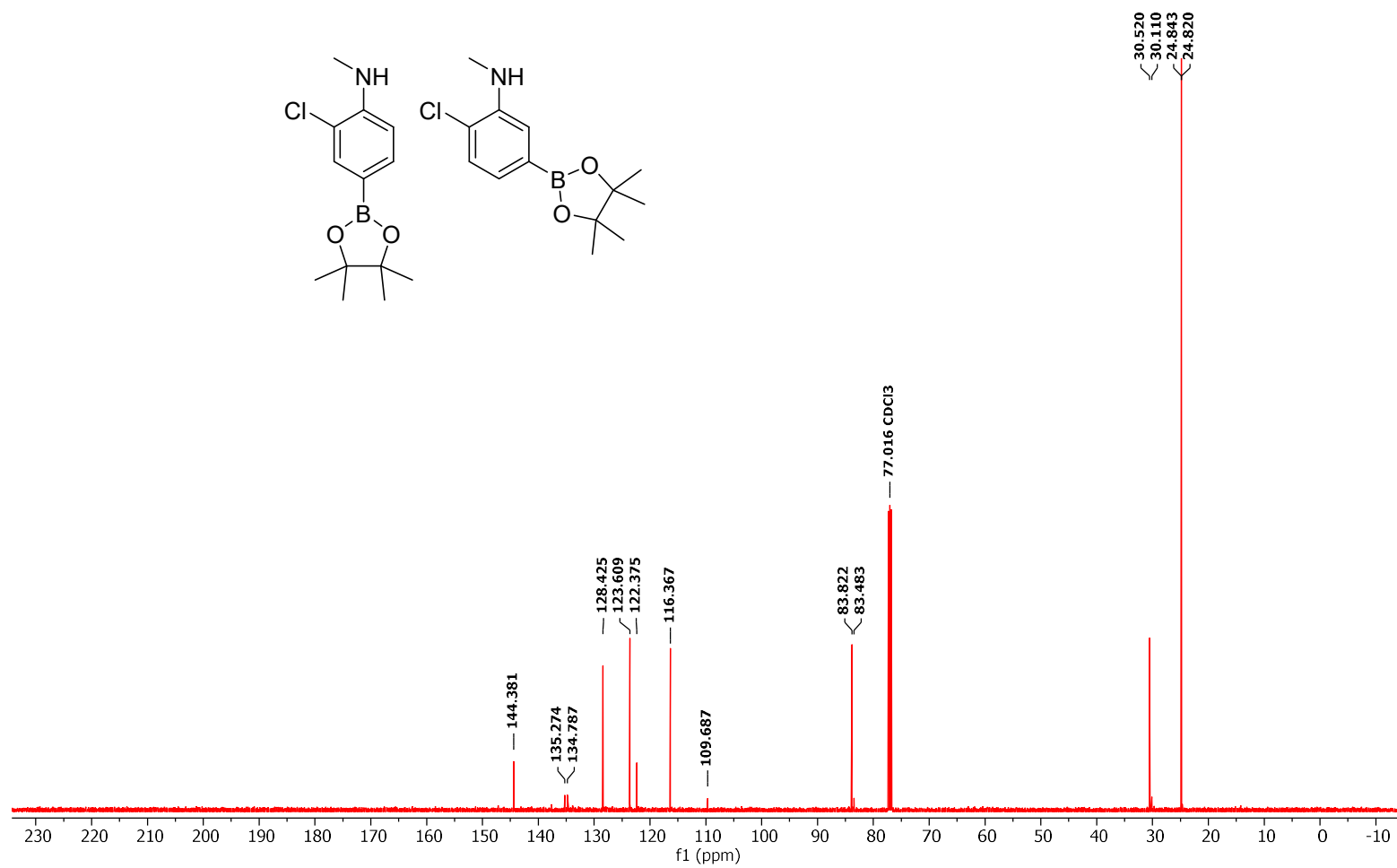


Figure 8-7 Conditions: 25 °C, 126 MHz, CDCl<sub>3</sub>

**$^{11}\text{B}$  NMR Spectra of the Unselective Borylation of 2-chloro-N-methylaniline (14a) Fraction 3**

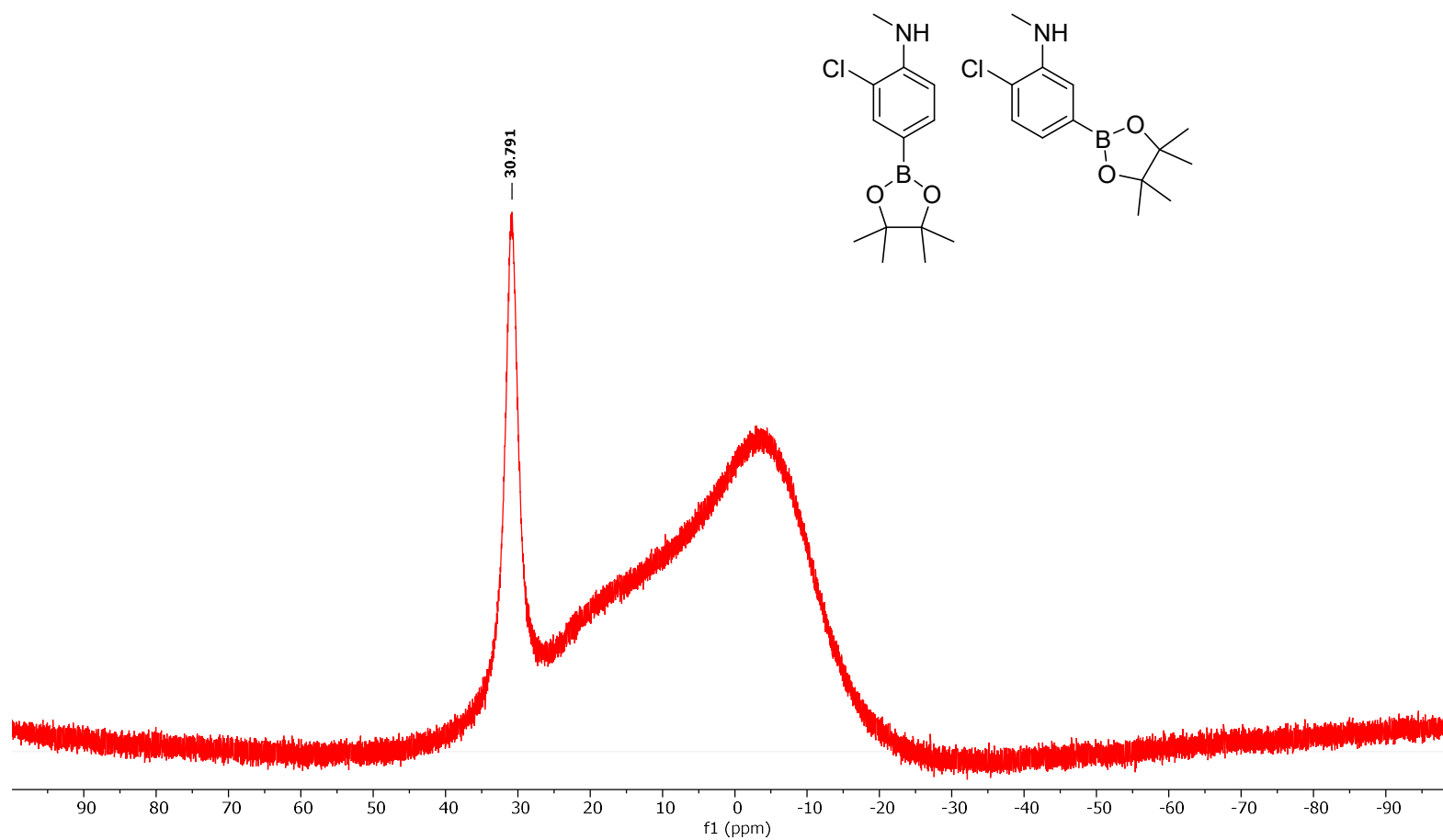


Figure 8-8 Conditions: 25 °C, 160 MHz,  $\text{CDCl}_3$

<sup>1</sup>H NMR Spectra of the Unselective Borylation of 2-chloro-N-methylaniline (14a) Fraction 4

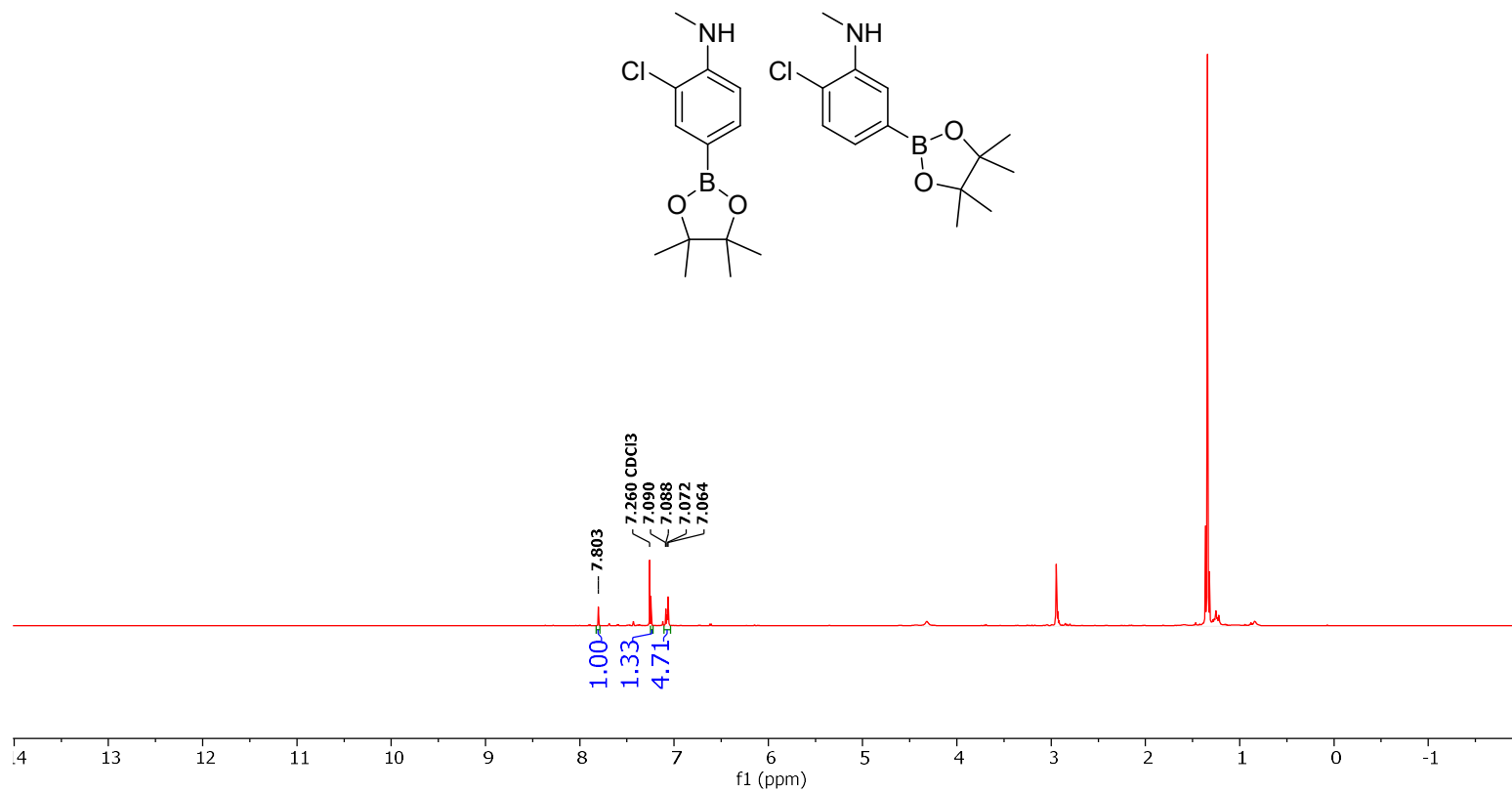


Figure 8-9 Conditions: 25 °C, 500 MHz, CDCl<sub>3</sub>

<sup>13</sup>C NMR Spectra of the Unselective Borylation of 2-chloro-N-methylaniline (14a) Fraction 4

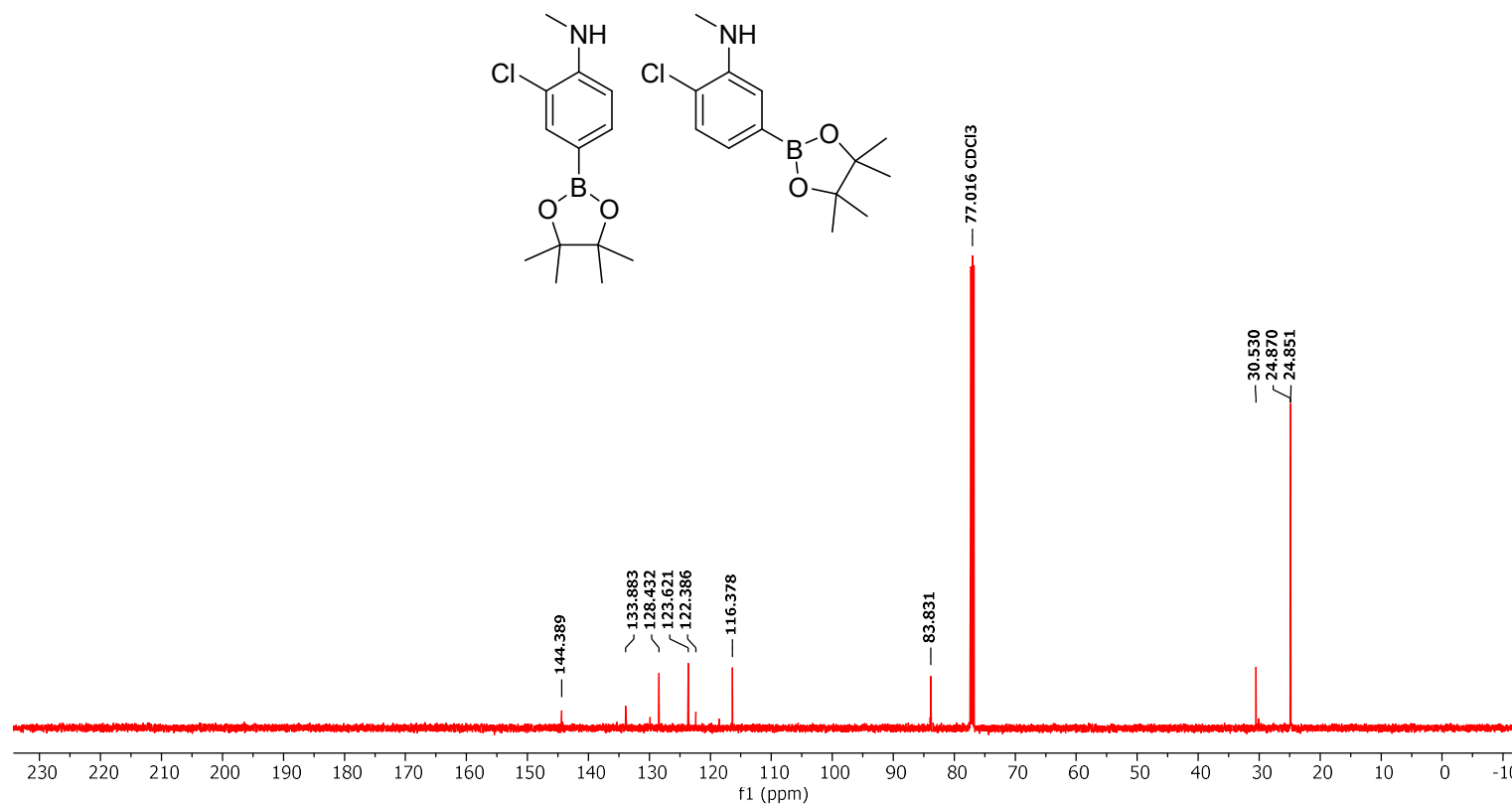
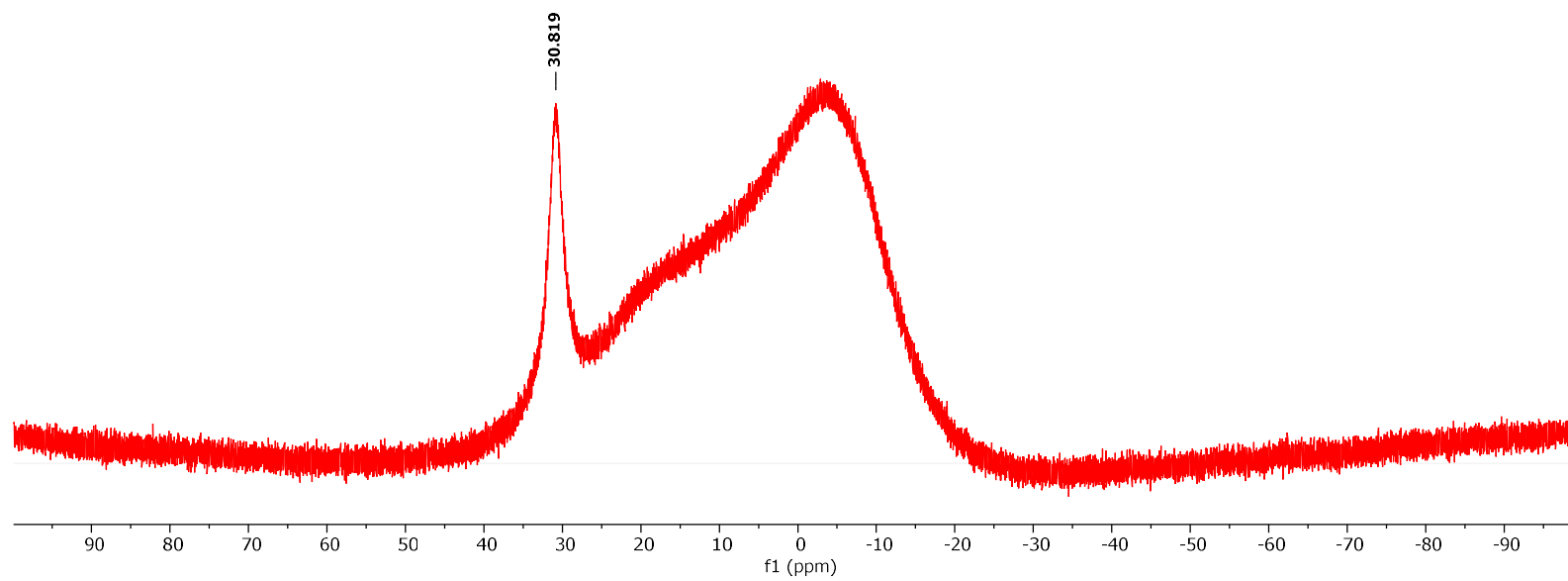
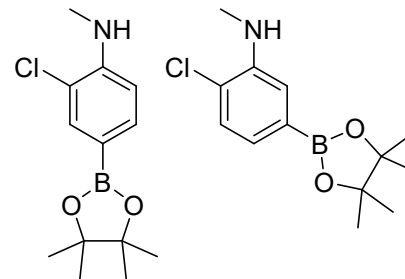


Figure 8-10 Conditions: 25 °C, 126 MHz, CDCl<sub>3</sub>

**$^{11}\text{B}$  NMR Spectra of the Unselective Borylation of 2-chloro-N-methylaniline (14a) Fraction 4**



8-11 Conditions: 25 °C, 160 MHz,  $\text{CDCl}_3$

**<sup>1</sup>H NMR of the Crude para borylated 1,2,3,4-tetrahydroquinoline (14d)**

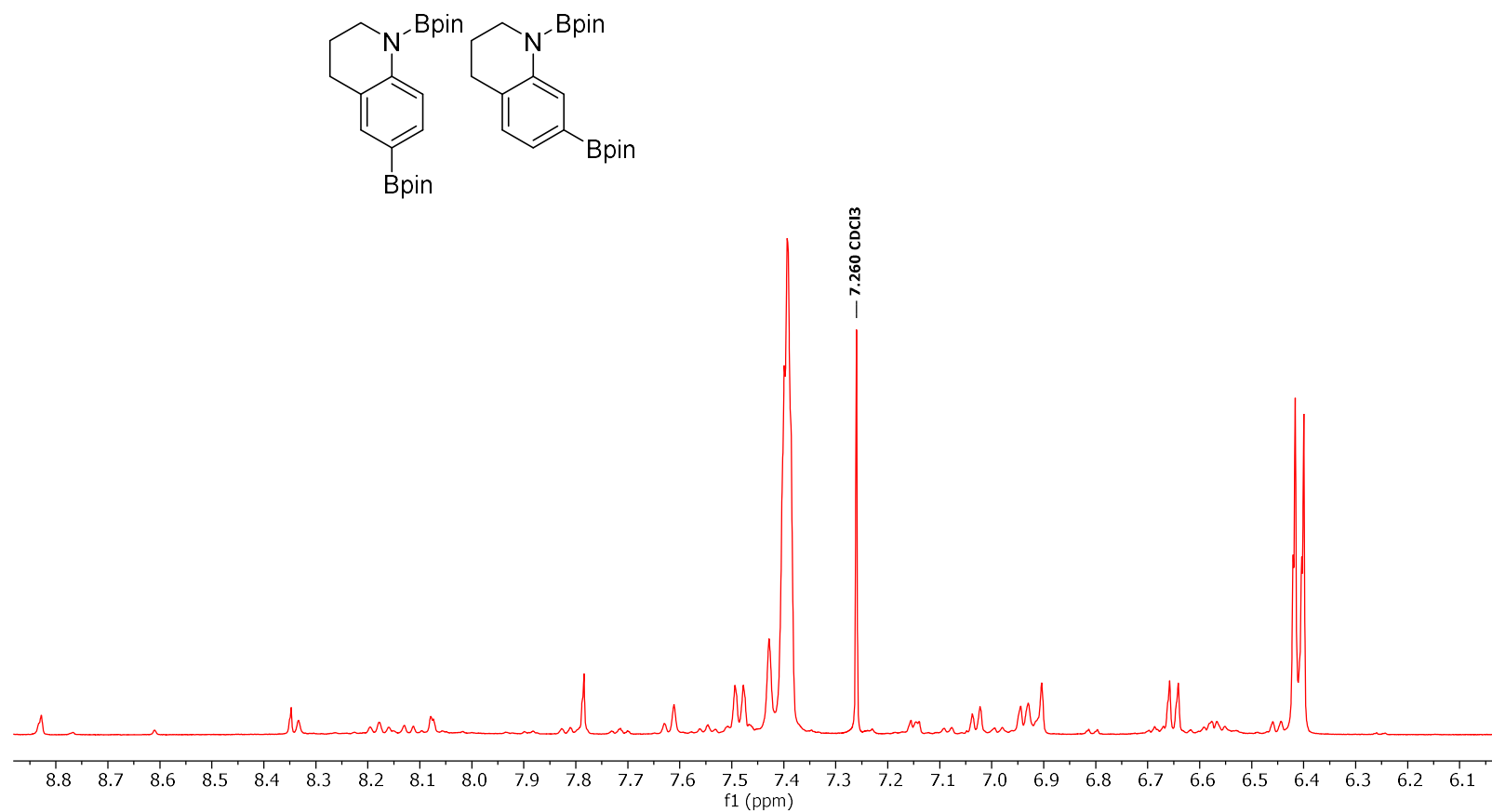


Figure 8-12 Conditions: 25 °C, 500 MHz, CDCl<sub>3</sub>



<sup>1</sup>H NMR of para borylated 1,2,3,4-tetrahydroquinoline Fraction 1 (14d)

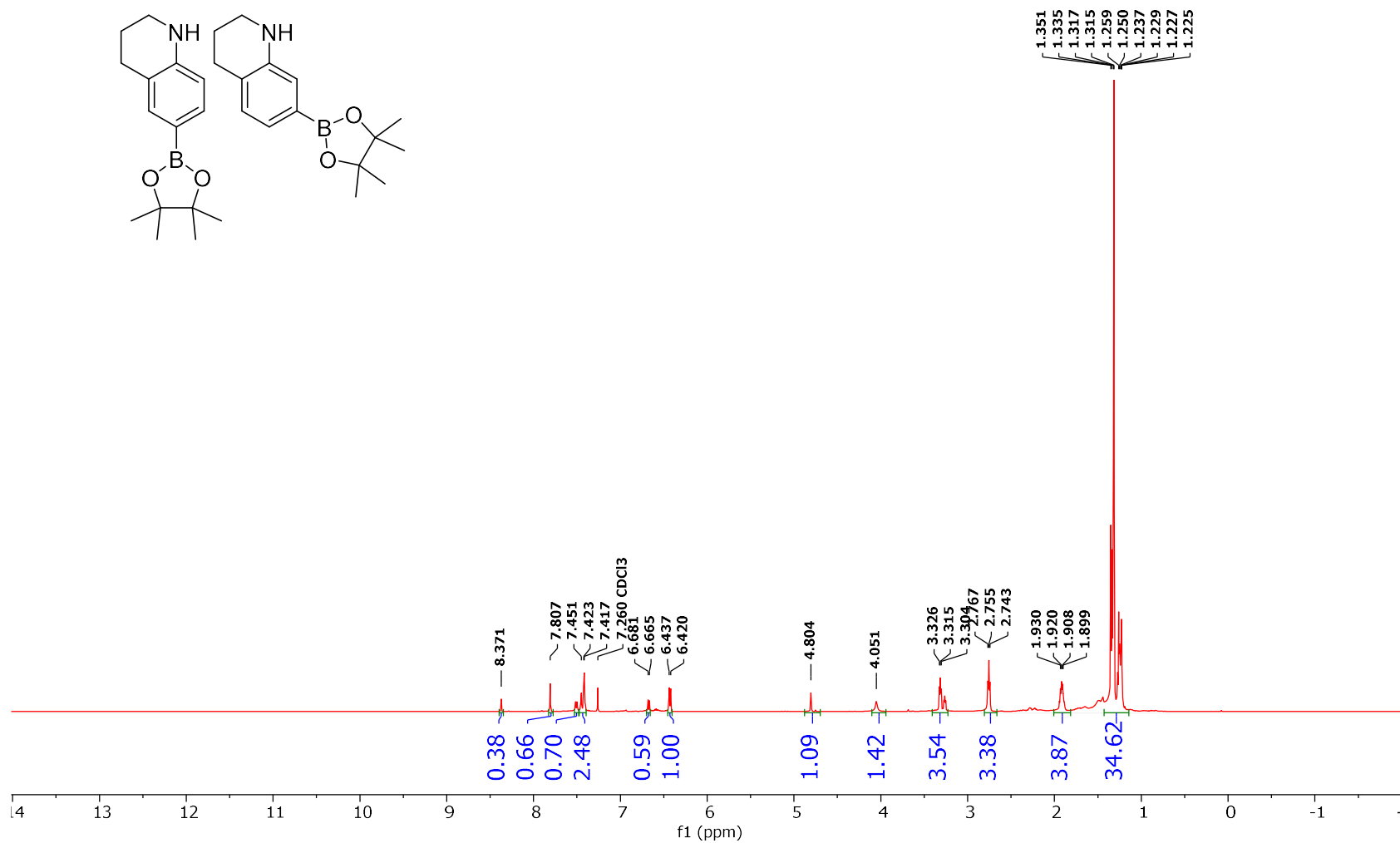


Figure 8-13 Conditions: 25 °C, 500 MHz, CDCl<sub>3</sub>

<sup>13</sup>C NMR of para borylated 1,2,3,4-tetrahydroquinoline (14d) Fraction 1

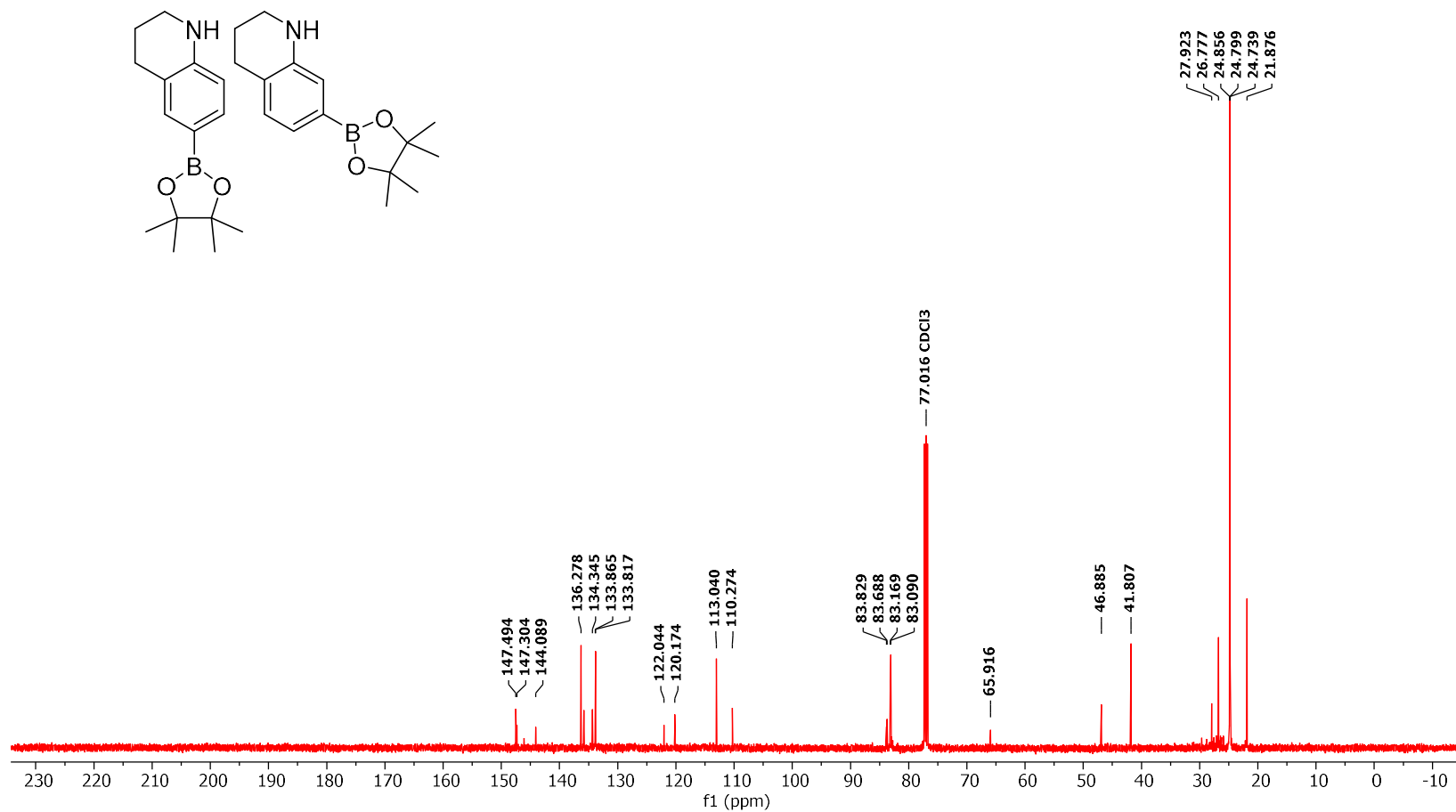


Figure 8-14 Conditions: 25 °C, 126 MHz, CDCl<sub>3</sub>

**$^{11}\text{B}$  NMR of para borylated 1,2,3,4-tetrahydroquinoline (14d) Fraction 1**

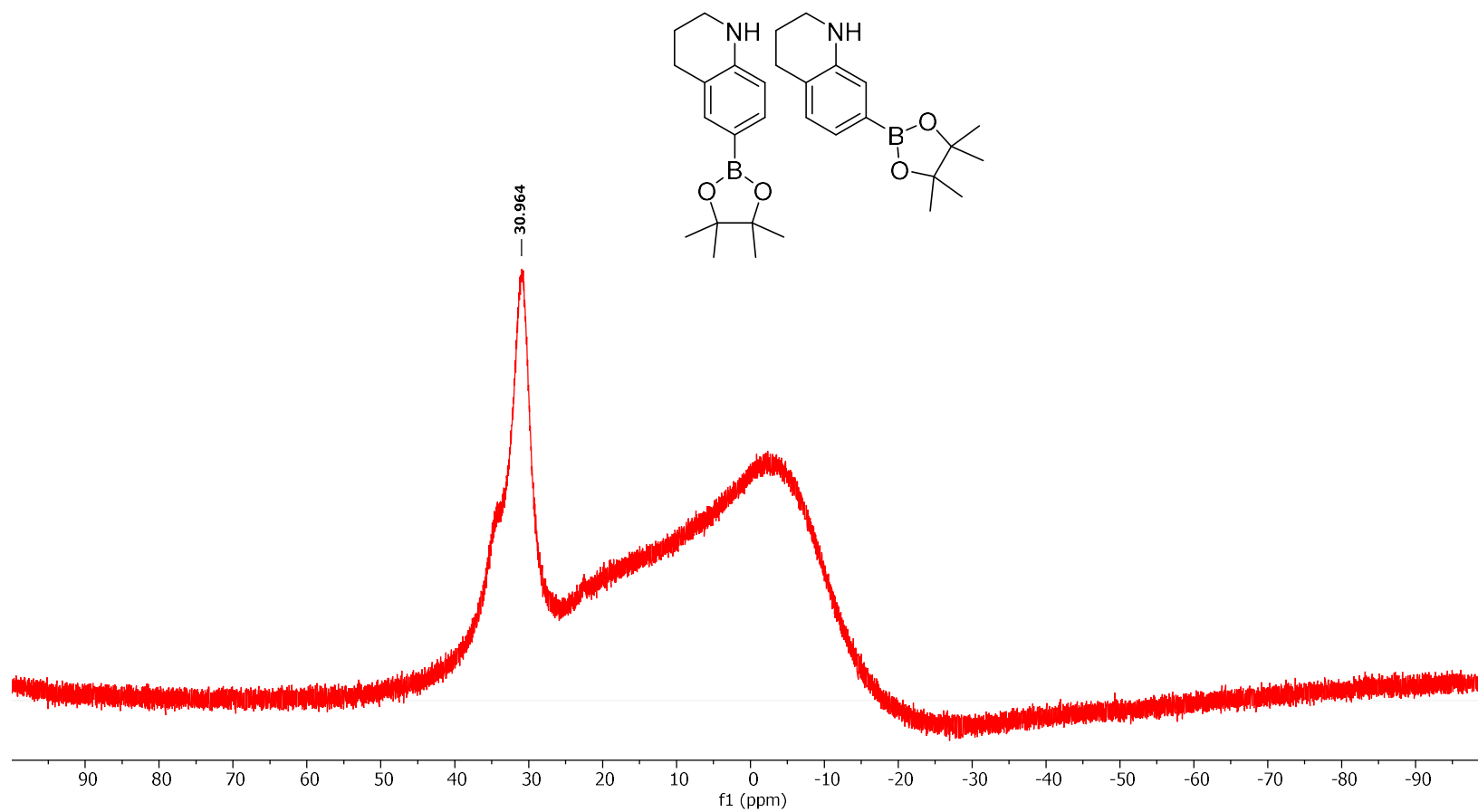


Figure 8-15 Conditions: 25 °C, 160 MHz,  $\text{CDCl}_3$

<sup>1</sup>H NMR of para borylated 1,2,3,4-tetrahydroquinoline (14d) Fraction 2

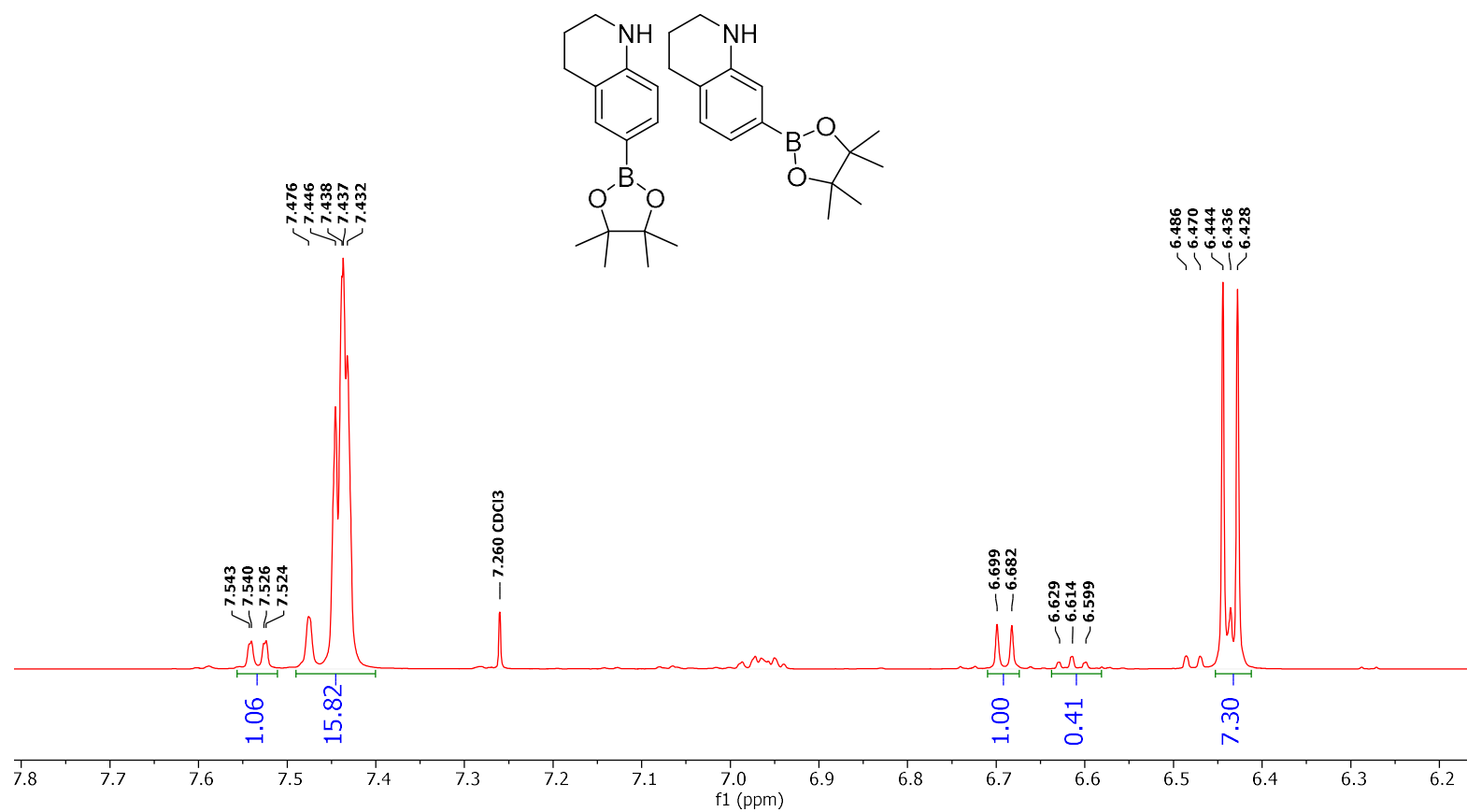


Figure 8-16 Conditions: 25 °C, 500 MHz, CDCl<sub>3</sub>

<sup>13</sup>C NMR of para borylated 1,2,3,4-tetrahydroquinoline (14d) Fraction 2

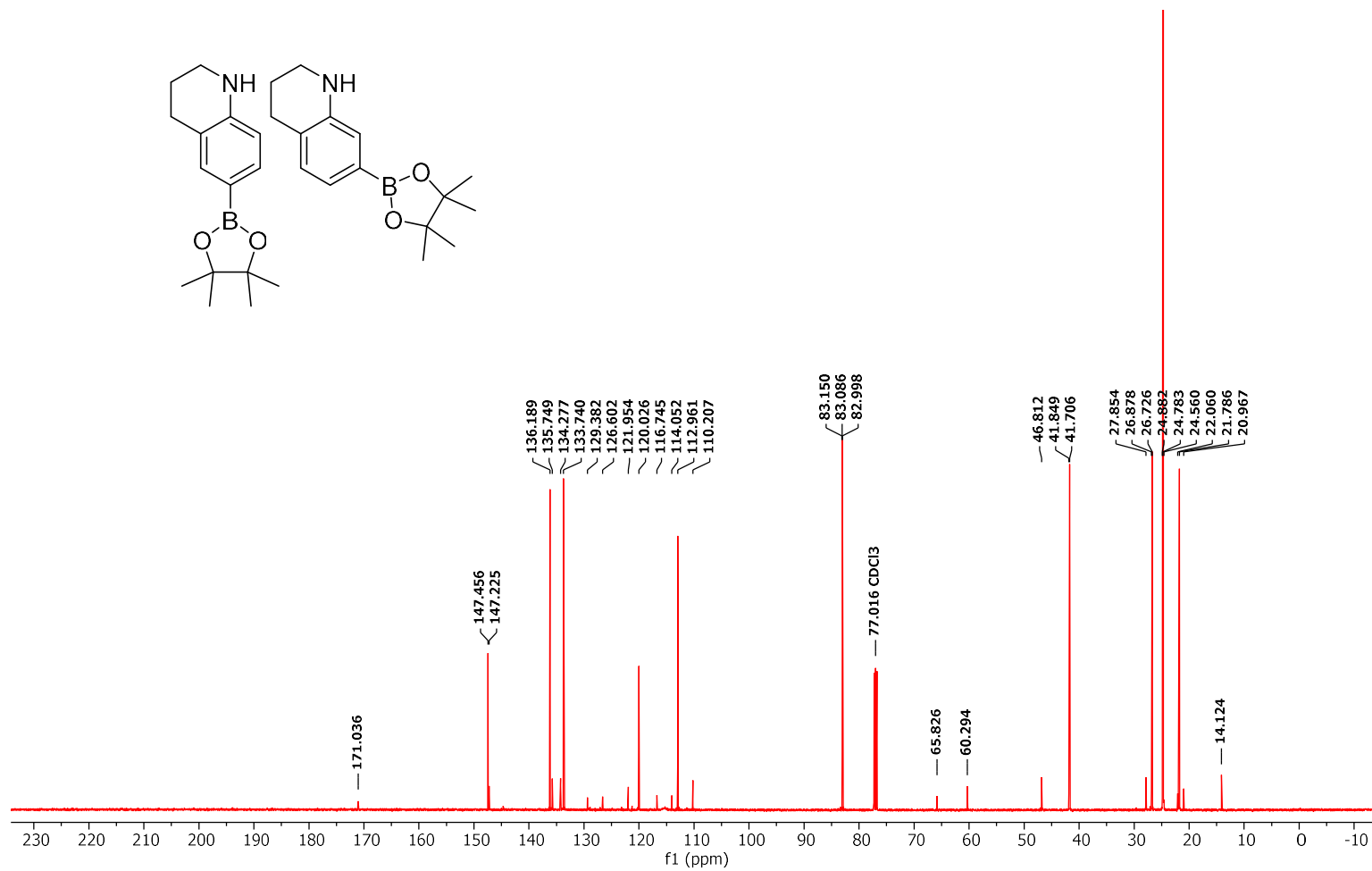


Figure 8-17 Conditions: 25 °C, 126 MHz, CDCl<sub>3</sub>

**$^{11}\text{B}$  NMR of para borylated 1,2,3,4-tetrahydroquinoline (14d) Fraction 2**

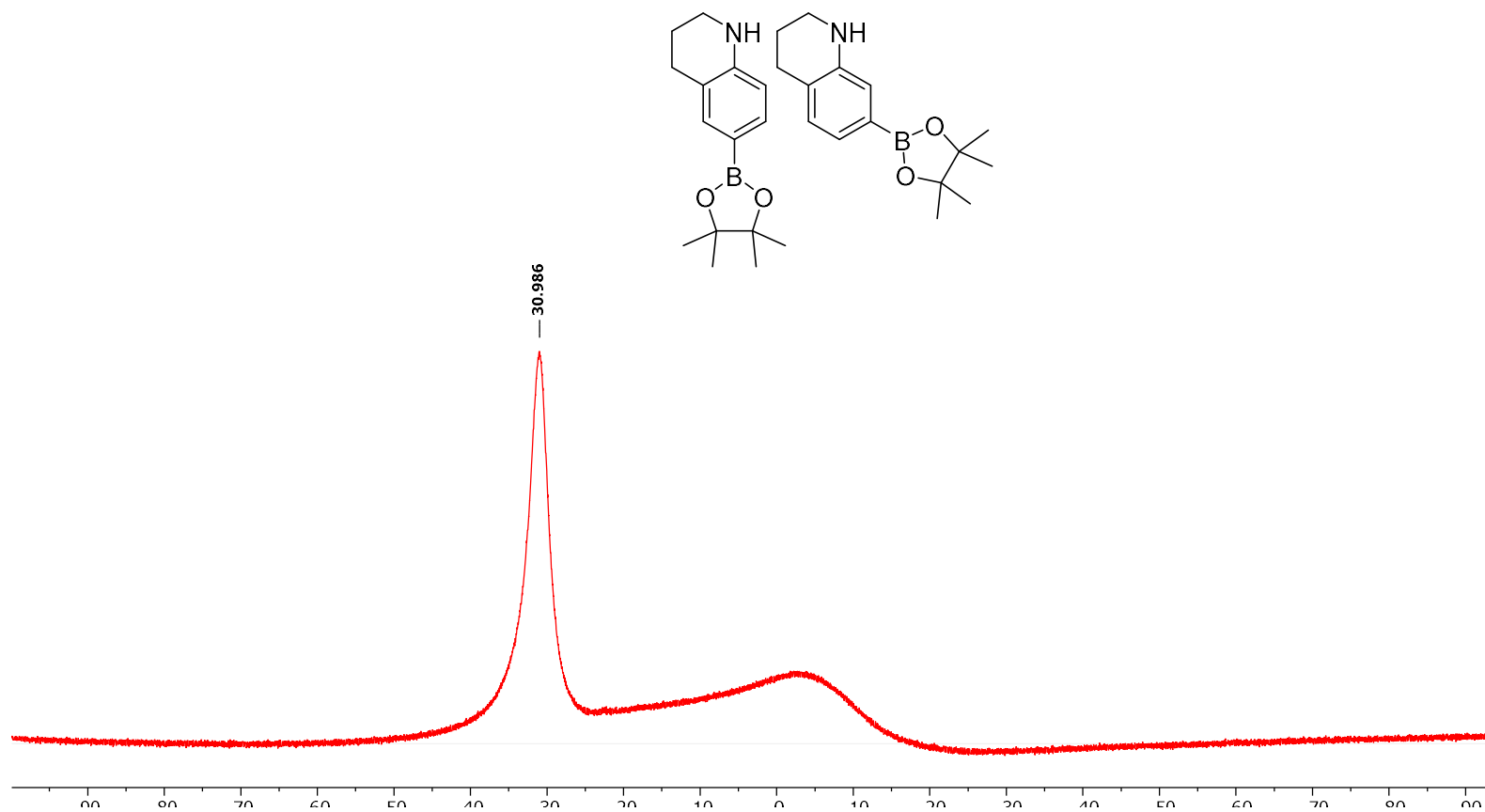


Figure 8-18 Conditions: 25 °C, 160 MHz,  $\text{CDCl}_3$

<sup>1</sup>H NMR of para borylated 1,2,3,4-tetrahydroquinoline (14d) Fraction 3

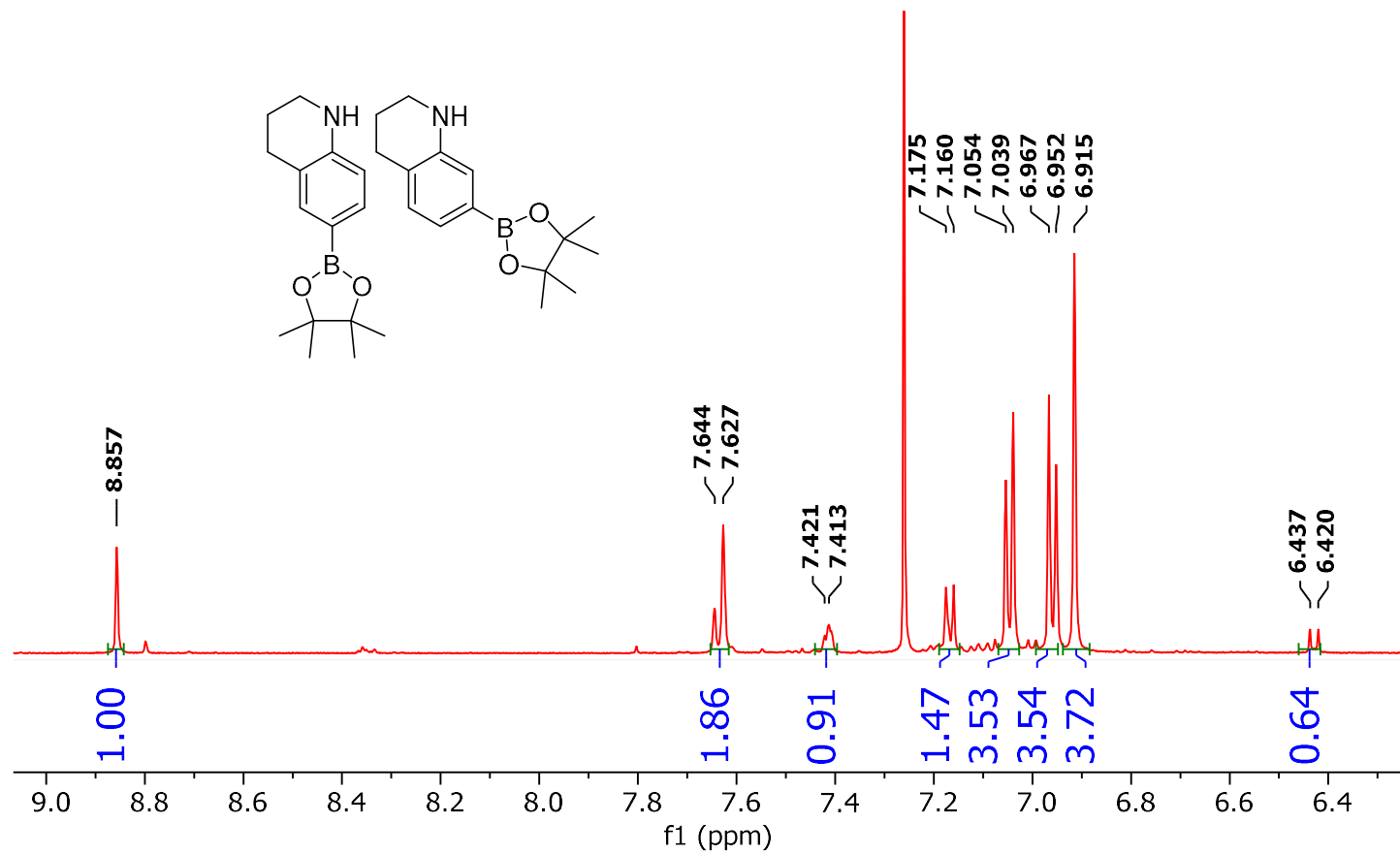


Figure 8-19 Conditions: 25 °C, 500 MHz, CDC

<sup>13</sup>C NMR of para borylated 1,2,3,4-tetrahydroquinoline (14d) Fraction 3

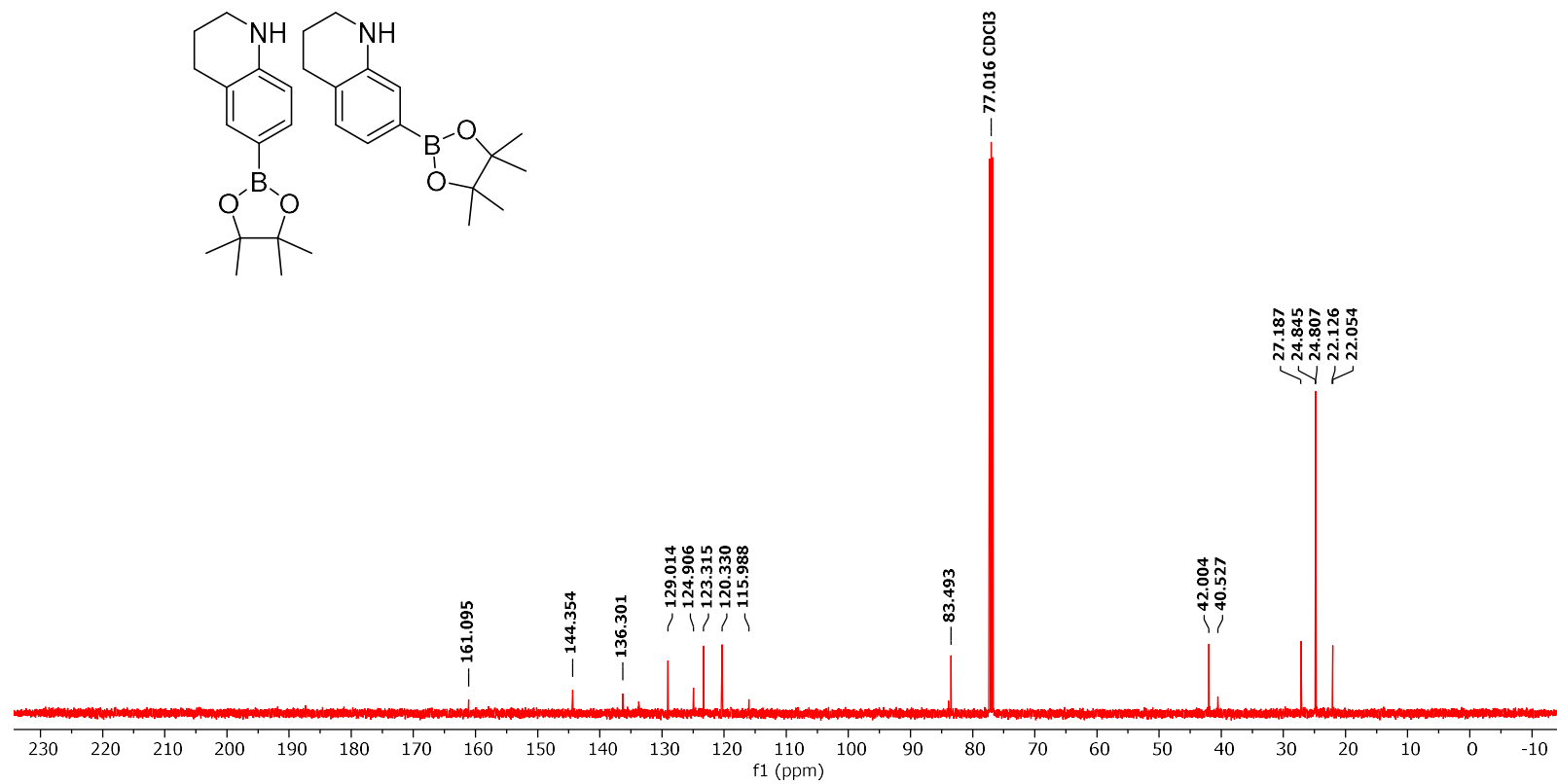


Figure 8-20 Conditions: 25 °C, 126 MHz, CDCl<sub>3</sub>



**$^{11}\text{B}$  NMR of para borylated 1,2,3,4-tetrahydroquinoline (14d) Fraction 3**

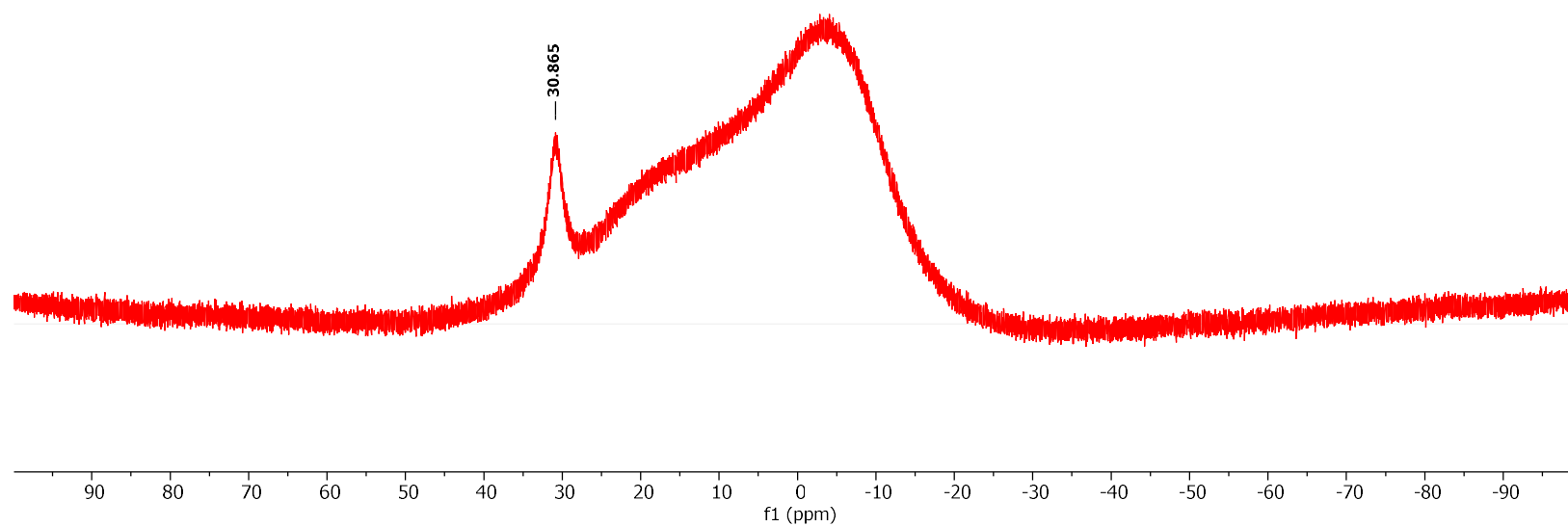
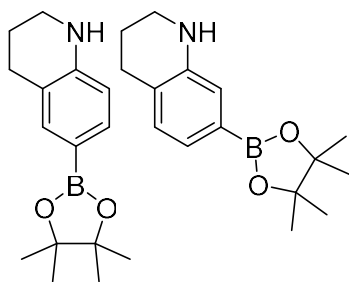


Figure 8-21 Conditions: 25 °C, 160 MHz,  $\text{CDCl}_3$

<sup>1</sup>H NMR of the Para CHB of 8-fluoro-3,4-dihydro-2H-benzo[b][1,4]oxazine (14i)

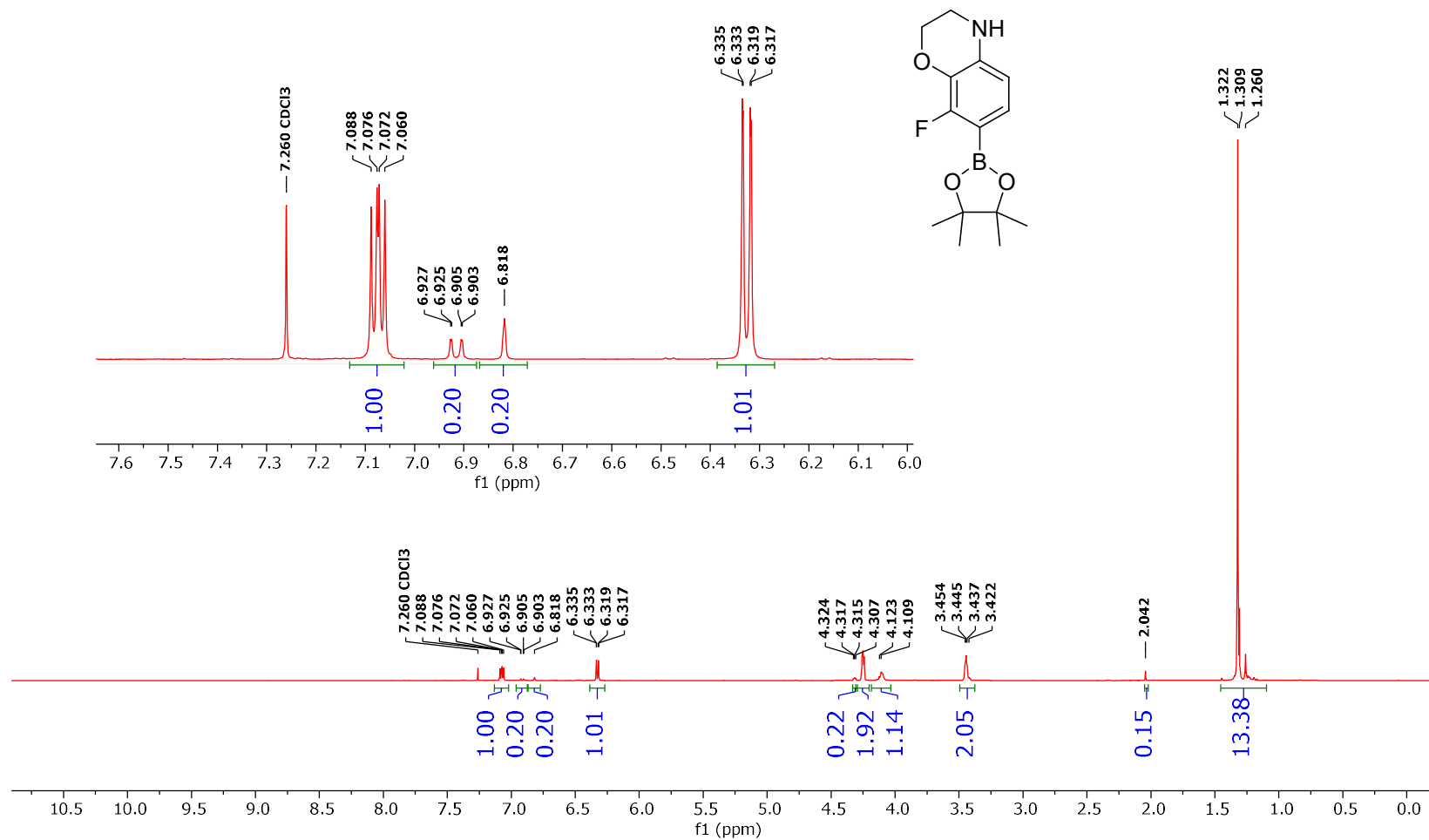


Figure 8-22 Conditions: 25 °C, 500 MHz, CDCl<sub>3</sub>

<sup>19</sup>F NMR of the Para CHB of 8-fluoro-3,4-dihydro-2H-benzo[b][1,4]oxazine (14i)

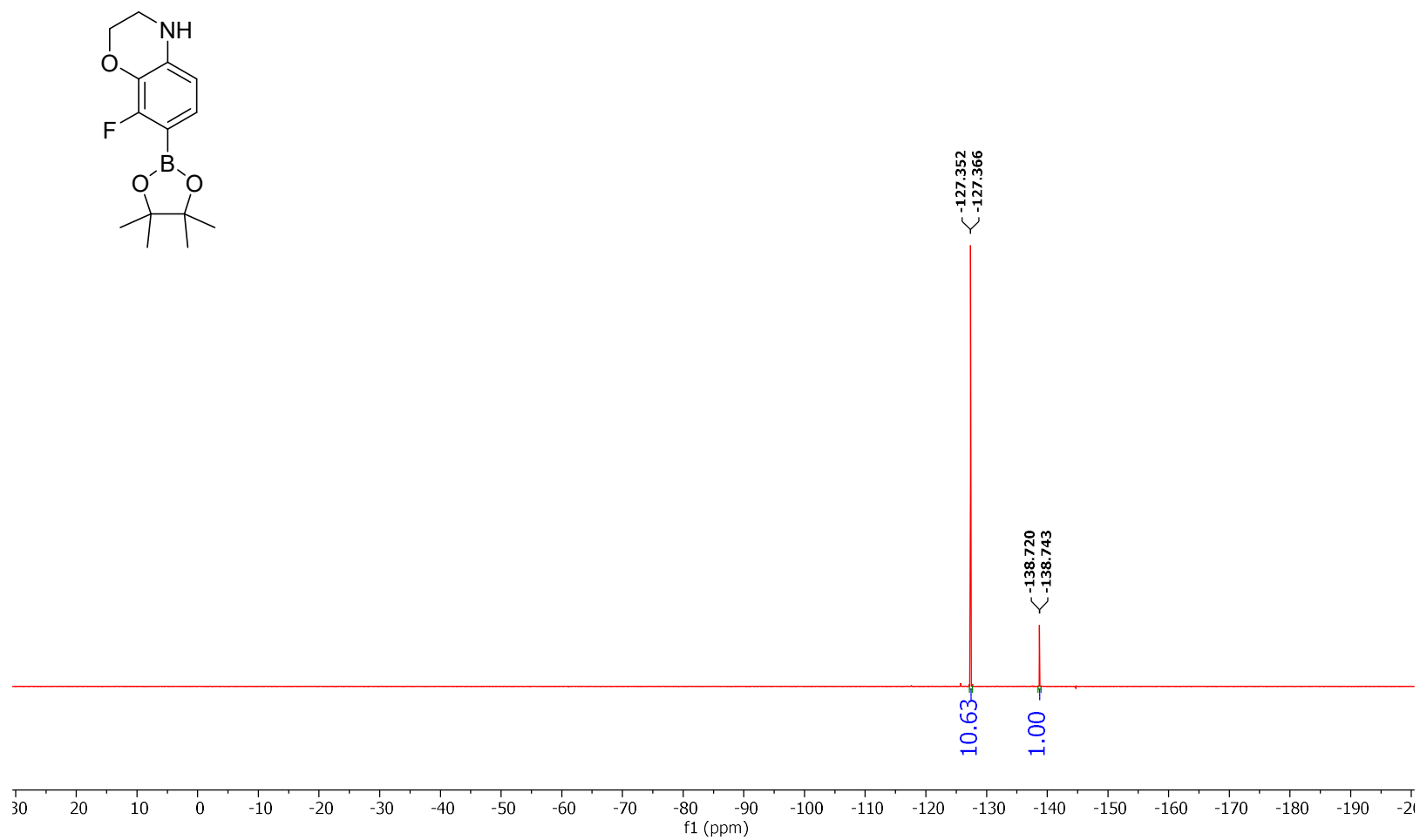


Figure 8-23 Conditions: 25 °C, 470 MHz, CDCl<sub>3</sub>

<sup>13</sup>C NMR of the Para CHB of 8-fluoro-3,4-dihydro-2H-benzo[b][1,4]oxazine (14i)

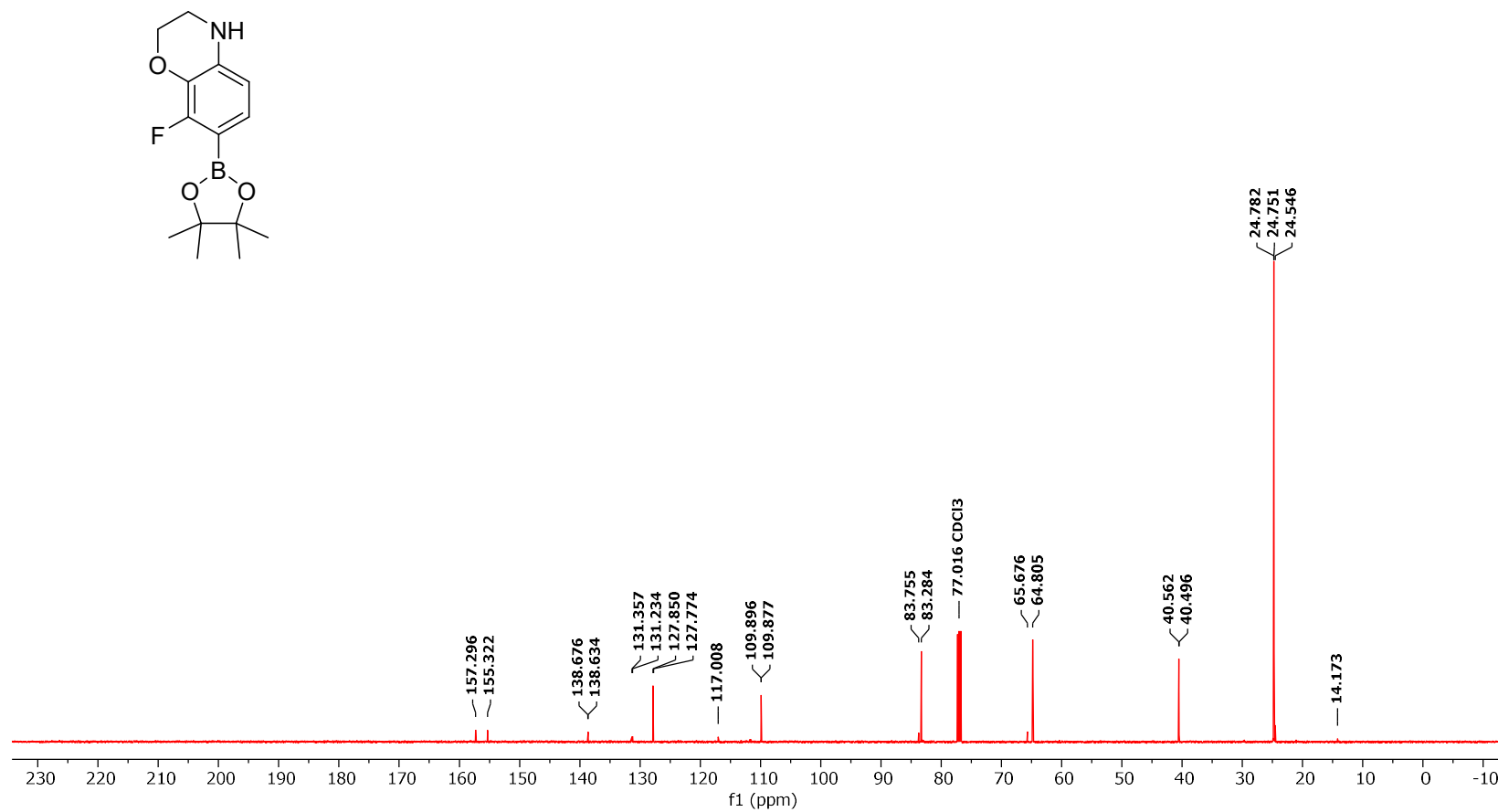


Figure 8-24 Conditions: 25 °C, 126 MHz, CDCl<sub>3</sub>

**$^{11}\text{B}$  NMR of the Para CHB of 8-fluoro-3,4-dihydro-2H-benzo[b][1,4]oxazine (14i)**

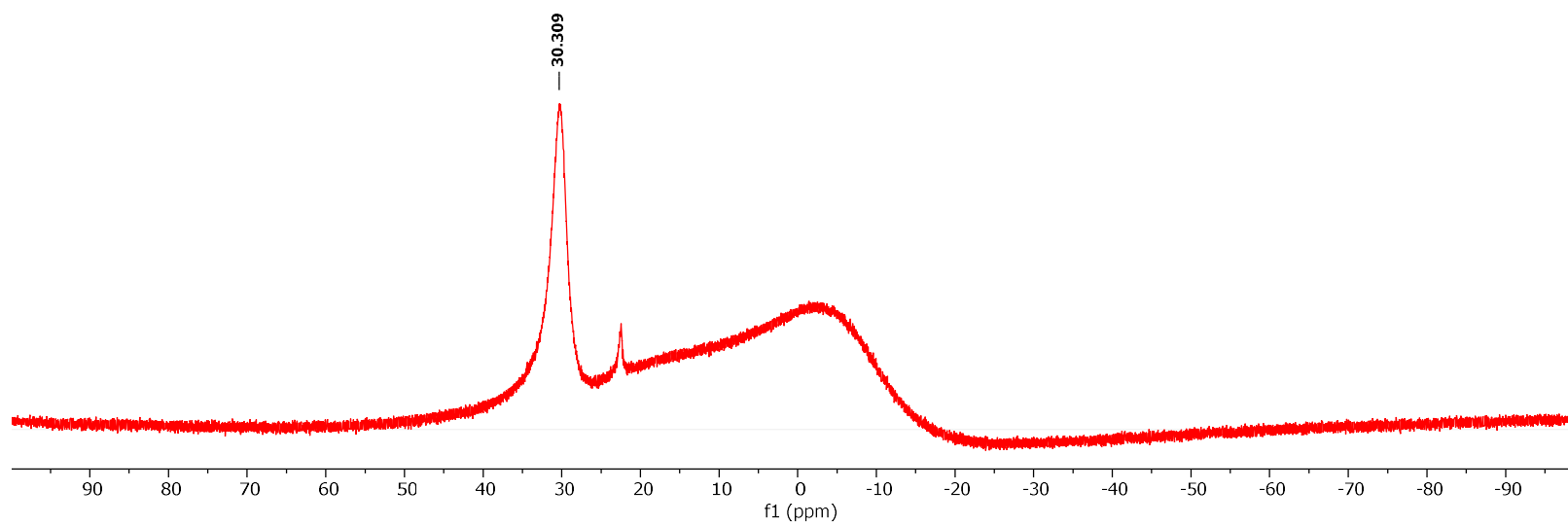
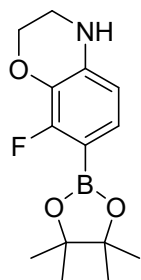


Figure 8-25 Conditions: 25 °C, 160 MHz,  $\text{CDCl}_3$

## Chapter 5 NMR Spectra

**$^{19}\text{F}$  NMR Spectra of the addition of Phenolphthalein to Sodium Tetrafluoroborate (Reaction 2)**

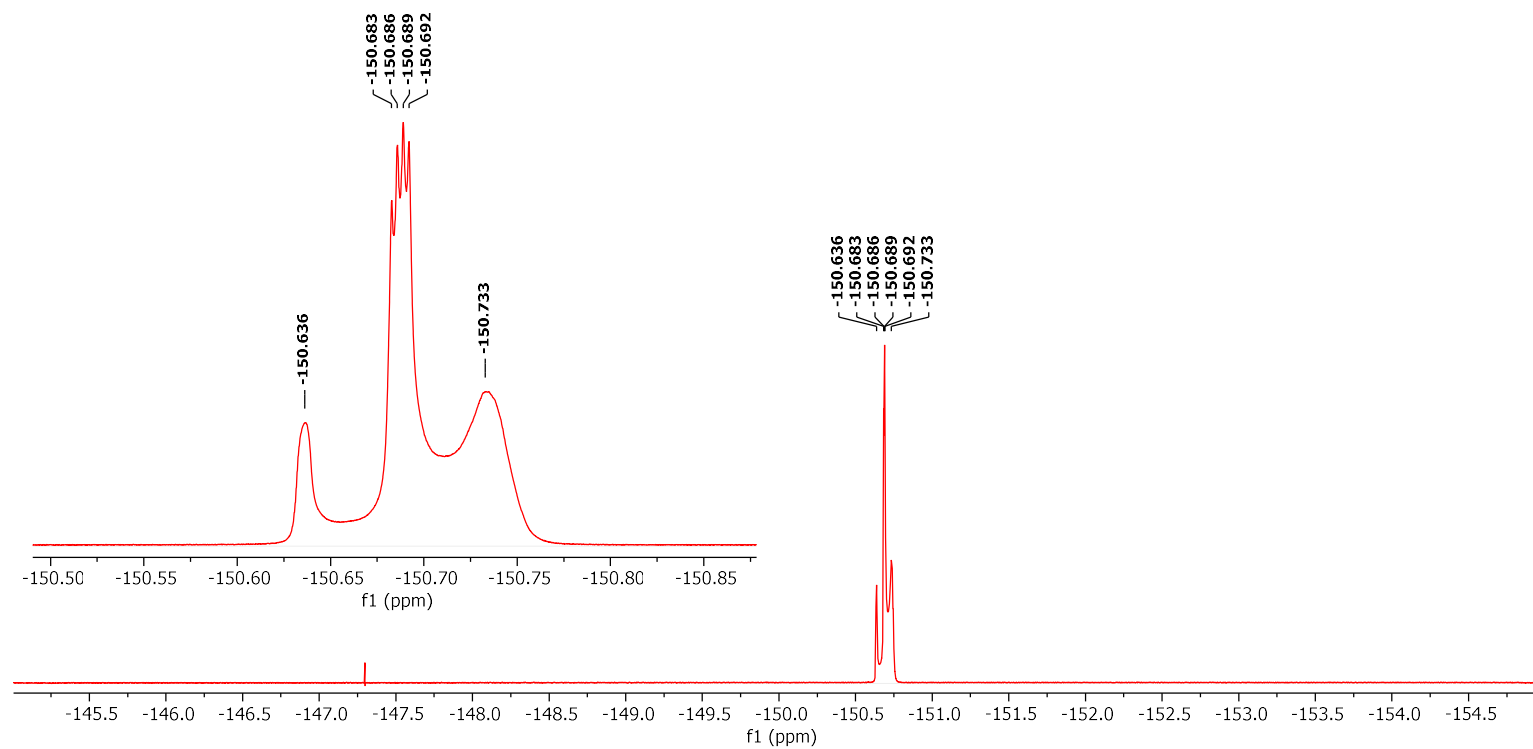


Figure 9-1 Conditions: 25 °C, 470 MHz,  $\text{D}_2\text{O}$

**$^{19}\text{F}$  NMR Spectra of the addition of Phenolphthalein then Sodium Chloride to Sodium Tetrafluoroborate (Reaction 2)**

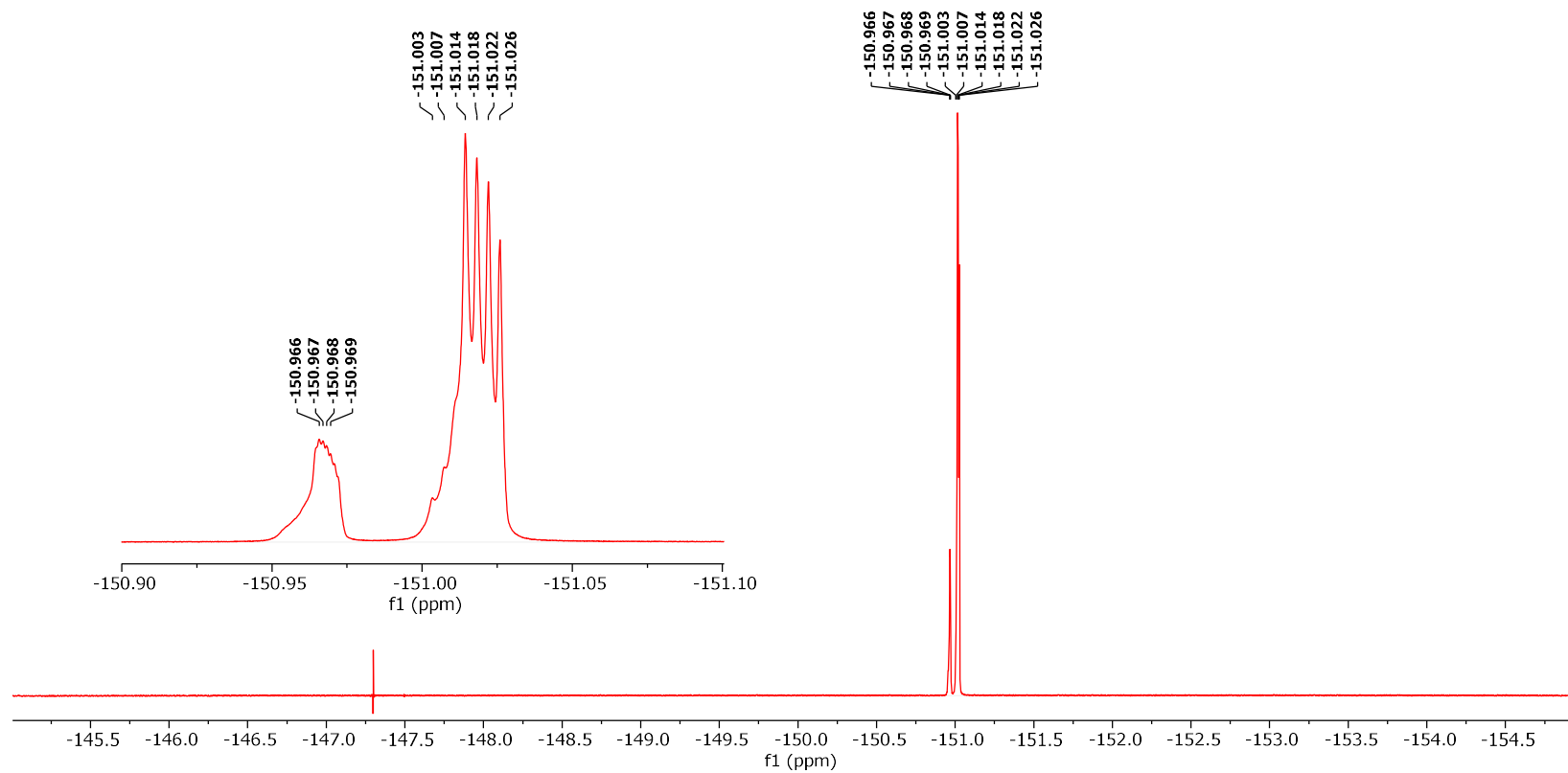


Figure 9-2 Conditions: 25 °C, 470 MHz,  $\text{D}_2\text{O}$



**$^{19}\text{F}$  NMR Spectra of the crude reaction mixture of the oxidation of (2-fluorophenyl)boronic acid in 1,4-dioxane (Reaction 3)**

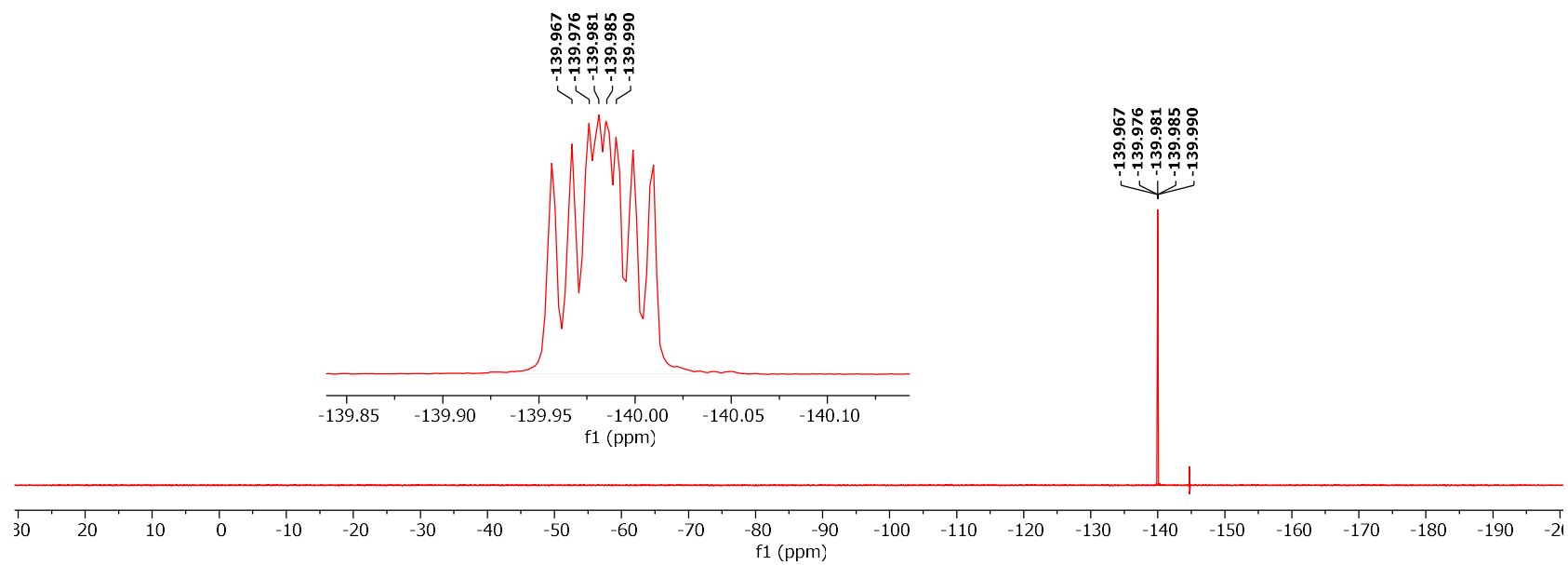


Figure 9-3 Conditions: 25 °C, 470 MHz,  $\text{D}_2\text{O}$

**$^{19}\text{F}$  NMR Spectra of the homogenized product of fluorination of boric acid to synthesize sodium tetrafluoroborate (Reaction 3)**

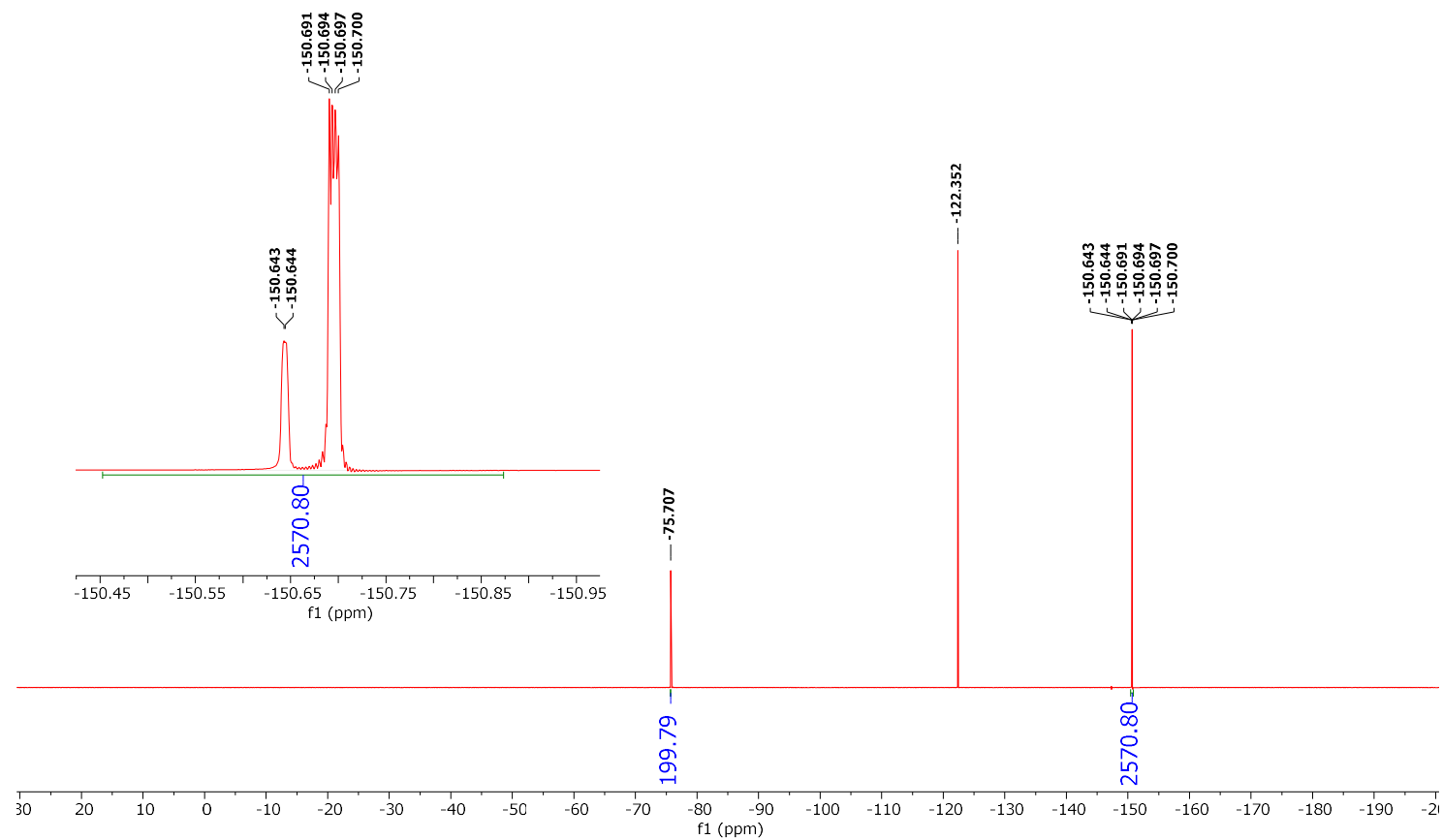


Figure 9-4 Conditions: 25 °C, 470 MHz,  $\text{D}_2\text{O}$

**$^{19}\text{F}$  NMR Spectra of the homogenized product of fluorination of boric acid to synthesize sodium tetrafluoroborate (Reaction 3)**

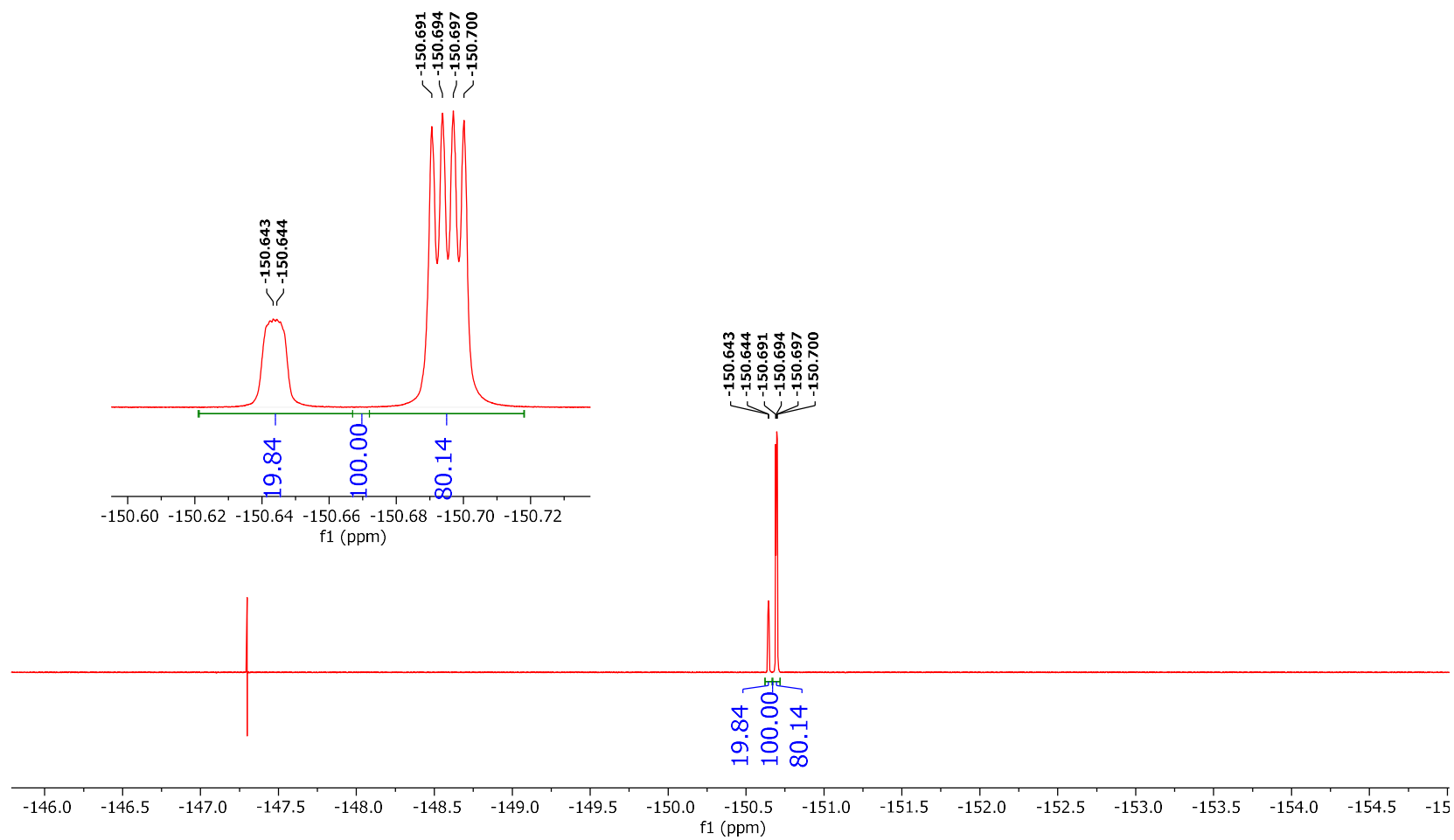


Figure 9-5 Conditions: 25 °C, 470 MHz, D<sub>2</sub>O

**$^{19}\text{F}$  NMR Spectra of synthesis of sodium tetrafluoroborate from boric acid (Reaction 4)**

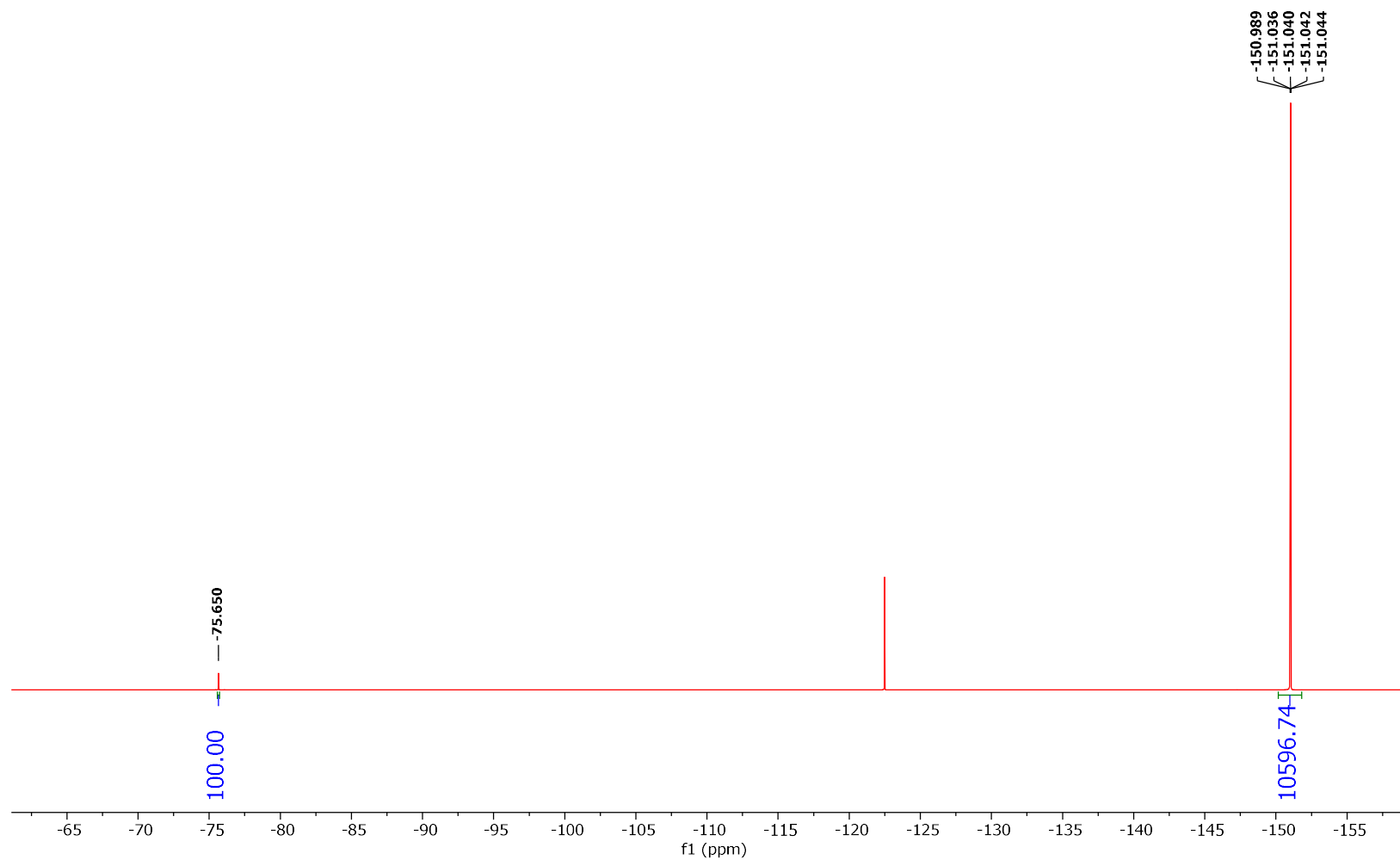


Figure 9-6 Conditions: 25 °C, 470 MHz,  $\text{D}_2\text{O}$

**$^{19}\text{F}$  NMR Spectra of synthesis of sodium tetrafluoroborate from boric acid (Reaction 4)**

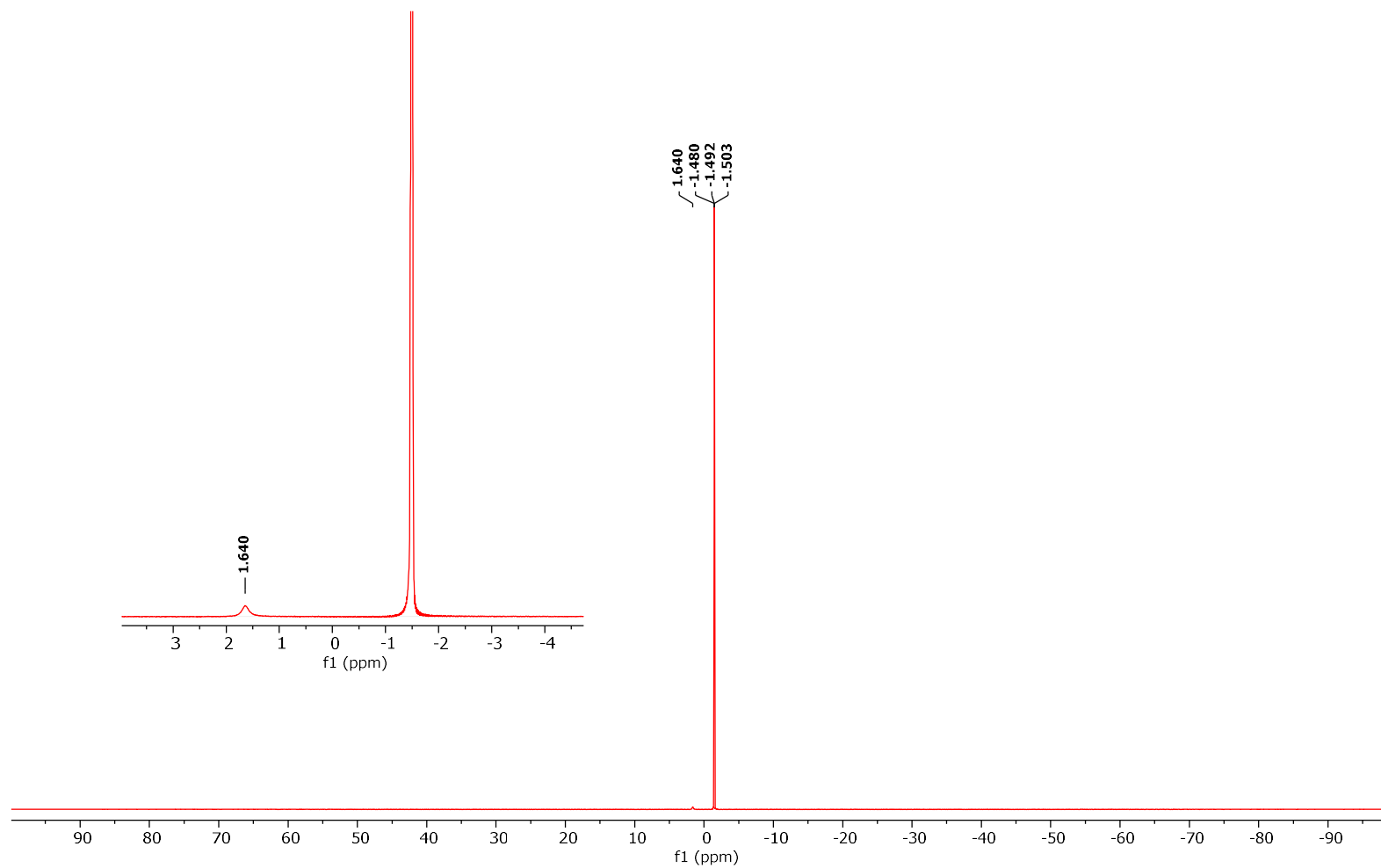


Figure 9-7 Conditions: 25 °C, 160 MHz,  $\text{CDCl}_3$

**$^{19}\text{F}$  NMR Spectra of the Primary Oxidation of 1 (Reaction 5)**

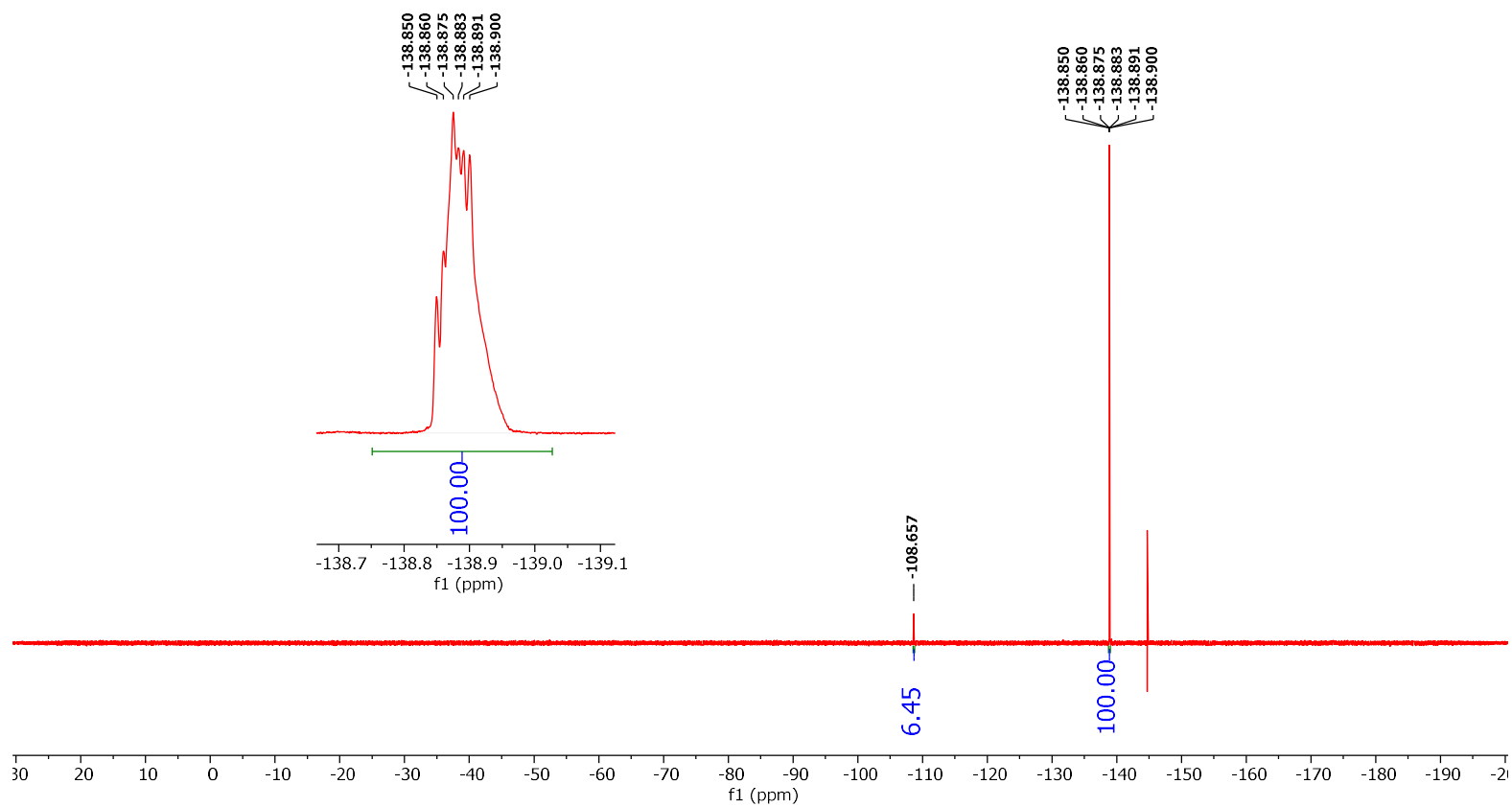


Figure 9-8 Conditions: 25 °C, 470 MHz,  $\text{D}_2\text{O}$

**$^{19}\text{F}$  NMR Spectra of the Primary Fluorination (Reaction 5)**

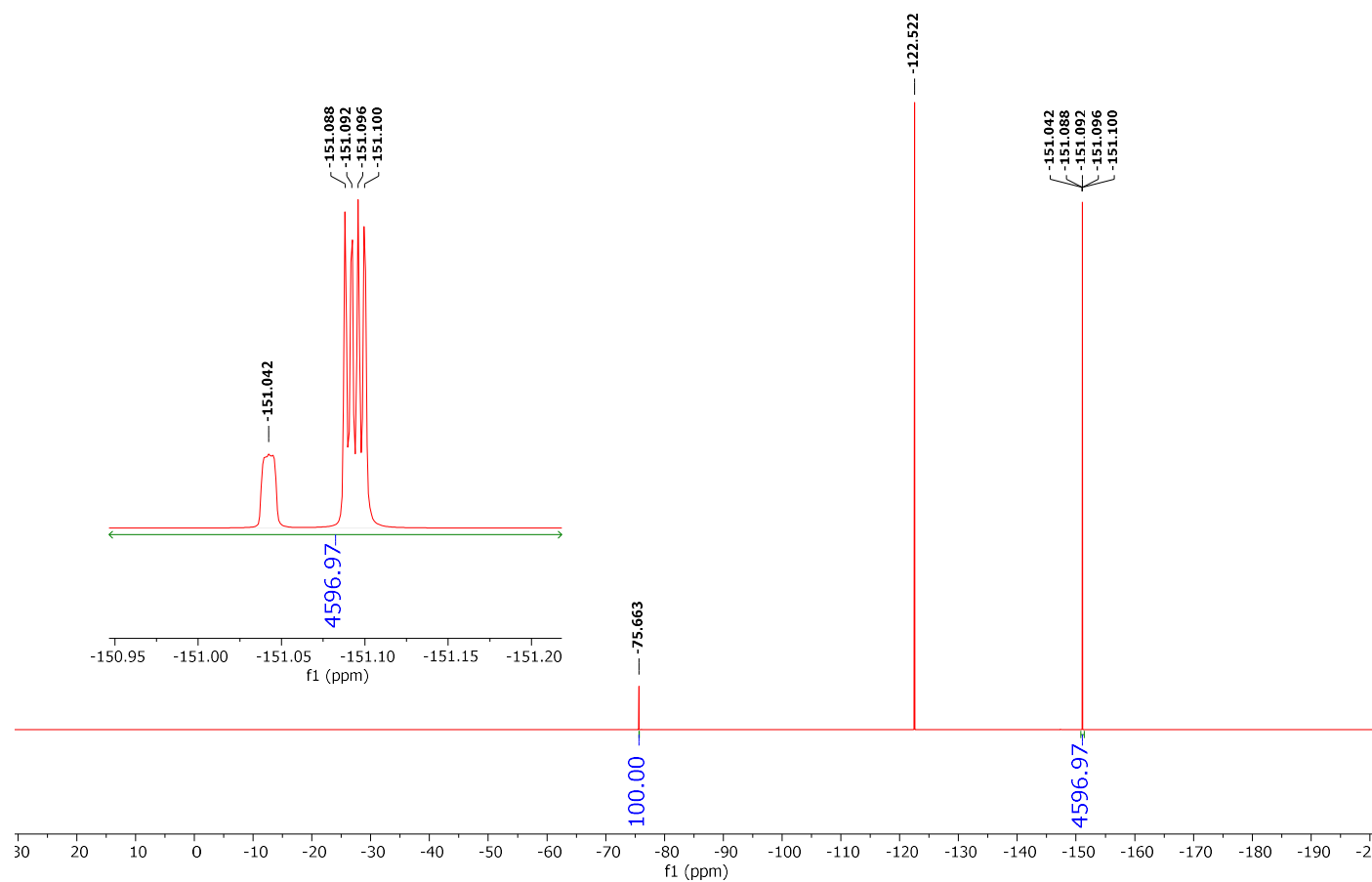


Figure 9-9 Conditions: 25 °C, 470 MHz,  $\text{D}_2\text{O}$

**$^{19}\text{F}$  NMR Spectra of the Secondary Fluorination (Reaction 5)**

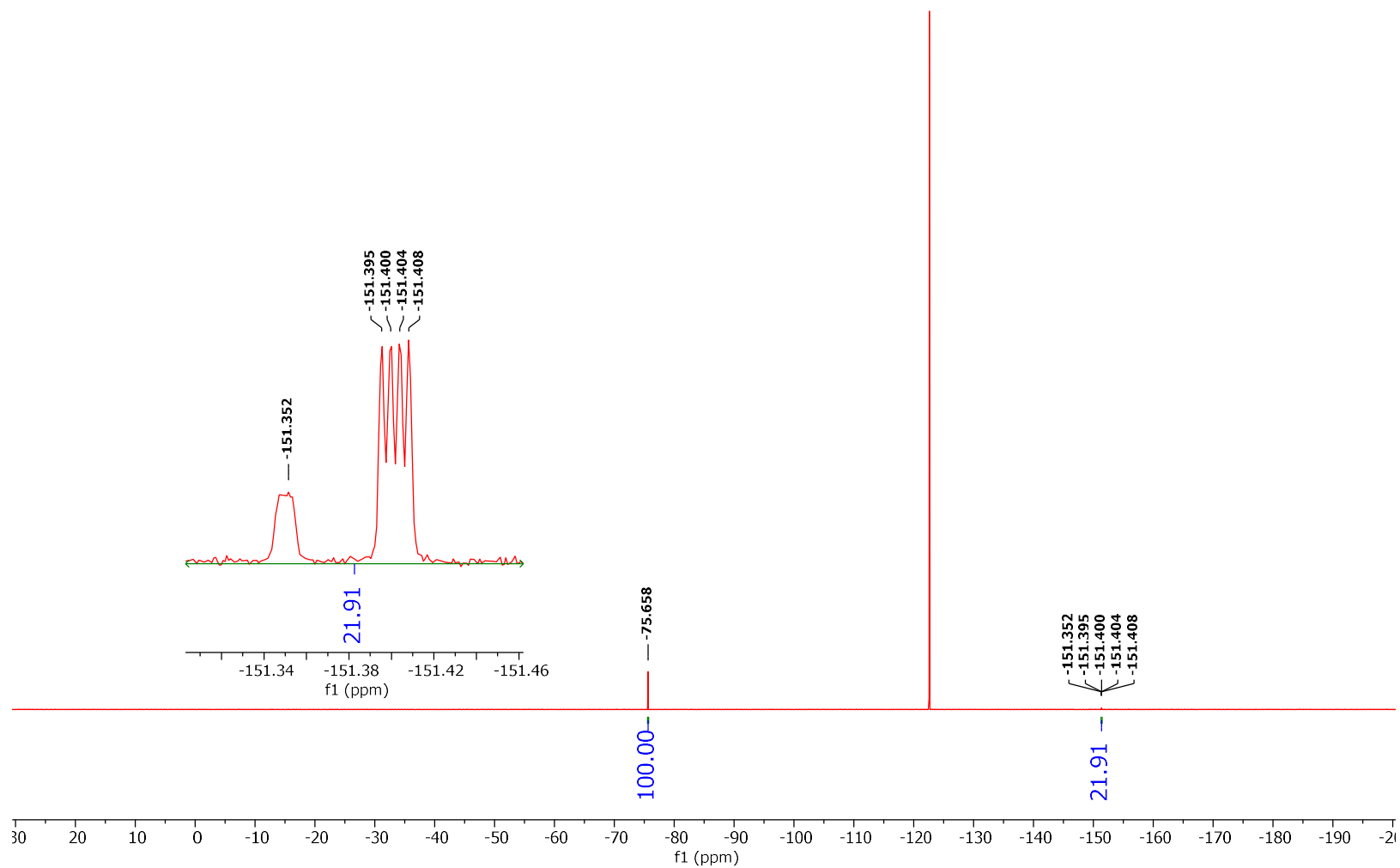


Figure 9-10 Conditions: 25 °C, 470 MHz,  $\text{D}_2\text{O}$



**$^{19}\text{F}$  NMR Small Window Spectra of the Primary Fluorination (Reaction 5)**

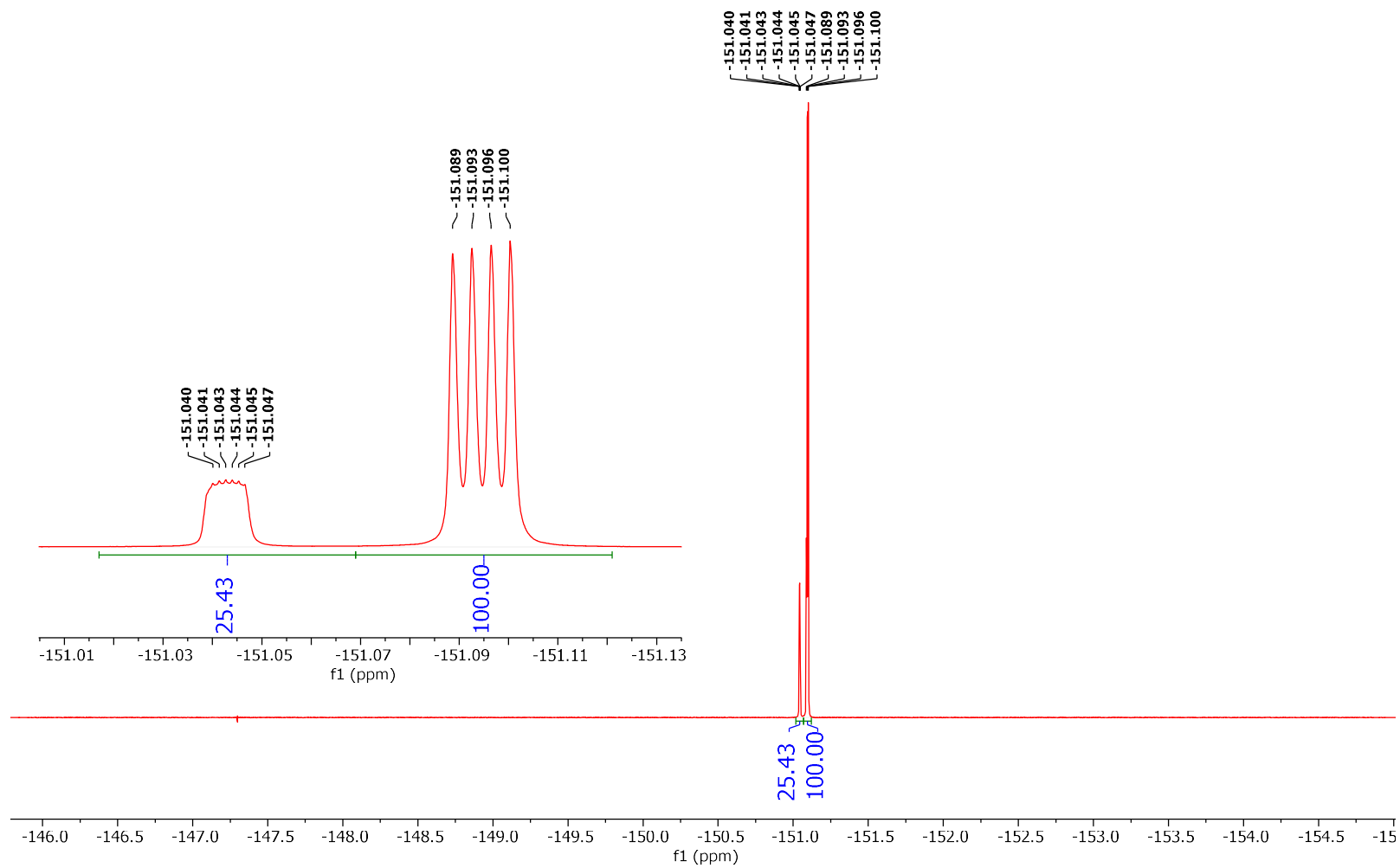


Figure 9-11 Conditions: 25 °C, 470 MHz,  $\text{D}_2\text{O}$

**$^{19}\text{F}$  NMR Small Window Spectra of the Secondary Fluorination (Reaction 5)**

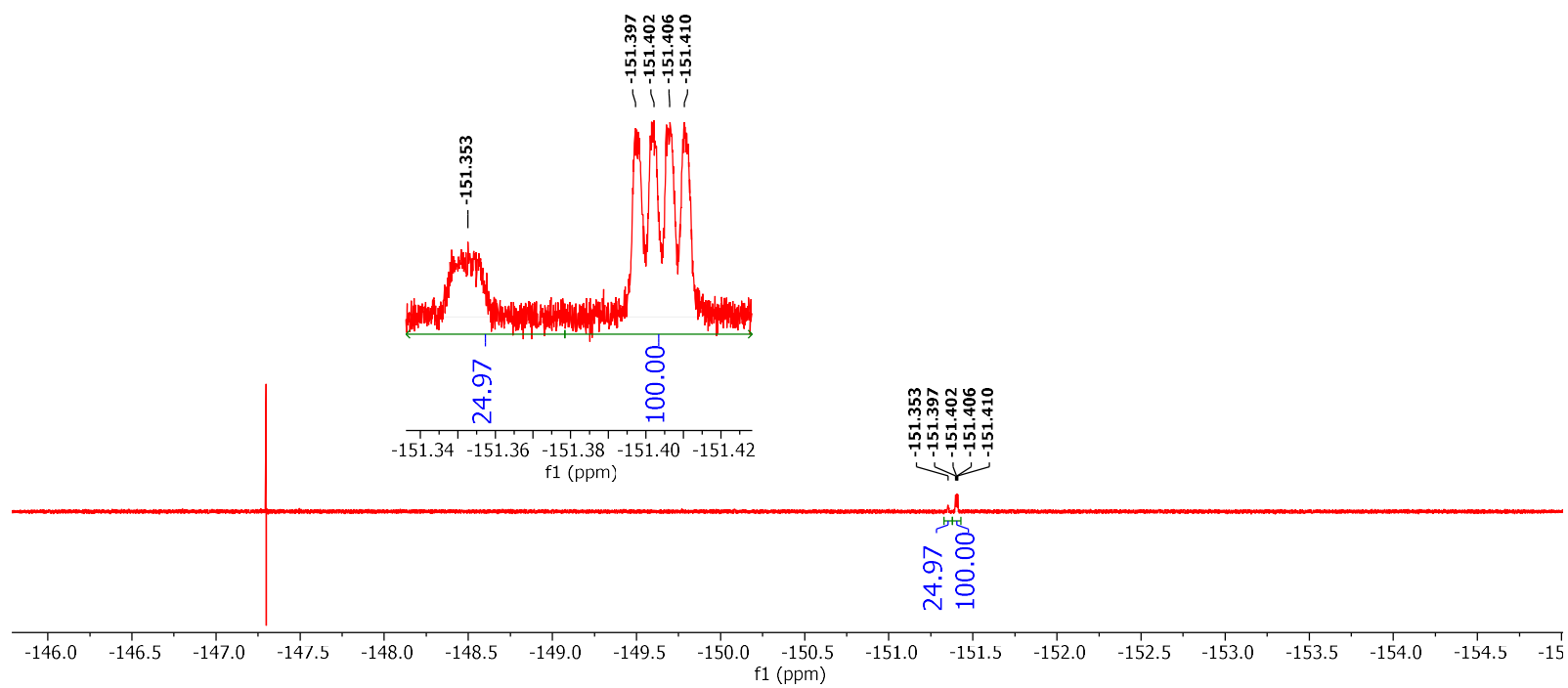


Figure 9-12 Conditions: 25 °C, 470 MHz,  $\text{D}_2\text{O}$

**$^{19}\text{F}$  NMR Spectra of  $\text{NaBF}_4$  (Reaction 6)**

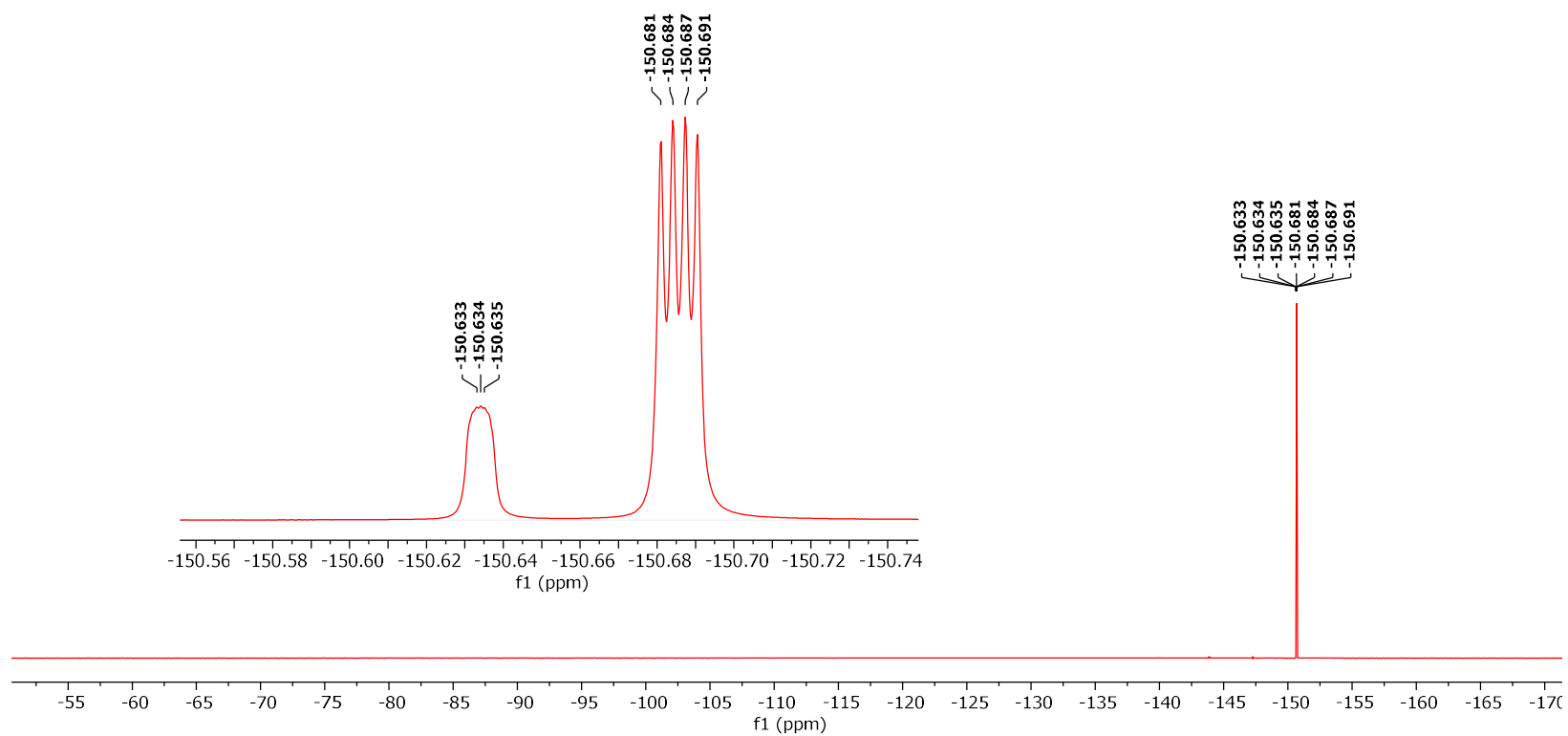


Figure 9-13 Conditions: 25 °C, 470 MHz,  $\text{D}_2\text{O}$

Small Spectral Window  $^{19}\text{F}$  NMR Spectra of  $\text{NaBF}_4$  (Reaction 6)

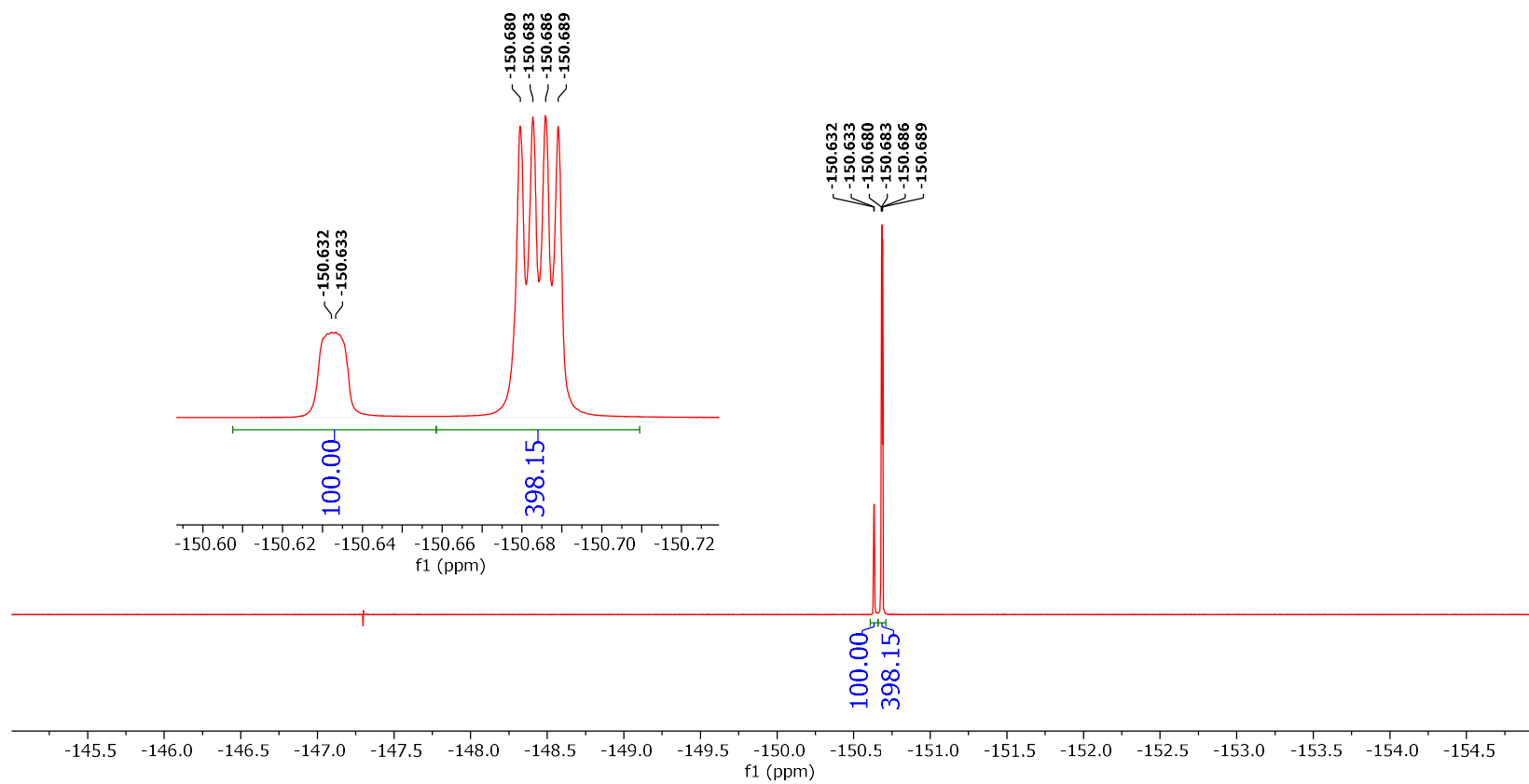


Figure 9-14 Conditions: 25 °C, 470 MHz,  $\text{D}_2\text{O}$

**$^{19}\text{F}$  NMR Spectra of  $\text{NaBF}_4$  with Sodium Trifluoro Acetate (Reaction 6)**

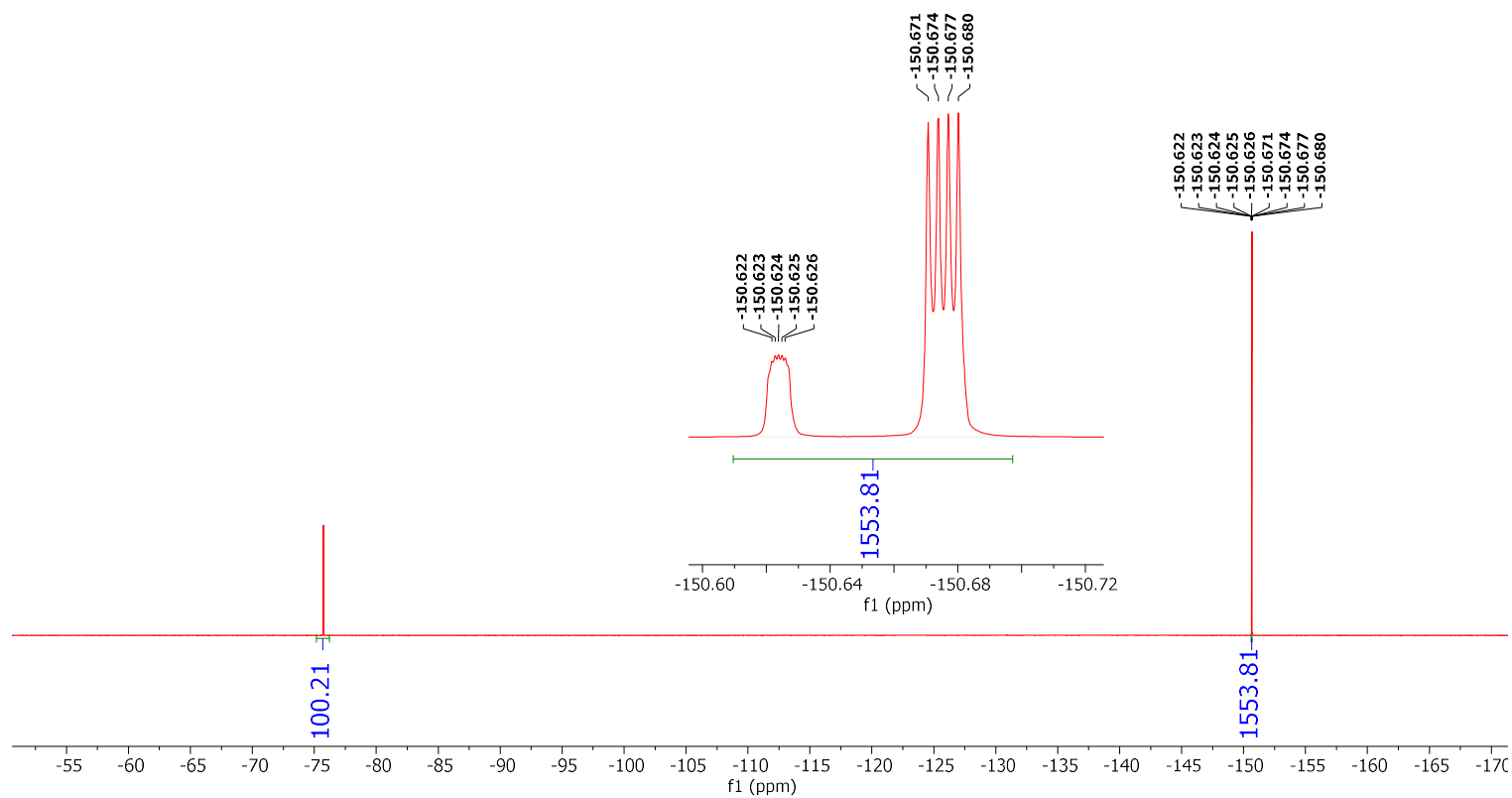


Figure 9-15 Conditions: 25 °C, 470 MHz,  $\text{D}_2\text{O}$

Small Spectral Window  $^{19}\text{F}$  NMR Spectra of  $\text{NaBF}_4$  and Sodium Trifluoroacetate Focusing on the  $\text{NaBF}_4$  Peak (Reaction 6)

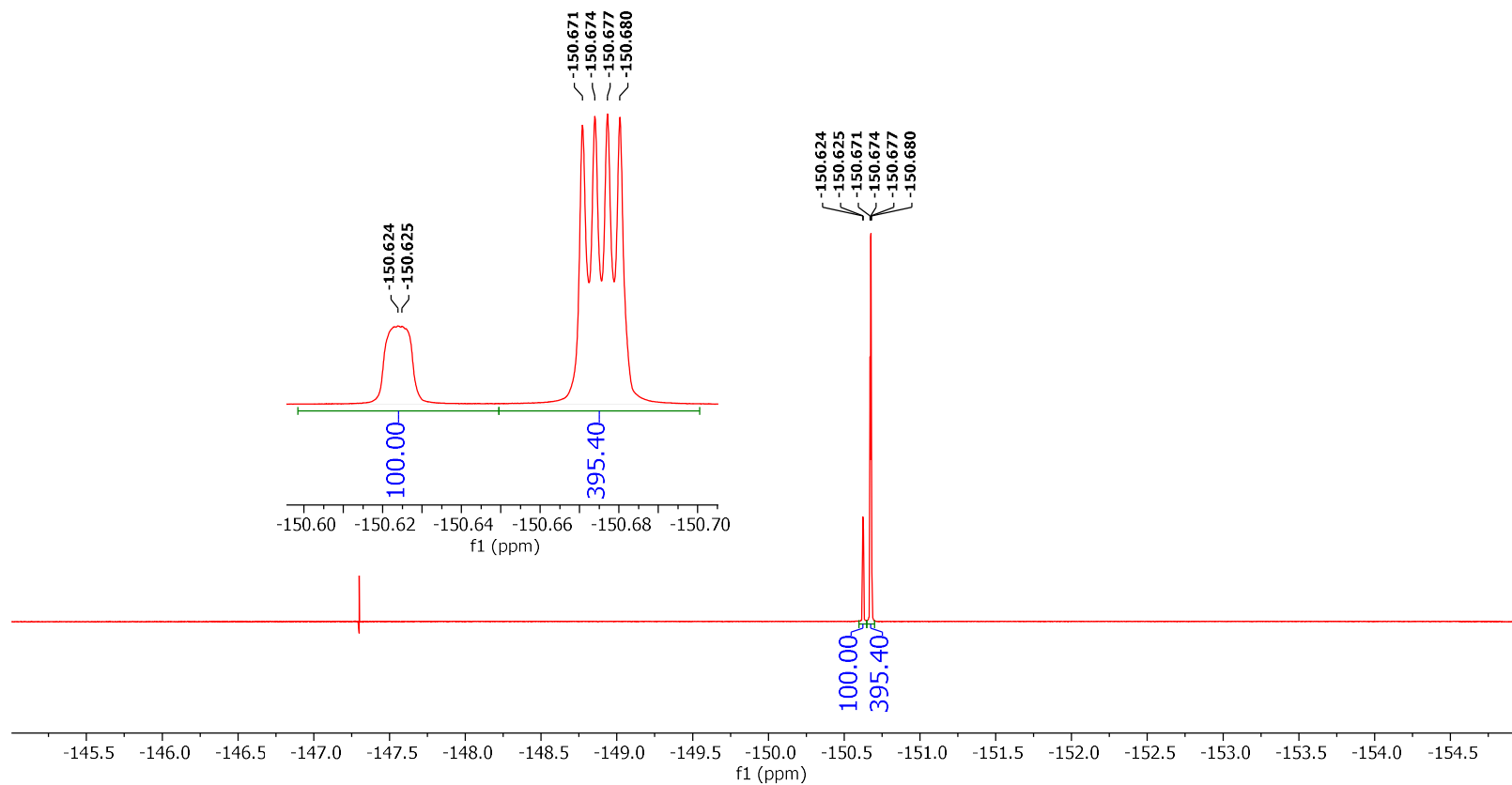


Figure 9-16 Conditions: 25 °C, 470 MHz,  $\text{D}_2\text{O}$

**$^{19}\text{F}$  NMR Spectra of  $\text{NaBF}_4$ , Sodium Trifluoro Acetate, and Phenolphthalein (Reaction 6)**

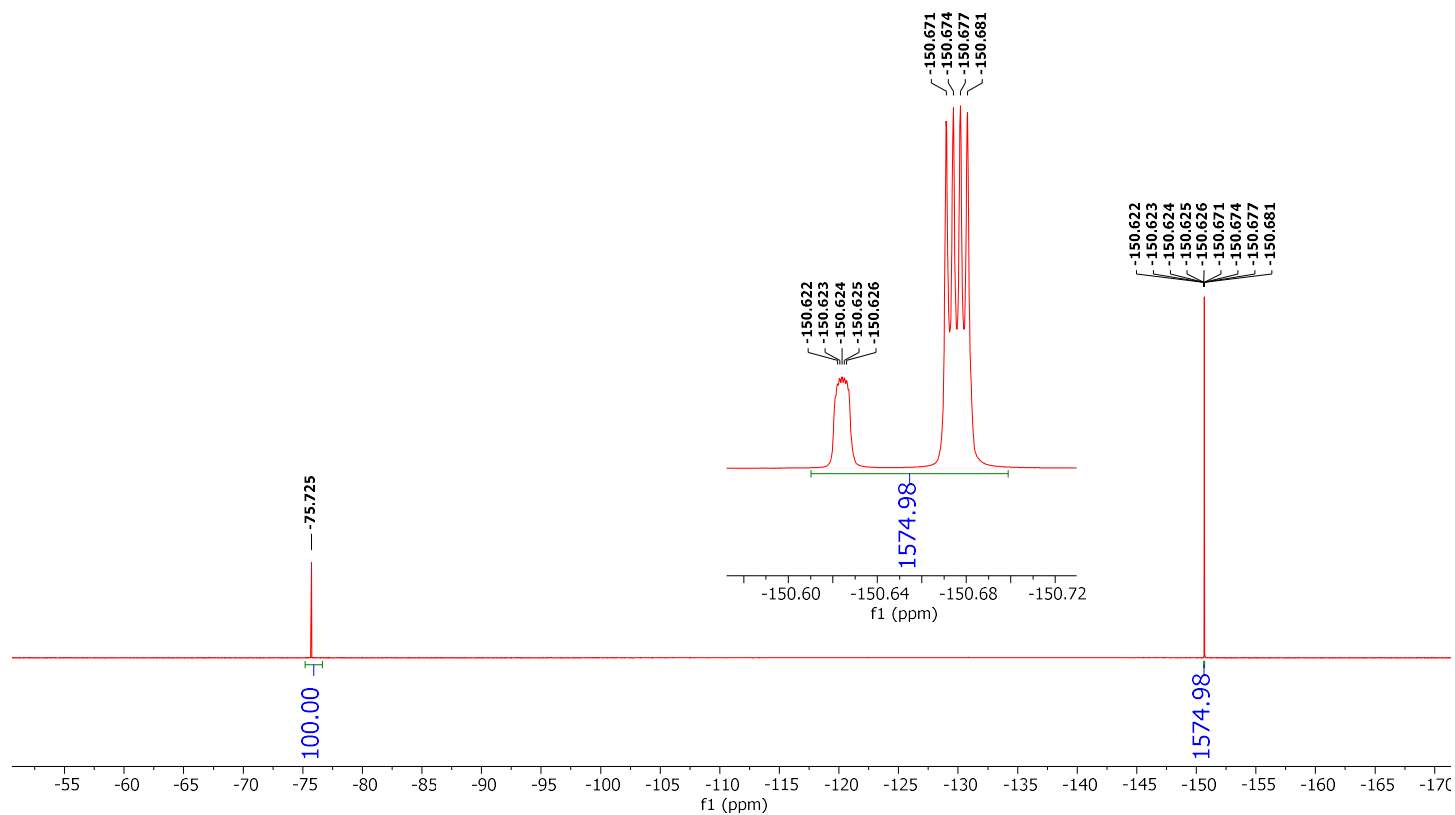


Figure 9-17 Conditions:  $25^\circ\text{C}$ ,  $470\text{ MHz}$ ,  $\text{D}_2\text{O}$

**$^{19}\text{F}$  NMR Spectra of  $\text{NaBF}_4$ , Sodium Trifluoro Acetate, Phenolphthalein, and Acetic Acid (Reaction 6)**

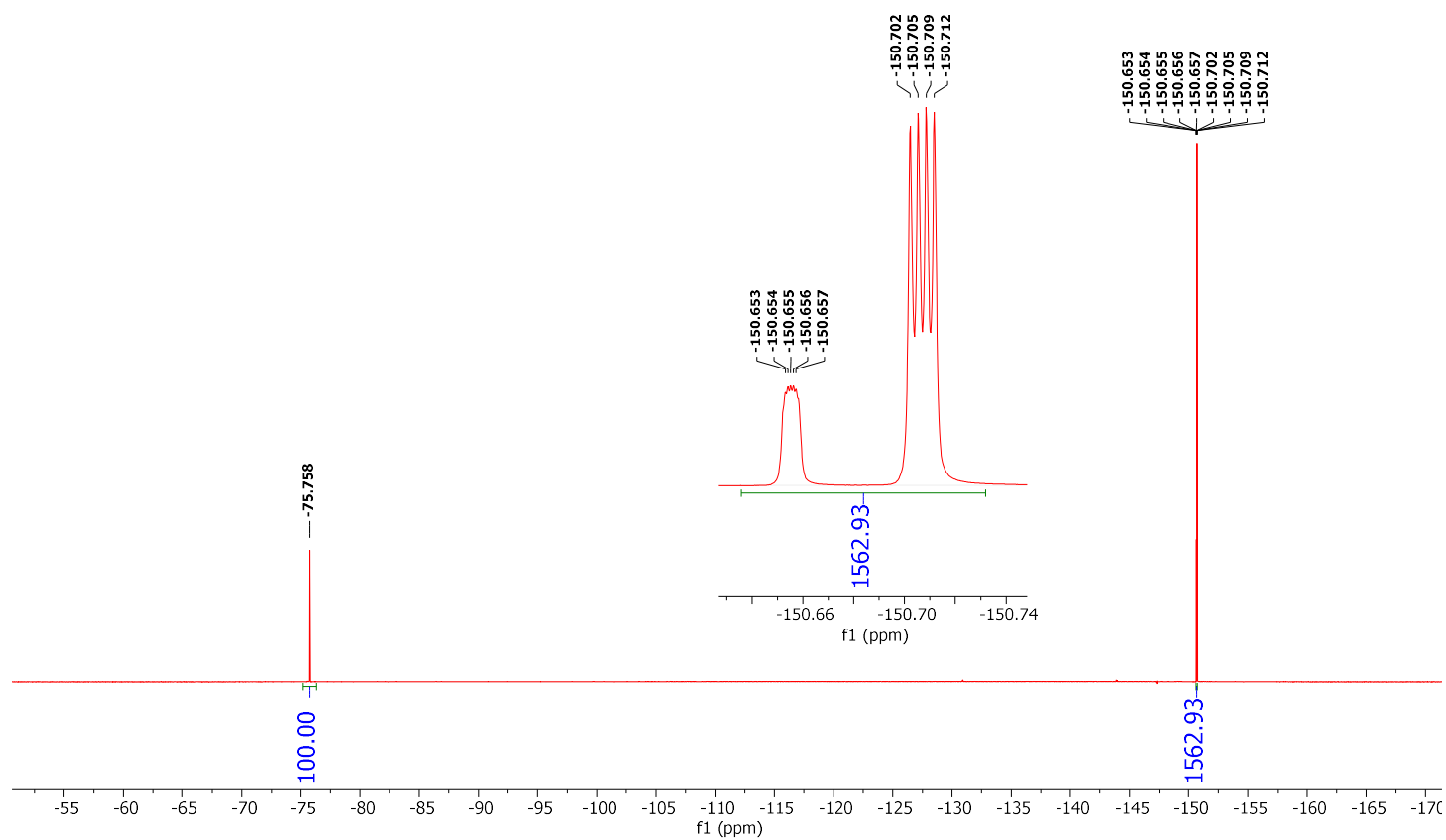


Figure 9-18 Conditions: 25 °C, 470 MHz,  $\text{D}_2\text{O}$



Small Spectral Window  $^{19}\text{F}$  NMR Spectra of  $\text{NaBF}_4$ , Sodium Trifluoroacetate, Phenolphthalein, and Acetic Acid Focusing on the  $\text{NaBF}_4$  Peak  
(Reaction 6)

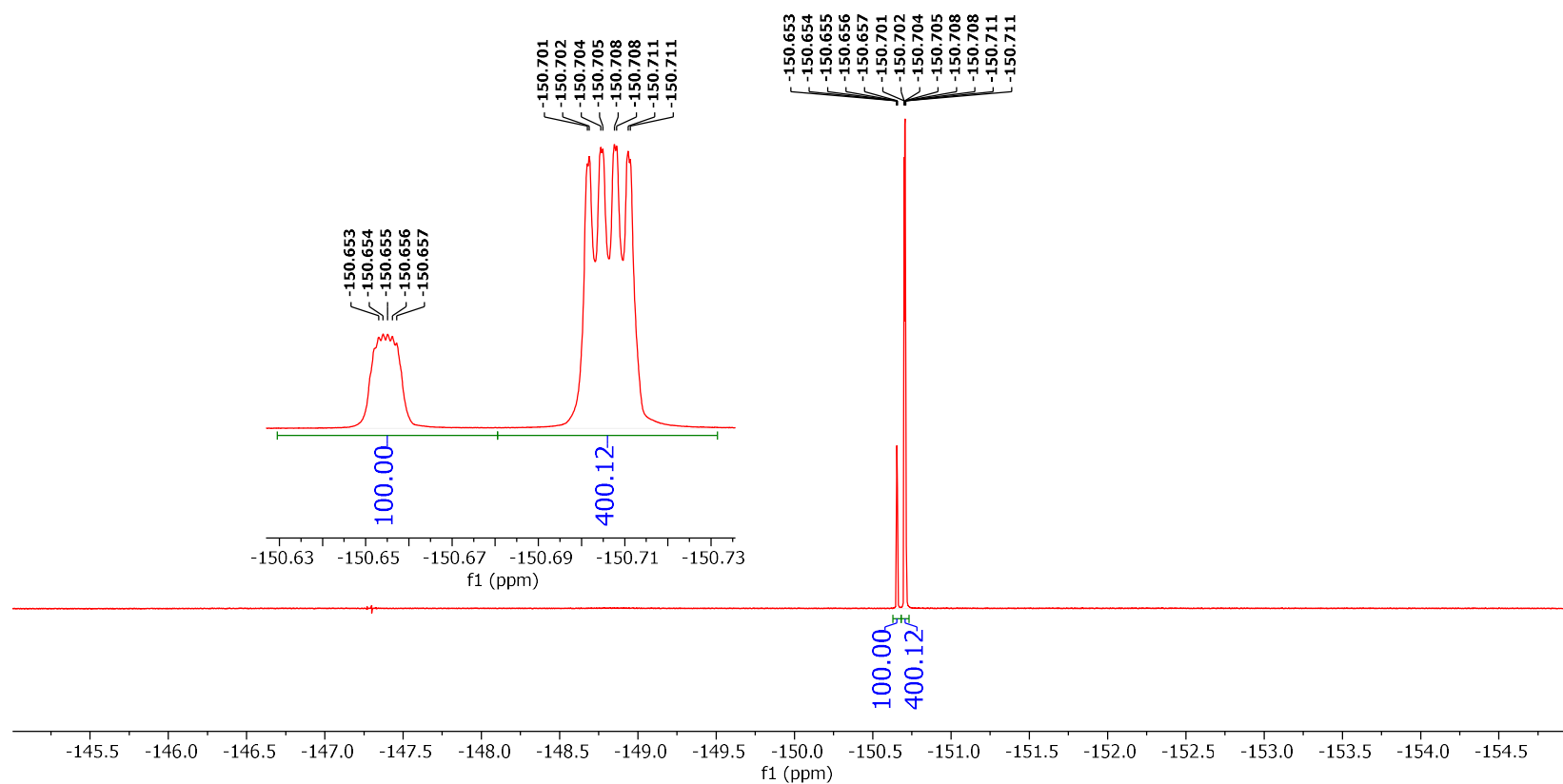


Figure 9-19 Conditions: 25 °C, 470 MHz,  $\text{D}_2\text{O}$

## APPENDIX B: CRYSTALLOGRAPHIC DATA

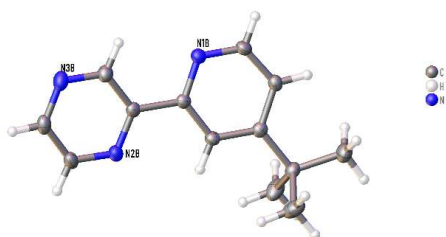


Figure 10-1 Structure of **Ligand-213**

Formula	C <sub>52</sub> H <sub>60</sub> N <sub>12</sub>
CCDC	2169118
$D_{calc.}/\text{g cm}^{-3}$	1.212
$m/\text{mm}^{-1}$	0.581
Formula Weight	853.12
Color	colourless
Shape	block-shaped
Size/ $\text{mm}^3$	0.24×0.20×0.09
$T/\text{K}$	100.00(10)
Crystal System	monoclinic
Space Group	$P2_1/c$
$a/\text{\AA}$	23.0373(2)
$b/\text{\AA}$	9.76616(9)
$c/\text{\AA}$	20.8418(2)
$a/^\circ$	90
$b/^\circ$	94.2447(9)
$g/^\circ$	90
$V/\text{\AA}^3$	4676.23(8)
$Z$	4
$Z'$	1
Wavelength/ $\text{\AA}$	1.54184
Radiation type	Cu $K_\alpha$
$Q_{min}/^\circ$	3.848
$Q_{max}/^\circ$	77.218
Measured Refl's.	32059
Indep't Refl's	9402
Refl's $I \geq 2\sigma(I)$	7893
$R_{int}$	0.0288
Parameters	589
Restraints	0
Largest Peak	0.441
Deepest Hole	-0.223
$wR_2$ (all data)	0.1236
$wR_2$	0.1152
$R_1$ (all data)	0.0507
$R_1$	0.0426

Table 10-1 General Crystal Structure Data for **Ligand-213**.

Atom	x	y	z	$U_{eq}$
N1A	-808.5(5)	4166.9(12)	3771.8(6)	29.8(2)
N2A	537.2(4)	5729.4(11)	4385.9(5)	24.9(2)
N3A	-253.3(5)	7806.3(12)	4631.0(6)	32.5(3)
C1	-29.9(5)	5610.0(12)	4201.2(6)	21.9(2)
C1A	-227.2(5)	4323.8(12)	3874.4(6)	22.4(2)
C2	-419.2(6)	6657.7(13)	4322.5(7)	28.7(3)
C2A	170.2(5)	3352.6(12)	3696.8(6)	21.8(2)
C3A	-21.8(6)	2133.0(13)	3401.3(6)	23.7(3)
C4A	-623.3(6)	1969.1(14)	3306.8(7)	30.1(3)
C5A	-989.7(6)	2997.4(15)	3493.2(7)	34.2(3)
C6A	411.6(6)	1080.4(13)	3184.7(6)	27.8(3)
C7A	114.2(8)	-270.0(16)	2973.5(8)	42.7(4)
C8A	705.7(8)	1676.7(17)	2610.2(8)	46.5(4)
C9A	869.5(8)	765.1(16)	3733.8(9)	47.8(4)
C12A	310.5(6)	7903.8(13)	4818.2(7)	28.1(3)
C13A	701.6(6)	6879.3(13)	4693.6(6)	27.2(3)
N1B	2937.5(4)	7125.6(10)	5228.4(5)	21.1(2)
N2B	1715.7(5)	9426.8(10)	5018.2(5)	23.5(2)
N3B	2066.5(5)	9884.9(11)	6317.4(5)	28.3(2)
C1B	2464.4(5)	7711.8(11)	4928.2(6)	18.5(2)
C2B	2251.7(5)	7376.6(11)	4304.9(5)	19.3(2)
C3B	2528.1(5)	6364.7(12)	3964.0(6)	19.7(2)
C4B	3017.6(5)	5761.9(12)	4276.5(6)	21.5(2)
C5B	3202.8(5)	6170.8(12)	4898.5(6)	22.8(2)
C6B	2297.4(5)	5963.2(12)	3280.1(6)	22.0(2)
C7B	2641.7(7)	4757.3(14)	3023.4(7)	33.3(3)
C8B	1661.7(6)	5510.6(17)	3278.7(7)	38.2(3)
C9B	2353.9(8)	7175.5(14)	2832.0(6)	36.9(3)
C10B	2166.4(5)	8749.8(11)	5310.5(6)	19.0(2)
C11B	2341.4(6)	8997.8(12)	5956.7(6)	24.2(3)
C12B	1617.4(6)	10546.8(12)	6019.1(6)	26.4(3)
C13B	1447.8(5)	10333.8(12)	5375.4(6)	25.3(3)
N1C	2097.4(4)	2988.4(10)	4571.5(5)	19.9(2)
N2C	3304.7(4)	632.8(10)	4746.8(5)	22.3(2)
N3C	2920.9(5)	167.9(11)	3459.2(5)	27.2(2)
C1C	2552.9(5)	2323.1(11)	4864.4(5)	17.5(2)
C2C	2754.2(5)	2545.8(11)	5504.6(5)	18.3(2)
C3C	2486.3(5)	3517.9(11)	5869.4(5)	18.4(2)
C4C	2015.3(5)	4216.0(12)	5562.1(6)	20.6(2)
C5C	1838.3(5)	3915.1(12)	4927.8(6)	21.4(2)

Table 10-2 Fractional Atomic Coordinates ( $\times 10^4$ ) and Equivalent Isotropic Displacement Parameters ( $\text{\AA}^2 \times 10^3$ ) for **Ligand-213**.  $U_{eq}$  is defined as 1/3 of the trace of the orthogonalized  $U_{ij}$ .

Table 10-2 (cont'd)

Atom	x	y	z	$U_{eq}$
C6C	2685.0(5)	3825.5(12)	6571.8(6)	21.0(2)
C7C	3174.4(6)	2876.1(14)	6829.4(6)	30.1(3)
C8C	2166.5(6)	3655.2(14)	6986.8(6)	29.3(3)
C9C	2902.4(7)	5306.2(13)	6624.9(6)	33.5(3)
C10C	2845.2(5)	1301.9(11)	4468.1(5)	18.4(2)
C11C	2655.5(6)	1056.6(12)	3827.2(6)	22.9(2)
C12C	3376.3(6)	-496.0(12)	3745.8(6)	25.5(3)
C13C	3563.7(5)	-277.4(12)	4383.4(6)	24.7(3)
N1D	4265.6(5)	4105.1(11)	3730.5(5)	25.5(2)
N2D	5576.9(4)	5710.8(10)	4414.4(5)	23.4(2)
N3D	4766.8(5)	7791.4(11)	4586.0(6)	29.3(2)
C1D	4843.0(5)	4288.2(12)	3854.8(6)	20.8(2)
C2D	5256.3(5)	3326.9(12)	3704.9(6)	21.2(2)
C3D	5082.0(5)	2089.8(12)	3412.3(6)	22.4(2)
C4D	4484.4(6)	1900.1(13)	3290.0(6)	26.1(3)
C5D	4102.9(6)	2920.5(14)	3453.0(6)	28.5(3)
C6D	5534.7(6)	1044.2(13)	3232.7(7)	29.0(3)
C7D	5953.8(7)	743.0(16)	3823.2(9)	45.3(4)
C8D	5868.3(8)	1651.2(17)	2688.4(9)	49.3(4)
C9D	5255.0(7)	-313.4(14)	3004.0(8)	36.5(3)
C10D	5020.0(5)	5588.1(12)	4185.2(6)	20.1(2)
C11D	4622.1(5)	6640.1(13)	4267.4(6)	25.7(3)
C12D	5318.7(6)	7885.8(13)	4823.3(6)	26.7(3)
C13D	5720.2(5)	6861.5(13)	4733.0(6)	25.0(3)

Atom	$U_{11}$	$U_{22}$	$U_{33}$	$U_{23}$	$U_{13}$	$U_{12}$
N1A	19.6(5)	34.7(6)	35.0(6)	-3.9(5)	1.5(4)	-1.6(4)
N2A	20.1(5)	25.6(5)	29.3(6)	-2.8(4)	3.0(4)	0.3(4)
N3A	25.3(6)	27.5(6)	45.2(7)	-3.5(5)	5.7(5)	3.0(4)
C1	19.6(6)	23.9(6)	22.6(6)	2.8(4)	4.0(4)	0.5(4)
C1A	19.4(6)	26.5(6)	21.3(6)	2.0(5)	1.3(4)	-0.9(5)
C2	21.0(6)	28.0(6)	37.1(7)	-0.7(5)	3.0(5)	1.8(5)
C2A	20.4(6)	24.3(6)	20.6(6)	1.8(4)	1.0(4)	-1.7(5)
C3A	27.2(6)	25.8(6)	17.9(6)	1.7(4)	0.3(5)	-2.6(5)
C4A	28.4(7)	32.0(7)	29.9(7)	-4.8(5)	1.2(5)	-7.7(5)
C5A	21.0(6)	41.3(8)	39.9(8)	-7.2(6)	0.0(5)	-7.2(5)
C6A	32.3(7)	22.4(6)	28.3(7)	-3.6(5)	0.0(5)	-0.2(5)
C7A	48.6(9)	33.6(8)	45.7(9)	-13.2(7)	3.2(7)	-4.7(7)
C8A	52.9(10)	39.6(8)	50.0(10)	-2.5(7)	23.8(8)	4.8(7)
C9A	52.2(10)	33.2(8)	55.0(10)	-9.0(7)	-16.0(8)	10.8(7)
C12A	28.2(7)	24.1(6)	32.5(7)	-3.3(5)	5.4(5)	-1.2(5)
C13A	21.6(6)	26.9(6)	32.8(7)	-3.7(5)	1.7(5)	-2.3(5)
N1B	21.9(5)	18.6(5)	22.4(5)	0.7(4)	-0.8(4)	1.5(4)
N2B	23.1(5)	19.4(5)	27.7(5)	-3.2(4)	0.0(4)	2.1(4)
N3B	37.8(6)	22.6(5)	24.7(5)	-3.1(4)	4.0(5)	1.5(4)
C1B	19.1(5)	15.5(5)	20.8(5)	1.5(4)	0.8(4)	-1.5(4)
C2B	19.9(5)	18.1(5)	19.6(5)	2.5(4)	-0.1(4)	0.7(4)
C3B	20.8(5)	18.5(5)	20.1(6)	1.2(4)	2.5(4)	-2.8(4)
C4B	21.6(6)	18.7(5)	24.6(6)	-0.9(4)	3.7(5)	1.2(4)
C5B	21.0(6)	20.7(6)	26.1(6)	1.6(5)	-1.9(5)	3.1(4)
C6B	25.6(6)	22.0(6)	18.3(6)	-1.1(4)	1.2(4)	-0.9(5)
C7B	40.4(8)	30.4(7)	28.8(7)	-6.8(5)	0.2(6)	4.3(6)
C8B	31.1(7)	57.0(9)	26.2(7)	-7.3(6)	-1.0(6)	-7.0(6)
C9B	60.9(10)	27.2(7)	21.8(6)	1.0(5)	-2.2(6)	-2.7(6)
C10B	20.4(5)	14.6(5)	22.0(6)	0.8(4)	1.1(4)	-2.4(4)
C11B	29.9(6)	20.1(6)	22.6(6)	0.2(4)	1.6(5)	1.3(5)
C12B	28.6(6)	19.7(6)	31.6(7)	-5.0(5)	7.2(5)	-1.3(5)
C13B	22.0(6)	19.7(6)	34.2(7)	-4.1(5)	1.2(5)	2.2(5)
N1C	20.7(5)	17.5(5)	21.0(5)	0.2(4)	-0.6(4)	1.3(4)
N2C	22.2(5)	18.4(5)	26.2(5)	-3.0(4)	0.3(4)	2.8(4)
N3C	37.4(6)	21.5(5)	23.0(5)	-3.2(4)	3.5(4)	2.4(4)
C1C	18.1(5)	14.3(5)	19.9(5)	1.4(4)	1.3(4)	-1.1(4)
C2C	18.2(5)	16.5(5)	20.0(5)	1.8(4)	1.0(4)	0.8(4)
C3C	20.1(5)	16.2(5)	19.0(6)	1.2(4)	2.3(4)	-1.5(4)
C4C	21.7(6)	18.2(5)	22.3(6)	0.0(4)	4.5(4)	2.1(4)
C5C	19.4(5)	19.6(5)	24.7(6)	2.3(4)	-0.4(4)	3.5(4)

Table 10-3 Anisotropic Displacement Parameters ( $\times 10^4$ ) for **Ligand-213**. The anisotropic displacement factor exponent takes the form:  $-2p^2[h^2a^{*2} \times U_{11} + \dots + 2hka^* \times b^* \times U_{12}]$ .

Table 10-3 (cont'd)

Atom	$U_{11}$	$U_{22}$	$U_{33}$	$U_{23}$	$U_{13}$	$U_{12}$
C6C	25.5(6)	20.2(6)	17.3(5)	-0.4(4)	1.3(4)	-0.3(4)
C7C	33.0(7)	36.1(7)	20.4(6)	-2.0(5)	-3.6(5)	7.2(6)
C8C	31.3(7)	37.2(7)	19.7(6)	-0.7(5)	4.3(5)	-0.4(5)
C9C	50.9(9)	26.0(6)	23.0(6)	-1.7(5)	-1.9(6)	-9.5(6)
C10C	20.0(5)	14.9(5)	20.3(6)	0.6(4)	2.0(4)	-2.3(4)
C11C	28.1(6)	19.0(6)	21.3(6)	-0.3(4)	0.5(5)	1.9(5)
C12C	29.3(6)	19.1(6)	29.1(6)	-5.8(5)	8.3(5)	0.1(5)
C13C	21.6(6)	20.0(6)	32.7(7)	-3.9(5)	2.8(5)	1.9(5)
N1D	19.8(5)	28.5(5)	27.9(5)	-1.7(4)	0.1(4)	-0.7(4)
N2D	19.2(5)	24.5(5)	26.3(5)	-2.2(4)	0.9(4)	0.9(4)
N3D	25.2(5)	25.0(5)	37.5(6)	-3.2(4)	1.5(5)	3.0(4)
C1D	19.8(6)	23.2(6)	19.3(6)	2.3(4)	0.7(4)	-0.4(4)
C2D	19.1(5)	23.6(6)	20.7(6)	1.3(4)	-0.1(4)	-0.9(4)
C3D	26.3(6)	22.6(6)	18.1(5)	1.2(4)	1.1(5)	-0.5(5)
C4D	27.3(6)	26.3(6)	24.3(6)	-2.3(5)	0.1(5)	-4.5(5)
C5D	20.9(6)	32.7(7)	31.5(7)	-2.6(5)	-1.1(5)	-4.5(5)
C6D	29.2(7)	24.3(6)	33.5(7)	-6.1(5)	2.0(5)	1.0(5)
C7D	41.9(9)	29.8(7)	60.7(10)	-13.8(7)	-18.8(8)	12.7(6)
C8D	53.5(10)	38.5(8)	59.9(11)	-11.7(8)	31.6(8)	-1.1(7)
C9D	41.9(8)	26.5(7)	40.5(8)	-11.6(6)	-0.9(6)	1.1(6)
C10D	19.4(5)	22.3(6)	18.8(5)	2.7(4)	2.4(4)	0.3(4)
C11D	20.6(6)	24.6(6)	31.6(7)	0.5(5)	0.2(5)	2.4(5)
C12D	27.8(6)	22.9(6)	29.5(7)	-3.2(5)	2.9(5)	-1.0(5)
C13D	20.1(6)	26.6(6)	28.2(6)	-2.2(5)	0.3(5)	-1.7(5)

Atom	Atom	Length/Å
N1A	C1A	1.3491(16)
N1A	C5A	1.3341(18)
N2A	C1	1.3396(16)
N2A	C13A	1.3342(17)
N3A	C2	1.3347(18)
N3A	C12A	1.3317(18)
C1	C1A	1.4841(17)
C1	C2	1.3960(17)
C1A	C2A	1.3875(17)
C2A	C3A	1.3976(17)
C3A	C4A	1.3944(18)
C3A	C6A	1.5244(18)
C4A	C5A	1.386(2)
C6A	C7A	1.5355(19)
C6A	C8A	1.534(2)
C6A	C9A	1.529(2)
C12A	C13A	1.3838(18)
N1B	C1B	1.3439(15)
N1B	C5B	1.3335(16)
N2B	C10B	1.3388(15)
N2B	C13B	1.3371(16)
N3B	C11B	1.3369(16)
N3B	C12B	1.3339(17)
C1B	C2B	1.3931(16)
C1B	C10B	1.4883(16)
C2B	C3B	1.3977(16)
C3B	C4B	1.3906(17)
C3B	C6B	1.5349(16)
C4B	C5B	1.3929(17)
C6B	C7B	1.5379(17)
C6B	C8B	1.5295(18)
C6B	C9B	1.5195(18)
C10B	C11B	1.3982(17)
C12B	C13B	1.3851(18)
N1C	C1C	1.3419(15)
N1C	C5C	1.3388(15)
N2C	C10C	1.3394(15)
N2C	C13C	1.3367(16)
N3C	C11C	1.3360(16)
N3C	C12C	1.3359(17)
C1C	C2C	1.3969(16)
C1C	C10C	1.4874(15)
C2C	C3C	1.3892(16)

Table 10-4 Bond Lengths in Å for **Ligand-213**.

Table 10-4 (cont'd)

Atom	Atom	Length/Å
C3C	C4C	1.3963(16)
C3C	C6C	1.5309(16)
C4C	C5C	1.3858(17)
C6C	C7C	1.5263(17)
C6C	C8C	1.5348(17)
C6C	C9C	1.5316(17)
N2D	C13D	1.3343(16)
N3D	C11D	1.3354(17)
N3D	C12D	1.3331(17)
C1D	C2D	1.3891(17)
C1D	C10D	1.4867(16)
C2D	C3D	1.3987(17)
C3D	C4D	1.3937(18)
C3D	C6D	1.5260(17)
C4D	C5D	1.3875(19)
C6D	C7D	1.536(2)
C6D	C8D	1.536(2)
C6D	C9D	1.5345(18)
C10D	C11D	1.3959(17)
C12D	C13D	1.3847(18)



Atom	Atom	Atom	Angle/°
C5A	N1A	C1A	116.17(11)
C13A	N2A	C1	116.58(11)
C12A	N3A	C2	116.08(11)
N2A	C1	C1A	117.68(11)
N2A	C1	C2	120.68(11)
C2	C1	C1A	121.63(11)
N1A	C1A	C1	115.82(11)
N1A	C1A	C2A	123.16(11)
C2A	C1A	C1	121.02(11)
N3A	C2	C1	122.57(12)
C1A	C2A	C3A	120.44(11)
C2A	C3A	C6A	120.83(11)
C4A	C3A	C2A	116.03(12)
C4A	C3A	C6A	123.13(11)
C5A	C4A	C3A	119.78(12)
N1A	C5A	C4A	124.41(12)
C3A	C6A	C7A	112.08(12)
C3A	C6A	C8A	108.18(11)
C3A	C6A	C9A	110.17(11)
C8A	C6A	C7A	108.41(12)
C9A	C6A	C7A	108.06(12)
C9A	C6A	C8A	109.91(14)
N3A	C12A	C13A	121.86(12)
N2A	C13A	C12A	122.22(12)
C5B	N1B	C1B	116.40(10)
C13B	N2B	C10B	116.62(11)
C12B	N3B	C11B	115.81(11)
N1B	C1B	C2B	123.46(11)
N2B	C10B	C1B	117.76(10)
N2B	C10B	C11B	120.76(11)
C11B	C10B	C1B	121.47(10)
N3B	C11B	C10B	122.62(12)
N3B	C12B	C13B	122.15(11)
N2B	C13B	C12B	122.01(12)
C5C	N1C	C1C	116.15(10)
C13C	N2C	C10C	116.77(10)
C11C	N3C	C12C	115.87(11)
N1C	C1C	C2C	123.52(10)
N1C	C1C	C10C	116.29(10)
C2C	C1C	C10C	120.18(10)
C3C	C2C	C1C	119.98(10)
C2C	C3C	C4C	116.37(10)
C2C	C3C	C6C	122.96(10)
C4C	C3C	C6C	120.67(10)

Table 10-5 Bond Angles in ° for **Ligand-213**.

Table 10-5 (cont'd)

Atom	Atom	Atom	Angle/°
C5C	C4C	C3C	119.86(11)
N1C	C5C	C4C	124.10(11)
C3C	C6C	C8C	109.12(10)
C3C	C6C	C9C	109.11(10)
C7C	C6C	C3C	112.21(10)
C7C	C6C	C8C	108.75(10)
C7C	C6C	C9C	108.61(11)
C9C	C6C	C8C	109.00(11)
N2C	C10C	C1C	117.53(10)
N2C	C10C	C11C	120.86(11)
C11C	C10C	C1C	121.61(10)
N3C	C11C	C10C	122.47(11)
N3C	C12C	C13C	122.25(11)
N2C	C13C	C12C	121.76(11)
C5D	N1D	C1D	116.08(11)
C13D	N2D	C10D	116.59(10)
C12D	N3D	C11D	116.02(11)
N1D	C1D	C2D	123.37(11)
N1D	C1D	C10D	115.80(10)
C2D	C1D	C10D	120.81(10)
C1D	C2D	C3D	120.17(11)
C2D	C3D	C6D	120.38(11)
C4D	C3D	C2D	116.25(11)
C4D	C3D	C6D	123.36(11)
C5D	C4D	C3D	119.65(12)
N1D	C5D	C4D	124.48(12)
C3D	C6D	C7D	109.40(11)
C3D	C6D	C8D	108.15(11)
C3D	C6D	C9D	112.05(11)
C7D	C6D	C8D	110.28(14)
C9D	C6D	C7D	107.94(12)
C9D	C6D	C8D	109.01(12)
N2D	C10D	C1D	117.63(10)
N2D	C10D	C11D	120.68(11)
C11D	C10D	C1D	121.68(11)
N3D	C11D	C10D	122.60(11)
N3D	C12D	C13D	121.87(12)
N2D	C13D	C12D	122.21(12)

Atom	Atom	Atom	Atom	Angle/°
N1A	C1A	C2A	C3A	-0.58(19)
N2A	C1	C1A	N1A	171.66(11)
N2A	C1	C1A	C2A	-7.65(17)
N2A	C1	C2	N3A	-0.9(2)
N3A	C12A	C13A	N2A	-0.8(2)
C1	N2A	C13A	C12A	-0.04(19)
C1	C1A	C2A	C3A	178.67(11)
C1A	N1A	C5A	C4A	-0.3(2)
C1A	C1	C2	N3A	178.15(12)
C1A	C2A	C3A	C4A	-0.49(17)
C1A	C2A	C3A	C6A	177.99(11)
C2	N3A	C12A	C13A	0.7(2)
C2	C1	C1A	N1A	-7.46(18)
C2	C1	C1A	C2A	173.23(12)
C2A	C3A	C4A	C5A	1.12(19)
C2A	C3A	C6A	C7A	170.83(12)
C2A	C3A	C6A	C8A	-69.70(15)
C2A	C3A	C6A	C9A	50.46(16)
C3A	C4A	C5A	N1A	-0.8(2)
C4A	C3A	C6A	C7A	-10.80(18)
C4A	C3A	C6A	C8A	108.67(15)
C4A	C3A	C6A	C9A	-131.17(14)
C5A	N1A	C1A	C1	-178.33(12)
C5A	N1A	C1A	C2A	0.96(19)
C6A	C3A	C4A	C5A	-177.32(13)
C12A	N3A	C2	C1	0.2(2)
C13A	N2A	C1	C1A	-178.29(11)
C13A	N2A	C1	C2	0.84(18)
N1B	C1B	C2B	C3B	1.18(17)
N1B	C1B	C10B	N2B	175.74(10)
N1B	C1B	C10B	C11B	-5.43(16)
N2B	C10B	C11B	N3B	1.51(19)
N3B	C12B	C13B	N2B	1.6(2)
C1B	N1B	C5B	C4B	-0.17(18)
C1B	C2B	C3B	C4B	-1.15(16)
C1B	C2B	C3B	C6B	179.18(10)
C1B	C10B	C11B	N3B	-177.28(11)
C2B	C1B	C10B	N2B	-5.19(16)
C2B	C1B	C10B	C11B	173.63(11)
C2B	C3B	C4B	C5B	0.55(17)
C2B	C3B	C6B	C7B	-175.61(11)
C2B	C3B	C6B	C8B	-56.79(15)
C2B	C3B	C6B	C9B	64.70(15)
C3B	C4B	C5B	N1B	0.13(19)

Table 10-6 Torsion Angles in ° for **Ligand-213**.

Table 10-6 (cont'd)

Atom	Atom	Atom	Atom	Angle/°
C5B	N1B	C1B	C2B	-0.48(17)
C5B	N1B	C1B	C10B	178.56(10)
C6B	C3B	C4B	C5B	-179.80(11)
C10B	N2B	C13B	C12B	-1.34(18)
C10B	C1B	C2B	C3B	-177.81(10)
C11B	N3B	C12B	C13B	-0.28(19)
C12B	N3B	C11B	C10B	-1.23(18)
C13B	N2B	C10B	C1B	178.68(10)
C13B	N2B	C10B	C11B	-0.15(17)
N1C	C1C	C2C	C3C	-1.24(17)
N1C	C1C	C10C	N2C	179.35(10)
N1C	C1C	C10C	C11C	0.18(16)
N2C	C10C	C11C	N3C	-0.80(18)
N3C	C12C	C13C	N2C	-1.2(2)
C1C	N1C	C5C	C4C	0.47(17)
C1C	C2C	C3C	C4C	0.69(16)
C1C	C2C	C3C	C6C	-179.56(10)
C1C	C10C	C11C	N3C	178.35(11)
C2C	C1C	C10C	N2C	-0.74(16)
C2C	C1C	C10C	C11C	-179.91(11)
C2C	C3C	C4C	C5C	0.33(16)
C2C	C3C	C6C	C7C	-4.18(16)
C2C	C3C	C6C	C8C	-124.77(12)
C2C	C3C	C6C	C9C	116.24(13)
C3C	C4C	C5C	N1C	-0.97(18)
C4C	C3C	C6C	C7C	175.57(11)
C4C	C3C	C6C	C8C	54.98(14)
C4C	C3C	C6C	C9C	-64.02(15)
C5C	N1C	C1C	C2C	0.64(16)
C5C	N1C	C1C	C10C	-179.46(10)
C6C	C3C	C4C	C5C	-179.43(10)
C10C	N2C	C13C	C12C	1.54(18)
C10C	C1C	C2C	C3C	178.86(10)
C11C	N3C	C12C	C13C	-0.16(18)
C12C	N3C	C11C	C10C	1.13(18)
C13C	N2C	C10C	C1C	-179.75(10)
C13C	N2C	C10C	C11C	-0.57(17)
N1D	C1D	C2D	C3D	-0.31(18)
N1D	C1D	C10D	N2D	168.98(10)
N1D	C1D	C10D	C11D	-9.82(17)
N2D	C10D	C11D	N3D	-1.63(19)
N3D	C12D	C13D	N2D	-1.3(2)
C1D	N1D	C5D	C4D	-0.09(19)

Table 10-6 (cont'd)

Atom	Atom	Atom	Atom	Angle/°
C1D	C2D	C3D	C4D	-0.26(17)
C1D	C2D	C3D	C6D	178.60(11)
C1D	C10D	C11D	N3D	177.14(11)
C2D	C3D	C4D	C5D	0.62(18)
C2D	C3D	C6D	C7D	52.53(16)
C2D	C3D	C6D	C8D	-67.62(16)
C2D	C3D	C6D	C9D	172.20(11)
C3D	C4D	C5D	N1D	-0.5(2)
C4D	C3D	C6D	C7D	-128.70(14)
C4D	C3D	C6D	C8D	111.16(15)
C4D	C3D	C6D	C9D	-9.02(18)
C5D	N1D	C1D	C2D	0.49(18)
C5D	N1D	C1D	C10D	-177.89(11)
C6D	C3D	C4D	C5D	-178.20(12)
C10D	N2D	C13D	C12D	-0.24(18)
C10D	C1D	C2D	C3D	177.98(10)
C11D	N3D	C12D	C13D	1.25(19)
C12D	N3D	C11D	C10D	0.14(19)
C13D	N2D	C10D	C1D	-177.22(11)
C13D	N2D	C10D	C11D	1.60(17)

Atom	x	y	z	$U_{eq}$
H2	-817.83	6548.98	4179.86	34
H2A	575.48	3517.69	3776.68	26
H4A	-781.44	1155.08	3115.24	36
H5A	-1397.25	2860.42	3417.49	41
H7AA	-90.82	-644.74	3329.81	64
H7AB	408.52	-926.27	2851.79	64
H7AC	-164.97	-100.72	2604.07	64
H8AA	409.85	1878.62	2260.82	70
H8AB	984.24	1011.14	2461.03	70
H8AC	911.1	2521.49	2741.78	70
H9AA	1088.93	1599.25	3850.76	72
H9AB	1136.28	61.14	3595.01	72
H9AC	676.69	432.84	4107.51	72
H12A	448.12	8699.12	5043.67	34
H13A	1100.67	6998.77	4831.92	33
H2B	1919.4	7834.89	4111.86	23
H4B	3224.94	5073.56	4066.54	26
H5B	3538.98	5743.17	5100.09	27
H7BA	2603.47	3957.81	3301.25	50
H7BB	3053.15	5009.93	3020.51	50
H7BC	2487.72	4535.77	2584.7	50
H8BA	1426	6269.19	3424.59	57
H8BB	1632.62	4728.11	3568.96	57
H8BC	1519.1	5244.65	2841.8	57
H9BA	2763.49	7448.97	2836.05	55
H9BB	2122.9	7943.13	2976.9	55
H9BC	2211.93	6916.15	2393.95	55
H11B	2668.71	8516.63	6147.1	29
H12B	1407.04	11185.09	6255.96	32
H13B	1131.4	10847.75	5181.71	30
H2C	3074.2	2032.56	5690.48	22
H4C	1816.53	4895.75	5787.32	25
H5C	1512.75	4396.57	4733.57	26
H7CA	3515.71	3012.34	6582.61	45
H7CB	3044.64	1922.54	6787.33	45
H7CC	3277.09	3083.75	7283.7	45
H8CA	2038.47	2698.06	6974.06	44
H8CB	1845.91	4244.75	6819.51	44
H8CC	2284.07	3914.19	7431.83	44
H9CA	2588.81	5929.15	6471.17	50
H9CB	3234.76	5421.93	6362.4	50
H9CC	3022.68	5514.89	7075.15	50

Table 10-7 Hydrogen Fractional Atomic Coordinates ( $\times 10^4$ ) and Equivalent Isotropic Displacement Parameters ( $\text{\AA}^2 \times 10^3$ ) for **Ligand-213**.  $U_{eq}$  is defined as 1/3 of the trace of the orthogonalized  $U_{ij}$ .

Table 10-7 (cont'd)

Atom	x	y	z	$U_{eq}$
H11C	2325.1	1539.69	3645.54	27
H12C	3578.29	-1140.2	3503.32	31
H13C	3885.09	-787.85	4568.01	30
H5D	3698.25	2765.32	3360.87	34
H7DA	5733.46	393.75	4173.04	68
H7DB	6156.1	1586.72	3962.54	68
H7DC	6239.48	56.12	3711.02	68
H8DA	6056.2	2507.65	2834.7	74
H8DB	5596.57	1834.27	2314.07	74
H8DC	6165.19	998.91	2569.13	74
H9DA	5004.21	-156.95	2610.27	55
H9DB	5021.67	-679.09	3339.27	55
H9DC	5560.55	-971.16	2916.44	55
H11D	4233.03	6532.71	4089.74	31
H12D	5440.13	8678.43	5061.1	32
H13D	6110.74	6981.92	4903.7	30

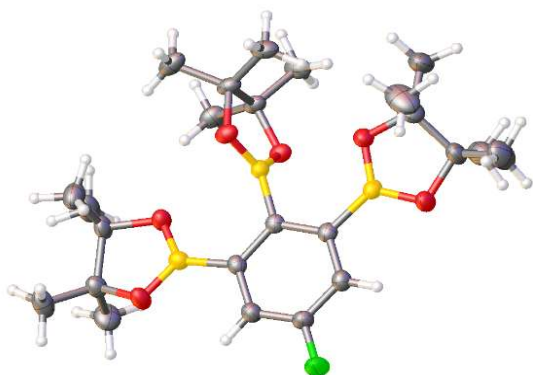


Figure 10-2 Structure of Compound 3a

Formula	C <sub>48</sub> H <sub>76</sub> B <sub>6</sub> F <sub>2</sub> O <sub>12</sub>
CCDC	2112718
Dcalc	1.198
<i>m</i> /mm <sup>-1</sup>	0.705
Formula Weight	947.94
Colour	colourless
Shape	irregular-shaped
Size/mm <sup>3</sup>	0.17×0.11×0.05
<i>T</i> /K	100(1)
Crystal System	orthorhombic
Flack Parameter	-0.03(9)
Hooft Parameter	-0.03(9)
Space Group	<i>Pca</i> 2 <sub>1</sub>
<i>a</i> /Å	13.32991(18)
<i>b</i> /Å	13.67698(18)
<i>c</i> /Å	28.8179(4)
<i>a</i> /°	90
<i>b</i> /°	90
<i>g</i> /°	90
<i>V</i> /Å <sup>3</sup>	5253.88(12)
<i>Z</i>	4
<i>Z</i> '	1
Wavelength/Å	1.54184
Radiation type	Cu K <sub>α</sub>
<i>Q</i> <sub>min</sub> /°	3.067
<i>Q</i> <sub>max</sub> /°	84.312
Measured Refl's.	18248
Indep't Refl's	18248
Refl's <i>I</i> ≥2 <i>s</i> ( <i>I</i> )	16984
<i>R</i> <sub>int</sub>	.
Parameters	715
Restraints	203
Largest Peak	0.377
Deepest Hole	-0.408
GooF	1.048
<i>wR</i> <sub>2</sub> (all data)	0.1902
<i>wR</i> <sub>2</sub>	0.1780
<i>R</i> <sub>1</sub> (all data)	0.0683
<i>R</i> <sub>1</sub>	0.0629

Table 10-8 General Crystal Structure Data for Compound **3a**.



Atom	x	y	z	$U_{eq}$
F1	2520(3)	2471(2)	7765.7(10)	47.0(8)
O1	4229(3)	255(2)	6594.7(12)	37.9(8)
O2	4207(2)	1074(2)	5906.8(12)	34.8(7)
O3	2158(2)	1838(2)	5530.0(10)	28.0(6)
O4	3155(2)	3197(2)	5519.1(10)	29.7(6)
O5	1163(2)	4029(2)	5873.8(11)	32.4(7)
O6	907(3)	4744(2)	6578.2(12)	35.0(7)
C1	3165(3)	1819(3)	6583.4(14)	25.9(8)
C2	2629(3)	2533(3)	6332.1(15)	24.1(8)
C3	2042(3)	3224(3)	6578.0(15)	26.1(8)
C4	2018(3)	3201(3)	7060.0(16)	30.9(9)
C5	2549(4)	2495(3)	7295.8(15)	31.9(10)
C6	3124(3)	1797(3)	7065.6(15)	29.6(9)
C7	4787(4)	-346(4)	6270.4(18)	40.2(11)
C8	5013(4)	363(4)	5873(2)	43.4(11)
C9	5646(6)	-818(6)	6516(2)	66.0(19)
C10	4035(5)	-1152(4)	6118(2)	52.2(14)
C11	6006(5)	915(6)	5961(3)	70(2)
C12	5038(6)	-68(5)	5395(2)	58.1(16)
C13	2239(3)	2095(3)	5042.0(15)	29.5(9)
C14	3113(4)	2872(3)	5036.5(14)	31.0(9)
C15	2453(4)	1173(4)	4766.5(17)	37.5(10)
C16	1221(4)	2520(4)	4901.8(16)	36.1(10)
C17	4139(4)	2441(4)	4931.7(17)	38.1(10)
C18	2916(4)	3747(4)	4725.2(17)	40.0(11)
C19	639(4)	4950(4)	5781.8(16)	34.4(10)
C20	189(4)	5204(3)	6263.6(16)	34.3(10)
C21	1428(4)	5678(4)	5622(2)	49.8(14)
C22	-134(5)	4785(4)	5406.7(18)	48.2(14)
C23	125(4)	6282(4)	6371(2)	44.0(12)
C24	-815(4)	4724(5)	6350(2)	50.0(13)
B1	3871(4)	1037(3)	6350.9(17)	27.0(9)
B2	2642(3)	2529(3)	5782.1(16)	25.3(9)
B3	1369(4)	4012(3)	6335.4(17)	27.3(9)
F1A	2787(3)	7566(2)	5270.8(10)	45.3(7)
O1A	850(3)	9613(3)	4085.1(13)	46.0(10)
O2A	788(2)	8660(2)	3441.2(11)	34.8(7)
O3A	2270(3)	6762(2)	3022.6(10)	33.2(7)
O4A	2948(2)	8281(2)	3041.3(10)	32.4(7)
O5A	4259(12)	6126(10)	3372(6)	33(2)
O5B	4511(12)	6375(11)	3429(6)	31(2)

Table 10-9 Fractional Atomic Coordinates ( $\times 10^4$ ) and Equivalent Isotropic Displacement Parameters ( $\text{\AA}^2 \times 10^3$ ) for **3a**.  $U_{eq}$  is defined as 1/3 of the trace of the orthogonalised  $U_{ij}$ .

Table 10-9 (cont'd)

Atom	x	y	z	$U_{eq}$
O6A	4607(8)	5446(10)	4083(4)	36(2)
O6B	4254(8)	5272(11)	4004(5)	40(2)
C1A	2007(3)	8129(3)	4091.2(14)	24.5(8)
C2A	2633(3)	7489(3)	3836.7(14)	21.8(7)
C3A	3297(3)	6868(3)	4077.5(14)	24.9(8)
C4A	3333(3)	6890(3)	4563.6(15)	29.8(9)
C13A	2251(3)	7081(3)	2541.9(14)	27.8(9)
C14A	2920(3)	8030(3)	2552.4(14)	26.4(8)
C15A	2671(4)	6259(4)	2244.8(18)	37.7(10)
C16A	1170(4)	7275(4)	2417.9(18)	36.5(10)
C17A	4017(4)	7856(4)	2410.7(19)	39.0(11)
C18A	2506(4)	8897(4)	2288(2)	42.2(12)
C19A	4819(8)	5234(8)	3270(4)	41.4(13)
C19B	5303(8)	5642(8)	3370(3)	39.5(13)
C20A	5268(8)	4977(8)	3764(4)	39.8(13)
C20B	4890(9)	4779(8)	3650(4)	44.3(13)
C21A	4032(9)	4490(10)	3113(5)	51(2)
C21B	6234(8)	6034(10)	3608(5)	50.9(19)
C22A	5634(11)	5477(16)	2904(6)	41(2)
C22B	5397(12)	5384(16)	2857(5)	40(2)
C23A	5295(10)	3869(9)	3839(5)	45(2)
C23B	4096(10)	4203(10)	3347(5)	54(2)
C24A	6284(9)	5421(10)	3848(5)	54.9(19)
C24B	5608(11)	4119(11)	3909(5)	53(2)
B1A	1211(3)	8816(3)	3861.0(17)	25.5(9)
B2A	2609(3)	7505(3)	3287.9(16)	22.7(9)
B3A	4042(4)	6158(3)	3830.5(16)	24.8(9)

Atom	$U_{11}$	$U_{22}$	$U_{33}$	$U_{23}$	$U_{13}$	$U_{12}$
F1	64(2)	53.0(19)	23.5(14)	1.5(12)	3.6(11)	18.8(16)
O1	45(2)	38.4(18)	30.2(16)	3.7(13)	1.3(14)	17.0(15)
O2	36.4(18)	35.0(16)	33.0(16)	5.6(13)	8.4(14)	9.8(13)
O3	31.4(16)	28.7(15)	23.8(14)	-0.4(11)	-1.5(12)	-5.0(11)
O4	35.3(16)	29.8(15)	24.1(14)	-0.2(11)	0.6(12)	-8.3(12)
O5	39.2(17)	30.4(15)	27.6(15)	-0.4(12)	-4.8(13)	9.2(13)
O6	39.2(18)	36.0(17)	30.0(15)	-5.2(13)	-6.1(13)	14.0(13)
C1	22.7(19)	26.3(19)	29(2)	1.3(15)	0.0(15)	-2.4(14)
C2	20.9(19)	24.6(19)	26.6(19)	-0.3(14)	-2.2(14)	-2.4(14)
C3	22(2)	26.0(19)	30(2)	-0.3(15)	-0.2(15)	0.2(15)
C4	32(2)	30(2)	30(2)	-1.8(16)	1.5(17)	3.7(17)
C5	38(2)	34(2)	24(2)	-0.4(16)	1.4(16)	2.5(18)
C6	29(2)	29(2)	31(2)	1.2(16)	-2.8(17)	2.5(16)
C7	47(3)	38(3)	36(2)	-1.5(18)	3(2)	17(2)
C8	34(2)	48(3)	48(3)	3(2)	11(2)	8(2)
C9	69(4)	75(5)	55(4)	-3(3)	-9(3)	36(4)
C10	60(4)	40(3)	56(3)	-4(2)	17(3)	-3(2)
C11	42(3)	67(4)	102(6)	-11(4)	26(4)	-10(3)
C12	76(4)	57(3)	41(3)	4(3)	19(3)	26(3)
C13	36(2)	30(2)	21.8(19)	-0.6(15)	0.6(17)	-6.1(16)
C14	37(2)	35(2)	20.6(19)	0.1(16)	2.6(17)	-8.2(17)
C15	42(3)	36(2)	35(2)	-10.3(18)	6(2)	-12(2)
C16	36(3)	43(3)	29(2)	2.9(18)	-6.2(18)	-7.6(19)
C17	35(2)	48(3)	31(2)	-3.9(19)	8.1(19)	-9(2)
C18	52(3)	40(3)	27(2)	5.3(18)	-6(2)	-13(2)
C19	35(2)	32(2)	37(2)	0.9(17)	-5.1(18)	12.8(18)
C20	34(2)	36(2)	33(2)	-3.7(17)	-5.3(17)	8.3(18)
C21	42(3)	45(3)	62(4)	18(2)	7(2)	9(2)
C22	61(4)	47(3)	37(3)	-8(2)	-18(2)	20(3)
C23	46(3)	39(3)	47(3)	-10(2)	-19(2)	14(2)
C24	31(3)	54(3)	65(4)	5(3)	6(2)	4(2)
B1	24(2)	28(2)	29(2)	5.4(17)	1.0(18)	1.1(17)
B2	25(2)	25(2)	27(2)	2.5(15)	1.0(16)	2.5(16)
B3	29(2)	28(2)	25(2)	-2.5(17)	-0.4(18)	-0.1(17)
F1A	60.4(19)	53.0(18)	22.4(13)	1.6(11)	1.3(13)	19.1(14)
O1A	55(2)	41(2)	42(2)	-13.9(15)	-16.6(17)	24.6(16)
O2A	34.2(18)	41.0(17)	29.1(16)	-6.0(13)	-5.6(13)	13.9(13)
O3A	46(2)	30.8(15)	22.8(14)	0.9(12)	-1.0(13)	-11.2(13)
O4A	38.5(18)	35.5(16)	23.2(14)	-1.6(12)	2.8(12)	-11.9(13)
O5A	42(7)	31(7)	26(4)	0(4)	3(4)	17(4)
O5B	38(7)	29(6)	26(4)	3(4)	5(4)	7(4)
O6A	36(6)	43(5)	30(4)	7(3)	1(4)	18(4)

Table 10-10 Anisotropic Displacement Parameters ( $\times 10^4$ ) for **3a**. The anisotropic displacement factor exponent takes the form:  $-2p^2[h^2a^{*2} \times U_{11} + \dots + 2hka^* \times b^* \times U_{12}]$ .

Table 10-10 (cont'd)

Atom	$U_{11}$	$U_{22}$	$U_{33}$	$U_{23}$	$U_{13}$	$U_{12}$
O6B	42(7)	43(5)	35(5)	11(4)	15(4)	22(5)
C1A	21.2(19)	25.2(19)	27.0(19)	0.4(14)	2.5(15)	-0.4(14)
C2A	19.5(18)	21.3(18)	24.6(18)	0.9(13)	1.2(13)	-3.6(14)
C5A	36(2)	33(2)	22(2)	-1.3(15)	1.5(16)	2.5(17)
C6A	32(2)	25.7(19)	28(2)	-0.2(15)	2.0(16)	5.7(15)
C7A	49(3)	37(3)	53(3)	-8(2)	-18(2)	19(2)
C8A	29(2)	41(2)	35(2)	-0.8(18)	-1.7(18)	13.1(18)
C9A	77(5)	46(4)	134(8)	28(4)	-51(5)	-15(3)
C10A	71(4)	78(5)	59(4)	-18(3)	-12(3)	47(4)
C11A	49(3)	56(3)	33(2)	4(2)	-4(2)	22(2)
C12A	35(3)	61(4)	69(4)	19(3)	-8(3)	1(2)
C13A	34(2)	29(2)	20.4(18)	-0.3(15)	-0.2(16)	-2.9(16)
C14A	28(2)	30(2)	21.0(18)	-0.2(14)	0.0(15)	-1.5(15)
C15A	35(2)	37(2)	41(3)	-9.9(19)	4.2(19)	-6.4(18)
C16A	30(2)	40(2)	39(2)	3.4(19)	-2.9(19)	-6.8(18)
C17A	33(2)	39(2)	45(3)	-5(2)	14(2)	-4.4(19)
C18A	42(3)	36(2)	48(3)	11(2)	-11(2)	-4(2)
C19A	40(3)	43(3)	41(3)	-5(2)	5(2)	15(2)
C19B	37(3)	44(3)	38(3)	-5(2)	5(2)	16(2)
C20A	37(3)	43(3)	39(3)	-6(2)	2(2)	15(2)
C20B	43(3)	46(3)	44(3)	-3(2)	7(2)	16(2)
C21A	50(4)	51(4)	53(4)	-14(4)	-2(4)	11(4)
C21B	39(4)	63(4)	51(4)	-20(3)	3(3)	5(3)
C22A	42(5)	45(4)	38(4)	0(3)	7(4)	12(4)
C22B	40(5)	46(4)	34(4)	-3(3)	5(4)	15(4)
C23A	43(4)	45(4)	47(4)	-6(3)	-1(4)	14(4)
C23B	54(4)	51(4)	58(4)	-10(4)	13(4)	4(4)
C24A	46(4)	63(4)	56(4)	-11(3)	-3(3)	10(3)
C24B	50(4)	56(4)	54(4)	0(3)	3(4)	21(4)
B1A	22(2)	25(2)	30(2)	-2.8(17)	2.9(17)	2.2(16)
B2A	19(2)	24(2)	25(2)	0.2(15)	1.2(16)	2.4(16)
B3A	25(2)	24(2)	25(2)	1.1(16)	-1.4(17)	-0.4(16)

Atom	Atom	Length/Å
F1	C5	1.355(5)
O1	C7	1.450(6)
O1	B1	1.366(6)
O2	C8	1.452(6)
O2	B1	1.357(6)
O3	C13	1.454(5)
O3	B2	1.356(5)
O4	C14	1.461(5)
O4	B2	1.370(5)
O5	C19	1.465(5)
O5	B3	1.358(6)
O6	C20	1.461(5)
O6	B3	1.367(6)
C1	C2	1.410(6)
C1	C6	1.391(6)
C1	B1	1.574(6)
C2	C3	1.417(6)
C2	B2	1.585(6)
C3	C4	1.390(6)
C3	B3	1.567(6)
C4	C5	1.377(6)
C5	C6	1.392(6)
C7	C8	1.532(8)
C7	C9	1.493(8)
C7	C10	1.553(8)
C8	C11	1.545(9)
C8	C12	1.497(8)
C13	C14	1.577(6)
C13	C15	1.517(6)
C13	C16	1.531(7)
C14	C17	1.519(7)
C14	C18	1.519(7)
C19	C20	1.552(7)
C19	C21	1.519(8)
C19	C22	1.511(7)
C20	C23	1.509(7)
C20	C24	1.512(7)
F1A	C5A	1.361(5)
O1A	C7A	1.468(6)
O1A	B1A	1.355(6)
O2A	C8A	1.461(5)
O2A	B1A	1.352(6)

Table 10-11 Bond Lengths in Å for **3a**.

Table 10-11 (cont'd)

Atom	Atom	Length/Å
O3A	C13A	1.453(5)
O3A	B2A	1.350(5)
O4A	C14A	1.451(5)
O4A	B2A	1.354(5)
O5A	C19A	1.460(19)
O5A	B3A	1.353(17)
O5B	C19B	1.46(2)
O5B	B3A	1.349(17)
O6A	C20A	1.426(18)
O6A	B3A	1.430(13)
O6B	C20B	1.489(18)
O6B	B3A	1.341(15)
C1A	C2A	1.414(5)
C1A	C6A	1.400(6)
C1A	B1A	1.565(6)
C2A	C3A	1.409(6)
C2A	B2A	1.582(6)
C3A	C4A	1.402(6)
C3A	B3A	1.561(6)
C4A	C5A	1.381(6)
C5A	C6A	1.375(6)
C7A	C8A	1.534(7)
C7A	C9A	1.514(11)
C7A	C10A	1.520(9)
C8A	C11A	1.515(7)
C8A	C12A	1.526(8)
C13A	C14A	1.575(6)
C13A	C15A	1.521(6)
C13A	C16A	1.508(7)
C14A	C17A	1.536(6)
C14A	C18A	1.514(6)
C19A	C20A	1.583(16)
C19A	C21A	1.530(15)
C19A	C22A	1.551(17)
C19B	C20B	1.532(17)
C19B	C21B	1.515(14)
C19B	C22B	1.527(16)
C20A	C23A	1.531(15)
C20A	C24A	1.504(15)
C20B	C23B	1.583(16)
C20B	C24B	1.512(15)

Atom	Atom	Atom	Angle/°
B1	O1	C7	107.0(4)
B1	O2	C8	106.5(4)
B2	O3	C13	108.3(3)
B2	O4	C14	107.7(3)
B3	O5	C19	106.7(3)
B3	O6	C20	107.0(3)
C2	C1	B1	123.7(4)
C6	C1	C2	120.5(4)
C6	C1	B1	115.7(4)
C1	C2	C3	119.0(4)
C1	C2	B2	120.4(4)
C3	C2	B2	120.5(4)
C2	C3	B3	123.5(4)
C4	C3	C2	119.8(4)
C4	C3	B3	116.6(4)
C5	C4	C3	119.8(4)
F1	C5	C4	119.7(4)
F1	C5	C6	118.4(4)
C4	C5	C6	121.9(4)
C1	C6	C5	118.9(4)
O1	C7	C8	102.9(4)
O1	C7	C9	109.4(4)
O1	C7	C10	104.7(4)
C8	C7	C10	111.4(5)
C9	C7	C8	118.5(5)
C9	C7	C10	108.8(5)
O2	C8	C7	103.2(4)
O2	C8	C11	107.2(5)
O2	C8	C12	110.0(5)
C7	C8	C11	110.8(6)
C12	C8	C7	116.2(5)
C12	C8	C11	109.0(6)
O3	C13	C14	103.2(3)
O3	C13	C15	108.6(4)
O3	C13	C16	106.3(3)
C15	C13	C14	114.6(4)
C15	C13	C16	110.1(4)
C16	C13	C14	113.3(4)
O4	C14	C13	102.9(3)
O4	C14	C17	105.8(4)
O4	C14	C18	109.2(4)
C17	C14	C13	113.9(4)
O6	C20	C24	106.9(4)

Table 10-12 Bond Angles in Å for **3a**.

Table 10-12 (cont'd)

Atom	Atom	Atom	Angle/°
C23	C20	C19	115.1(4)
C23	C20	C24	109.9(4)
C24	C20	C19	113.1(4)
O1	B1	C1	121.5(4)
O2	B1	O1	113.5(4)
O2	B1	C1	125.0(4)
O3	B2	O4	114.0(4)
O3	B2	C2	122.2(4)
O4	B2	C2	123.8(4)
O5	B3	O6	113.5(4)
O5	B3	C3	124.3(4)
O6	B3	C3	122.2(4)
B1A	O1A	C7A	106.5(4)
B1A	O2A	C8A	106.5(3)
B2A	O3A	C13A	108.6(3)
B2A	O4A	C14A	108.4(3)
B3A	O5A	C19A	109.4(12)
B3A	O5B	C19B	106.4(12)
C20A	O6A	B3A	107.6(10)
B3A	O6B	C20B	105.8(10)
C2A	C1A	B1A	123.5(4)
C6A	C1A	C2A	119.9(4)
C6A	C1A	B1A	116.6(4)
C1A	C2A	B2A	119.9(3)
C3A	C2A	C1A	119.2(4)
C3A	C2A	B2A	120.9(3)
C2A	C3A	B3A	123.4(4)
C4A	C3A	C2A	120.0(4)
C4A	C3A	B3A	116.6(4)
C5A	C4A	C3A	119.1(4)
F1A	C5A	C4A	118.3(4)
F1A	C5A	C6A	119.3(4)
C6A	C5A	C4A	122.4(4)
C5A	C6A	C1A	119.3(4)
O1A	C7A	C8A	102.1(4)
O1A	C7A	C9A	106.4(5)
O1A	C7A	C10A	107.6(5)
C9A	C7A	C8A	113.2(6)
C9A	C7A	C10A	112.1(6)
C10A	C7A	C8A	114.5(5)
O2A	C8A	C7A	102.3(4)
O2A	C8A	C11A	109.9(4)
O2A	C8A	C12A	106.0(4)



Atom	Atom	Atom	Atom	Angle/°
F1	C5	C6	C1	-179.5(4)
O1	C7	C8	O2	-25.9(5)
O1	C7	C8	C11	88.5(5)
O1	C7	C8	C12	-146.4(5)
O3	C13	C14	O4	-19.3(4)
O3	C13	C14	C17	94.7(4)
O3	C13	C14	C18	-137.6(4)
O5	C19	C20	O6	28.5(4)
O5	C19	C20	C23	146.7(4)
O5	C19	C20	C24	-85.8(5)
C1	C2	C3	C4	1.2(6)
C1	C2	C3	B3	-176.5(4)
C1	C2	B2	O3	71.2(5)
C1	C2	B2	O4	-107.1(5)
C2	C1	C6	C5	-0.4(6)
C2	C1	B1	O1	-167.9(4)
C2	C1	B1	O2	14.2(7)
C2	C3	C4	C5	-1.3(7)
C2	C3	B3	O5	9.9(7)
C2	C3	B3	O6	-171.8(4)
C3	C2	B2	O3	-105.9(5)
C3	C2	B2	O4	75.8(5)
C3	C4	C5	F1	-179.7(4)
C3	C4	C5	C6	0.5(7)
C4	C3	B3	O5	-167.9(4)
C4	C3	B3	O6	10.4(6)
C4	C5	C6	C1	0.3(7)
C6	C1	C2	C3	-0.3(6)
C6	C1	C2	B2	-177.5(4)
C6	C1	B1	O1	14.5(6)
C6	C1	B1	O2	-163.4(4)
C7	O1	B1	O2	-5.9(6)
C7	O1	B1	C1	176.0(4)
C8	O2	B1	O1	-11.8(5)
C8	O2	B1	C1	166.2(4)
C9	C7	C8	O2	-146.8(5)
C9	C7	C8	C11	-32.4(7)
C9	C7	C8	C12	92.8(7)
C10	C7	C8	O2	85.8(5)
C10	C7	C8	C11	-159.8(5)
C10	C7	C8	C12	-34.6(6)
C13	O3	B2	O4	-6.8(5)
C13	O3	B2	C2	174.8(4)

Table 10-13 Torsion Angles in ° for **3a**.

Table 10-13 (cont'd)

Atom	Atom	Atom	Atom	Angle/°
C14	O4	B2	O3	-6.8(5)
C14	O4	B2	C2	171.6(4)
C15	C13	C14	O4	-137.2(4)
C15	C13	C14	C17	-23.2(5)
C15	C13	C14	C18	104.5(5)
C20	O6	B3	O5	10.1(5)
C20	O6	B3	C3	-168.4(4)
C21	C19	C20	O6	-86.0(4)
C21	C19	C20	C23	32.2(6)
C21	C19	C20	C24	159.7(4)
C22	C19	C20	O6	146.3(4)
C22	C19	C20	C23	-95.6(5)
C22	C19	C20	C24	31.9(6)
B1	O1	C7	C8	19.7(5)
B1	O1	C7	C9	146.6(5)
B1	O1	C7	C10	-96.9(5)
B1	O2	C8	C7	23.2(5)
B1	O2	C8	C11	-93.9(6)
B1	O2	C8	C12	147.8(5)
B1	C1	C2	C3	-177.8(4)
B1	C1	C2	B2	5.0(6)
B1	C1	C6	C5	177.3(4)
B2	O3	C13	C14	16.2(4)
B2	O3	C13	C15	138.2(4)
B2	O3	C13	C16	-103.4(4)
B2	O4	C14	C13	16.1(4)
B2	O4	C14	C17	-103.8(4)
B2	O4	C14	C18	137.7(4)
B2	C2	C3	C4	178.3(4)
B2	C2	C3	B3	0.6(6)
B3	O5	C19	C20	-23.7(5)
B3	O5	C19	C21	95.3(5)
B3	O5	C19	C22	-145.0(4)
B3	O6	C20	C19	-23.9(5)
B3	O6	C20	C23	-146.1(4)
B3	O6	C20	C24	95.0(5)
B3	C3	C4	C5	176.6(4)
F1A	C5A	C6A	C1A	179.9(4)
O1A	C7A	C8A	O2A	-28.9(5)
O1A	C7A	C8A	C11A	-148.4(4)
O1A	C7A	C8A	C12A	84.7(5)

Table 10-13 (cont'd)

Atom	Atom	Atom	Atom	Angle/°
O3A	C13A	C14A	O4A	-17.6(4)
O3A	C13A	C14A	C17A	96.5(4)
O3A	C13A	C14A	C18A	-135.4(4)
O5A	C19A	C20A	O6A	23.7(12)
O5A	C19A	C20A	C23A	143.9(11)
O5A	C19A	C20A	C24A	-90.8(11)
O5B	C19B	C20B	O6B	-27.9(11)
O5B	C19B	C20B	C23B	80.8(11)
O5B	C19B	C20B	C24B	-145.9(12)
C2A	C3A	B3A	O5B	35.8(8)
C2A	C3A	B3A	O6A	-171.4(6)
C2A	C3A	B3A	O6B	-143.5(7)
C3A	C2A	B2A	O3A	69.1(5)
C3A	C2A	B2A	O4A	-110.0(5)
C3A	C4A	C5A	F1A	-178.0(4)
C3A	C4A	C5A	C6A	-0.1(7)
C4A	C3A	B3A	O5A	-168.4(7)
C4A	C3A	B3A	O5B	-142.4(7)
C4A	C3A	B3A	O6A	10.5(8)
C4A	C3A	B3A	O6B	38.3(8)
C4A	C5A	C6A	C1A	2.0(7)
C6A	C1A	C2A	C3A	1.9(6)
C6A	C1A	C2A	B2A	-175.8(4)
C6A	C1A	B1A	O1A	21.2(6)
C6A	C1A	B1A	O2A	-155.5(4)
C7A	O1A	B1A	O2A	-9.0(6)
C7A	O1A	B1A	C1A	173.9(4)
C8A	O2A	B1A	O1A	-10.8(5)
C8A	O2A	B1A	C1A	166.2(4)
C9A	C7A	C8A	O2A	85.0(5)
C9A	C7A	C8A	C11A	-34.4(7)
C9A	C7A	C8A	C12A	-161.4(5)
C10A	C7A	C8A	O2A	-144.8(5)
C10A	C7A	C8A	C11A	95.7(6)
C10A	C7A	C8A	C12A	-31.2(7)
C13A	O3A	B2A	O4A	-7.5(5)
C13A	O3A	B2A	C2A	173.3(4)
C14A	O4A	B2A	O3A	-5.0(5)
C14A	O4A	B2A	C2A	174.2(4)
C15A	C13A	C14A	O4A	-134.2(4)
C15A	C13A	C14A	C17A	-20.1(5)
C15A	C13A	C14A	C18A	107.9(5)

Table 10-13 (cont'd)

Atom	Atom	Atom	Atom	Angle/°
C16A	C13A	C14A	O4A	97.8(4)
C16A	C13A	C14A	C17A	-148.1(4)
C16A	C13A	C14A	C18A	-20.0(5)
C19A	O5A	B3A	O6A	13.0(11)
C19A	O5A	B3A	C3A	-168.0(7)
C19B	O5B	B3A	O6B	-13.6(11)
C19B	O5B	B3A	C3A	167.1(6)
B1A	O1A	C7A	C8A	23.6(6)
B1A	O1A	C7A	C9A	-95.3(6)
B1A	O1A	C7A	C10A	144.5(5)
B1A	O2A	C8A	C7A	24.7(5)
B1A	O2A	C8A	C11A	148.0(5)
B1A	O2A	C8A	C12A	-94.2(5)
B1A	C1A	C2A	C3A	-177.3(4)
B1A	C1A	C2A	B2A	4.9(6)
B1A	C1A	C6A	C5A	176.4(4)
B2A	O3A	C13A	C14A	15.4(4)
B2A	O3A	C13A	C15A	136.5(4)
B2A	O3A	C13A	C16A	-104.6(4)
B2A	O4A	C14A	C13A	14.1(4)
B2A	O4A	C14A	C17A	-105.8(4)
B2A	O4A	C14A	C18A	136.9(4)
B2A	C2A	C3A	C4A	177.7(4)
B2A	C2A	C3A	B3A	-0.4(6)
B3A	O5A	C19A	C20A	-22.3(11)
B3A	O5A	C19A	C21A	94.8(11)
B3A	O5A	C19A	C22A	-141.7(10)
B3A	O5B	C19B	C20B	25.6(10)
B3A	O5B	C19B	C21B	-89.1(10)
B3A	O5B	C19B	C22B	143.3(11)
B3A	O6A	C20A	C19A	-17.2(11)
B3A	O6A	C20A	C23A	-136.9(10)
B3A	O6A	C20A	C24A	102.6(10)
B3A	O6B	C20B	C19B	21.1(11)
B3A	O6B	C20B	C23B	-92.5(10)
B3A	O6B	C20B	C24B	147.6(10)
B3A	C3A	C4A	C5A	177.3(4)

Atom	x	y	z	$U_{eq}$
H4	1636.18	3671.44	7226.4	37
H6	3481.28	1313.68	7234.96	36
H9A	6065.16	-312.76	6659.82	99
H9B	6047.73	-1191.37	6293.15	99
H9C	5389.73	-1258.39	6756.55	99
H10D	3787.92	-1499.99	6392.51	78
H10E	4374	-1615.01	5910.93	78
H10F	3469.74	-850.84	5954.55	78
H11D	6053.17	1473.97	5749.41	106
H11E	6572.94	473.31	5907.65	106
H11F	6021.55	1148.63	6282.63	106
H12D	4368.48	-308.99	5313.56	87
H12E	5517.27	-610.88	5387.66	87
H12F	5244.02	434.04	5172.09	87
H15D	3066.6	864.76	4883.87	56
H15E	2541.08	1339.89	4438.39	56
H15F	1889.64	717.63	4799.46	56
H16D	693.03	2039.32	4964.58	54
H16E	1227.35	2677.01	4569.98	54
H16F	1091.15	3115.63	5080.94	54
H17D	4656.6	2936.2	4987.23	57
H17E	4163.77	2232.64	4606.54	57
H17F	4258.04	1876.5	5133.71	57
H18D	2311.78	4088.42	4831.53	60
H18E	2817.59	3523.37	4405.23	60
H18F	3490.24	4192.98	4737.77	60
H21G	1909.31	5791.8	5873.69	75
H21H	1102.53	6296.72	5539.49	75
H21I	1780.5	5416.4	5351.11	75
H22G	202.76	4717.86	5106.19	72
H22H	-595.34	5342.5	5396.4	72
H22I	-512.12	4186.83	5474.32	72
H23G	-202.24	6375.16	6672.11	66
H23H	-266.35	6611.34	6129.02	66
H23I	802.27	6560.42	6380.96	66
H24G	-775.43	4029.88	6267.82	75
H24H	-1328.92	5042.8	6159.48	75
H24I	-992.12	4788.3	6678.64	75
H4A	3772.42	6466.79	4728.11	36
H6A	1678.57	8608.86	4747.87	34
H9AA	1209.85	11286.11	3778.2	129
H9AB	452.59	11358.66	3348.65	129
H9AC	1371.33	10606.22	3332.45	129

Table 10-14 Hydrogen Fractional Atomic Coordinates ( $\times 10^4$ ) and Equivalent Isotropic Displacement Parameters ( $\text{\AA}^2 \times 10^3$ ) for **3a**.  $U_{eq}$  is defined as 1/3 of the trace of the orthogonalised  $U_{ij}$ .

Table 10-14 (cont'd)

Atom	x	y	z	$U_{eq}$
H10A	-938.63	10078.53	4228.16	104
H10B	-1181.72	10780.56	3798.36	104
H10C	-429.26	11136.03	4196.84	104
H12A	-1066.02	8158.32	3365.24	83
H12B	-1581.39	9133.44	3558.59	83
H12C	-870.35	8497.56	3888.95	83
H15A	3337.38	6075.09	2359.53	57
H15B	2724.62	6479.04	1922.15	57
H15C	2223.15	5691.79	2261.24	57
H16A	775.99	6678.15	2465.01	55
H16B	1126.26	7474.95	2092.01	55
H16C	905.93	7796.98	2616.07	55
H17A	4406.75	8452.3	2465.07	58
H17B	4046.39	7683.93	2080.86	58
H17C	4296.57	7320.19	2595.83	58
H18A	1842.96	9066.6	2410.2	63
H18B	2448.58	8729.03	1958.26	63
H18C	2959.58	9455.86	2323.67	63
H21A	3580.92	4340.84	3371.94	77
H21B	4366.68	3889.73	3010.76	77
H21C	3642.96	4763.68	2854.94	77
H21D	6382.96	6689.84	3490.02	76
H21E	6801.59	5599.1	3543.96	76
H21F	6118.64	6065.43	3943.47	76
H22A	5327.01	5507.01	2595.33	62
H22B	6151.39	4967.79	2907.55	62
H22C	5939.8	6110.07	2977.59	62
H22D	4751.7	5140.27	2742.08	60
H22E	5910.32	4877.74	2817.19	60
H22F	5589.68	5968.28	2681.15	60
H23A	5500.25	3729.34	4158.9	67
H23B	5775.56	3573.63	3623.44	67
H23C	4626.2	3595.49	3783.54	67
H23D	3757.42	3714.97	3540.27	81
H23E	4439.53	3875.08	3089.65	81
H23F	3599.96	4662.9	3222.97	81
H24A	6755.12	5187.27	3611.42	82
H24B	6524.74	5229.81	4156.05	82
H24C	6234.55	6134.97	3830.75	82
H24D	6122.45	4517.09	4062.09	80
H24E	5929.09	3669.3	3689.94	80
H24F	5238.32	3743.96	4142.75	80

Atom	Occupancy
O5A	0.5
O5B	0.5
O6A	0.5
O6B	0.5
C19A	0.5
C19B	0.5
C20A	0.5
C20B	0.5
C21A	0.5
H21A	0.5
H21B	0.5
H21C	0.5
C21B	0.5
H21D	0.5
H21E	0.5
H21F	0.5
C22A	0.5
H22A	0.5
H22B	0.5
H22C	0.5
C22B	0.5
H22D	0.5
H22E	0.5
H22F	0.5
C23A	0.5
H23A	0.5
H23B	0.5
H23C	0.5
C23B	0.5
H23D	0.5
H23E	0.5
H23F	0.5
C24A	0.5
H24A	0.5
H24B	0.5
H24C	0.5
C24B	0.5
H24D	0.5
H24E	0.5
H24F	0.5

Table 10-15 Atomic Occupancies for all atoms that are not fully occupied in **3a**.

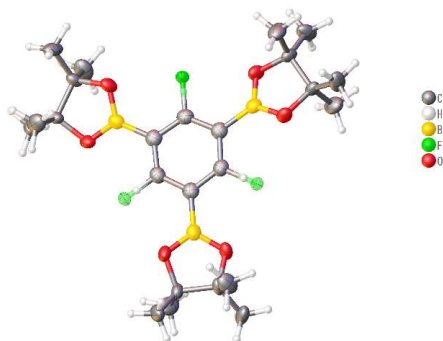


Figure 10-3 Structure of **3a''**

Formula	C <sub>24</sub> H <sub>38</sub> B <sub>3</sub> FO <sub>6</sub>
CCDC	2126641
<i>D</i> <sub>calc.</sub> /g cm <sup>-3</sup>	1.185
<i>m</i> /mm <sup>-1</sup>	0.697
Formula Weight	473.97
Color	colourless
Shape	block-shaped
Size/mm <sup>3</sup>	0.21×0.12×0.03
<i>T</i> /K	100.00(10)
Crystal System	trigonal
Space Group	<i>R</i> -3 <i>c</i>
<i>a</i> /Å	12.7356(3)
<i>b</i> /Å	12.7356(3)
<i>c</i> /Å	28.3761(7)
<i>a</i> /°	90
<i>b</i> /°	90
<i>g</i> /°	120
<i>V</i> /Å <sup>3</sup>	3985.8(2)
<i>Z</i>	6
<i>Z</i> '	0.166667
Wavelength/Å	1.54184
Radiation type	Cu K <sub>α</sub>
<i>Q</i> <sub>min</sub> /°	5.079
<i>Q</i> <sub>max</sub> /°	79.643
Measured Refl's.	11224
Indep't Refl's	971
Refl's <i>I</i> ≥2 <i>s</i> ( <i>I</i> )	930
<i>R</i> <sub>int</sub>	0.0585
Parameters	59
Restraints	0
Largest Peak	0.546
Deepest Hole	-0.319
GooF	1.045
<i>wR</i> <sub>2</sub> (all data)	0.1672
<i>wR</i> <sub>2</sub>	0.1654
<i>R</i> <sub>1</sub> (all data)	0.0691
<i>R</i> <sub>1</sub>	0.0673

Table 10-16 General Crystal Structure Data for Compound **3a''**.



Atom	x	y	z	$U_{eq}$
F1	0	2258(3)	7500	29.4(9)
O1	3423.9(13)	2445.9(13)	7629.4(5)	37.1(5)
C1	0	1080(2)	7500	33.1(7)
C2	1118(2)	1118(2)	7500	34.6(7)
C3	4369.3(19)	3666.7(18)	7496.1(7)	33.5(5)
C4	4816(3)	3561(2)	7015.2(9)	54.7(7)
C5	5401(2)	4138(2)	7851.7(10)	51.0(7)
B1	2342(3)	2342(3)	7500	31.7(7)

Table 10-17 Fractional Atomic Coordinates ( $\times 10^4$ ) and Equivalent Isotropic Displacement Parameters ( $\text{\AA}^2 \times 10^3$ ) for **3a''**.  $U_{eq}$  is defined as 1/3 of the trace of the orthogonalised  $U_{ij}$ .

Atom	$U_{11}$	$U_{22}$	$U_{33}$	$U_{23}$	$U_{13}$	$U_{12}$
F1	28(2)	23.4(15)	38(2)	0.7(9)	1.4(18)	13.8(11)
O1	39.3(8)	35.1(8)	43.5(8)	11.8(6)	6.2(6)	23.7(7)
C1	44.9(16)	37.6(11)	19.1(11)	0.0(5)	0.0(10)	22.4(8)
C2	42.6(12)	42.6(12)	18.8(11)	0.2(5)	-0.2(5)	21.3(14)
C3	36.8(11)	34.3(10)	38.5(10)	9.3(8)	8.3(8)	24.7(9)
C4	62.0(17)	52.4(15)	54.9(15)	3.4(11)	25.4(12)	32.5(13)
C5	35.6(12)	52.7(14)	68.3(16)	19.0(12)	-4.0(11)	24.8(11)
B1	39.2(13)	39.2(13)	22.3(12)	-1.2(5)	1.2(5)	23.8(14)

Table 10-18 Anisotropic Displacement Parameters ( $\times 10^4$ ) for **3a''**. The anisotropic displacement factor exponent takes the form:  $-2p^2[h^2a^{*2} \times U_{11} + \dots + 2hka^* \times b^* \times U_{12}]$ .

Atom	Atom	Length/Å
F1	C1	1.501(5)
O1	C3	1.462(3)
O1	B1	1.367(2)
C1	C21	1.400(2)
C1	C2	1.400(2)
C2	B1	1.559(5)
C3	C32	1.550(4)
C3	C4	1.510(3)
C3	C5	1.522(3)

Table 10-19 Bond Lengths in Å for **3a''**.

Atom	Atom	Atom	Angle/°
B1	O1	C3	106.73(16)
C2 <sup>1</sup>	C1	F1	118.27(15)
C2	C1	F1	118.27(15)
C2	C1	C2 <sup>1</sup>	123.5(3)
C1	C2	C1 <sup>2</sup>	116.5(3)
C1	C2	B1	121.73(15)
C12	C2	B1	121.73(15)
O1	C3	C33	101.77(10)
O1	C3	C4	106.59(18)
O1	C3	C5	109.71(16)
C4	C3	C33	114.6(2)
C4	C3	C5	110.2(2)
C5	C3	C33	113.35(18)
O1	B1	O13	112.9(3)
O1	B1	C2	123.55(13)
O13	B1	C2	123.55(13)

Table 10-20 Bond Angles in ° for **3a''**.

Atom	Atom	Atom	Atom	Angle/°
F1	C1	C2	C11	180.0
F1	C1	C2	B1	0.000(0)
C11	C2	B1	O12	161.20(8)
C1	C2	B1	O1	161.20(8)
C11	C2	B1	O1	-18.80(8)
C1	C2	B1	O12	-18.80(8)
C23	C1	C2	C11	0.000(0)
C23	C1	C2	B1	180.000(0)
C3	O1	B1	O12	-10.72(9)
C3	O1	B1	C2	169.28(9)
B1	O1	C3	C32	25.8(2)
B1	O1	C3	C4	-94.54(18)
B1	O1	C3	C5	146.16(16)

Table 10-21 Torsion Angles in ° for **3a''**.

Atom	x	y	z	$U_{eq}$
H1	0	1825.47	7500	40
H4A	4175.49	3359.21	6781.72	82
H4B	5029.25	2920.8	7020.73	82
H4C	5532.11	4333.91	6931.14	82
H5A	6017.77	4967.88	7768.14	76
H5B	5763.26	3616.65	7848.82	76
H5C	5085.47	4132.71	8167.29	76

Table 10-22 Hydrogen Fractional Atomic Coordinates ( $\times 10^4$ ) and Equivalent Isotropic Displacement Parameters ( $\text{\AA}^2 \times 10^3$ ) for **3a''**.  $U_{eq}$  is defined as 1/3 of the trace of the orthogonalised  $U_{ij}$ .

Atom	Occupancy
F1	0.3333
H1	0.6667

Table 10-23 Atomic Occupancies for all atoms that are not fully occupied in **3a''**.

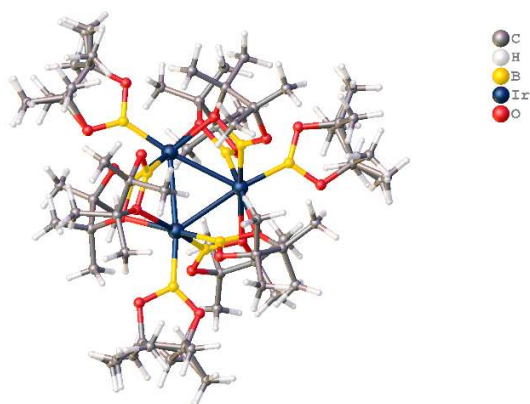


Figure 10-4 Structure of **[Ir(Bpin)<sub>3</sub>]<sub>3</sub>**

Formula	C <sub>54</sub> H <sub>108</sub> B <sub>9</sub> Ir <sub>3</sub> O <sub>18</sub>
CCDC	2250220
<i>D</i> <sub>calc.</sub> / g cm <sup>-3</sup>	1.562
<i>m</i> /mm <sup>-1</sup>	10.834
Formula Weight	1719.29
Color	red
Shape	octahedral-shaped
Size/mm <sup>3</sup>	0.24×0.19×0.15
<i>T</i> /K	100(2)
Crystal System	hexagonal
Space Group	<i>P</i> 6 <sub>3</sub> / <i>m</i>
<i>a</i> /Å	14.9030(3)
<i>b</i> /Å	14.9030(3)
<i>c</i> /Å	19.0012(4)
<i>a</i> /°	90
<i>b</i> /°	90
<i>g</i> /°	120
<i>V</i> /Å <sup>3</sup>	3654.75(15)
<i>Z</i>	2
<i>Z</i> '	0.166667
Wavelength/Å	1.54184
Radiation type	Cu K <sub>α</sub>
<i>Q</i> <sub>min</sub> /°	3.424
<i>Q</i> <sub>max</sub> /°	79.784
Measured Refl's.	18124
Indep't Refl's	2718
Refl's I ≥ 2 <i>s</i> (I)	2590
<i>R</i> <sub>int</sub>	0.0538
Parameters	147
Restraints	1
Largest Peak	1.705
Deepest Hole	-1.597
GooF	1.222
<i>wR</i> <sub>2</sub> (all data)	0.1647
<i>wR</i> <sub>2</sub>	0.1629
<i>R</i> <sub>1</sub> (all data)	0.0588
<i>R</i> <sub>1</sub>	0.0565

Table 10-24 General Crystal Structure Data for **[Ir(Bpin)<sub>3</sub>]<sub>3</sub>**.

Atom	x	y	z	$U_{eq}$
Ir <sup>1</sup>	4192.5(4)	6284.6(4)	7500	29.7(2)
O <sup>1</sup>	6569(7)	7259(8)	7500	51(2)
O <sup>2</sup>	5688(7)	5533(8)	7500	48(2)
O <sup>3</sup>	3264(5)	4906(5)	6770(3)	43.1(14)
O <sup>4</sup>	1903(7)	4663(8)	6122(4)	69(3)
C <sup>1</sup>	7325(14)	6941(16)	7256(11)	55(5)
C <sup>2</sup>	6766(13)	5780(14)	7500	59(4)
C <sup>3</sup>	7446(19)	6900(20)	6470(16)	76(4)
C <sup>4</sup>	8380(12)	7718(16)	7500	76(4)
C <sup>5</sup>	6951(18)	5060(20)	7224(15)	76(4)
C <sup>6</sup>	6955(19)	5780(20)	8345(17)	76(4)
C <sup>7</sup>	3226(8)	4240(8)	6192(5)	46(2)
C <sup>8</sup>	2479(12)	4326(13)	5677(7)	79(4)
C <sup>9</sup>	4290(10)	4540(11)	5932(7)	70(3)
C <sup>10</sup>	2736(17)	3152(12)	6506(9)	103(6)
C <sup>11</sup>	3110(20)	5209(19)	5145(8)	136(10)
C <sup>12</sup>	1755(15)	3444(19)	5266(9)	130(9)
B <sup>1</sup>	5610(11)	6423(13)	7500	39(3)
B <sup>2</sup>	2420(8)	5060(7)	6744(5)	35.0(19)

Table 10-25 Fractional Atomic Coordinates ( $\times 10^4$ ) and Equivalent Isotropic Displacement Parameters ( $\text{\AA}^2 \times 10^3$ ) for **[Ir(Bpin)<sub>3</sub>]<sub>3</sub>**.  $U_{eq}$  is defined as 1/3 of the trace of the orthogonalised  $U_{ij}$ .

Atom	$U_{11}$	$U_{22}$	$U_{33}$	$U_{23}$	$U_{13}$	$U_{12}$
Ir <sup>1</sup>	33.5(3)	34.5(3)	22.3(3)	0	0	18.0(2)
O <sup>1</sup>	30(4)	55(6)	70(7)	0	0	23(4)
O <sup>2</sup>	44(5)	50(5)	55(6)	0	0	28(4)
O <sup>3</sup>	46(3)	55(4)	33(3)	-18(3)	-8(3)	29(3)
O <sup>4</sup>	88(6)	125(7)	31(4)	-38(4)	-28(4)	82(6)
C <sup>1</sup>	61(12)	73(13)	45(10)	-6(9)	-11(8)	45(11)
C <sup>2</sup>	54(8)	76(11)	44(8)	0	0	30(8)
C <sup>3</sup>	49(6)	98(9)	89(9)	33(9)	4(7)	42(6)
C <sup>4</sup>	49(6)	98(9)	89(9)	33(9)	4(7)	42(6)
C <sup>5</sup>	49(6)	98(9)	89(9)	33(9)	4(7)	42(6)
C <sup>6</sup>	49(6)	98(9)	89(9)	33(9)	4(7)	42(6)
C <sup>7</sup>	58(6)	50(5)	35(5)	-16(4)	-5(4)	30(4)
C <sup>8</sup>	100(10)	121(12)	51(7)	-36(7)	-28(7)	82(10)
C <sup>9</sup>	65(7)	80(8)	66(8)	-20(7)	6(6)	38(7)
C <sup>10</sup>	176(19)	76(10)	78(10)	16(8)	37(11)	78(12)
C <sup>11</sup>	240(30)	220(30)	49(8)	58(12)	50(12)	190(20)
C <sup>12</sup>	129(15)	220(20)	94(12)	-120(15)	-65(11)	127(17)
B <sup>1</sup>	40(7)	61(9)	24(6)	0	0	31(7)
B <sup>2</sup>	46(5)	35(4)	27(4)	-2(4)	4(4)	22(4)

Table 10-26 Anisotropic Displacement Parameters ( $\times 10^4$ ) for **[Ir(Bpin)<sub>3</sub>]<sub>3</sub>**. The anisotropic displacement factor exponent takes the form:  $-2p^2[h^2a^{*2} \times U_{11} + \dots + 2hka^* \times b^* \times U_{12}]$ .

Atom	Atom	Length/Å
Ir <sup>1</sup>	Ir <sup>11</sup>	2.8423(8)
Ir <sup>1</sup>	Ir <sup>12</sup>	2.8423(8)
Ir <sup>1</sup>	O <sup>33</sup>	2.284(6)
Ir <sup>1</sup>	O <sup>3</sup>	2.284(6)
Ir <sup>1</sup>	B <sup>1</sup>	2.018(14)
Ir <sup>1</sup>	B <sup>24</sup>	2.022(9)
Ir <sup>1</sup>	B <sup>21</sup>	2.022(9)
O <sup>1</sup>	C <sup>1</sup>	1.50(2)
O <sup>1</sup>	B <sup>1</sup>	1.346(18)
O <sup>2</sup>	C <sup>2</sup>	1.459(19)
O <sup>2</sup>	B <sup>1</sup>	1.388(18)
O <sup>3</sup>	C <sup>7</sup>	1.463(10)
O <sup>3</sup>	B <sup>2</sup>	1.388(12)
O <sup>4</sup>	C <sup>8</sup>	1.462(14)
O <sup>4</sup>	B <sup>2</sup>	1.371(11)
C <sup>1</sup>	C <sup>2</sup>	1.57(3)
C <sup>1</sup>	C <sup>3</sup>	1.51(4)
C <sup>1</sup>	C <sup>4</sup>	1.486(17)
C <sup>2</sup>	C <sup>5</sup>	1.34(3)
C <sup>2</sup>	C <sup>6</sup>	1.63(3)
C <sup>7</sup>	C <sup>8</sup>	1.536(16)
C <sup>7</sup>	C <sup>9</sup>	1.499(16)
C <sup>7</sup>	C <sup>10</sup>	1.528(18)
C <sup>8</sup>	C <sup>11</sup>	1.55(3)
C <sup>8</sup>	C <sup>12</sup>	1.44(2)

Table 10-27 Bond Lengths in Å for [Ir(Bpin)<sub>3</sub>]<sub>3</sub>.

Atom	Atom	Atom	Angle/°
Ir <sup>11</sup>	Ir <sup>1</sup>	Ir <sup>12</sup>	60.0
O <sup>33</sup>	Ir <sup>1</sup>	Ir <sup>12</sup>	117.95(16)
O <sup>3</sup>	Ir <sup>1</sup>	Ir <sup>12</sup>	117.95(16)
O <sup>3</sup>	Ir <sup>1</sup>	Ir <sup>11</sup>	71.25(16)
O <sup>33</sup>	Ir <sup>1</sup>	Ir <sup>11</sup>	71.25(16)
O <sup>33</sup>	Ir <sup>1</sup>	O <sup>3</sup>	74.8(4)
B <sup>1</sup>	Ir <sup>1</sup>	Ir <sup>11</sup>	172.6(5)
B <sup>1</sup>	Ir <sup>1</sup>	Ir <sup>12</sup>	127.4(5)
B <sup>1</sup>	Ir <sup>1</sup>	O <sup>3</sup>	103.0(4)
B <sup>1</sup>	Ir <sup>1</sup>	O <sup>33</sup>	103.0(4)
B <sup>1</sup>	Ir <sup>1</sup>	B <sup>22</sup>	77.6(4)
B <sup>1</sup>	Ir <sup>1</sup>	B <sup>24</sup>	77.6(4)
B <sup>24</sup>	Ir <sup>1</sup>	Ir <sup>11</sup>	107.4(3)
B <sup>22</sup>	Ir <sup>1</sup>	Ir <sup>11</sup>	107.4(3)
B <sup>22</sup>	Ir <sup>1</sup>	Ir <sup>12</sup>	66.3(3)
B <sup>24</sup>	Ir <sup>1</sup>	Ir <sup>12</sup>	66.3(3)
B24	Ir1	Ir12	66.3(3)
B22	Ir1	O33	172.0(3)
B24	Ir1	O3	172.0(3)
B22	Ir1	O3	97.3(3)
B24	Ir1	O33	97.3(3)
B24	Ir1	B22	90.6(6)
B1	O1	C1	109.0(12)
B1	O2	C2	111.5(12)
C7	O3	Ir1	150.1(6)
B2	O3	Ir1	93.7(5)
B2	O3	C7	110.8(7)
B2	O4	C8	110.3(8)
O1	C1	C2	100.9(14)
O1	C1	C3	116.4(16)
C3	C1	C2	104.8(17)
C4	C1	O1	109.1(15)
C4	C1	C2	122.6(16)
C4	C1	C3	103.8(17)
O2	C2	C1	100.8(13)
O2	C2	C6	99.6(11)
C1	C2	C6	107.0(16)
C5	C2	O2	116.0(16)
C5	C2	C1	124.1(16)
C5	C2	C6	106.4(19)
O3	C7	C8	101.8(8)
O3	C7	C9	111.6(8)
O3	C7	C10	105.2(9)
C9	C7	C8	117.8(11)
C9	C7	C10	108.6(11)
C10	C7	C8	110.9(13)

Table 10-28 Bond Angles in ° for [Ir(Bpin)<sub>3</sub>]<sub>3</sub>.



Table 10-28 (cont'd)

Atom	Atom	Atom	Angle/°
O4	C8	C7	103.5(9)
O4	C8	C11	107.3(12)
C7	C8	C11	109.3(14)
C12	C8	O4	109.0(13)
C12	C8	C7	120.8(14)
C12	C8	C11	106.3(16)
O1	B1	Ir1	131.8(11)
O1	B1	O2	109.1(11)
O2	B1	Ir1	119.0(10)
O3	B2	Ir11	123.6(6)
O4	B2	Ir11	127.7(7)
O4	B2	O3	108.7(7)

Atom	Atom	Atom	Atom	Angle/°
Ir <sup>1</sup>	O <sup>3</sup>	C <sup>7</sup>	C <sup>8</sup>	-123.9(12)
Ir <sup>1</sup>	O <sup>3</sup>	C <sup>7</sup>	C <sup>9</sup>	2.7(17)
Ir <sup>1</sup>	O <sup>3</sup>	C <sup>7</sup>	C <sup>10</sup>	120.3(13)
Ir <sup>1</sup>	O <sup>3</sup>	B <sup>2</sup>	Ir <sup>11</sup>	-24.1(7)
Ir <sup>1</sup>	O <sup>3</sup>	B <sup>2</sup>	O <sup>4</sup>	153.6(7)
O <sup>1</sup>	C <sup>1</sup>	C <sup>2</sup>	O <sup>2</sup>	26.3(10)
O <sup>1</sup>	C <sup>1</sup>	C <sup>2</sup>	C <sup>5</sup>	158.3(17)
O <sup>1</sup>	C <sup>1</sup>	C <sup>2</sup>	C <sup>6</sup>	-77.4(16)
O <sup>3</sup>	C <sup>7</sup>	C <sup>8</sup>	O <sup>4</sup>	-21.3(13)
O <sup>3</sup>	C <sup>7</sup>	C <sup>8</sup>	C <sup>11</sup>	92.8(12)
O <sup>3</sup>	C <sup>7</sup>	C <sup>8</sup>	C <sup>12</sup>	-143.6(15)
C <sup>1</sup>	O <sup>1</sup>	B <sup>1</sup>	Ir <sup>1</sup>	-160.9(8)
C <sup>1</sup>	O <sup>1</sup>	B <sup>1</sup>	O <sup>2</sup>	19.1(8)
C <sup>2</sup>	O <sup>2</sup>	B <sup>1</sup>	Ir <sup>1</sup>	180.000(0)
C <sup>2</sup>	O <sup>2</sup>	B <sup>1</sup>	O <sup>1</sup>	0.000(0)
C <sup>3</sup>	C <sup>1</sup>	C <sup>2</sup>	O <sup>2</sup>	-94.9(14)
C <sup>3</sup>	C <sup>1</sup>	C <sup>2</sup>	C <sup>5</sup>	37(2)
C <sup>3</sup>	C <sup>1</sup>	C <sup>2</sup>	C <sup>6</sup>	161.3(16)
C <sup>4</sup>	C <sup>1</sup>	C <sup>2</sup>	O <sup>2</sup>	147.6(15)
C <sup>4</sup>	C <sup>1</sup>	C <sup>2</sup>	C <sup>5</sup>	-80(2)
C <sup>4</sup>	C <sup>1</sup>	C <sup>2</sup>	C <sup>6</sup>	44(2)
C <sup>7</sup>	O <sup>3</sup>	B <sup>2</sup>	Ir <sup>11</sup>	173.4(7)
C <sup>7</sup>	O <sup>3</sup>	B <sup>2</sup>	O <sup>4</sup>	-8.9(11)
C <sup>8</sup>	O <sup>4</sup>	B <sup>2</sup>	Ir <sup>11</sup>	171.3(10)
C <sup>8</sup>	O <sup>4</sup>	B <sup>2</sup>	O <sup>3</sup>	-6.3(13)
C <sup>9</sup>	C <sup>7</sup>	C <sup>8</sup>	O <sup>4</sup>	-143.8(11)
C <sup>9</sup>	C <sup>7</sup>	C <sup>8</sup>	C <sup>11</sup>	-29.7(15)
C <sup>9</sup>	C <sup>7</sup>	C <sup>8</sup>	C <sup>12</sup>	93.9(18)
C <sup>10</sup>	C <sup>7</sup>	C <sup>8</sup>	O <sup>4</sup>	90.2(13)
C <sup>10</sup>	C <sup>7</sup>	C <sup>8</sup>	C <sup>11</sup>	-155.7(12)
C <sup>10</sup>	C <sup>7</sup>	C <sup>8</sup>	C <sup>12</sup>	-32.0(19)
B <sup>1</sup>	O <sup>1</sup>	C <sup>1</sup>	C <sup>2</sup>	-28.7(11)
B <sup>1</sup>	O <sup>1</sup>	C <sup>1</sup>	C <sup>3</sup>	84(2)
B <sup>1</sup>	O <sup>1</sup>	C <sup>1</sup>	C <sup>4</sup>	-159.1(10)
B <sup>1</sup>	O <sup>2</sup>	C <sup>2</sup>	C <sup>1</sup>	-17.5(8)
B <sup>1</sup>	O <sup>2</sup>	C <sup>2</sup>	C <sup>5</sup>	-154.2(14)
B <sup>1</sup>	O <sup>2</sup>	C <sup>2</sup>	C <sup>6</sup>	92.1(14)
B <sup>2</sup>	O <sup>3</sup>	C <sup>7</sup>	C <sup>8</sup>	19.1(12)
B <sup>2</sup>	O <sup>3</sup>	C <sup>7</sup>	C <sup>9</sup>	145.7(10)
B <sup>2</sup>	O <sup>3</sup>	C <sup>7</sup>	C <sup>10</sup>	-96.7(12)
B <sup>2</sup>	O <sup>4</sup>	C <sup>8</sup>	C <sup>7</sup>	17.8(15)
B <sup>2</sup>	O <sup>4</sup>	C <sup>8</sup>	C <sup>11</sup>	-97.7(14)
B <sup>2</sup>	O <sup>4</sup>	C <sup>8</sup>	C <sup>12</sup>	147.6(14)

Table 10-29 Torsion Angles in ° for [Ir(Bpin)<sub>3</sub>]<sub>3</sub>.

Atom	x	y	z	$U_{eq}$
H <sup>3A</sup>	6791.25	6364.77	6266.44	115
H <sup>3B</sup>	7991.82	6732.07	6371.11	115
H <sup>3C</sup>	7635.58	7573.34	6263.56	115
H <sup>4A</sup>	8608.61	8374.55	7252.74	115
H <sup>4B</sup>	8860.97	7466.37	7400.4	115
H <sup>4C</sup>	8365.11	7826.04	8007.69	115
H <sup>5A</sup>	6537.85	4401.5	7474.25	115
H <sup>5B</sup>	7688.21	5283.56	7272.08	115
H <sup>5C</sup>	6760.33	4963.53	6724.91	115
H <sup>6A</sup>	6487.15	5956.58	8595	115
H <sup>6B</sup>	7674.46	6296.51	8455.86	115
H <sup>6C</sup>	6815.89	5093.85	8492.35	115
H <sup>9A</sup>	4534.01	5134.87	5613.84	104
H <sup>9B</sup>	4266.24	3955.82	5679.31	104
H <sup>9C</sup>	4763.88	4727.21	6332.85	104
H <sup>10A</sup>	3018.9	3188.66	6977.67	155
H <sup>10B</sup>	2891.45	2712.56	6204.85	155
H <sup>10C</sup>	1983.95	2855.61	6536.94	155
H <sup>11A</sup>	2647.6	5200.08	4774.96	204
H <sup>11B</sup>	3652.86	5107.76	4934.26	204
H <sup>11C</sup>	3427.39	5876.74	5389.96	204
H <sup>12A</sup>	1204.6	2941.46	5572.49	196
H <sup>12B</sup>	2118.17	3120.03	5046.49	196
H <sup>12C</sup>	1451.92	3672.73	4898.68	196

Table 10-30 Hydrogen Fractional Atomic Coordinates ( $\times 10^4$ ) and Equivalent Isotropic Displacement Parameters ( $\text{\AA}^2 \times 10^3$ ) for **[Ir(Bpin)<sub>3</sub>]**.  $U_{eq}$  is defined as 1/3 of the trace of the orthogonalised  $U_{ij}$ .

Atom	Occupancy
C <sup>1</sup>	0.5
C <sup>3</sup>	0.5
H <sup>3A</sup>	0.5
H <sup>3B</sup>	0.5
H <sup>3C</sup>	0.5
H <sup>4A</sup>	0.5
H <sup>4B</sup>	0.5
H <sup>4C</sup>	0.5
C <sup>5</sup>	0.5
H <sup>5A</sup>	0.5
H <sup>5B</sup>	0.5
H <sup>5C</sup>	0.5
C <sup>6</sup>	0.5
H <sup>6A</sup>	0.5
H <sup>6B</sup>	0.5
H <sup>6C</sup>	0.5

Table 10-31 Atomic Occupancies for all atoms that are not fully occupied in **[Ir(Bpin)<sub>3</sub>]<sub>3</sub>**.